OCS Study
BOEM 2020-021

Cross-Shelf Habitat Suitability Modeling: Characterizing Potential Distributions of Deep-Sea Corals, Sponges, and Macrofauna Offshore of the US West Coast

US Department of the Interior
Bureau of Ocean Energy Management
Pacific OCS Region

BOEM
Bureau of Ocean Energy Management

OCS Study
BOEM 2020-021

Cross-Shelf Habitat Suitability Modeling: Characterizing Potential Distributions of Deep-Sea Corals, Sponges, and Macrofauna Offshore of the US West Coast

October 2020

Authors:
Matthew Poti[1,2], Sarah K. Henkel[3], Joseph J. Bizzarro[4], Thomas F. Hourigan[5], M. Elizabeth Clarke[6], Curt E. Whitmire[7], Abigail Powell[8], Mary M. Yoklavich[4], Laurie Bauer[1,2], Arliss J. Winship[1,2], Michael Coyne[1,2], David J. Gillett[9], Lisa Gilbane[10], John Christensen[2], and Christopher F.G. Jeffrey[1,2]

1. CSS, Inc., 10301 Democracy Ln, Suite 300, Fairfax, VA 22030
2. National Centers for Coastal Ocean Science (NCCOS), National Oceanic and Atmospheric Administration (NOAA), National Ocean Service, 1305 East West Hwy SSMC4, Silver Spring, MD 20910
3. Oregon State University, Hatfield Marine Science Center, 2030 Marine Science Drive, Newport, OR 97365
4. Institute of Marine Sciences, University of California, Santa Cruz & Fisheries Ecology Division, Southwest Fisheries Science Center (SWFSC), NOAA National Marine Fisheries Service (NMFS), Santa Cruz, CA 95060
5. Deep Sea Coral Research & Technology Program, NOAA NMFS, 1315 East West Hwy, Silver Spring, MD 20910
6. Northwest Fisheries Science Center (NWFSC), NOAA NMFS, 2725 Montlake Blvd East, Seattle, WA 98112
7. Fishery Resource Analysis and Monitoring Division, NWFSC, NOAA NMFS, 99 Pacific St, Bldg 255-A, Monterey, CA 93940
8. Lynker Technologies under contract to the NWFSC, NOAA NMFS, 2725 Montlake Blvd East, Seattle, WA 98112
9. Southern California Coastal Water Research Project, 3535 Harbor Blvd, Suite 110, Costa Mesa, CA, 92626
10. Bureau of Ocean Energy Management, 770 Paso Camarillo, Suite 102, Camarillo, CA 93010

Prepared under NCCOS IAA MOA-2016-055/10325, BOEM OCS Study 2020-021, and NCCOS BOEM IAA M16PG00014
By
U.S. Department of Commerce
National Oceanic and Atmospheric Administration
National Ocean Service
National Centers for Coastal Ocean Science
Marine Spatial Ecology Division
1305 East-West Hwy, SSMC-4, N/SCI-1
Silver Spring, MD 20910

US Department of the Interior
Bureau of Ocean Energy Management
Pacific OCS Region

DISCLAIMER

This study was funded, in part, by the US Department of the Interior, Bureau of Ocean Energy Management (BOEM), Environmental Studies Program, Washington, DC, through Interagency Agreement Number M16PG00014 with the US Department of Commerce, National Oceanic and Atmospheric Administration, National Ocean Service, National Centers for Coastal Ocean Science, Silver Spring, MD. This report has been technically reviewed by BOEM, and it has been approved for publication. The views and conclusions contained in this document are those of the authors and should not be interpreted as representing the opinions or policies of the US Government, nor does mention of trade names or commercial products constitute endorsement or recommendation for use.

REPORT AVAILABILITY

To download a PDF file of this report, go to the US Department of the Interior, Bureau of Ocean Energy Management Data and Information Systems webpage (http://www.boem.gov/Environmental-Studies-EnvData/), click on the link for the Environmental Studies Program Information System (ESPIS), and search on 2020-021. The report is also available at the National Technical Reports Library at https://ntrl.ntis.gov/NTRL/.

CITATION

Poti, M., S.K. Henkel, J.J. Bizzarro, T.F. Hourigan, M.E. Clarke, C.E. Whitmire, A. Powell, M.M. Yoklavich, L. Bauer, A.J. Winship, M. Coyne, D.J. Gillett, L. Gilbane, J. Christensen, and C.F.G. Jeffrey. 2020. Cross-Shelf Habitat Suitability Modeling: Characterizing Potential Distributions of Deep-Sea Corals, Sponges, and Macrofauna Offshore of the US West Coast. Camarillo (CA): US Department of the Interior, Bureau of Ocean Energy Management. OCS Study BOEM 2020-021. 267 p.

ABOUT THE COVER

Cover photos: (Top Left) *Stylaster californicus* with a Blacksmith (*Chromis punctipinnis*) and many Squarespot (*Sebastes hopkinsi*) at 41 m depth on Farnsworth Bank. Credit: NOAA Southwest Fisheries Science Center, Advanced Survey Technologies Group (Top Right) *Nutricola lordi*. Credit: Sarah Henkel, Oregon State University (Middle Right) *Alia gausapata*. Credit: Sarah Henkel, Oregon State University (Bottom Right) *Primnoa pacifica*, *Lophelia pertusa*, and *Desmophyllum* at 278 m depth observed by the remotely operated vehicle *ROPOS* in 2008. Credit: NOAA Olympic Coast National Marine Sanctuary (Bottom Left) *Magelona berkeleyi*. Credit: Sarah Henkel, Oregon State University

ACKNOWLEDGMENTS

We dedicate this report to Brian Kinlan, our friend and colleague who passed away before this study was completed. This study began through a conversation Brian had with Lisa Gilbane at a conference in Oxnard, California in 2013. Brian had a vision for improving deep-sea coral modeling across all US waters, and we think this report is one step closer to that vision.

We thank the many scientists who contributed their data, time, and expertise over the course of this study. Robert McGuinn (NOAA National Centers for Environmental Information) provided assistance in using data from the NOAA National Database for Deep-Sea Corals and Sponges. Gregory Boland (BOEM), Peter Etnoyer (NOAA NCCOS), Meredith Everett (NOAA NWFSC), Samuel Georgian (Marine Conservation Institute), Enrique Salgado (NOAA NCCOS), and Brian Tissot (Humboldt State University) participated in a discussion of the available deep-sea coral and sponge data in our study area and the use of these data in species distribution models. John King (University of Rhode Island), Bridgette Lohrman (Environmental Protection Agency), and Walter Nelson (Environmental Protection Agency) participated in a discussion of the available macrofauna survey data in our study area and the use of these data in species distribution models. Guy Cochrane (United States Geological Survey), David Huff (NOAA NWFSC), and Chris Jenkins (University of Colorado) provided advice on the source data and methods used to develop environmental predictor variables depicting depth, seafloor topography, and seafloor substrate. Steven Bograd (NOAA SWFSC), Andrew Moore (University of California, Santa Cruz), Rachel Simons (University of California, Santa Barbara), Libe Washburn (University of California, Santa Barbara), Yizhen Li (CSS Inc. and NOAA NCCOS), Susan Zaleski (BOEM), and Brian Zelenke (formerly BOEM) provided advice on the source data and methods used to develop the oceanographic variables used in the models. Andrew Moore and Changming Dong (University of California, Los Angeles) shared outputs from a hindcast ocean circulation model for us to use in developing environmental predictor variables. Samuel Georgian, David Huff, Christopher Rooper (Department of Fisheries and Oceans Canada), and James Thorson (NOAA Alaska Fisheries Science Center) reviewed early drafts of model outputs and modeling methods and offered suggestions for improvements. Thomas Laidig (NOAA SWFSC), Diana Watters (NOAA SWFSC), and Linda Kuhnz (Monterey Bay Aquarium Research Institute) provided data from recent visual surveys for our exploration of ground-truthing the deep-sea coral and sponge models. Heather Coleman (NOAA Deep Sea Coral Research & Technology Program) and Elizabeth Duncan (Channel Islands National Marine Sanctuary) provided valuable advice and feedback throughout the study. Catherine Dunkel (BOEM), Peter Etnoyer, Matthew Kendall (NOAA NCCOS), Sarah Hile (CSS, Inc. and NOAA NCCOS), Thomas Laidig (NOAA SWFSC), Mark Mueller (BOEM), Timothy White (BOEM), and Susan Zaleski (BOEM) reviewed this report and provided helpful comments and suggestions.

This study was funded by the Bureau of Ocean Energy Management through Interagency Agreement Number M16PG00014 with the US Department of Commerce, National Oceanic and Atmospheric Administration, National Ocean Service, National Centers for Coastal Ocean Science. Matthew Poti, Laurie Bauer, Michael Coyne, Christopher Jeffrey, and Arliss Winship were supported by NOAA Contracts No. EA133C-17-BA-0062 with CSS, Inc.

Contents

List of Figures

List of Tables

List of Abbreviations and Acronyms

AICc	Akaike's Information Criterion, corrected for small sample size
ATSML	Active Tectonics and Seafloor Mapping Lab
AUC	Area Under the Receiver Operating Characteristic Curve
AUV	Autonomous Underwater Vehicle
BHC	Benthic Habitat Characterization
BOEM	Bureau of Ocean Energy Management
BRT	Boosted Regression Tree
C	Celsius
CCLEAN	Central Coast Long-term Environmental Assessment Network
CRM	Coastal Relief Model
CSUMB	California State University, Monterey Bay
CV	Coefficient of Variation
°	Degree
DSCS	Deep-sea Corals and Sponges
EFH	Essential Fish Habitat
EPA	US Environmental Protection Agency
GEBCO	General Bathymetric Chart of the Oceans
GLM	Generalized Linear Model
HOODS	Humboldt Open Ocean Disposal Site
HYCOM	HYbrid Coordinate Ocean Model
km	Kilometer
m	Meter
m/s	Meter per Second
MaxEnt	Maximum Entropy
MBARI	Monterey Bay Aquarium Research Institute
mg/m^3	Milligram per Cubic Meter
MLML	Moss Landing Marine Laboratory
mm	Millimeter
MODIS	Moderate Resolution Imaging Spectroradiometer
NASA	National Aeronautics and Space Administration
NCCOS	National Centers for Coastal Ocean Science
NEPA	National Environmental Policy Act
nm	Nanometer
NMFS	National Marine Fisheries Service
NOAA	National Oceanic and Atmospheric Administration
NOS	National Ocean Service
OCNMS	Olympic Coast National Marine Sanctuary
OCS	Outer Continental Shelf
ODFW	Oregon Department of Fish and Wildlife
ODMDS	Ocean Dredged Material Disposal Sites
OER	Office of Exploration and Research
OET	Ocean Exploration Trust

OSU	Oregon State University
OWET	Oregon Wave Energy Trust
PDE	Percentage of Deviance Explained
PMEL	Pacific Marine Environmental Laboratory
POORT	Port Orford Ocean Research Team
psu	Practical Salinity Unit
ROMS	Regional Ocean Modeling System
ROV	Remotely Operated Vehicle
SCB	Southern California Bight
SCCWRP	Southern California Coastal Water Research Project
SeaWiFS	Sea-Viewing Wide Field-of-View Sensor
SFPUC	San Francisco Public Utility Commission
SIMPER	Similarity Percentages Analysis
SIMPROF	Similarity Profile Routine
sr	Steradian
UCLA	University of California, Los Angeles
UCSC	University of California, Santa Cruz
USACE	US Army Corps of Engineers
USGS	US Geological Survey
UW	University of Washington
VIIRS	Visible Infrared Imaging Radiometer Suite
WEMAP	Western Environmental Monitoring and Assessment Program
WoRMS	World Register of Marine Species

1 Introduction

Through the passage of the Energy Policy Act of 2005, the Bureau of Ocean Energy Management (BOEM) acquired responsibilities for overseeing development of renewable energy in US federal waters in an economically and environmentally responsible manner. As part of these management responsibilities, BOEM must evaluate possible direct, indirect, and cumulative impacts of renewable energy activities to disclose and minimize their negative impacts on human, coastal, and oceanic communities. To accomplish this, the agency requires up-to-date information to address such potential impacts when developing environmental analysis documents and outreach under the National Environmental Policy Act (NEPA) and other consultation regulations. Along the continental US West Coast, the states of California, Oregon, and Washington are also evaluating siting alternatives for developing offshore energy projects within their state waters and adjacent BOEM Outer Continental Shelf (OCS) regions (Porter and Phillips 2016). In fact, in situ tests of commercial-scale wave energy converters began in Oregon in 2012, and the first utility-scale marine wave energy converter to be connected to the grid via an underwater cable in US federal waters is on schedule to be permitted in 2020 (ODOE 2018, US DOE 2020).

Offshore energy projects include activities that physically disturb the seafloor. At a commercial scale, the intensity and extent could have profound consequences for deep-sea corals, sponges, benthic macrofauna, commercially fished species, and other ecological marine resources (i.e., benthic habitats) associated with the seafloor. For example, installation of anchors and energy transmission cables for wind turbines as well as the altered hydrodynamic flow caused by wave generators redistribute sediments around these projects and likely alter biological species and abundance near the area. Many corals and sponges add structural complexity to seafloor habitats, provide refuge and substrate, increase the number and availability of microhabitats for other organisms, and thereby create hotspots of biological diversity that serve as foraging oases for pelagic species in deep sea areas (Roberts et al. 2009). The Food and Agriculture Organization considers deep-sea corals and sponges (DSCS) to be vulnerable marine ecosystems in need of protection from adverse impacts of deep-sea bottom fishing on the high seas (FAO 2009). They also have been identified as key components of "Ecologically and Biologically Significant Areas" in the deep sea that need protection under the auspices of the United Nations Convention on Biological Diversity (Convention on Biological Diversity 2009). Thus, BOEM has a critical need for information on the spatial distribution of these organisms and benthic habitats to make enviornmetnally responsible decisions regarding offshore energy projects.

BOEM funded the National Oceanic and Atmospheric Administration (NOAA) National Centers for Coastal Ocean Science (NCCOS) and the NOAA National Marine Fisheries Service (NMFS) to model and map the distributions of DSCS and benthic macrofauna to improve knowledge of benthic habitats across the continental US West Coast for ocean planning purposes. The study area encompassed an extensive area offshore of the states of California, Oregon, and Washington out to a depth of 1,200 m (Figure 1.1). The study area included three BOEM Call Areas for wind energy development offshore of California: Humboldt, Morro Bay, and the Diablo Canyon (Federal Register 2018). This study compiled and synthesized available DSCS and macrofauna survey data and also defined the physical and environmental characteristics of the study area that are likely to be correlated with the occurrence of these organisms. Finally, statistical models that related the locations of deep-sea corals, sponges, and macrofauna to spatially co-occurring environmental predictor variables were used to predict and map the distribution of their occurrence across the study area, including at unexplored locations.

This report summarizes the approach used for this study. Chapter 1 introduces the study, describes the management rationale for the analyses, and sets the stage for the subsequent chapters. Chapter 2 describes datasets depicting depth and seafloor topography, seafloor substrate composition, oceanography, and geographic location for the study area. These datasets represented potential drivers (or best available

proxies) of the spatial distribution of habitats for deep-sea corals, sponges, and macrofauna, and were included as environmental predictor variables in the statistical models predicting distributions of these organisms. Chapter 3 describes the development of maximum entropy (MaxEnt) models that were used to predict and map the distribution of suitable habitat for selected taxa of DSCS. Chapter 4 describes the development of boosted regression tree (BRT) models that were used to predict and map the distribution of suitable habitat for selected taxa of macrofauna. Chapters 3 and 4 also describe measures of model performance and provide spatially explicit depictions of prediction uncertainty. The modeled spatial patterns of habitat suitability for DSCS and benthic macrofauna will help identify unique areas that could be biologically impaired by offshore renewable energy projects.

Figure 1.1. Map of the study area offshore of the continental US West Coast from 0 to 1,200 m depth.

2 Environmental Predictor Variables

2.1 Introduction

Datasets depicting measures of depth and seafloor topography, seafloor substrate, oceanography, and geography were generated for the study area. These datasets represented potential drivers (or proxies for drivers) of the spatial distribution of DSCS and benthic macrofauna and were used in statistical models predicting the occurrence of these organisms. Selection of the initial set of 66 environmental predictor variables was based on literature review and input from experts in DSCS and benthic macrofauna ecology. Additional environmental predictor variables describing ocean chemistry, including total organic carbon and total nitrogen, were also considered for inclusion in the models. However, in situ and modeled measures of these variables had insufficient spatial coverage. This chapter describes decisions about data sources and methods used to generate the environmental predictor datasets. In addition, maps are presented in Appendix A for each of the 66 environmental predictor variables.

2.2 Methods

2.2.1 Study Area

The study area encompassed an area of approximately 136,336 km^2 within the Pacific OCS Region that extended from the California-Mexico border to northern Washington (approximately 47.755 °N) and offshore to a depth of 1,200 m (Figure 1.1). It did not extend northward to the Washington-Canada border because the ocean circulation model (see Section 2.2.5.2) used to develop several of the environmental predictor variables had a northern extent of approximately 48 °N. The study area did not extend farther offshore than 1,200 m for a few reasons. First, there was considerably less coverage of multibeam bathymetry in the deeper waters offshore of California, Oregon, and Washington. In addition, there were fewer DSCS occurrence records in the NOAA National Database for Deep-Sea Corals and Sponges in deeper waters, and many of the records in deeper waters were not identified to the species or genus level. No macrofauna sampling stations were located in waters deeper than 1,200 m. Finally, most human uses and planning along the continental US West Coast are currently inshore of 1,200 m. BOEM identified the area offshore to 1,200 m as a high priority for its management needs, particularly in relation to three Call Areas (Humboldt, Morro Bay, Diablo Canyon) for offshore wind energy development (Federal Register 2018).

2.2.2 Map Projection and Spatial Grid Resolution

All datasets used as environmental predictors were projected onto an oblique Mercator coordinate system (origin = 39°N 125°W, azimuth = 75°, scale = 0.9996, datum = WGS84). This specific coordinate system was selected to minimize area distortion at the edges of the study area. The spatial resolution of the model grid differed for DSCS and benthic macrofauna, primarily because of differences in the accuracy of the spatial locations of the occurrence data used in the models. Additional information about these data is provided in Sections 3.2.1 and 4.2.1 of the report. For DSCS, the model grid had a spatial resolution of 200 x 200 m, while for benthic macrofauna the model grid had a spatial resolution of 25 x 25 m.

During the development of environmental predictor datasets, source data were initially processed in their native coordinate systems and at their native spatial grid resolution prior to projection onto the model grids. Bilinear interpolation was used to resample the predictor values onto the model grids unless otherwise specified. As described in Sections 2.2.3, environmental predictor datasets for depth and seafloor topography were initially created on the 25 x 25 m model grid. For the DSCS models, the values of these environmental predictors were assigned to the 200 x 200 m model grid by averaging the values of the 25 x 25 m grids within each of the 200 x 200 m grid cells. Similarly, as described in Section 2.2.4.1,

the classified substrate datasets were projected and resampled (using nearest neighbor resampling) onto the 25 x 25 m model grid. Values were assigned to the 200 x 200 m model grid by finding the most common value of the 25 x 25 m grids within each of the 200 x 200 m grid cells. Environmental predictor datasets generated directly from point data (e.g., through interpolation) were created on the model grids.

2.2.3 Depth and Seafloor Topography

Environmental predictor variables representing depth and seafloor topography (Table 2.1) were included in the models to account for variation in the occurrence of DSCS and benthic macrofauna resulting from the direct and indirect effects of the depth and shape of the seafloor. For example, although seafloor depth does not directly influence the distributions of marine species, it can have an indirect effect as a proxy for other measures (e.g., temperature, salinity) that may directly relate to species distributions (Wiltshire et al. 2018). Variables depicting the shape and complexity of the seafloor can identify areas of exposed hard substrate, which provides habitat (e.g., for attachment) for many benthic invertebrates (Huff et al. 2013, Guinotte and Davies 2014). For species distribution models of DSCS occurrence, it is important to derive depth and seafloor topography variables from high-resolution bathymetry data collected using multibeam acoustic sonar when possible to capture the fine-scale features on the seafloor that may provide habitat (Winship et al. 2020). Studies have also shown that depth is an important variable for explaining spatial patterns in macrofauna species distributions, species richness, and community composition (Hyland et al. 1991, Bergen et al. 2001, Henkel et al. 2020).

For this study, all available bathymetry data from multibeam sonar surveys in the waters offshore of the continental US West Coast were obtained and reviewed to build a comprehensive inventory of high-resolution bathymetry datasets. This inventory was used to create a single, gridded depth dataset, from which environmental predictor datasets depicting depth and measures of seafloor topography were derived.

2.2.3.1 Synthesis of Bathymetry Data

The final inventory included 455 high-resolution bathymetry datasets (see Appendix B for more information about specific datasets) and covered approximately 51% (approximately 70,000 km^2) of the study area, as well as some parts of the Pacific OCS Region outside the study area. Many of these datasets were obtained from a data catalog compiled for the 2012 review of essential fish habitat (EFH) for Pacific Coast Groundfish (NOAA NWFSC 2016) and from the NOAA National Centers for Environmental Information (NOAA NCEI 2020). Additional datasets were obtained from the US Geological Survey (USGS) and from Ocean Exploration Trust (OET). Sources of these datasets included the California State University, Monterey Bay (CSUMB) Seafloor Mapping Lab; Fugro Pelagos, Inc.; Monterey Bay Aquarium Research Institute (MBARI); NOAA National Ocean Service (NOS); NOAA Office of Exploration and Research (OER); NOAA Pacific Marine Environmental Laboratory (PMEL); NOAA Olympic Coast National Marine Sanctuary (OCNMS); Oregon Department of Fish and Wildlife (ODFW); OET; Oregon State University Active Tectonics and Seafloor Mapping Lab (OSU ATSML); Port Orford Ocean Research Team (POORT); USGS; and University of Washington (UW). In addition to the data from multibeam bathymetry, data from the NOAA Coastal Relief Models (CRMs) and the General Bathymetric Chart of the Oceans (GEBCO) were used in the bathymetry synthesis (Figure 2.1).

Only previously gridded datasets were included in the inventory of multibeam datasets (i.e., no raw or unprocessed data were included). Prior to inclusion in the inventory, bathymetry datasets were evaluated for inconsistencies, artifacts, spatial coverage, and spatial resolution. Some datasets under consideration were excluded from the inventory following this evaluation. For example, datasets from vessel transits were omitted when broader areas surrounding the transit lines had not been mapped by multibeam sonar. This was done to minimize boundary effects where the contrast in depth values between the multibeam-derived bathymetry and coarser surrounding bathymetry could result in identification of false seafloor

features in the seafloor topography variables (e.g., areas incorrectly appearing to have high slope). It is also important to note that the inventory of multibeam bathymetry datasets did not include recently conducted surveys for which data had not been processed into a final gridded dataset prior to the start of the modeling component of this study.

Each bathymetry dataset in the final inventory was projected and bilinearly resampled onto the 25 x 25 m model grid. This spatial resolution represented a typical resolution of the available multibeam bathymetry datasets. However, some datasets had a native spatial resolution finer than 25 x 25 m. Resampling these datasets onto the coarser model grid resulted in the loss of some finer-scale information. In addition, some datasets, particularly from the deeper waters of the study area, had a native spatial resolution coarser than 25 x 25 m. Although these datasets were resampled onto the model grid, they did not include information at the resolution of the model grid. As a result, seafloor topography variables did not capture finer-scale features (e.g., those indicative of exposed hard substrate) in areas represented by these datasets.

The projected and resampled datasets were merged together using the 'raster' package in R (Hijmans and van Etten 2018). In areas where datasets overlapped, depth values for the merged dataset generally were selected from the input dataset that had finer native spatial resolution or that was most recently collected. Where no multibeam bathymetry data existed, depth values were obtained from the 3 arc-second NOAA CRMs (NOAA NGDC 2003a, 2003b, 2003c) or from the 30 arc-second GEBCO 2014 grid (Weatherall et al. 2015). A Gaussian smoothing filter (sigma = 5) was used to remove some remaining artifacts (e.g., visible survey lines) in the merged dataset.

It is important to note that nearly half of the study area had not been mapped by multibeam sonar (Figure 2.1). In the areas represented in the bathymetry synthesis by the CRMs or GEBCO, finer-scale seafloor features that could be associated with DSCS or benthic macrofauna habitat were not resolved in the depth and seafloor topography variables. Additional mapping of the seafloor in these areas would be useful for assessing model predictions. GIS data layers for each of the multibeam bathymetry datasets included in the synthesis were provided with this report and can be used to identify areas that need additional mapping effort.

2.2.3.2 Seafloor Topography

Environmental predictor variables representing seafloor topography (Table 2.1) were derived from the merged depth dataset using focal statistics, where the value for each grid cell was calculated from the values of the eight neighboring grid cells in a 3 x 3 cell neighborhood. All datasets were generated using the 'raster' package in R (Hijmans and van Etten 2018). Seafloor slope and aspect (slope direction) were calculated using the 'terrain' function. Because aspect is a directional measure (i.e., it is a circular variable), it was converted to measures of the north-south and east-west gradients of aspect by calculating the cosine and sine, respectively, of aspect.

Two methods were used to create datasets depicting seafloor rugosity. The widely used surface ratio method measures rugosity as the ratio of surface area to the horizontal planar area (Jenness 2013). Because the surface ratio method can produce inflated rugosity values in areas of high slope, Du Preez (2015) developed the arc-chord ratio method that decouples rugosity from slope by calculating rugosity as the ratio of surface area to the area of a plane of best fit.

Several measures of seafloor curvature were derived to characterize the shape of the seafloor (e.g., whether it is convex or concave). The first, slope of slope, was calculated from the slope dataset using the 'terrain' function in the 'raster' package in R (Hijmans and van Etten 2018). The remaining measures were calculated following two commonly used approaches that differ in the polynomial used to fit a curve to the depth values in each 3 x 3 grid cell neighborhood (see Jenness 2013 for a detailed description of

these approaches) and included total curvature, general curvature, plan curvature, cross-sectional curvature, profile curvature, and longitudinal curvature.

Additional measures of seafloor topography (e.g., bathymetric position index, terrain ruggedness) were considered but are not included in this report. Previous experience indicated that these measures were generally highly correlated with other measures of seafloor topography and were not highly influential in fitting models to predict habitat suitability for DSCS.

2.2.4 Seafloor Substrate

Environmental predictor variables representing seafloor substrate (Table 2.2) included a classified map depicting areas of hard, soft, and mixed substrate and measures of surficial sediment characteristics.

2.2.4.1 Classified Substrate Map

Substrate data, and specifically induration type (i.e., 'hardness'), represent a critical habitat input for the spatial modeling of groundfishes and structure-forming marine invertebrates such as deep-sea corals. To facilitate these types of modeling efforts, as well as broader scientific and fisheries management needs, a West Coast seafloor substrate map was produced in 2005 as part of the five-year review of EFH by the NOAA NMFS (NOAA NMFS 2005). This contiguous polygon map spanned coastal waters from the Canadian to Mexican borders, and, where data were available, offshore to the US Exclusive Economic Zone. It was interpreted by experienced geologists using a four-category, hierarchical scheme after Greene et al. (1999). Induration was defined as hard (rock pavement, outcrops/reefs, or boulders), soft (silt to cobbles), or mixed (one hard and one soft induration type) substrate; however, only hard and soft induration types were identified in California waters, based on the predominant induration type. In 2011, as part of the subsequent EFH review, new or missing datasets (e.g., habitat maps) that depicted induration type were compiled. These newer files were merged into the 2005 map to produce a 25 x 25 m gridded raster dataset, with the highest resolution data depicted when different coverages overlapped (PFMC 2012).

There are some limitations to this 2011 substrate map that made it inadequate for the objectives of this study. One problem stems from inconsistent data type and accuracy between the regions north and south of Fort Bragg, California. To the north, the original map was updated periodically since its creation in 2005 and depicts hard, mixed, and soft substrate types (see Goldfinger et al. 2014). By contrast, the region south of Fort Bragg distinguishes only hard and soft substrate types, and was not formally updated since 2005. In addition, although data of various types and resolutions are embedded in the 2011 map, there is no data quality information included. Therefore, each raster cell is inherently assumed to have the same predictive ability. These incongruities create significant limitations and biases to coast-wide modeling efforts.

To address the biases inherent to the 2011 map, a new substrate map was created that is more consistent and accurate at depicting seafloor induration. A secondary goal was to compile and embed new induration data. This second component was more important for California waters south of Fort Bragg, which had not been updated since the 2011 effort.

Data sources from the 2005 and 2011 mapping efforts south of Fort Bragg were located and inspected to determine if a mixed component could be added. Unfortunately, none of the original data sources from the 2005 mapping effort contained this information and these datasets remain restricted to hard and soft designations. Several datasets compiled during 2011 did include a mixed induration category and were incorporated to replace the original (hard and soft) coverages. All polygon coverages were converted to (25 x 25 m) raster grids using the maximum combined area method with snapping set to the 2011 map to ensure proper grid cell alignment. Raster coverages often were present in a variety of resolutions (e.g., 2 x

2 m, 5 x 5 m, and 10 x 10 m cell sizes) and were resampled to a 25 x 25 m grid resolution using nearest neighbor interpolation. Input raster grids were snapped to the original 2011 map extents during resampling, and then merged using the Mosaic to New Raster tool in ArcGIS, with higher resolution data taking priority when coverages overlapped.

New induration data were added throughout the extent of the 2011 substrate map. North of Fort Bragg, this information was derived from Goldfinger et al. (2014). South of Fort Bragg, 33 new coverages were compiled from the CSUMB Seafloor Mapping Lab, the USGS State Mapping Project, and Moss Landing Marine Laboratories (MLML) Center for Habitat Studies. Most new data coverages, especially south of Fort Bragg, were located in state waters. All new datasets were processed as previously described, and a new map was produced that depicts hard, mixed, and soft substrate. Because mixed substrate was not always identified on input maps, a second map was created by incorporating all mixed types into the 'hard' category.

Accounting for differential quality of induration data is a crucial element of the map upgrade and required the creation of an appropriate scheme. This scheme has three fundamental components (or categories): data type, interpretation type, and ground-truthing type. Scores ranged from 0–3 in each category, and differential scoring among categories was based on their perceived relative importance in accurately distinguishing hard, mixed, and soft substrate. An overall, weighted data quality score was calculated as a weighted sum of the scores. Categories were weighted based on perceived relative importance as follows: data type = 3, interpretation type = 1, ground-truthing type = 1.5. Eighteen different data quality scores were possible based on this scheme. Weighted data quality scores were rescaled to final data quality scores ranging from 1–10 (Table 2.3).

Associated data quality maps were constructed for the substrate maps by compiling or creating footprint maps to match the original seafloor datasets, then scoring those datasets for data quality. This process was conducted in the same stages as the original mapping effort; 2005 input data were first compiled, then 2011 data, then the data included in the current upgrade. For each subsequent compilation, footprint maps that overlapped were merged to match the orientation of the associated substrate maps ('best' data on top of lesser data). All processing (i.e., resampling, mosaicking, snapping) was conducted as previously described. For the map version that distinguished only hard and soft induration types, the original data quality scores of all mixed induration cells were reduced by half during analysis to reflect added uncertainty in converting them to hard induration cells. While these data quality maps can be used to identify areas where the substrate maps could be improved (e.g., by additional mapping or ground-truthing), these data quality datasets were not used in the models of DSCS or benthic macrofauna occurrence. Including measures of environmental predictor data quality or uncertainty would necessitate a different class of models than were used in this study.

The gridded datasets depicting the classified substrate maps (hard-soft and hard-mixed-soft) were initially created in a transverse Mercator coordinate system (origin = 0°N 123°W, false easting = 500000, false northing = 0, scale = 0.9996, datum = WGS84). The datasets were projected and resampled onto the 25 x 25 m model grid by assigning each grid cell the value from the nearest grid cell center in the original datasets. For the DSCS models, values were assigned to the 200 x 200 m model grid by finding the most common value of the projected and resampled datasets within each of the 200 x 200 m grid cells.

2.2.4.2 Surficial Sediment Characteristics

Point data records from seabed surveys (typically grab samples) were obtained from the USGS usSEABED database for the US West Coast (Reid et al. 2006) to extract information for environmental predictor variables describing surficial sediment characteristics (Table 2.2). This database includes records containing information from analytical measurements as well as records containing information inferred from text descriptions of samples (Reid et al. 2006). Records were filtered to remove duplicate

data and data not pertaining to surficial sediments. Additional records were obtained from the Henkel Laboratory at OSU, the Southern California Coastal Water Research Project (SCCWRP), and published data in reports from the US Department of the Interior Minerals Management Service (now BOEM).

A number of statistical methods have been used to create spatially continuous datasets from point samples of environmental data (see Li and Heap 2014 for a review of 25 commonly applied methods). In this study, gridded spatial datasets depicting surficial sediment mean grain size (phi units) and sediment composition (percent gravel, percent sand, percent mud) were interpolated from values (grain size and composition measures as described in Reid et al. 2006) in the original point data described above using the Empirical Bayesian Kriging tool in ArcGIS Pro (Krivoruchko 2012). Kriging is a stochastic interpolation method that assumes values are more similar for neighboring data than for data farther apart (i.e., data are spatially autocorrelated) and uses this assumption to fit a statistical model to the data in order to estimate values at locations that do not have data (Tobler 1970, Cressie 1993). Spatial gridded datasets were created on the 25 x 25 m and 200 x 200 m models grids.

In addition to providing a gridded prediction from the point data, kriging also provides a measure of prediction uncertainty (i.e., standard error) at each grid cell that can be used to assess confidence in the predictions. However, these measures of uncertainty were not incorporated directly into the models of DSCS and benthic macrofauna occurrence, as this would require a different class of models than were used in this study. Nonetheless, these maps of prediction uncertainty in sediment characteristics can be used to evaluate the quality of the datasets depicting mean grain size and sediment composition and to identify areas where these environmental predictor datasets could be improved through additional collection of sediment grab samples.

2.2.5 Oceanography

Environmental predictor variables representing aspects of oceanography (Table 2.4) were included in the models to account for variation in the occurrence of DSCS and benthic macrofauna resulting from direct and indirect effects of ocean productivity or the physical state and dynamics of the ocean.

2.2.5.1 Ocean Productivity

Gridded spatial datasets describing long-term climatological patterns in sea surface chlorophyll-a concentration and sea surface reflectance (water leaving radiance at 547 nm) at 4 x 4 km grid resolution were generated from remotely sensed ocean color data to serve as proxies for measures of ocean productivity (Table 2.4). Daily sea surface chlorophyll-a concentration data from multiple satellites were downloaded from the National Aeronautics and Space Administration (NASA) Ocean Biology Processing Group (NASA 2018). This included data from the Visible Infrared Imaging Radiometer Suite (VIIRS) collected from 2012 to 2017, data from the Moderate Resolution Imaging Spectroradiometer (MODIS) instruments collected from 2002 to 2017, and data from the Sea-Viewing Wide Field-of-View Sensor (SeaWiFS) collected from 1997 to 2001 (Table 2.4). Daily data from VIIRS and MODIS were blended together for best spatial coverage. Data from SeaWiFS were resampled from a native spatial resolution of 9 x 9 km to a spatial resolution of 4 x 4 km to match the resolution of the VIIRS and MODIS data. A long-term annual mean climatology of sea surface chlorophyll-a concentration was calculated from these daily data. Daily data were also binned by date into spring/summer, fall, and winter subsets. Long-term seasonal mean climatologies were calculated from the daily data in each seasonal bin. Daily sea surface reflectance data from MODIS were also downloaded from NASA (NASA 2018), and long-term annual and seasonal mean climatologies were calculated from these data. The gridded datasets depicting the climatologies described in this section were all projected and bilinearly resampled onto the 25 x 25 m and 200 x 200 m model grids.

2.2.5.2 Ocean Circulation Models

Data describing long-term trends in the physical properties of bottom ocean water (temperature, salinity, currents; Table 2.4) were obtained from three data assimilating ocean circulation models (Table 2.5). Daily data were obtained from a global 0.08° (approximately 9 x 9 km spatial grid resolution) approximately 20 year (1992–2012) hindcast model from the HYbrid Coordinate Ocean Model (HYCOM; HYCOM Consortium 2018). In addition, approximately 27 years of daily data from a regional 0.1° (approximately 10 x 10 km spatial grid resolution) 31 year (1980–2010) hindcast model developed by the University of California, Santa Cruz (UCSC) in the Regional Ocean Modeling System (ROMS) were provided by Dr. Andrew Moore from the UCSC Ocean Modeling Group (UCSC 2018). Finally, daily data from a 0.013° (approximately 1 x 1 km spatial grid resolution) approximately 10 year (2004–2013) hindcast model for Southern California developed by the University of California, Los Angeles (UCLA) in the ROMS were provided by BOEM (Dong et al. 2017).

For each model, long-term annual mean climatologies were calculated from daily data for bottom temperature, bottom salinity, bottom current east-west velocity, and bottom current north-south velocity. In addition, daily data were binned by date into spring/summer, fall, and winter subsets. Long-term seasonal mean climatologies were calculated from the daily data in each seasonal bin for the bottom ocean water variables. Long-term annual and seasonal mean climatologies were also calculated for bottom current vertical velocity for the UCSC ROMS and UCLA ROMS models. The gridded datasets depicting the climatologies described in this section were all projected and bilinearly resampled onto the 25 x 25 m and 200 x 200 m model grids.

Although gridded climatological datasets were developed for each of the three ocean circulation models, only datasets derived from the UCSC ROMS model were used in models predicting DSCS and benthic macrofauna occurrence. The UCLA ROMS model had the finest spatial grid resolution of the three models but did not cover the entire study area. Merging or blending the data from the UCLA ROMS model with data from HYCOM was investigated. However, there were considerable differences in the data values at the boundary between the UCLA ROMS model and HYCOM that resulted in an edge artifact. Data from the UCLA ROMS model were not merged or blended with data from the UCSC ROMS model because there were only three years of overlap between the models. While the HYCOM and UCSC ROMS models had similar spatial grid resolution, the UCSC ROMS model was preferred because it was developed specifically for the US West Coast and was more accurate on the continental shelf and slope (Y. Li, pers. comm.). The UCSC ROMS model also included bottom current vertical velocity, which was not in the HYCOM model. It is important to note that the study area extent was constrained by the selection of the UCSC ROMS model, which extended only to 48°N and not to the Washington-Canada border.

2.2.5.3 Ocean Waves

Gridded spatial datasets describing long-term trends in ocean wave properties (Table 2.4) were derived from the 4 arc-minute (approximately 7 x 7 km) NOAA WAVEWATCH III 30 year (1979–2009) hindcast model for the US West Coast (NOAA NWS 2018). Annual mean and maximum climatologies were calculated for significant wave height and primary wave mean period from daily data. Daily data were also binned by date into spring/summer, fall, and winter subsets. Seasonal mean and maximum climatologies were calculated from the daily data in each seasonal bin for the ocean wave variables. In addition, mean and maximum climatologies for wave power were derived from significant wave height and wave period (Sheng and Li 2017). The gridded datasets depicting the climatologies described in this section were all projected and bilinearly resampled onto the 25 x 25 m and 200 x 200 m model grids.

2.2.6 Geography

Gridded spatial datasets depicting the Euclidean straight-line distance to shoreline, longitude, and latitude were generated on the model grids to provide variables that could account for variation in the distributions of benthic invertebrates arising from spatial location.

Table 2.1. Environmental predictor variables depicting depth and seafloor topography.

Dataset	Description	Unit	Source
Depth	Seafloor depth derived from a synthesis of bathymetry datasets	Meters	Multibeam Bathymetry (Appendix B), NOAA CRM Vol. 6 - Southern California, NOAA CRM Vol. 7 - Central Pacific, NOAA CRM Vol. 8 - Northwest Pacific, GEBCO_2014 grid version 20150318
Slope	Steepness of the seafloor, calculated as the magnitude of the maximum gradient in depth	Degrees	Derived from Depth
North-South Aspect	Cosine of the direction of slope	Unitless	Derived from Depth
East-West Aspect	Sine of the direction of slope	Unitless	Derived from Depth
Rugosity (surface ratio)	Roughness of the seafloor, calculated as the ratio of the area of the contoured depth surface to the horizontal planar area	Unitless	Derived from Depth
Rugosity (arc-chord ratio)	Roughness of the seafloor, calculated as the ratio of the area of the contoured depth surface to the area of a plane of best fit that accounts for slope	Unitless	Derived from Depth
Slope of Slope	Curvature of the seafloor, calculated as the magnitude of the maximum gradient in slope	Degrees	Derived from Depth
Total Curvature	Roughness of the seafloor; higher values indicate an area is more rugged; all values ≥ 0	Radians/100m^2	Derived from Depth
General Curvature	Extent to which the seafloor is convex (e.g., ridges, >0) or concave (e.g., valleys, <0)	Radians/100m	Derived from Depth
Plan Curvature	Curvature of the seafloor along the line of intersection between the depth surface and the horizontal plane; indicates whether seafloor is convex (>0), concave (<0), or flat (0)	Radians/100m	Derived from Depth
Cross-Sectional Curvature	Curvature of the seafloor along the line of intersection between the depth surface and the plane formed by the slope normal and direction of slope; indicates whether the seafloor is convex (>0), concave (<0), or flat (0)	Radians/100m	Derived from Depth
Profile Curvature	Curvature of the seafloor along the line of intersection between the depth surface and the plane formed by the direction of slope and the Z-axis; indicates whether the seafloor is convex (<0), concave (>0), or flat (0)	Radians/100m	Derived from Depth
Longitudinal Curvature	Curvature of the seafloor along the line of intersection between the depth surface and the plane formed by the slope and direction of slope; indicates whether the seafloor is convex (<0), concave (>0), or flat (0)	Radians/100m	Derived from Depth

Table 2.2. Environmental predictor variables depicting seafloor substrate.

Dataset	Description	Unit	Source
Hard-Soft	Categorical map dividing seafloor into hard substrate and soft substrate	N/A	Sources described in Goldfinger et al. 2014; also CSUMB Seafloor Mapping Lab, USGS State Mapping Project, and MLML Center for Habitat Studies
Hard-Mixed-Soft	Categorical map dividing seafloor into hard substrate, mixed substrate, and soft substrate	N/A	Sources described in Goldfinger et al. 2014; also CSUMB Seafloor Mapping Lab, USGS State Mapping Project, and MLML Center for Habitat Studies
Mean Grain Size	Mean grain size (phi units) of the surficial sediments, interpolated from point samples	Phi units	USGS usSEABED, OSU, SCCWRP, BOEM
Percent Gravel	Percentage composition of the gravel fraction in surficial sediments, interpolated from point samples	Percent	USGS usSEABED, OSU, SCCWRP, BOEM
Percent Sand	Percentage composition of the sand fraction in surficial sediments, interpolated from point samples	Percent	USGS usSEABED, OSU, SCCWRP, BOEM
Percent Mud	Percentage composition of the mud fraction in surficial sediments, interpolated from point samples	Percent	USGS usSEABED, OSU, SCCWRP, BOEM

Table 2.3. Scheme for assigning data quality scores to classified substrate maps.

Data Type	Data Score	Interpretation Type	Interpretation Score	Ground-truthing Type	Ground-truthing Score	Weighted Score	Final Score
Low Resolution	0.25	Unsupervised	1.5	None	0	2.25	1.0
Low Resolution	0.25	Supervised	3	None	0	3.75	1.9
Low Resolution	0.25	Unsupervised	1.5	Limited	1.5	4.50	2.4
Low Resolution	0.25	Supervised	3	Limited	1.5	6.00	3.3
Medium Resolution	1.5	Unsupervised	1.5	None	0	6.00	3.3
Low Resolution	0.25	Unsupervised	1.5	Comprehensive	3	6.75	3.8
Medium Resolution	1.5	Supervised	3	None	0	7.50	4.3
Low Resolution	0.25	Supervised	3	Comprehensive	3	8.25	4.8
Medium Resolution	1.5	Unsupervised	1.5	Limited	1.5	8.25	4.8
Medium Resolution	1.5	Supervised	3	Limited	1.5	9.75	5.7
High Resolution	3	Unsupervised	1.5	None	0	10.50	6.2
Medium Resolution	1.5	Unsupervised	1.5	Comprehensive	3	10.50	6.2
High Resolution	3	Supervised	3	None	0	12.00	7.1
Medium Resolution	1.5	Supervised	3	Comprehensive	3	12.00	7.1
High Resolution	3	Unsupervised	1.5	Limited	1.5	12.75	7.6
High Resolution	3	Supervised	3	Limited	1.5	14.25	8.6
High Resolution	3	Unsupervised	1.5	Comprehensive	3	15.00	9.0
High Resolution	3	Supervised	3	Comprehensive	3	16.50	10.0

Data Type
Low Resolution: cores, >100 m gridded or >1:100,000 scale multibeam bathymetry or sidescan/backscatter, seismic lines, bathymetric contour maps
Medium Resolution: >10–100 m gridded or >1:10,000–100,000 scale multibeam bathymetry or sidescan/backscatter
High Resolution: <10 m gridded or 1 :<10,000 scale multibeam bathymetry or sidescan/backscatter.

Interpretation Type
Unsupervised: e.g., terrain ruggedness such as vector ruggedness measure
Supervised: e.g., machine learning or expert interpretation

Ground-truthing Type
Limited: a posteriori use of video data or limited and opportunistic grab samples
Comprehensive: incorporated two or more methods and conducted with an a priori survey design based on pre-existing habitat map; e.g., coordinated use of grab samples and seafloor video data to verify the substrate composition of different interpreted seafloor habitats and to check boundary regions

Table 2.4. Environmental predictor variables depicting measures of oceanography.

Dataset	Description	Statistics	Unit	Native Spatial Resolution (Approximate)	Source
Surface Chlorophyll	Satellite-derived concentration of chlorophyll-a at the ocean surface	Annual, spring/summer, fall, winter climatological mean	mg/m^3	4 x 4 km, 9 x 9 km	SeaWiFS (1997–2001), MODIS Aqua and Terra (2000–2017), VIIRS (2012–2017)
Surface Reflectance	Satellite-derived mean normalized water-leaving radiance at 547 nm	Annual, spring/summer, fall, winter climatological mean	sr^{-1}	4 x 4 km	MODIS Aqua and Terra (2000–2017)
East-West Bottom Current Velocity	East-west component (u) of current speed at the deepest level of an ocean circulation model	Annual, spring/summer, fall, winter climatological mean	m/s	10 x 10 km	UCSC 31 year hindcast ocean circulation model (1980–2010)
North-South Bottom Current Velocity	North-south component (v) of current speed at the deepest level of an ocean circulation model	Annual, spring/summer, fall, winter climatological mean	m/s	10 x 10 km	UCSC 31 year hindcast ocean circulation model (1980–2010)
Vertical Bottom Current Velocity	Vertical component (w) of current speed at the deepest level of an ocean circulation model	Annual, spring/summer, fall, winter climatological mean	m/s	10 x 10 km	UCSC 31 year hindcast ocean circulation model (1980–2010)
Bottom Salinity	Ocean water salinity at the deepest level of an ocean circulation model	Annual, spring/summer, fall, winter climatological mean	psu	10 x 10 km	UCSC 31 year hindcast ocean circulation model (1980–2010)
Bottom Temperature	Ocean water temperature at the deepest level of an ocean circulation model	Annual, spring/summer, fall, winter climatological mean	°C	10 x 10 km	UCSC 31 year hindcast ocean circulation model (1980–2010)
Wave Height	Significant height of combined wind waves and swell	Annual, spring/summer, fall, winter climatological max and mean	Meters	7 x 7 km	NOAA WAVEWATCH III 30 year hindcast Phase 2, US West Coast (1979–2009)
Wave Power	Energy flux per unit of wave-crest length	Annual, spring/summer, fall, winter climatological max and mean	Watts/ meter	7 x 7 km	NOAA WAVEWATCH III 30 year hindcast Phase 2, US West Coast (1979–2009)

Table 2.5. Comparison of ocean circulation models considered.

Model	Spatial Extent	Spatial Grid Resolution	Temporal Extent	Variables
HYCOM	Global	0.08 x 0.08°	Approximately 20 years 1 Aug 1992–31 Jul 2012	Temperature, Salinity, East-West Current Velocity (u), North-South Current Velocity (v)
UCSC ROMS	US West Coast Longitude: 113°W–134°W Latitude: 30°N– 48°N	0.1 x 0.1°	Approximately 27 years 8 Jan 1980–17 Mar 2007	Temperature, Salinity, East-West Current Velocity (u), North-South Current Velocity (v), Vertical Current Velocity (w)
UCLA ROMS	Southern California	0.013 x 0.013°	Approximately 10 years 21 Jan 2004–21 Nov 2013	Temperature, Salinity, East-West Current Velocity (u), North-South Current Velocity (v), Vertical Current Velocity (w)

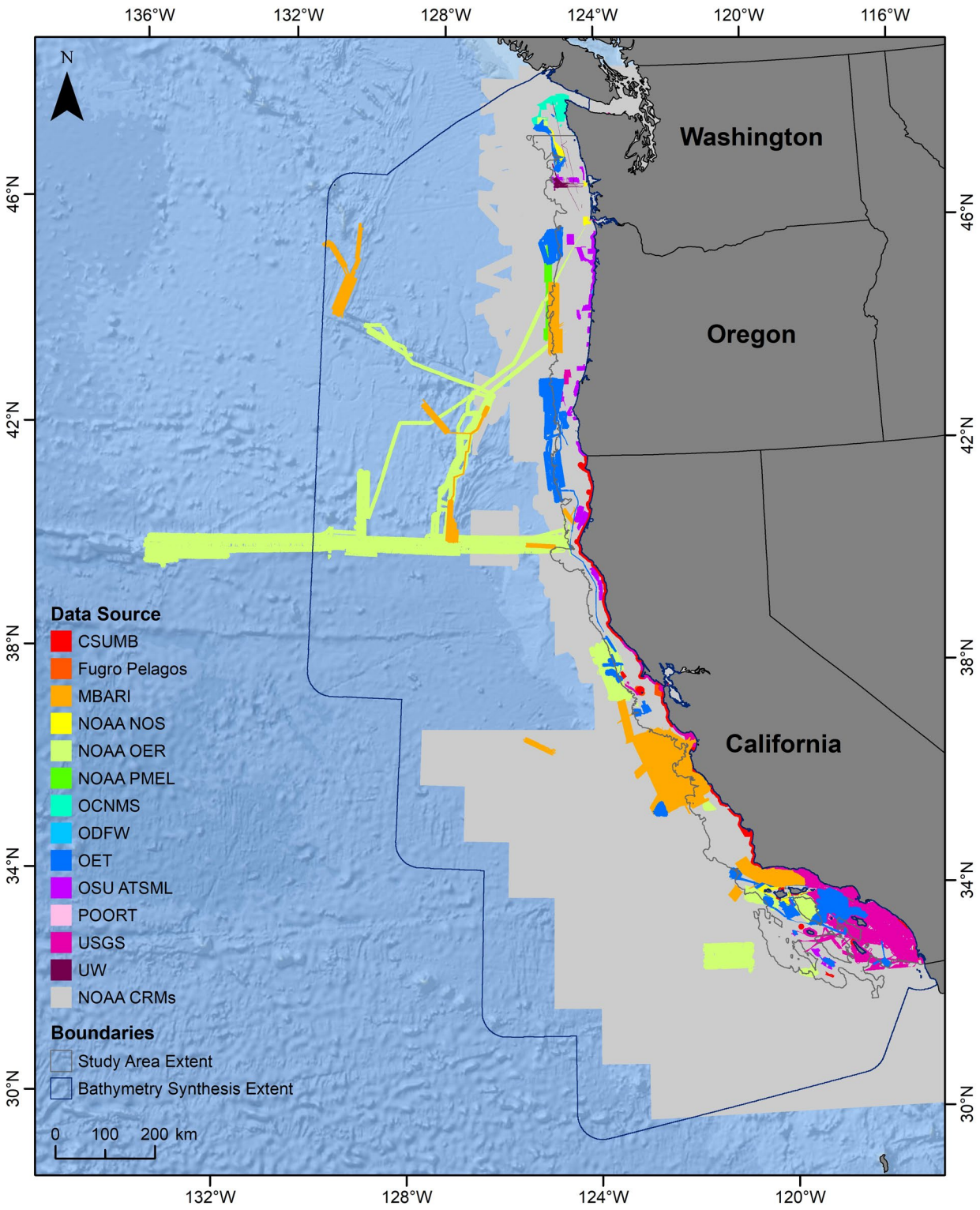

Figure 2.1. Coverage of available bathymetry datasets offshore of the continental US West Coast. Areas within the bathymetry synthesis extent used data from GEBCO when no other bathymetry data were available. See Appendix B for legend explanation and specific datasets.

3 Deep-Sea Corals and Sponges

3.1 Introduction

DSCS are generally long-lived, slow-growing, and fragile, making them and their associated communities vulnerable to human impacts. Consequently, understanding the spatial distribution of these vulnerable organisms and their habitats is key to minimizing potential human impacts to these resources. Corals and sponges are the most important groups of benthic organisms that form biogenic habitats in the deep sea. Many DSCS contribute three-dimensional structural complexity to seafloor habitats, provide refuge and substrate, increase the number and availability of microhabitats for other organisms, and thereby create hotspots of biological diversity (Roberts et al. 2009, Buhl-Mortensen et al. 2010, Hogg et al. 2010, Rossi et al. 2017).

Deep-sea corals, also known as cold-water corals or deepwater corals, have become a major focus of new deep-sea research and conservation, both in the US and worldwide. Recent reviews (Roberts et al. 2009, Cordes et al. 2016, Hourigan et al. 2017) have highlighted the value of the habitats they create and their vulnerability to anthropogenic impacts. Offshore of the continental US West Coast, most deep-sea coral taxa are found on hard substrate, often associated with seamounts, banks, and canyons (Etnoyer and Morgan 2005, Whitmire and Clarke 2007, Clarke et al. 2017). In this region, hard and mixed seabed types represent only around 10% of the substrata from the continental shelf to depths of 3,000 m (NOAA NMFS 2013) and only around 7% of the substrata within the study area (based on the classified substrate maps described in Section 2.2.4.1).

Gorgonian octocorals (Order Alcyonacea) and black corals (Order Antipatharia) often have a branching morphology and a number of species can reach large sizes, which increases their capacity to provide habitat for other species. Other taxa, including larger unbranched gorgonians and black corals, as well as branching colonial stony corals (Order Scleractinia) and stylasterid lace corals (Class Hydrozoa, Family Stylasteridae) are also considered structure-forming or habitat-forming corals (Etnoyer and Morgan 2005, Whitmire and Clarke 2007, NOAA CRCP 2010). The branching stony coral *Lophelia pertusa* (= *Desmophyllum pertusum*), which is the dominant reef-forming deep-sea coral in the Atlantic, also occurs off the US West Coast, but it does not appear to form reefs (i.e., bioherms) in this region (Salgado et al. 2018). Sea pens (Order Pennatulacea) are the most abundant group of deep-sea corals in the region (Whitmire and Clarke 2007). In contrast to other corals, nearly all sea pens are adapted to live in soft substrata, and a number of species in the region form aggregations or ‘groves.’ Twenty-eight species of pennatulaceans are known from the US West Coast region (Whitmire et al. 2017), ranging from very shallow waters (e.g., *Stylatula elongata*) to very deep (e.g., *Umbellula lindahli*, recorded from nearly 4,000 m).

In contrast to deep-sea coral habitats, until recently deep-sea sponge grounds have been relatively overlooked and poorly understood (Hogg et al. 2010, Maldonado et al. 2016). New research has highlighted the extent and importance of these habitats in shaping community structure and biodiversity of associated species (Stone 2014, Hawkes et al. 2019). Sponge aggregations also appear to serve important ecosystem functions in carbon and nutrient recycling and benthic-pelagic coupling in the food-limited deep ocean (Kutti et al. 2013, Maldonado et al. 2016). Sponges and octocorals are currently the most important targets for marine natural product research (Leal et al. 2012). Deep-sea sponges are also widespread in the region to depths over 4,000 m. They have been recorded as bycatch in about one quarter of all trawls by the NMFS West Coast Groundfish Bottom Trawl Survey (Clarke et al. 2017), though most could only be identified as ‘Porifera’. There is no comprehensive list of deep-sea sponge species for any US region. However, the NOAA National Database for Deep-Sea Corals and Sponges (NOAA DSCRTP 2019) includes 119 species of deepwater sponges from the US West Coast region (73 demosponges, 40 glass sponges, four calcareous sponges, and two homoscleromorph sponges). This

number is certainly an underestimate. In general, demosponges (Class Demospongiae) are most abundant in shallower water, while in deeper water glass sponges (Class Hexactinellida) predominate. There are, however, important habitats dominated by glass sponges in relatively shallow water (e.g., Grays Canyon, off Washington; Salmi et al. 2011, Powell et al. 2018).

Clarke et al. (2017) recently reviewed the state of DSCS ecosystems offshore of the US West Coast. Both corals and sponges occur along the entire length of the coast to depths of over 4,000 m. Seventy percent of DSCS records from the region in the NOAA National Database for Deep-Sea Corals and Sponges (NOAA DSCRTP 2019) occur between 50–1,000 m, though this is undoubtedly biased due to increased sampling effort in this depth range. Corals are a morphologically and taxonomically diverse group. More than 135 unique species are known from US waters deeper than 50 m off California, Oregon, and Washington (Whitmire et al. 2017), with nearly 75% being octocorals (Orders Alcyonacea and Pennatulacea). While many coral species occur throughout the entire region, for other species there is a distinct biogeographic transition zone between the California and Oregon ecoregions around Point Conception, California.

Octocorals, black corals, and sponges off the US West Coast are known to provide habitat for numerous invertebrate species (Clarke et al. 2017). Strong associations between rockfishes and DSCS in the eastern North Pacific have been documented from visual surveys conducted in Alaska (e.g., corals and sponges in the Aleutian Islands: Stone 2014; red tree octocoral in the Gulf of Alaska: Stone et al. 2014) and British Columbia (Du Preez and Tunnicliffe 2011). In the US West Coast region, similar strong associations have been observed between rockfishes and sponges in Grays Canyon off Washington (Powell et al. 2018). Henderson et al. (in revision) recently used modeling approaches to show that eight DSCS taxa increased the probability of presence for the commercially important rockfish species Bank Rockfish (*Sebastes rufus*) and Bocaccio (*S. paucipinis*) as well as young-of-year *Sebastes* spp., after accounting for depth and seafloor relief. Many of the recent revisions to areas off the West Coast to protect Groundfish EFH that were implemented by the Pacific Fishery Management Council and NOAA Fisheries in 2020 reflected new information on the spatial distribution of DSCS. Sea pens generally have fewer associated invertebrates than do other corals (De Clippele 2015). The role of sea pen aggregations as habitat for fishes off the US West Coast has not been well studied. In Alaska, commercially important Pacific Ocean Perch (*Sebastes alutus*) has been observed to shelter in groves of *Halipteris willemoesi* (Brodeur 2001), a sea pen also found off the US West Coast. Baillon et al. (2012, 2014) found evidence that several species of sea pens may serve as nursery habitat for larval redfish (*Sebastes* spp.) off eastern Canada, but this has not been examined in the Pacific.

With the designation of the Oculina Banks Habitat Area of Particular Concern off eastern Florida in 1984 to protect corals as EFH, the US became the first country to designate a deepwater coral protected area. Conservation of deep-sea corals has since become central to US deep-sea conservation efforts (Hourigan et al. 2017). In 2007, the reauthorization of the Magnuson-Stevens Fisheries Conservation and Management Act provided additional authorities to protect deep-sea coral areas from fishing. NOAA's 2010 "Strategic Plan for Deep-Sea Coral and Sponge Ecosystems: Research, Management, and International Cooperation" (NOAA CRCP 2010) highlighted the importance of both DSCS ecosystems and identified goals, objectives, and approaches to improve their conservation and management.

BOEM has identified deep-sea coral communities as sensitive deep-water biological communities and included guidance for oil and gas developers to avoid such habitats. Internationally, DSCS have been identified as vulnerable marine ecosystems in need of protection from adverse impacts of deep-sea bottom fishing on the high seas (FAO 2009). They have also been identified as key components of "Ecologically and Biologically Significant Areas" (Convention on Biological Diversity 2009) in need of protection under the auspices of the United Nations Convention on Biological Diversity. While these international agreements do not carry legal or regulatory requirements in US waters, they reflect the growing consensus on the value and vulnerability of these communities.

Two previous efforts have modeled the spatial distribution of deep-sea corals at a regional scale for the US West Coast. Bryan and Metaxas (2006, 2007) modeled the distribution of two gorgonian families, Primnoidae and Paragorgiidae, along the northeast Pacific coast from California to Alaska. Guinotte and Davies (2014) developed predictive models of habitat suitability for black corals (Order Antipatharia), stony corals (Order Scleractinia), and four suborders of alcyonaceans for the entire continental US West Coast. Results from the MaxEnt models by Guinotte and Davies (2014) were considered in the Pacific Fishery Management Council's EFH review. These earlier efforts used presence-only models, with relatively fewer coral records and more limited environmental predictor information than are now available. Additional studies have modeled distributions of deep-sea corals at local (i.e., sub regional) scales (Etherington et al. 2011, Huff et al. 2013). The authors of this study were not aware of any studies that have modeled the distribution of deep-sea sponges for the continental US West Coast. Modeling the distribution of DSCS has now become a central approach in US efforts to understand the distributions of these species (Guinotte et al. 2017).

In this study, statistical models were used to predict and map the distribution of suitable habitat for 32 species and genera of deep-sea corals, 13 species and genera of deep-sea sponges, and two classes of deep-sea sponges. These models build upon previous modeling efforts in the region by incorporating the considerable number of new DSCS occurrence records from high-resolution visual surveys (e.g., from remotely operated vehicles) that have been archived in the NOAA National Database for Deep-Sea Corals and Sponges (NOAA DSCRTP 2019) in the past few years. In addition, the models take advantage of the increased coverage of multibeam bathymetry data in the region. As a result, the models were developed at both a finer taxonomic resolution (primarily at the species and genus level) and at a finer spatial resolution (200 x 200 m) than previously possible at the regional scale. The objectives for this study were to develop models with high predictive performance and to produce maps showing areas likely to contain suitable habitat for DSCS across the study area with corresponding maps showing the variability in the predictions to demonstrate the degree of confidence in the predictions at any given model grid cell. This chapter describes the data and statistical modeling approach used to produce the models and presents the results of the models, including maps depicting the distribution of predicted suitable habitat for each DSCS taxon modeled.

3.2 Methods

3.2.1 Deep-Sea Coral and Sponge Occurrence Data

Records of DSCS occurrence were obtained from the NOAA National Database for Deep-Sea Corals and Sponges (version 20190208; NOAA DSCRTP 2019; Figure 3.1). The National Database was created to serve as a repository of DSCS observational data. It includes historical records from samples housed in museum collections and at research institutions, records reported in the scientific literature, catch records from dredge and trawl surveys, and observations from in situ visual surveys (Hourigan et al. 2015). It is important to note the differences in the resolution and accuracy of taxonomic identification as well as in the accuracy of location data associated with records collected using different survey platforms and equipment. Records in the National Database are reviewed for potential location errors, and all taxonomic names are standardized using the World Register of Marine Species (WoRMS; WoRMS Editorial Board 2019). However, records in the National Database may be decades old with limited taxonomic and spatial resolution. Records from museum specimens likely have the best taxonomic resolution; however, many were collected from dredge and trawl surveys conducted in the last century with less accurate positional information. NOAA bottom trawl surveys are conducted with a systematic approach across the entire study area, but are generally limited to low relief, soft and mixed substrate habitats. Spatial positions assigned to these records are typically reported as the midpoint of an approximately 1 km survey, and taxonomic resolution varies depending on the expertise of onboard biologists. Recent observations collected by visual surveys using equipment such as autonomous underwater vehicles (AUVs) and

remotely operated vehicles (ROVs) have the most accurate spatial locations. These surveys often include rocky habitats that are important for most DSCS, but survey effort across the region is uneven and the taxonomic resolution of these records can still be variable because of the difficulty in identifying taxa without collection of physical specimens. In particular, sponge observations have often been identified at coarse taxonomic resolution (e.g., only to phylum) or by morphotype. As a result, records of sponge species and genera are likely underrepresented in the National Database.

Within the study area, the National Database contained approximately 250,000 records of DSCS occurrence from 1888–2017 across 87 datasets (Table 3.1). The majority of these records were from visual surveys using ROVs, manned submersibles, towed cameras, and AUVs. NOAA SWFSC submitted the largest number of records to the database collected across many expeditions using several types of survey equipment. MBARI submitted 82,972 records collected by ROV from multiple cruises over 25 years. Additional information on DSCS datasets and individual records used in this study is available from the NOAA Deep Sea Coral Research and Technology Program Data Portal (NOAA DSCRTP 2019). Some records within the study area were not used in the models because of insufficient taxonomic resolution or because of spatial sampling bias. Methods for determining which records to retain for modeling are described in Section 3.2.3.2.

3.2.2 Environmental Predictor Variables

As described in Chapter 2, an initial set of 66 environmental predictor variables were generated on the 200 x 200 m model grid for use in the DSCS models. A pairwise correlation analysis was performed on the environmental predictor variables to identify and remove predictor variables that were highly correlated (Spearman rank correlation coefficient $|\rho| > 0.7$) with each other. This resulted in a final set of 22 environmental predictor variables that were used in the statistical modeling framework (Table 3.2).

3.2.3 Statistical Modeling Framework

3.2.3.1 Overview

A statistical modeling framework using MaxEnt models was implemented to identify locations within the study area that are likely to contain habitat for the selected DSCS taxa. MaxEnt has been widely used for modeling species distributions from presence-only data, including for DSCS globally (Tittensor et al. 2009, Davies and Guinotte 2011, Yesson et al. 2012) and at regional scales (Guinotte and Davies 2014, Anderson et al. 2016, Howell et al. 2016, Gullage et al. 2017). MaxEnt models estimate functional relationships between occurrence and the environmental predictor variables, constrained by the mean value of the environmental predictors at the occurrence locations (Phillips et al. 2004, 2006, Elith et al. 2011). These relationships, known as features in MaxEnt, include linear and non-linear functions of the environmental predictor variables (Elith et al. 2011, Merow et al. 2013). MaxEnt uses these relationships to predict the relative probability of occurrence, often referred to as habitat suitability, across the study area (Phillips et al. 2004, 2006, Elith et al. 2011, Merow et al. 2013). This section describes the methods for each stage of the modeling framework: data preparation, model fitting and model selection, spatial prediction, and evaluating model performance (Figure 3.2).

3.2.3.2 Data Preparation

DSCS occurrence records from the National Database were summarized by taxon to identify species and genera with sufficient numbers of occurrences for modeling. Models were generated at the species and genus level to avoid combining taxa with different habitat requirements, as models for broader taxonomic groups (e.g., suborder, order) may overpredict the extent of suitable habitat (Guinotte and Davies 2014, Kinlan et al. 2020, Winship et al. 2020). Deep-sea coral records not identified to the species or genus

level were excluded from the analysis. Sponge records identified to the class level were retained, although sponge models were at the species or genus level except for two class level models.

As is often the case for databases compiled from numerous sources, spatial sampling bias was apparent in the occurrence records extracted from the National Database (Varela et al. 2014, Vierod et al. 2014). Spatial sampling bias results from some locations being more heavily surveyed than others. Survey effort for DSCS tends to focus on specific areas of interest because of the logistical challenges of conducting deep-sea surveys or to inform specific management needs (Vierod et al. 2014). In addition, annotations from visual surveys may result in high numbers of DSCS observations in a small area (Guinotte and Davies 2014). For example, there was a high number of records clustered in and around Monterey Bay (Figure 3.1) because of the intensive survey effort by MBARI relative to other areas. Other locations with relatively high numbers of records included the Southern California Bight (SCB) predominantly offshore of the Channel Islands, Cordell Bank offshore of Point Reyes, California, and the Brush Patch Groundfish EFH conservation area offshore of Crescent City in northern California.

Spatial sampling bias can result in models that are fit too closely (i.e., overfit) to the environmental conditions represented in the occurrence data and not the full range of environmental conditions. Models that are overfit to the data used to train the model will be less successful at predicting the data withheld to test the model or at estimating occurrence in unsampled locations (Phillips et al. 2009, Boria et al. 2014). Modeling approaches such as MaxEnt that use presence but not absence data (i.e., presence-only or presence-background models) may confuse the distribution of sampling effort with the distribution of occurrence if they do not account for spatial sampling bias in the occurrence data (Phillips et al. 2009, Elith et al. 2011).

Several methods for thinning or filtering occurrence data have been used to minimize the effects of sampling bias on model predictions (Boria et al. 2014, Varela et al. 2014). Here, DSCS occurrence records for each taxon were thinned by removing spatial duplicate records within the same model grid cell (200 x 200 m). Although removing records reduces sample size, it can help reduce the effects of sampling bias in heavily sampled areas (Aiello-Lammens et al. 2015). Following the removal of records in the same model grid cell, taxa were selected for modeling that had >50 model grid cells containing occurance records. Some studies have demonstrated the successful use of MaxEnt to model species distributions with lower numbers of records (Hernandez et al. 2006, Pearson et al. 2007). However, the minimum number of records needed is likely to vary with prevalence, or the proportion of the study area occupied by the species/taxon (van Proosdij et al. 2016). Based on previous experience modeling DSCS occurrence using MaxEnt, a minimum sample size of 50 grid cells was selected for this study. In total, 44 taxa of DSCS with sufficient numbers of occurrences were selected for modeling.

The 44 selected deep-sea coral taxa included three species and one genus of stony corals, two species and one genus of black corals, 10 species and two genera of gorgonian corals, one species and one genus of soft corals, six species and three genera of sea pens, and one species of stylasterid coral (Table 3.3). Sponge taxa included two species and five genera of demosponges and four species and two genera of glass sponges (Table 3.4). In addition to the selected species and genera, demosponges (Class Demospongiae) and glass sponges (Class Hexactinellida) were also modeled at the class level. These models included all records identified to the class level plus records identified to the species, genus, family, suborder, or order level within each class. Therefore, sponge records identified to the species or genus level were used in both a species/genus level model and a class level model.

In addition to the records of occurrence (i.e., presence), MaxEnt uses a set of locations termed background (sometimes called pseudo-absence) locations to sample the environmental conditions across the entire study area (Phillips et al. 2009, Elith et al. 2011, Merow et al. 2013). MaxEnt compares the environmental conditions at the background locations to the conditions at the locations of occurrence. While background locations are commonly selected by randomly sampling the study area, this neglects

the issue of spatial sampling bias and will affect model performance and the extent of predicted suitable habitat (Phillips et al. 2009, Elith et al. 2011, Merow et al. 2013). Alternative approaches to background sample selection that attempt to address sampling bias include directly using information about the spatial distribution of sampling effort (although this is not often available) or selecting background locations from occurrence records for a broader group of related species. The latter approach, based on target group sampling, assumes that spatial sampling effort for the broader target group is similar to that of the taxon to be modeled (Phillips et al. 2009, Elith et al. 2011, Merow et al. 2013). In this study, background locations were selected using an approach similar to target group sampling. For each DSCS taxon, 10,000 background locations were randomly selected from the full set of model grid cells containing any DSCS occurrence records, except for grid cells containing the taxon to be modeled.

Values of the environmental predictor variables were extracted from grid cells containing DSCS occurrence records and background locations.

3.2.3.3 Model Fitting and Model Selection

MaxEnt fits models using functions and transformations of the environmental predictor variables, known as features, which are constrained by the values of the environmental predictor variables at the locations of the occurrence records. Feature types include linear and non-linear (e.g., quadratic, hinge, threshold) functions of the environmental predictor variables as well as product features that allow interactions between environmental predictor variables (Phillips et al. 2004, Elith et al. 2011).

MaxEnt uses a model selection approach called regularization to choose the features that are most important for model fit (i.e., how closely the model matches the data) while applying a penalty to less informative features to avoid models that are overly complex. Models that are overly complex (i.e., that include too many features) can be fit too closely to the data used to train the model (i.e., overfit) and less successful at predicting the data withheld to test the model (Phillips et al. 2004, Elith et al. 2011, Merow et al. 2013). In addition, overly complex models can limit the ability to make inferences about the relationships between individual environmental predictors and habitat suitability (Warren and Seifort 2011). In spite of its use of regularization, under its default settings MaxEnt may still be prone to fitting models that are too complex, and alternative methods for model selection have been proposed (Warren and Seifort 2011, Halvorsen et al. 2015). In this study, an iterative model selection approach based on information criteria (Warren and Seifort 2011) was used to choose the subset of environmental predictor variables that maximized predictive performance for each DSCS taxon.

MaxEnt models were fit as logistic regression models using the ‘maxnet’ package in R (Phillips et al. 2017) following the recent interpretation of MaxEnt as an inhomogeneous Poisson process (Fithian and Hastie 2013, Renner and Warton 2013). The ‘maxnet’ package provides the same options for feature classes and regularization as the commonly used Java software, but uses the ‘glmnet’ package in R (Friedman et al. 2010) to fit the models.

At each iteration of the model selection procedure, models were fit using cross-validation. In this process, data were assigned to subsets (i.e., folds) of approximately equal size. Each fold was then used to test the performance of a model fit using the data in all of the other folds. Instead of random assignment to the cross-validation folds, DSCS occurrence records and background locations were assigned to spatially separated cross-validation folds, or spatial blocks, to account for spatial sampling bias in the occurrence records (i.e., to avoid overfitting to clustered occurrence records). The size of each spatial block (32,536 x 32,536 m) was determined by the spatial autocorrelation in the environmental predictor variables (Valavi et al. 2018).

For the initial iteration of the model selection procedure, models were fit using the full set of 22 environmental predictor variables. Model predictive performance was measured using the area under the

receiver operating characteristic curve (AUC; Fielding and Bell 1997) and Akaike's information criterion corrected for small sample size (AICc; Akaike 1974, Burnham and Anderson 2002). The most redundant environmental predictor in this iteration was identified as the predictor whose omission from model fitting resulted in the smallest reduction in mean AUC across the cross-validation folds. This environmental predictor variable was then removed for the next iteration of the model selection procedure, and new models were fit using the updated set of predictor variables. This process was repeated until a single environmental predictor variable remained. Model iterations were then ranked from best to worst in terms of mean cross-validation AUC (highest mean AUC = rank 1, lowest mean AUC = rank 22) and AICc (lowest AICc = rank 1, highest AICc = rank 22). The model iteration (i.e., subset of environmental predictor variables) with the lowest average rank was selected as the best model iteration.

3.2.3.4 Spatial Prediction

Bootstrapping was used to create spatial gridded predictions of habitat suitability and to estimate variability (i.e., uncertainty) in model predictions. For each DSCS taxon, occurrence records were sampled with replacement to create 100 bootstrap samples of the original sample size for the taxon. For example, each bootstrap sample for *Acanthogorgia* contained a set of 105 records drawn with replacement (i.e., a record could be selected multiple times) from the original 105 *Acanthogorgia* records. A model was fit for each bootstrap sample using the subset of environmental predictor variables from the best model iteration. A spatial gridded prediction of the estimated relative probability of occurrence, referred to here as habitat suitability, was calculated for each bootstrap model using the complementary log-log transformation of the MaxEnt model output (Phillips et al. 2017).The bootstrapping procedure generated a set of 100 predictions of habitat suitability at each grid cell. Since each bootstrap sample could include a different set of records drawn from the original data, this set of predictions could be used to assess sensitivity to variation in the original data.

From the bootstrapped set of 100 spatial gridded predictions, the mean of the predicted habitat suitability (hereafter, mean habitat suitability) was calculated at each grid cell. As a measure of variability, the coefficient of variation (CV) was also calculated at each grid cell as the standard deviation of the predicted habitat suitability divided by the mean habitat suitability. A higher value indicated greater variability in the predictions for the 100 bootstrap samples, while a lower value indicated less variability. It is important to note that in addition to areas of high variability (high standard deviation), high values of the CV can also result from extremely low values of the mean habitat suitability. Therefore, the CV should be interpreted in conjunction with the mean habitat suitability. The CV can also provide information about locations where variability in model predictions was high because of limited occurrence records.

Predictions of habitat suitability are sometimes converted into binary maps, where grid cells with values above a selected breakpoint are defined as suitable habitat and all other grid cells are defined as unsuitable habitat. While this allows direct comparison of predictions from different MaxEnt models (e.g., for different taxa), it is difficult to select an appropriate (e.g., ecologically meaningful) breakpoint (Merow et al. 2013). In this study, the mean habitat suitability for each taxon was classified into a map with four habitat suitability classes ('very low', 'low', 'medium', 'high') using a series of breakpoints identified through receiver operating characteristic curve analysis. Each breakpoint was calculated using a ratio of the cost of a false positive error to the cost of a false negative error. For example, with a 1:2 cost ratio, a false negative error (i.e., predicting unsuitable habitat in a location that is actually suitable habitat) is twice as costly as a false positive error (i.e., predicting suitable habitat in a location that is actually unsuitable habitat). The cost ratio was increased for each successive breakpoint such that each successive breakpoint resulted in a habitat suitability class with a more constrained prediction of the area containing suitable habitat, with the high habitat suitability class the least likely to overpredict the area of suitable habitat. All receiver operating characteristic curve analyses were performed using the 'ROCR' package in

R (Sing et al. 2005). In addition, the grid cells for which all 100 bootstrap predictions were classified in the high habitat suitability class were labeled as a fifth 'robust high' habitat suitability class.

For each taxon, a map page was created to depict the occurrence records, the classified mean habitat suitability, and the CV of the predicted habitat suitability. Note that fine-scale features may be difficult to discern in the map pages given the resolution of the model predictions and the extent of the map display. However, these features can be examined using the GIS data products associated with the report.

3.2.3.5 Model Performance

For each taxon, model performance for the best model iteration was assessed using four measures (Table 3.5). First, AUC was calculated for a model fit to the full set of occurrence records (training AUC). In addition, the mean AUC was calculated across the ten cross-validation folds (cross-validation mean AUC). AUC values range from 0 to 1, with an AUC value of 0.5 indicating that the model does no better than a random model at discriminating presence from absence (here, background locations). AUC values were categorized as high, medium, and low using similar breakpoints as in Hosmer and Lemeshow (2000). While AUC is often used to evaluate the accuracy of species distribution models, there are considerable concerns about the use of AUC, in particular for presence-only models, for which AUC values may overestimate model performance (Lobo et al. 2008, Jiménez-Valverde 2012, Yackulic et al. 2013).

Because of these limitations with using AUC to evaluate performance for presence-only models, additional measures of model fit and model stability were also calculated (Table 3.5) to assess model performance using the classified mean habitat suitability. Model fit was calculated as the percentage of occurrence records that were in grid cells where the classified mean habitat suitability was in the high habitat suitability class. This measure provides an indication of how well the model predictions matched the occurrence data used to fit the models, with higher model fit values indicating that more of the grid cells containing occurrence records were also predicted to have high habitat suitability. Model stability was calculated as the percentage of grid cells predicted in the high habitat suitability class that were also predicted to be in the robust high class. This measure reflects how sensitive the model predictions were to variation in the occurrence records selected for each bootstrap sample. Higher values for model stability indicated that there was less variability in the predicted habitat suitability at grid cells predicted to be in the high habitat suitability class. Model fit and model stability values were categorized relative to their observed values as high (top 25% of the values), medium (middle 50% of the values), or low (lowest 25% of the values) (Table 3.5).

3.2.4 Aggregated Maps for Taxa Associated with Hard Substrate

In addition to maps identifying areas likely to contain suitable habitat for individual DSCS taxa, maps depicting areas that provide habitat for multiple taxa may also be important for making management decisions. For example, BOEM identified a need for information on the distribution of DSCS habitat in relation to the Humboldt Call Area offshore of northern California. Specifically, BOEM was interested in maps showing areas with predicted suitable habitat for multiple taxa associated with hard substrate, as hard seafloor features at differing spatial scales (ranging from rocks and boulders to ridges and seamounts) can be home to a number of DSCS taxa and may also provide habitat for other organisms. While the models developed in this study did not directly predict distributions of DSCS communities or provide direct, spatial information about taxonomic richness, the classified mean habitat suitability maps can be combined to suggest areas where taxa are likely to co-occur. Deep-sea coral taxa considered to be associated with hard substrate included the 22 taxa that were not sea pens (Table 3.3; P. Etnoyer, pers. comm.). Sea pens were excluded because all the sea pen taxa modeled here are associated with soft, unconsolidated sediments.

For each of the 22 included taxa, the classified mean habitat suitability was converted into a binary map where one was assigned to all model grid cells classified as high habitat suitability and zero was assigned to all other grid cells. The binary maps were summed across the taxa to produce a map depicting the number of taxa predicted to have high habitat suitability for each grid cell. An additional map with the number of taxa predicted to have robust high habitat suitability was also created. All 22 taxa considered to be associated with hard substrate were included in these maps regardless of model performance, so these maps combined taxa with varying levels of model performance.

It is important to note that these maps do not directly represent or estimate taxonomic richness and are only intended to demonstrate areas where multiple taxa are more likely to occur. Furthermore, the maps are only representative of the deep-sea coral taxa selected for modeling and may reflect any taxonomic biases in the records included in the National Database for the study area. Nevertheless, these maps can be used to identify areas where multiple taxa of interest for management are likely to co-occur.

3.2.5 Environmental Predictor Variable Importance

The Java software commonly used to fit MaxEnt models provides multiple measures that can be used to evaluate the importance of each environmental predictor variable to model fitting (Phillips 2017). However, these measures are not generated by the 'maxnet' package in R. For this study, the possibility of evaluating environmental predictor importance from the coefficients of the logistic regression models fit by 'maxnet' was explored. However, results of this exploration were not sufficient to provide measures of environmental predictor variable importance comparable to the outputs from the Java software. It is important to note that for this study MaxEnt models were fit to maximize predictive performance rather than to determine the ecological drivers and mechanisms behind the occurrence of DSCS in the study area. Without the standard measures of environmental predictor variable importance, information about which environmental predictor variables may be most important for predicting habitat suitability for each DSCS taxon was limited to the list of environmental predictor variables included in the best model iteration from the model selection procedure.

3.2.6 Model Validation

Presence-only models of DSCS spatial distributions, such as those presented in this report, represent estimates or predictions of relative habitat suitability with inherent uncertainty. Model predictions should be validated to verify their accuracy using independent DSCS occurrence data, either existing data that were held aside from model fitting or new data collected after the models were developed. Ideally, data used for model validation should be collected following a sampling design that provides for a robust statistical analysis of the accuracy of model predictions. While the additional survey effort required for model validation can be logistically challenging and costly, it has been achieved in some previous studies (e.g., Anderson et al. 2016, Rooper et al. 2018). Here a proof of concept example is presented to demonstrate how model predictions from this study might be validated through the collection of additional DSCS occurrence data.

The example analysis used occurrence data collected using an AUV during an expedition by the NOAA Ship *Bell M. Shimada* along the continental US West Coast in fall 2018 as part of the Expanding Pacific Research and Exploration of Submerged Systems (EXPRESS) campaign. For this expedition, a set of sampling locations was proposed for model validation purposes by identifying areas of interest where multiple taxa had high predicted habitat suitability. These locations were used to inform survey planning, but it is important to note that the primary objective of the expedition was not model validation. Thus, the data were not collected in sufficient number or following a sampling design (e.g., stratified across habitat suitability classes) that would permit a robust statistical validation of the model predictions. Nevertheless, these data do provide an example of the type of data that might be used for model validation. Here

methods that might be applied to such 'opportunistic' data collections are described, with the goal of validating predictions of habitat suitability from presence-only models.

The data from the AUV surveys were composed of individual still images of the seafloor covering approximately 4.5 m^2 each collected along dive transects every 8 seconds with a separation of approximately 2 m between images. The presence or absence of DSCS taxa were noted for each image. Four modeled taxa with sufficient numbers of occurrences in the AUV data were selected for this analysis: Demospongiae, Hexactinellida, *Paragorgia*, and *Swiftia pacifica*. The first two taxa represent classes of sponges while the latter two taxa represent a genus and a species of deep-sea coral, respectively.

The goal of this analysis was to assess the agreement between the occurrences of the chosen taxa in the AUV data and the predicted habitat suitability from the presence-only MaxEnt models. Model grid cells where AUV surveys were conducted were chosen as the replicates, or sample units, for analysis. The number of images where a given taxon was present was treated as the response variable, thus the response variable was essentially a count at the spatial resolution of image field of view (4.5 m^2). The number of images in each grid cell represented the sampling effort. The 'raw' or 'exponential' prediction values (rather than the complementary log-log transformation of the MaxEnt prediction depicted in the map pages) from the MaxEnt models were used as the explanatory variable since these predictions are proportional to predicted density and thus are appropriate for modeling count data (Phillips et al. 2017). Specifically, the mean bootstrapped prediction values were used.

As an approximate initial assessment of the agreement between the numbers of AUV images where the chosen taxa were present and the model prediction values, the Spearman rank correlation coefficient was calculated. In order to account for sampling effort, the correlation between the proportion of images where the taxa were present and the model predictions was calculated.

As a more robust analysis of the agreementbetween the numbers of AUV images where the chosen taxa were present and the model prediction values, a generalized linear model (GLM) was fit for each taxon. Given that the response variable was treated as a count, a quasi-Poisson model with the log link function was used. The quasi-Poisson model was chosen over a Poisson model due to the almost certain overdispersion in the data relative to the simple model, which was confirmed by the estimated dispersion in the GLM. The linear predictor in the model was composed of an intercept and a linear effect of predicted habitat suitability ('raw' MaxEnt prediction). The log of the number of images in each grid cell was included as an effort 'offset.' The offset enforced a proportional relationship between sampling effort in a grid cell (i.e., the number of images) and the number of images in that cell where the taxon would be expected present. For example, if a taxon would be expected to be present in 5 out of 10 images in a given cell, then it would be expected to be present in 10 out of 20 images in another cell with identical predicted habitat suitability.

3.3 Results and Discussion

3.3.1 Predicted Spatial Distributions and Model Performance

This section describes the mapped spatial predictions of suitable habitat for each of the selected DSCS taxa in relation to the locations of occurrence records and, for corals, the reported depth range from Whitmire et al. (2017). Taxa are organized by category (stony corals, black corals, gorgonian corals, soft corals, sea pens, stylasterid corals, demosponges, glass sponges) to facilitate comparisons of the spatial distributions of occurrences and predicted suitable habitat among taxa within the same category. In addition to examining spatial patterns or trends in the areas likely to contain suitable habitat, the maps can also be used to identify potential targets for future exploration (e.g., an area predicted to have high habitat

suitability that has not been previously explored). Maps of the CV can be used to identify areas with greater variability (i.e., less precision) in the model predictions. In addition to areas of greater variability, higher values of the CV can also result from extremely low values of the mean habitat suitability. Therefore, maps of the CV should be interpreted in conjunction with the mean habitat suitability. The CV can also provide information about locations where variability in model predictions was high because of limited occurrence records, which may suggest potential targets for future surveys.

This section also summarizes the measures of model performance, which can be used to assess the relative level of confidence one can have in the model predictions for each taxon. For example, if cross-validation mean AUC, model fit, and model stability are all high, this suggests that model performance is excellent with predictions of suitable habitat that match the occurrence records and relatively low variability in model predictions for grid cells with a high classified mean habitat suitability. High cross-validation mean AUC and/or model fit but low model stability indicates that while model predictions may closely match the occurrence data, there is relatively higher variability in the predictions. If cross-validation mean AUC, model fit, and model stability are all low, mapped predictions should be used with more caution as model predictions do not fit the occurrence records as well and have relatively higher variability.

3.3.1.1 Stony Corals (Class Anthozoa; Order Scleractinia)

Distributions of three of the four taxa of stony corals modeled had little predicted suitable habitat north of Monterey Bay. The colonial cup coral *Coenocyathus bowersi* (Figure 3.3), the solitary cup coral *Desmophyllum dianthus* (Figure 3.4), and the structure-forming stony coral *Lophelia pertusa* (Figure 3.5) were generally restricted to the SCB and offshore of central California. Although *C. bowersi* had a reported depth range of 12–708 m, occurrence records and areas of high predicted habitat suitability (i.e., from the classified mean habitat suitability) were generally found near the offshore southern California islands in the shallower end of this depth range (Figure 3.3a–b). Variability in model predictions (i.e., the CV) for *C. bowersi* was generally greatest in deeper waters farther offshore and in the SCB, and relatively low in the areas with high predicted habitat suitability (Figure 3.3c). For *D. dianthus*, on the other hand, occurrence records and areas of high predicted habitat suitability were often in the southernmost part of the study area and at the deeper end of its reported depth range (37–293 m) (Figure 3.4a–b). Model predictions for *D. dianthus* were more variable offshore of Washington, particularly areas closer to shore, and had releative low variability in areas predicted to have higher habitat suitability (Figure 3.4c). *L. pertusa* had the widest reported depth range (390–2,775 m) of the stony corals modeled, but occurrence records were concentrated at depths <300 m on the continental shelf break and around the Channel Islands in the SCB and on the upper slopes of canyon walls in central California (Figure 3.5a). Areas of high predicted habitat suitability for *L. pertusa* were similarly constrained to the continental shelf break and upper slope in these locations and were generally too small to see on the map page (Figure 3.5b). Variability in model predictions for *L. pertusa* was relatively high north of Cape Mendocino, just outside of San Francisco Bay, and in some parts of the SCB, but was lowest in the areas with higher predicted habitat suitability (Figure 3.5c). The cross-validation mean AUC was high for *C. bowersi*, *D. dianthus*, and *L. pertusa*, and model fit was medium for all three species, with *D. dianthus* having the best model fit of the three (Table 3.6). This suggested that predictions of suitable habitat for these taxa matched the occurrence records. Model stability was medium for *C. bowersi* and *D. dianthus* but was low for *L. pertusa* (Table 3.6), which indicated that for *L. pertusa* there was greater variability in model predictions at grid cells predicted to have high habitat suitability.

Similar to the other stony corals, occurrences of cup corals in the genus *Paracyathus* were primarily located in the SCB and offshore of central California (Figure 3.6a). Although there are two known species of *Paracyathus* in the study area, the National Database included only records of *P. stearnsii* and records identified to the genus level. While occurrence records for *Paracyathus* spanned its full reported depth range (6–835 m), occurrences in deeper waters (>300 m) were limited to a few areas on the walls of

Monterey Canyon (Figure 3.6a). Areas of medium and high predicted habitat suitability included only small patches in shallower areas that were too small to see on the map page (Figure 3.6b). Variability in model predictions for *Paracyathus* was relatively high offshore of Oregon and Washington, particularly closer to shore on the continental shelf, and in some deeper areas off central and southern California. Model predictions had relatively low variability in the limited areas predicted to have medium or high habitat suitability (Figure 3.6c). The cross-validation mean AUC for *Paracyathus* was medium. However, model fit was low, as no model grid cells containing occurrence data were classified as high habitat suitability, and model stability was low, as no grid cells with high habitat suitability were also classified as robust (Table 3.6). Additional observations of this genus are needed to improve model performance. In particular, because deeper records of *Paracyathus* were clustered in a few small areas in Monterey Canyon, additional records of *Paracyathus* from surveys in deeper waters (300–1,000 m) may help models predict suitable habitat in areas like the walls of Monterey Canyon. Alternatively, additional observations may enable separate models for the shallower records on the continental shelf and the deeper records in places like canyons.

3.3.1.2 Black Corals (Class Anthozoa; Order Antipatharia)

As expected, the three taxa of black corals modeled had distinct distributional patterns. For the Christmas tree coral *Antipathes dendrochristos*, which has a reported depth range of 91–427 m, occurrence data and areas predicted to have high habitat suitability were limited to the SCB, with the exception of a single observation in the Gulf of the Farallones (Figure 3.7a–b). Patchy areas with relatively high variability in model predictions for *A. dendrochristos* were found throughout the study area, but model predictions had relatively low variability in areas in the SCB predicted to have high habitat suitability (Figure 3.7c). In contrast to *A. dendrochristos*, occurrence data and areas of high predicted habitat suitability for *Chrysopathes speciosa*, which has a reported depth range of 225–1,400 m, were mostly in deeper waters offshore of Oregon and Washington (Figure 3.8a–b). Variability in model predictions for *C. speciosa* was relatively high south of Cape Mendocino and in some areas on the continental shelf offshore of northern California and Washington. Model predictions had relatively low variability in the deeper waters offshore of Oregon and Washington where suitable habitat was predicted to occur (Figure 3.8c). Finally, observations and areas of medium and high predicted habitat suitability for the genus *Bathypathes* were more widespread, in deeper waters along the entire latitudinal extent of the study area (Figure 3.9a–b). Model predictions for *Bathypathes* had relatively low variability in the areas of medium and high predicted habitat suitability and higher variability in areas on the continental shelf where predicted habitat suitability was very low (Figure 3.9c). *Bathypathes* has a wide reported depth range (225–4,868 m) that extends considerably deeper than the study area. In fact, >80% of the *Bathypathes* records in the National Database were deeper than 1,200 m. The cross-validation mean AUC and model fit were high for *A. dendrochristos*, while model stability was medium (Table 3.6). Although cross-validation mean AUC was also high for *C. speciosa* and *Bathypathes*, model fit and model stability were low (Table 3.6). The low numbers of occurrences of *C. speciosa* and *Bathypathes* likely affected model performance, and these occurrences were also at the edge of the study area extent in deeper waters. Additional observations and/or models generated for an extent that includes deeper waters would be beneficial for characterizing the spatial distributions of these species.

3.3.1.3 Gorgonian Corals (Class Anthozoa; Order Alcyonacea; Suborders Calcaxonia, Holaxonia, Scleraxonia)

The genus *Acanthogorgia*, the only taxon modeled from the family Acanthogorgiidae, has a broad reported depth range (49–2,301 m) offshore of the continental US West Coast. The distribution of occurrence data and areas of high predicted habitat suitability for *Acanthogorgia* included both the SCB as well as some small areas offshore of central California (Figure 3.10a–b). This may reflect differences in the species that comprise the genus *Acanthogorgia* within the study area, with one species occurring in shallower waters (approximately 300–600 m) and only in the SCB and the rest of the species occurring in

deeper waters (>1,000 m), such as offshore of Monterey (T. Laidig, pers. comm.). Variability in model predictions for *Acanthogorgia* was generally highest offshore of Oregon and Washington and lowest in areas of higher predicted habitat suitability (Figure 3.10c). The cross-validation mean AUC was high for *Acanthogorgia*, while model fit was medium and model stability was low (Table 3.6). Separate models for the shallower and deeper species may perform better but would likely require additional observations of *Acanthogorgia* in each depth zone.

Species in the family Gorgoniidae generally occur in shallower waters within the study area. Three species in family Gorgoniidae were modeled. Occurrences and areas predicted to have high predicted habitat suitability for *Adelogorgia phyllosclera* (reported depth range: 9–595 m) were only found in the SCB (Figure 3.11a–b). Model predictions for *A. phyllosclera* had relatively low variability in the areas with higher predicted habitat suitability in the SCB, and highest variability in model predictions generally occurred in the deeper waters of the study area outside the reported depth range for *A. phyllosclera* (Figure 3.11c). *Eugorgia rubens* has a slightly shallower reported depth range (50–200+ m), but similar to *A. pyllosclera* areas of high (and sometimes robust high) predicted habitat suitability were also found only in the SCB (Figure 3.12b), although there were a couple of occurrences just south of Monterey Bay in addition to the observations in the SCB (Figure 3.12a). Variability in model predictions for *E. rubens* was highest offshore of Oregon and Washington, where predicted habitat suitability was very low. Model predictions had relatively low variability in the areas predicted to have high and robust high habitat suitability in the SCB (Figure 3.12c). Occurrence data for *Leptogorgia chilensis* (reported depth range: 5–231 m) were primarily in the SCB and offshore of central California (Figure 3.13a). There were areas of medium, high, and robust high predicted habitat suitability in these locations, but also in the Gulf of the Farallones and offshore of Washington where there were no occurrence records (Figure 3.13b). Suitable habitat for *L. chilensis* could exist in these areas (e.g., because the environmental conditions were similar to other locations of *L. chilensis* occurrence) where there were no occurrences of *L. chilensis* and few observations of any DSCS (Figure 3.1), but some caution should be used until these areas are ground-truthed. Model predictions for *L. chilensis* were most variable in deeper parts of the study areas and had lower variability in the areas with higher predicted habitat suitability (Figure 3.13c). Cross-validation mean AUC was high for all three species of Gorgoniids (Table 3.6). Model fit was high for *A. phyllosclera*, medium for *E. rubens*, and low for *L. chilensis*, while model stability was high for *E. rubens* and *L. chilensis* and medium for *A. phyllosclera*.

Offshore of the continental US West Coast, species in the family Isididae are generally found in waters deeper than the 1,200 m limit of the study area. Hence, *Isidella tentaculum* was the only taxon from the family Isididae modeled in this study. Consistent with its reported depth range of 720–1,050 m, occurrence data and areas of medium and high predicted habitat suitability for *I. tentaculum* were typically found in relatively deeper waters coastwide (Figure 3.14a–b). Variability in model predictions for *I. tentaculum* was highest in patches around the SCB and offshore of Washington, and lowest in deeper waters where there was higher predicted habitat suitability (Figure 3.14c). Cross-validation mean AUC was high for *I. tentaculum*, while model fit was medium and model stability was low (Table 3.6).

Occurrence data for the genus *Paragorgia* in the family Paragorgiidae were distributed coastwide (Figure 3.15a), and there were areas of high predicted habitat suitability throughout the SCB and in deeper waters offshore along the entire latitudinal extent of the study area (Figure 3.15b). The reported depth range for *Paragorgia* is 18–2,936 m, but most records in the National Database were deeper than the 1,200 m depth limit of the study area. Model predictions for *Paragorgia* had relatively low variability throughout much of the study area, including where models predicted high habitat suitability. Areas with the highest variability in model predictions (e.g., offshore of central Oregon) occurred where models predicted very low habitat suitability (Figure 3.15c). Cross-validation mean AUC was medium for *Paragorgia*, while model fit was high and model stability was medium (Table 3.6). Although model performance for

Paragorgia was generally good, a model generated for an extent that includes deeper waters where *Paragorgia* is known to occur may perform better.

Four species in the family Plexauridae were modeled in this study. This included the relatively shallow *Chromoplexaura marki* (reported depth range: 9–200 m) and three species in the genus *Swiftia* that have broader reported depth ranges extending from relatively shallow waters to deeper than the 1,200 m limit of the study area. *C. marki* observations, including some records deeper than its reported depth range, were found coastwide from the SCB north to offshore of Washington (Figure 3.16a). However, areas predicted as having medium or high habitat suitability for *C. marki* were sparse and very small (not easily visible in the map page, but sometimes surrounded by larger patches of low predicted habitat suitability), and typically were found on or near the edge of the continental shelf (Figure 3.16b). Variability in model predictions for *C. marki* was generally low throughout much of the study area, with highest variability outside San Francisco Bay and close to shore off northern California, northern Oregon, and Washington (Figure 3.16c). The reported depth ranges for *Swiftia kofoidi* (91–2,393 m), *Swiftia pacifica* (89–2,904 m), and *Swiftia simplex* (147–2,123 m) were similar, and observations of all three species were found coastwide. *S. kofoidi* observations and areas of medium and high predicted habitat suitability were found in the SCB, offshore of central California including in Monterey Canyon, and offshore of northern California (Figure 3.17a–b). Variability in model predictions for *S. kofoidi* was highest both nearshore and in deeper waters farther offshore of Oregon and Washington, as well as an area in the southernmost part of the study area in the SCB, while variability was relatively low in the areas predicted to have medium and high habitat suitability (Figure 3.17c). *S. pacifica* occurrences and areas of high predicted habitat suitability were also found in the SCB and to a lesser extent offshore of central California but were more likely to be found offshore of northern California and Oregon (Figure 3.18a–b). Model predictions for *S. pacifica* had highest variability close to shore, particularly north of Cape Mendocino, while variability was relatively low in areas with high predicted habitat suitability (Figure 3.18c). Occurrences and areas of high predicted habitat suitability for *S. simplex* were most concentrated offshore of central California, particularly Monterey Canyon, and offshore of northern California (Figure 3.19a–b). Although only a few observations of *S. simplex* existed in the SCB, there were some areas predicted to have high habitat suitability (Figure 3.19a–b). Variability in model predictions for *S. simplex* was relatively low, except in a few patches in the SCB and parts of the continental shelf offshore of Oregon and Washington. Model predictions generally had relatively low variability at the areas predicted to have high habitat suitability (Figure 3.19c). Cross-validation mean AUC was medium for all four species of Plexauridae. Model fit was medium for *S. kofoidi* and *S. pacifica* and low for *C. marki* and *S. simplex*. Model stability was medium for *S. pacifica* and *S. simplex* and low for *C. marki* and *S. kofoidi*.

Similar to the family Isididae, many of the species in the family Primnoidae found off the continental US West Coast occur deeper than the 1,200 m depth limit of the study area. Consequently, only two species in the family Primnoidae were modeled. *Parastenella ramosa* has a broad reported depth range (619–3,427 m). Occurrence data for *P. ramosa* were either in deeper waters (>600 m) offshore of northern California or in the SCB, where many of the records were considerably shallower than its reported depth range (Figure 3.20a). A few small patches (too small to be easily seen in the map page) of medium and high predicted habitat suitability were found in these areas in the SCB, but larger areas of high predicted habitat suitability were located in deeper waters offshore of northern California (Figure 3.20b). Variability in model predictions for *P. ramosa* was highest offshore of Washington and in a few small patches in the southernmost part of the study area. Model predictions had relatively low variability where models predicted medium and high habitat suitability (Figure 3.20c). In contrast, *Plumarella longispina* has a reported depth range of 80–732 m. Most of the occurrence data and areas of high predicted habitat suitability for *P. longispina* were in the SCB, but there were also a number of observations farther north near Cordell Bank and an area predicted to have high habitat suitability that spanned from Cordell Bank to Fanny Shoal (Figure 3.21a–b). Model predictions for *P. longispina* generally had the highest variability on the continental slope offshore of northern California, Oregon, and Washington, although there were

also some areas with higher variability in the SCB. Variability in model predictions was relatively low in the areas predicted to have high habitat suitability (Figure 3.21c). Cross-validation mean AUC was high and model fit and model stability were medium for both species of Primnoidae.

3.3.1.4 Soft Corals (Class Anthozoa; Order Alcyonacea; Suborders Alcyoniina, Stolonifera)

The mushroom soft coral *Heteropolypus ritteri* has a broad reported depth range (35–3,330 m) off the continental US West Coast that extends well past the 1,200 m depth limit of the study area. Occurrence data for *H. ritteri* were widespread from the California-Mexico border to northern Washington and were found predominantly on the continental slope as well as deeper areas within the SCB (Figure 3.22a). Areas predicted to have high and robust high habitat suitability for *H. ritteri* were also widespread in these locations (Figure 3.22b). Model predictions for *H. ritteri* generally had low variability, with some areas of higher variability offshore of Washington (Figure 3.22c). Stoloniferan corals in the genus *Clavularia* also have a reported depth range (0–1,529 m) that extends past the depth limit of the study area, but *Clavularia* was not as widely distributed. Records of *Clavularia* occurrence and areas of high predicted habitat suitability were generally at depths >500 m in three areas, the SCB, near Monterey Bay, and offshore of northern California (Figure 3.23a–b). Variability in model predictions for *Clavularia* was relatively high, particularly along the edge of the continental shelf from central California north to Washington. Model predictions had lower variability in the areas predicted to have high habitat suitability (Figure 3.23c). For both taxa of soft corals, the cross-validated mean AUC was high. Model fit was high for *H. ritteri* and medium for *Clavularia*. Model stability was medium for both *H. ritteri* and *Clavularia* (Table 3.6).

3.3.1.5 Sea Pens (Class Anthozoa; Order Pennatulacea)

Occurrence data for *Anthoptilum grandiflorum* (reported depth range: 72–3,651 m), the only member of the family Anthoptilidae modeled in this study, were widespread but generally farther offshore on the continental slope and deeper parts of the SCB (Figure 3.24a). There were large areas of high and robust high predicted habitat suitability for *A. grandiflorum* in the deeper waters of the study area (Figure 3.24b). Model predictions for *A. grandiflorum* had relatively low variability throughout the study area, including areas predicted to have higher habitat suitability, and highest variability on the continental shelf offshore of Oregon and Washington (Figure 3.24c). Cross-validation mean AUC and model fit were medium for *A. grandiflorum*, while model stability was high (Table 3.6).

The genus *Funiculina* in the family Funiculinidae includes three known species (combined reported depth range: 200–2,740 m) in the study area. Observations of *Funiculina* were typically farther offshore (Figure 3.25a), and areas of high and robust high predicted habitat suitability were found throughout the SCB and in a narrow band along the offshore edge of the study area (Figure 3.25b). Variability in model predictions for *Funiculina* was highest on the continental shelf offshore of Oregon and Washington and on some of the banks in the SCB, but was lower in the deeper waters farther offshore and areas predicted to have higher habitat suitability (Figure 3.25c). Cross-validation mean AUC and model fit were high for *Funiculina*, while model stability was medium (Table 3.6).

Of the two known species in the family Halipteridae in the study area, only *Halipteris californica* had sufficient numbers of records for modeling. While *H. californica* has a broad reported depth range (46–2,780 m), occurrences were typically found from 500–1,000 m. Occurrence data were coastwide (Figure 3.26a), but areas predicted to have high habitat suitability for *H. californica* were predominantly in the SCB and offshore of central and northern California (Figure 3.26b). Model predictions for *H. californica* were most variable on the continental shelf from northern California to Washington, while variability in model predictions was lowest in the areas of the continental slope with high predicted habitat suitability

(Figure 3.26c). Cross-validation mean AUC, model fit, and model stability were all medium for *H. californica* (Table 3.6).

In the family Pennatulidae, *Pennatula phosphorea* (reported depth range: 519–2,825 m) is found in deeper waters while *Ptilosarcus gurneyi* (reported depth range: 16–475 m) is found in relatively shallower waters. There were some observations of *P. phosphorea* offshore of Oregon and Washington, but occurrences and areas of high predicted habitat suitability were mostly in the western part of the SCB and offshore of central California (Figure 3.27a–b). Variability in model predictions for *P. phosphorea* was highest in the southernmost part of the SCB, on the edge of the continental shelf offshore of central and northern California, and on the continental shelf offshore of Oregon and Washington (Figure 3.27c). Variability was lower, however, in the areas predicted to have higher habitat suitability (Figure 3.27c). Occurrences of *P. gurneyi* were located all along the coast and predominantly on the continental shelf or upper slope, although some records were found slightly deeper on the slope offshore of Oregon and Washington (Figure 3.28a). Large areas on the continental shelf and upper slope were predicted to have high or robust high habitat suitability north of the northernmost Channel Islands, around Point Conception, and from Monterey Bay to the Gulf of the Farallones (Figure 3.28b). Offshore of Oregon, a long band closer to shore on the continental shelf was predicted to have high or robust high habitat suitability (Figure 3.28b). Model predictions for *P. gurneyi* had highest variability in some deeper parts of the SCB, near Santa Lucia Bank off central California, just outside San Francisco Bay, and at the mouth of the Columbia River (Figure 3.28c). Variability in model predictions was again lower in the areas with high predicted habitat suitability (Figure 3.28c). Cross-validation mean AUC was medium for both species in Pennatulidae, while model fit was high for *P. phosphorea* and medium for *P. gurneyi* and model stability was high for *P. gurneyi* and medium for *P. phosphorea* (Table 3.6).

Although *Umbellula lindahli* in the family Umbellulidae has a narrow reported depth range (914–927 m), records in the National Database were found across a broader depth range with most records occurring between 500–1,000 m depth. Observations and areas of high and robust high predicted habitat suitability for *U. lindahli* were found in deeper waters in the eastern part of the SCB and offshore of central and northern California (Figure 3.29a–b). Variability in model predictions for *U. lindahli* was highest in the southernmost part of the SCB, near Santa Lucia Bank off central California, on parts of the continental shelf from northern California to Washington, and in deeper waters offshore of Washington (Figure 3.29c). Model predictions had lowest variability in the areas predicted to have high and robust high habitat suitability (Figure 3.29c). Cross-validation mean AUC, model fit, and model stability were all high for *U. lindahli* (Table 3.6).

One species and two genera in the family Virgularidae were modeled. *Acanthoptilum gracile* has a reported depth range of 5–1,981 m, but most observations were closer to shore on the continental shelf (Figure 3.30a). There was a long stretch of high and robust high predicted habitat suitability offshore of Oregon in addition to other areas of high predicted habitat suitability along the coast and in the SCB (Figure 3.30b). Model predictions for *A. gracile* had relatively low variability on the continental shelf, but variability was slightly higher in deeper waters on the continental slope (Figure 3.30c). While cross-validation mean AUC and model stability were medium for *A. gracile*, model fit was low (Table 3.6). For the genus *Stylatula*, occurrence data were widespread across the continental shelf and slope north of Point Conception. Records were fewer in the SCB and were mostly on the continental shelf (Figure 3.31a). Large areas on the continental shelf offshore of Oregon and Washington were predicted to have high or robust high habitat suitability (Figure 3.31b). Areas of high predicted habitat suitability were also found on the deepest edge of the study area from Point Conception to Washington (Figure 3.31b). Although there were records of *Stylatula* occurrence on the continental shelf in the SCB, there were no areas of medium or high predicted habitat suitability (Figure 3.31b). Variability in model predictions for *Stylatula* was relatively low throughout the study area, but was slightly higher in the deeper parts of the SCB where there were no occurrence data (Figure 3.31c). Cross-validation mean AUC was medium for *Stylatula*,

while model fit was low and model stability was high (Table 3.6). *Stylatula* includes two known species within the study area. *Stylatula gracilis* occurs in shallower waters (reported depth range: 50–261 m), while *Stylatula elongata* has a broader reported depth range (2–820 m). Models developed separately for the two species would likely have better performance, but there were insufficient numbers of records identified at the species level. Occurrence data for the genus *Virgularia* were sparse but were found from the SCB north to Washington. Records in the SCB were primarily close to shore on the continental shelf and around the Channel Islands. Farther north, occurrences were more evenly distributed between the continental shelf and on the slope (Figure 3.32a). Very few areas were predicted to have low or medium habitat suitability for *Virgularia*, and there were no areas classified as high predicted habitat suitability (Figure 3.32b). Model predictions for *Virgularia* generally had relatively low variability throughout the study area (Figure 3.32c). Cross-validation mean AUC, model fit, and model stability were all low for *Virgularia* (Table 3.6). Similar to *Stylatula*, the genus *Virgularia* includes a shallower species, *V. bromleyi* (reported depth range: 5–90 m) and a more widely distributed species, *V. agassizi* Studer (reported depth range: 30–1,000 m). Model performance may improve for models at the species level, but additional observations are needed to support these models.

3.3.1.6 Stylasterid Corals (Class Hydrozoa; Order Anthoathecatae)

The only stylasterid coral modeled, *Stylaster californicus* (reported depth range: 4–126 m) was observed closer to shore on the continental shelf off California as well as on banks in the SCB, but was not recorded north of California (Figure 3.33a). Areas of high predicted habitat suitability were small and generally patchy in the SCB and along the continental shelf, and extended north to Oregon and Washington even though no occurrence data were found that far north (Figure 3.33b). Slightly larger bands of high habitat suitability were predicted very close to shore just south of Monterey Bay and around Cape Mendocino (Figure 3.33b). Variability in model predictions for *S. californicus* was highest in deeper waters on the continental slope as well as some parts of the continental shelf offshore of Washington, but was lower on the parts of the continental shelf south of Cape Mendocino where there were occurrence records (Figure 3.33c). Cross-validation mean AUC was high, while model fit and model stability were medium (Table 3.6).

3.3.1.7 Demosponges (Class Demospongiae)

Demosponge observations and areas predicted to have high or robust high habitat suitability spanned the entire coast and were typically found on the continental shelf and on features like banks and shoals (Figure 3.34a–b). Model predictions for Demonspongiae had relatively low variability throughout the study area, with highest variability in the deepest edge of the study area and some parts of the continental shelf offshore of Oregona and Washington (Figure 3.34c). The cross-validation mean AUC was medium, and model fit and model stability were high for the class level model of demosponges (Table 3.7).

Occurrences and areas of high predicted habitat suitability for the genus *Asbestopluma* were primarily found in the eastern part of the SCB and near Monterey Bay, as well as in a small area in deeper waters offshore of Oregon (Figure 3.35a–b). Variability in model predictions for *Asbestopluma* was highest in deeper waters south of Cape Mendocino and on the continental shelf and slope offshore of Oregon and Washington, but was lower in the SCB where higher habitat suitability was predicted (Figure 3.35c). Cross-validation mean AUC, model fit, and model stability were all medium for *Asbestopluma* (Table 3.7).

For *Craniella arb*, observations were found close to shore along the continental shelf offshore of California, with only a few occurrences south of Point Conception (Figure 3.36a). Small patches and narrow bands of high predicted habitat suitability were found very close to shore along the continental shelf from Point Conception to northern California and to the north of the northernmost Channel Islands (Figure 3.36b). Model predictions for *C. arb* had lowest variability in the narrow band close to shore

along the continental shelf were high habitat suitability was predicted, but variability was higher on the rest of the continental shelf and on the continental slope, particularly in deeper waters (Figure 3.36c). While cross-validation mean AUC was high for *C. arb*, model fit was medium and model stability was low (Table 3.7).

Similar to *Asbestopluma*, occurrences for the genus *Haliclona* were mostly restricted to the SCB and near Monterey Bay, although *Haliclona* was also observed at Cordell Bank (Figure 3.37a). Areas predicted to have high habitat suitability for *Haliclona* were concentrated on edges of banks in the SCB and on the rim of Monterey Canyon, with medium habitat suitability predicted on the edges of Cordell Bank (Figure 3.37b). Variability in model predictions for *Haliclona* was lower in areas predicted to have higher habitat suitability, but variability was relatively high in many areas, including some of the deeper parts of the study area (Figure 3.37c). While cross-validation mean AUC was high for *Haliclona*, model fit was medium and model stability was low (Table 3.7).

For the genus *Mycale*, observations were located in relatively shallow waters on banks in the SCB and northern California (Fanny Shoal, Rittenburg Bank, Cordell Bank) as well as in deeper waters on the edge of the continental shelf and on the slope coastwide (Figure 3.38a). Areas of high habitat suitability were predicted in many of the areas where Mycale was observed, and no areas of medium or high habitat suitability were predicted north of California (Figure 3.38b). Model predictions for *Mycale* had the highest variability in the deeper parts of the SCB, while areas with lower variability included the places with high predicted habitat suitability (Figure 3.38c). Cross-validation mean AUC was medium, model fit was high, and model stability was medium (Table 3.7).

Records of *Polymastia* occurrence were concentrated on banks in the SCB and on the rim of Monterey Canyon, but were also found in some locations on the continental shelf and upper continental slope off California (Figure 3.39a). Areas of high predicted habitat suitability for *Polymastia* were very small (difficult to see on the map page) and patchy, and generally near the most concentrated occurrence records (Figure 3.39b). Variability in model predictions for *Polymastia* was highest in deeper waters offshore of northern California and offshore of Oregon and California, and was lower in the areas predicted to have high habitat suitability (Figure 3.39c). Cross-validation mean AUC, model fit, and model stability were all medium for *Polymastia* (Table 3.7).

Rhizaxinella gadus observations and areas of high predicted habitat suitability were almost exclusively in the SCB with only a couple of observations (but no predicted suitable habitat) in Monterey Bay and an area of high habitat suitability (but no occurrence data) on the edge of Heceta Bank offshore of Oregon (Figure 3.40a–b). Model predictions for *R. gadus* had highest variability in parts of the SCB, outside San Francisco Bay, closer to shore on the continental shelf off northern California, and offshore of Washington. Variability in model predictions was lower in the locations with higher predicted habitat suitability (Figure 3.40c). Cross-validation mean AUC was high for *R. gadus*, while model fit and model stability were medium (Table 3.7).

Most of the occurrence data and high and robust high predicted habitat suitability for the genus *Thenea* were in the SCB (Figure 3.41a–b). Some observations of *Thenea* were found in Monterey Bay, but only small patches (too small to be seen in the map page) of high habitat suitability were predicted elsewhere offshore of central and northern California (Figure 3.41a–b). Variability in model predictions for *Thenea* was lowest in the areas of the SCB predicted to have higher habitat suitability and was higher in some deeper parts of the SCB, near Santa Lucia Bank, near Delgada Canyon south of Cape Mendocino, and in areas offshore of Oregon and Washington (Figure 3.41c). Cross-validation mean AUC, model fit, and model stability were all high for *Thenea* (Table 3.7).

3.3.1.8 Glass Sponges (Class Hexactinellida)

Like demosponges, glass sponges were widespread along the entire coast but generally occurred farther offshore and deeper than demosponges. Occurrence records and large swaths of high and robust high predicted habitat suitability extended from the basins and slopes of banks in the SCB along the continental slope to Washington (Figure 3.42a–b). North of Cape Mendocino, most of the area deeper than 200 m was predicted to have robust high habitat suitability. Similarly, much of the SCB deeper than 200 m was predicted to have high or robust high habitat suitability (Figure 3.42b). Model predictions for Hexactinellida generally had relatively low variability throughout the study area, but were most variable on the continental shelf offshore of Washington (Figure 3.43c). Cross-validation mean AUC and model fit were medium, while model stability was high for the class-level glass sponge model (Table 3.7).

Almost all occurrence data and a large area of high predicted habitat suitability for *Aphrocallistes vastus* were in deeper waters offshore of Oregon and Washington, although there were also some smaller areas of medium and high habitat suitability predicted in deeper waters offshore of northern California and off of Santa Lucia Bank in central California (Figure 3.43a–b). Variability in model predictions for *A. vastus* was relatively low in deeper waters on the continental slope, but was higher in the SCB and on the continental shelf offshore of Oregon and Washington (Figure 3.43c). Cross-validation mean AUC and model stability were high for *A. vastus*, while model fit was medium (Table 3.7).

Farrea occa was not as widespread, with observations and high and robust high predicted habitat suitability primarily in the SCB as well as a large area in deeper waters on the continental slope at the California-Oregon border (Figure 3.44a–b). Model predictions for *F. occa* had the highest variability offshore of Washington, and were lower in the areas predicted to have higher habitat suitability (Figure 3.44c). Cross-validation mean AUC was high for *F. occa*, while model fit and model stability were medium (Table 3.7).

For *Heterochone calyx*, occurrence data and areas of high and robust high predicted habitat suitability were patchy but spanned the coast, particularly in the SCB, near Cordell Bank, and offshore of Oregon and Washington (Figure 3.45a–b). Variability in model predictions for *H. calyx* was highest near Santa Lucia Bank, around Cape Mendocino, and in some areas offshore of Oregon and Washington. However, variability was relatively low in the areas predicted to have higher habitat suitability (Figure 3.45c). Cross-validation mean AUC, model fit, and model stability were all medium for *H. calyx* (Table 3.7).

The distribution of the genus *Hyalonema* appeared to be divided primarily into two distinct locations — deeper waters in the southern part of the SCB and on the continental slope offshore of Washington. In each location, there were many occurrences and large areas predicted to have high and robust high habitat suitability (Figure 3.46a–b). Model predictions for *Hyalonema* had relatively low variability in these locations, but had somewhat higher variability on the continental shelf north of Monterey Bay (Figure 3.46c). In spite of having two distinct areas of occurrence, cross-validation mean AUC, model fit, and model stability were all high for *Hyalonema* (Table 3.7).

Rhabdocalyptus dawsoni observations and areas predicted to have high habitat suitability were concentrated in the SCB, along the rim of Monterey Canyon, and on the edge of the continental shelf just south of Monterey Bay, although patches of high predicted habitat suitability were smaller and difficult to discern in the map page for the latter locations (Figure 3.47a–b). Variability in model predictions for *R. dawsoni* was higher in some deeper parts of the SCB and offshore of Oregon and Washington, but was lower in areas predicted to have higher habitat suitability and other parts of the shelf in southern and central California (Figure 3.47c). Cross-validation mean AUC was high for *R. dawsoni*, while model fit and model stability were medium (Table 3.7).

For the genus *Staurocalyptus*, occurrence data and patches of high predicted habitat suitability were found on shallower banks in the SCB and off northern California (Rittenburg Bank, Fanny Shoal) as well as on the deeper slopes off the northernmost Channel Islands and along the continental slope to the California-Oregon border (Figure 3.48a–b). High habitat suitability was also predicted at similar banks, such as Santa Lucia Bank in central California, where there were no occurrence records (Figure 3.48b). Model predictions for *Staurocalyptus* had higher variability in deeper waters of the SCB and on the continental shelf offshore of Oregon and Washington, but variability was lower for the banks and parts of the continental slope where high habitat suitability was predicted (Figure 3.48c). Cross-validation mean AUC and model fit were medium for *Staurocalyptus*, while model stability was low (Table 3.7).

3.3.2 Aggregated Predictions for Taxa Associated with Hard Substrate

The 22 deep-sea coral taxa associated with hard substrate that were included in aggregated maps of habitat suitability included all of the stony corals, black corals, soft corals, and stylasterid corals selected for modeling in this study (Table 3.3). The aggregated maps depict how many of these taxa were predicted to have high or robust high habitat suitability at each grid cell from models developed for individual taxa.

General patterns of predicted habitat suitability may be similar for some of these taxa, but there was considerable variability in which model grid cells were predicted to have high or robust high habitat suitability. Consequently, while 520,912 grid cells (21.6% of the study area) had predicted high habitat suitability for at least one taxon, only 125,248 grid cells (<4% of the study area) had predicted high habitat suitability for two or more taxa and 5,737 grid cells (<0.2% of the study area) had high habitat suitability for four or more taxa (Figure 3.49). The maximum number of taxa predicted to have high habitat suitability at the same grid cell was eight, but this occurred at only five grid cells. Similar to high habitat suitability, robust high habitat suitability was predicted for at least one taxon at 176,313 grid cells (5.2% of the study area), but <1% of the grid cells had robust high habitat suitability for two or more taxa (Figure 3.50). The maximum number of taxa with co-occurring robust high habitat suitability was six, at only 13 grid cells.

The soft coral *H. ritteri* and gorgonian coral *Paragorgia* were the taxa most frequently predicted to co-occur (i.e., both taxa had high habitat suitability), but at only 36,480 grid cells (1.1% of the study area). *H. ritteri* was also predicted to co-occur with the gorgonian coral *S. simplex* at 15,231 grid cells (0.4% of the study area) and with the gorgonian coral *P. ramosa* at 9,504 grid cells (0.3% of the study area). *Paragorgia* was also predicted to co-occur with the gorgonian coral *S. pacifica* at 9,877 grid cells (0.3% of the study area). The stony coral taxa were predicted to co-occur with each other at <0.1% of model grid cells. Only *L. pertusa* was most frequently predicted to co-occur with another stony coral taxon, but it only co-occurred with *D. dianthus* at 1,628 grid cells. *C. bowersi* was most frequently predicted to co-occur with the gorgonian coral *E. rubens*, at 9,164 grid cells (0.3% of the study area), while *D. dianthus* most frequently was predicted to co-occur with the black coral *A. dendrochristos*, but only at 3,205 grid cells (<0.1% of the study area). Among the black corals, *Bathypathes* and *C speciosa* were predicted to co-occur at only 656 grid cells. *A. dendrochristos* was not predicted to co-occur with either of the other black coral taxa but was predicted to co-occur with the gorgonian coral *P. longispina* at 7,808 grid cells (0.2% of the study area).

Although the number of co-occurring taxa at each grid cell was generally low, the aggregated maps can nevertheless provide useful information about the locations where these taxa may co-occur to support management decision making. In the SCB, areas with high and robust high habitat suitability for multiple taxa were found on the shelf and upper slope around many of the Channel Islands and offshore banks (Figure 3.49, Figure 3.50). North of Point Conception, California, these areas were generally on the continental slope, including in submarine canyons that incise the slope (e.g., Monterey Canyon) and on rugose features such as the Brush Patch Groundfish EFH conservation area. In addition to identifying

these patterns, the aggregated maps can be used to evaluate the potential impacts to deep-sea coral habitat at a wind energy planning area, such as the Humboldt Call Area offshore of northern California, by suggesting which areas (e.g., lease blocks) may contain suitable habitat for multiple taxa (Figure 3.49b, Figure 3.50b).

Again, it is important to note that the aggregated maps presented here are only representative of the deep-sea coral taxa selected for modeling and may reflect any taxonomic biases in the records included in the National Database for the study area. In addition, the maps may reflect spatial sampling bias in the records, as areas identified as having suitable habitat for multiple taxa coincided with areas having greater numbers of records in the National Database. Finally, because the MaxEnt models developed in this study provide only a measure of the relative probability of occurrence (i.e., relative habitat suitability), the aggregated maps do not intend to depict taxonomic richness or community composition but rather only to examine patterns of habitat suitability across multiple taxa.

3.3.3 Trends in Selected Environmental Predictor Variables

The number and composition of environmental predictor variables in the best model iteration varied across the DCSC taxa. The environmental predictor variables most commonly included in DSCS models following the model selection procedure were depth (43 out of 46 taxa), latitude (29 taxa), and slope (26 taxa) (Figure 3.51). These environmental predictors were also the most common when considering just the deep-sea coral models or just the sponge models. Interestingly, while the hard-soft substrate classification was included in the best model iteration for 18 DSCS taxa, it was only included for nine of the 22 deep-sea coral taxa associated with hard substrate. This could indicate that other environmental predictors (e.g., seafloor slope) that were more commonly included for these taxa were sufficient at the resolution of the models for characterizing areas of the seafloor likely to contain hard substrate.

Although the model selection procedure was implemented to avoid fitting overly complex models, the median number of environmental predictors included in models was 7.5 and several models still included >10 predictors. Without the standard measures of environmental predictor variable importance provided by the Java software, it was not possible to determine which of the environmental predictors used in the selected models were contributing most to model fitting.

3.3.4 Model Validation

A total of 20,575 images from the AUV surveys conducted in fall 2018 during the expedition by the NOAA Ship *Bell Shimada* were available for the ground-truthing analysis. These surveys spanned from southern California to Oregon, but images were collected in only 220 of the 200 x 200 m model grid cells. Most grid cells had 1–150 images, while a few grid cells had substantially more (up to 525) images (Figure 3.52). There were 3,408,393 model grid cells total, so <0.01% of cells had an AUV image.

The distribution of AUV images across predicted habitat suitability classes varied among the four taxa selected for the model validation exercise (Table 3.8). Sample sizes were spread more evenly across habitat suitability classes for the sponges than for the deep-sea corals. Most of the AUV images were from grid cells with very low predicted habitat suitability for *Paragorgia* or *S. pacifica*, and only a few images were from grid cells with medium or high habitat suitability.

The correlation coefficient was positive for all four taxa ranging from 0.14–0.44 (Table 3.9). However, there was a lot of variability in the relationship between the number of AUV images with presences and the predicted habitat suitability, with only weak visual agreement except perhaps for Demospongiae (Figure 3.53).

The estimated relationship between the number of images where a taxon was present and the model predictions was positive for all four taxa but was only significant ($\alpha = 0.05$) for Demospongiae and *S.*

pacifica (Table 3.9). The percentage of deviance explained by the GLM was low for all four taxa, ranging from 0–9% (Table 3.9).

The analysis presented here was intended as a proof of concept example of how newly collected DSCS data might be used to validate the model predictions of relative habitat suitability presented in this report. Unfortunately, at this time there are insufficient data to conduct a thorough validation of the model predictions. Nevertheless, the analytical methods presented here may be useful when such data do become available.

The GLM framework in particular has several desirable features including appropriate model structures for different data types (e.g., presence-absence or count) and proper accounting for sampling effort. The GLM framework could also accommodate multiple data types (e.g., AUV and ROV), potentially with estimated survey-specific effects on detection probability. A feature not incorporated in this analysis, but worthy of further consideration, is explicit accounting for spatial autocorrelation both within and across model grid cells. The sequential nature of the AUV data and the proximity of images to each other will almost certainly result in correlations in the response between nearby images given non-random patterns of DSCS spatial distributions. In this analysis, a quasi-Poisson model was employed in an attempt to adjust *p*-values appropriately for remaining correlations in residual errors, but an explicit accounting for spatial autocorrelation would be better.

Collection of new DSCS data to validate predictions of species distribution models is logistically challenging and expensive. Data should be collected across the full range of predicted habitat suitability for a given taxon, and this task becomes especially challenging when models for multiple taxa with varying distributions are to be validated. When model predictions cover a large area, as was the case with the models presented in this report, large samples are required for a robust statistical analysis of the accuracy of model predictions. The AUV data analyzed here were not sufficient for a thorough validation of the model predictions. For example, the predicted most suitable habitat for the two deep-sea coral taxa analyzed was not well sampled by the AUV survey. Nevertheless, the methodological approach outlined here provides a starting point for future validation of the model predictions once sufficient new data are available. It is promising that there was some evidence of correspondence between the model predictions and observed occurrences on this new survey, at least for a couple of taxa.

It is important to note that the predictions of habitat suitability from the presence-only models are relative, not absolute, so validation is also limited to relative terms. The strength of correlation or the relationship between the model predictions and new occurrence data represents the measure of model validation. In contrast, it is not possible to validate the model predicted values themselves because they do not represent absolute quantities like probability of occurrence or density. Validation of the model predictions will only indicate how well a model distinguishes areas where a taxon is more likely to occur from areas where a taxon is less likely to occur. The models by design do not predict how likely a taxon is to occur in an absolute sense, and therefore cannot be validated in that sense.

3.3.5 Comparison to Existing US West Coast Models

Models produced for this study included more taxa and were at a finer taxonomic resolution than those developed in previous regional-scale modeling efforts (e.g., Bryan and Metaxas 2006, 2007 modeled two families of corals, Guinotte and Davies 2014 modeled two orders and three suborders of corals). This was made possible by the large number of additional records of DSCS occurrences that have been submitted to the NOAA National Database over the past several years. Many of these recent records were collected using high-resolution visual surveys (e.g., by AUVs and ROVs) and were identified at the species or genus level. Because individual taxa that comprise a broader taxonomic group (e.g., genera in a family) can have different habitat requirements, models fit at a coarser taxonomic level may perform poorly in resolving the habitat features for the unique taxa within the broader group. Therefore, it is preferable to

develop models for taxa at the finest taxonomic level that is practical, especially when there are known differences in habitat between the taxa. If needed for specific management questions, taxa may later be combined into broader groups for modeling if there are indications that they are expected to respond to similar environmental conditions.

In addition to the increase in the number of occurrence records, this study incorporated environmental data that was not available for previous modeling efforts. This included the extensive seafloor mapping with multibeam sonar that has occurred over the past decade. Incorporating fine-scale seafloor depth information into the development of environmental predictor variables can allow models to be developed at finer spatial resolution (although it is also important to consider the limitations of the positional accuracy of the occurrence data). The seafloor features inhabited by DSCS can be quite small, and regional or coarse bathymetry compilations will not likely resolve these features. As a result, models fit using environmental predictor variables derived from coarser bathymetry data may not predict suitable habitat in areas with these fine-scale, hard seafloor features. Previous regional-scale models also did not incorporate environmental predictor variables depicting hard substrate or bottom ocean currents because data for these variables did not exist for the entire model domain or at sufficient resolution (Guinotte and Davies 2014).

Finally, previous regional-scale models have not presented measures of prediction uncertainty and have not been validated using independent data. Maps presented in this study include measures of prediction variability (i.e., uncertainty), which provide information about confidence in model predictions and could be used to identify locations where additional survey effort would be beneficial. Similar to previous models, the models presented in this study have relied on cross-validation to assess model performance. However, as part of this study initial efforts have been made to collect 'opportunistic' survey data for model ground-truthing through collaboration with other studies and field efforts. Although it would be ideal to design a sampling effort for field validation that is focused solely on evaluating model performance, this is not typically feasible, particularly for the large geographic extent of this study. Efforts to assess model performance using similar data collections and methods as described in Sections 3.2.6 and 3.3.4 will continue in the future.

3.4 Conclusions

The presence-only models developed for this study utilized the increased availability of both DSCS observations and environmental data to produce predictions of the distribution of DSCS habitat across the continental shelf and slope offshore of the continental US West Coast. While the models did not directly predict distributions of DSCS communities or provide direct, spatial information about taxonomic richness, the maps presented here can be used to infer patterns in predicted habitat suitability across taxa.

The maps presented in this chapter provide information about the likely spatial distribution of suitable habitat offshore of the continental US West Coast to 1,200 m depth for 46 taxa of DSCS. The maps of the classified mean habitat suitability are accompanied by corresponding maps of the CV of the predicted mean habitat suitability, which provide a measure of prediction variability (i.e., uncertainty) that can be used to assess the level of confidence in the predictions at each model grid cell. It is important that the CV maps are considered alongside the classified mean habitat suitability maps. In addition to areas of greater variability in model predictions, higher values of the CV can also result from extremely low values of the mean habitat suitability. In this study, the CV was generally lower in areas of higher predicted habitat suitability and higher in areas with very low predicted habitat suitability. In areas where both the CV and mean habitat suitability are high, predictions should be interpreted with more caution. The maps can also help identify locations where variability in model predictions is high but occurrence records are limited, which may suggest potential targets for future surveys.

In addition to maps of predicted suitable habitat for DSCS, this chapter provides measures of model performance. These measures indicate how well the models fit the occurrence records (i.e., how closely the model predictions match the data used to fit the models) and how variable predictions were in areas of high habitat suitability. These measures indicate the relative level of confidence one can have in the model predictions for each taxon. For example, if cross-validation mean AUC, model fit, and model stability are all high, this suggests that model performance is excellent with predictions of suitable habitat that match the occurrence records and relatively low variability in the predictions. High cross-validation mean AUC and/or model fit but low model stability indicates that while model predictions may closely match the occurrence data, there is relatively higher variability in the predictions. If cross-validation mean AUC, model fit, and model stability are all low, mapped predictions should be used with caution as model predictions do not fit the occurrence records as well and have relatively higher variability. In general, taxa with low model performance tended to have fewer occurrence records. Taxa with greater numbers of records distributed over the entire study area (e.g., *Paragorgia* and *H. ritteri*) tended to have the best model performance. It should be noted that the high, medium, and low rankings assigned for model fit and model stability are only relative to the models developed in this study. All models included in this report had sufficient performance to inform management.

Maps of predicted suitable habitat for deep-sea coral taxa considered to be associated with hard substrate were aggregated to identify locations where these taxa may co-occur. In the SCB, areas with high and robust high habitat suitability for multiple taxa were found on the shelf and upper slope around many of the Channel Islands and offshore banks. North of Point Conception, these areas were generally on the continental slope, including in submarine canyons that incise the slope (e.g., Monterey Canyon) and on rugose features such as the Brush Patch Groundfish EFH conservation area. Predicted suitable habitat for sea pens was generally more widespread and either on or near the edge of the continental shelf or in deeper waters on the continental slope. Demosponges typically were predicted to occur on the continental shelf and on features like banks and shoals, while predicted suitable habitat for glass sponges was farther offshore and deeper along the continental slope.

A few of the DSCS taxa modeled in this study were reported to occur only in one biogeographic province (i.e., either the California Province south of Point Conception or the Oregon Province to the north; Whitmire et al. 2017). While the reported biogeographic divisions were reflected in occurrence records in the National Database and predictions of suitable habitat for some taxa (e.g., the gorgonian coral *A. phyllosclera*), this was not always the case. For example, the black coral *Bathypathes* was reported to occur only in the Oregon Province, but observations and predicted suitable habitat were coastwide. In addition, a few taxa (e.g., *Bathypathes*, *Paragorgia*) included in this study had reported depth ranges and distributions of occurrence records that extended deeper than the offshore extent of the study area. Expanding the model domain to include deeper waters would likely improve model performance for these taxa. A model domain that extended deeper would also allow models to be fit for some taxa (e.g., in the gorgonian coral families Chrysogorgiidae and Isididae) that were excluded from this study because there were insufficient numbers of records (or in some cases no records) in the study area. However, as stated previously, there was considerably less coverage of multibeam bathymetry in the deeper waters offshore of California, Oregon, and Washington, and efforts to increase the coverage of multibeam bathymetry in deeper waters are needed.

While the models presented in this study took advantage of the increased availability of both DSCS observations and bathymetry data from multibeam sonar surveys, there are still limitations that need to be considered. While efforts have been made to increase the coverage of multibeam bathymetry in the region, at the time of this study nearly half of the study area had not been mapped by multibeam sonar. Environmental predictor variables depicting seafloor topography and seafloor substrate could not capture finer-scale features (e.g., those indicative of exposed hard substrate) in areas not mapped by multibeam. Collection of additional data from multibeam sonar surveys would improve these predictors for future

models of DSCS habitat suitability. Maps of the existing coverage of multibeam bathymetry (Figure 2.1) and the data quality maps associated with the hard-soft and hard-mixed-soft maps can be used to identify targets for mapping efforts. Similarly, the utility of the environmental predictor variables representing surficial sediment characteristics was limited by the available coverage of sediment grab samples. The uncertainty maps associated with these variables can be used to identify locations where additional samples would be most beneficial for improving the characterization of surficial sediments. Finally, the environmental predictor variables depicting measures of oceanography were all derived from remotely sensed data and/or models. These datasets may have insufficient resolution to depict the fine-scale patterns that may be helpful in predicting habitat suitability for DSCS. In this study, a smaller model domain limited to the SCB was considered for some taxa restricted to or more common in the SCB, as this would allow the bottom current variables to be derived from the higher-resolution UCLA ROMS. Ultimately, a single model domain was used in this study so that maps of predicted habitat suitability could be compared across all the DSCS taxa.

Although model performance was assessed using cross-validation, limited ground-truthing with independent data has been performed at this time. Spatial sampling bias, reflected here by the proportionately large number of records in Monterey Canyon, is a major challenge for presence-only models such as the models used in this study, which do not account for sampling effort in ways that other models do. As more data on absence or other measures of DSCS occurrence (e.g., abundance) are collected, future modeling efforts should incorporate these data into new approaches that account for sampling effort (Winship et al. 2020).

The maps presented in this chapter can be used to inform planning and management decisions in the study area by providing information about the locations of likely habitat for DSCS and by indicating locations where additional information needs to be collected. In addition to providing information to meet the needs of BOEM for renewable energy siting, it is hoped that outputs from this study will be used more broadly to inform marine resource management for the continental US West Coast, including fisheries management and future ocean exploration and research. The products presented here were not designed to replace but to help inform additional analyses required by law under NEPA and other environmental statutes. For more information about how these products may be used, please contact BOEM's Pacific OCS Region: http://www.boem.gov/Pacific-Region/.

Table 3.1. Datasets in the NOAA National Database for Deep-Sea Corals and Sponges, listed in order of the total number of DSCS occurrence records in each dataset found within the study area offshore of the continental US West Coast to 1,200 m depth.

Data Provider	Dataset ID	Principal Investigator(s)	Year(s)	Sample Type	Number of Records
MBARI	MBARI	Many	1989–2015	ROV	82,972
NOAA, SWFSC	NOAA_SWFSC_Submersible	M. Yoklavich; M. Love	1992–2011	Submersible	31,600
NOAA, SWFSC	NOAA_PU-11-08	M. Yoklavich	2014	Towed camera	14,504
NOAA, SWFSC	NOAA_M2-10-06-L3	M. Yoklavich	2010	ROV	13,156
NOAA, SWFSC	NOAA_VO-02-10	M. Yoklavich	2002	Submersible	11,914
NOAA, SWFSC	NOAA_VO-07-10	M. Yoklavich; R. Starr	2007	Submersible	8,069
NOAA, SWFSC	NOAA_VO-08-09	M. Yoklavich; R. Starr	2008	Submersible	6,089
NOAA, SWFSC	NOAA_VO-08-10	M. Yoklavich; R. Starr	2008	Submersible	5,563
NOAA, SWFSC	NOAA_RL-16-06	M. Yoklavich; M.E. Clarke	2016	AUV	5,126
NOAA, NWFSC	NOAA_NWFSC_Bottom_Trawl_Survey	Many	2001–2013	Trawl	5,090
NOAA, SWFSC	NOAA_VO-10-10	T. Laidig	2010	Submersible	4,650
NOAA, NWFSC	NOAA_PU-14-13	M.E. Clarke	2014	AUV	4,554
NOAA, SWFSC	NOAA_VO-07-09	M. Yoklavich; R. Starr	2007	Submersible	4,550
NOAA, NWFSC	NOAA_PS-10-01-L1	M.E. Clarke	2010	AUV	4,360
NOAA, SWFSC	NOAA_SW-12-08	S. Johnson; G. Cochrane; M. Yoklavich	2012	Towed camera	4,043
NOAA, SWFSC	NOAA_SWFSC_AST	K. Stierhoff; P. Etnoyer; J. Butler	2004–2011	ROV	3,989
NOAA, CINMS	NOAA-SH-15-03	P. Etnoyer	2015	ROV	3,365
Oceana; MARE	Oceana_SW_16-08	G. Shester	2016	ROV	3,149
NOAA, CBNMS	NOAA_M2-04-02	D. Roberts	2004	Towed camera	2,939
NOAA, SWFSC	NOAA_OL-11-12	J. Butler	2011	ROV	2,506
NOAA, AFSC	NOAA_AFSC_Bottom_Trawl_Survey	Many	1975–2004	Trawl	2,505
NOAA, SWFSC	NOAA_SW-11-08	S. Johnson; G. Cochrane; M. Yoklavich	2011	Towed camera	2,183
NOAA, SWFSC	OET_NA072	R. Embley; N. Raineault	2016	ROV	1,977
NOAA, CINMS	NOAA_SW-15-08	P. Etnoyer	2015	ROV	1,914
NOAA, SWFSC	NOAA_SW_10-07	S. Johnson; G. Cochrane; M. Yoklavich	2010	Towed camera	1,834
NOAA, SWFSC	NOAA_SW-09-08	S. Johnson; G. Cochrane; M. Yoklavich	2009	Towed camera	1,484
NOAA, GFNMS	NOAA_FM-12-10	P. Etnoyer	2012	ROV	1,281
NOAA, NWFSC	NOAA_M2-10-02	M. Yoklavich	2010	AUV	1,259
NOAA, CCMA	NOAA_SW-13-06	S. Katz	2013	ROV	1,209
NOAA, SWFSC	NOAA_SW-08-10	S. Johnson; G. Cochrane; M. Yoklavich	2008	Towed camera	1,121
NOAA, SWFSC	NOAA_SW-07-09	S. Johnson; G. Cochrane; M. Yoklavich	2007	Towed camera	972
NOAA, SWFSC	NOAA_SW-08-08	S. Johnson; G. Cochrane; M. Yoklavich	2008	Towed camera	782
NOAA, CBNMS	NOAA_FM-07-05	D. Roberts	2007	Towed camera	647
NOAA, SWFSC	NOAA_OL-05-04	J. Butler	2005	ROV	488

Table 3.1. Continued

Data Provider	Dataset ID	Principal Investigator(s)	Year(s)	Sample Type	Number of Records
NOAA, SWFSC	NOAA_SW-09-07	S. Johnson; G. Cochrane; M. Yoklavich	2009	Towed camera	462
NOAA, SWFSC	NOAA_SW-08-09	S. Johnson; G. Cochrane; M. Yoklavich	2008	Towed camera	448
NOAA, CBNMS	NOAA_VO-05-09	D. Howard	2005	Submersible	440
NOAA, CBNMS	NOAA_FM-14-09	D. Lipski	2014	ROV	406
CAS	CAS	Many	1890–2011	Dredge; Grab; Hook and line; ROV; SCUBA; Submersible; Trawl	391
NOAA, NWFSC	NOAA_NWFSC_FRAM	J. McVeigh	2007–2009	Trawl	346
Smithsonian Institution, NMNH	NMNH_IZ	Many	1888–2010	Dredge; Net; ROV; Submersible; Trawl	299
NOAA, SWFSC	NOAA_OL-05-06	J. Butler	2005	ROV	273
NOAA, SWFSC	NOAA_OL-11-09	J. Butler	2011	ROV	264
NOAA, CBNMS	NOAA_VO-01-09	D. Howard	2001	Submersible	261
NOAA, SWFSC	NOAA_OL-05-01	J. Butler	2005	ROV	260
NOAA, CCMA	NOAA_SW-16-08	P. Etnoyer	2016	ROV	255
NOAA, CBNMS	NOAA_VO-03-09	D. Howard	2003	Submersible	245
NOAA, SWFSC	NOAA_OL-05-02	J. Butler	2005	ROV	238
NOAA, SWFSC	NOAA_OL-04-10	J. Butler	2004	ROV	224
NOAA, CBNMS	NOAA_M2-10-06-L2	D. Howard	2010	ROV	195
NOAA, SWFSC	NOAA_OL-05-03	J. Butler	2005	ROV	174
NOAA, SWFSC	NOAA_OL-05-11	J. Butler	2005	ROV	154
MCZ, Harvard University	MCZ_IZ	NA	1888–2017	Dredge; ROV	153
NOAA, SWFSC	NOAA_OL-07-08	J. Butler	2007	ROV	149
NOAA, SWFSC	NAA_DS-11-10	J. Butler	2011	ROV	145
NOAA, CBNMS	NOAA_VO-02-09	D. Howard	2002	Submersible	126
NOAA, SWFSC	NOAA_OL-06-05	J. Butler	2006	ROV	124
NOAA, SWFSC	NOAA_OL-07-12	J. Butler	2007	ROV	120
NOAA, OER	NOAA_EX-11-02	K. Elliott	2011	ROV	117
NOAA, SWFSC	NOAA_OL-07-10	J. Butler	2007	ROV	112
NOAA, SWFSC	NOAA_OL-03-11	J. Butler	2003	ROV	100
OBIS	OBIS	S. Clark; NA	1999–2009	Grab; NA	94
SBMNH	SBMNH	Many	1938–2010	Dredge; Multiple gears; Net; Submersible; Trawl; Other	88
Oceana	Oceana_ML-11-06	B. Enticknap	2011	ROV	80
NOAA, CINMS	NOAA_SH-10-11	J. Butler	2010	ROV	63
NOAA, NWFSC	NOAA_FM-11-01	D. Howard	2011	AUV	59
NOAA, SWFSC	NOAA_OL-06-02	J. Butler	2006	ROV	56

Table 3.1. Continued

Data Provider	Dataset ID	Principal Investigator(s)	Year(s)	Sample Type	Number of Records
NOAA, SWFSC	NOAA_OL-10-10	J. Butler	2010	ROV	52
WSU	Pirtle_J_2002	B. Tissot; D. Roberts	2002	Submersible	51
NOAA, CBNMS	NOAA_VO-04-08	D. Howard	2004	Submersible	43
NOAA, SWFSC	NOAA_DS-04-10	J. Butler	2004	ROV	39
NOAA, SWFSC	NOAA_OL-08-04	J. Butler	2008	ROV	38
NOAA, SWFSC	NOAA_OL-04-09	J. Butler	2004	ROV	37
Oceana	Oceana	G. Shester	2010	ROV	36
WSU	Bianchi_C_2001	B. Tissot; W. Wakefield; C. Goldfinger; B. Embley	2001	ROV	33
NOAA, SWFSC	NOAA_OL-08-02	J. Butler	2007	ROV	30
NOAA, SWFSC	NOAA_OL-08-03	J. Butler	2008	ROV	30
NOAA, SWFSC	NOAA_OL-04-03	J. Butler	2004	ROV	29
NOAA, SWFSC	NOAA_OL-11-04	J. Butler	2007-2011	ROV	28
NOAA, SWFSC	NOAA_OL-08-06	J. Butler	2008	ROV	21
NOAA, SWFSC	NOAA_OL-10-11	J. Butler	2010	ROV	11
Hexacorallians of the World; OBIS	Hexacoral	NA	NA	NA	8
NOAA, SWFSC	NOAA_OL-07-01	J. Butler	2006-2007	ROV	7
NOAA, SWFSC	NOAA_OL-08-10	J. Butler	2008	ROV	7
Daniel Wagner	Wagner_D_2011	Many	NA	NA	7
NOAA, CCMA	NOAA_NBI	NA	2006	Grab	6
NOAA, NWFSC	NOAA_TN174	M.E. Clarke; W. Wakefield	2004	ROV	1

AFSC–Alaska Fisheries Science Center
CAS–California Academy of Sciences
CBNMS–Cordell Bank National Marine Sanctuary
CCMA–Center for Coastal Monitoring and Assessment (now Marine Spatial Ecology Division)
CINMS–Channel Islands National Marine Sanctuary
GFNMS–Greater Farallones National Marine Sanctuary
MARE–Marine Applied Research and Exploration
MBARI–Monterey Bay Aquarium Research Institute
MCZ–Museum of Comparative Zoology
NMNH–National Museum of Natural History
NWFSC–Northwest Fisheries Science Center
OBIS– Ocean Biodiversity Information System
OER–Office of Ocean Exploration
SBMNH–Santa Barbara Museum of Natural History
SWFSC–Southwest Fisheries Science Center
WSU–Washington State University

Table 3.2. Subset of environmental predictor variables used to fit models of DSCS occurrence, selected following pairwise correlation analysis.

Environmental Predictor Variable	Category
East-West Aspect	Depth and Seafloor Topography
North-South Aspect	Depth and Seafloor Topography
Depth	Depth and Seafloor Topography
General Curvature	Depth and Seafloor Topography
Cross-Sectional Curvature	Depth and Seafloor Topography
Slope	Depth and Seafloor Topography
Hard-Soft	Seafloor Substrate
Percent Gravel	Seafloor Substrate
Percent Sand	Seafloor Substrate
Spring/Summer East-West Bottom Current Velocity	Oceanography
Winter East-West Bottom Current Velocity	Oceanography
Spring/Summer North-South Bottom Current Velocity	Oceanography
Winter North-South Bottom Current Velocity	Oceanography
Fall Vertical Bottom Current Velocity	Oceanography
Spring/Summer Vertical Bottom Current Velocity	Oceanography
Winter Vertical Bottom Current Velocity	Oceanography
Spring/Summer Surface Reflectance	Oceanography
Winter Surface Reflectance	Oceanography
Annual Max Wave Power	Oceanography
Spring/Summer Mean Wave Power	Oceanography
Distance to Shore	Geography
Latitude	Geography

Table 3.3. Deep-sea coral taxa (n = 31) selected for modeling. * denotes used for aggregated predictions in Section 3.3.2.

Taxon	Category	Class	Order	Family	Number of Occurrences	Number of Grid Cells with Occurrences
*Acanthogorgia**	Gorgonian Corals	Anthozoa	Alcyonacea	Acanthogorgiidae	1,469	105
Acanthoptilum gracile	Sea Pens	Anthozoa	Pennatulacea	Virgulariidae	242	155
*Adelogorgia phyllosclera**	Gorgonian Corals	Anthozoa	Alcyonacea	Gorgoniidae	4,130	194
Anthoptilum grandiflorum	Sea Pens	Anthozoa	Pennatulacea	Anthoptilidae	1,509	868
*Antipathes dendrochristos**	Black Corals	Anthozoa	Antipatharia	Antipathidae	2,532	237
*Bathypathes**	Black Corals	Anthozoa	Antipatharia	Schizopathidae	74	68
*Chromoplexaura marki**	Gorgonian Corals	Anthozoa	Alcyonacea	Plexauridae	226	70
*Chrysopathes speciosa**	Black Corals	Anthozoa	Antipatharia	Cladopathidae	70	67
*Clavularia**	Soft Corals	Anthozoa	Alcyonacea	Clavulariidae	264	98
*Coenocyathus bowersi**	Stony Corals	Anthozoa	Scleractinia	Caryophylliidae	363	124
*Desmophyllum dianthus**	Stony Corals	Anthozoa	Scleractinia	Caryophylliidae	651	183
*Eugorgia rubens**	Gorgonian Corals	Anthozoa	Alcyonacea	Gorgoniidae	2,103	296
Funiculina	Sea Pens	Anthozoa	Pennatulacea	Funiculinidae	10,895	346
Halipteris californica	Sea Pens	Anthozoa	Pennatulacea	Halipteridae	3,951	393
*Heteropolypus ritteri**	Soft Corals	Anthozoa	Alcyonacea	Alcyoniidae	13,040	1,107
*Isidella tentaculum**	Gorgonian Corals	Anthozoa	Alcyonacea	Isididae	433	84
*Leptogorgia chilensis**	Gorgonian Corals	Anthozoa	Alcyonacea	Gorgoniidae	2,242	211
*Lophelia pertusa**	Stony Corals	Anthozoa	Scleractinia	Caryophylliidae	851	146
*Paracyathus**	Stony Corals	Anthozoa	Scleractinia	Caryophylliidae	106	50
*Paragorgia**	Gorgonian Corals	Anthozoa	Alcyonacea	Paragorgiidae	5,757	486
*Parastenella ramosa**	Gorgonian Corals	Anthozoa	Alcyonacea	Primnoidae	614	77
Pennatula phosphorea	Sea Pens	Anthozoa	Pennatulacea	Pennatulidae	1,035	103
*Plumarella longispina**	Gorgonian Corals	Anthozoa	Alcyonacea	Primnoidae	2,942	207
Ptilosarcus gurneyi	Sea Pens	Anthozoa	Pennatulacea	Pennatulidae	667	380
*Stylaster californicus**	Stylasterid Corals	Hydrozoa	Anthoathecata	Stylasteridae	1,219	178
Stylatula	Sea Pens	Anthozoa	Pennatulacea	Virgulariidae	772	452
*Swiftia kofoidi**	Gorgonian Corals	Anthozoa	Alcyonacea	Plexauridae	1,205	142
*Swiftia pacifica**	Gorgonian Corals	Anthozoa	Alcyonacea	Plexauridae	3,716	115
*Swiftia simplex**	Gorgonian Corals	Anthozoa	Alcyonacea	Plexauridae	1,659	186
Umbellula lindahli	Sea Pens	Anthozoa	Pennatulacea	Umbellulidae	7,730	585
Virgularia	Sea Pens	Anthozoa	Pennatulacea	Virgulariidae	95	70

Table 3.4. Sponge taxa (n = 15) selected for modeling.

Taxon	Category	Class	Order	Family	Number of Occurrences	Number of Grid Cells with Occurrences
Aphrocallistes vastus	Glass Sponges	Hexactinellida	Sceptrulophora	Aphrocallistidae	739	384
Asbestopluma	Demosponges	Demospongiae	Poecilosclerida	Cladorhizidae	2,588	386
Craniella arb	Demosponges	Demospongiae	Tetractinellida	Tetillidae	101	80
Demospongiae	Demosponges	Demospongiae	NA	NA	12,446	1245
Farrea occa	Glass Sponges	Hexactinellida	Sceptrulophora	Farreidae	844	176
Haliclona	Demosponges	Demospongiae	Haplosclerida	Chalinidae	615	102
Heterochone calyx	Glass Sponges	Hexactinellida	Sceptrulophora	Aphrocallistidae	1,556	217
Hexactinellida	Glass Sponges	Hexactinellida	NA	NA	8,193	1975
Hyalonema	Glass Sponges	Hexactinellida	Amphidiscosida	Hyalonematidae	331	235
Mycale	Demosponges	Demospongiae	Poecilosclerida	Mycalidae	3,173	165
Polymastia	Demosponges	Demospongiae	Polymastiida	Polymastiidae	465	93
Rhabdocalyptus dawsoni	Glass Sponges	Hexactinellida	Lyssacinosida	Rossellidae	643	209
Rhizaxinella gadus	Demosponges	Demospongiae	Suberitida	Suberitidae	242	57
Staurocalyptus	Glass Sponges	Hexactinellida	Lyssacinosida	Rossellidae	705	165
Thenea	Demosponges	Demospongiae	Tetractinellida	Theneidae	1,363	184

Table 3.5. Metrics used to evaluate model performance.

Metric	Description	Categories
Training AUC	AUC calculated for a model fit to the full set of occurrence records.	H: ≥ 0.90 M: 0.70 - 0.90 L: < 0.70
Cross-validation Mean AUC	The mean AUC calculated across the ten cross-validation folds. During cross-validation, the AUC for each cross-validation fold was calculated by using it to test the performance of a model fit using the data in the nine other folds.	H: ≥ 0.90 M: 0.70 - 0.90 L: < 0.70
Model Fit	The percentage of grid cells containing occurrence records that were predicted to be in the high habitat suitability class.	H: > 86% M: 64 - 86% L: < 64%
Model Stability	The percentage of grid cells predicted in the high habitat suitability class that were also predicted to be in the robust high class.	H: > 36% M: 11 - 36% L: < 11%

H = High, M = Medium, L = Low

Table 3.6. Measures of model performance for deep-sea coral taxa.

Taxon	Training AUC	Cross-validation Mean AUC	Model Fit	Model Stability
Acanthogorgia	0.98	0.90	81.69	9.38
Acanthoptilum gracile	0.90	0.88	13.22	30.74
Adelogorgia phyllosclera	0.99	0.96	94.62	33.55
Anthoptilum grandiflorum	0.91	0.89	67.33	59.39
Antipathes dendrochristos	0.99	0.95	96.13	21.29
Bathypathes	0.93	0.92	1.35	0.09
Chromoplexaura marki	0.89	0.78	37.61	0.00
Chrysopathes speciose	0.97	0.95	30.00	8.41
Clavularia	0.99	0.92	77.27	19.67
Coenocyathus bowersi	0.98	0.96	69.42	19.34
Desmophyllum dianthus	0.98	0.92	83.87	20.99
Eugorgia rubens	0.98	0.96	78.46	46.31
Funiculina	0.97	0.93	95.87	31.54
Halipteris californica	0.92	0.84	76.34	30.53
Heteropolypus ritteri	0.93	0.90	94.71	36.58
Isidella tentaculum	0.96	0.91	39.26	4.94
Leptogorgia chilensis	0.96	0.91	18.69	44.17
Lophelia pertusa	0.97	0.94	67.10	5.60
Paracyathus	0.92	0.82	0.00	0.00
Paragorgia	0.94	0.87	91.49	23.14
Parastenella ramosa	0.99	0.93	80.62	11.87
Pennatula phosphorea	0.98	0.89	88.02	11.84
Plumarella longispina	0.97	0.91	75.63	20.58
Ptilosarcus gurneyi	0.93	0.87	65.37	40.29
Stylaster californicus	0.98	0.95	86.22	17.74
Stylatula	0.85	0.80	25.00	39.04
Swiftia kofoidi	0.95	0.80	76.02	9.05
Swiftia pacifica	0.96	0.83	85.17	15.62
Swiftia simplex	0.93	0.84	31.46	15.03
Umbellula lindahli	0.98	0.95	98.03	42.06
Virgularia	0.76	0.65	0.00	0.00

Table 3.7. Measures of model performance for sponge taxa.

Taxon	Training AUC	Cross-validation Mean AUC	Model Fit	Model Stability
Aphrocallistes vastus	0.95	0.91	80.24	37.87
Asbestopluma	0.95	0.89	78.59	25.02
Craniella arb	0.98	0.97	50.50	8.66
Demospongiae	0.87	0.81	90.07	43.41
Farrea occa	0.98	0.91	86.26	36.58
Haliclona	0.98	0.93	63.90	9.58
Heterochone calyx	0.97	0.80	83.55	13.07
Hexactinellida	0.87	0.82	86.46	61.38
Hyalonema	0.98	0.97	89.12	38.52
Mycale	0.97	0.84	95.05	22.42
Polymastia	0.98	0.86	80.00	19.39
Rhabdocalyptus dawsoni	0.97	0.90	66.10	20.24
Rhizaxinella gadus	0.99	0.94	76.86	17.02
Staurocalyptus	0.96	0.84	64.54	10.99
Thenea	0.98	0.91	92.66	37.60

Table 3.8. Sample size (number of model grid cells with ≥1 image) by predicted habitat suitability class for each taxon included in the example model validation exercise. There were a total of 220 grid cells with images from AUV surveys.

Taxon	Predicted habitat suitability class									
	Very low					Low	Med	High		
	1	2	3	4	5	6	7	8	9	10
Demospongiae	0	0	12	20	38	81	44	25	0	0
Hexactinellida	0	0	8	9	20	6	56	79	33	9
Paragorgia	89	15	69	14	23	1	2	5	2	0
Swiftia pacifica	24	49	52	69	17	0	9	0	0	0

Table 3.9. Results of statistical analyses of the relationship between taxon occurrence and predicted habitat suitability (MaxEnt 'raw' predictions) from the example model validation exercise.

Taxon	*r*	GLM	
		PDE	*p*
Demospongiae	0.2	9	<0.01
Hexactinellida	0.3	1	0.135
Paragorgia	0.4	0	0.894
Swiftia pacifica	0.1	5	<0.01

Spearman rank correlation coefficient (*r*) between proportion of images where taxa were present and predicted habitat suitability and quasi-Poisson generalized linear model (GLM) of number of images where taxa were present as function of predicted habitat suitability. For the GLM, the percent deviance explained (PDE) by the model and the *p*-value of the positive effect of predicted habitat suitability are presented.

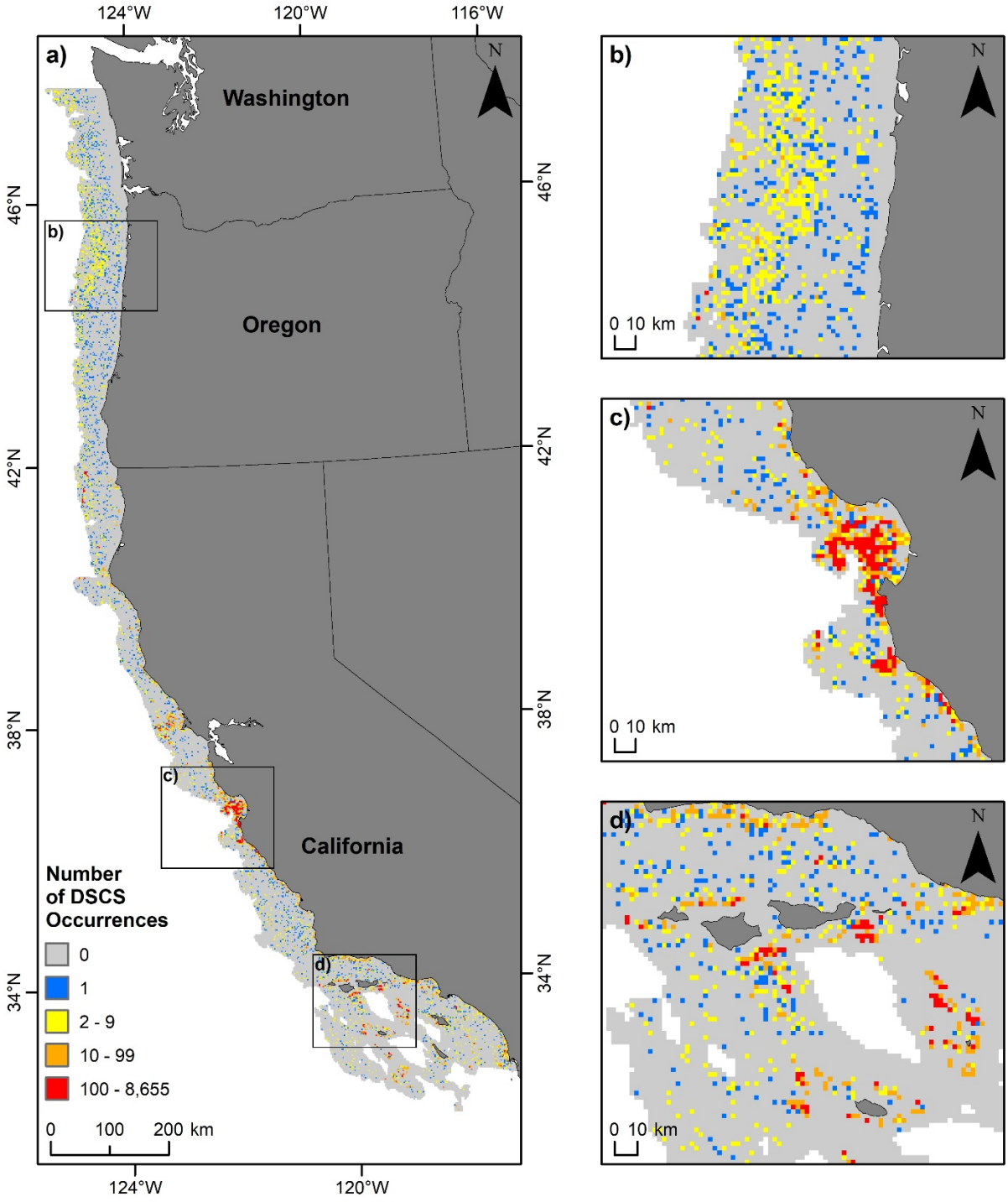

Figure 3.1. Density of DSCS occurrences in the NOAA National Database for Deep-Sea Corals and Sponges, calculated as the number of occurrences in 2 x 2 km grid cells, for a) the entire study area offshore of the continental US West Coast to 1,200 m depth, b) offshore of northern Oregon, c) near Monterey Bay, and d) part of the Southern California Bight.

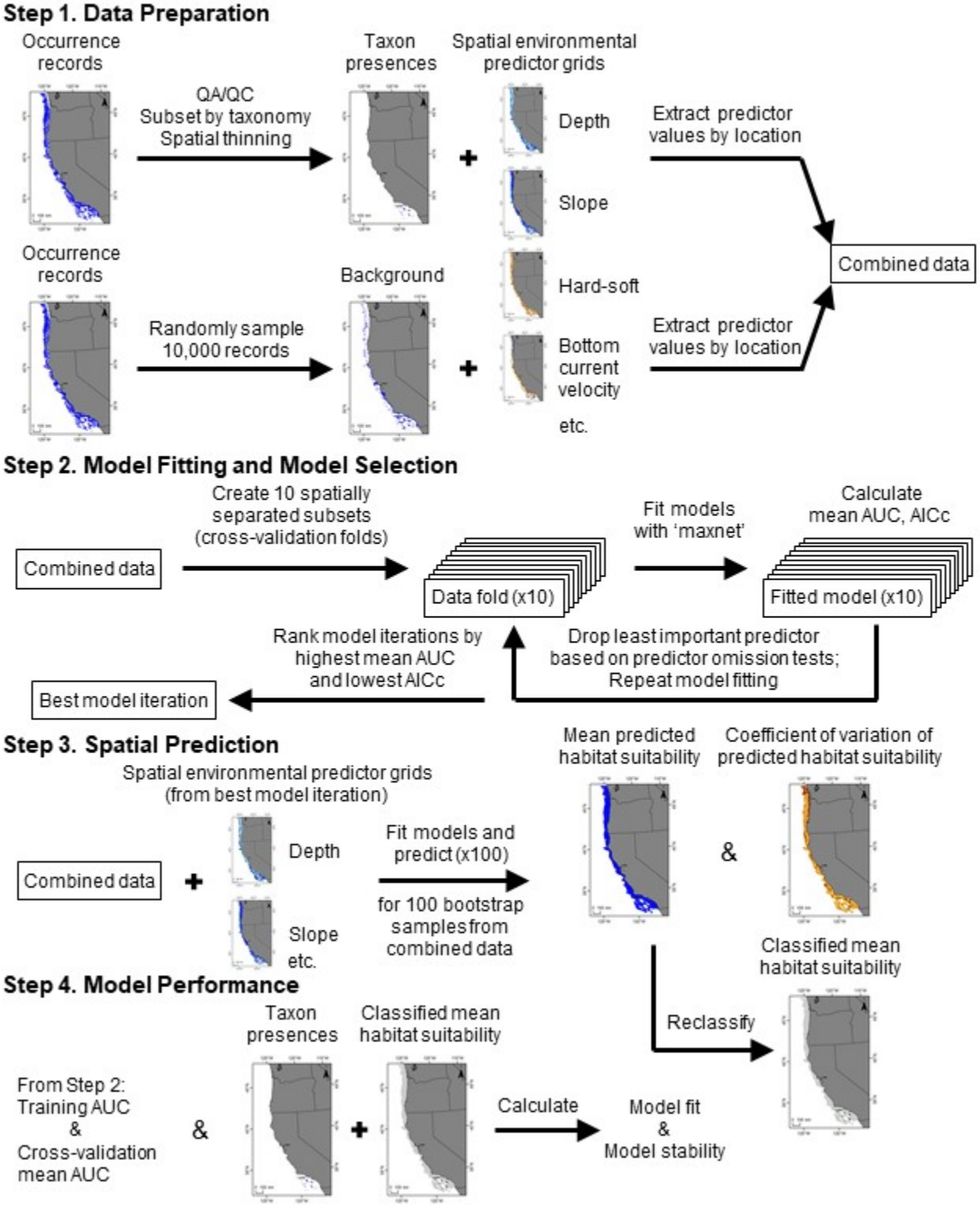

Figure 3.2. Maximum entropy modeling framework, including data preparation, model fitting and model selection, spatial prediction, and evaluation of model performance.

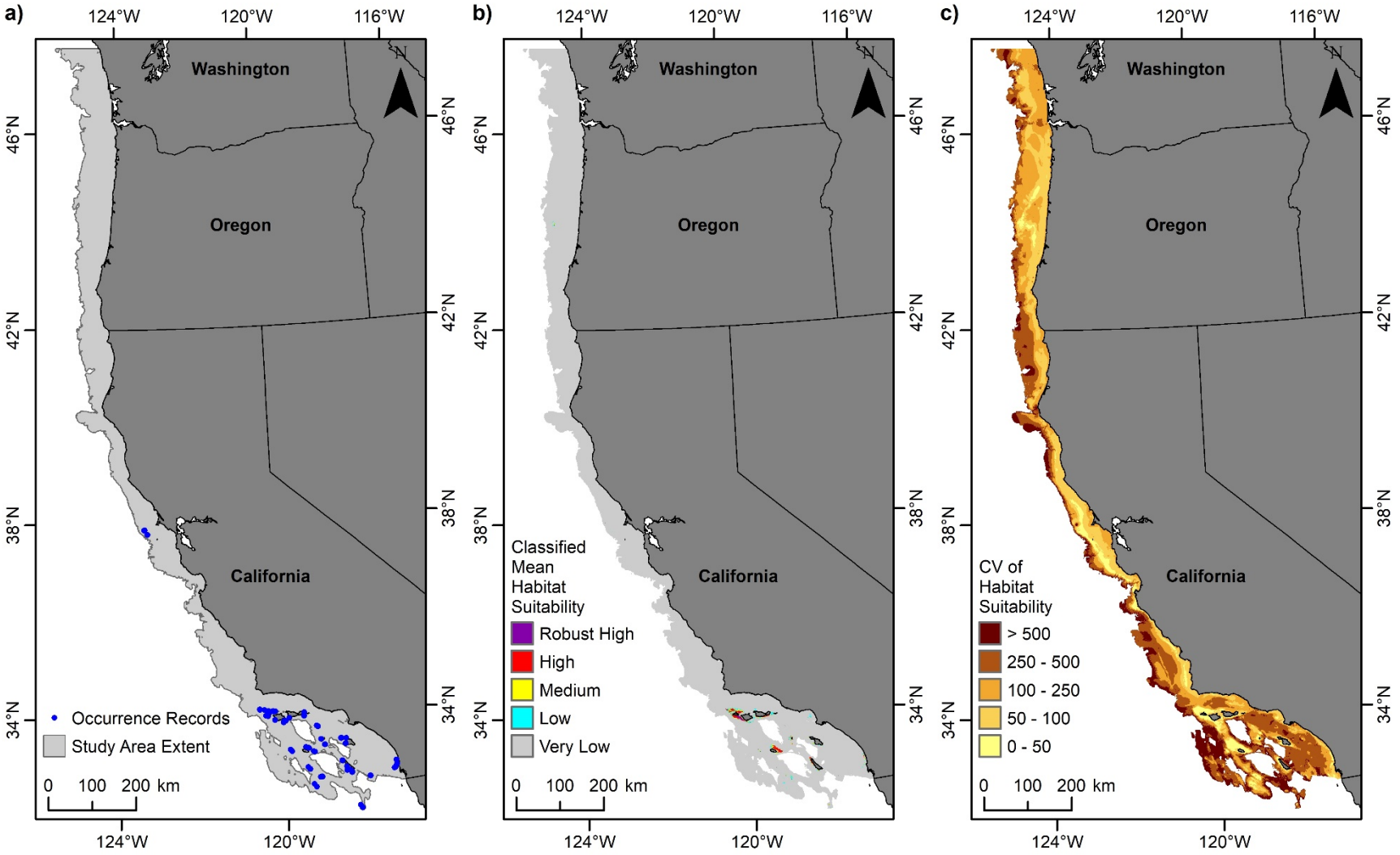

Figure 3.3. Predicted habitat suitability for the stony coral *Coenocyathus bowersi* (Scleractinia, Caryophylliidae).
(a) Records of *C. bowersi* occurrence from the NOAA National Database for Deep-Sea Corals and Sponges within the study area offshore to 1,200 m depth; (b) classified mean habitat suitability for *C. bowersi*; and (c) coefficient of variation of the mean habitat suitability for *C. bowersi*.

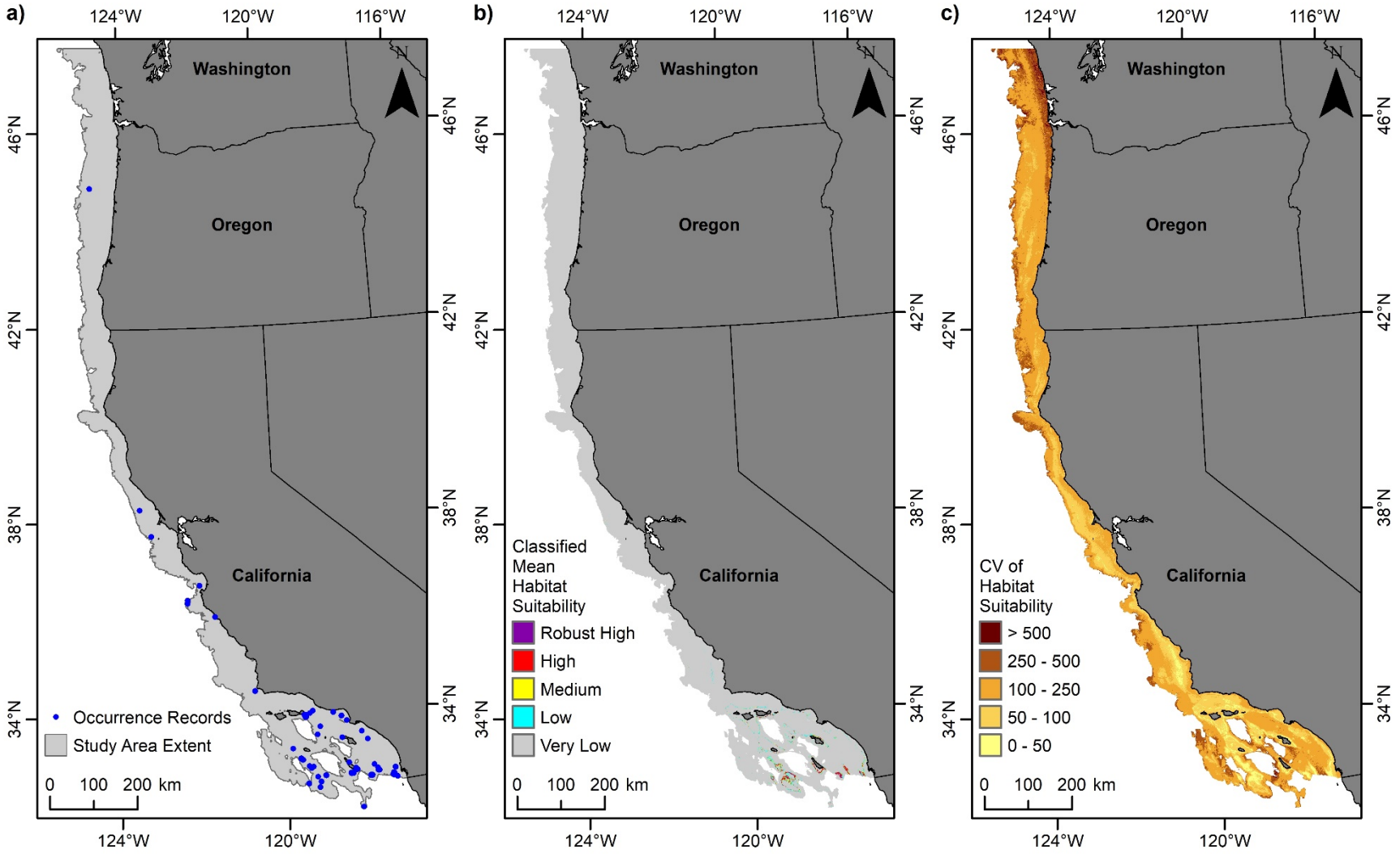

Figure 3.4. Predicted habitat suitability for the stony coral *Desmophyllum dianthus* (Scleractinia, Caryophylliidae).
(a) Records of *D. dianthus* occurrence from the NOAA National Database for Deep-Sea Corals and Sponges within the study area offshore to 1,200 m depth; (b) classified mean habitat suitability for *D. dianthus*; and (c) coefficient of variation of the mean habitat suitability for *D. dianthus*.

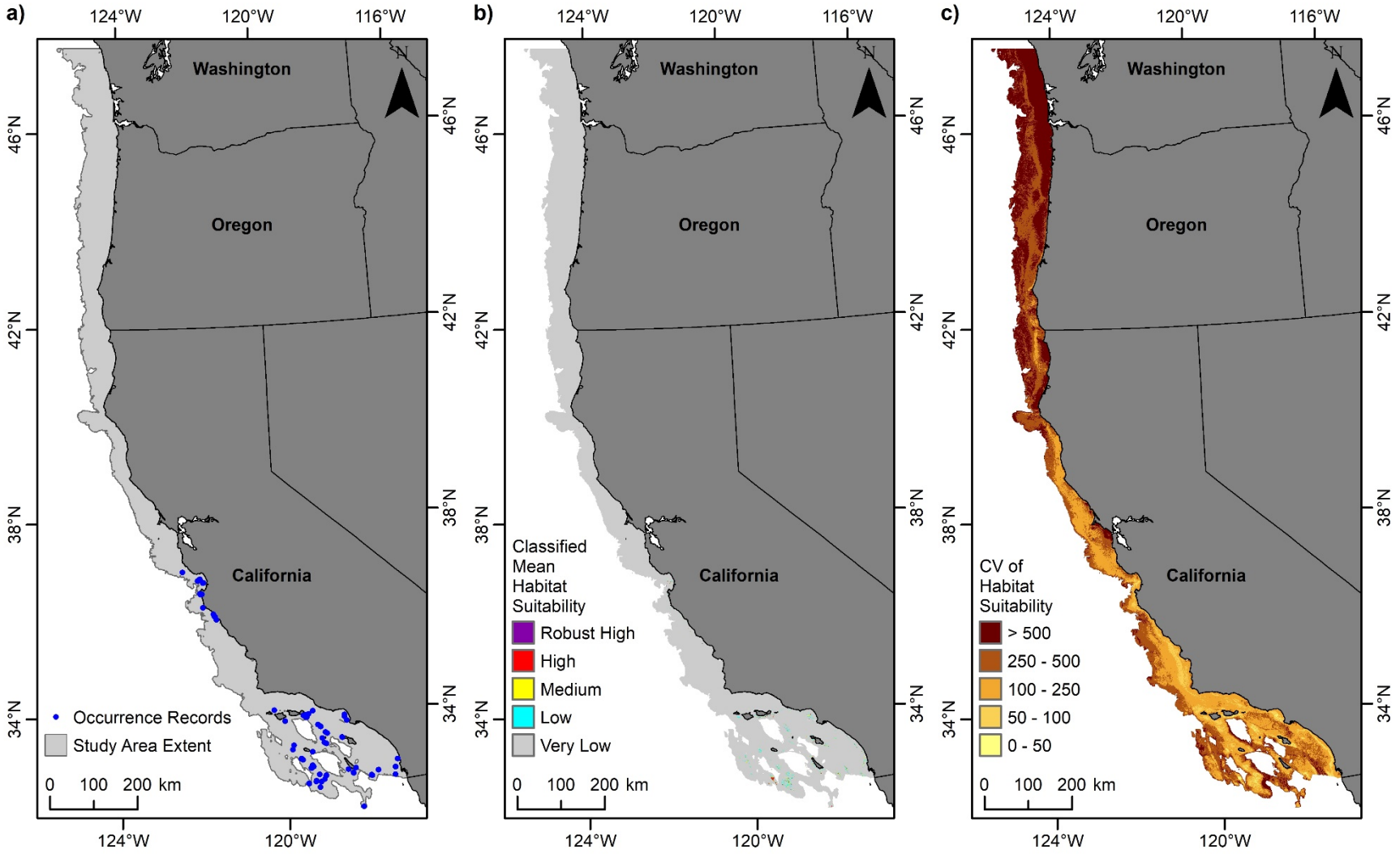

Figure 3.5. Predicted habitat suitability for the stony coral *Lophelia pertusa* (Scleractinia, Caryophylliidae).
(a) Records of *L. pertusa* occurrence from the NOAA National Database for Deep-Sea Corals and Sponges within the study area offshore to 1,200 m depth; (b) classified mean habitat suitability for *L. pertusa*; and (c) coefficient of variation of the mean habitat suitability for *L. pertusa*.

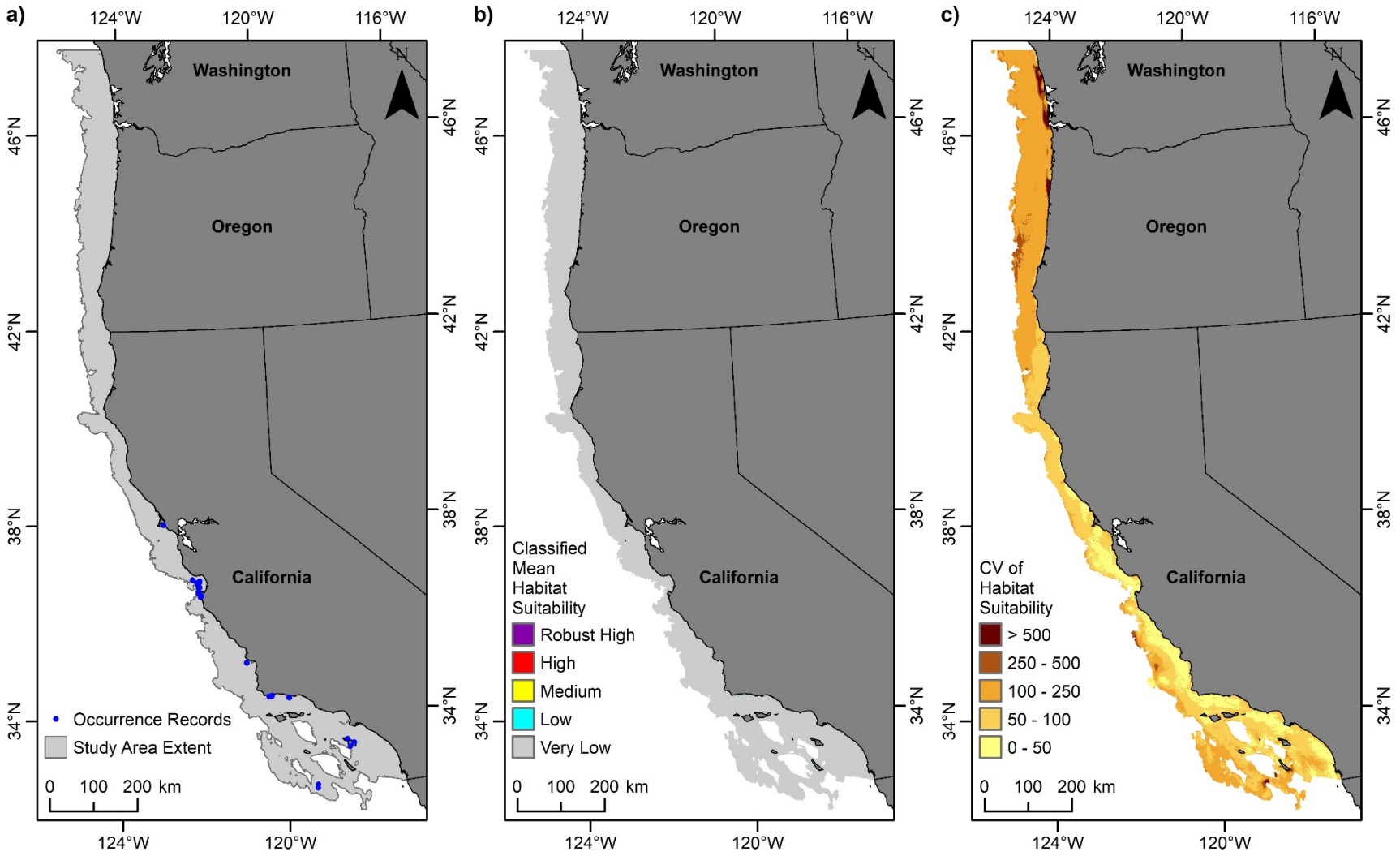

Figure 3.6. Predicted habitat suitability for the stony coral *Paracyathus* (Scleractinia, Caryophylliidae).
(a) Records of *Paracyathus* occurrence from the NOAA National Database for Deep-Sea Corals and Sponges within the study area offshore to 1,200 m depth; (b) classified mean habitat suitability for *Paracyathus*; and (c) coefficient of variation of the mean habitat suitability for *Paracyathus*.

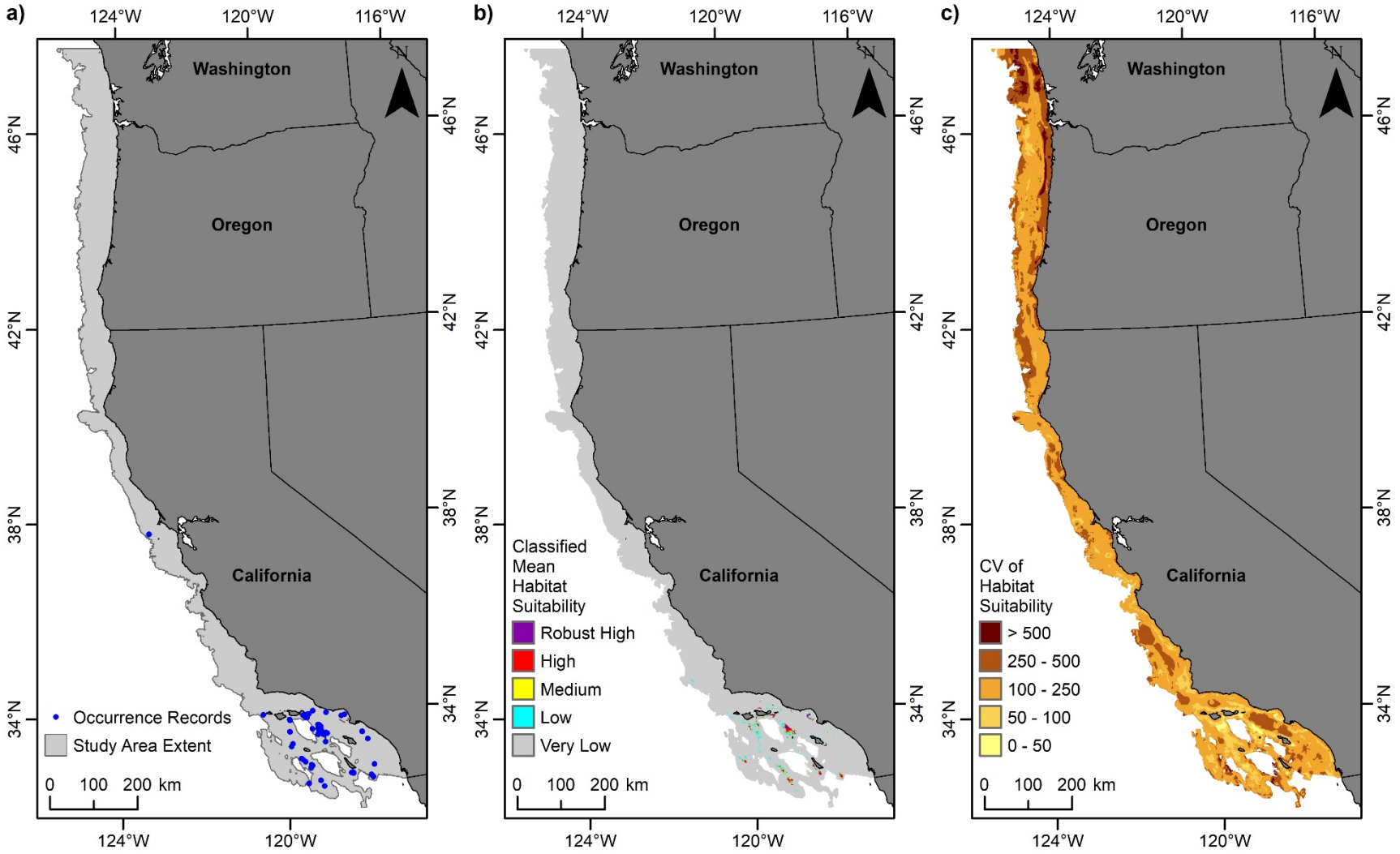

Figure 3.7. Predicted habitat suitability for the black coral *Antipathes dendrochristos* (Antipatharia, Antipathidae).
(a) Records of *A. dendrochristos* occurrence from the NOAA National Database for Deep-Sea Corals and Sponges within the study area offshore to 1,200 m depth; (b) classified mean habitat suitability for *A. dendrochristos*; and (c) coefficient of variation of the mean habitat suitability for *A. dendrochristos*.

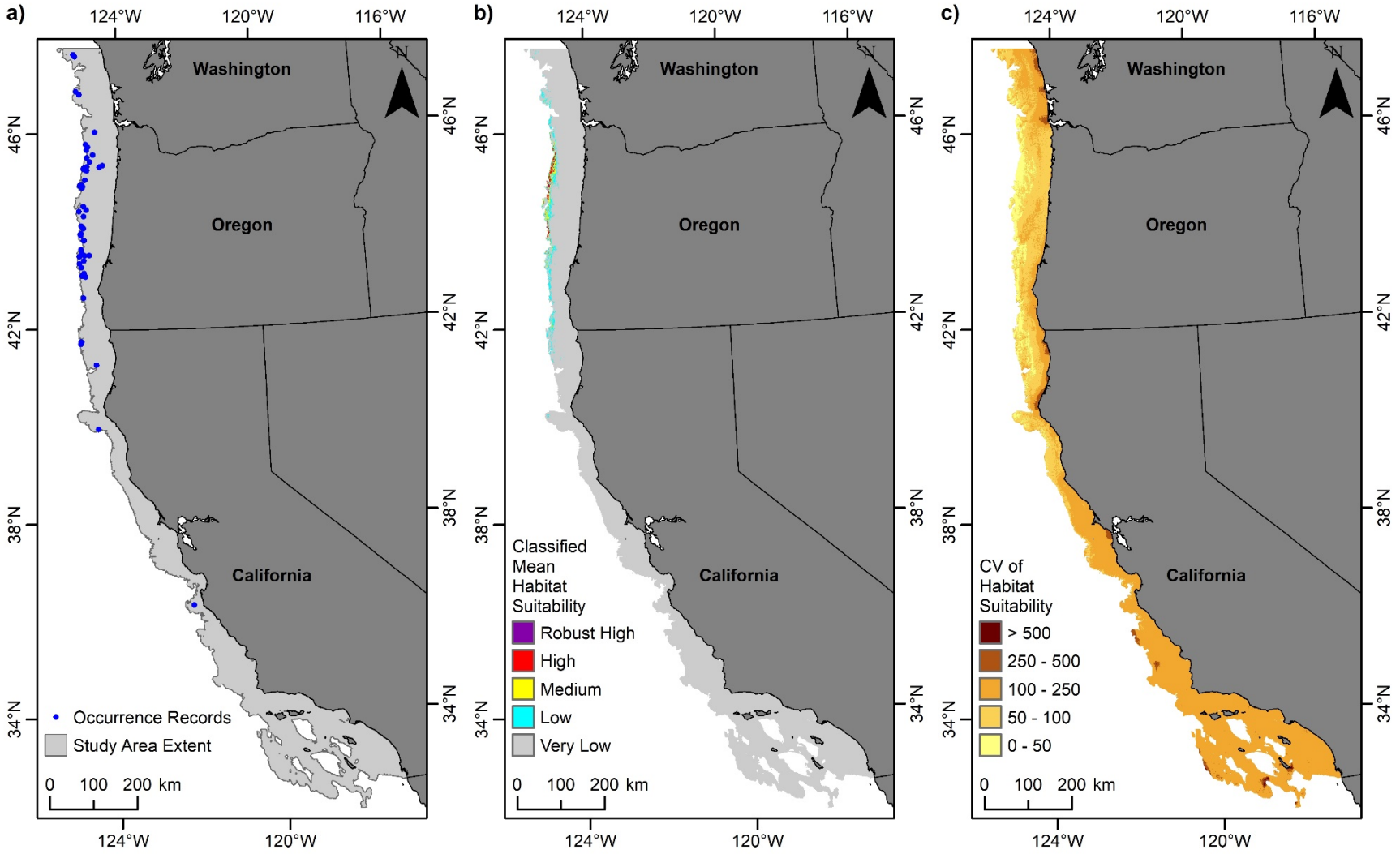

Figure 3.8. Predicted habitat suitability for the black coral *Chrysopathes speciosa* (Antipatharia, Cladopathidae).
(a) Records of *C. speciosa* occurrence from the NOAA National Database for Deep-Sea Corals and Sponges within the study area offshore to 1,200 m depth; (b) classified mean habitat suitability for *C. speciosa*; and (c) coefficient of variation of the mean habitat suitability for *C. speciosa*.

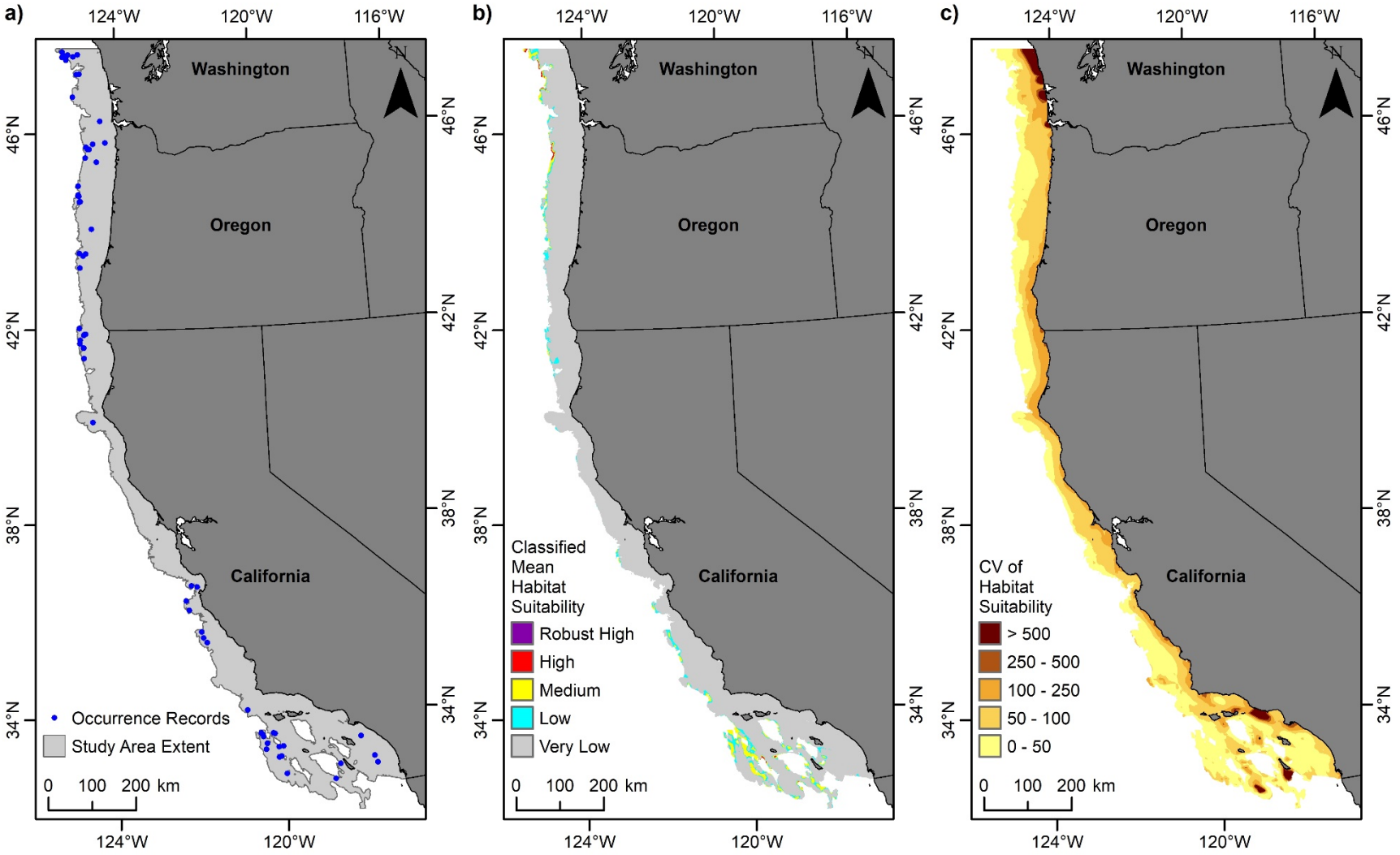

Figure 3.9. Predicted habitat suitability for the black coral *Bathypathes* (Antipatharia, Schizopathidae).
(a) Records of *Bathypathes* occurrence from the NOAA National Database for Deep-Sea Corals and Sponges within the study area offshore to 1,200 m depth; (b) classified mean habitat suitability for *Bathypathes*; and (c) coefficient of variation of the mean habitat suitability for *Bathypathes*.

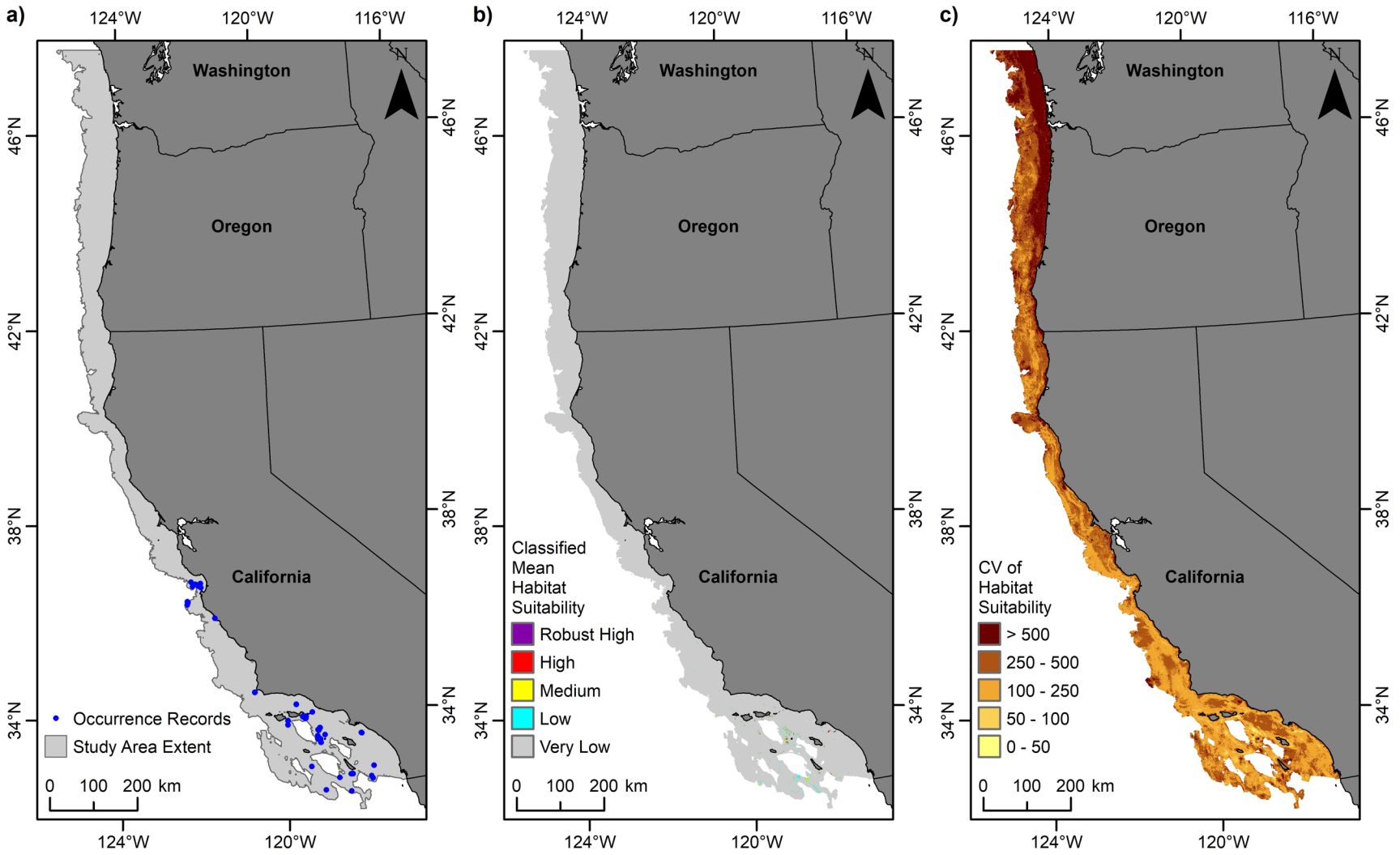

Figure 3.10. Predicted habitat suitability for the gorgonian coral *Acanthogorgia* (Alcyonacea, Acanthogorgiidae).
(a) Records of *Acanthogorgia* occurrence from the NOAA National Database for Deep-Sea Corals and Sponges within the study area offshore to 1,200 m depth; (b) classified mean habitat suitability for *Acanthogorgia*; and (c) coefficient of variation of the mean habitat suitability for *Acanthogorgia*.

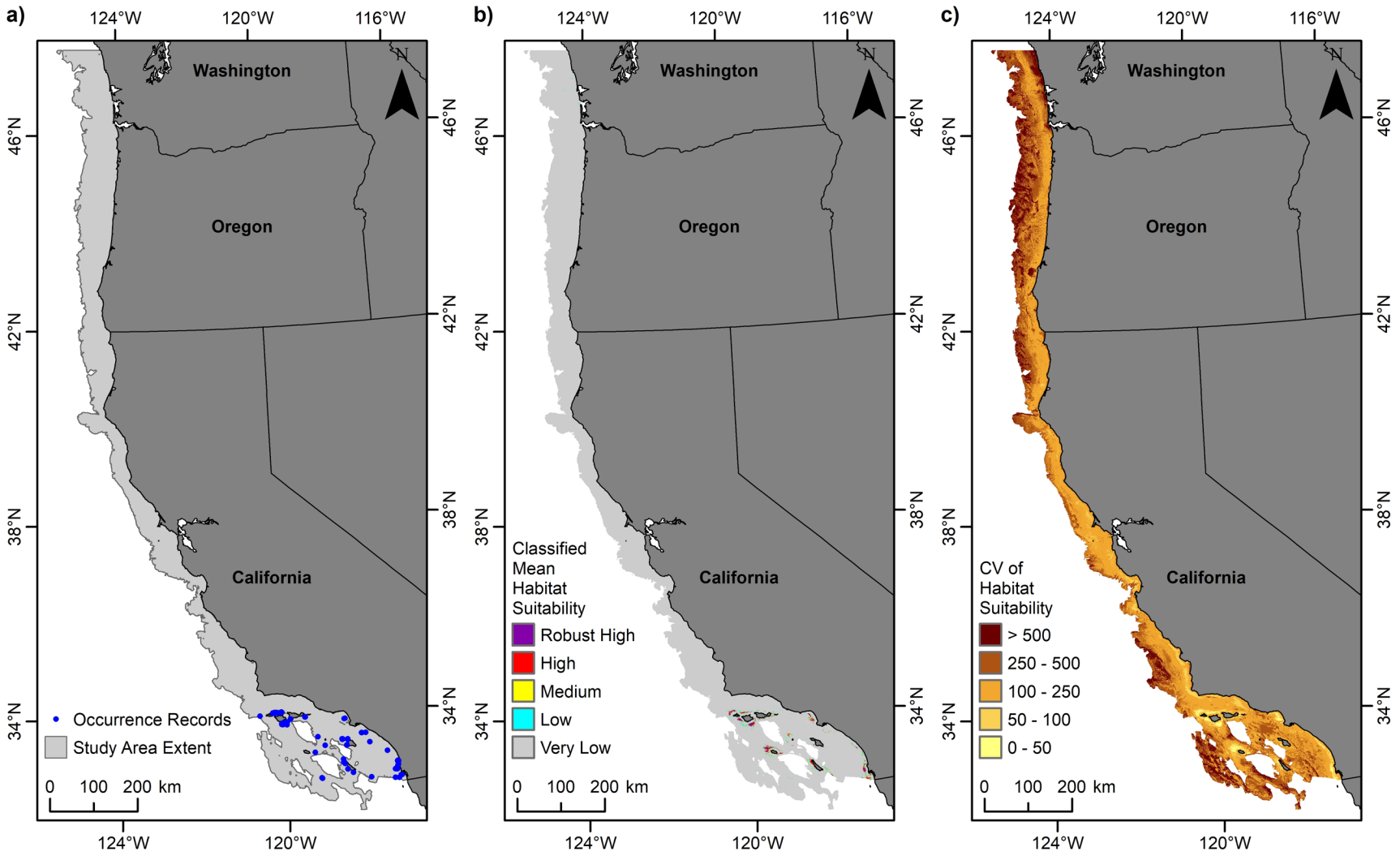

Figure 3.11. Predicted habitat suitability for the gorgonian coral *Adelogorgia phyllosclera* (Alcyonacea, Gorgoniidae).
(a) Records of *A. phyllosclera* occurrence from the NOAA National Database for Deep-Sea Corals and Sponges within the study area offshore to 1,200 m depth; (b) classified mean habitat suitability for *A. phyllosclera*; and (c) coefficient of variation of the mean habitat suitability for *A. phyllosclera*.

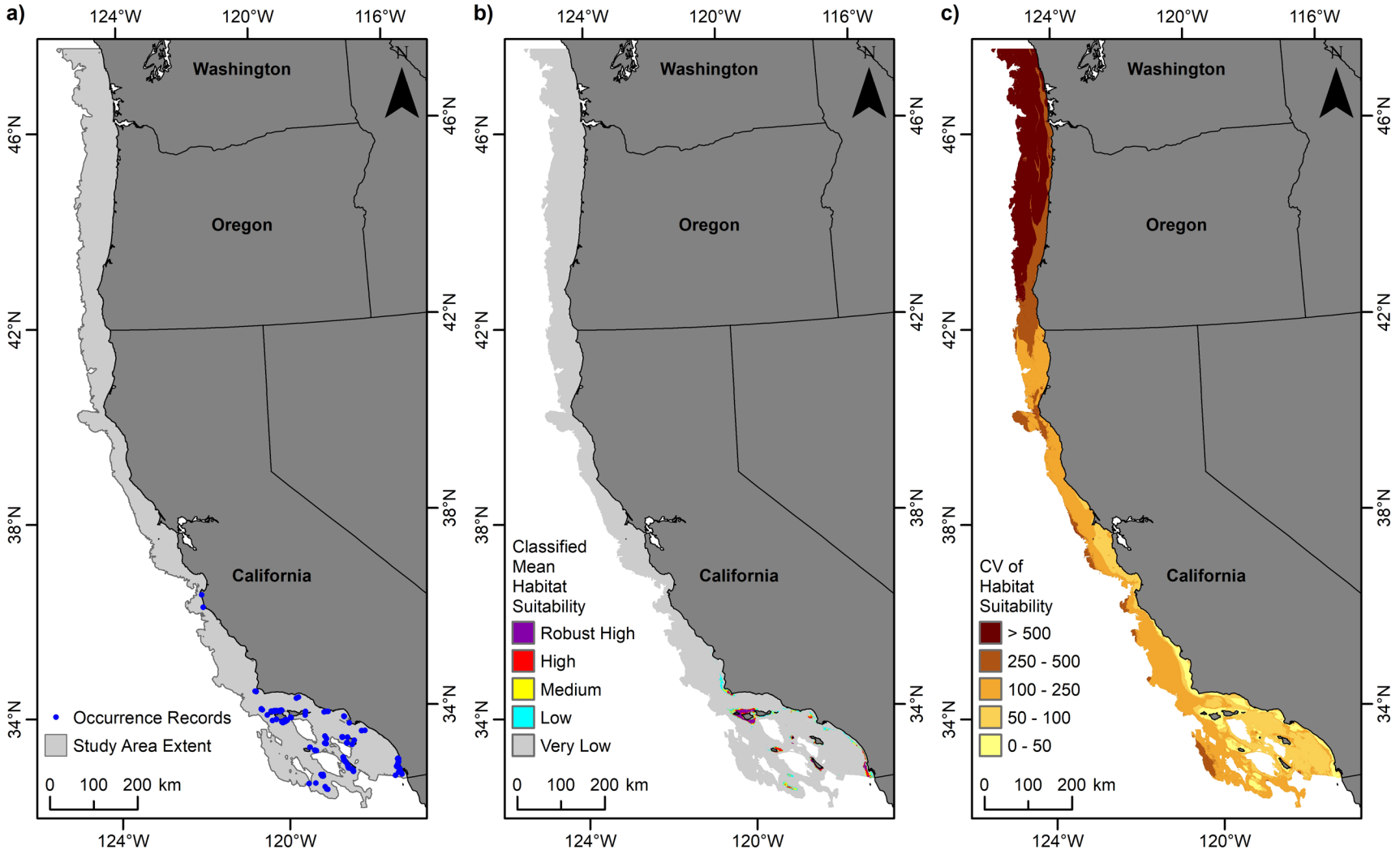

Figure 3.12. Predicted habitat suitability for the gorgonian coral *Eugorgia rubens* (Alcyonacea, Gorgoniidae).
(a) Records of *E. rubens* occurrence from the NOAA National Database for Deep-Sea Corals and Sponges within the study area offshore to 1,200 m depth; (b) classified mean habitat suitability for *E. rubens*; and (c) coefficient of variation of the mean habitat suitability for *E. rubens*.

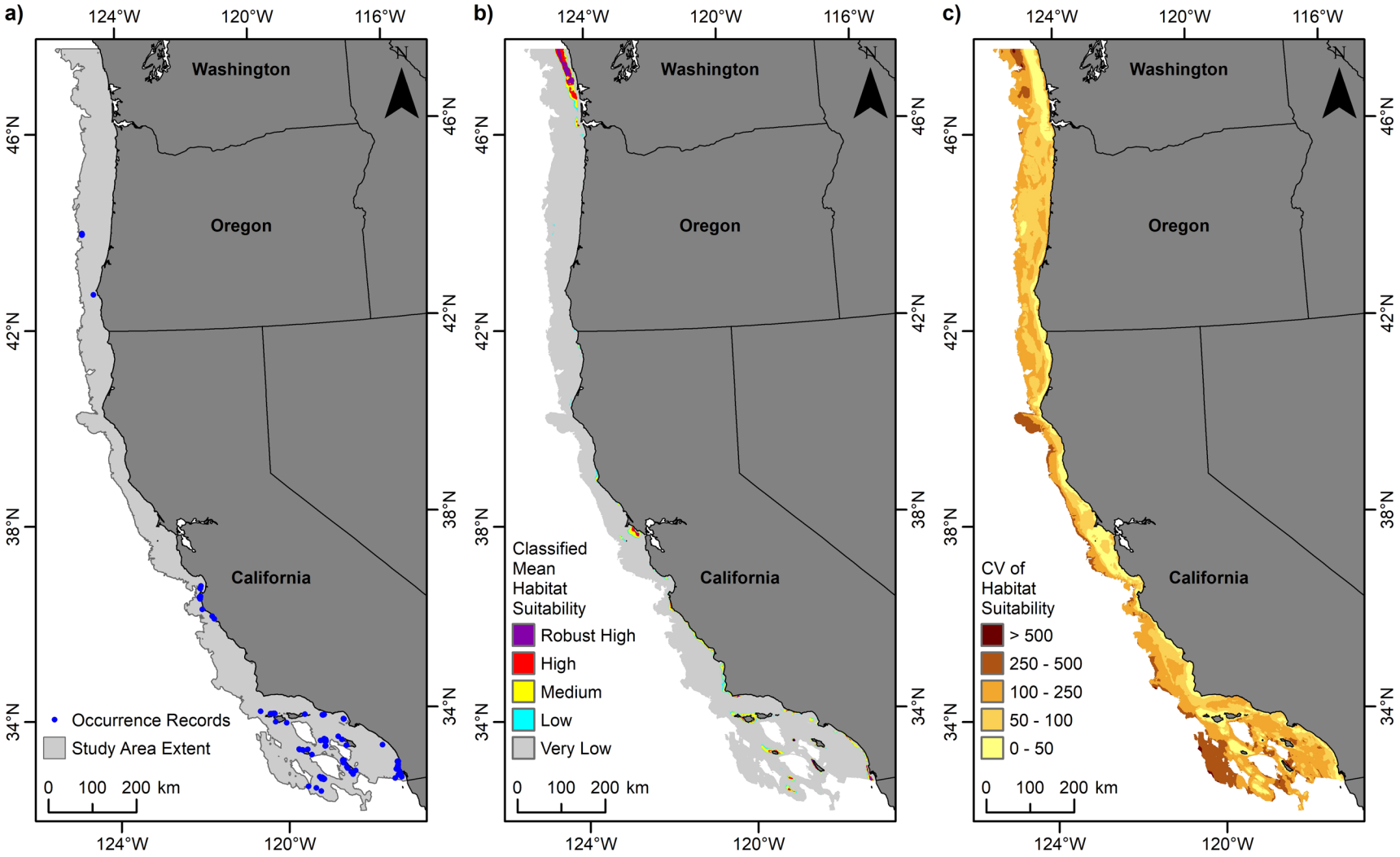

Figure 3.13. Predicted habitat suitability for the gorgonian coral *Leptogorgia chilensis* (Alcyonacea, Gorgoniidae).
(a) Records of *L. chilensis* occurrence from the NOAA National Database for Deep-Sea Corals and Sponges within the study area offshore to 1,200 m depth; (b) classified mean habitat suitability for *L. chilensis*; and (c) coefficient of variation of the mean habitat suitability for *L. chilensis*.

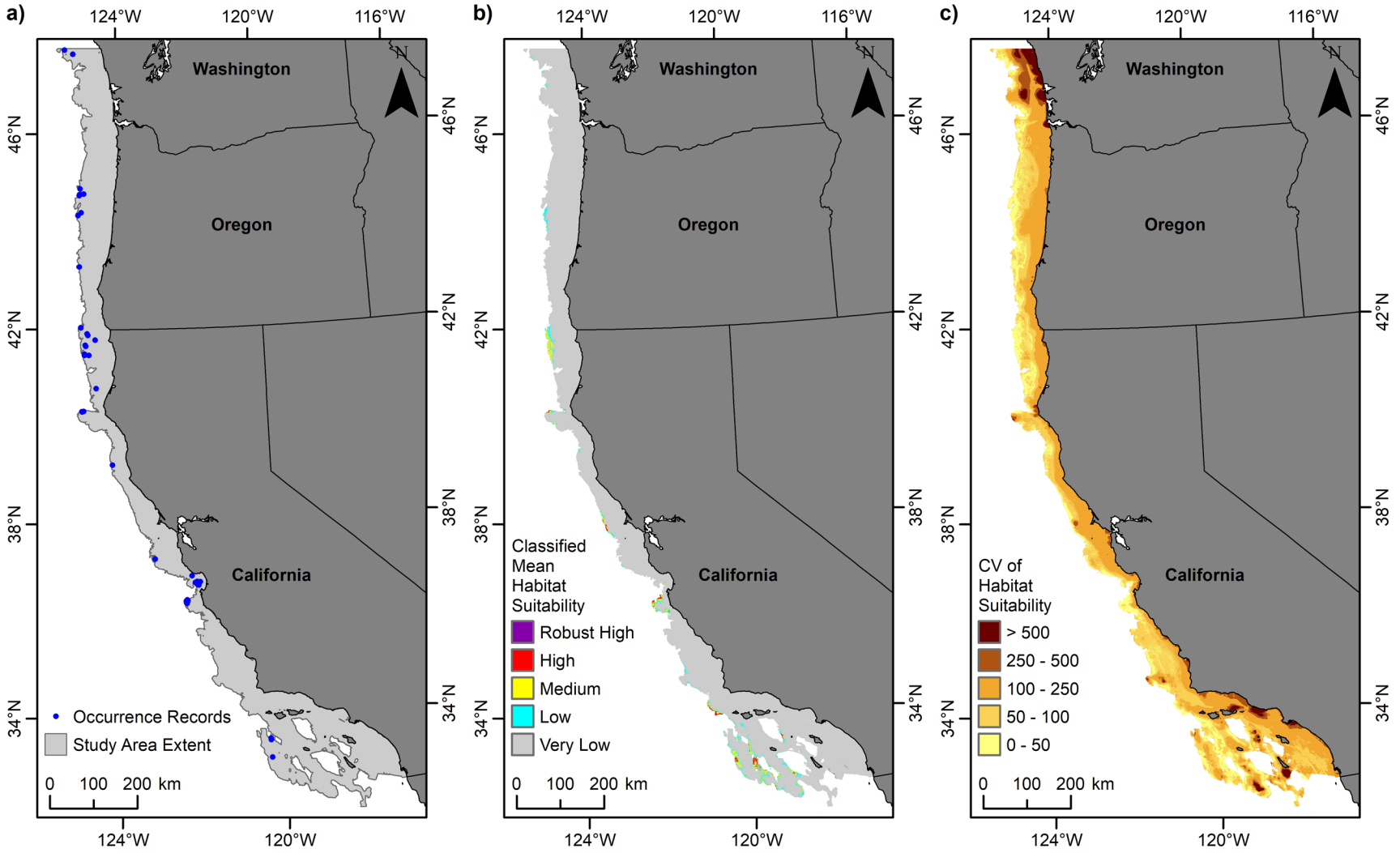

Figure 3.14. Predicted habitat suitability for the gorgonian coral *Isidella tentaculum* (Alcyonacea, Isididae).
(a) Records of *I. tentaculum* occurrence from the NOAA National Database for Deep-Sea Corals and Sponges within the study area offshore to 1,200 m depth; (b) classified mean habitat suitability for *I. tentaculum*; and (c) coefficient of variation of the mean habitat suitability for *I. tentaculum*.

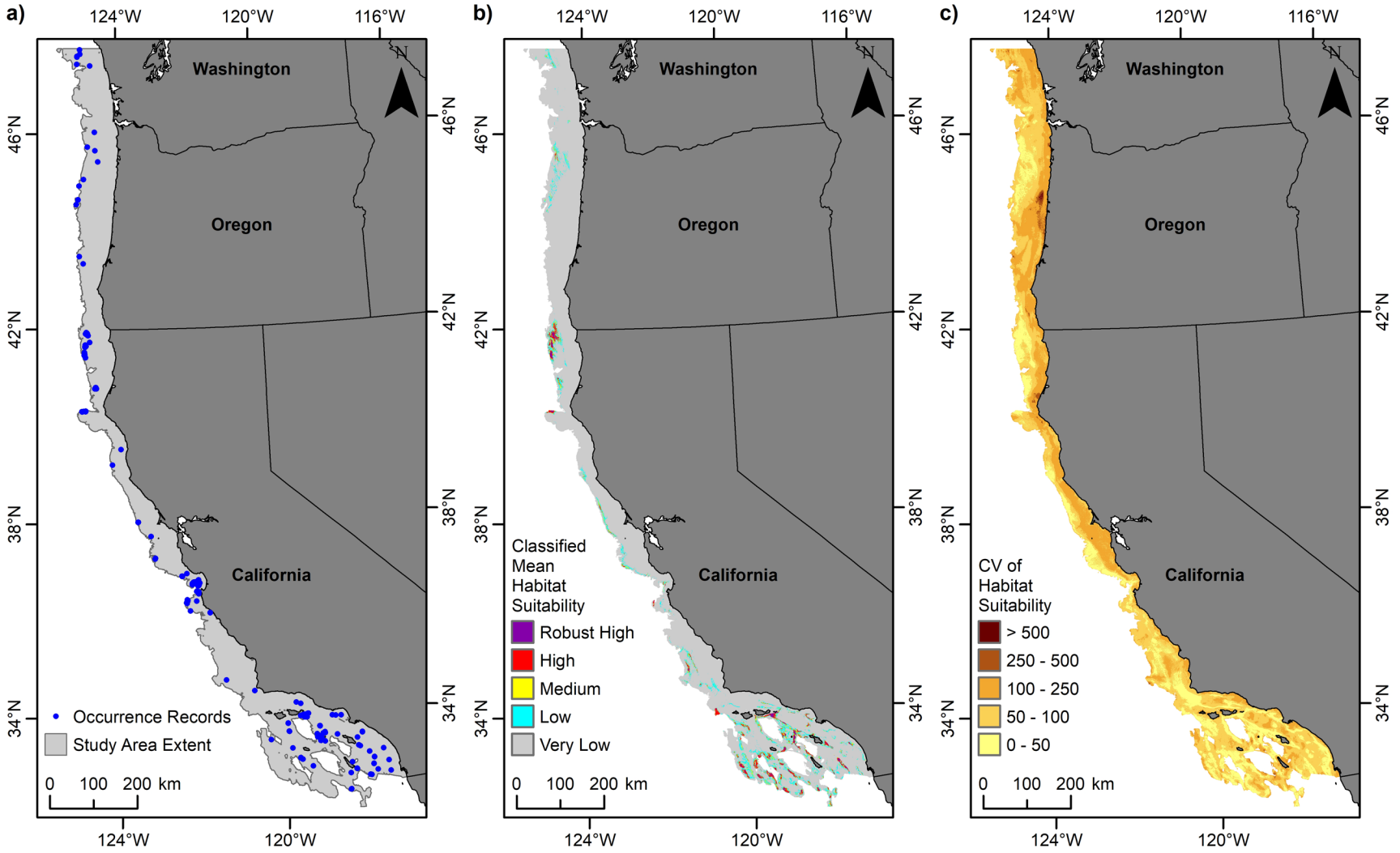

Figure 3.15. Predicted habitat suitability for the gorgonian coral *Paragorgia* (Alcyonacea, Paragorgiidae).
(a) Records of *Paragorgia* occurrence from the NOAA National Database for Deep-Sea Corals and Sponges within the study area offshore to 1,200 m depth; (b) classified mean habitat suitability for *Paragorgia*; and (c) coefficient of variation of the mean habitat suitability for *Paragorgia*.

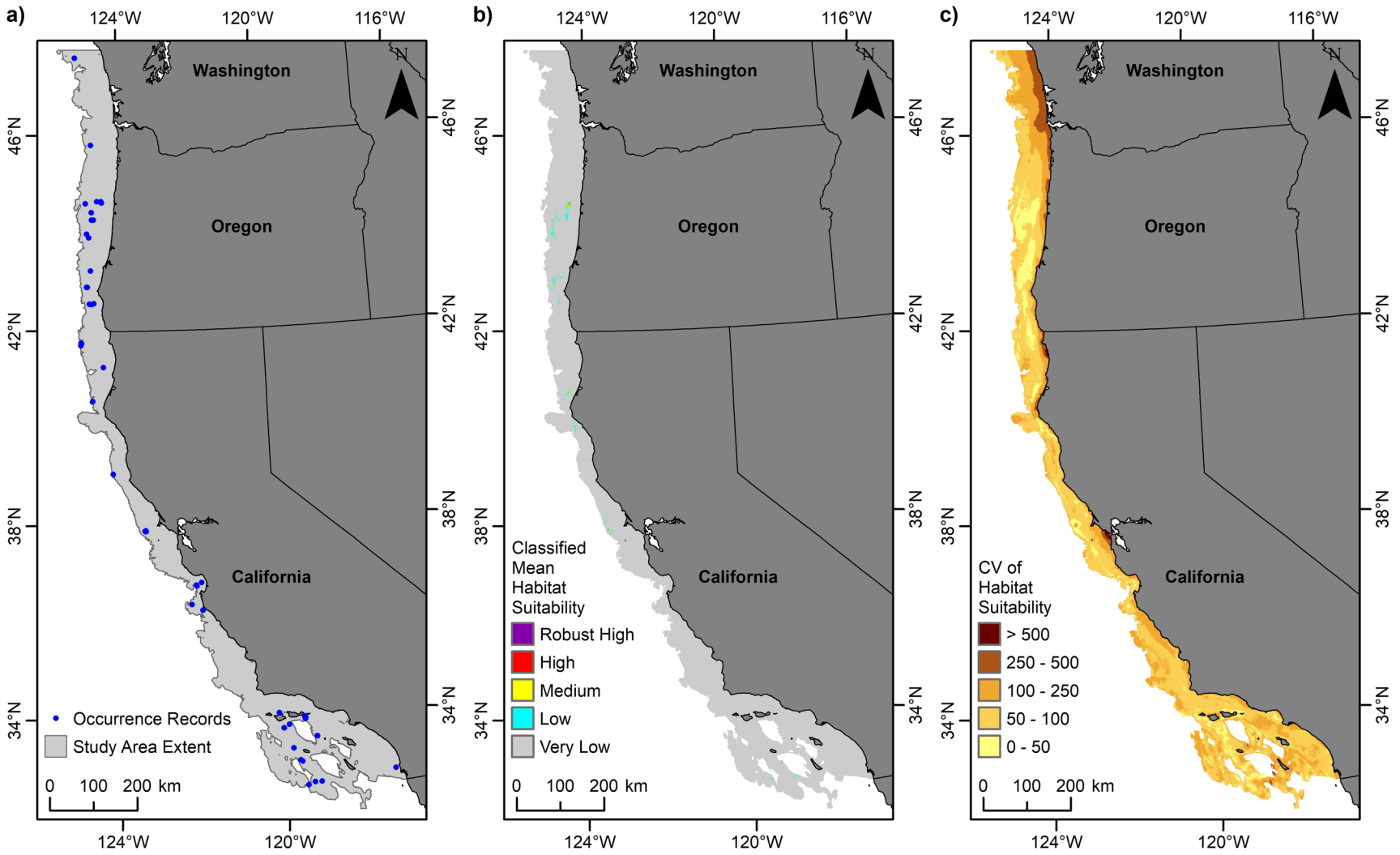

Figure 3.16. Predicted habitat suitability for the gorgonian coral *Chromoplexaura marki* (Alcyonacea, Plexauridae).
(a) Records of *C. marki* occurrence from the NOAA National Database for Deep-Sea Corals and Sponges within the study area offshore to 1,200 m depth; (b) classified mean habitat suitability for *C. marki*; and (c) coefficient of variation of the mean habitat suitability for *C. marki*.

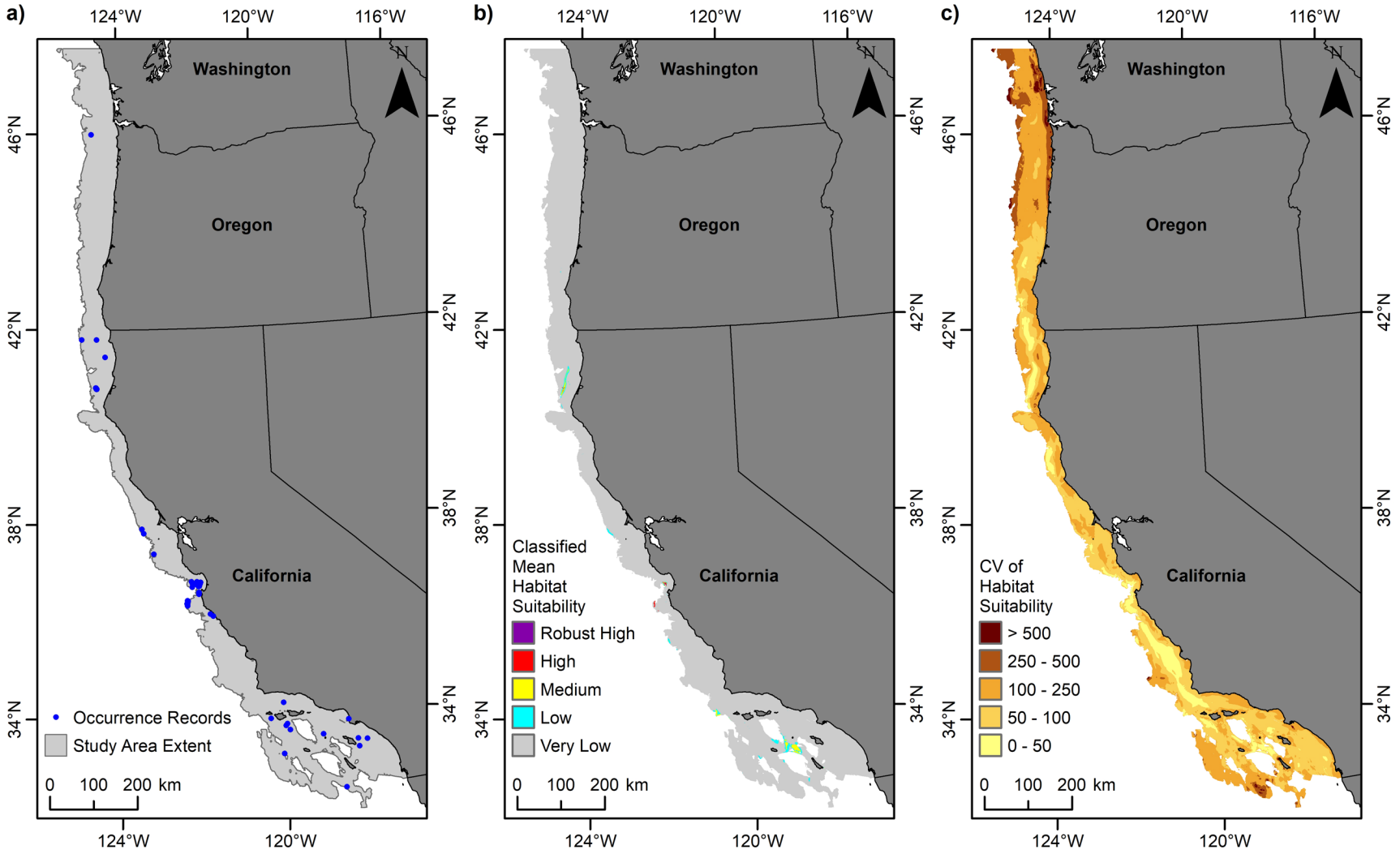

Figure 3.17. Predicted habitat suitability for the gorgonian coral *Swiftia kofoidi* (Alcyonacea, Plexauridae).
(a) Records of *S. kofoidi* occurrence from the NOAA National Database for Deep-Sea Corals and Sponges within the study area offshore to 1,200 m depth; (b) classified mean habitat suitability for *S. kofoidi*; and (c) coefficient of variation of the mean habitat suitability for *S. kofoidi*.

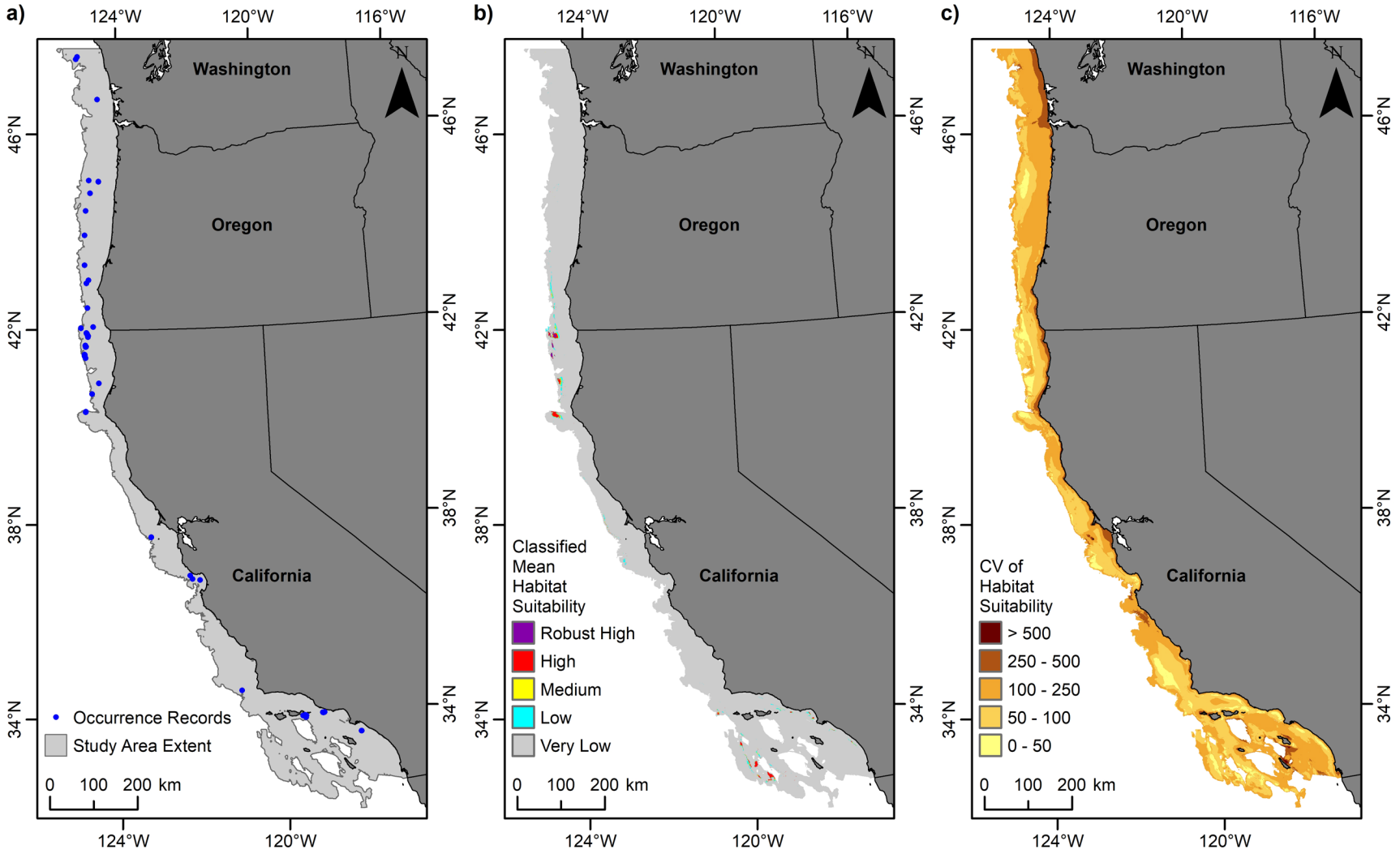

Figure 3.18. Predicted habitat suitability for the gorgonian coral *Swiftia pacifica* (Alcyonacea, Plexauridae).
(a) Records of *S. pacifica* occurrence from the NOAA National Database for Deep-Sea Corals and Sponges within the study area offshore to 1,200 m depth; (b) classified mean habitat suitability for *S. pacifica*; and (c) coefficient of variation of the mean habitat suitability for *S. pacifica*.

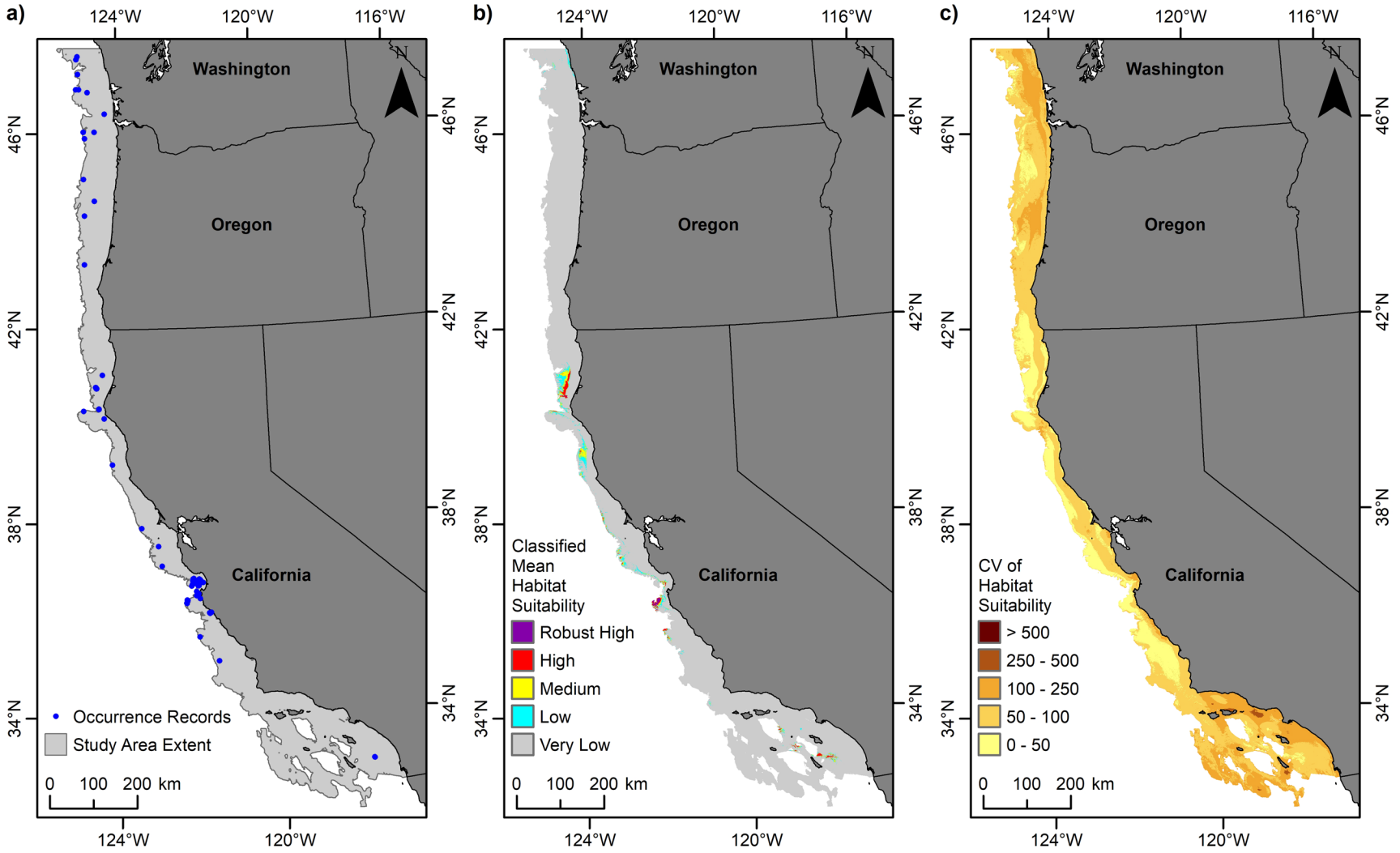

Figure 3.19. Predicted habitat suitability for the gorgonian coral *Swiftia simplex* (Alcyonacea, Plexauridae).
(a) Records of *S. simplex* occurrence from the NOAA National Database for Deep-Sea Corals and Sponges within the study area offshore to 1,200 m depth; (b) classified mean habitat suitability for *S. simplex*; and (c) coefficient of variation of the mean habitat suitability for *S. simplex*.

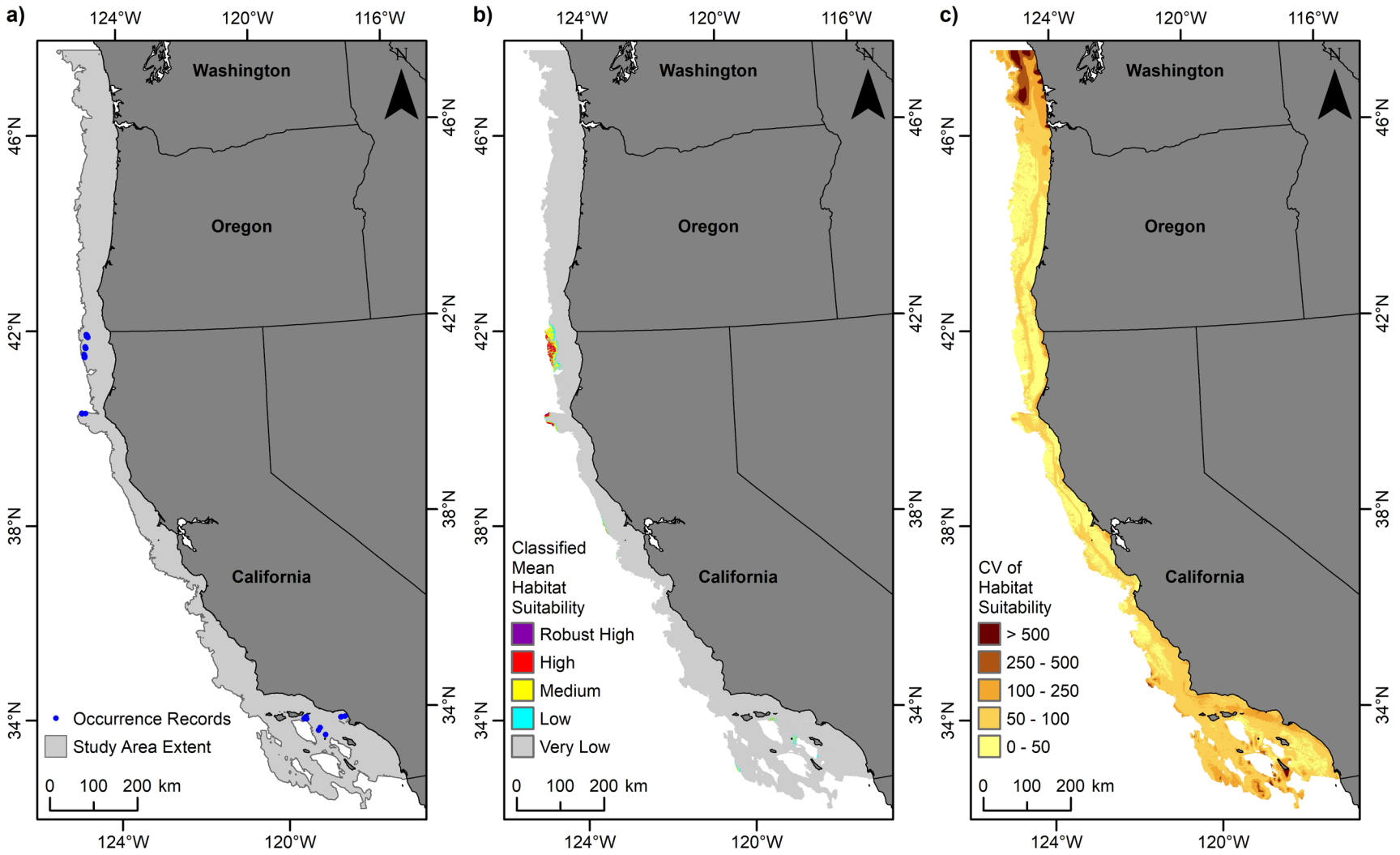

Figure 3.20. Predicted habitat suitability for the gorgonian coral *Parastenella ramosa* (Alcyonacea, Primnoidae).
(a) Records of *P. ramosa* occurrence from the NOAA National Database for Deep-Sea Corals and Sponges within the study area offshore to 1,200 m depth; (b) classified mean habitat suitability for *P. ramosa*; and (c) coefficient of variation of the mean habitat suitability for *P. ramosa*.

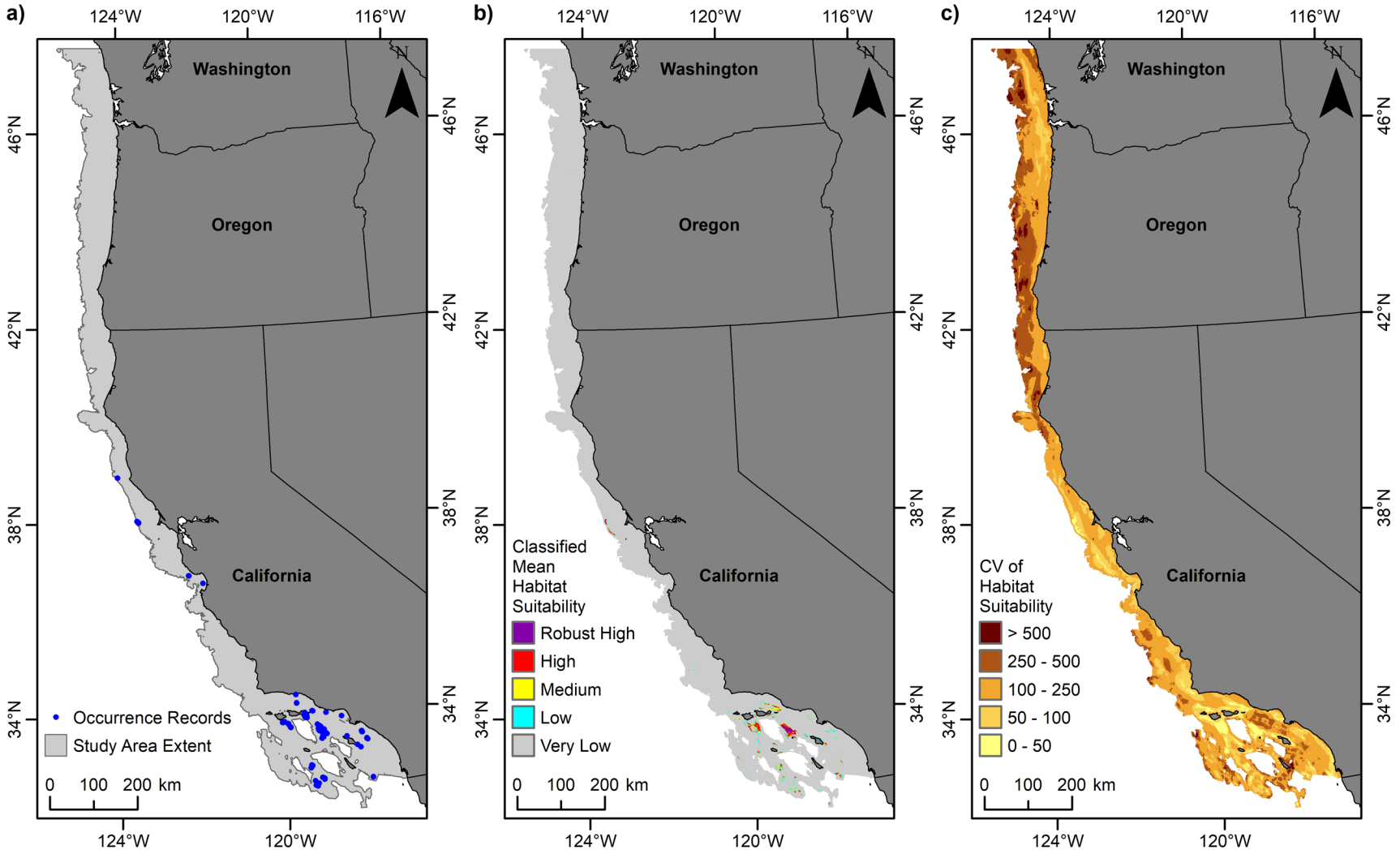

Figure 3.21. Predicted habitat suitability for the gorgonian coral *Plumarella longispina* (Alcyonacea, Primnoidae).
(a) Records of *P. longispina* occurrence from the NOAA National Database for Deep-Sea Corals and Sponges within the study area offshore to 1,200 m depth; (b) classified mean habitat suitability for *P. longispina*; and (c) coefficient of variation of the mean habitat suitability for *P. longispina*.

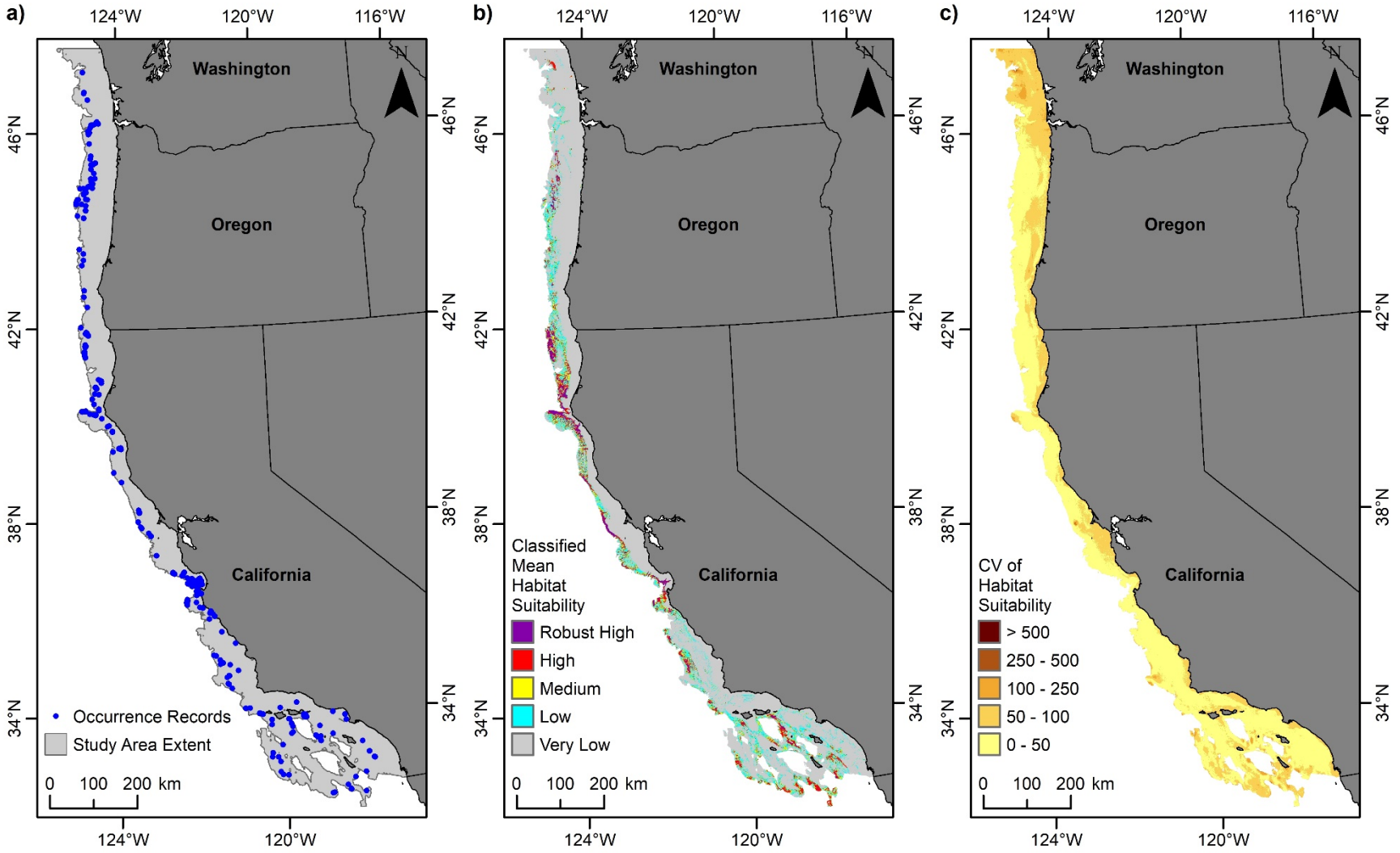

Figure 3.22. Predicted habitat suitability for the soft coral *Heteropolypus ritteri* (Alcyonacea, Alcyoniidae).
(a) Records of *H. ritteri* occurrence from the NOAA National Database for Deep-Sea Corals and Sponges within the study area offshore to 1,200 m depth; (b) classified mean habitat suitability for *H. ritteri*; and (c) coefficient of variation of the mean habitat suitability for *H. ritteri*.

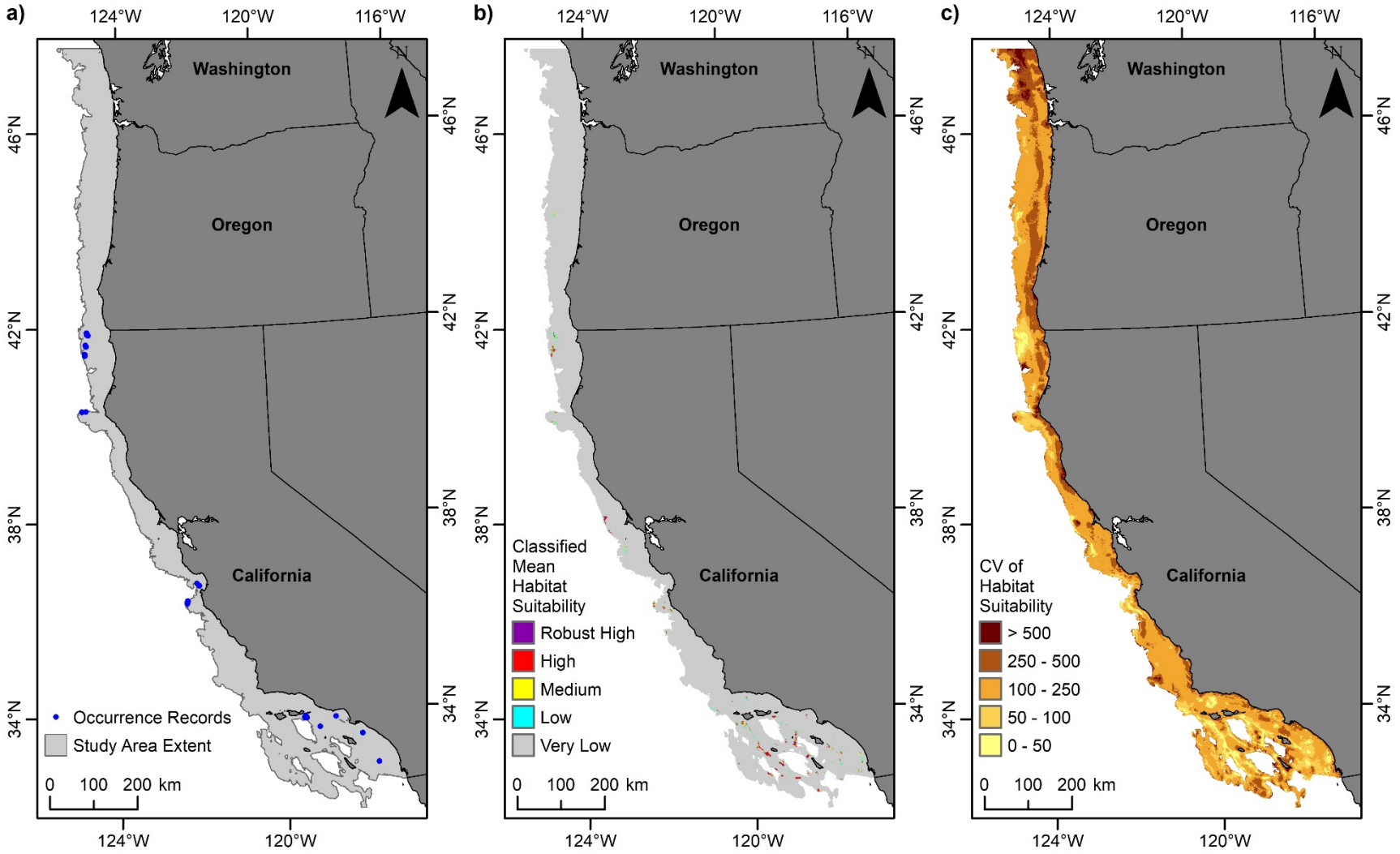

Figure 3.23. Predicted habitat suitability for the soft coral *Clavularia* (Alcyonacea, Clavulariidae).
(a) Records of *Clavularia* occurrence from the NOAA National Database for Deep-Sea Corals and Sponges within the study area offshore to 1,200 m depth; (b) classified mean habitat suitability for *Clavularia*; and (c) coefficient of variation in the mean habitat suitability for *Clavularia*.

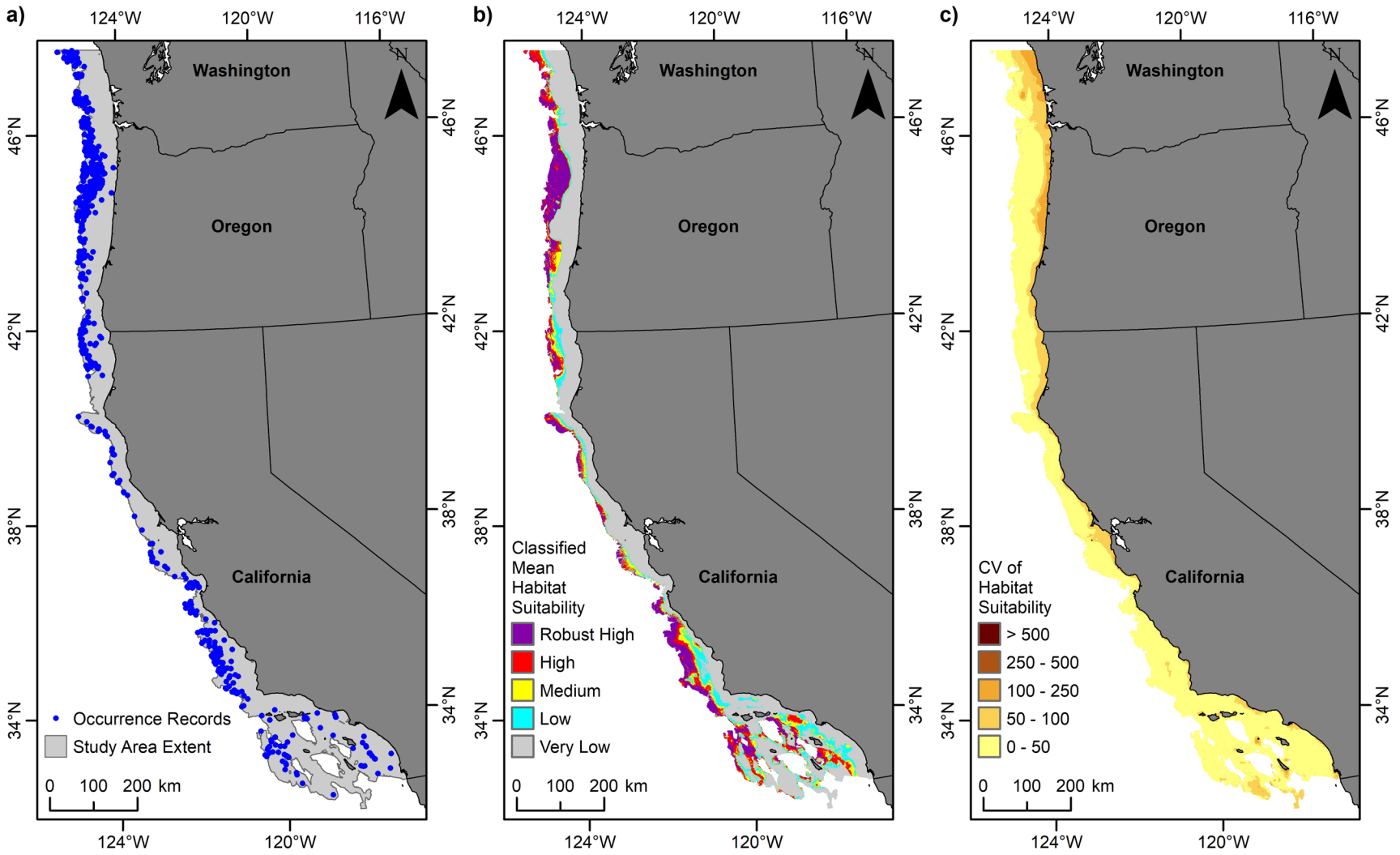

Figure 3.24. Predicted habitat suitability for the sea pen *Anthoptilum grandiflorum* (Pennatulacea, Anthoptilidae).
(a) Records of *A. grandiflorum* occurrence from the NOAA National Database for Deep-Sea Corals and Sponges within the study area offshore to 1,200 m depth; (b) classified mean habitat suitability for *A. grandiflorum*; and (c) coefficient of variation of the mean habitat suitability for *A. grandiflorum*.

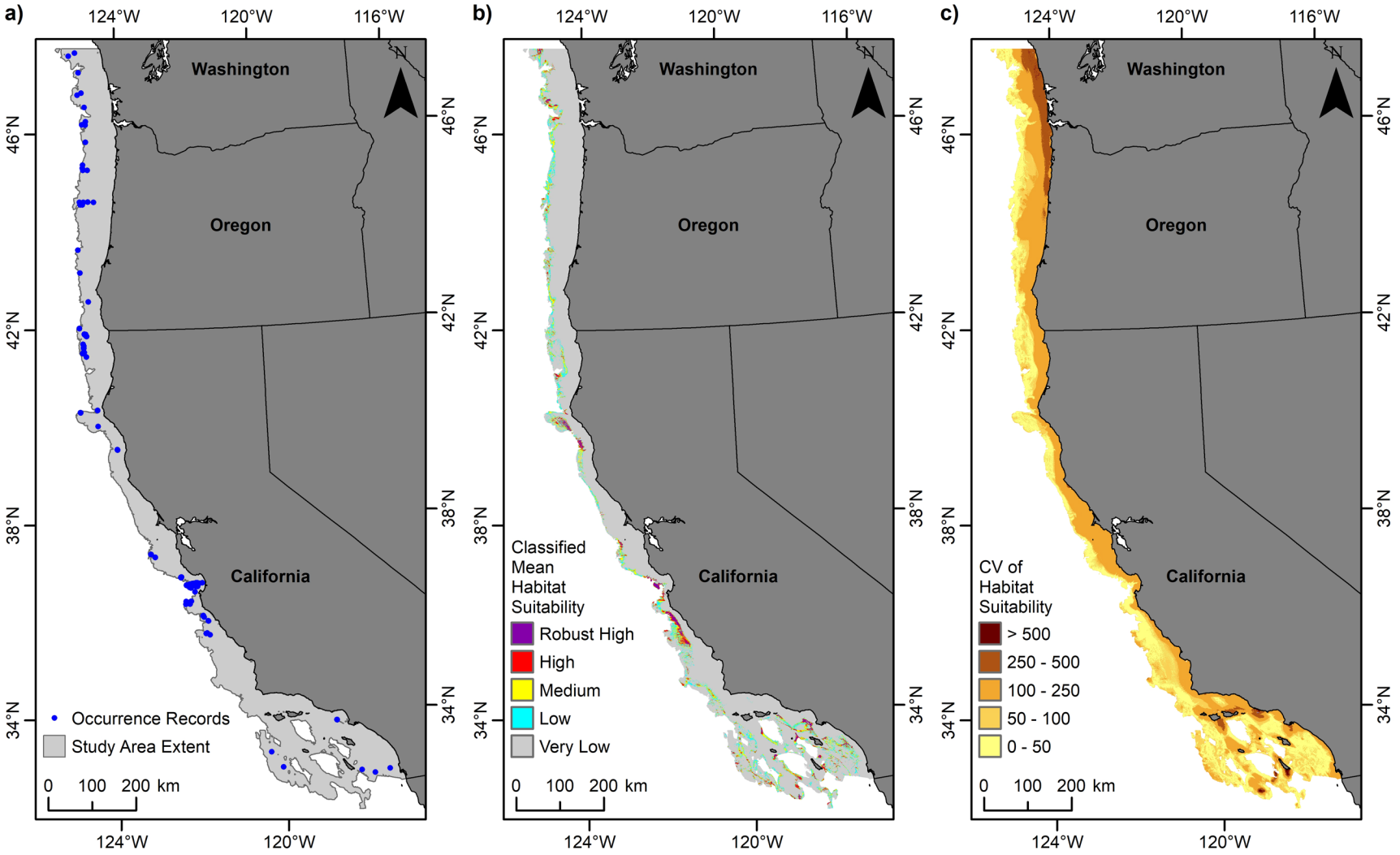

Figure 3.25. Predicted habitat suitability for the sea pen *Funiculina* (Pennatulacea, Funiculinidae).
(a) Records of *Funiculina* occurrence from the NOAA National Database for Deep-Sea Corals and Sponges within the study area offshore to 1,200 m depth; (b) classified mean habitat suitability for *Funiculina*; and (c) coefficient of variation of the mean habitat suitability for *Funiculina*.

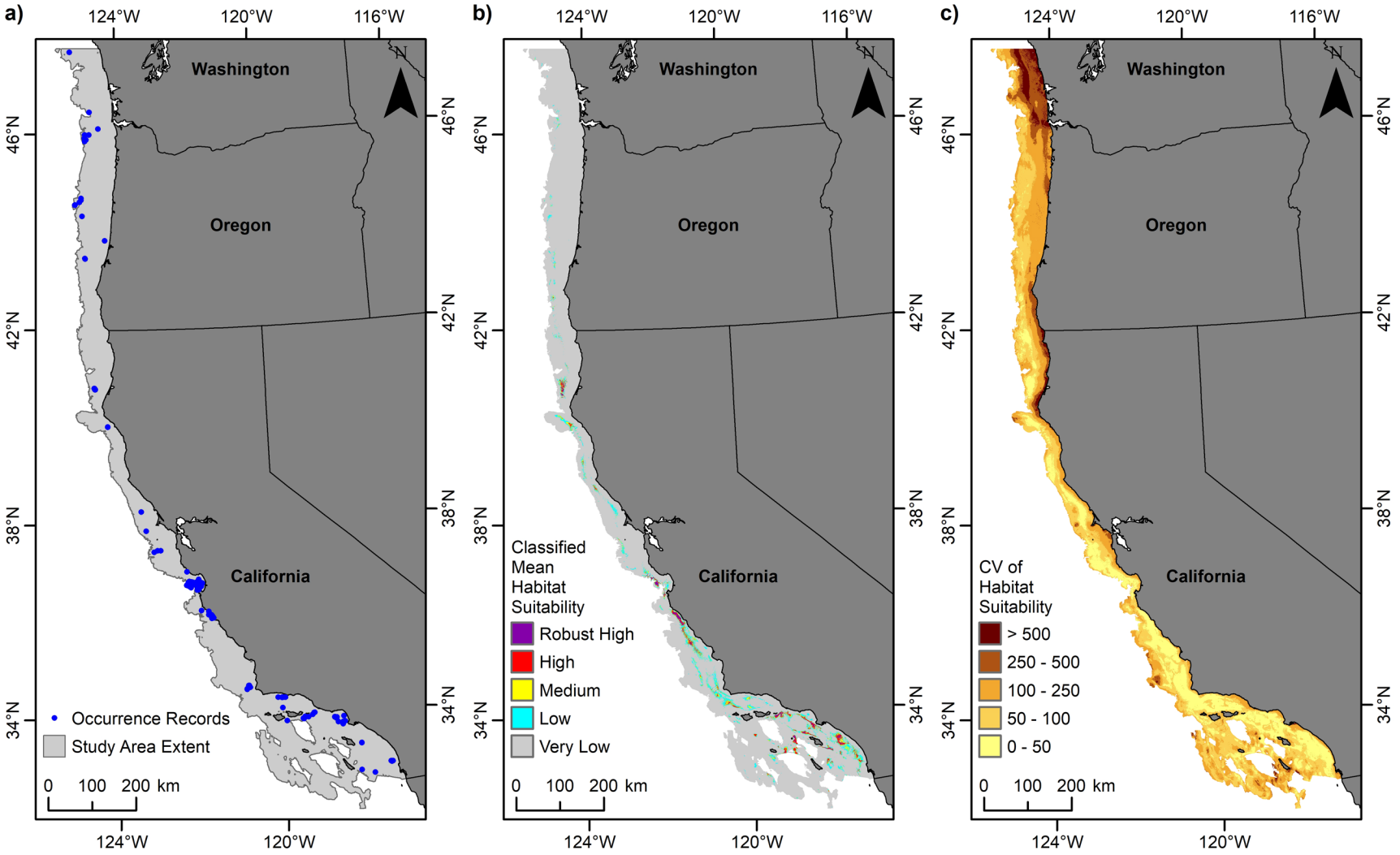

Figure 3.26. Predicted habitat suitability for the sea pen *Halipteris californica* (Pennatulacea, Halipteridae).
(a) Records of *H. californica* occurrence from the NOAA National Database for Deep-Sea Corals and Sponges within the study area offshore to 1,200 m depth; (b) classified mean habitat suitability for *H. californica*; and (c) coefficient of variation of the mean habitat suitability for *H. californica*.

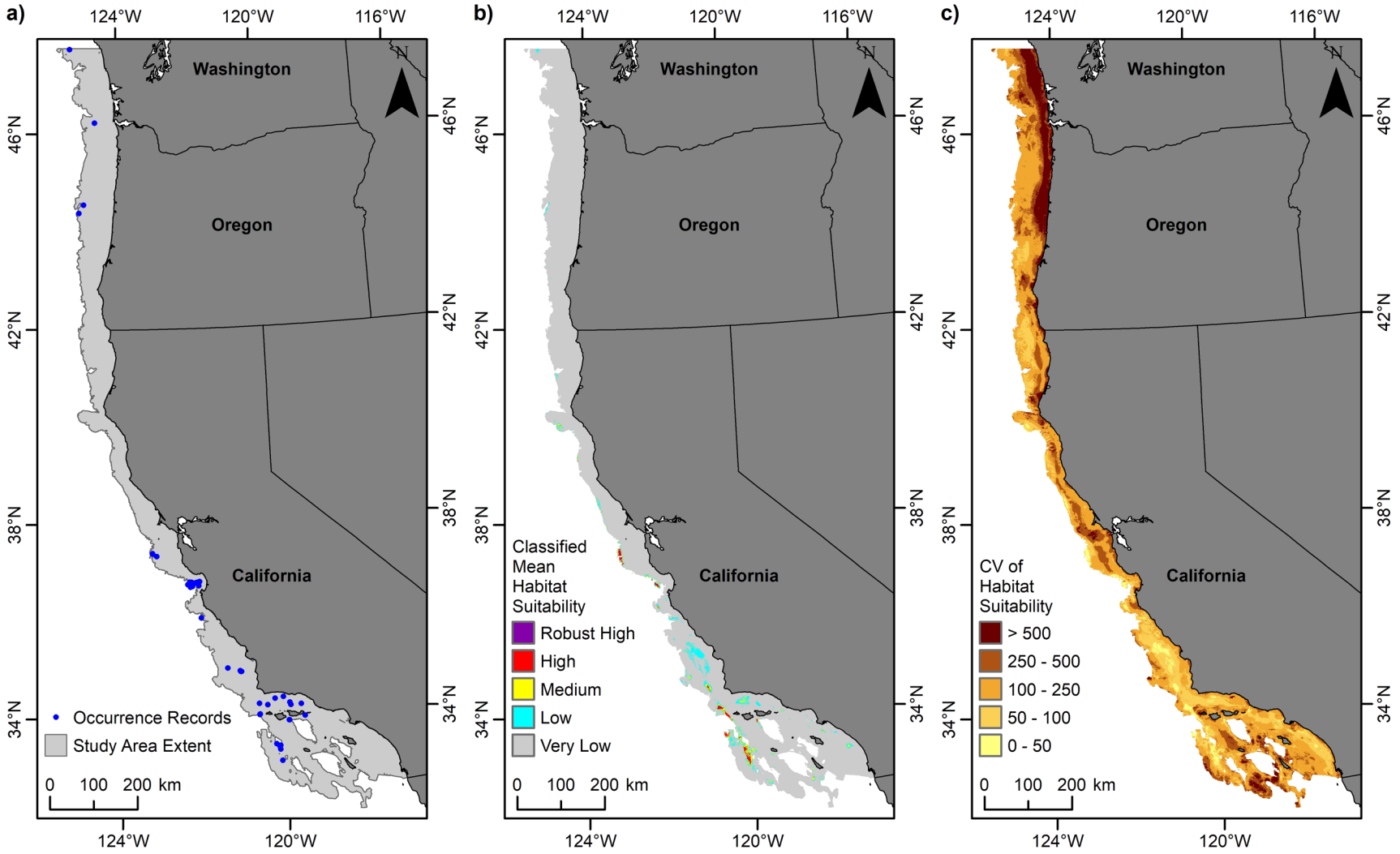

Figure 3.27. Predicted habitat suitability for the sea pen *Pennatula phosphorea* (Pennatulacea, Pennatulidae).
(a) Records of *P. phosphorea* occurrence from the NOAA National Database for Deep-Sea Corals and Sponges within the study area offshore to 1,200 m depth; (b) classified mean habitat suitability for *P. phosphorea*; and (c) coefficient of variation in the mean habitat suitability for *P. phosphorea*.

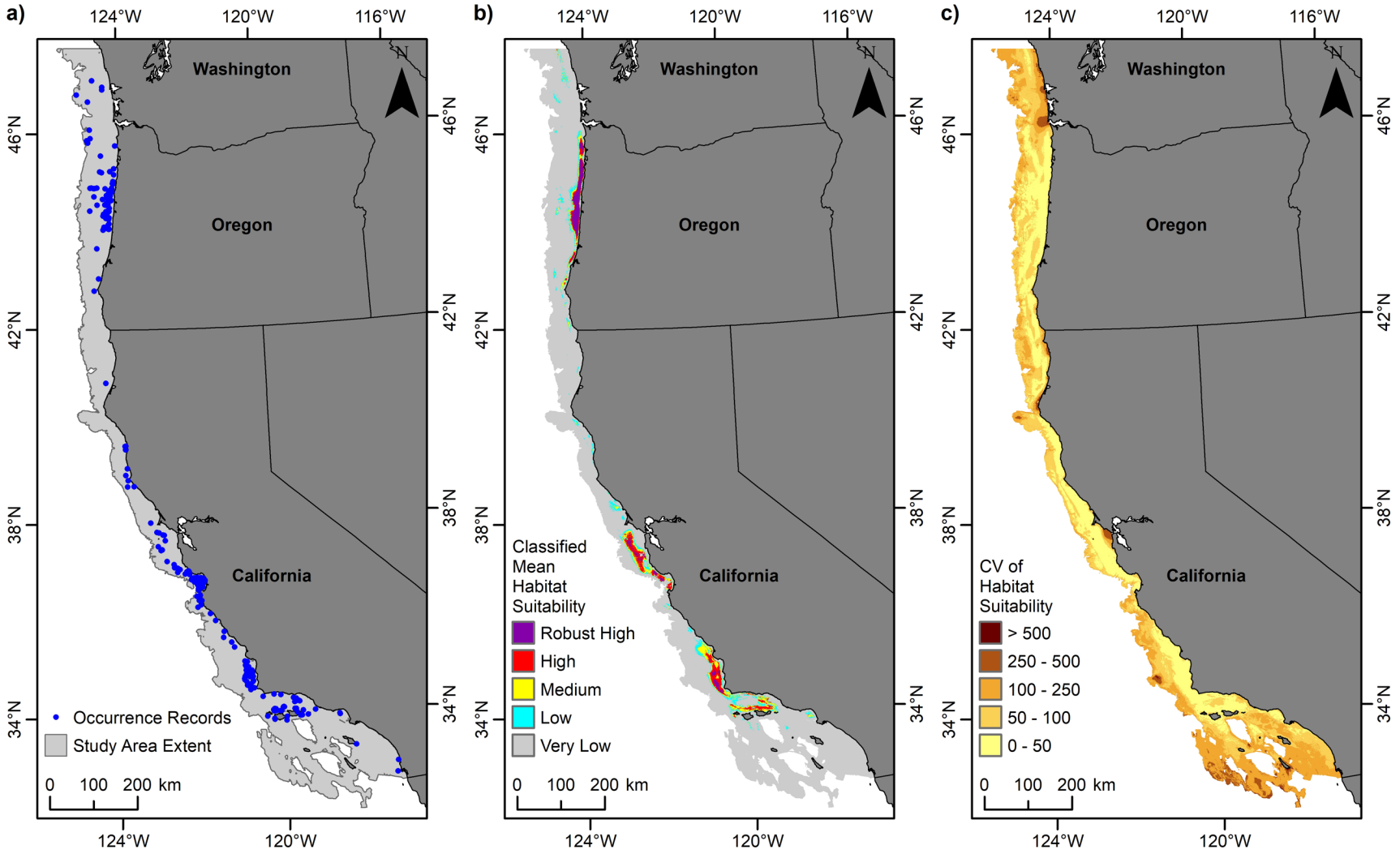

Figure 3.28. Predicted habitat suitability for the sea pen *Ptilosarcus gurneyi* (Pennatulacea, Pennatulidae).
(a) Records of *P. gurneyi* occurrence from the NOAA National Database for Deep-Sea Corals and Sponges within the study area offshore to 1,200 m depth; (b) classified mean habitat suitability for *P. gurneyi*; and (c) coefficient of variation of the mean habitat suitability for *P. gurneyi*.

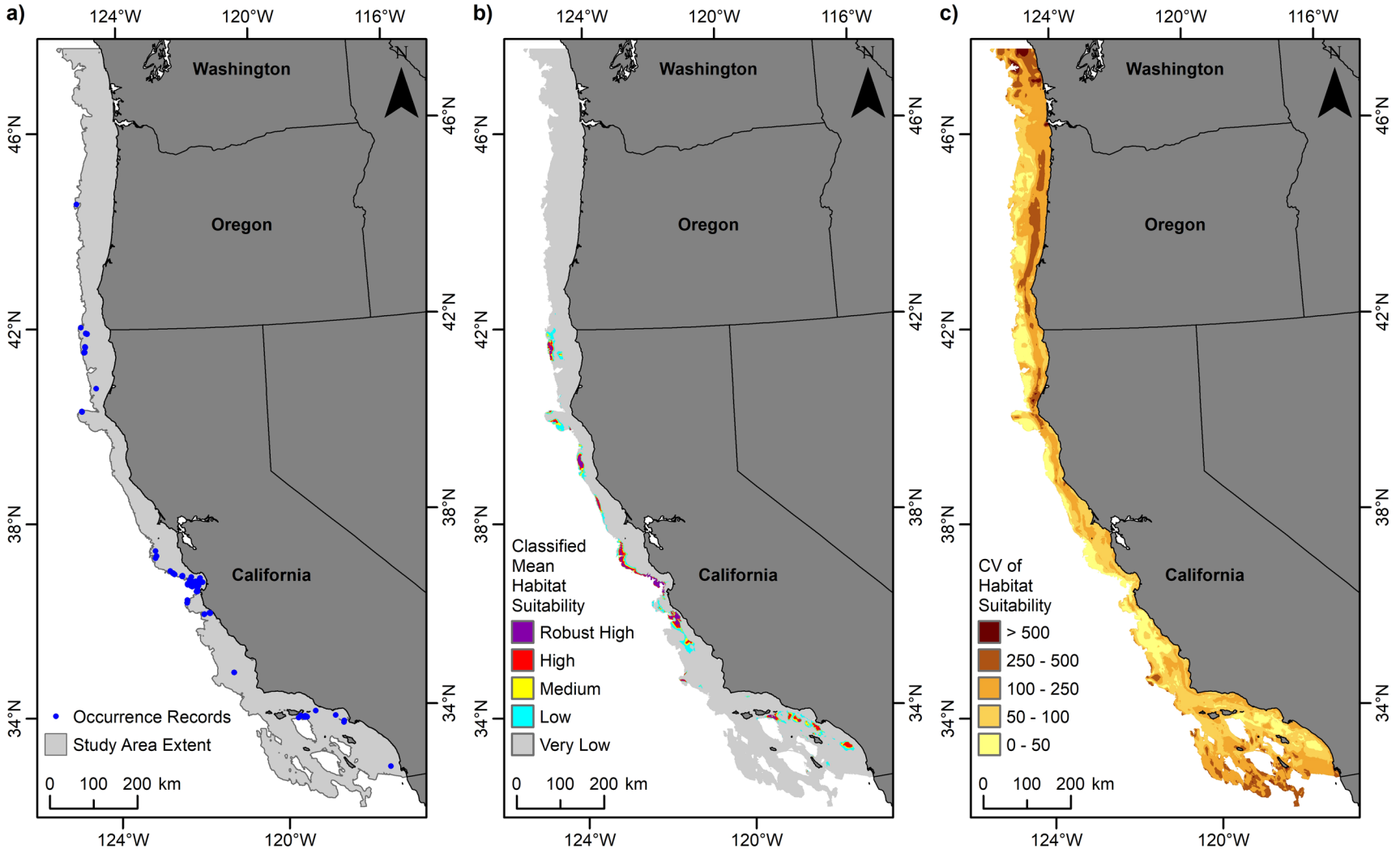

Figure 3.29. Predicted habitat suitability for the sea pen *Umbellula lindahli* (Pennatulacea, Umbellulidae).
(a) Records of *U. lindahli* occurrence from the NOAA National Database for Deep-Sea Corals and Sponges within the study area offshore to 1,200 m depth; (b) classified mean habitat suitability for *U. lindahli*; and (c) coefficient of variation of the mean habitat suitability for *U. lindahli*.

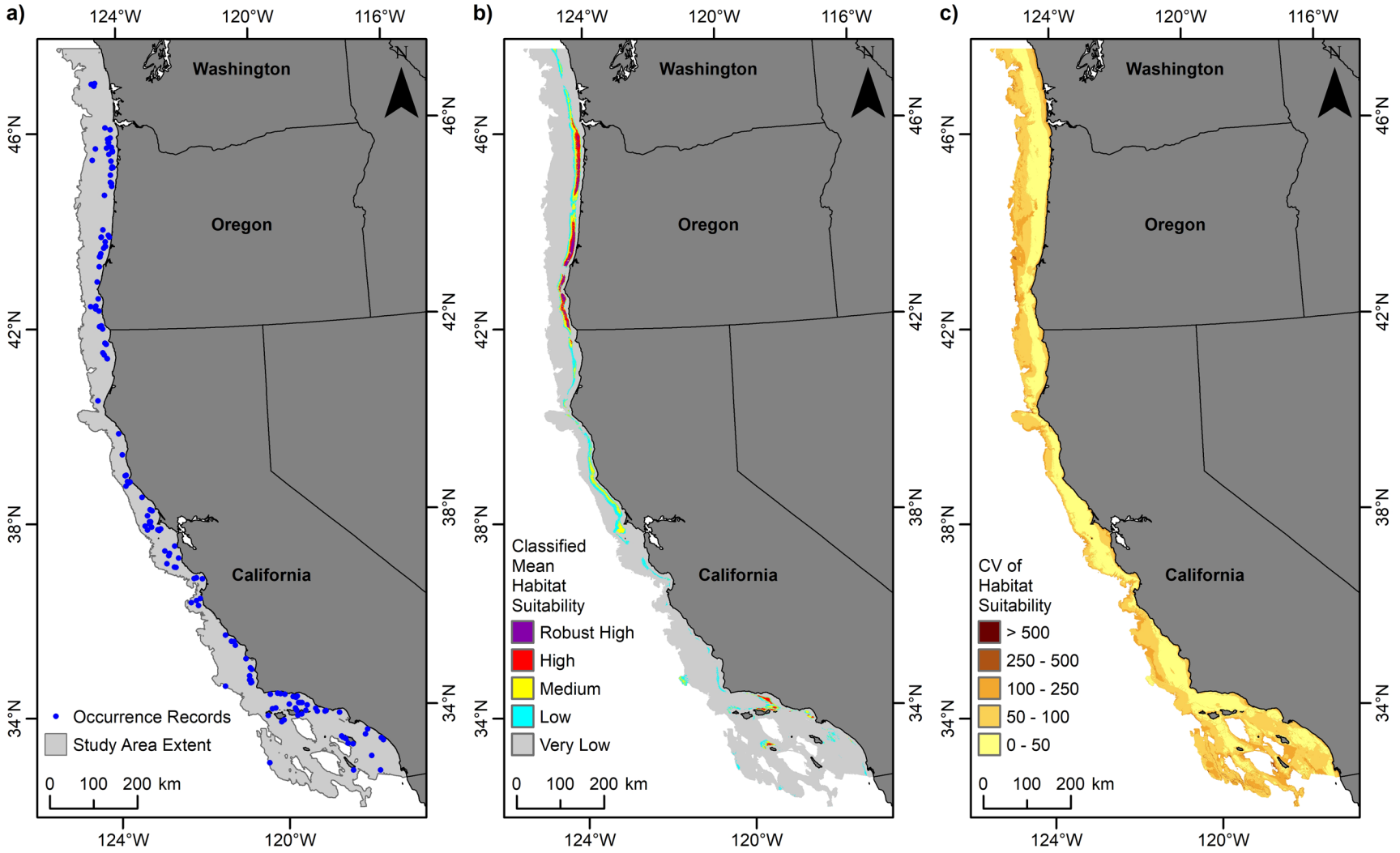

Figure 3.30. Predicted habitat suitability for the sea pen *Acanthoptilum gracile* (Pennatulacea, Virgularidae).
(a) Records of *A. gracile* occurrence from the NOAA National Database for Deep-Sea Corals and Sponges within the study area offshore to 1,200 m depth; (b) classified mean habitat suitability for *A. gracile*; and (c) coefficient of variation of the mean habitat suitability for *A. gracile*.

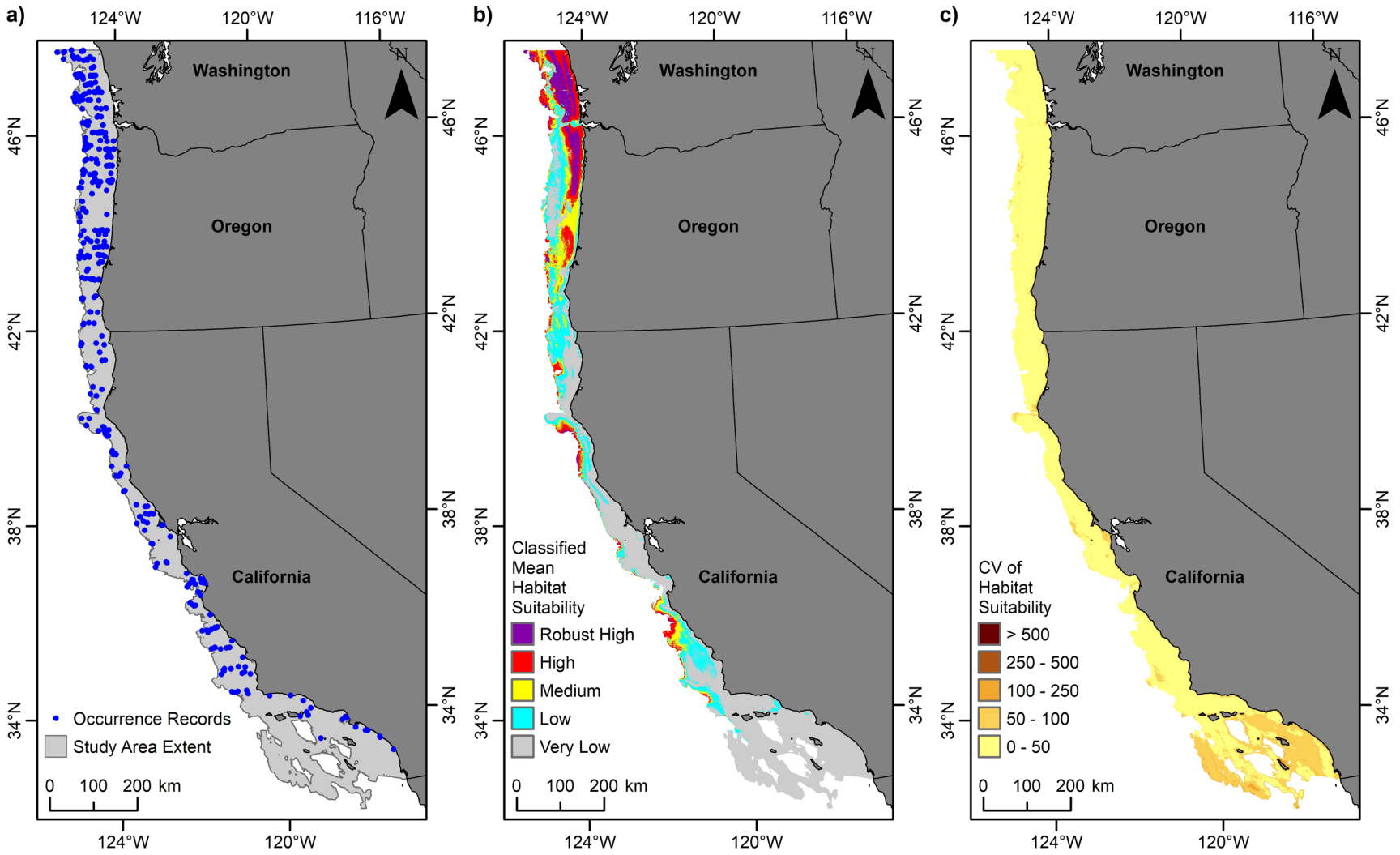

Figure 3.31. Predicted habitat suitability for the sea pen *Stylatula* (Pennatulacea, Virgulariidae).
(a) Records of *Stylatula* occurrence from the NOAA National Database for Deep-Sea Corals and Sponges within the study area offshore to 1,200 m depth; (b) classified mean habitat suitability for *Stylatula*; and (c) coefficient of variation of the mean habitat suitability for *Stylatula*.

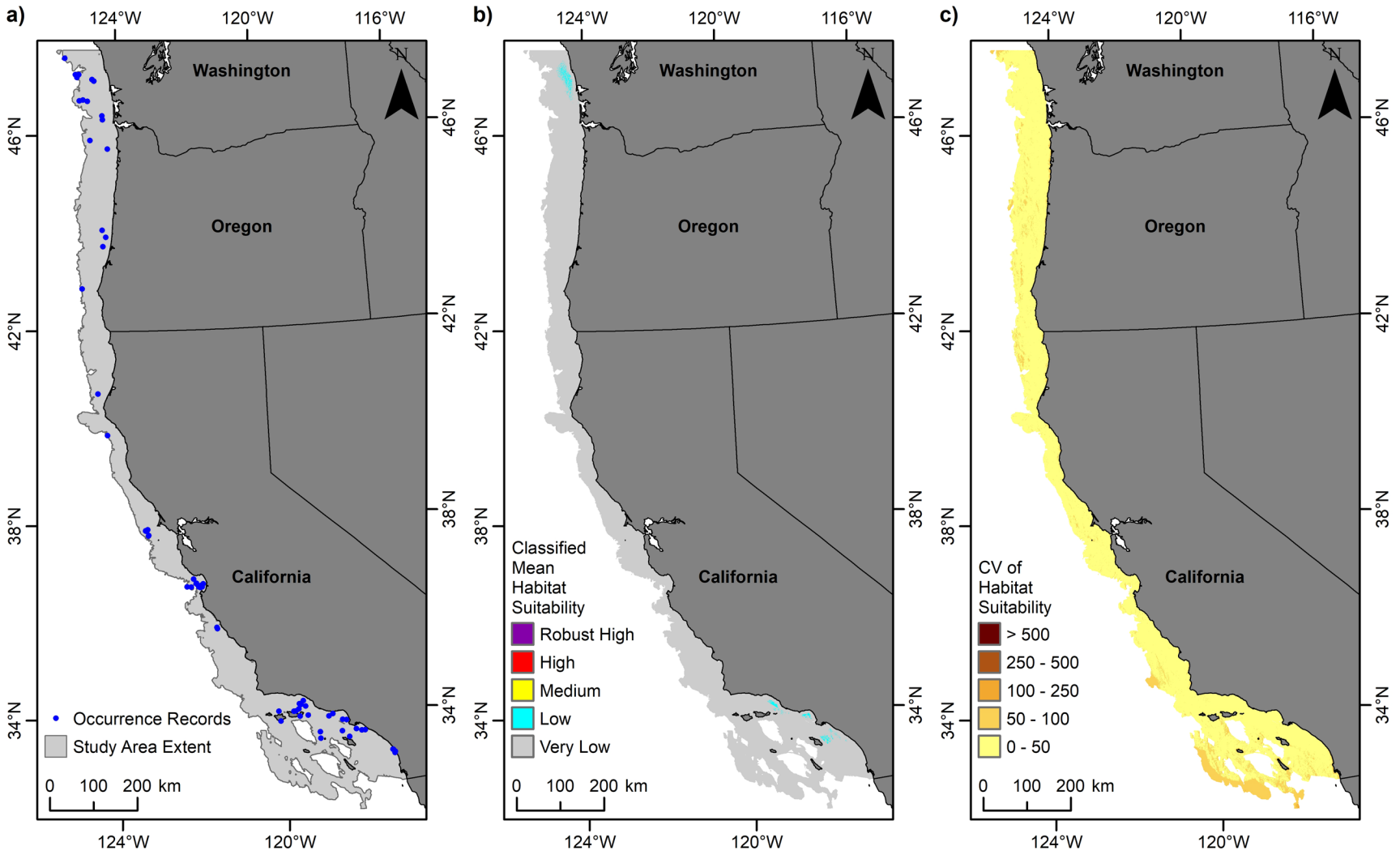

Figure 3.32. Predicted habitat suitability for the sea pen *Virgularia* (Pennatulacea, Virgularidae).
(a) Records of *Virgularia* occurrence from the NOAA National Database for Deep-Sea Corals and Sponges within the study area offshore to 1,200 m depth; (b) classified mean habitat suitability for *Virgularia*; and (c) coefficient of variation of the mean habitat suitability for *Virgularia*.

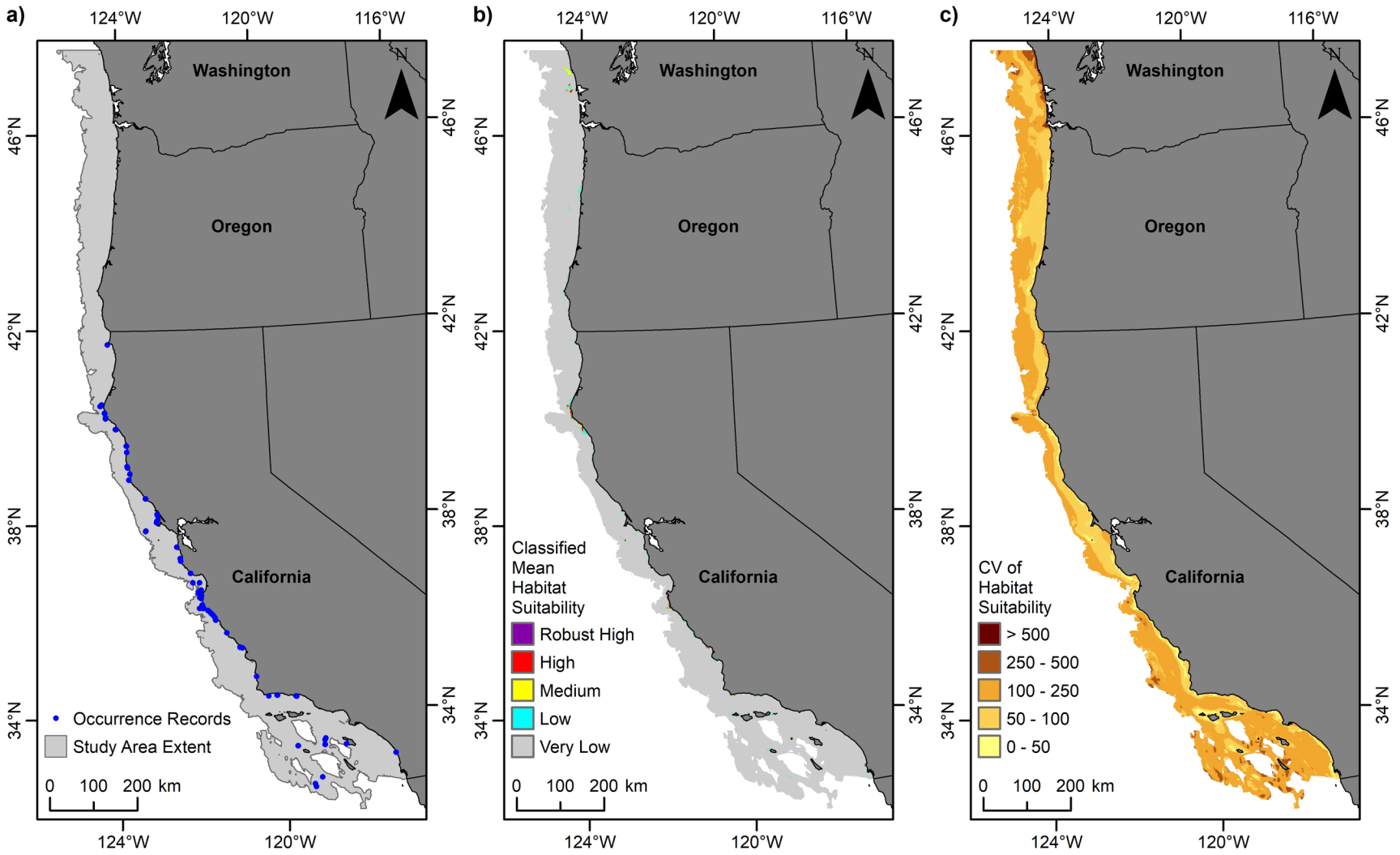

Figure 3.33. Predicted habitat suitability for the stylasterid coral *Stylaster californicus* (Anthoathecata, Stylasteridae).
(a) Records of *S. californicus* occurrence from the NOAA National Database for Deep-Sea Corals and Sponges within the study area offshore to 1,200 m depth; (b) classified mean habitat suitability for *S. californicus*; and (c) coefficient of variation of the mean habitat suitability for *S. californicus*.

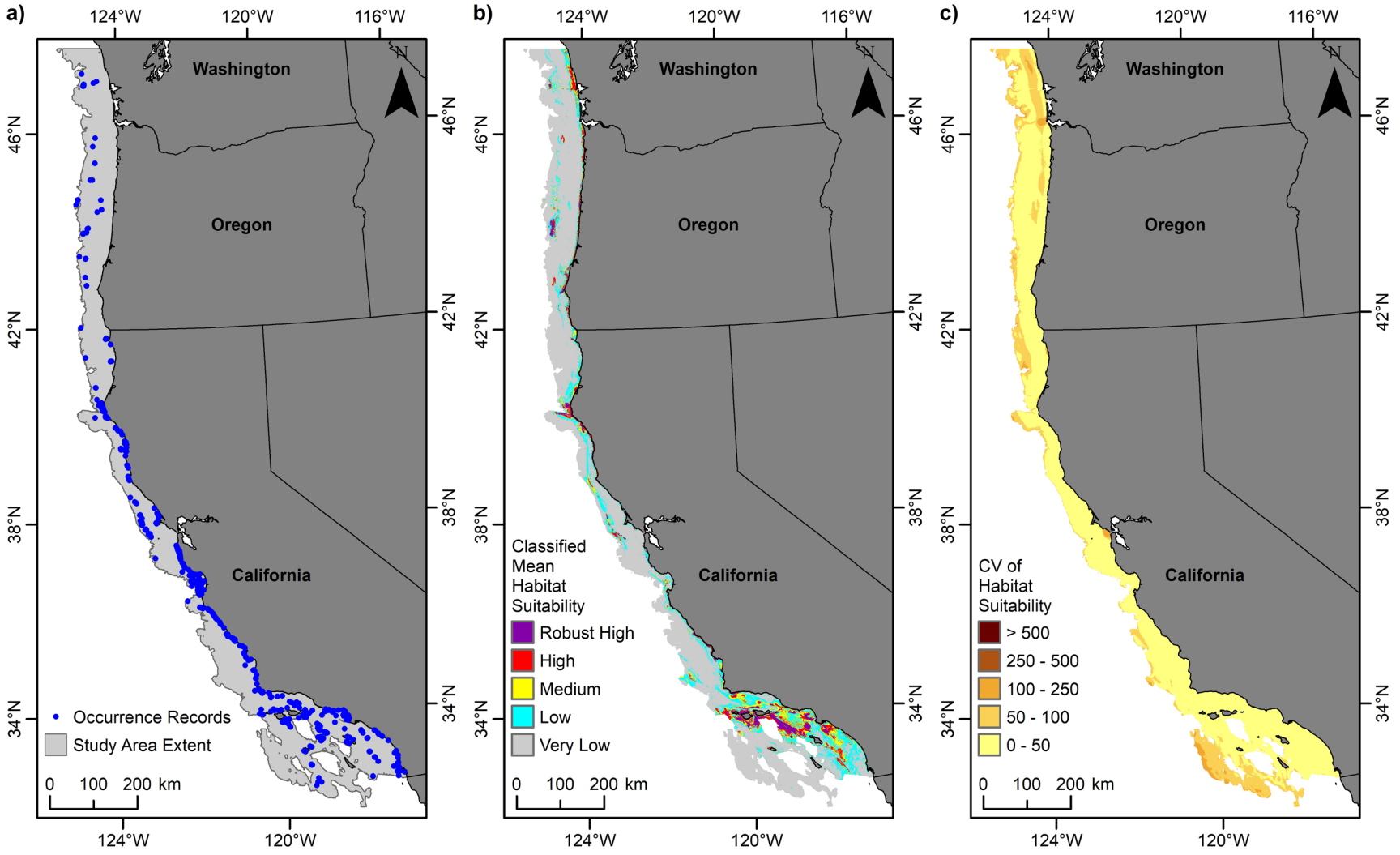

Figure 3.34. Predicted habitat suitability for Demosponges (Class Demospongiae).
(a) Records of Demospongiae occurrence from the NOAA National Database for Deep-Sea Corals and Sponges within the study area offshore to 1,200 m depth; (b) classified mean habitat suitability for Demospongiae; and (c) coefficient of variation of the mean habitat suitability for Demospongiae.

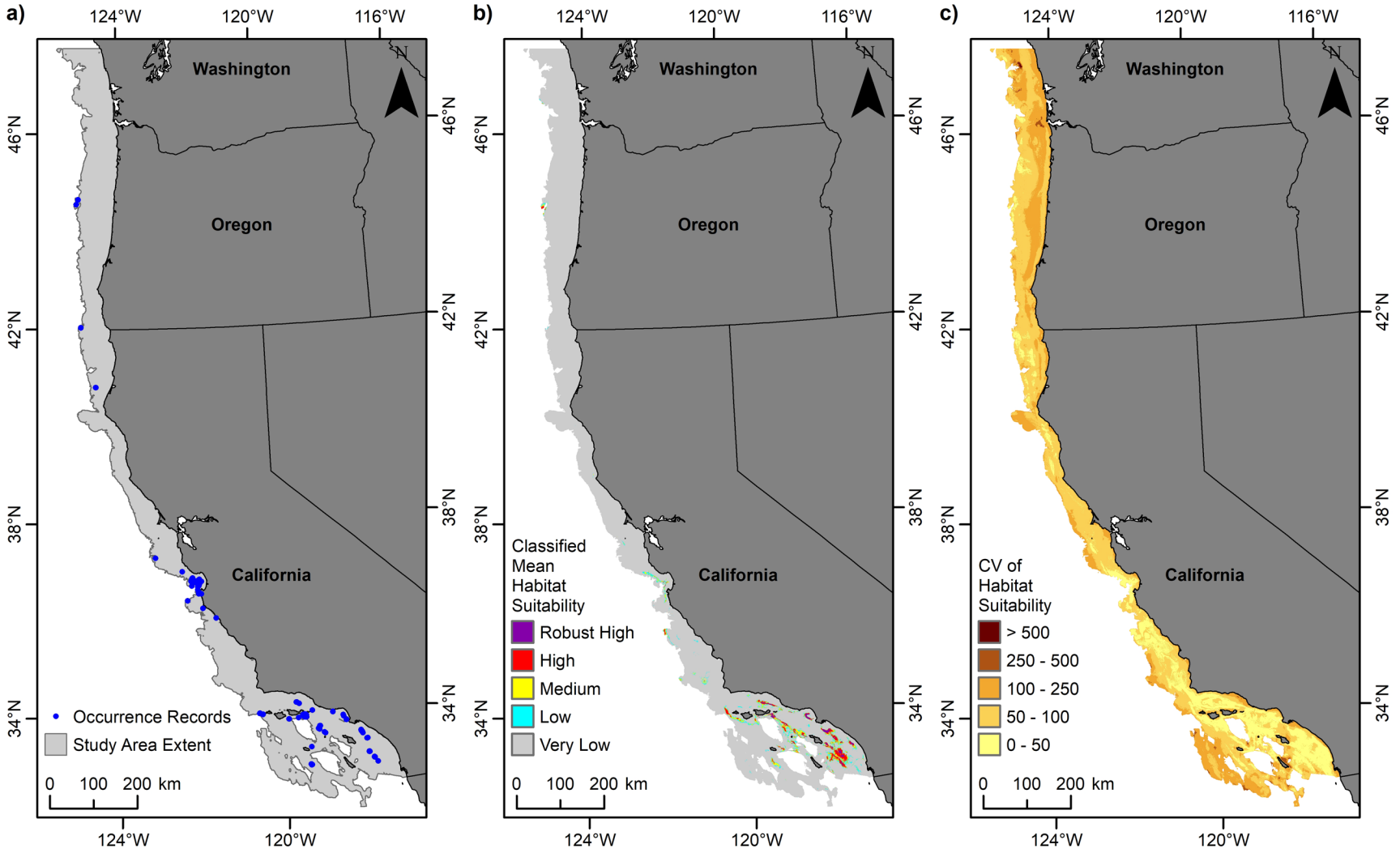

Figure 3.35. Predicted habitat suitability for the demosponge *Asbestopluma* (Poecilosclerida, Cladorhizidae).
(a) Records of *Asbestopluma* occurrence from the NOAA National Database for Deep-Sea Corals and Sponges within the study area offshore to 1,200 m depth; (b) classified mean habitat suitability for *Asbestopluma*; and (c) coefficient of variation of the mean habitat suitability for *Asbestopluma*.

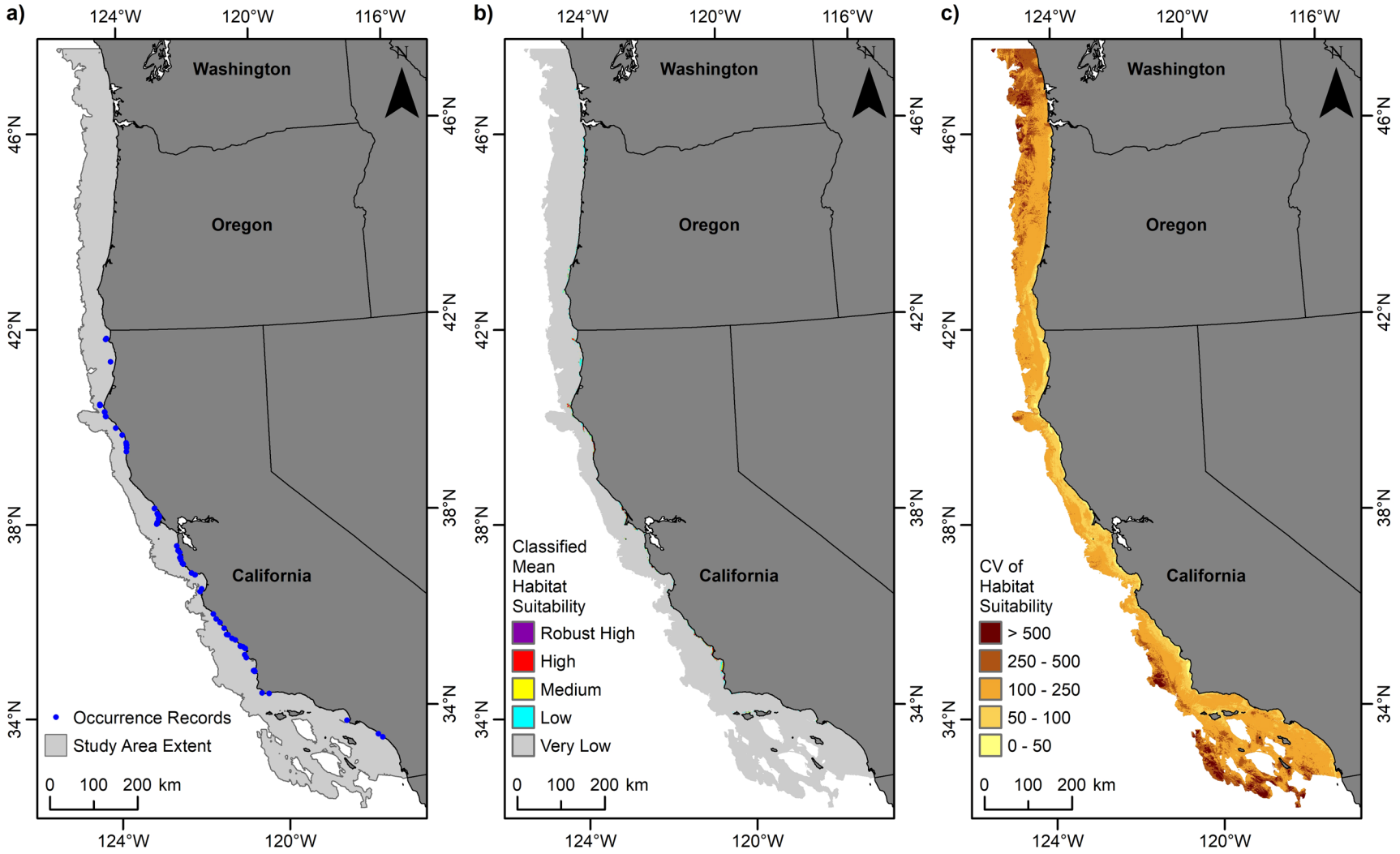

Figure 3.36. Predicted habitat suitability for the demosponge *Craniella arb* (Tetractinellida, Tetillidae).
(a) Records of *C. arb* occurrence from the NOAA National Database for Deep-Sea Corals and Sponges within the study area offshore to 1,200 m depth; (b) classified mean habitat suitability for *C. arb*; and (c) coefficient of variation of the mean habitat suitability for *C. arb*.

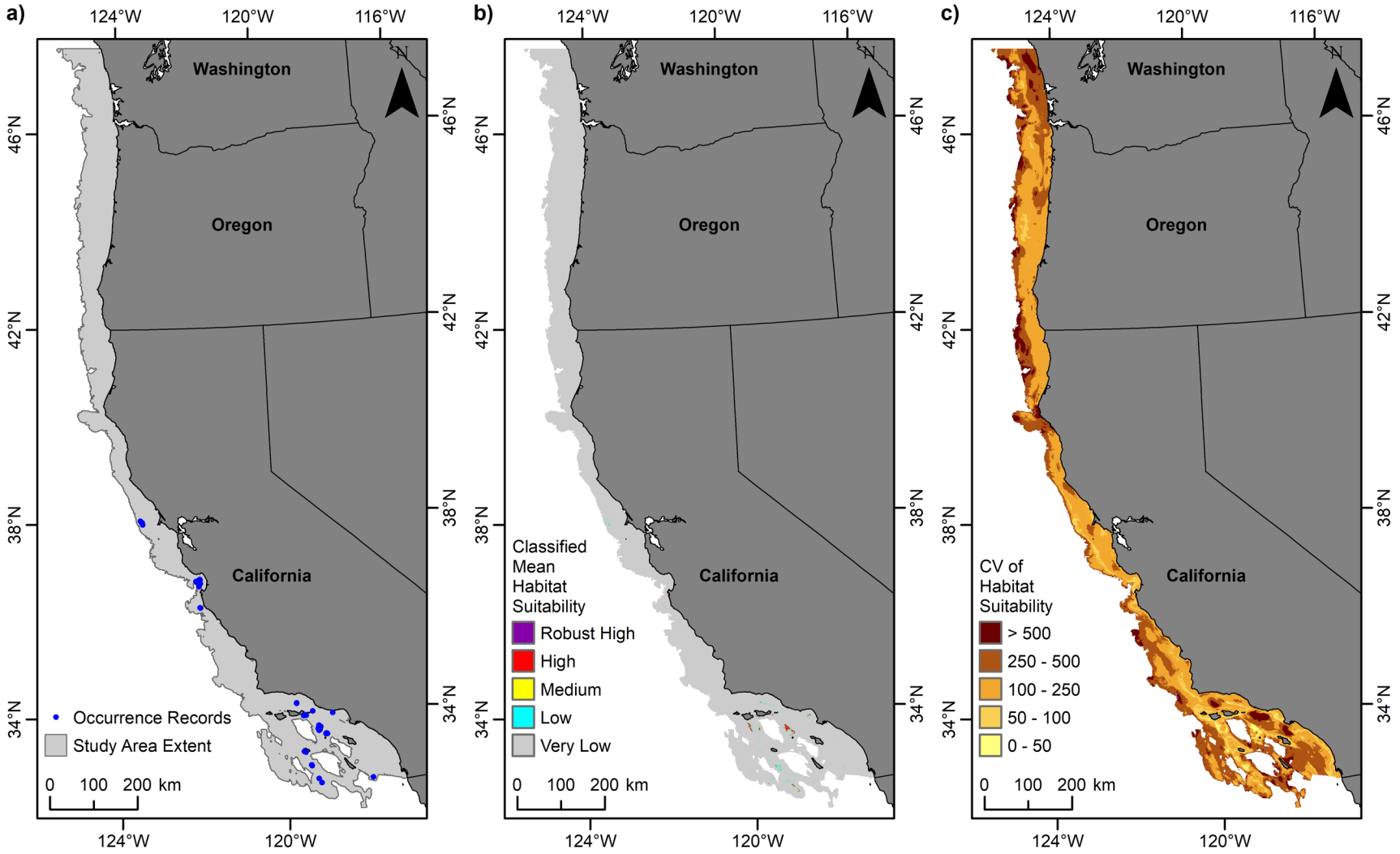

Figure 3.37. Predicted habitat suitability for the demosponge *Haliclona* (Haplosclerida, Chalinidae).
(a) Records of *Haliclona* occurrence from the NOAA National Database for Deep-Sea Corals and Sponges within the study area offshore to 1,200 m depth; (b) classified mean habitat suitability for *Haliclona*; and (c) coefficient of variation of the mean habitat suitability for *Haliclona*.

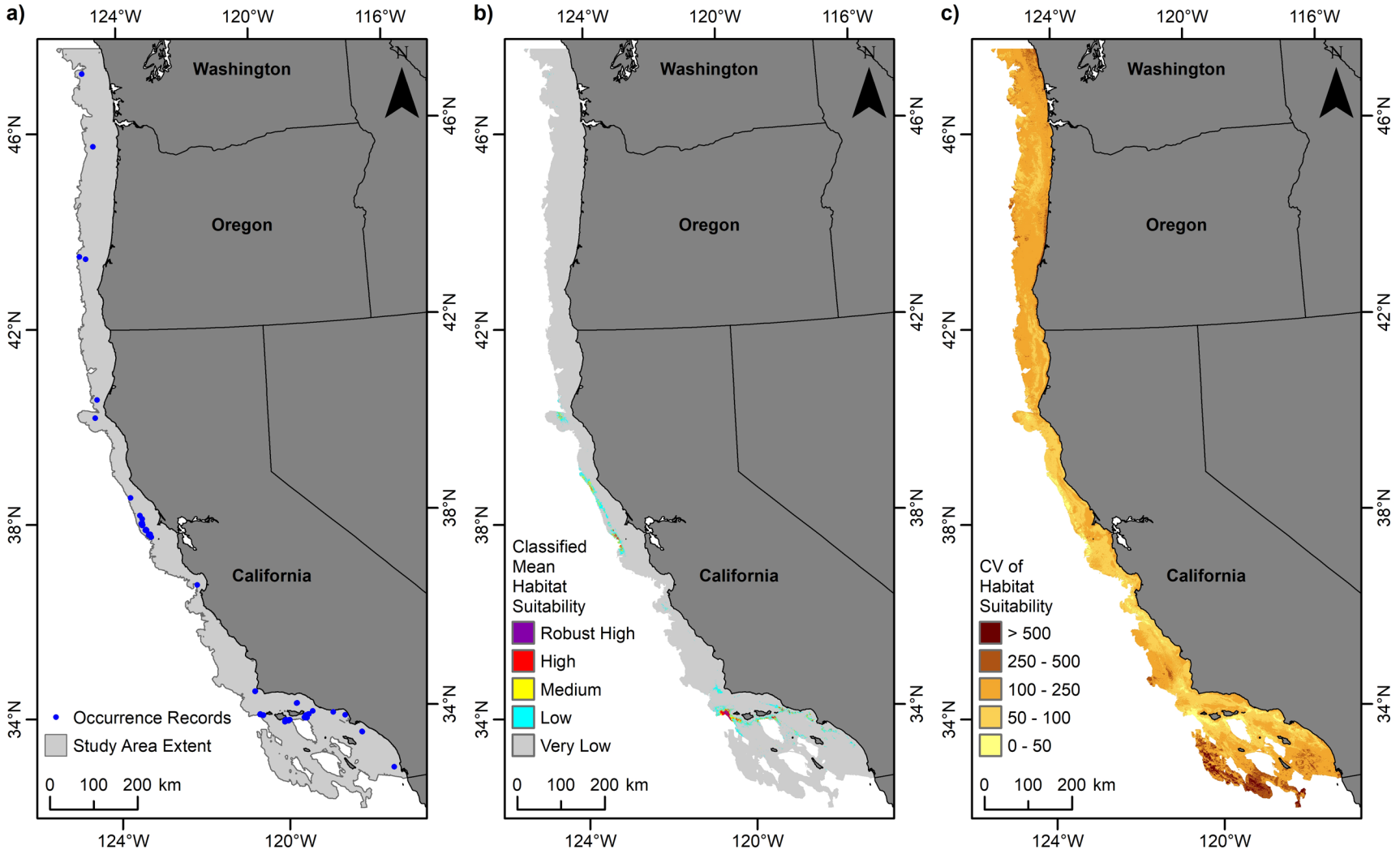

Figure 3.38. Predicted habitat suitability for the demosponge *Mycale* (Poecilosclerida, Mycalidae).
(a) Records of *Mycale* occurrence from the NOAA National Database for Deep-Sea Corals and Sponges within the study area offshore to 1,200 m depth; (b) classified mean habitat suitability for *Mycale*; and (c) coefficient of variation of the mean habitat suitability for *Mycale*.

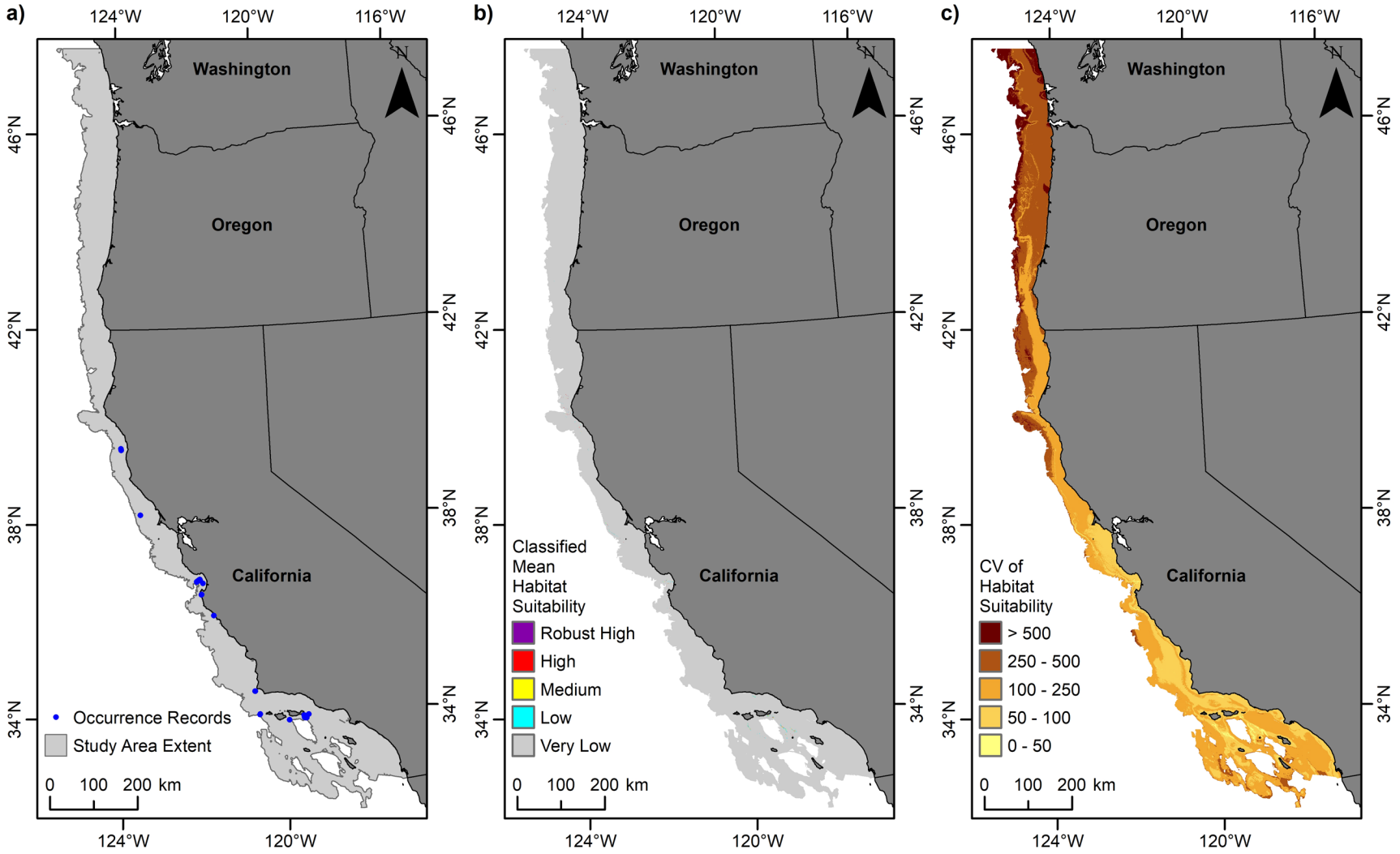

Figure 3.39. Predicted habitat suitability for the demosponge *Polymastia* (Polymastiida, Polymastiidae).
(a) Records of *Polymastia* occurrence from the NOAA National Database for Deep-Sea Corals and Sponges within the study area offshore to 1,200 m depth; (b) classified mean habitat suitability for *Polymastia*; and (c) coefficient of variation of the mean habitat suitability for *Polymastia*.

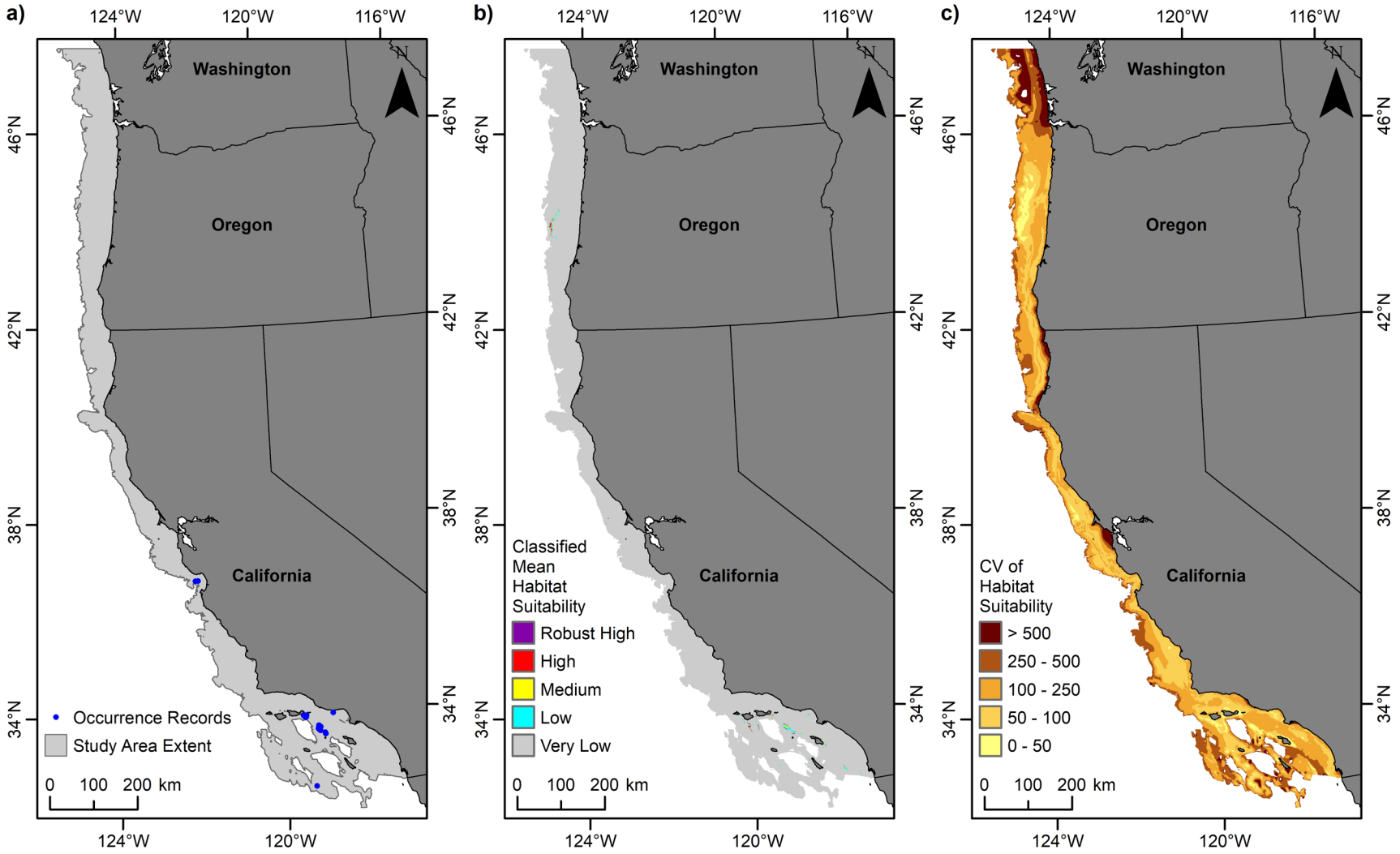

Figure 3.40. Predicted habitat suitability for the demosponge *Rhizaxinella gadus* (Suberitida, Suberitidae).
(a) Records of *R. gadus* occurrence from the NOAA National Database for Deep-Sea Corals and Sponges within the study area offshore to 1,200 m depth; (b) classified mean habitat suitability for *R. gadus*; and (c) coefficient of variation of the mean habitat suitability for *R. gadus*.

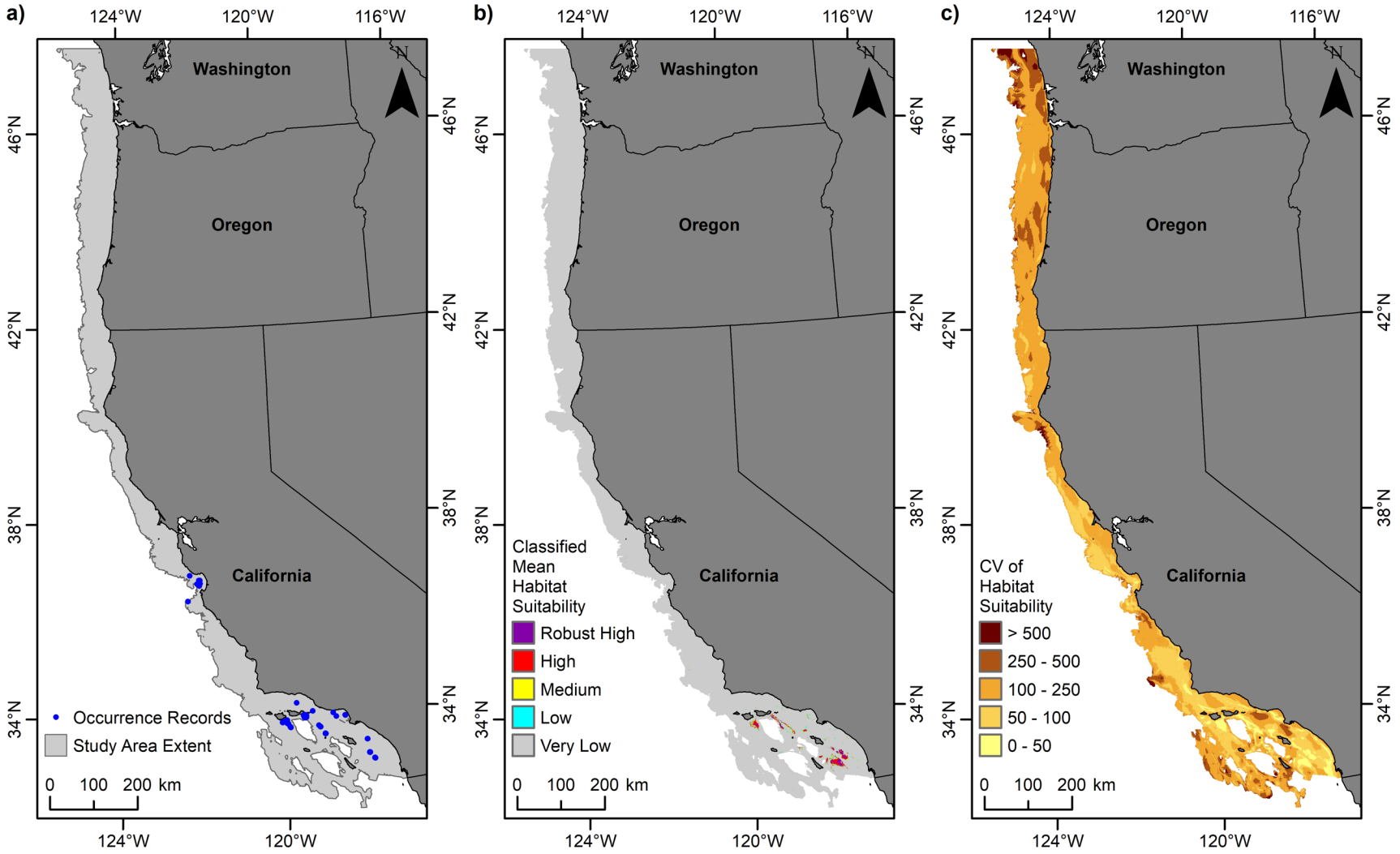

Figure 3.41. Predicted habitat suitability for the demosponge *Thenea* (Tetractinellida, Theneidae).
(a) Records of *Thenea* occurrence from the NOAA National Database for Deep-Sea Corals and Sponges within the study area offshore to 1,200 m depth; (b) classified mean habitat suitability for *Thenea*; and (c) coefficient of variation of the mean habitat suitability for *Thenea*.

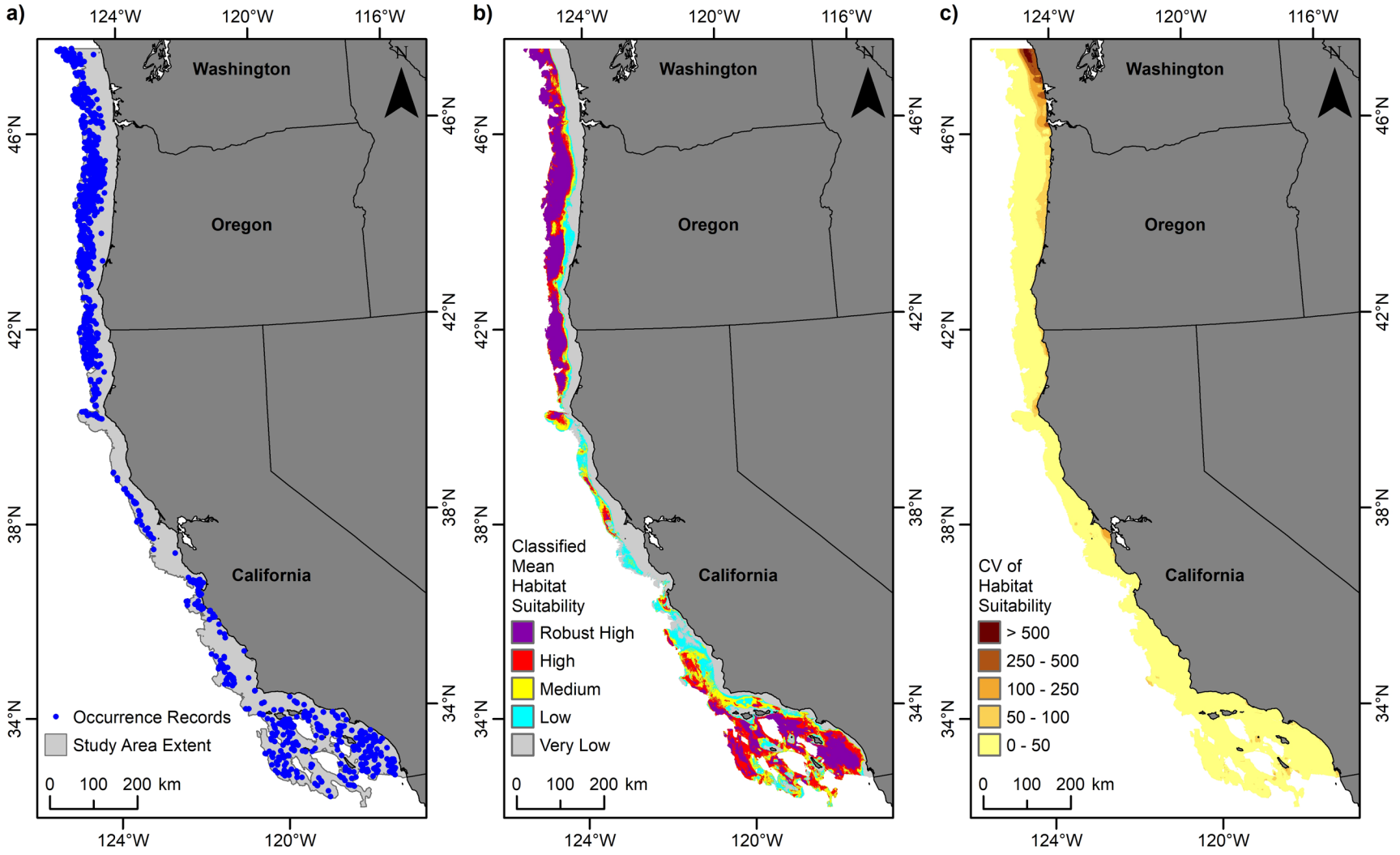

Figure 3.42. Predicted habitat suitability for glass sponges (Class Hexactinellida).
(a) Records of Hexactinellida occurrence from the NOAA National Database for Deep-Sea Corals and Sponges within the study area offshore to 1,200 m depth; (b) classified mean habitat suitability for Hexactinellida; and (c) coefficient of variation of the mean habitat suitability for Hexactinellida.

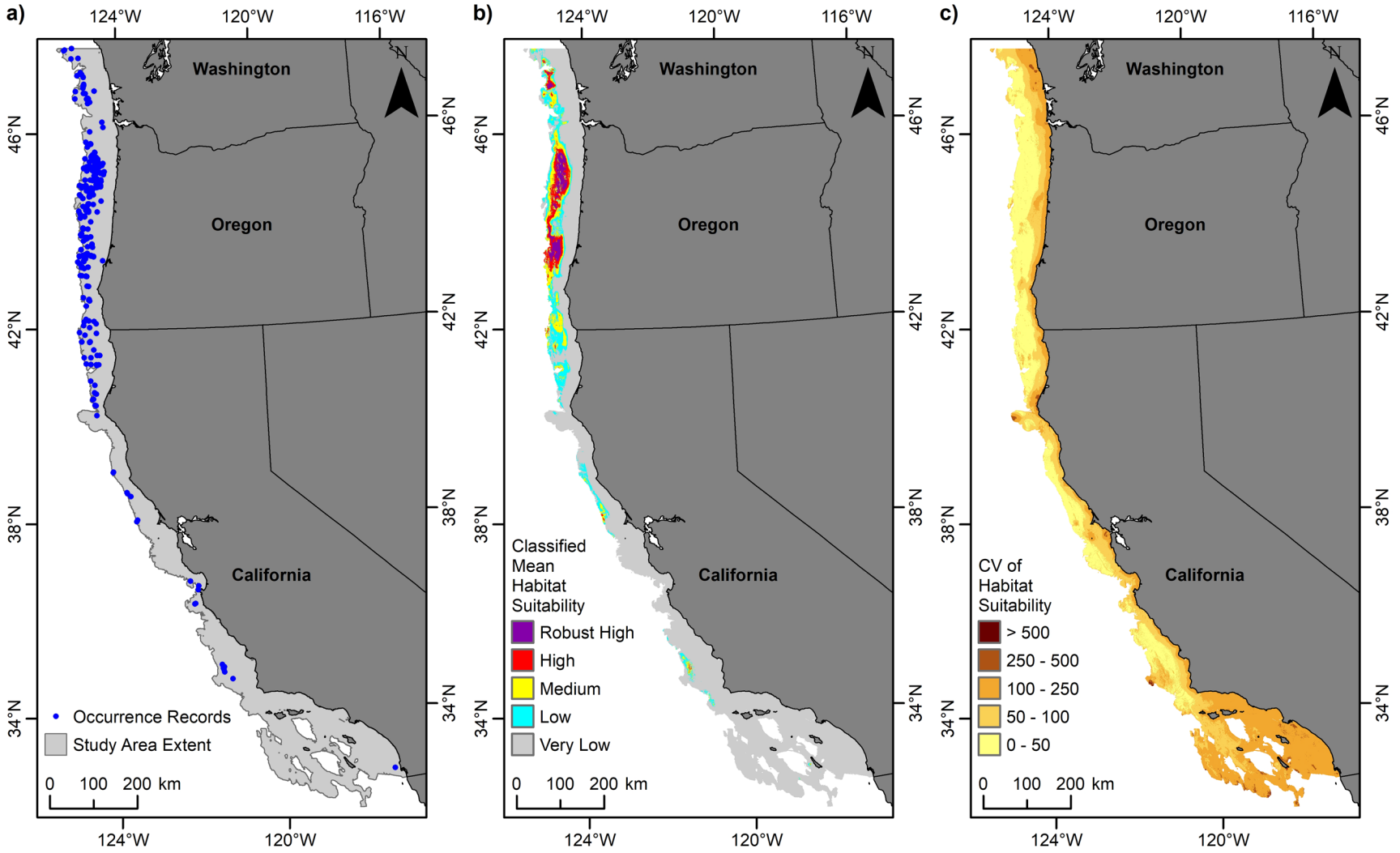

Figure 3.43. Predicted habitat suitability for the glass sponge *Aphrocallistes vastus* (Sceptrulophora, Aphrocallistidae).
(a) Records of *A. vastus* occurrence from the NOAA National Database for Deep-Sea Corals and Sponges within the study area offshore to 1,200 m depth; (b) classified mean habitat suitability for *A. vastus*; and (c) coefficient of variation of the mean habitat suitability for *A. vastus*.

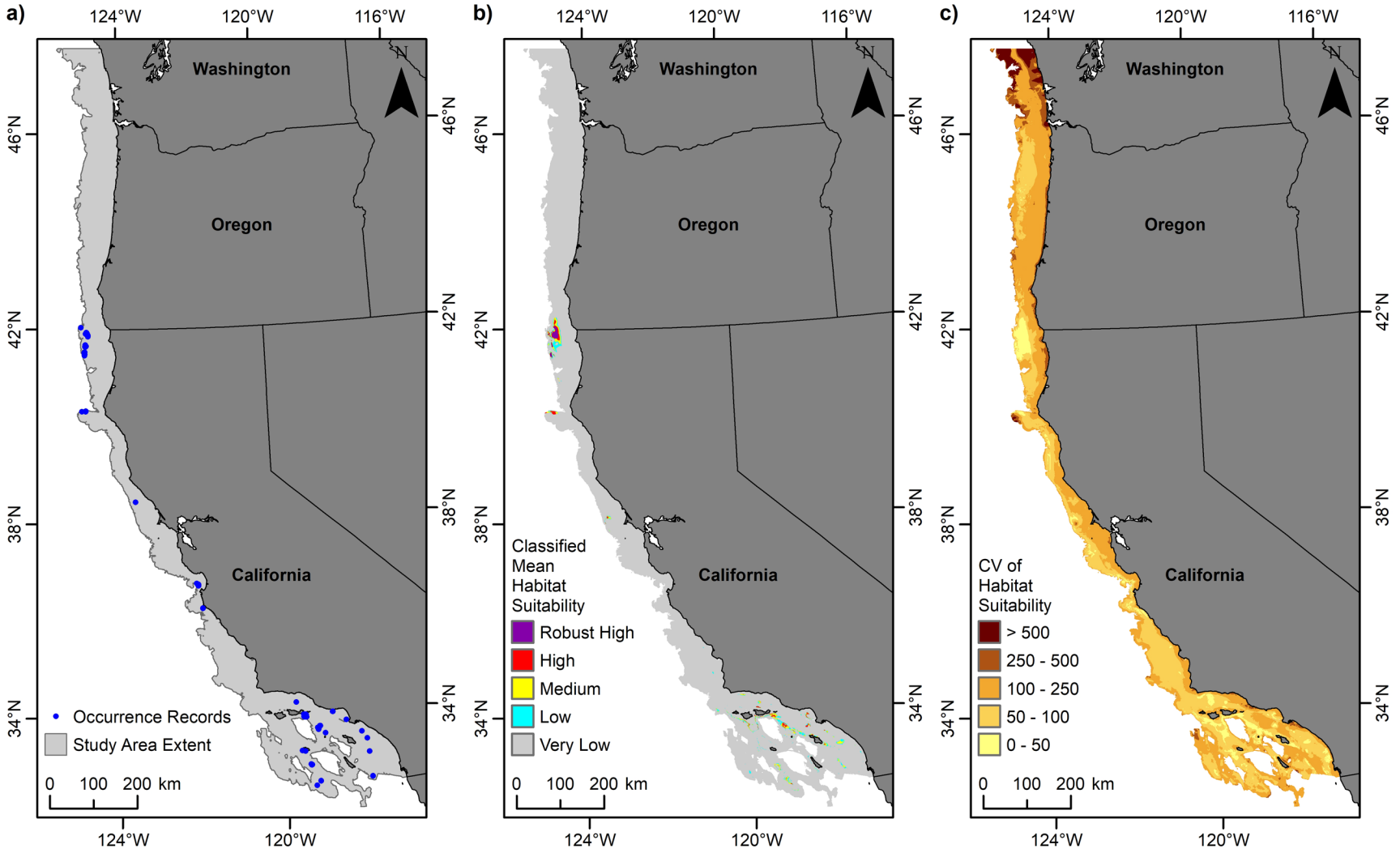

Figure 3.44. Predicted habitat suitability for the glass sponge *Farrea occa* (Sceptrulophora, Farreidae).
(a) Records of *F. occa* occurrence from the NOAA National Database for Deep-Sea Corals and Sponges within the study area offshore to 1,200 m depth; (b) classified mean habitat suitability for *F. occa*; and (c) coefficient of variation of the mean habitat suitability for *F. occa*.

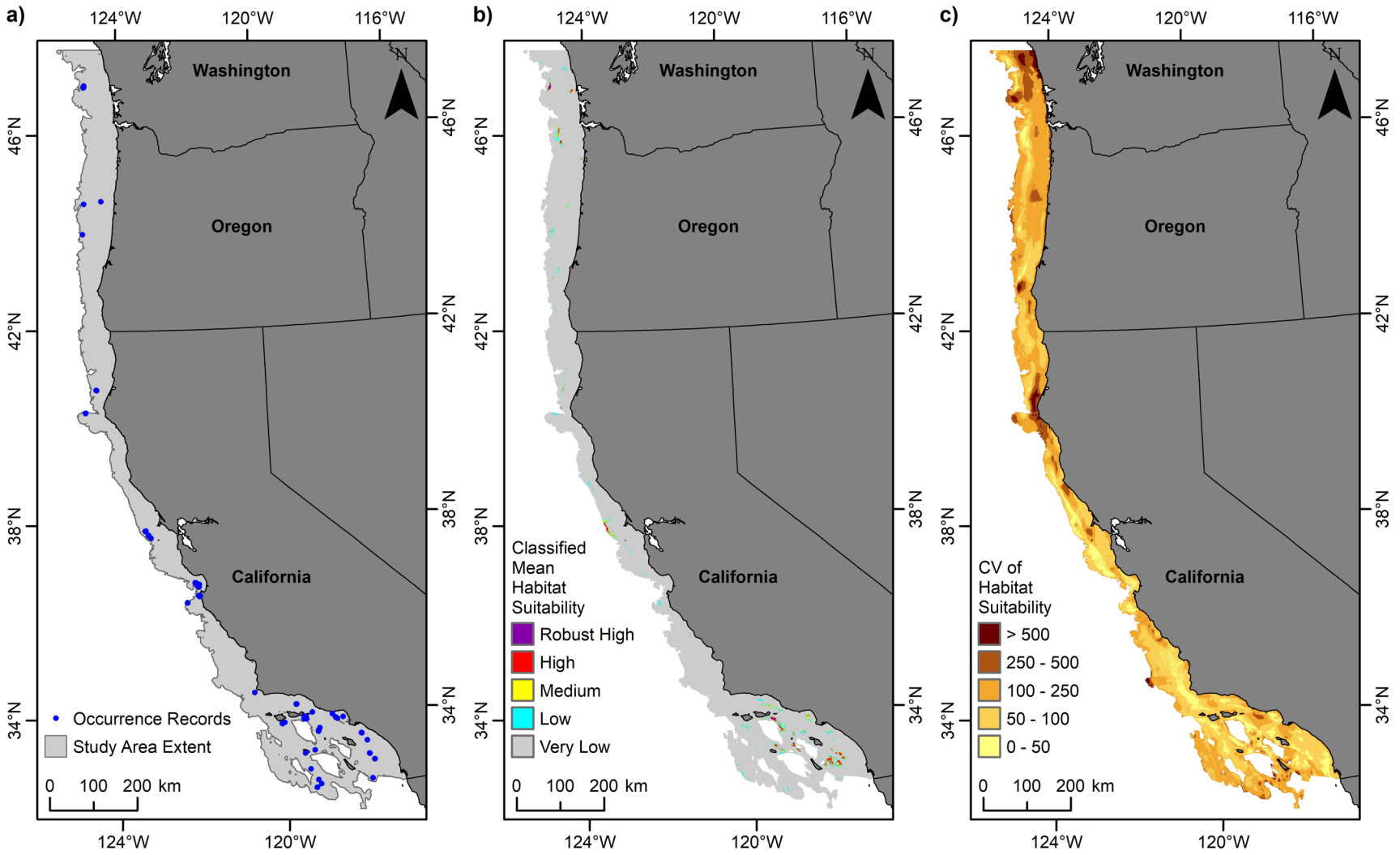

Figure 3.45. Predicted habitat suitability for the glass sponge *Heterochone calyx* (Sceptrulophora, Aphrocallistidae).
(a) Records of *H. calyx* occurrence from the NOAA National Database for Deep-Sea Corals and Sponges within the study area offshore to 1,200 m depth; (b) classified mean habitat suitability for *H. calyx*; and (c) coefficient of variation of the mean habitat suitability for *H. calyx*.

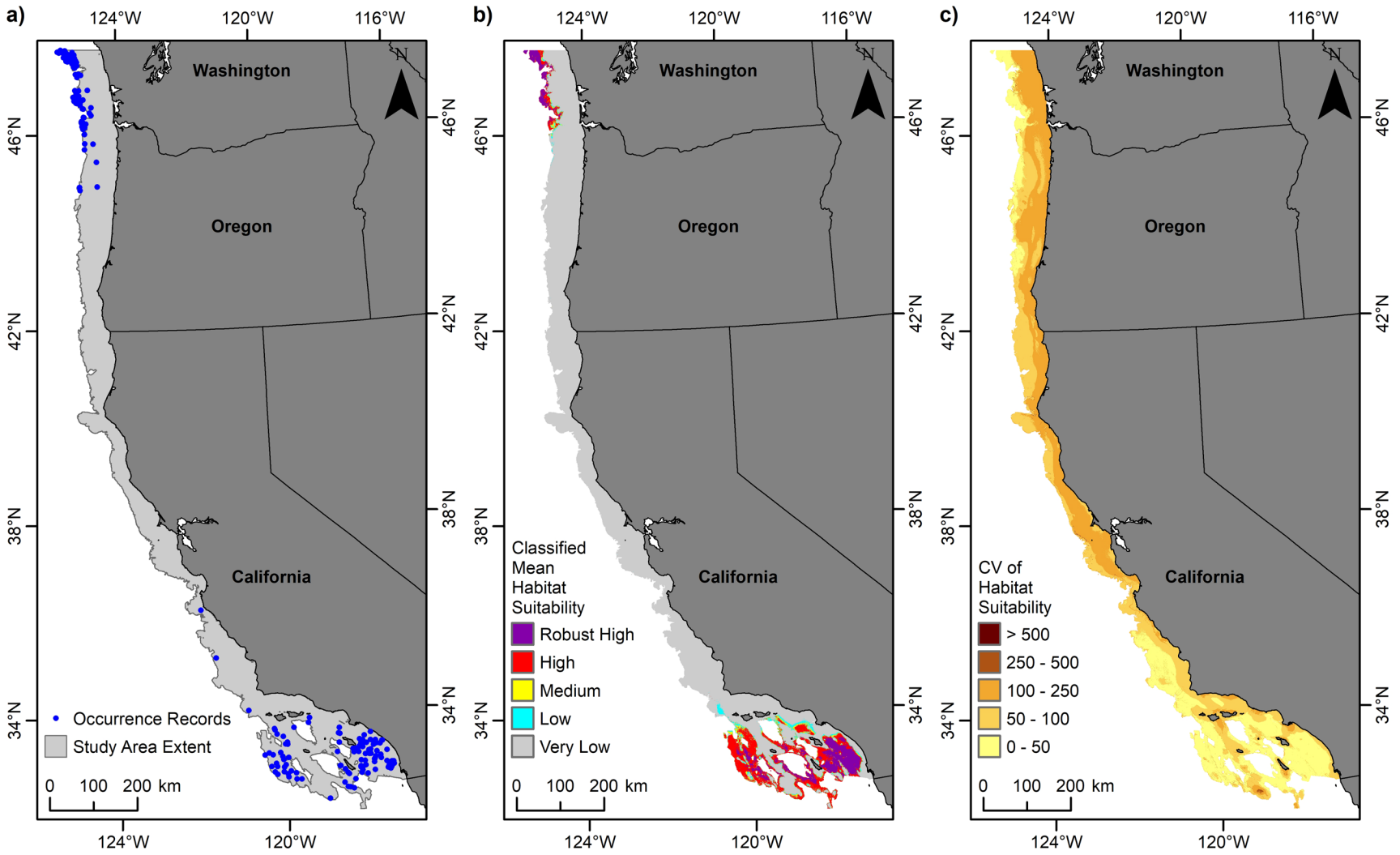

Figure 3.46. Predicted habitat suitability for the glass sponge *Hyalonema* (Amphidiscosida, Hyalonematidae).
(a) Records of *Hyalonema* occurrence from the NOAA National Database for Deep-Sea Corals and Sponges within the study area offshore to 1,200 m depth; (b) classified mean habitat suitability for *Hyalonema*; and (c) coefficient of variation of the mean habitat suitability for *Hyalonema*.

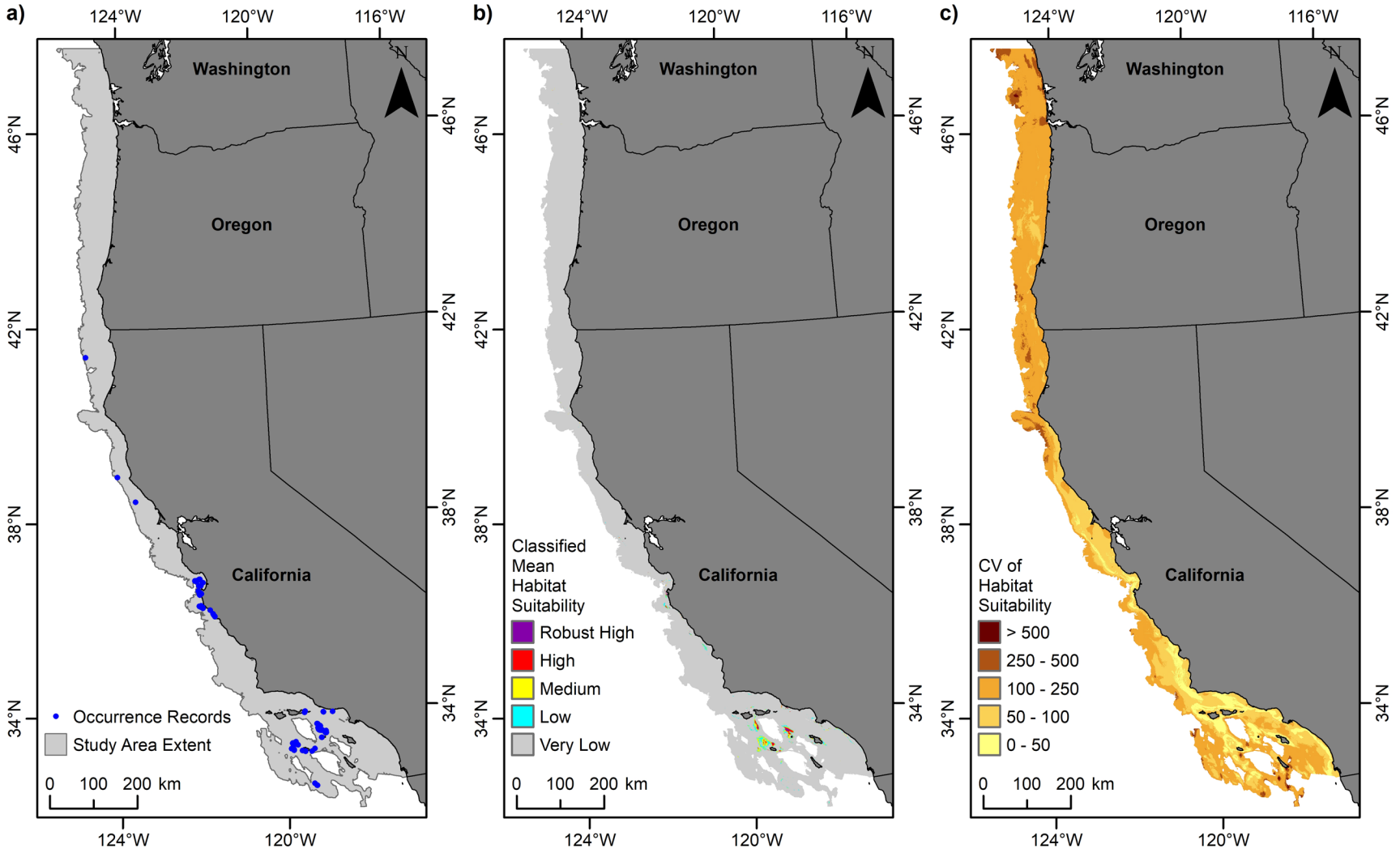

Figure 3.47. Predicted habitat suitability for the glass sponge *Rhabdocalyptus dawsoni* (Lyssacinosida, Rossellidae).
(a) Records of *R. dawsoni* occurrence from the NOAA National Database for Deep-Sea Corals and Sponges within the study area offshore to 1,200 m depth; (b) classified mean habitat suitability for *R. dawsoni*; and (c) coefficient of variation of the mean habitat suitability for *R. dawsoni*.

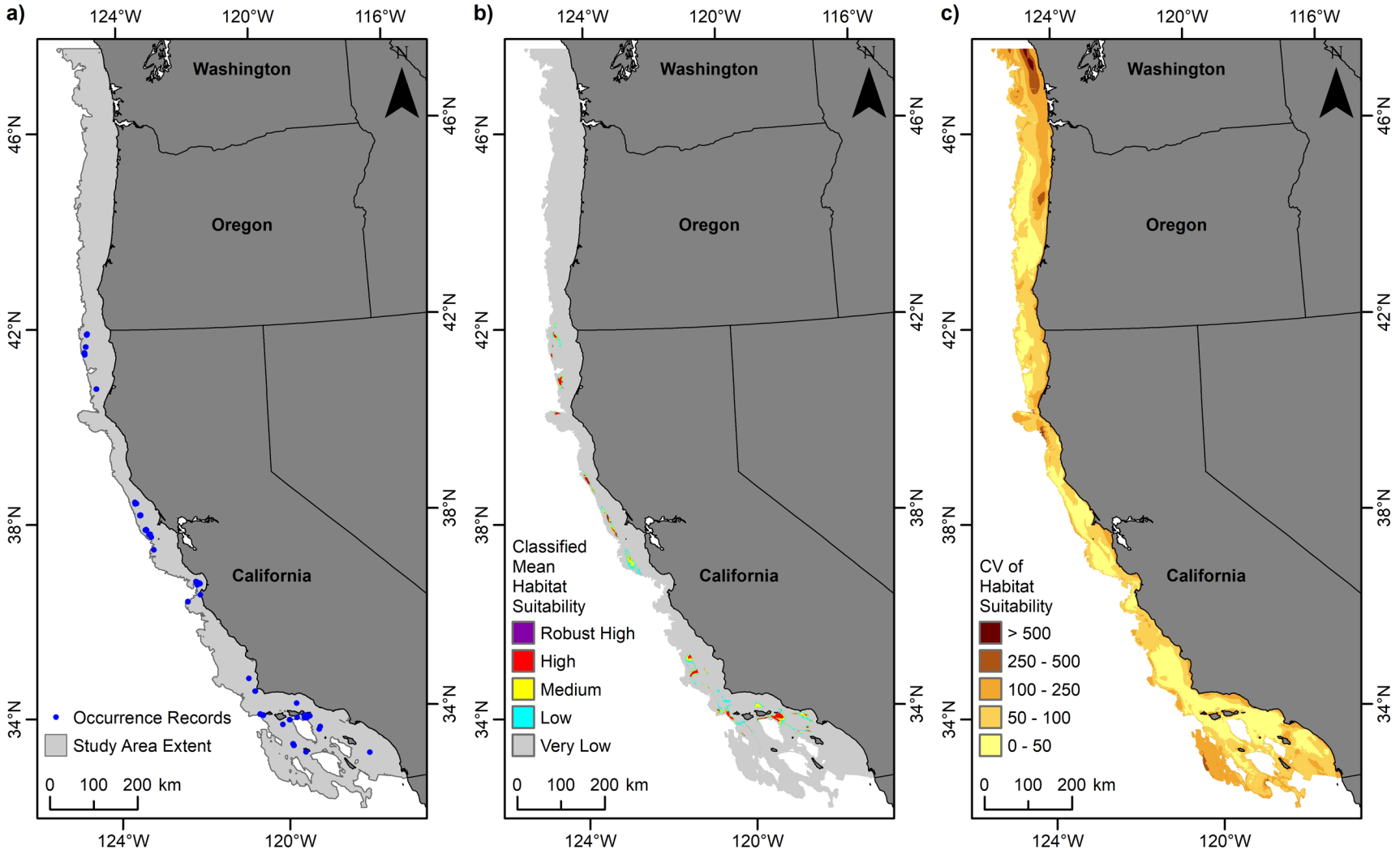

Figure 3.48. Predicted habitat suitability for the glass sponge *Staurocalyptus* (Lyssacinosida, Rossellidae).
(a) Records of *Staurocalyptus* occurrence from the NOAA National Database for Deep-Sea Corals and Sponges within the study area offshore to 1,200 m depth; (b) classified mean habitat suitability for *Staurocalyptus*; and (c) coefficient of variation of the mean habitat suitability for *Staurocalyptus*.

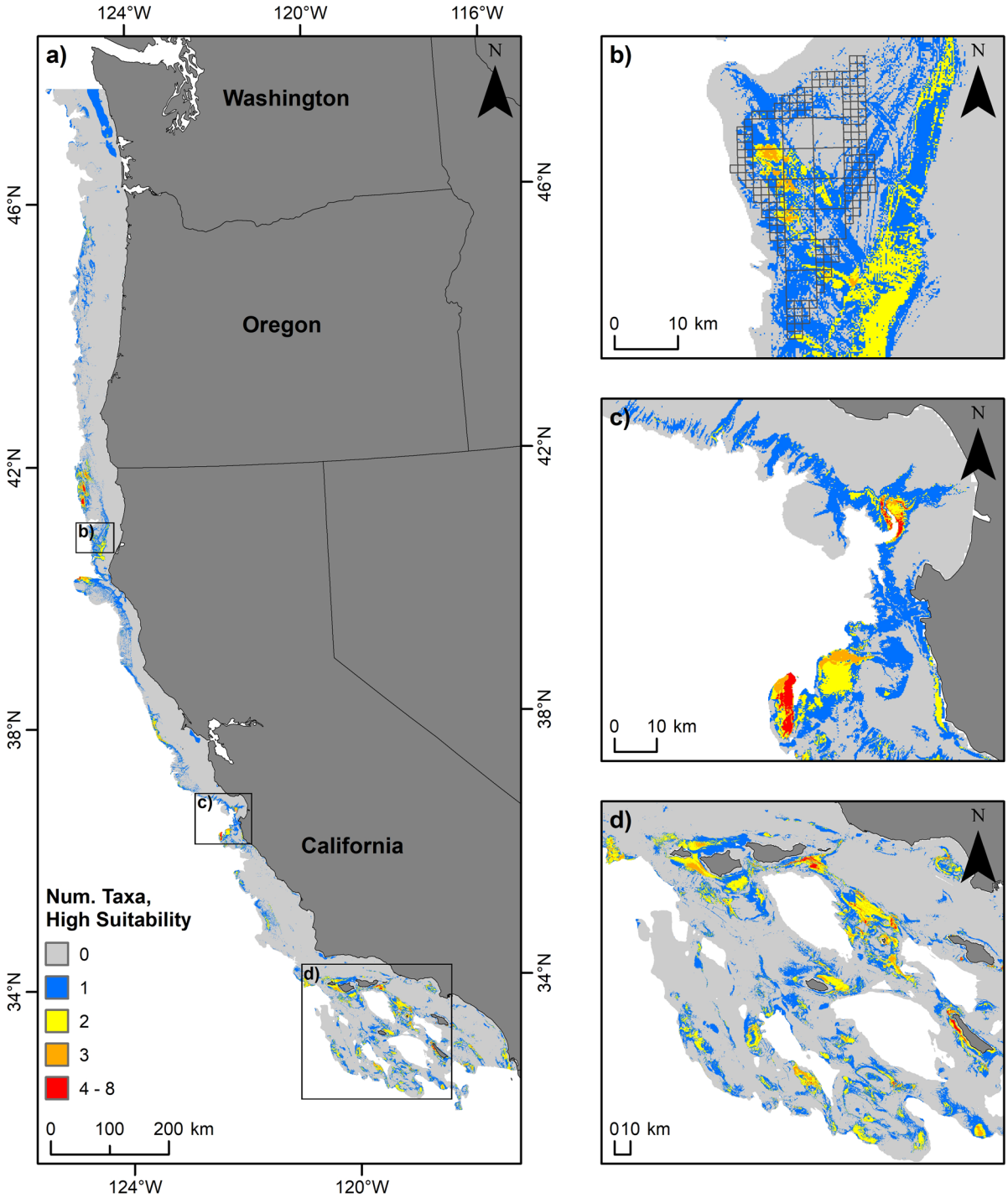

Figure 3.49. Number of deep-sea coral taxa associated with hard substrate that were predicted to have high habitat suitability for a) the entire study area offshore the continental US West Coast to 1,200 m depth, b) a BOEM wind energy planning area (lease blocks depicted with gray lines) offshore of Humboldt County, California, c) Monterey Bay, California, and d) the Southern California Bight.

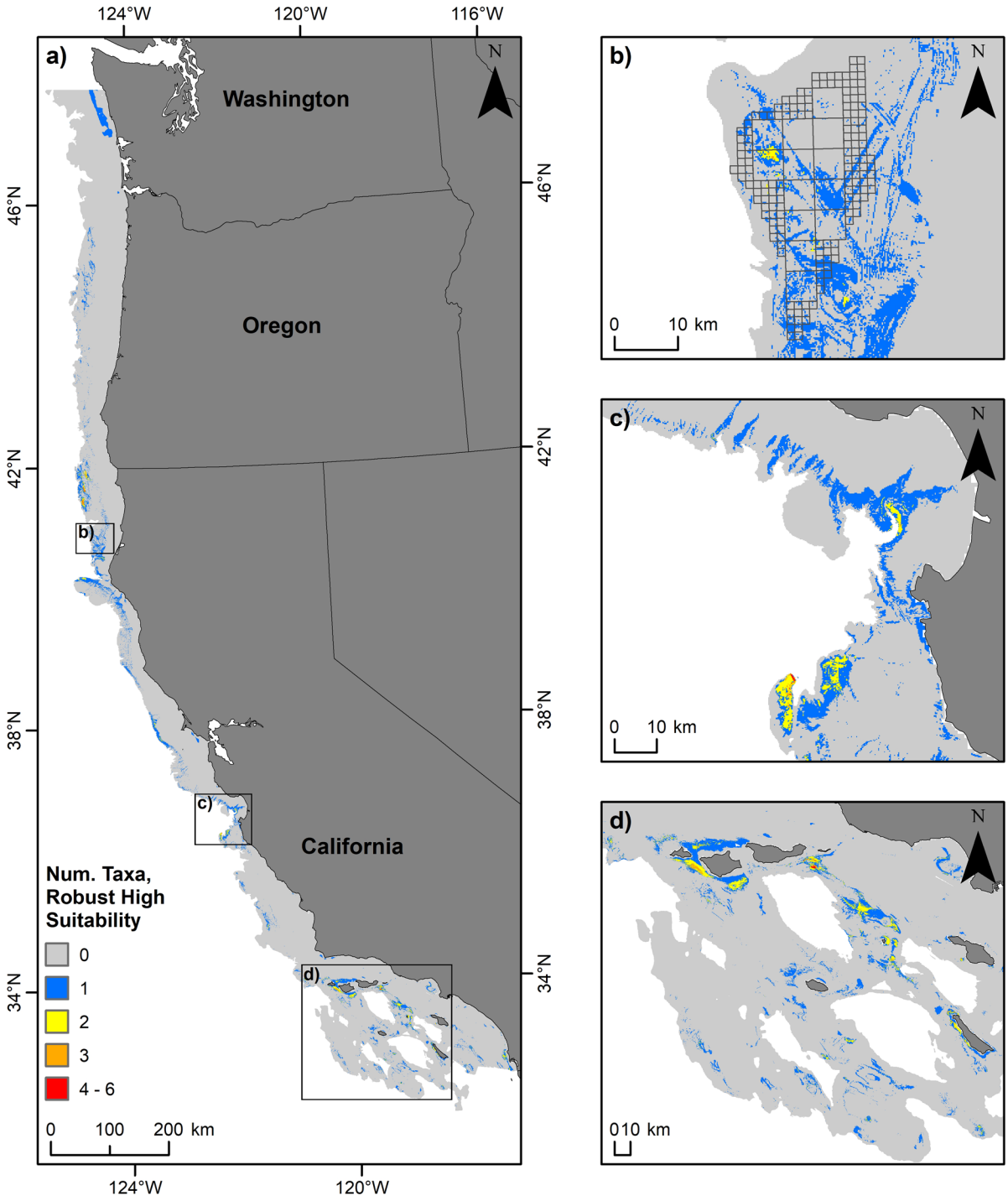

Figure 3.50. Number of deep-sea coral taxa associated with hard substrate that were predicted to have robust high habitat suitability for a) the entire study area offshore the continental US West Coast to 1,200 m depth, b) a BOEM wind energy planning area (lease blocks depicted with gray lines) offshore of Humboldt County, California, c) Monterey Bay, California, and d) the Southern California Bight.

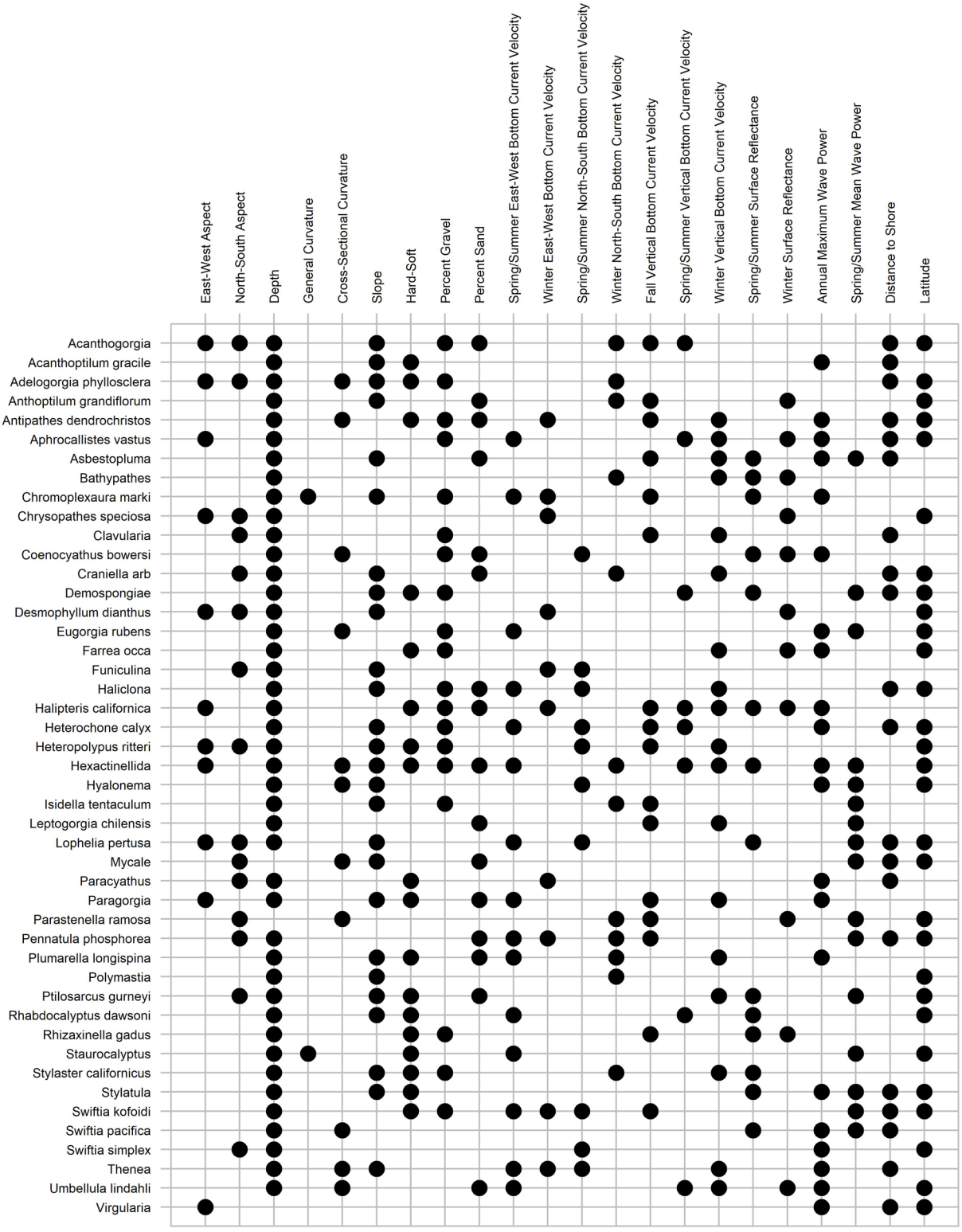

Figure 3.51. Environmental predictor variables in the best model iteration for each DSCS taxon.

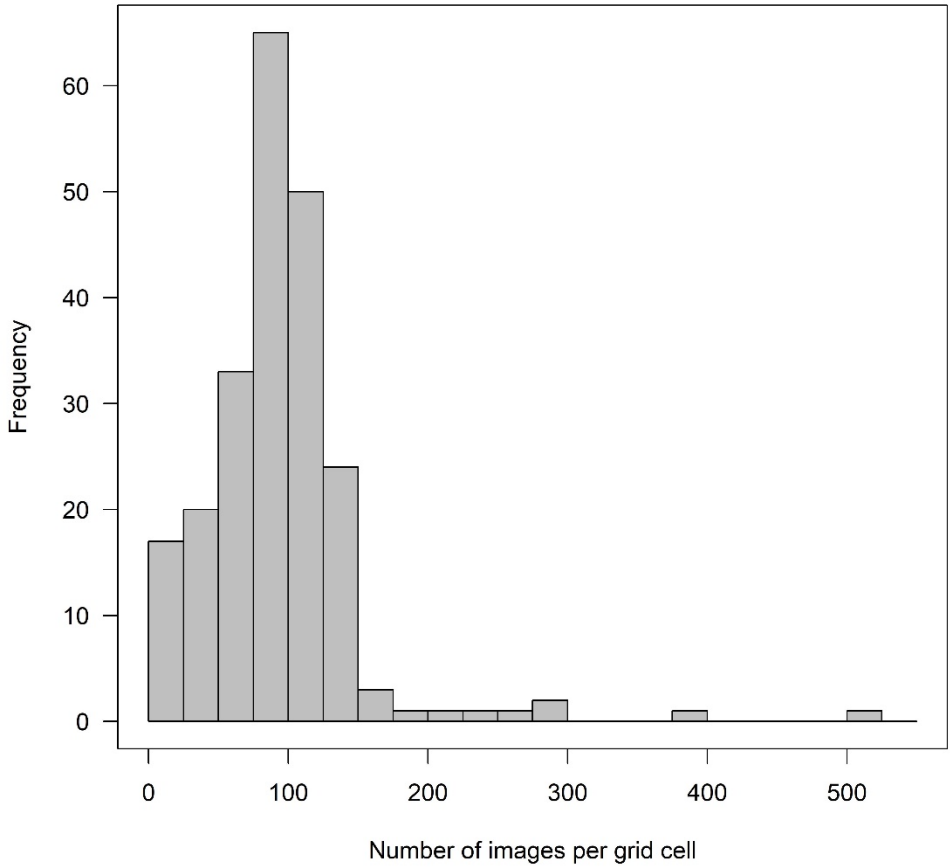

Figure 3.52. Distribution of AUV images across model grid cells.
There were 20,575 total images across 220 grid cells from AUV surveys used in the model validation exercise.

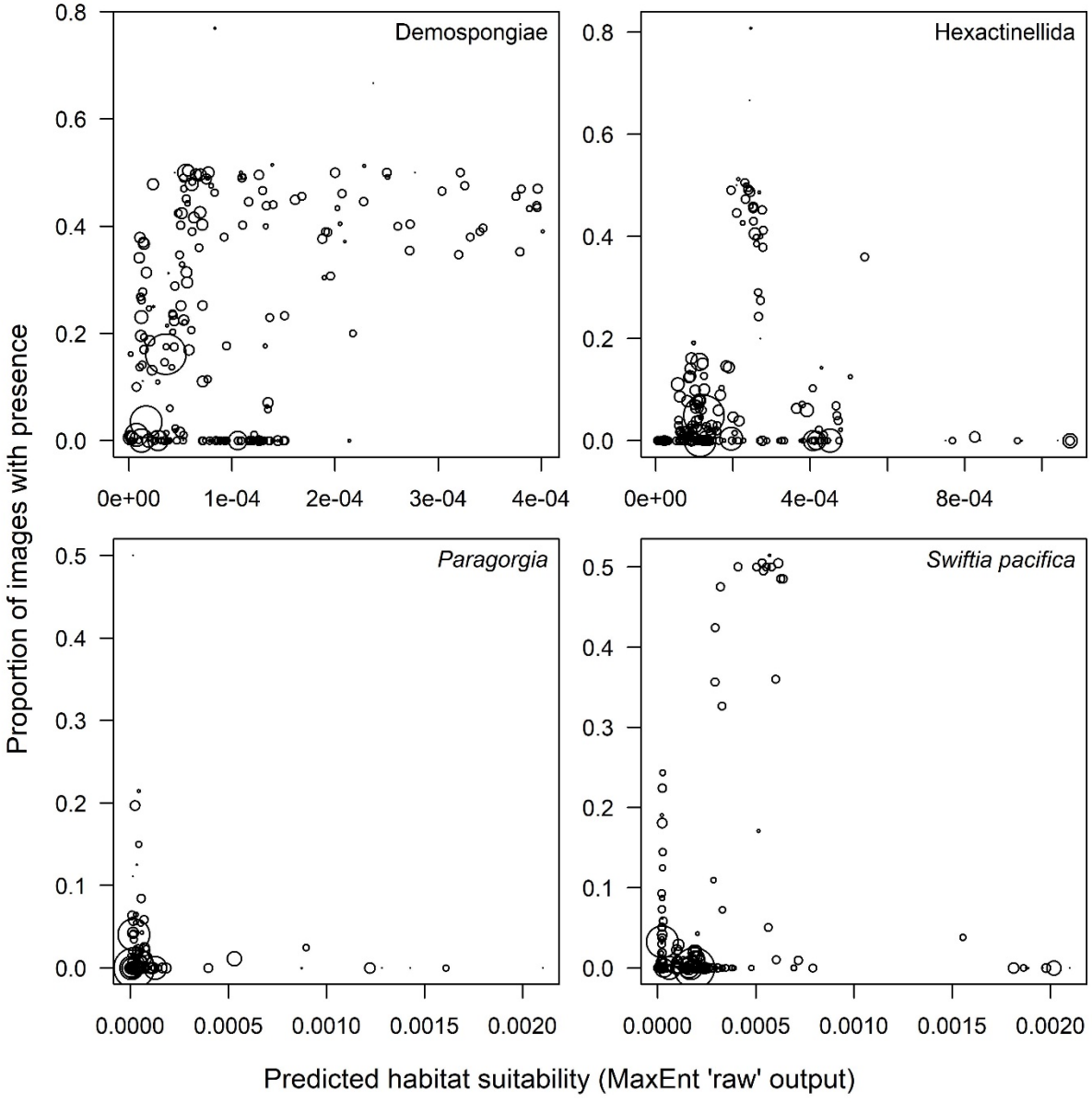

Figure 3.53. Proportion of AUV images with presence for four selected taxa in relation to predicted habitat suitability.
Each data point represents a single study grid cell with ≥1 image (*n* = 220), and the diameter of a data point is proportional to the number of images in that cell.

4 Macrofauna

4.1 Introduction

Benthic macrofauna include a variety of fauna >1 mm in size that live on the seafloor, often in sedimentary habitats. On the continental shelf of the continental US West Coast, predominant macrofauna taxa include polychaete worms and crustaceans with molluscs and echinoderms also present (Henkel and Nelson 2018). Macrofauna assemblages represent the biological community most likely to be directly impacted by offshore energy development as the seafloor habitat directly under the anchors or foundations of renewable energy devices will be lost. Further, the area of impact to benthic organisms could be larger than the direct footprint of these installations. Device components at these installations, and in the case of wave energy devices, energy removal, can change the local hydrodynamics leading to scour or deposition of sediment in the vicinity. Changes to sediment condition may affect the distribution of invertebrate species that are dependent on grain size, near-bottom sedimentation, and particle loads (Etnoyer and Morgan 2003).

In this study, models predicting the probability of occurrence (sometimes referred to as habitat suitability models) were generated for an assortment of selected macrofauna taxa to assist with planning for renewable energy development offshore of the continental US West Coast. A prior analysis of benthic habitat distribution (referenced as Benthic Habitat Characterization BOEM-BHC; Henkel et al. 2014) was motivated by wave energy project proposals in northern California and Oregon. Since that analysis, there has been interest in siting other renewable energy projects in the deeper waters of the continental slope, as well as waters farther south. In response to this increase in geographic scope, the aim of this study was to expand the depth and latitudinal range of habitat suitability models, like those developed in the BOEM-BHC study, by incorporating sampling data from additional survey programs.

Existing habitat maps on the continental shelf and slope primarily distinguish only hard from soft bottom. In areas with higher resolution mapping and ground-truthing, soft sediment habitats are further classified into sub-categories based on the relative portions of sand and mud. Unfortunately, the boundaries between sediment classes have not been defined based on any known correlation with benthic communities, which has hindered consideration of macrofauna in the renewable energy siting process. Therefore, habitat suitability models were developed to understand which species would most likely be impacted by a project sited in a particular place.

Forty-three taxa, primarily at the species level, were selected for modeling. Most of these taxa were chosen based on the results of multivariate statistical analyses to identify taxa representative of macrofauna communities. This chapter describes the data and statistical modeling approach used to produce the models of macrofauna occurrence and presents the results of the models, including maps depicting the distribution of predicted probability of occurrence for each macrofauna taxon modeled. The collection and compilation of macrofauna occurrence data and analyses used to select taxa for modeling are presented in more detail in a separate report funded under BOEM Cooperative Agreement M16AC00014 (Henkel et al. 2020).

4.2 Methods

4.2.1 Macrofauna Survey Data

This section describes the compilation of macrofauna occurrence data from benthic grab samples for use in the macrofauna models. This compilation was funded under BOEM Cooperative Agreement M16AC00014 and included the collection of new samples as well as the incorporation of data from previous sampling programs. Additional details not provided here can be found in Henkel et al. (2020).

Data were obtained from fourteen offshore survey datasets spanning from the California-Mexico border to Grays Harbor, Washington. The datasets were named Benthic Habitat Characterization (BHC), Western Environmental Monitoring and Assessment Program (WEMAP), Ocean Dredged Material Disposal Sites (ODMDS), Humboldt Open Ocean Disposal Site (HOODS), Farallones, San Francisco Public Utility Commission (SFPUC), MCI Communications, Central Coast Long-term Environmental Assessment Network (CCLEAN), NOAA-MLML, Morro Bay, PacWave, Oregon Wave Energy Trust (OWET), OSU-BOEM, and SCCWRP (Table 4.1). In total, the datasets included records from 2,905 stations within the study area ranging from 3 to 1,023 m deep (Figure 4.1). All records contained macrofauna abundance (i.e., count) data, station location, and depth. Additional measures (e.g., sediment composition) were available for some or all of the records but were not used in the models of macrofauna occurrence.

Samples from OSU's Henkel Laboratory projects span the northern portion of the study area from Fort Bragg, California, to Grays Harbor, Washington and were collected between 2010 and 2016. In addition to the OSU-BOEM dataset collected under BOEM Cooperative Agreement M16AC00014 and the BOEM-funded BHC dataset (Henkel et al. 2014), the Henkel lab also provided many of the other datasets from the northern portion of the study area. This included the PacWave dataset collected in and around the PacWave facilities operated by OSU's Pacific Marine Energy Center and from a project off Reedsport and Coos Bay, Oregon, funded by the OWET. The US Environmental Protection Agency (EPA) conducted an Environmental Monitoring and Assessment Program survey on the shelf in 2003 (Nelson et al. 2008). These data are available for download from the EPA National Coastal Assessment's Coastal Data Search Engine (EPA NCA 2016). The 2003 data for California (north of Point Conception), Oregon, and Washington were included in the MS Access database developed by the Henkel lab and are referred to here as the WEMAP dataset. The ODMDS dataset included monitoring data from Oregon and was obtained directly from the US Army Corps of Engineers (USACE), facilitated by previous collaborative projects between Henkel and USACE/EPA. The SCCWRP dataset was provided by David Gillett and included macrofaunal samples collected as part of the SCB Regional Monitoring Program (Schiff et al. 2016) beginning in 1994 and conducted approximately every five years thereafter.

To fill the gap in spatial coverage between the SCCWRP dataset in southern California and the datasets for the northern part of the study area in the Henkel lab data holdings, additional data were incorporated from previous sampling programs carried out by various entities in central and northern California. The MLML Benthic Lab provided the MCI, CCLEAN, and NOAA-MLML datasets. The SFPUC and HOODS datasets were provided by Walt Nelson, former Assistant to the Division Director of the Western Ecology Division of the EPA. The Morro Bay dataset included shallow water station data and were obtained from the City of Morro Bay and Cayucos Sanitary District Offshore Monitoring and Reporting Program (Marine Research Specialists 2016).

All data from north of Point Conception were entered into a Microsoft Access database and a 'taxon reduced' query was created from the various datasets. Because projects often had different spellings for the same animal (e.g., *Acteocina* sp. vs *Acteocina* spp vs *Acteocina* spp.) over 3,000 unique taxa were generated. Sometimes different scientific names were used, including older names no longer recognized as valid by the scientific community. Additionally, there were many misspelled entries and common names were occasionally used. In some instances, the stage of the animal was included in the text (e.g., Aeolidiacea sp. Juv.), and there were other name differences making merging the datasets difficult. Therefore, a secondary column was created and used in a query to aggregate all the similar species together. The World Register of Marine Species (WoRMS Editorial Board 2019) was used to cross check species names and select valid species names. In some instances, it was not possible to determine what the animal was at the species level and a taxon name was chosen at the finest possible level (e.g., Cuke-like Anemone became *Actiniaria* sp). It was from this query 'Total Taxon Reduced' that all data were pulled for the statistical analyses described below in Section 4.2.2.

4.2.2 Selection of Macrofauna Taxa for Modeling

Multivariate statistical analyses were conducted using the compilation of macrofauna occurrence data to help identify candidate taxa (primarily species) for macrofauna models by determining which taxa contributed most to similarities within and differences between groups of sampling stations. Analyses were performed using PRIMER v6 (Clarke and Gorley 2006). Additional details of the analysis methods and results not provided here can be found in Henkel et al. (2020).

Data were first subset to include only surveys that used 1.0 mm mesh size (the majority of the available data). This subset also used only data from 2003 from the SCCWRP dataset, as those data were temporally consistent with the rest of the samples from the WEMAP dataset, which was the major source of station data for central and northern California (Nelson et al. 2008). Using all the years of data in the SCCWRP dataset collected in essentially the same area would skew the selection of taxa to those found in southern California. After subsetting, the remaining dataset included abundance data from 1,483 sampling stations.

A cluster analysis was conducted using a similarity profile routine (SIMPROF; Clarke et al. 2008) set at the 1% significance level to determine statistically significant groups of the 1,483 stations. A similarity percentages (SIMPER) analysis was then performed to determine which taxa contributed to the similarities within groups and differences between them (Clarke and Gorley 2006).

The cluster analysis with a SIMPROF threshold of 1% resulted in 303 significantly different groups of sampling stations. There were 147 significant groups detected in the Pacific Northwest (Oregon and Washington), 29 groups in northern California (above Point Conception), and 127 groups in southern California (the SCCWRP data). The results of the SIMPER analysis were analyzed by determining the number of times each taxon was indicated as being a significant contributor to the similarities within groups overall and within each ecoregion (Oregon/Washington, northern California, the SCB). Taxa that were frequent contributors were selected as potential candidates for modeling. However, taxa that were significant contributors to the similarities within groups for only one ecoregion were only considered for modeling if there was additional evidence that their presence-absence contributed to differences among habitats within that region (and were not just defining the region). Additional taxa were then considered if they were frequently significant contributors to the similarities within or frequent distinguishers between the 12 major habitat groups determined by Henkel et al. (2020, Chapter 3). These taxa were added separately because they included taxa that were discriminating on the slope, where there was little coverage in the remainder of the study area and thus would not be identified as a frequently characteristic taxon in the coastwide analysis. Because samples were biased to the northern part of the region, when one species in a genus was a frequent distinguisher in the north and a conspecific was more common in the south, the southern conspecific was added to the list of taxa to be modeled. Species that had a p-code pollution tolerance score of less than 30 in the SCCWRP database were also prioritized, favoring species that were representative of non-impacted conditions (for the p-codes, a higher number indicates greater tolerance to pollution; Smith et al. 2001). Finally, if not already included, taxa that were previously modeled (Henkel et al. 2014) were added in order to compare model outputs between model approaches.

The frequency of occurrence of each of the selected taxa was checked to ensure there were enough occurrences (not just large abundances at a few stations) to be useful for modeling. In order to be considered for modeling, the target standard was a minimum of 10% occurrence in the northern study region; however, this was not always possible for slope species as the number of slope samples was low relative to the entire dataset. While the initial lists of potential model taxa were derived based only on the 1 mm mesh sieve studies, occurrence data was based on all the datasets.

As a result of the selection process, forty-three macrofauna taxa were chosen for modeling (Table 4.2). Polychaetes were the most frequent taxonomic group considered to be characteristic of and/or distinguishing between macrofaunal assemblages, and 23 taxa of polychaetes were initially selected for modeling. Taxonomic changes over the course of the sampling efforts resulted in some suspected synonyms being lumped together. Consequently, 21 polychaete taxa were modeled. Molluscs were the second most frequent characteristic/distinguishing taxa. Eight bivalves, three gastropods, three scaphopods, and the caudofoveatan *Chaetoderma argenteum* (which was a slope distinguishing species) were selected for modeling. The most frequently overall characteristic species (contributing to the similarity of the stations within a group) was the ubiquitous bivalve *Axinopsida serricata*, which was characteristic in 95 of the 303 groups. Thus, while widespread, it was expected that models would predict some unsuitable habitat for this species as it was not found to be highly characteristic of all macrofaunal assemblages. Only three crustacea were determined to be highly characteristic of assemblages or distinguishing among them: the mud-tolerant shelf amphipod *Ampelisca careyi*, the highly abundant pea crab *Pinnixa occidentalis* complex, and the ostracod *Euphilomedes carcharodonta*. Three echinoderms were also determined to be highly characteristic of assemblages or distinguishing among them: two ophiuroids and the heart urchin *Brisaster latifrons*, which was indicative of the outer shelf and slope with the smallest grain sizes. Finally, phoronids were included as a single model group as they discriminated deep slope stations off Oregon and were found to be characteristic across all three ecoregions.

4.2.3 Environmental Predictor Variables

As described in Chapter 2, an initial set of 66 environmental predictor variables were generated on the 25 x 25 m model grid for use in the macrofauna models. A pairwise correlation analysis was performed on the environmental predictor variables to identify and remove predictor variables that were highly correlated (Spearman rank correlation coefficient $|\rho| > 0.7$) with each other. This resulted in a set of 23 environmental predictor variables that were used in the models of macrofauna occurrence (Table 4.3).

4.2.4 Statistical Modeling Framework

4.2.4.1 Overview

A statistical modeling framework using boosted regression tree (BRT) models was implemented to identify areas within the study area that are most likely to contain habitat for the selected macrofauna taxa. Although abundance data were available for each sampling station, initial models fit to the abundance data performed poorly. Therefore, the models generated in this study were presence-absence models. These models related the occurrence (presence-absence) of each macrofauna taxon at each sampling station to the spatial environmental predictor variables and used these estimated relationships to predict the probability of occurrence across the entire study area (i.e., for each model grid cell, the probability of the taxon being observed in a sample taken in that grid cell).

In tree-based models, the relationships between the response variable and the predictor variables are estimated using a series of binary splits on the predictor variables that partition the data into groups that are as homogeneous as possible in terms of the response variable (Breiman et al. 1984, De'ath and Fabricious 2000). Tree-based approaches are particularly useful for the analysis of ecological data because they are able to incorporate nonlinear relationships and high-order interactions among the response and predictor variables (De'ath and Fabricious 2000). BRT models improve model predictive performance compared to single decision tree models by using a machine learning approach called boosting. In this approach, a large number of tree models are fit stagewise (i.e., after each tree model is fit, the next model is fit using the residual variation in the response variable) and then combined to create a final model (Freidman 2002, De'ath 2007, Elith et al. 2008).

This section describes the methods for each stage of the modeling framework: data preparation, model fitting and model selection, spatial prediction, and evaluating model performance (Figure 4.2).

4.2.4.2 Data Preparation

Abundance data were converted to presence-absence values. Values of the environmental predictor variables were extracted at the locations of the sampling stations. For each macrofauna taxon, data were randomly divided into subsets for model training and model testing such that the model training subset contained 70% of the presence data and 70% of the absence data and the model test subset contained 30% of the presence data and 30% of the absence data. The model training data were used to fit the BRT models. The model test data were withheld from model fitting and spatial prediction, and were used only to evaluate model performance.

4.2.4.3 Model Fitting

BRT models can accommodate different types of response variables through the selection of an error distribution (De'ath 2007, Elith et al. 2008). The response variable in this study, the presence or absence of a given macrofauna taxon, was modeled using a binomial distribution.

Similar to the MaxEnt models described in Chapter 3, BRT models use regularization to avoid fitting overly complex models that are fit too closely (i.e., overfit) to the data used to train the models (Elith et al. 2008). In this case, regularization is achieved by determining the optimal values for parameters that control the BRT model fitting process. These include the number of trees, learning rate, tree complexity, and bag fraction (Elith et al. 2008). The number of trees indicates how many individual tree models (i.e., iterations of the boosting procedure) will be included in the final, ensemble model. The learning rate, or shrinkage rate, determines the contribution of each individual tree model to the final model. Smaller values for the learning rate will result in a larger number of trees (Elith et al. 2008). The tree complexity controls the number of allowable nodes in a tree, which limits the number of possible interactions between environmental predictor variables. In general, greater tree complexity results in fewer trees (Elith et al. 2008). Stochastic gradient boosting, a version of boosting in which each new model is fit using only a random subsample of the data, was used to reduce overfitting further and improve model performance. The fraction of data drawn at random without replacement from the training data at each iteration is known as the bag fraction (Freidman 2002, Elith et al. 2008).

For each macrofauna taxon, the learning rate, tree complexity, and bag fraction were tuned over a range of values to identify the optimal combination and the corresponding number of boosting iterations (i.e., the number of tree-based models to fit). For each combination of parameter values, models were fit using 10-fold cross-validation. In this process, the model training data were divided into 10 random subsets (i.e., folds). Each fold was used to evaluate model performance for a BRT model fit using the data in the other nine folds. Model performance was measured using the percent deviance explained (PDE), which indicates the amount of variation in the response variable explained by the model. The combination of parameter values with the highest mean PDE across the 10 cross-validation folds was selected as the optimal combination. Statistical modeling was performed in R using the 'dismo' (Hijmans et al. 2017) and 'raster' (Hijmans and van Etten 2018) packages.

4.2.4.4 Spatial Prediction

Similar to the DSCS, bootstrapping was used to create spatial gridded predictions of the probability of occurrence and to estimate variability (i.e., uncertainty) in model predictions for macrofauna. For each macrofauna taxon, the model training data were randomly sampled with replacement to create 100 bootstrap samples of the original sample size of the training data. A BRT model was fit to each bootstrap sample using the optimal combination of model parameters and corresponding number of trees (i.e.,

boosting iterations). Each of these models was used to create a spatial gridded prediction of the probability of occurrence across the study area, where the probability of occurrence at each grid cell represented the probability of the taxon being observed in a sample taken in that grid cell. The bootstrapping procedure generated a set of 100 predictions of the probability of occurrence at each grid cell. Since each bootstrap sample could include a different set of records drawn from the original data, this set of predictions could be used to assess sensitivity to variation in the original data.

From the bootstrapped set of 100 spatial gridded predictions, the mean of the predicted probability of occurrence was calculated at each grid cell. As a measure of variability, the CV was also calculated at each grid cell as the standard deviation of the predicted probability of occurrence divided by the mean probability of occurrence. A higher value indicated greater variability in the predictions for the 100 bootstrap samples, while a lower value indicated less variability. It is important to note that in addition to areas of high variability (high standard deviation), high values of the CV can also result from extremely low values of the mean probability of occurrence. Therefore, the CV should be interpreted in conjunction with the mean probability of occurrence. The CV can also provide information about locations where variability in model predictions is high as a result of limited sampling.

A map page was created for each macrofauna taxon to depict the presence or absence of the taxon at each sampling station, the mean predicted probability of occurrence, and the coefficient of variation of the predicted probability of occurrence. Note that fine-scale features may be difficult to discern in the map pages given the resolution of the model predictions and the extent of the map display. However, these features can be examined using the GIS data products associated with the report.

4.2.4.5 Model Performance

Model performance was evaluated using several metrics (Table 4.4). The training PDE and cross-validation PDE were calculated during the process for tuning model parameter values described in Section 4.2.4.3. Values for training and cross-validation PDE are reported for models fit using the optimal combination of model parameters. The training PDE was calculated for a model fit to the full set of model training data, while the cross-validation PDE was the mean PDE for the 10 models fit during cross-validation. In addition, the test PDE was calculated as the percent deviance explained by the model when evaluated using the model test data. Each of the PDE metrics provides a measure of overall model fit (i.e., how well model predictions match actual data), but the test PDE specifically provides an assessment of how well the model performed when predicting data that was independent of model fitting. Higher PDE values indicate that models can be used with greater confidence to make predictions. Each measure of PDE was categorized relative to its observed values as high (top 25% of the values), medium (middle 50% of the values), or low (lowest 25% of the values) (Table 4.4).

Model predictive performance was also evaluated using the test AUC, defined as the area under the receiver operating characteristic curve (Fielding and Bell 1997) calculated using the model test data. Like the PDE metrics, the test AUC provides a measure of overall model fit, and higher values generally indicate better performance. Test AUC values were categorized as high, medium, and low (Table 4.4), using similar breakpoints as in Hosmer and Lemeshow (2000).

Although the training PDE is included here, in general it is preferable not to evaluate model performance using the training data (Elith et al. 2008). In addition, while AUC values were reported in this study, it is important to note that there is considerable criticism of the use of AUC to evaluate model performance for species distribution models (e.g., Lobo et al. 2008). Therefore, discussion of model performance in Section 4.3.1 below focused primarily on the cross-validation and test PDE.

4.2.5 Environmental Predictor Variable Importance

BRT models were fit to maximize predictive performance rather than to determine the ecological drivers and mechanisms behind the occurrence of macrofauna in the study area. Nonetheless, the BRT model outputs did provide a measure of the relative importance of each environmental predictor variable to model fitting derived from the number of times each predictor was used during tree splitting (Elith et al. 2008). The relative importance of the environmental predictor variables across the macrofauna taxa was summarized using a bubble plot. Inferences about the ecological drivers of macrofauna occurrence from the relative contributions of the environmental predictor variables to model fitting should be made with caution because of the high correlations between some environmental predictors.

4.2.6 Comparison to Existing Models

Havron et al. (2017) described models that predicted the probability of occurrence along the continental shelf from northern California to southern Washington for seven of the macrofauna species also modeled in this study. These models used occurrence data (presence-absence) from many of the same macrofauna sampling stations included in this study, but were fit using a different modeling approach (Bayesian networks), for a smaller spatial domain, and using some environmental predictor variables (e.g., total organic carbon, total nitrogen) not included in this study. In spite of these differences, model predictions from this study were compared to model predictions for two species (*Alia gausapata*, *Axinopsida serricata*) from Havron et al. (2017) to assess similarities and differences in the patterns of predicted macrofauna habitat.

Model predictions from this study were unprojected and bilinearly resampled from the 25 x 25 m grid to match the geographic coordinate system (WGS84) and 250 x 250 m grid used by Havron et al. (2017), and the Spearman rank correlation coefficient was calculated. Models were also compared by visual inspection of the patterns of predicted macrofauna occurrence. Again, it is important to note the differences in approaches used by this study and Havron et al. (2017) and only general inferences about the similarities and differences in the patterns of predicted macrofauna habitat should be made.

4.3 Results and Discussion

4.3.1 Predicted Spatial Distributions, Model Performance, and Insights from Important Environmental Predictor Variables

This section describes the mapped spatial predictions of probability of occurrence from the BRT models for each of the selected macrofauna taxa in relation to the locations of sample collections and known habitat preferences. Results are organized by taxonomic group to facilitate comparisons of the spatial distributions of occurrence (observed and predicted) among taxa within the same group. In addition to examining spatial patterns or trends in the areas with high predicted probability of occurrence, the maps can also be used to identify potential targets for future sampling (e.g., an area predicted to have high probability of occurrence that has not been previously sampled). Maps of the CV can be used to identify areas with greater variability (i.e., less precision) in the model predictions. Again, it is important to note that in addition to areas of greater variability, higher values of the CV can also result from extremely low values of the mean predicted probability of occurrence. Therefore, maps of the CV should be interpreted in conjunction with the mean probability of occurrence. The CV can also provide information about locations where variability in model predictions is high because of limited sampling effort, which may suggest potential targets for future surveys.

This section also summarizes the measures of model performance, which can be used to assess the relative level of confidence one can have in the model predictions for each taxon. For example, if training, cross-validation, and test PDE are all high, this suggests that the models performed well at predicting the

occurrence of the taxon at both sampling stations used to fit the models and stations withheld for testing model performance. If training PDE is high but cross-validation and/or test PDE is low, this indicates that the model was less successful at predicting occurrence at sampling stations withheld for model testing and may not generalize well to new data. For taxa with low training, cross-validation, and test PDE, caution should be taken when using mapped predictions.

Finally, this section indicates the environmental predictor variables that were most important to model fitting for each taxon and provides the relative contribution value for each of these predictors. These generally included all environmental predictors with relative contribution values >10%. It is important to note again that care must be taken when making inferences about the ecological drivers of macrofauna occurrence from the relative contributions because of correlations between the environmental predictors. In some instances, the relationship between the predicted probability of occurrence and the values of an environmental predictor is described. These relationships were inferred from marginal effects plots (sometimes called partial dependence plots) that depict how the predicted probability of occurrence varied across the range of environmental predictor values while holding each of the other environmental predictors at its mean value at the sampling stations. These plots must be interpreted carefully when environmental predictors are highly correlated or have interaction effects (Elith et al. 2008).

4.3.1.1 Mollusca

Bivalves

All measures of model performance were high for *Nutricola lordi* and *Huxleyia munita* (Table 4.5). The *N. lordi* model predicted occurrence in only very specific locations, primarily nearshore of Oregon and Washington and in deeper waters offshore of southern Oregon (Figure 4.3). Annual maximum wave power (33.5%) and percent sand (22.6%) were the most important environmental predictors for the *N. lordi* model, followed by depth (7.0%) (Figure 4.46). The highest predicted probability of occurrence was associated with higher values for annual maximum wave power and percent sand. While deep-water sampling was limited to areas offshore of Oregon and in the SCB, *H. munita* was predicted to occur offshore in relatively deeper waters throughout the study region (Figure 4.4). Spring/summer mean wave power was the greatest contributor to the *H. munita* model (31.0%) with highest probability of occurrence at highest values for wave power. Distance to shore (13.5%) and depth (9.7%) were secondary (Figure 4.46).

Cross-validation PDE and test PDE were medium for *Acila castrensis*, *Adontorhina cyclia*, *Axinopsida serricata*, and *Ennucula tenuis* (Table 4.5). Depth (44.1%) was the most important environmental predictor for the *A. serricata* model, with all other environmental predictor variables having similar relative contributions near 5% (Figure 4.46). This species is rarely found shallower than 50 m and persists beyond the shelf break, tapering off with depth just past 400 m throughout the entire study area (Figure 4.5). Depth (25.6%) was also the most important environmental predictor for *A. cyclia*, which has the broadest depth range of the bivalves modeled (Figure 4.46). The second most important environmental predictor for the *A. cyclia* model was latitude (14.5%), which was surprising given the observations and predicted occurrences of it throughout the study area. However, the predicted probability of occurrence for *A. cyclia* was high in the SCB in the deepest part of the study area where there were no sampling stations, and it was not predicted to occur closer to the mainland where there were observations (Figure 4.6). Samples should be collected in these deeper areas in the SCB to validate the model for *A. cyclia*. For *E. tenuis* depth (23.4%) was again the most important environmental predictor, with a much more restricted depth range. Highest probability of occurrence corresponded to depths around 100 m. Winter surface reflectance (12.4%) was the second most important environmental predictor followed by percent sand (8.4%) and latitude (7.3%) (Figure 4.46). *E. tenuis* was not predicted to occur much past 100 m, and it was predicted to have low probability of occurrence south of Monterey Bay, despite having numerous observations at sampling stations in the SCB because there were also many more absences (Figure 4.7).

Spring/summer vertical bottom current velocity (15.7%) and depth (14.2%) were the most important environmental predictors for *A. castrensis*, followed by winter surface reflectance, latitude, and other measures of bottom current velocity with <10% contribution each (Figure 4.46). This is a strictly shelf species predicted to occur mostly north of San Francisco Bay but with occasional observations off central and southern California (Figure 4.8).

Training PDE, cross-validation PDE, and test PDE were low for *Kurtiella tumida* and *Macoma carlottensis* (Table 4.5). Caution should be taken when using the mapped predictions for these taxa. Areas with the highest predicted probability of occurrence for *K. tumida* extended in a narrow band along the coastline from the SCB to central Oregon (Figure 4.9). Depth (18.3%) and latitude (8.1%) were the most important environmental predictors (Figure 4.46). Depth was also the most important environmental predictor for the *M. carlottensis* model, but with only 10.8% relative contribution, and was followed by spring/summer mean wave power (9.8%) (Figure 4.46). While *M. carlottensis* was observed at sampling stations coastwide, the areas with the highest predicted probability of occurrence for *M. carlottensis* were across the shelf break off northern California, Oregon, and Washington (Figure 4.10).

Caudofoveata

The bristleworm *Chaetoderma argenteum* was observed at a small number (n = 62) of sampling stations in deeper waters offshore of Oregon. Nearly all measures of model performance were high for *C. argenteum* (Table 4.5). It was predicted to occur in deeper waters offshore of Washington but was not likely to occur offshore of California (Figure 4.11). The most important environmental predictors for this model were annual maximum wave power (18.9%) and spring/summer mean wave power (17.0%), with occurrence predicted only at the highest values for wave power, followed by distance to shore (14.2%) and latitude (7.6%) (Figure 4.46).

Gastropods

None of the three gastropod species modeled were found south of Monterey Bay, and latitude was the most important environmental predictor for *Alia gausapata* and *Cylichna attonsa* (Figure 4.46). Areas of highest predicted probability of occurrence for *A. gausapata* closely matched the areas where it was observed in samples, with a small area off Cape Mendocino without samples also predicted to be suitable (Figure 4.12). The second and third most important environmental predictors for the *A. gausapata* model were distance to shore (11.9%) and depth (6.9%) (Figure 4.46). Cross-validation PDE and test PDE values were low and medium, respectively, for *A. gausapata*, and were medium for *Callianax pycna* and *C. attonsa* (Table 4.5). For *C. pycna*, observations were almost exclusively at sampling stations nearshore of the Oregon coast, and the only area of predicted high probability of occurrence was a narrow nearshore band offshore of Oregon and northern California (Figure 4.13). However, depth was not an important environmental predictor for the *C. pycna* model. Instead, the most important predictors for the *C. pycna* model were percent sand (24.9%) and winter east-west bottom current velocity (18.8%), with highest predicted probability of occurrence associated with highest values for each of these predictors. Observations of *C. attonsa* were widespread offshore of Oregon and Washington and also nearshore at Eureka, San Francisco Bay, and Monterey Bay, California. The highest predicted probability of occurrence for *C. attonsa* was offshore of Oregon and Washington, with lower probabilities around the stations near Eureka and San Francisco Bay and no predicted occurrence off Monterey Bay (Figure 4.14). Latitude (30.9%) and spring/summer vertical bottom current velocity (11.9%) were the most important environmental predictors for the *C. attonsa* model (Figure 4.46).

Scaphopods

Cross-validation PDE and test PDE were medium for *Gadila tolmiei*, *Pulsellum salishorum*, and *Rhabdus rectius* (Table 4.5). *G. tolmiei* observations were uncommon (n = 94), occurring only at sampling stations

farther offshore in the SCB and offshore of Oregon (Figure 4.15). Depth (26.8%) and distance to shore (19.4%) were the most important environmental predictors for the *G. tolmiei* model (Figure 4.46). Areas of highest predicted probability of occurrence for *G. tolmiei* were found in deeper waters offshore of Oregon (where it was observed in samples) as well as offshore of Washington and in the SCB where it was predicted to occur deeper than any sampling stations included in this study (Figure 4.15). Additional samples should be collected in these deeper areas offshore of Washington and in the SCB to validate the model predictions for *G. tolmiei*. Observations of *P. salishorum* occurred across the shelf and slope off northern California, Oregon, and Washington, with a narrow band of highest predicted probability of occurrence on the shelf offshore of Oregon and Washington (Figure 4.16). While latitude (14.6%) was the second most important environmental predictor for this northern species, the most important predictor for the *G. tolmiei* model was spring/summer vertical bottom current velocity (15.4%) (Figure 4.46). *R. rectius* was observed at sampling stations coastwide, but was more commonly observed offshore of northern California, Oregon, and Washington. Areas of highest predicted probability of occurrence for *R. rectius* were two narrow mid- to outer-shelf bands, from northern California to central Oregon and northern Oregon to Washington (Figure 4.17). Depth (13.0%) and winter vertical bottom current velocity (12.8%) were the most important environmental predictors for *R. rectius* (Figure 4.46).

4.3.1.2 Crustacaea

Among the three crustaceans modeled, cross-validation PDE and test PDE were the highest for the ostracod *Euphilomedes carcharodonta* but still only medium (Table 4.5). Observations and areas with highest predicted probability of occurrence for *E. carcharodonta* were nearly coastwide, including nearshore in the SCB, around the Channel Islands, between Monterey Bay and the Gulf of the Farallones, and offshore of Oregon and Washington. Interestingly, *E. carcharodonta* was not observed or predicted to occur off northern California despite having been identified from stations both north and south of that region (Figure 4.18). The most important environmental predictors for the ostracod model were depth (18.1%), annual maximum wave power (10.2%), and percent sand (9.1%) (Figure 4.46). Highest predicted probability of occurrence corresponded with mid- to inner-shelf depths, lowest wave power, and surficial sediments with around 60% sand.

While pea crabs from the *Pinnixa occidentalis* complex were observed at stations throughout Oregon and Washington, predicted probability of occurrence was much lower off Oregon and Washington than off north central California (Figure 4.19). Latitude (16.1%) was by far the most important environmental predictor, followed by depth (9.2%) (Figure 4.46). Predicted probability of occurrence was greatest on the outer shelf and then declined down the slope. For this species, cross-validation PDE and test PDE were both low (Table 4.5).

Somewhat surprisingly, cross-validation PDE and test PDE were also low for the amphipod *Ampelisca careyi* (Table 4.5), even though this species was observed at a relatively large number of sampling stations (n = 980). The poor performance of the *A. careyi* model might be related to the relatively low predicted probability of occurrence in parts of the SCB where it was commonly observed (Figure 4.20). *A. careyi* is primarily a shelf species but can occur down the slope. The most important environmental predictor for the *A. careyi* model was depth (14.5%) followed by spring/summer east-west bottom current velocity (8.7%) (Figure 4.46).

4.3.1.3 Echinodermata

The heart urchin, *Brisaster latifrons* was only observed at deeper sampling stations on the outer shelf and upper slope from central California and to the north. Areas of highest predicted probability of occurrence extended to the deepest edge of the study area coastwide, including areas such as the SCB where the extent of sampling stations in the study did not extend as deep (Figure 4.21). Additional samples in these deeper areas would be beneficial for evaluating the performance of the *B. latifrons* model. Training PDE

and test PDE were high for this species, while the cross-validation PDE was medium (Table 4.5). The most important environmental predictors for the heart urchin model were spring/summer mean wave power (14.5%), latitude (10.8%), and depth (10.3%) (Figure 4.46). Highest predicted probability of occurrence corresponded with highest wave power values.

The two brittle stars modeled occupied different habitats on the shelf/slope, with *Amphiodia urtica* occurring more nearshore throughout the study area and *Amphioplus macraspis* offshore. Training PDE, cross-validation PDE, and test PDE were all low for *A. urtica* (Table 4.5). Although *A. urtica* was observed at sampling stations coastwide, the areas with the highest predicted probability of occurrence for this species were from Monterey Bay north to the Oregon-Washington border, with very low probability of occurrence in the SCB (Figure 4.22). The most important environmental predictors for the *A. urtica* model were depth (10.7%) and winter east-west bottom current velocity (8.2%) (Figure 4.46). *A. macraspis* was uncommon (n = 81), with observations and areas of higher predicted probability of occurrence only found farther offshore of Oregon and Washington (Figure 4.23). Distance to shore (33.5%) was the most important environmental predictor for the *A. macraspis* model (Figure 4.46). Training PDE was high for this species while cross-validation PDE and test PDE were medium (Table 4.5).

4.3.1.4 Phoronidae

Multiple taxa with differing spatial distributions may have been represented by the family level Phoronidae group, as observations were made at stations in the sandy areas nearshore and muddy areas offshore of Oregon as well as nearshore of southern California and around the Channel Islands. Areas of highest predicted probability of occurrence for Phoronidae were concentrated close to shore and around the Channel Islands. The areas near the observations of Phoronidae offshore of Oregon had low predicted probability of occurrence, while the area of central Oregon with more dense observations did not have any predicted occurrence (Figure 4.24). Depth (22.6%) and spring/summer mean wave power (20.4%) were the most important environmental predictors for the Phoronidae model (Figure 4.46). Training PDE, cross-validation PDE, and test PDE were all medium for Phoronidae (Table 4.5).

4.3.1.5 Polychaeta

Cross-validation PDE and test PDE were medium for *Chloeia pinnata* and *Galathowenia oculata* (Table 4.5). *C. pinnata* was most frequently observed at sampling stations nearshore in the SCB and Monterey Bay, and was also observed in the Gulf of the Farallones and offshore of northern California and Washington. Areas with the highest predicted probability of occurrence for *C. pinnata* were on the banks and ridges within the SCB as well as from central California up to Cape Mendocino (Figure 4.25). The most important environmental predictors for the *C. pinnata* model were winter surface reflectance (29.1%) and depth (18.8%) (Figure 4.46). Observations of *G. oculata* were widespread offshore of Washington, Oregon, and California down to Monterey Bay. The largest area of highest predicted probability of occurrence for *G. oculata* was in deeper waters offshore of northern Oregon and Washington, but relatively high predicted probability of occurrence extended south to just north of Monterey Bay. *G. oculata* was also predicted to occur in deep waters in the SCB, although there were no sampling stations in this area. (Figure 4.26). The most important environmental predictors for this model were latitude (19.7%) and spring/summer mean wave power (17.4%) (Figure 4.46).

Cross-validation PDE and test PDE were high for *Glycera nana* and *Glycera tesselata* (Table 4.5). *G. nana* was observed at sampling stations from Point Conception north to Washington, and areas with the highest predicted probability of occurrence were found from Monterey Bay north to the Gulf of the Farallones, around Cape Mendocino, and from northern Oregon to Washington (Figure 4.27). Latitude (21.8%) and percent sand (12.4%) were the most important environmental predictors for this model (Figure 4.46). Predicted probability of occurrence generally declined with increasing percent sand, which

could explain the relatively low predicted probability of occurrence off the central coast of Oregon. Observations and areas of highest predicted probability of occurrence for *G. tesselata*, on the other hand, were almost completely restricted to the continental shelf and shelf break in the SCB (Figure 4.28). Latitude (36.9%) and percent sand (13.6%) again were among the most important environmental predictors, along with depth (16.8%), for the *G. tesselata* model (Figure 4.46). The highest predicted probability of occurrence for *G. tesselata* corresponded with 40–50% sand. *Glycinde armigera* was widely observed (n = 1,096) at sampling stations coastwide. Patchy areas with the highest predicted probability of occurrence for *G. armigera* were found nearshore near Point Reyes, Cape Mendocino, Coos Bay, and the mouth of the Columbia River (Figure 4.29). However, cross-validation PDE and test PDE were low for *G. armigera*. The most important environmental predictors were winter surface reflectance (11.3%) and spring/summer north-south bottom current velocity (9.0%) (Figure 4.46).

Although *Leitoscoloplos pugettensis* was observed at sampling stations coastwide, areas of highest predicted probability of occurrence were limited to nearshore areas off northern California, southern Oregon, and Washington (Figure 4.30). Cross-validation PDE and test PDE were low for *L. pugettensis* (Table 4.5). The relative contributions of the environmental predictor variables to fitting the *L. pugettensis* model were all <10%. The most important environmental predictors were depth (8.7%) and spring/summer north-south bottom current velocity (8.4%) (Figure 4.46).

Cross-validation PDE and test PDE also were low for *Magelona berkeleyi*. Observations of *M. berkeleyi* were distributed coastwide. A small patch with the highest predicted probability of occurrence for *M. berkeleyi* was located offshore of northern Oregon. Areas of lower predicted probability of occurrence were also found in deeper waters coastwide (Figure 4.31). Again, the relative contributions were <10% for all the environmental predictor variables. The most important environmental predictors were fall vertical bottom current velocity (8.8%) and percent gravel (7.2%) (Figure 4.46). Highest predicted probability of occurrence for *M. berkeleyi* corresponded to percent gravel >10%. This could explain why it was infrequently observed at sampling stations and had limited areas of predicted occurrence, as few gravelly areas were sampled in the study area. In contrast, cross-validation PDE and test PDE were high for *Magelona sacculata*, which was observed at a relatively high number of sampling stations (n = 900), particularly closer to shore in the Gulf of the Farallones and central Oregon. Areas of highest predicted probability of occurrence for *M. sacculata* included the Gulf of the Farallones and a narrow nearshore band that extended from Cape Mendocino to the northern extent of the study area off Washington (Figure 4.32). Percent sand (40.1%) was the most important environmental predictor for the *M. sacculata* model, with highest predicted probability of occurrence for percent sand values >80%. Winter surface reflectance (18.0%) was also an important environmental predictor (Figure 4.46).

Cross-validation PDE and test PDE were medium for *Maldane sarsi* (Table 4.5). This species was observed coastwide, particularly nearshore in the SCB and Monterey Bay and farther offshore near Eureka, California, and central Oregon. Areas of highest predicted probability of occurrence for *M. sarsi* were widespread, including the SCB, Monterey Bay, the Gulf of the Farallones (but not directly offshore of San Francisco Bay), and northern California (Figure 4.33). Percent sand (25.3%) was the most important environmental predictor for *M. sarsi*, with predicted probability of occurrence generally decreasing with increasing percent sand. Depth (17.9%) was also an important environmental predictor for this model, with highest predicted probability of occurrence at around 90 m. Relative contributions for all other predictors were <5% (Figure 4.46).

Ninoe gemmea was only observed at sampling stations offshore of northern California, Oregon, and Washington. Areas of highest predicted probability of occurrence were limited to a narrow band extending from Cape Mendocino north to Washington (Figure 4.34). Cross-validation PDE and test PDE were high for *N. gemmea* (Table 4.5). The most important environmental predictors for the *N. gemmea* model were winter vertical bottom current velocity (23.1%) and spring/summer east-west bottom current velocity (14.9%) (Figure 4.46). Conversely, observations of *Ninoe tridentata* were found primarily at

sampling stations closer to shore near Monterey Bay and in southern California. The predicted probability of occurrence was fairly low for *N. tridentata* throughout the study area, and areas of highest predicted probability of occurrence were restricted to the areas where *N. tridentata* was observed in southern California and Monterey Bay (Figure 4.35). Cross-validation PDE and test PDE were medium (Table 4.5). The most important environmental predictors for the *N. tridentata* model were completely different from the *N. gemmea* model and included depth (21.6%), percent sand (17.0%), and latitude (8.6%) (Figure 4.46).

Onuphis iridescens was observed at sampling stations coastwide (n = 875), but was more commonly observed offshore of northern California, Oregon, and Washington. Areas of highest predicted probability of occurrence for *O. iridescens* were found from Cape Mendocino to central Oregon and near the Oregon-Washington border (Figure 4.36). The most important environmental predictors for the *O. iridescens* model were annual maximum wave power (15.3%), depth (10.8%), and spring/summer mean wave power (9.1%) (Figure 4.46). Predicted probability of occurrence was generally highest for higher values of wave power and for depths from 200 to 400 m. Cross-validation PDE and test PDE were low (Table 4.5).

Nearly all measures of model performance were high for both *Paraprionospio alata* and *Paraprionospio pinnata* (Table 4.5). Observations and areas of highest predicted probability of occurrence for *P. alata* were concentrated in the nearshore areas of southern California and around the Channel Islands, although some observations occurred along the rest of the coast (Figure 4.37). Not surprisingly, latitude (40.6%) was the most important environmental predictor for the *P. alata* model. Depth (14.4%) was also an important environmental predictor for the model (Figure 4.46). In contrast, *P. pinnata*, was never observed at sampling stations in the SCB, but was found at sampling stations just north of Point Conception, in Monterey Bay, the Gulf of the Farallones, and offshore of northern California, Oregon, and Washington. Areas of highest predicted probability of occurrence for *P. pinnata* included a large area extending from Monterey Bay past the Gulf of the Farallones, close to shore just to the south of Fort Bragg, around Cape Mendocino, in small patches extending from Cape Mendocino to central Oregon, and a large area offshore of Washington (Figure 4.38). Latitude (24.7%) was again the most important environmental predictor, followed by percent gravel (8.7%), percent sand (8.2%), and depth (7.4%) (Figure 4.46). Highest predicted probability of occurrence for *P. pinnata* corresponded to higher values for percent gravel and lower values for percent sand.

Cross-validation PDE was medium for *Polycirrus*, but test PDE was low (Table 4.5). Observations of *Polycirrus* were patchy, with it being present at some stations and absent at others in areas with a high density of sampling stations off San Francisco and Eureka, California, as well as central Oregon. *Polycirrus* was not observed at any sampling stations south of Point Conception. Highest predicted probability of occurrence for *Polycirrus* was found from Monterey Bay to Cape Mendocino, and again off northern Oregon (Figure 4.39). Latitude (14.3%) was the most important environmental predictor for the *Polycirrus* model, followed by spring/summer east-west bottom current velocity (12.2%) and spring/summer mean wave power (8.7%) (Figure 4.46).

Praxillella gracilis was observed infrequently (n = 130), but was found coastwide. Cross-validation PDE was medium, but test PDE was low (Table 4.5). Narrow patches of highest predicted probability of occurrence for *P. gracilis* extended north from Cape Mendocino (Figure 4.40). The most important environmental predictors for the *P. gracilis* model were percent sand (13.0%), depth (11.4%), spring/summer east-west bottom current velocity (11.0%), spring/summer mean wave power (10.8%), and winter vertical bottom current velocity (8.8%) (Figure 4.46).

Most observations of *Prionospio jubata* were located in nearshore areas off southern California and around the Channel Islands, but it was observed throughout the entire study area. Areas of highest predicted probability for *P. jubata* were found throughout the SCB, off Point Reyes, and offshore of Washington (Figure 4.41). All measures of model performance were high for *P. jubata* (Table 4.5).

Latitude (32.9%) was the most important environmental predictor for the *P. jubata* model, with the highest predicted probability of occurrence at the lowest latitudes and a slightly higher predicted probability of occurrence at the highest latitudes. Depth (25.1%) and percent sand (6.9%) were also important environmental predictors (Figure 4.46).

Scoletoma luti was widely observed at sampling stations north of Point Conception. Locations with areas of highest predicted probability of occurrence for *S. luti* included the Gulf of the Farallones, around Cape Mendocino, and offshore of the Columbia River north into Washington (Figure 4.42). Cross-validation PDE and test PDE were high for the *S. luti* model (Table 4.5). Spring/summer surface reflectance (25.2%), winter surface reflectance (18.5%), and latitude (11.2%) were the most important environmental predictors (Figure 4.46).

Observations and areas of highest predicted probability of occurrence for *Spiophanes berkeleyorum* were located from Monterey Bay north to Cape Mendocino and offshore of Oregon and Washington (Figure 4.43). Cross-validation PDE and test PDE were medium (Table 4.5). Latitude (36.0%) was by far the most important environmental predictor for the *S. berkeleyorum* model. Depth (9.4%) was also an important environmental predictor for this model (Figure 4.46).

Sternaspis assimilis was only observed at a small number of sampling stations (n = 39) offshore of Oregon. However, in addition to a narrow strip with high predicted probability of occurrence offshore of Oregon in the vicinity of these sampling stations, areas of high predicted probability of occurrence for *S. assimilis* were also found in locations with no nearby sampling stations offshore of Washington and offshore of central and southern California (Figure 4.44). Cross-validation PDE was medium for *S. assimilis*, but test PDE was low (Table 4.5). Additional samples in unsampled deeper areas offshore of Washington and California are needed to validate the *S. assimilis* model. Winter vertical bottom current velocity (42.2%), spring/summer mean wave power (17.6%), and annual maximum wave power were the most important environmental predictors for the *S. assimilis* model (17.0%) (Figure 4.46). In contrast, cross-validation PDE and test PDE were both high for *Sternaspis fossor* (Table 4.5). Observations and areas of highest predicted probability of occurrence for *S. fossor* were closer to shore, extending from Monterey Bay to central Oregon and offshore of Washington (Figure 4.45). The most important environmental predictors for the *S. fossor* model were latitude (20.4%), percent sand (17.5%), depth (16.1%), and winter surface reflectance (14.2%) (Figure 4.46).

4.3.2 Comparison to Existing Models

Visual comparison of predicted probabilities of occurrence between the models produced by Havron et al. (2017) and models from this study suggested similar patterns in predicted occurrence for both *Alia gausapata* (Figure 4.46) and *Axinopsida serricata* (Figure 4.47). For both species, predicted probabilities appear to be slightly higher in Havron et al. (2017), particularly in areas with the highest predicted probabilities. Model predictions from the two studies were somewhat correlated, with $\rho = 0.38$ for *A. gausapata* and $\rho = 0.3$ for *A. serricata*. Havron et al. (2017) noted that the model for *A. gausapata* was the poorest performing model of the species modeled in their study and it was one of the poorest performing in this study as well.

While this comparison suggests general agreement in model predictions for the two species considered, it is important to note the differences in the modeling approaches for each study. Havron et al. (2017) fit models using Bayesian networks, while this study used BRTs. The spatial extent and resolution of the models were also different. Havron et al. (2017) developed models at 250 x 250 m resolution from northern California to southern Washington, while the models from this study were developed at 25 x 25 m resolution for nearly the entire continental US West Coast. By using the Bayesian networks approach, Havron et al. (2017) were able to incorporate additional environmental predictor variables related to water chemistry that were not available for the extent of this study.

It is difficult to make any broad conclusions about how the models from this study compare to those presented in Havron et al. (2017) given the limited number of species available for comparison. Further comparisons between the different modeling approaches would be beneficial to guide future modeling efforts for benthic macrofauna.

4.4 Conclusions

The maps presented in this chapter provide information about the distribution of likely habitat offshore of the continental US West Coast to depths of 1,200 m for a range of species of benthic macrofauna. In addition to identifying areas of likely habitat (i.e., having the highest predicted probability of occurrence) for each of the 43 selected taxa, the maps of predicted probability of occurrence are also accompanied by corresponding maps of the CV, which provide a measure of prediction variability (i.e., uncertainty) that indicates the confidence in the predictions at each model grid cell. It is important that the CV maps are considered alongside the maps of the mean predicted probability of occurrence. In addition to areas of greater variability, higher values of the CV can also result from extremely low values of the mean probability of occurrence. In areas where the CV is high and the mean is not very low, predictions should be interpreted cautiously. The maps can also help identify locations where variability in model predictions is high but sampling effort is limited, which may suggest locations for future sampling.

In addition to maps of predicted macrofauna habitat, this chapter also provides measures of model performance. These measures indicate how well the models fit the occurrence data (i.e., how closely the models match the data) for both data used to fit the models and data withheld for model testing. While high, medium, and low rankings assigned for each metric are only relative to the models developed in this study, these measures suggest the relative level of confidence one can have in the model predictions for each taxon. For example, if training, cross-validation, and test PDE are all high, this suggests that the models performed well at predicting the occurrence of the taxon at both sampling stations used to fit the models and stations withheld for testing model performance. If training PDE is high but cross-validation and/or test PDE is low, this indicates that the model was less successful at predicting occurrence at sampling stations withheld for model testing and may not generalize well to new data. For taxa with low training, cross-validation, and test PDE, more caution should be taken when using mapped predictions. In general, taxa with relatively low model performance tended to have fewer observations (i.e., they were absent at most sampling stations), so additional surveys in unexplored areas similar to where these taxa were observed may provide additional information that allows future models to perform better. It should be noted that all models included in this report had sufficient performance to inform management.

This study represents the first effort to combine multiple databases of macrofauna occurrence offshore of the US West Coast and, as discussed in Section 4.2, the models were possible because of the increased data from macrofauna sampling stations compiled by the Henkel lab at OSU. In addition, the use of bathymetry data from multibeam sonar surveys allowed models to be produced at finer spatial resolution (25 x 25 m) than previous models of macrofauna occurrence for this region.

While this effort represents the first attempt at predicting distributions of macrofauna habitat across the entire continental US West Coast, it is important to recognize that there are limitations that need to be considered. As described in Section 3.4, environmental predictor variables depicting seafloor topography and seafloor substrate could be improved through the collection of additional seafloor mapping data (i.e., multibeam sonar surveys, sediment grab samples). In addition, the environmental predictor variables depicting measures of oceanography were all derived from remotely sensed data and/or models. These datasets may have insufficient resolution to depict the fine-scale patterns that may be helpful in predicting the occurrence of macrofauna. Other oceanographic variables depicting measures of ocean chemistry, such as total organic carbon and total nitrogen, were considered for this study but not included because of

insufficient spatial coverage. Additional in situ data for these variables or the inclusion of these variables in a biogeochemical ROMS would benefit future models of macrofauna occurrence.

For many of the macrofauan taxa selected for modeling, observation data were potentially zero-inflated (i.e., most observations were absences). Zero-inflated abundance models were explored as part of this study, but they performed poorly. Additional research into the use of zero-inflated abundance models for macrofauna would be beneficial. Although model performance was assessed using cross-validation, model performance should also be evaluated using independent model validation data collected by future sampling at new locations. The models presented in this study provide some suggestions about the environmental predictor variables most important for predicting distributions of the selected macrofauna taxa. While in some cases these environmental predictor variables may only represent proxies for the actual ecological drivers of macrofauna distributions, these results may provide some interesting hypotheses to investigate about the habitat requirements for the macrofauna taxa modeled.

The maps presented in this chapter are intended to inform planning and management decisions for ocean activities in the study area, such as wave and wind energy development, by providing information about the locations of likely habitat for benthic macrofauna and by indicating locations where additional information needs to be collected to assess the potential impacts of these activities. These products were not designed to replace but to help inform additional analyses required by law under NEPA and other environmental statutes. For more information about how these products may be used, please contact BOEM's Pacific OCS Region: http://www.boem.gov/Pacific-Region/.

Table 4.1. Descriptions of macrofauna survey datasets included.

Dataset	Collection Type	Sieve Mesh Size (mm)	Region	Years	Depth Range (m)	Number of Stations	Dataset Sources
BHC	Box core	1	WA, OR, northern CA	2010–2012	49–133	150	Benthic habitat characterization surveys from OSU; Henkel et al. 2014
WEMAP	Van Veen	1	WA, OR, CA	2003	28–126	131	Environmental monitoring & assessment program data provided by EPA; Henkel and Nelson 2018
ODMDS	Box core	0.5	OR	2008, 2009, 2013, 2014, 2016	10–85	309	Designated ocean dredged material disposal sites from seven Oregon sites provided by EPA Region 10
HOODS	Van Veen	0.5	northern CA	2008, 2014	31–92	44	Humboldt open ocean disposal site data provided by EPA Region 9
Farallones	Van Veen	1	central CA	2009	8–34	2	Assessing potential resource utilization by Gray Whales in the Gulf of the Greater Farallones National Marine Sanctuary; data provided by EPA Region 9
SFPUC	Van Veen	0.5	central CA	2004, 2005, 2010	12–35	154	San Francisco offshore provided by the San Francisco Public Utility Commission
MCI	Smith-McIntyre	0.5	central CA	1999	10–450	83	Surveys in Monterey Bay National Marine Sanctuary for MCI/WorldCom (ABA Consultants 2000) data provided by MLML Benthic Lab
CCLEAN	Smith-McIntyre/ Van Veen	0.5	central CA	2001–2006, 2008–2010, 2015	80	90	Central Coast Long-term Environmental Assessment Network data provided by MLML Benthic Lab
NOAA-MLML	Smith-McIntyre	0.5	central CA	2004, 2005	80–476	53	Data collected by NOAA and provided by MLML Benthic Lab
Morro Bay	Young Modified Van Veen	1	central CA	2015	15	7	City of Morro Bay and Cayucos Sanitary District Offshore Monitoring and Reporting Program
PacWave	Box core	1	central OR	2010–2016	20-70	597	PacWave test sites data collected by Henkel (OSU) funded by various sources
OWET	Box core	1	southern OR	2011	24-90	42	Data collected by Henkel (OSU) funded by Oregon Wave Energy Trust
OSU–BOEM	Box core	1	OR	2014–2016	60–525	147	Data collected by Henkel (OSU) funded by BOEM
SCCWRP	Van Veen	1	southern CA	1994–2013	3–1,023	1096	Bight '13 regional survey provided by SCCWRP; Gillett et al. 2017

Table 4.2. Macrofauna taxa (n = 43) selected for modeling.

Taxon	Category	Number of Observations
Acila castrensis	Bivalves	323
Adontorhina cyclia	Bivalves	271
Alia gausapata	Gastropods	549
Ampelisca careyi	Crustaceans	980
Amphiodia urtica	Echinoderms	580
Amphioplus macraspis	Echinoderms	81
Axinopsida serricata	Bivalves	1,276
Brisaster latifrons	Echinoderms	156
Callianax pycna	Gastropods	419
Chaetoderma argenteum	Bristleworms	62
Chloeia pinnata	Polychaetes	568
Cylichna attonsa	Gastropods	800
Ennucula tenuis	Bivalves	538
Euphilomedes carcharodonta	Crustaceans	757
Gadila tolmiei	Scaphopods	94
Galathowenia oculata	Polychaetes	315
Glycera nana	Polychaetes	399
Glycera tesselata	Polychaetes	504
Glycinde armigera	Polychaetes	1,096
Huxleyia munita	Bivalves	150
Kurtiella tumida	Bivalves	916
Leitoscoloplos pugettensis	Polychaetes	785
Macoma carlottensis	Bivalves	521
Magelona berkeleyi	Polychaetes	176
Magelona sacculata	Polychaetes	900
Maldane sarsi	Polychaetes	661
Ninoe gemmea	Polychaetes	124
Ninoe tridentate	Polychaetes	168
Nutricola lordi	Bivalves	308
Onuphis iridescens	Polychaetes	875
Paraprionospio alata	Polychaetes	868
Paraprionospio pinnata	Polychaetes	359
Phoronidae	Phoronids	503
Pinnixa occidentalis complex	Crustaceans	313
Polycirrus	Polychaetes	232
Praxillella gracilis	Polychaetes	130
Prionospio jubata	Polychaetes	637
Pulsellum salishorum	Scaphopods	130
Rhabdus rectius	Scaphopods	262
Scoletoma luti	Polychaetes	438
Spiophanes berkeleyorum	Polychaetes	715
Sternaspis assimilis	Polychaetes	39
Sternaspis fossor	Polychaetes	272

Table 4.3. Subset of environmental predictor variables used to fit models of macrofauna occurrence, selected following pairwise correlation analysis.

Environmental Predictor Variable	Category
East-West Aspect	Depth and Seafloor Topography
North-South Aspect	Depth and Seafloor Topography
Depth	Depth and Seafloor Topography
General Curvature	Depth and Seafloor Topography
Plan Curvature	Depth and Seafloor Topography
Profile Curvature	Depth and Seafloor Topography
Slope	Depth and Seafloor Topography
Hard-Soft	Seafloor Substrate
Percent Gravel	Seafloor Substrate
Percent Sand	Seafloor Substrate
Spring/Summer East-West Bottom Current Velocity	Oceanography
Winter East-West Bottom Current Velocity	Oceanography
Spring/Summer North-South Bottom Current Velocity	Oceanography
Winter North-South Bottom Current Velocity	Oceanography
Fall Vertical Bottom Current Velocity	Oceanography
Spring/Summer Vertical Bottom Current Velocity	Oceanography
Winter Vertical Bottom Current Velocity	Oceanography
Spring/Summer Surface Reflectance	Oceanography
Winter Surface Reflectance	Oceanography
Annual Maximum Wave Power	Oceanography
Spring/Summer Mean Wave Power	Oceanography
Distance to Shore	Geography
Latitude	Geography

Table 4.4. Metrics used to evaluate model performance.

Metric	Description	Categories
Training PDE	Percent deviance explained (PDE) for a model fit using all the data in the model training dataset.	H: > 76% M: 59–76% L: < 59%
Cross-validation Mean PDE	Cross-validation estimate of the mean percent deviance explained, where each of the ten cross-validation folds was used to calculate the PDE for a model fit to the data in the nine other folds.	H: > 54% M: 36–54% L: < 36%
Test PDE	Percent deviance explained by the model when evaluated using the model test dataset.	H: > 55% M: 32–55% L: < 32%
Test AUC	Estimate of area under the receiver operating characteristic curve (AUC) when evaluated using the model test dataset.	H: $\geq$ 0.90 M: 0.70–0.90 L: < 0.70

H = High, M = Medium, L = Low

Table 4.5. Measures of model performance for models of macrofauna probability of occurrence.

Taxon	Number of Observations	Training PDE	Cross-validation PDE	Test PDE	Test AUC
Acila castrensis	323	73.39	50.30	53.28	0.94
Adontorhina cyclia	271	66.20	46.12	50.36	0.95
Alia gausapata	549	58.65	35.76	32.30	0.88
Ampelisca careyi	980	43.76	23.74	21.11	0.80
Amphiodia urtica	580	46.50	19.60	18.79	0.80
Amphioplus macraspis	81	84.30	50.94	40.39	0.96
Axinopsida serricata	1,276	63.77	41.07	41.18	0.90
Brisaster latifrons	156	77.39	52.13	56.05	0.97
Callianax pycna	419	71.85	50.93	50.80	0.95
Chaetoderma argenteum	62	78.95	59.32	65.54	0.99
Chloeia pinnata	568	59.85	47.76	47.95	0.93
Cylichna attonsa	800	67.71	51.65	50.73	0.94
Ennucula tenuis	538	64.83	41.98	41.33	0.91
Euphilomedes carcharodonta	757	61.69	35.52	37.86	0.89
Gadila tolmiei	94	71.46	46.54	43.43	0.94
Galathowenia oculata	315	74.21	53.31	51.51	0.95
Glycera nana	399	83.48	61.70	61.89	0.97
Glycera tesselata	504	75.90	56.81	55.29	0.96
Glycinde armigera	1,096	32.87	12.71	7.14	0.68
Huxleyia munita	150	83.29	58.70	66.88	0.99
Kurtiella tumida	916	55.37	30.26	28.80	0.85
Leitoscoloplos pugettensis	785	41.53	20.36	20.59	0.80
Macoma carlottensis	521	54.95	28.66	28.42	0.86
Magelona berkeleyi	176	43.95	13.91	16.08	0.79
Magelona sacculata	900	65.37	54.57	58.71	0.95
Maldane sarsi	661	69.82	43.68	44.64	0.92
Ninoe gemmea	124	82.52	54.12	55.13	0.98
Ninoe tridentata	168	63.86	45.56	45.81	0.95
Nutricola lordi	308	76.60	63.88	66.22	0.97
Onuphis iridescens	875	44.19	26.29	27.52	0.84
Paraprionospio alata	868	74.39	54.30	55.01	0.94
Paraprionospio pinnata	359	81.10	54.31	55.78	0.96
Phoronidae	503	61.20	39.66	35.93	0.90
Pinnixa occidentalis complex	313	51.58	31.81	31.93	0.89
Polycirrus	232	64.64	39.97	30.39	0.90
Praxillella gracilis	130	55.60	35.44	30.96	0.90
Prionospio jubata	637	79.83	57.91	60.10	0.96
Pulsellum salishorum	130	78.68	50.27	40.09	0.94
Rhabdus rectius	262	71.82	43.19	39.02	0.91
Scoletoma luti	438	71.93	56.09	60.14	0.97
Spiophanes berkeleyorum	715	69.24	48.03	49.42	0.93
Sternaspis assimilis	39	61.74	44.72	21.00	0.94
Sternaspis fossor	272	86.66	69.86	69.04	0.99

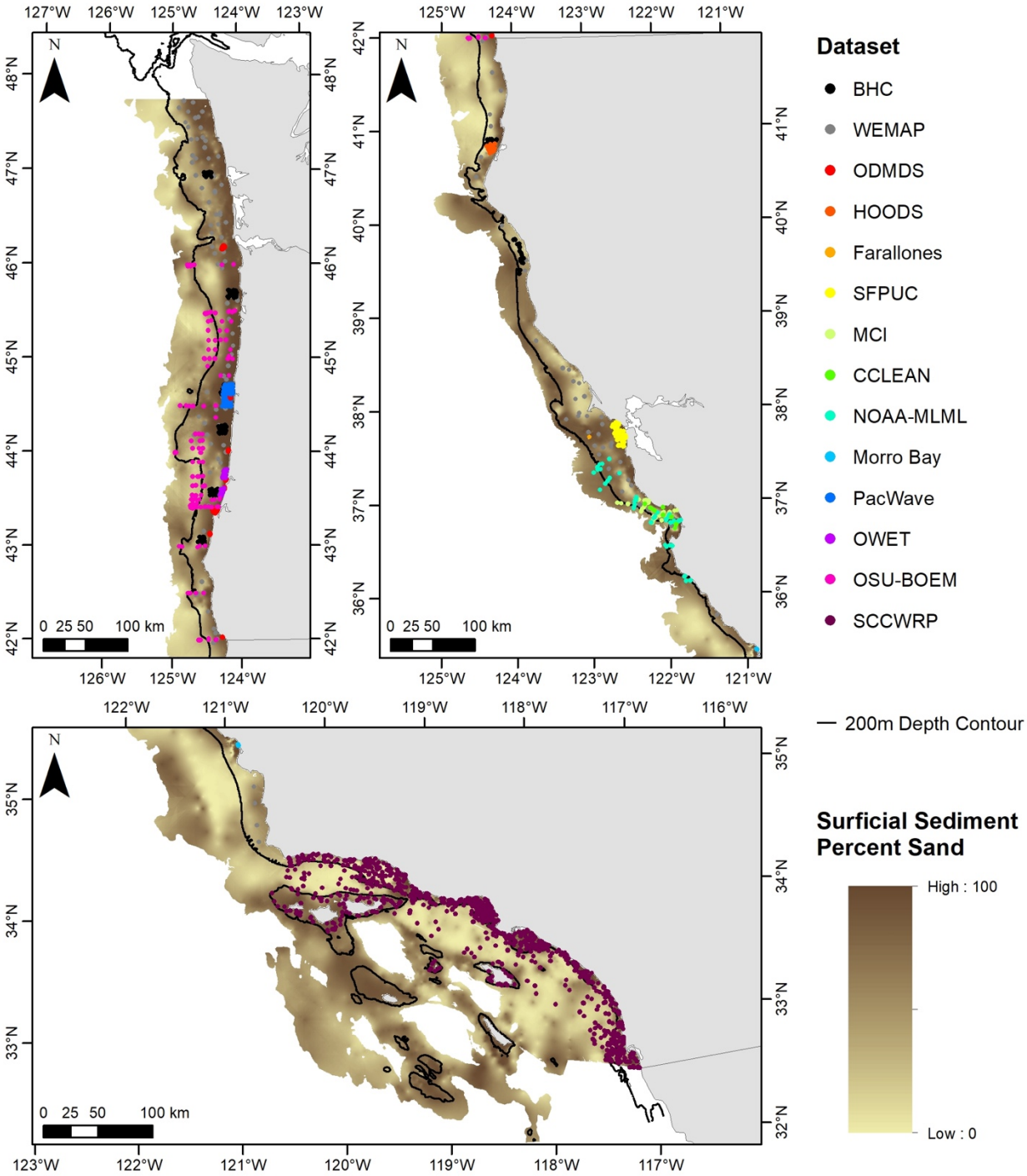

Figure 4.1. Locations of macrofauna sampling stations in the study areas offshore of the continental US West Coast to 1,200 m depth (from Henkel et al. 2020).

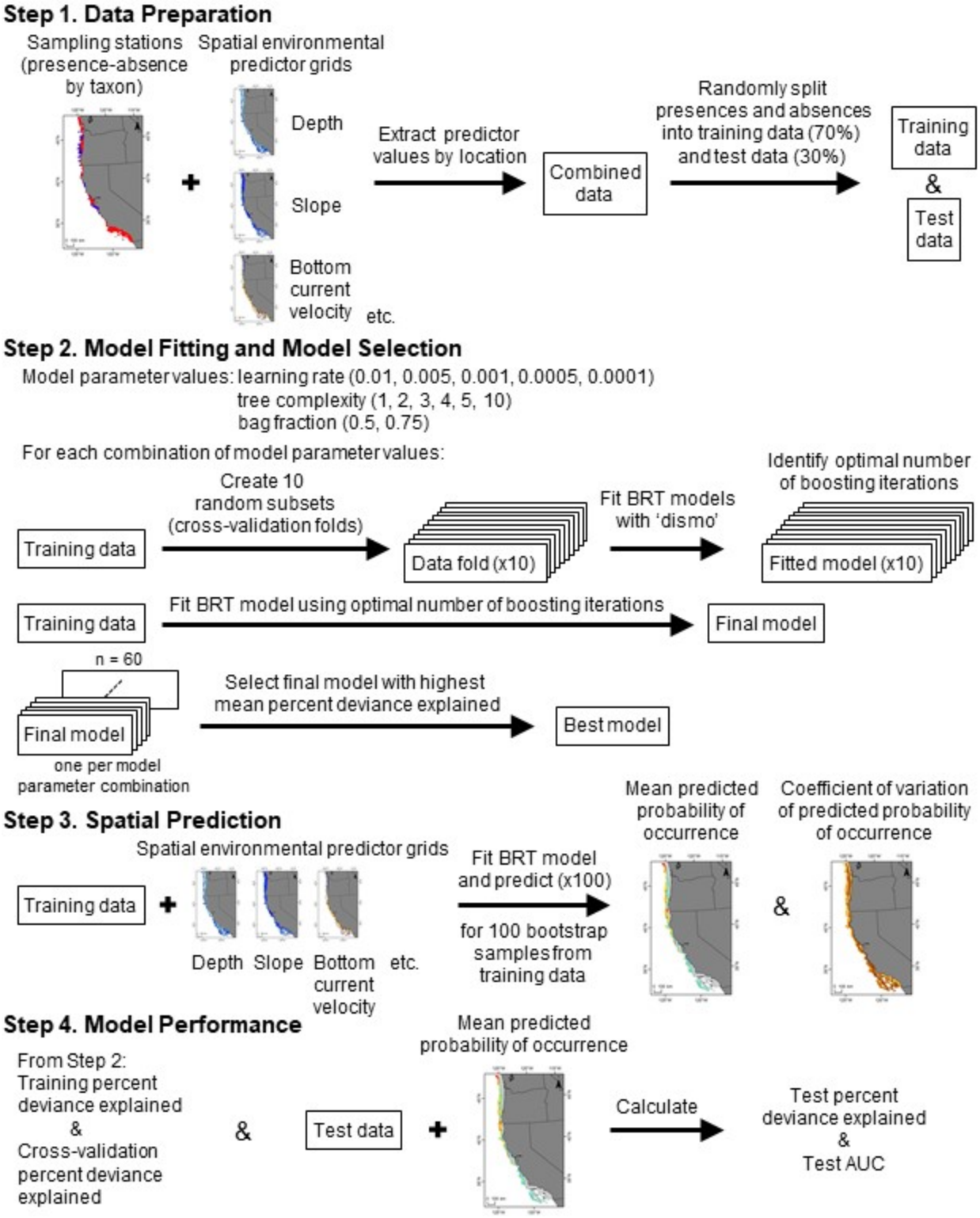

Figure 4.2. Boosted regression tree modeling framework, including data preparation, model fitting and model selection, spatial prediction, and evaluation of model performance.

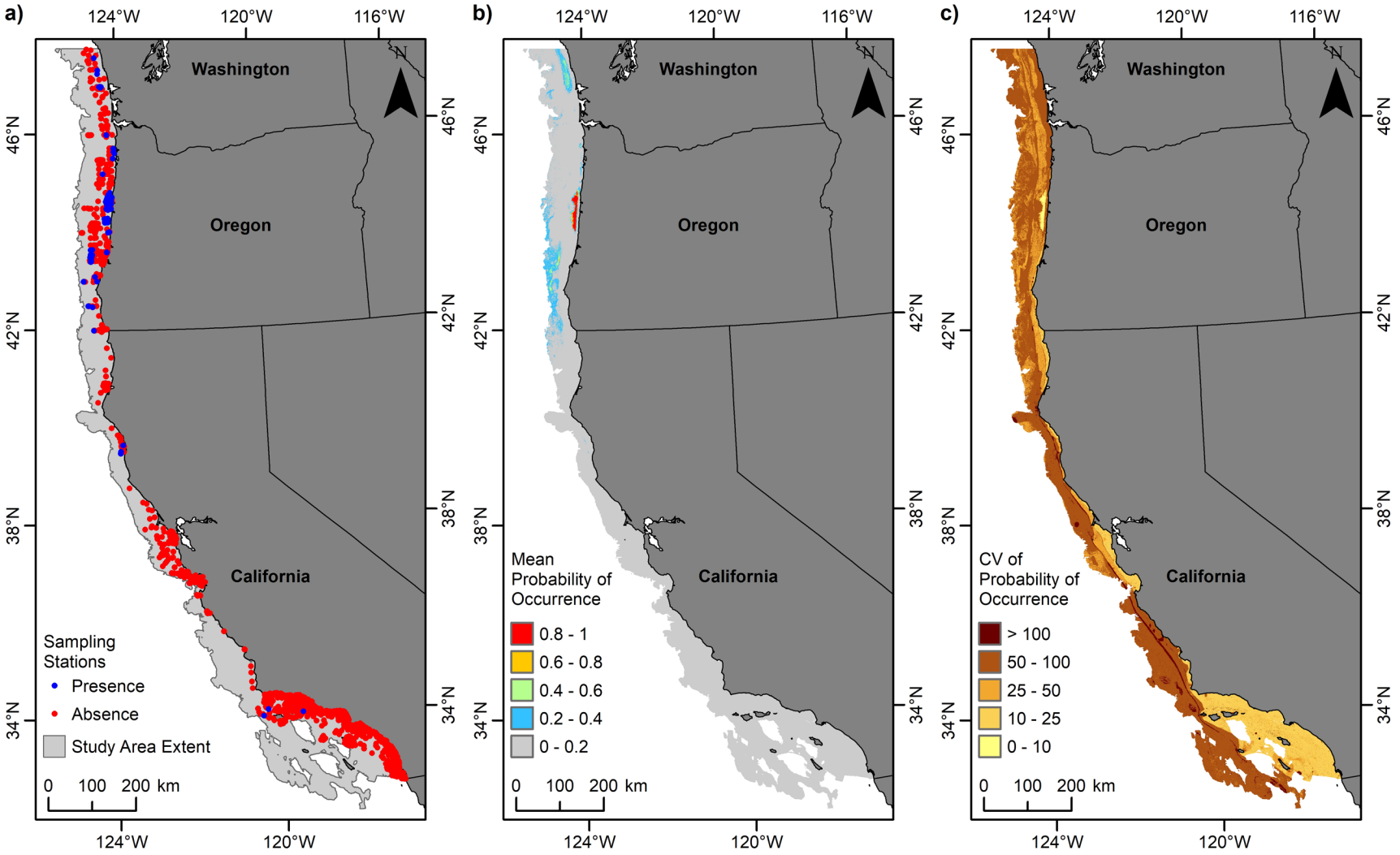

Figure 4.3. Predicted distribution of the bivalve *Nutricola lordi* (Bivalvia, Venerida, Veneridae).
(a) Presence or absence of *N. lordi* from grab samples at 2905 sampling stations within the study area offshore to 1,200 m depth; (b) mean predicted probability of occurrence for *N. lordi*; and (c) coefficient of variation of the predicted probability of occurrence for *N. lordi*.

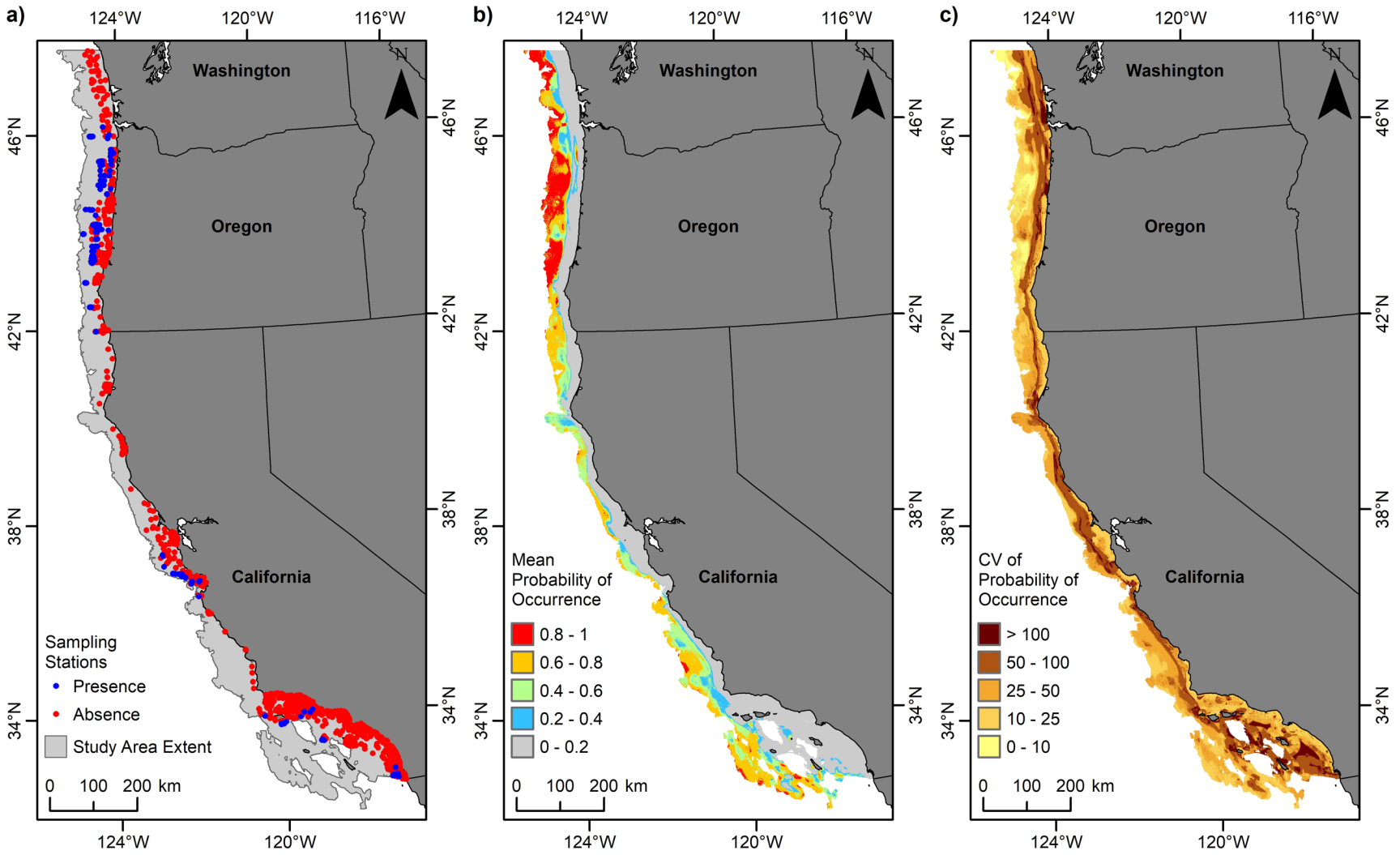

Figure 4.4. Predicted distribution of the bivalve *Huxleyia munita* (Bivalvia, Solemyida, Nucinellidae).
(a) Presence or absence of *H. munita* from grab samples at 2905 sampling stations within the study area offshore to 1,200 m depth; (b) mean predicted probability of *H. munita* occurrence; and (c) coefficient of variation of the predicted probability of *H. munita* occurrence.

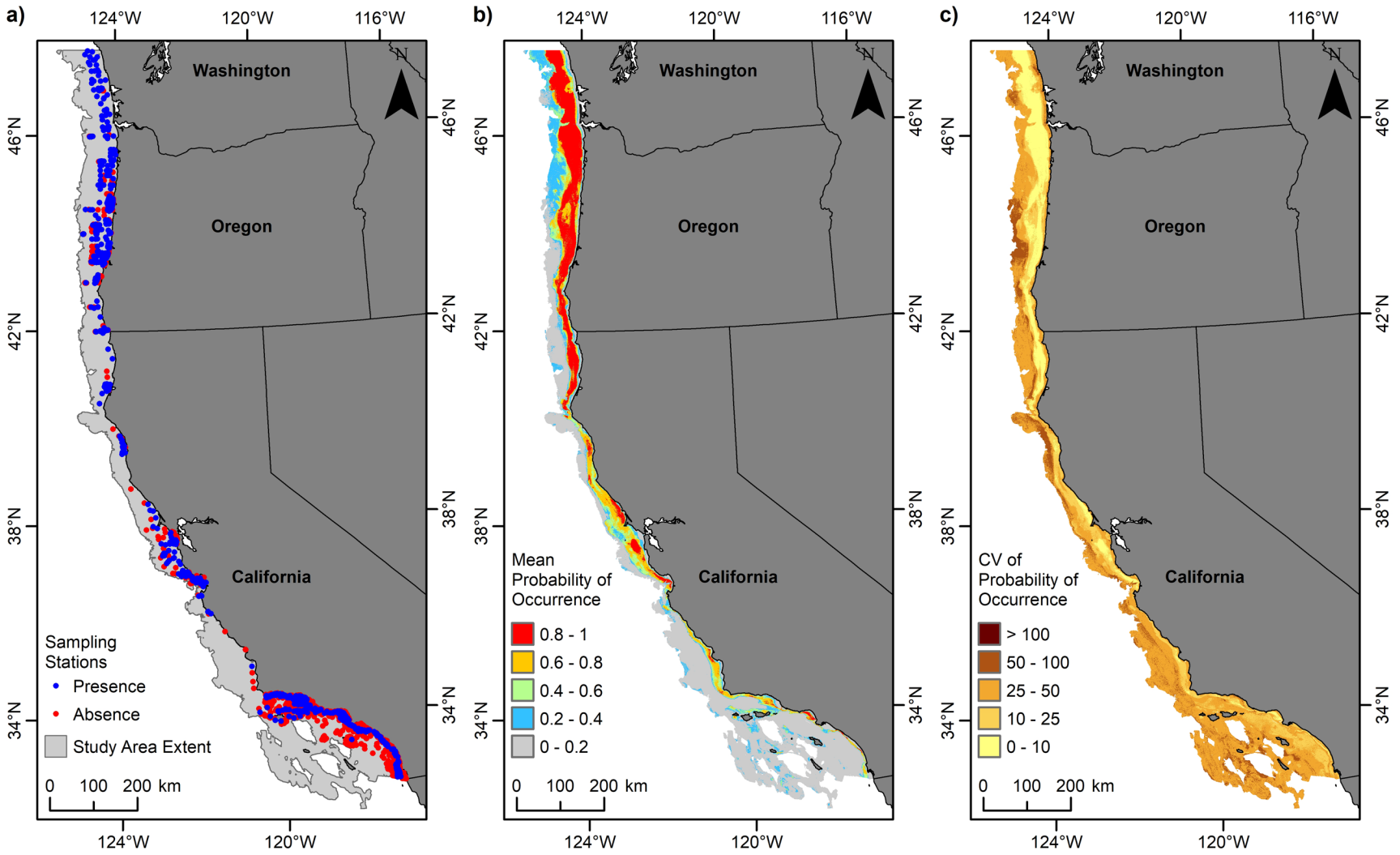

Figure 4.5. Predicted distribution of the bivalve *Axinopsida serricata* (Bivalvia, Lucinida, Thyasiridae).
(a) Presence or absence of *A. serricata* from grab samples at 2905 sampling stations within the study area offshore to 1,200 m depth; (b) mean predicted probability of *A. serricata* occurrence; and (c) coefficient of variation of the predicted probability of *A. serricata* occurrence.

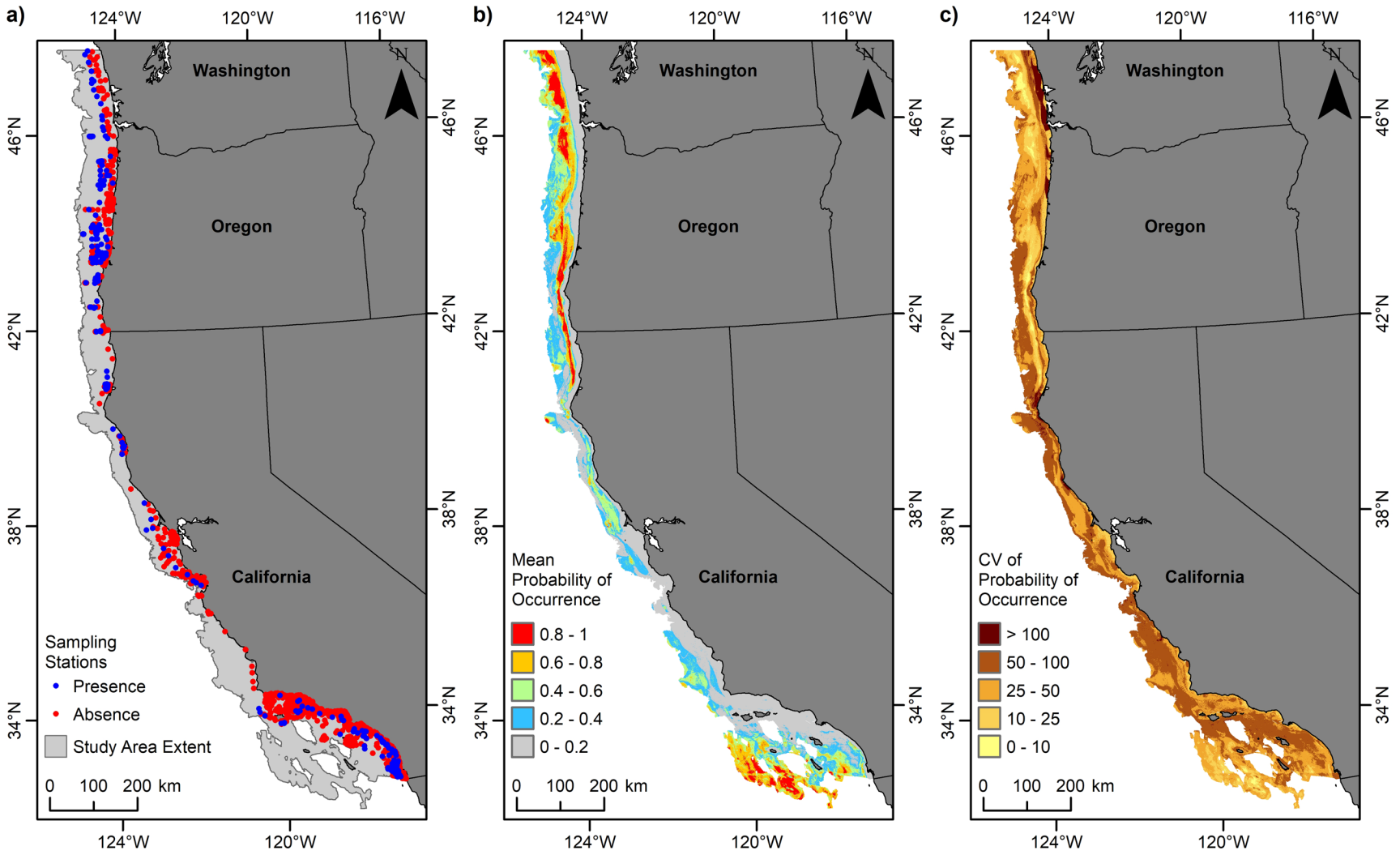

Figure 4.6. Predicted distribution of the bivalve *Adontorhina cyclia* (Bivalvia, Lucinida, Thyasiridae).
(a) Presence or absence of *A. cyclia* from grab samples at 2905 sampling stations within the study area offshore to 1,200 m depth; (b) mean predicted probability of *A. cyclia* occurrence; and (c) coefficient of variation of the predicted probability of *A. cyclia* occurrence.

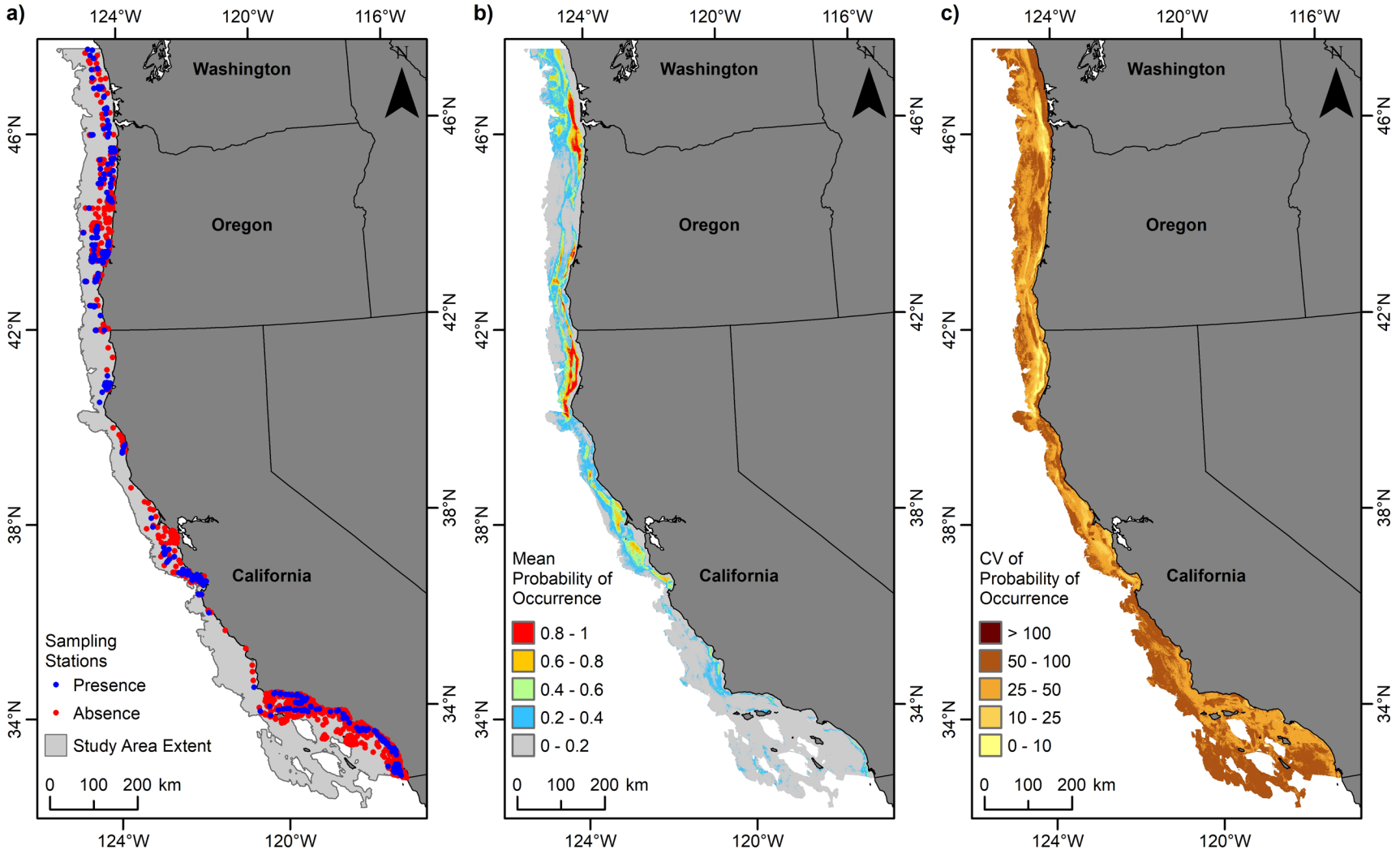

Figure 4.7. Predicted distribution of the bivalve *Ennucula tenuis* (Bivalvia, Nuculida, Nuculidae).
(a) Presence or absence of *E. tenuis* from grab samples at 2905 sampling stations within the study area offshore to 1,200 m depth; (b) mean predicted probability of *E. tenuis* occurrence; and (c) coefficient of variation of the predicted probability of *E. tenuis* occurrence.

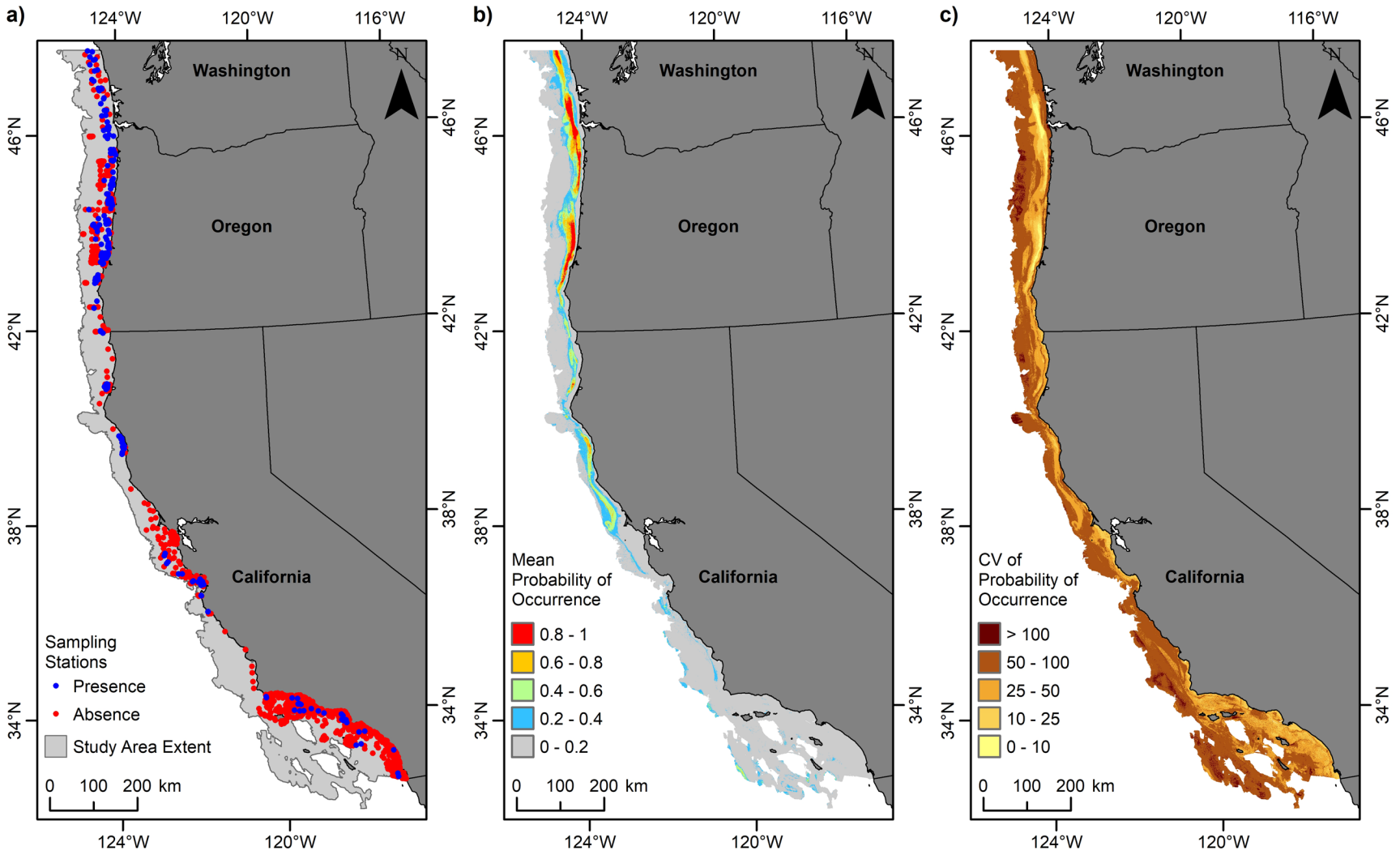

Figure 4.8. Predicted distribution of the bivalve *Acila castrensis* (Bivalvia, Nuculida, Nuculidae).
(a) Presence or absence of *A. castrensis* from grab samples at 2905 sampling stations within the study area offshore to 1,200 m depth; (b) mean predicted probability of *A. castrensis* occurrence; and (c) coefficient of variation of the predicted probability of *A. castrensis* occurrence.

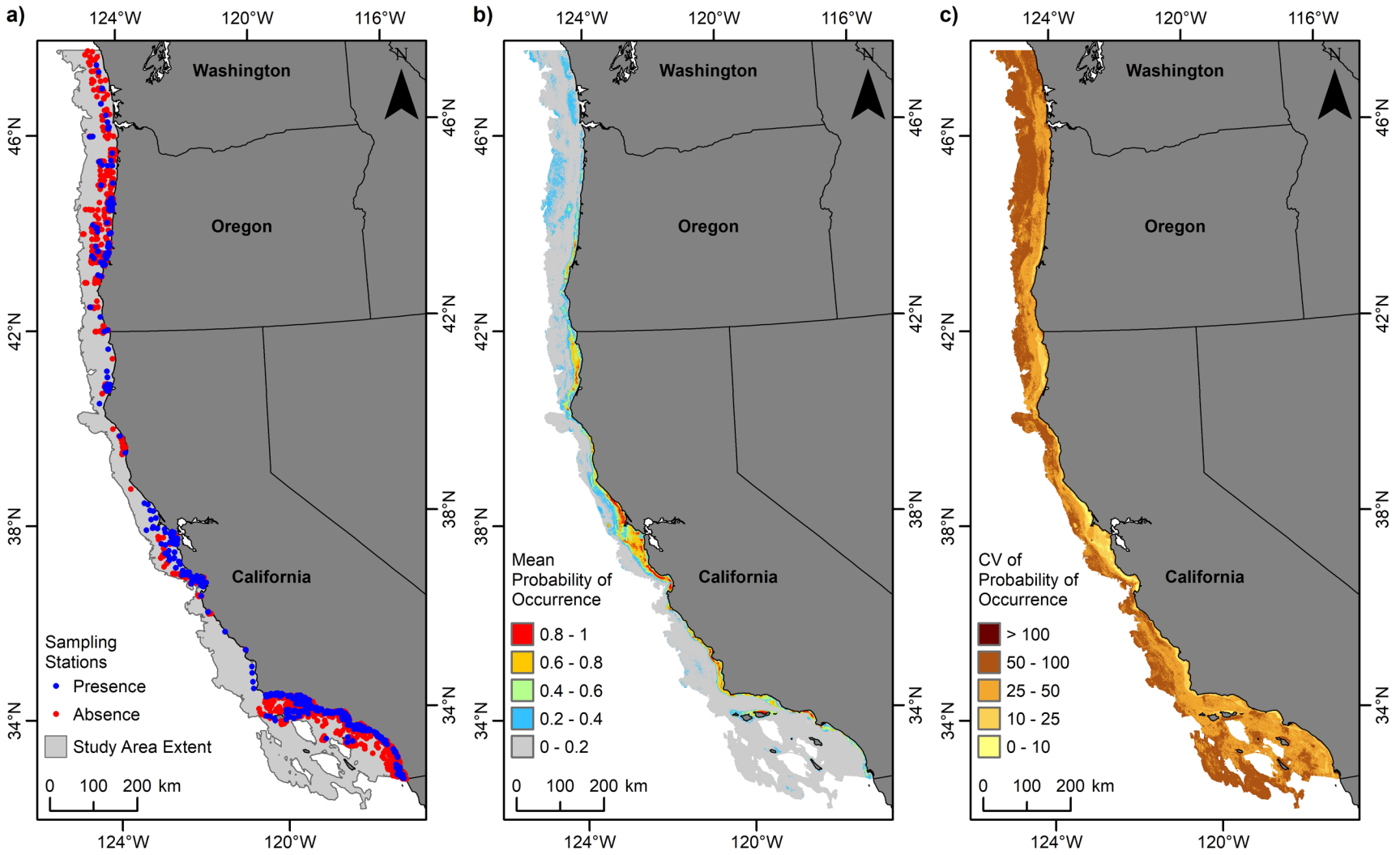

Figure 4.9. Predicted distribution of the bivalve *Kurtiella tumida* (Bivalvia, Galeommatida, Lasaeidae).
(a) Presence or absence of *K. tumida* from grab samples at 2905 sampling stations within the study area offshore to 1,200 m depth; (b) mean predicted probability of *K. tumida* occurrence; and (c) coefficient of variation of the predicted probability of *K. tumida* occurrence.

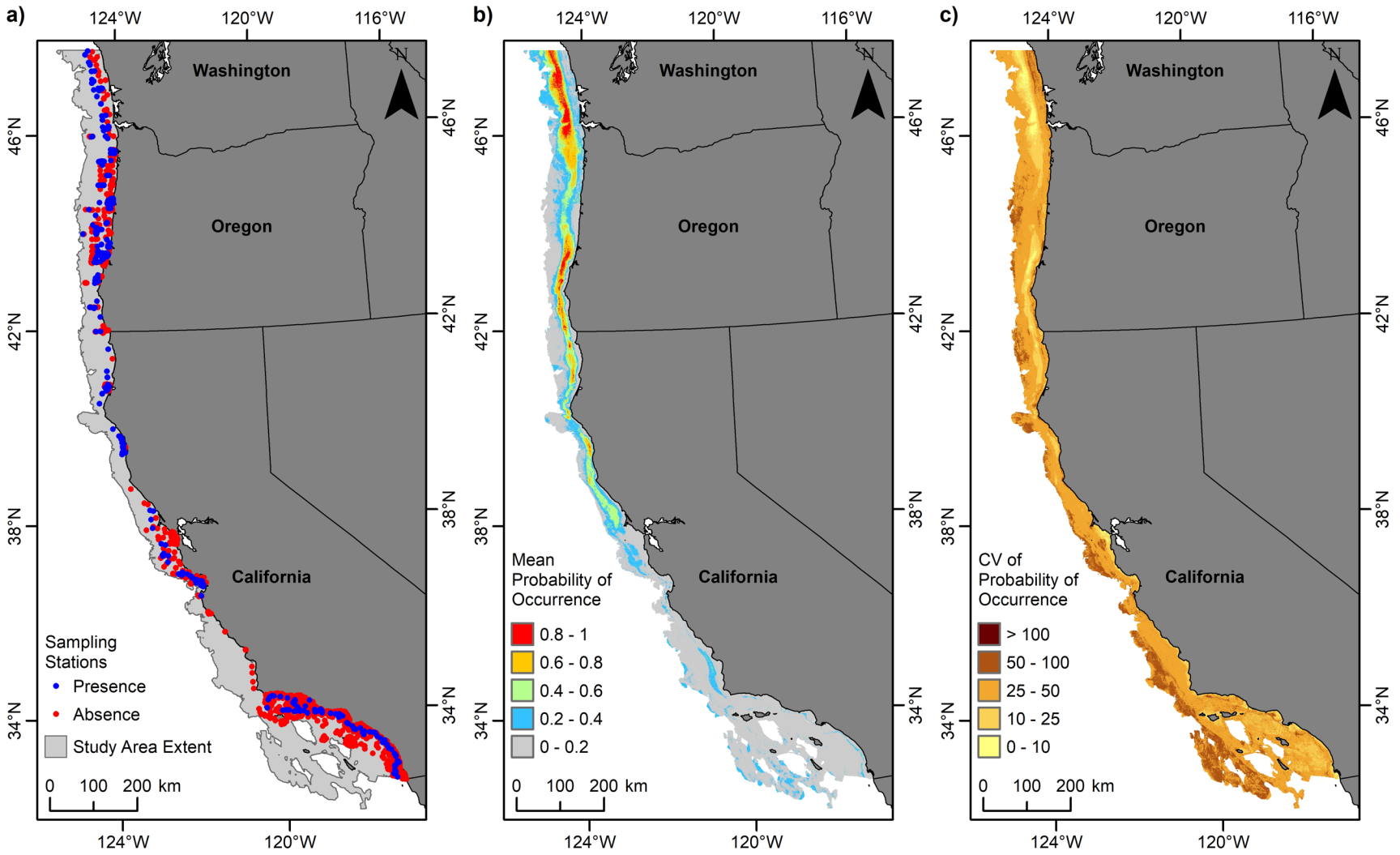

Figure 4.10. Predicted distribution of the bivalve *Macoma carlottensis* (Bivalvia, Cardiida, Tellinidae).
(a) Presence or absence of *M. carlottensis* from grab samples at 2905 sampling stations within the study area offshore to 1,200 m depth; (b) mean predicted probability of *M. carlottensis* occurrence; and (c) coefficient of variation of the predicted probability of *M. carlottensis* occurrence.

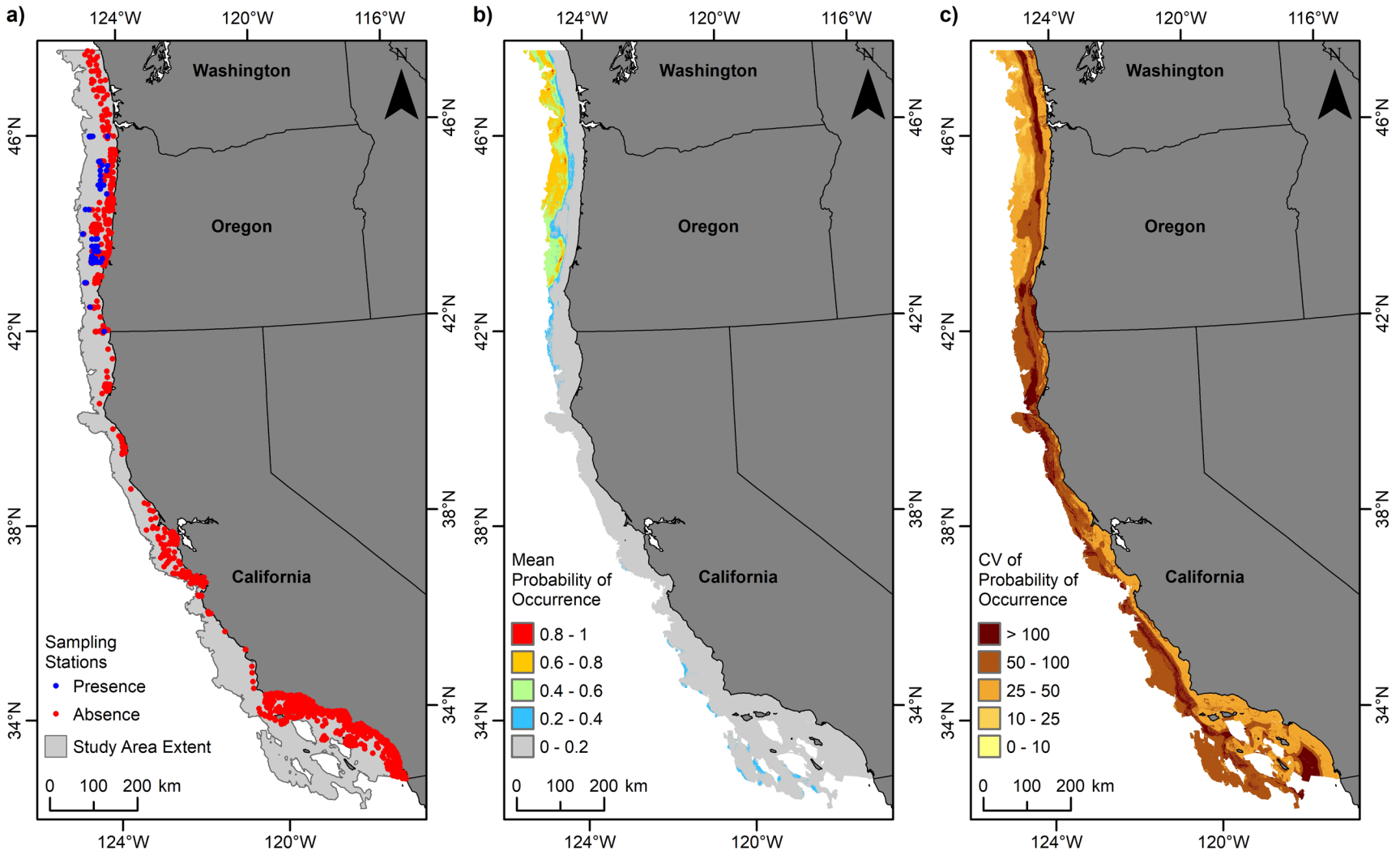

Figure 4.11. Predicted distribution of the bristleworm *Chaetoderma argenteum* (Caudofoveata, Chaetodermatida, Chaetodermatidae). (a) Presence or absence of *C. argenteum* from grab samples at 2905 sampling stations within the study area offshore to 1,200 m depth; (b) mean predicted probability of *C. argenteum* occurrence; and (c) coefficient of variation of the predicted probability of *C. argenteum* occurrence.

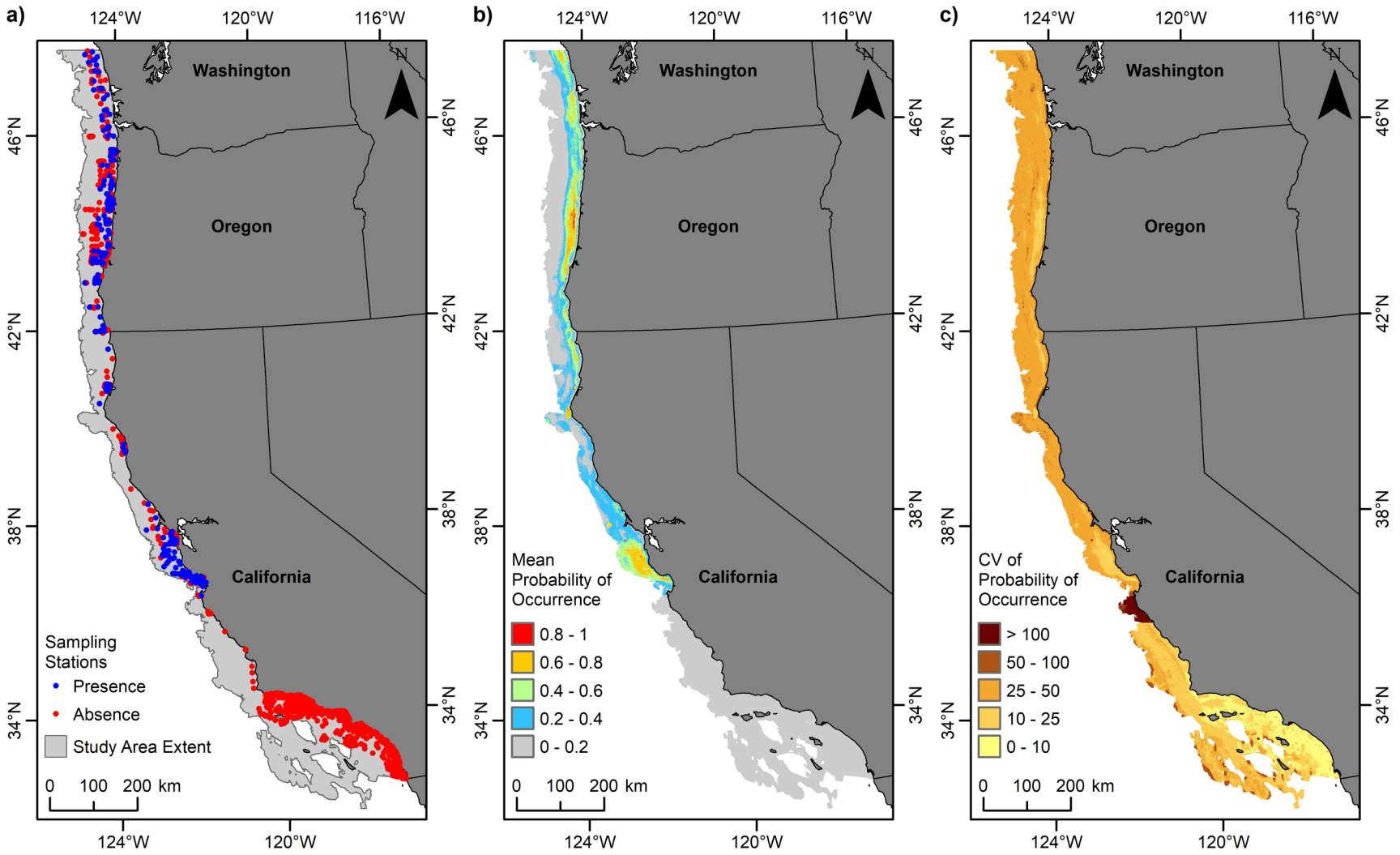

Figure 4.12. Predicted distribution of the gastropod *Alia gausapata* (Gastropoda, Neogastropoda, Columbellidae).
(a) Presence or absence of *A. gausapata* from grab samples at 2905 sampling stations within the study area offshore to 1,200 m depth; (b) mean predicted probability of *A. gausapata* occurrence; and (c) coefficient of variation of the predicted probability of *A. gausapata* occurrence.

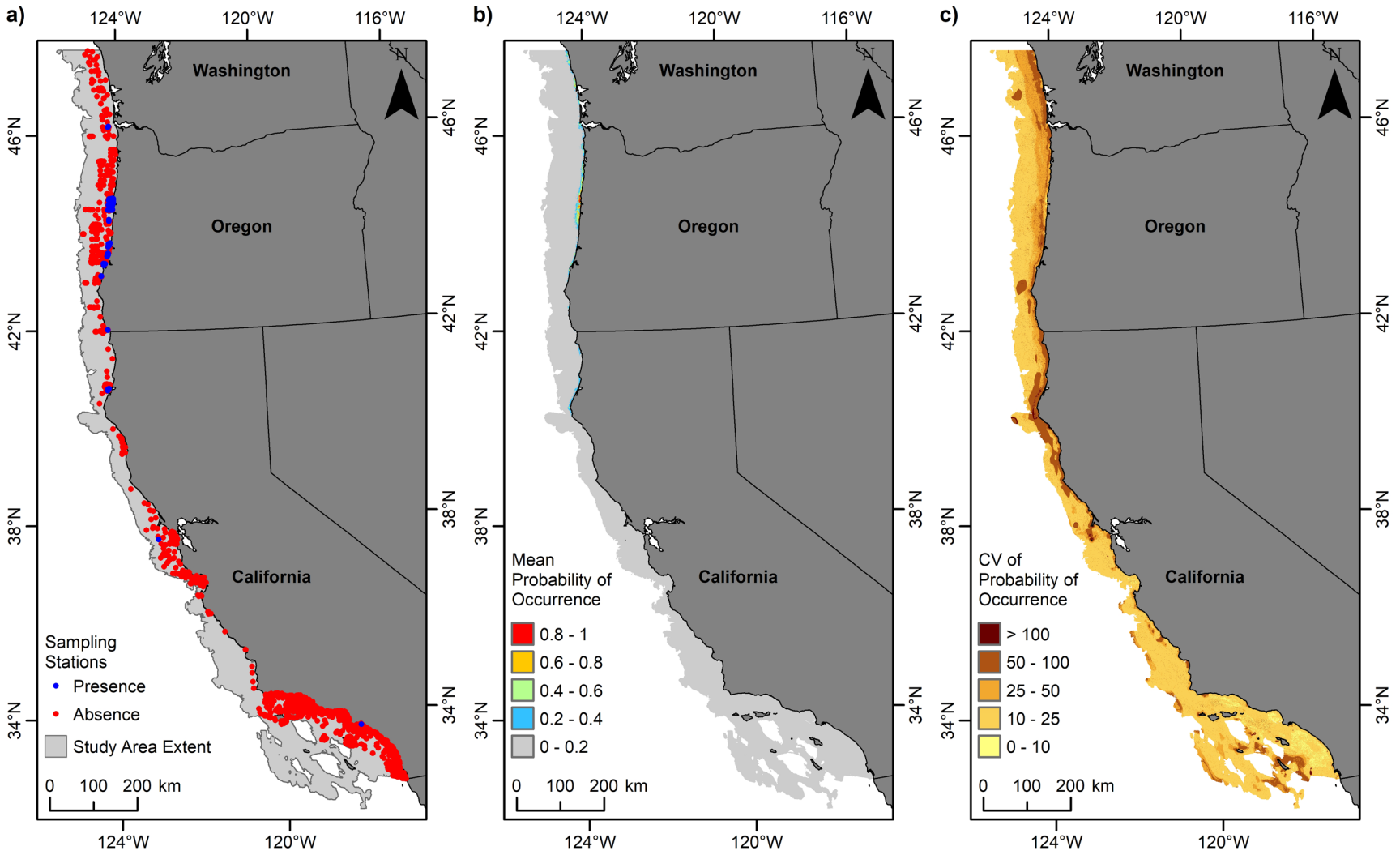

Figure 4.13. Predicted distribution of the gastropod *Callianax pycna* (Gastropoda, Neogastropoda, Olividae).
(a) Presence or absence of *C. pycna* from grab samples at 2905 sampling stations within the study area offshore to 1,200 m depth; (b) mean predicted probability of *C. pycna* occurrence; and (c) coefficient of variation of the predicted probability of *C. pycna* occurrence.

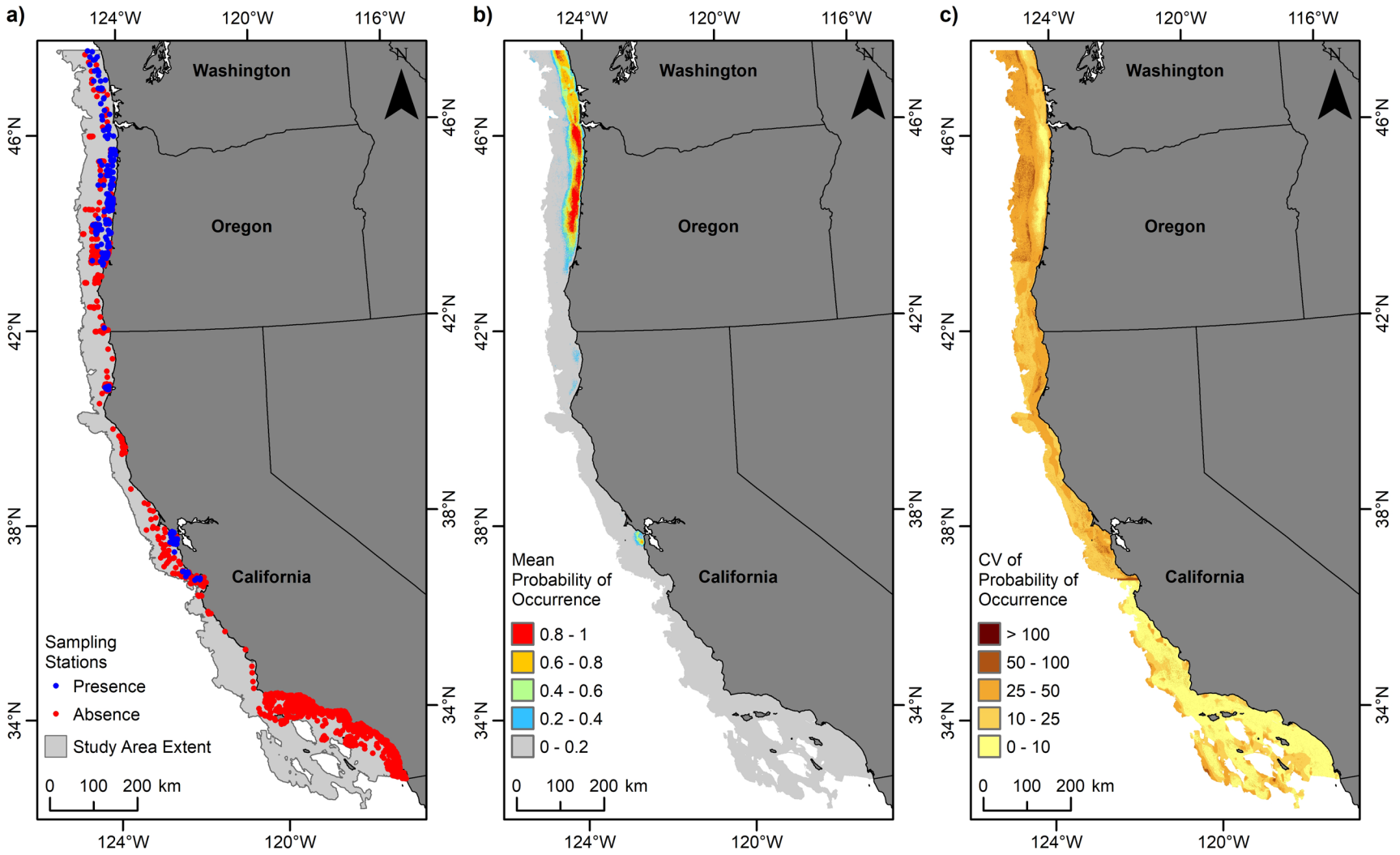

Figure 4.14. Predicted distribution of *Cylichna attonsa* (Gastropoda, Cephalaspidea, Cylichnidae).
(a) Presence or absence of *C. attonsa* from grab samples at 2905 sampling stations within the study area offshore to 1,200 m depth; (b) mean predicted probability of *C. attonsa* occurrence; and (c) coefficient of variation of the predicted probability of *C. attonsa* occurrence.

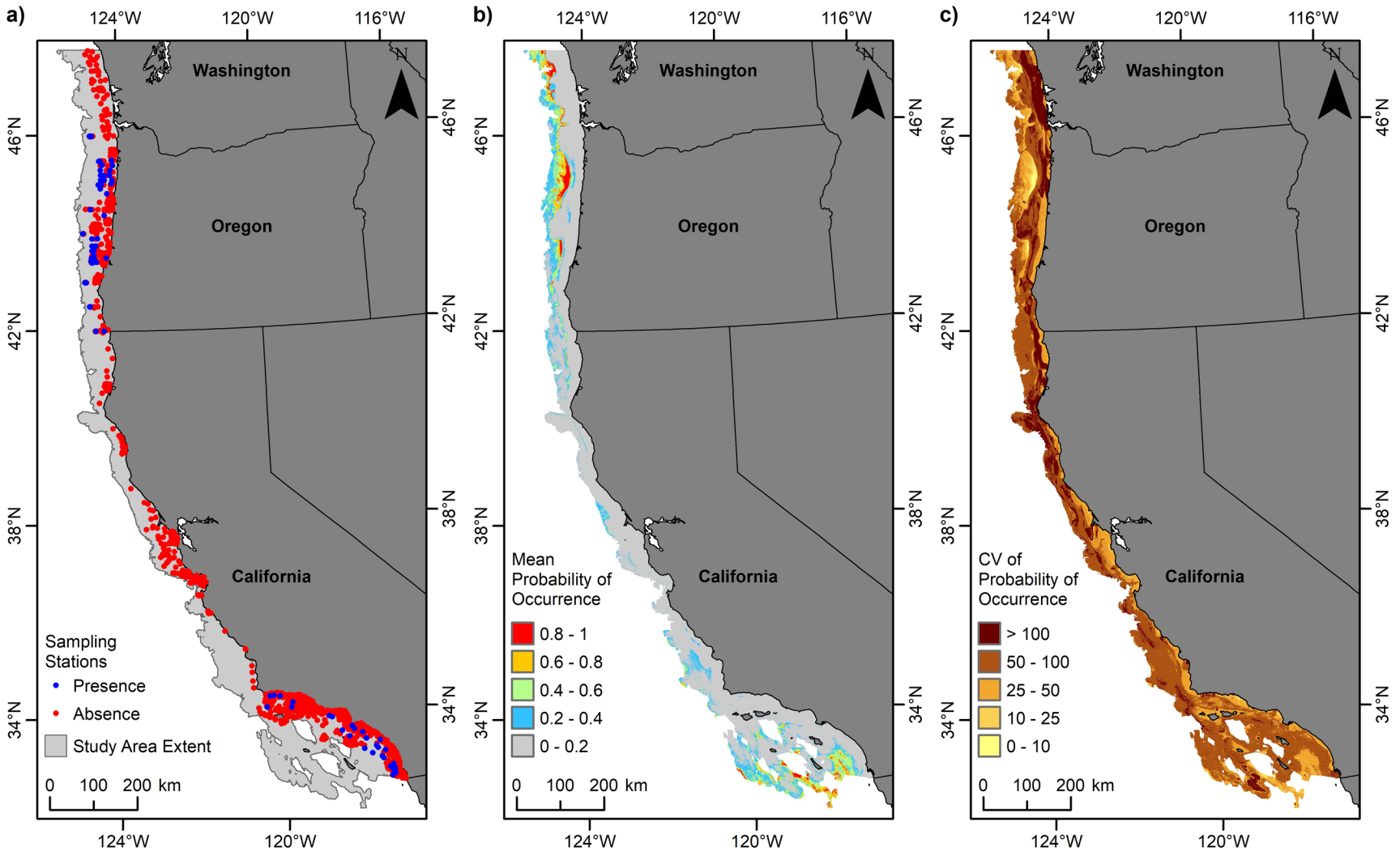

Figure 4.15. Predicted distribution of the scaphopod *Gadila tolmiei* (Scaphopoda, Gadilida, Gadilidae).
(a) Presence or absence of *G. tolmiei* from grab samples at 2905 sampling stations within the study area offshore to 1,200 m depth; (b) mean predicted probability of *G. tolmiei* occurrence; and (c) coefficient of variation of the predicted probability of *G. tolmiei* occurrence.

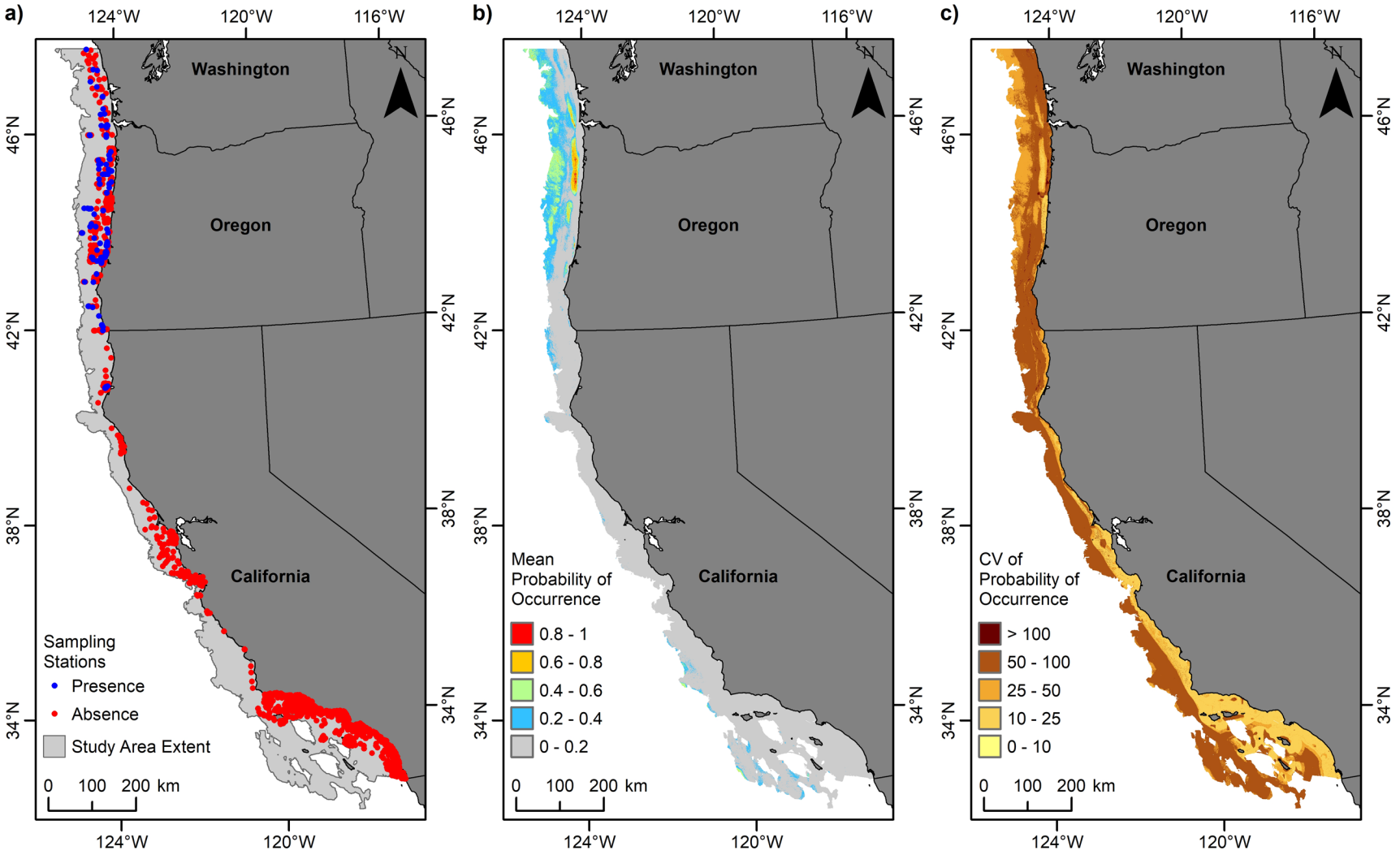

Figure 4.16. Predicted distribution of the scaphopod *Pulsellum salishorum* (Scaphopoda, Gadilida, Pulsellidae).
(a) Presence or absence of *P. salishorum* from grab samples at 2905 sampling stations within the study area offshore to 1,200 m depth; (b) mean predicted probability of *P. salishorum* occurrence; and (c) coefficient of variation of the predicted probability of *P. salishorum* occurrence.

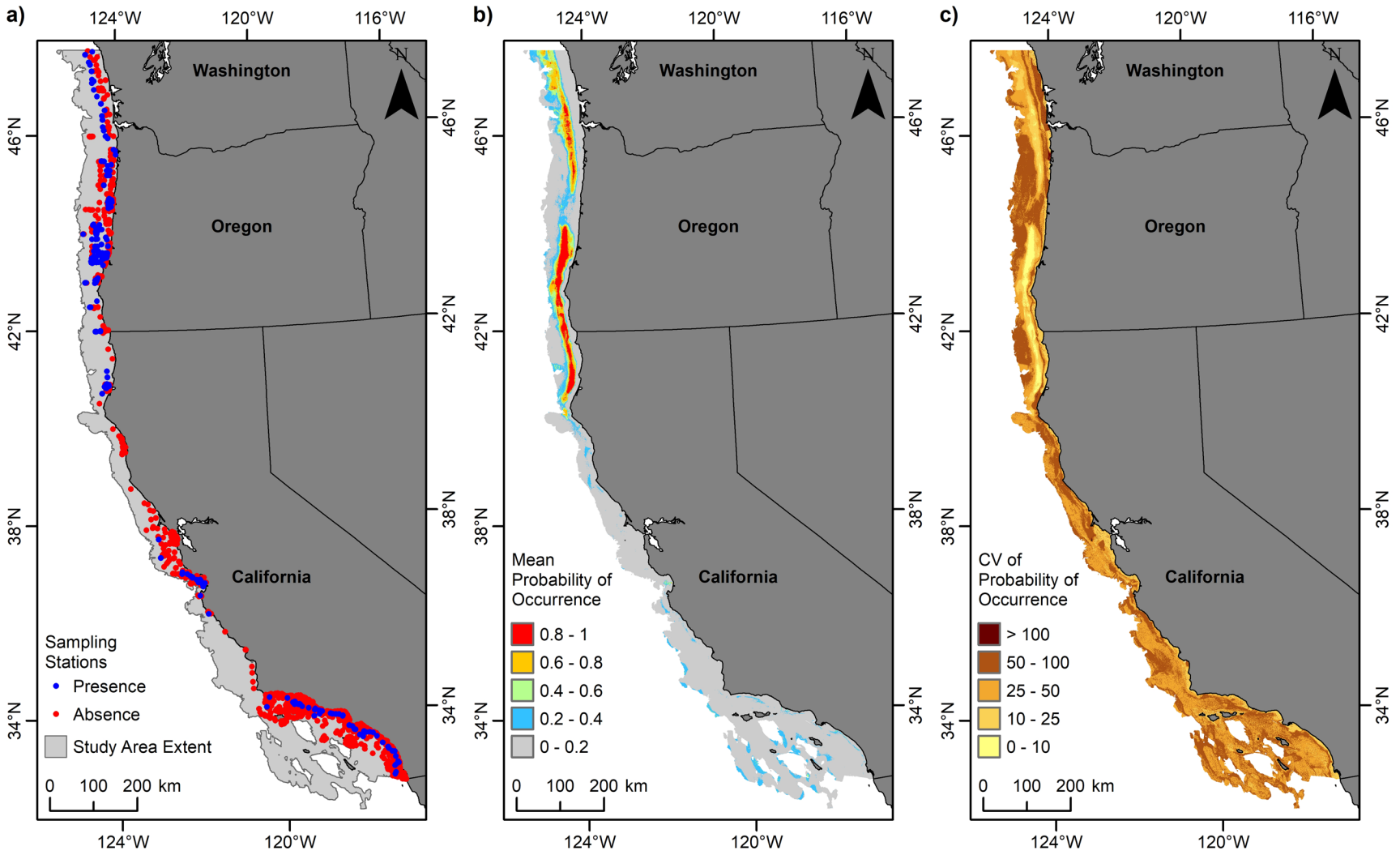

Figure 4.17. Predicted distribution of the scaphopod *Rhabdus rectius* (Scaphopoda, Dentaliida, Rabdidae).
(a) Presence or absence of *R. rectius* from grab samples at 2905 sampling stations within the study area offshore to 1,200 m depth; (b) mean predicted probability of *R. rectius* occurrence; and (c) coefficient of variation of the predicted probability of *R. rectius* occurrence.

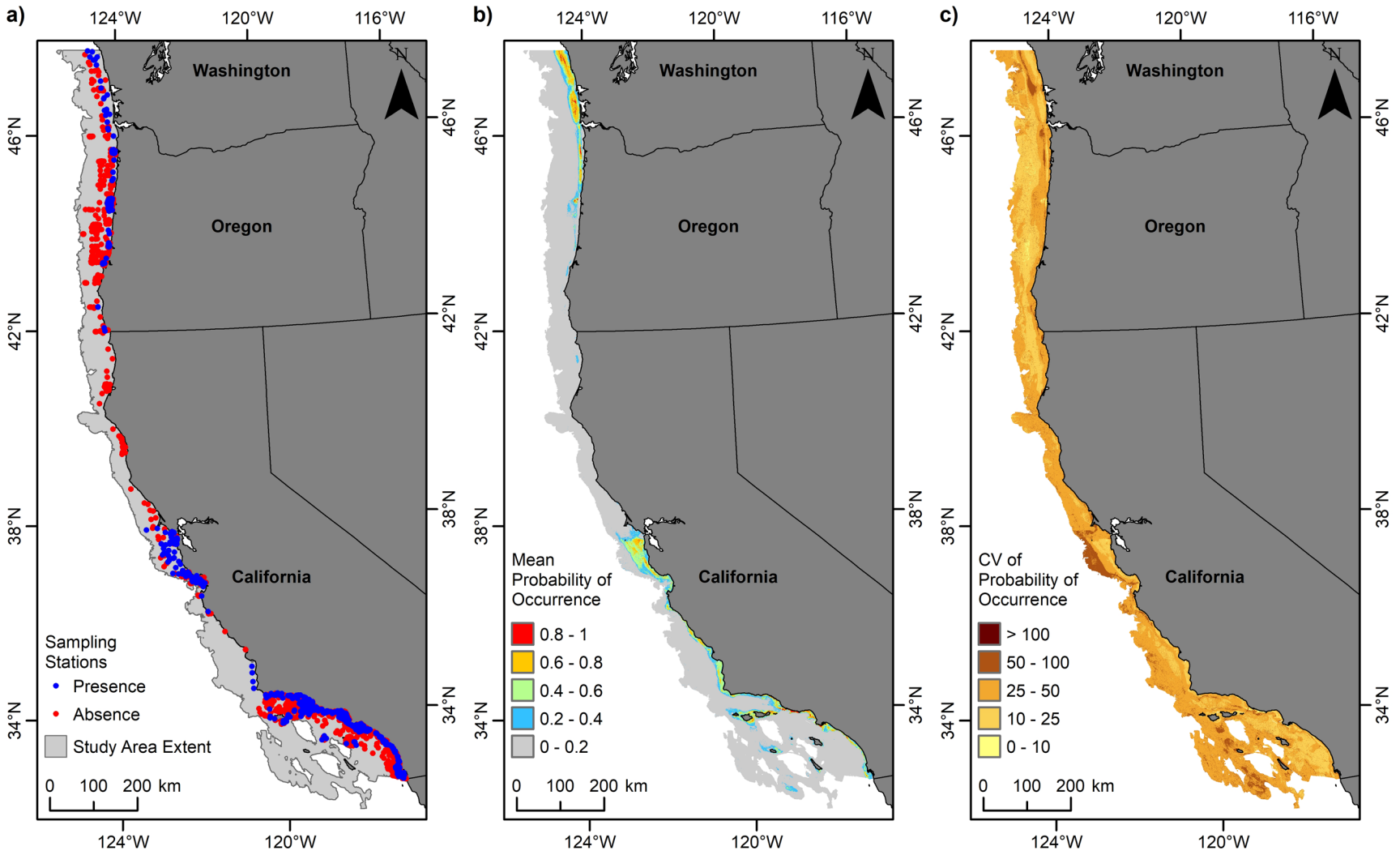

Figure 4.18. Predicted distribution of the ostracod *Euphilomedes carcharodonta* (Ostracoda, Myodocopida, Philomedidae).
(a) Presence or absence of *E. carcharodonta* from grab samples at 2905 sampling stations within the study area offshore to 1,200 m depth; (b) mean predicted probability of *E. carcharodonta* occurrence; and (c) coefficient of variation of the predicted probability of *E. carcharodonta* occurrence.

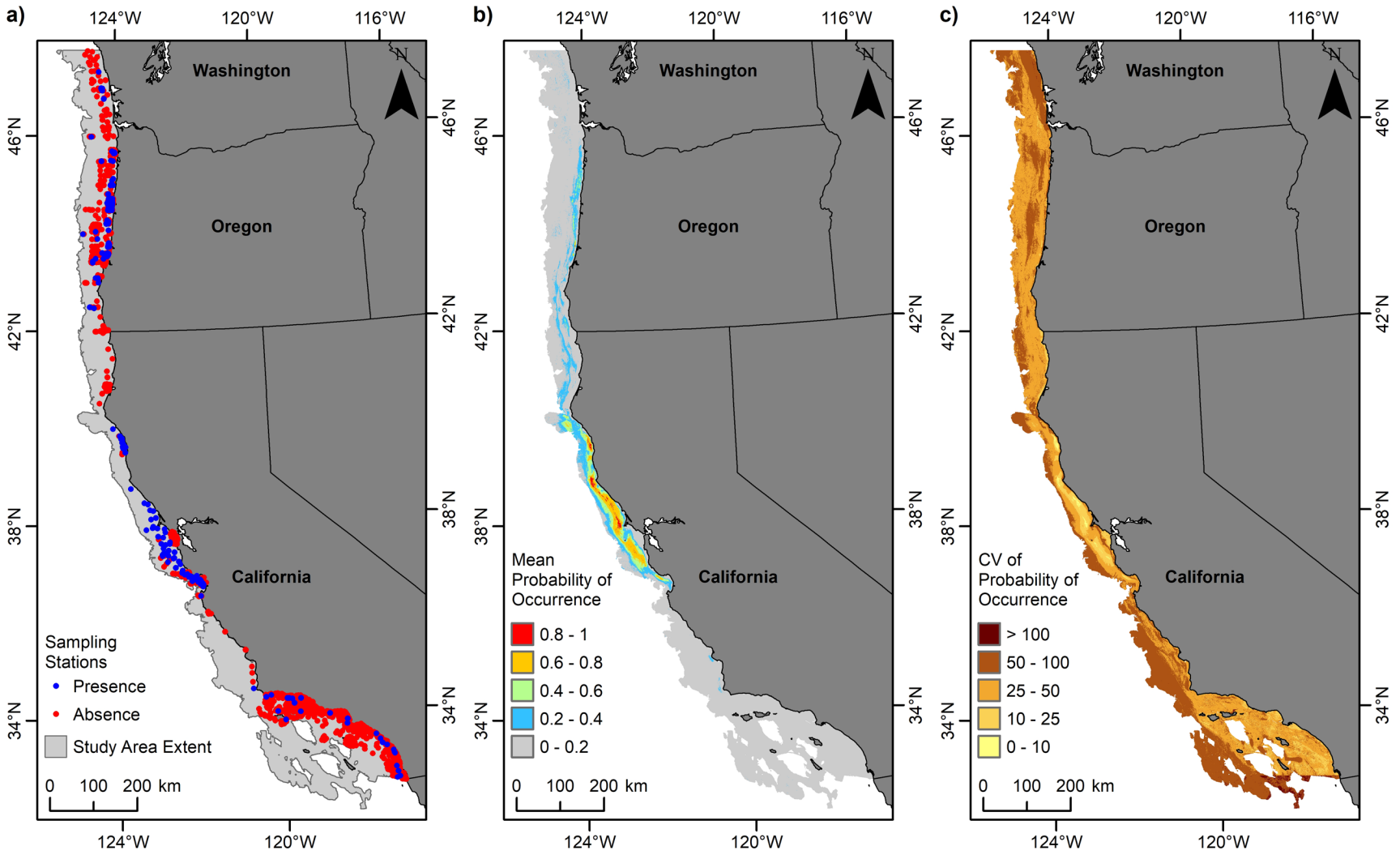

Figure 4.19. Predicted distribution of the pea crab *Pinnixa occidentalis* complex (Malacostraca, Decapoda, Pinnotheridae).
(a) Presence or absence of *P. occidentalis* complex from grab samples at 2905 sampling stations within the study area offshore to 1,200 m depth; (b) mean predicted probability of *P. occidentalis* complex occurrence; and (c) coefficient of variation of the predicted probability of *P. occidentalis* complex occurrence.

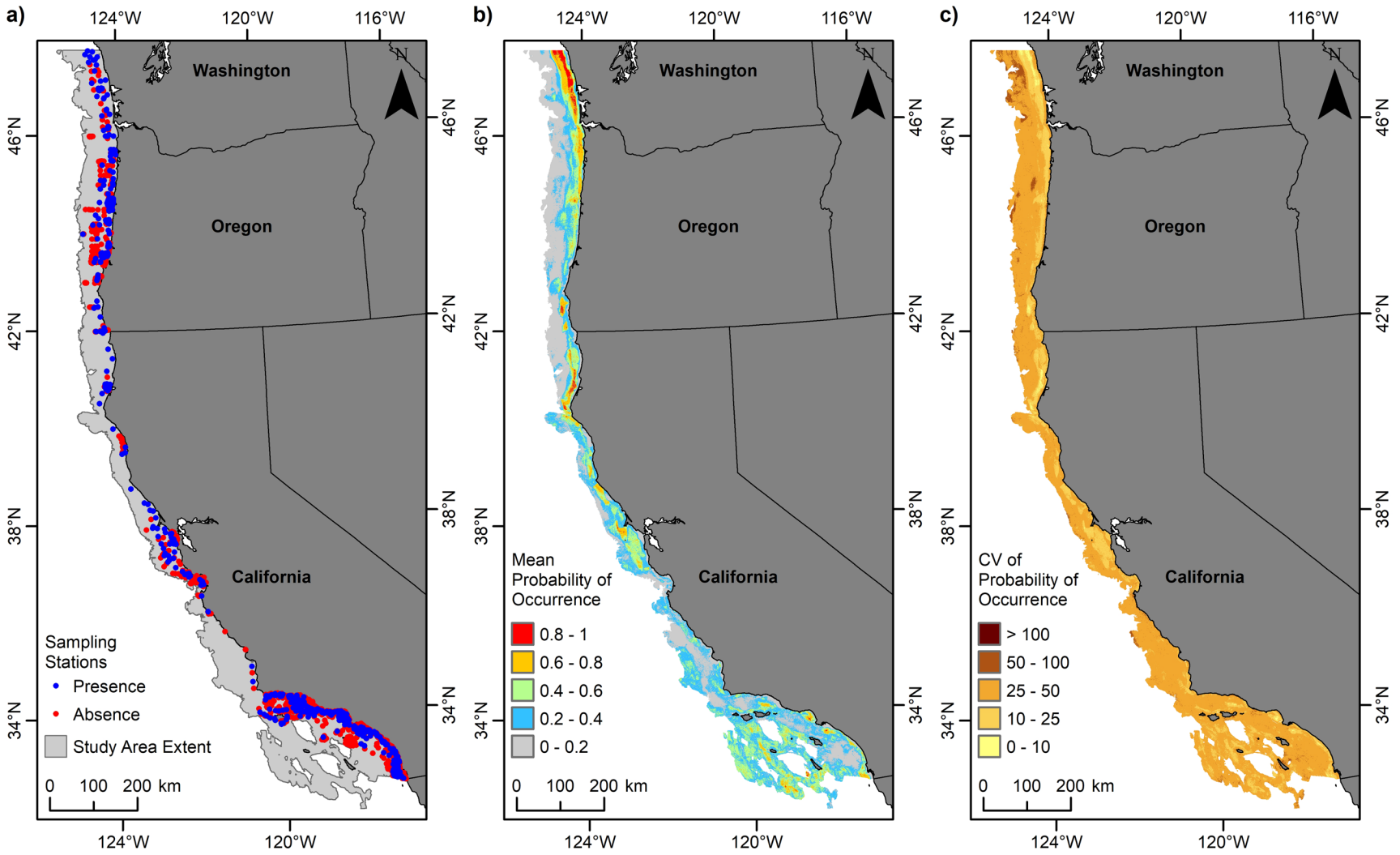

Figure 4.20. Predicted distribution of the amphipod *Ampelisca careyi* (Malacostraca, Amphipoda, Ampeliscidae).
(a) Presence or absence of *A. careyi* from grab samples at 2905 sampling stations within the study area offshore to 1,200 m depth; (b) mean predicted probability of *A. careyi* occurrence; and (c) coefficient of variation of the predicted probability of *A. careyi* occurrence.

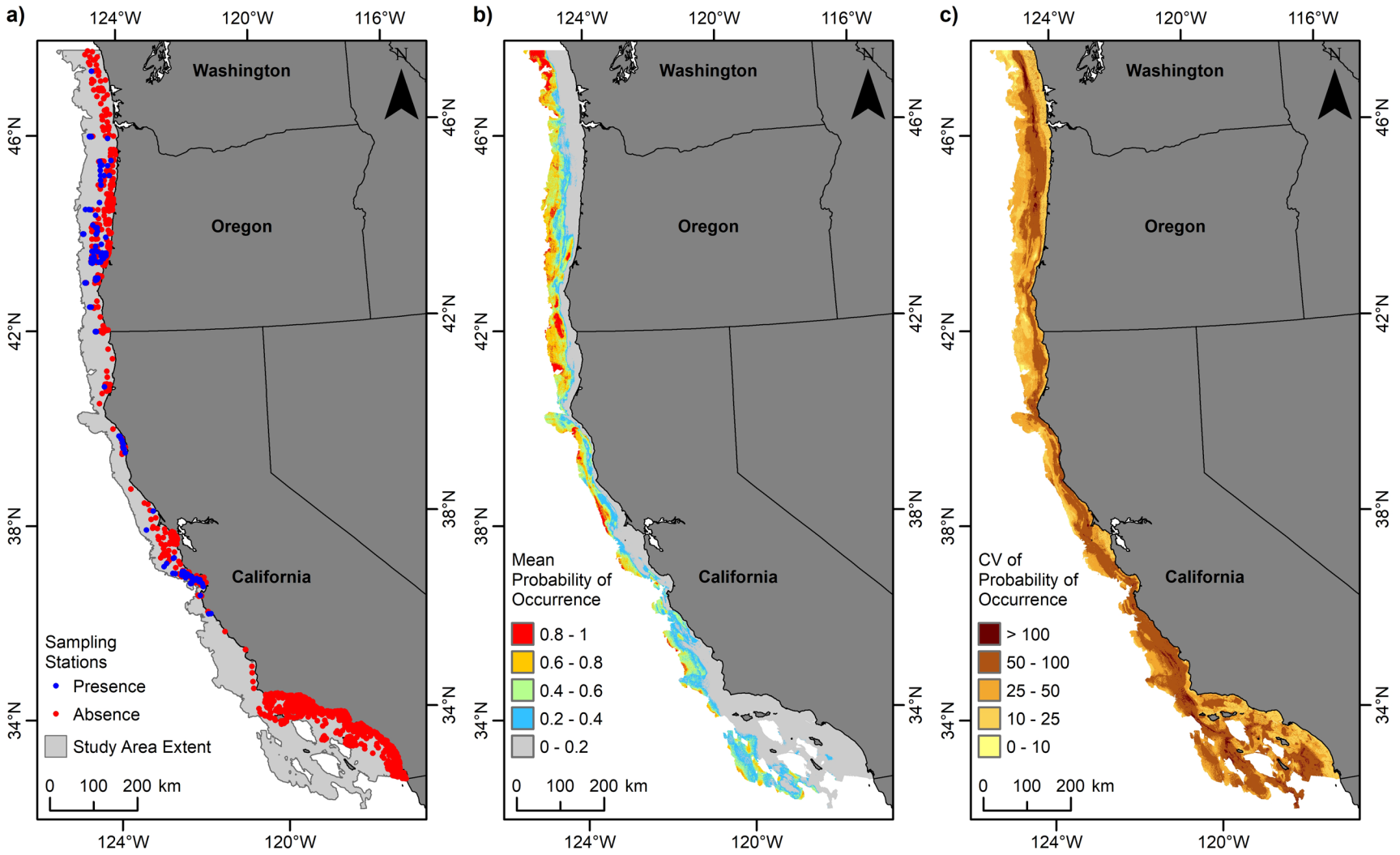

Figure 4.21. Predicted distribution of the heart urchin *Brisaster latifrons* (Echinoidea, Spatangoida, Schizasteridae).
(a) Presence or absence of *B. latifrons* from grab samples at 2905 sampling stations within the study area offshore to 1,200 m depth; (b) mean predicted probability of *B. latifrons* occurrence; and (c) coefficient of variation of the predicted probability of *B. latifrons* occurrence.

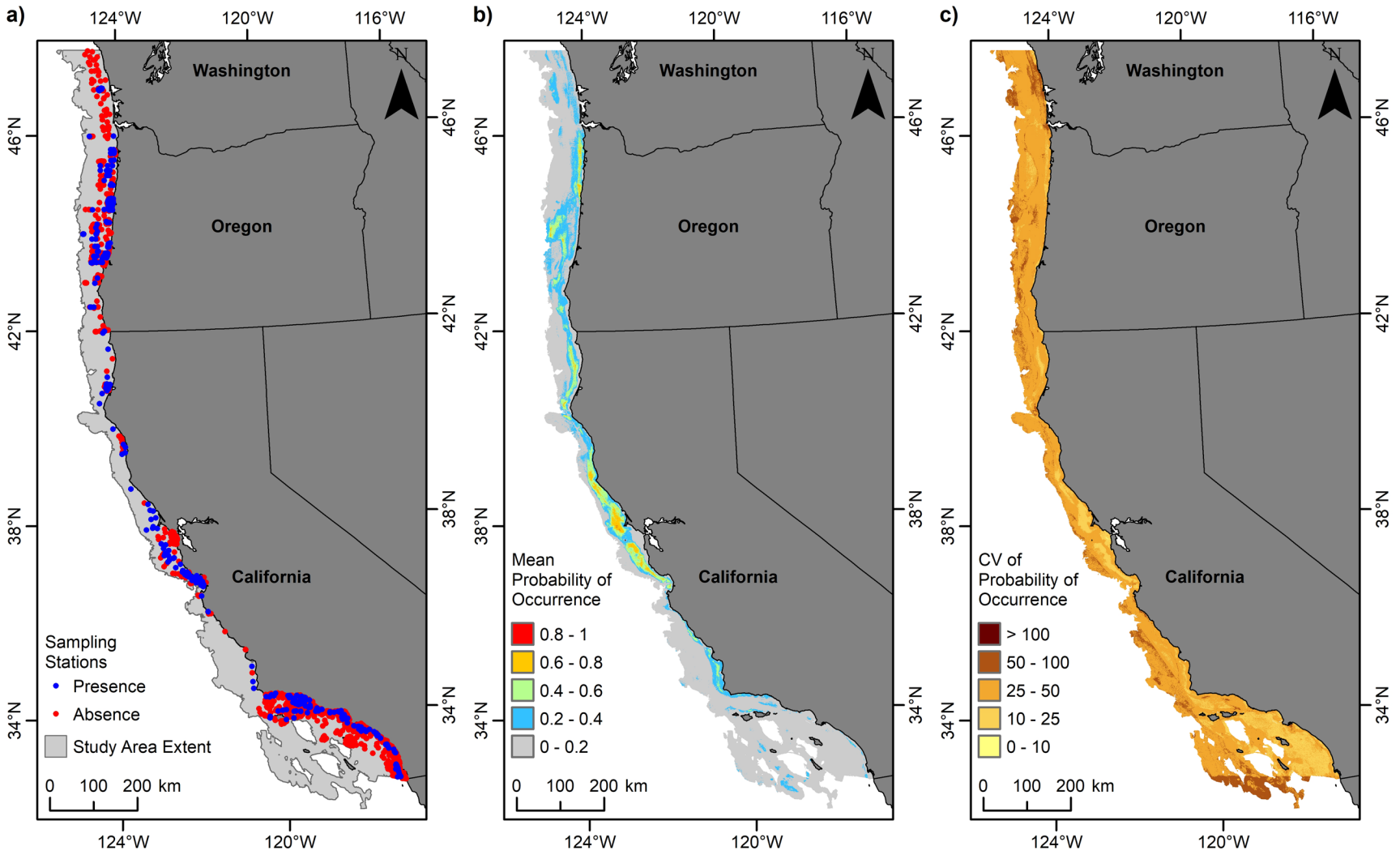

Figure 4.22. Predicted distribution of the brittle star *Amphiodia urtica* (Ophiuroidea, Ophiurida, Amphiuridae).
(a) Presence or absence of *A. urtica* from grab samples at 2905 sampling stations within the study area offshore to 1,200 m depth; (b) mean predicted probability of *A. urtica* occurrence; and (c) coefficient of variation of the predicted probability of *A. urtica* occurrence.

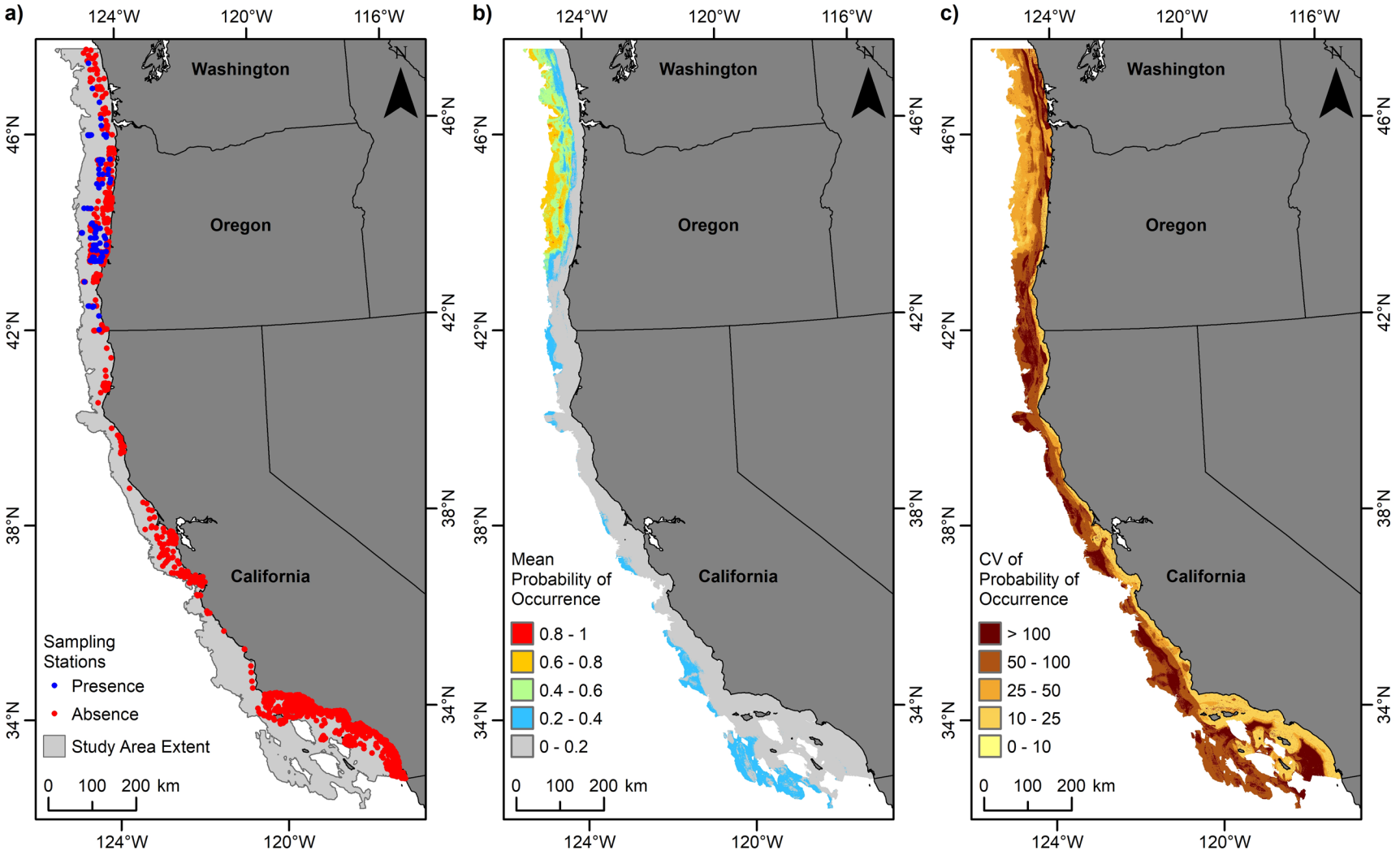

Figure 4.23. Predicted distribution of the brittle star *Amphioplus macraspis* (Ophiuroidea, Ophiurida, Amphiuridae).
(a) Presence or absence of *A. macraspis* from grab samples at 2905 sampling stations within the study area offshore to 1,200 m depth; (b) mean predicted probability of *A. macraspis* occurrence; and (c) coefficient of variation of the predicted probability of *A. macraspis* occurrence.

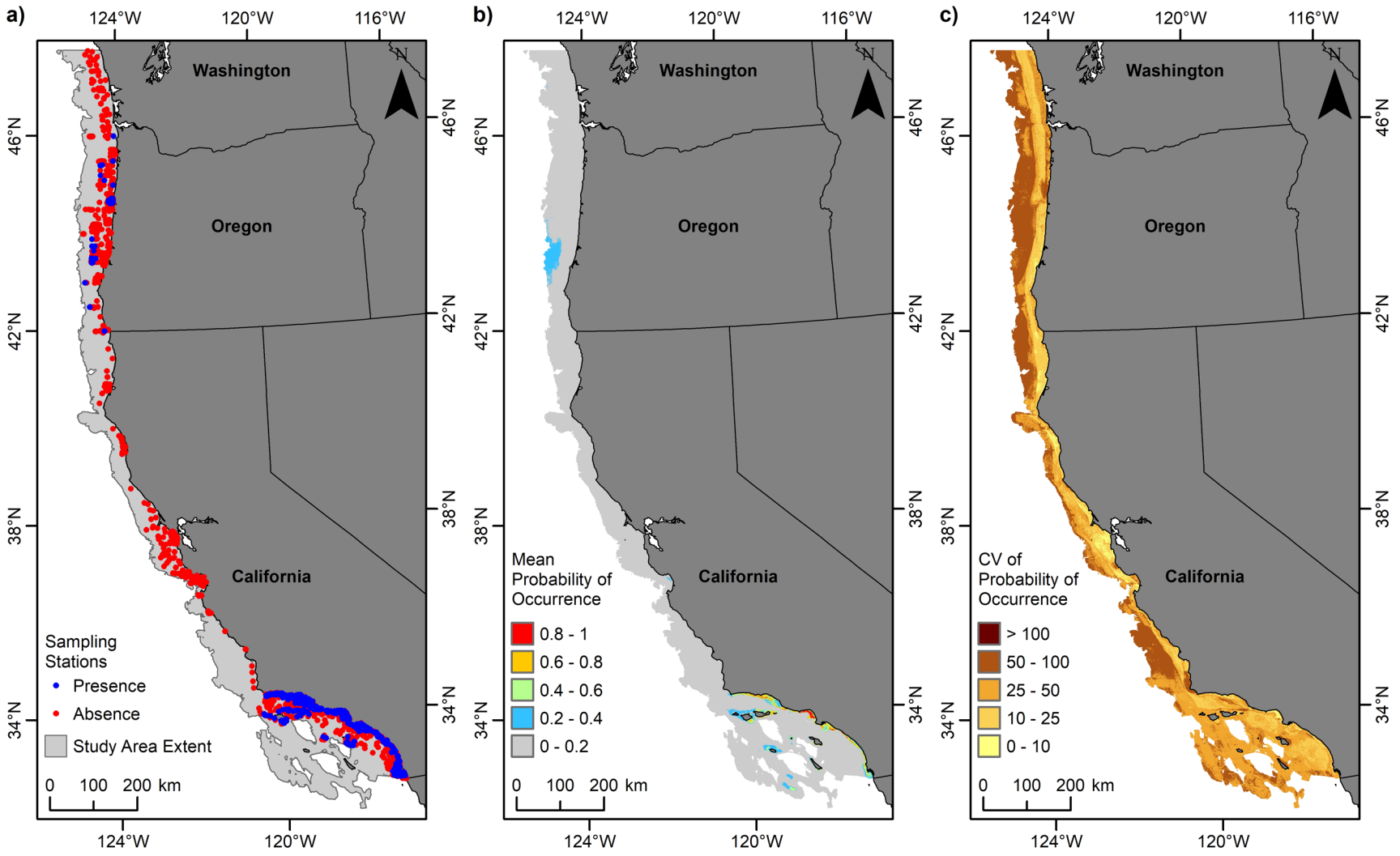

Figure 4.24. Predicted distribution of horseshoe worms in Family Phoronidae.
(a) Presence or absence of Phoronidae from grab samples at 2905 sampling stations within the study area offshore to 1,200 m depth; (b) mean predicted probability of Phoronidae occurrence; and (c) coefficient of variation of the predicted probability of Phoronidae occurrence.

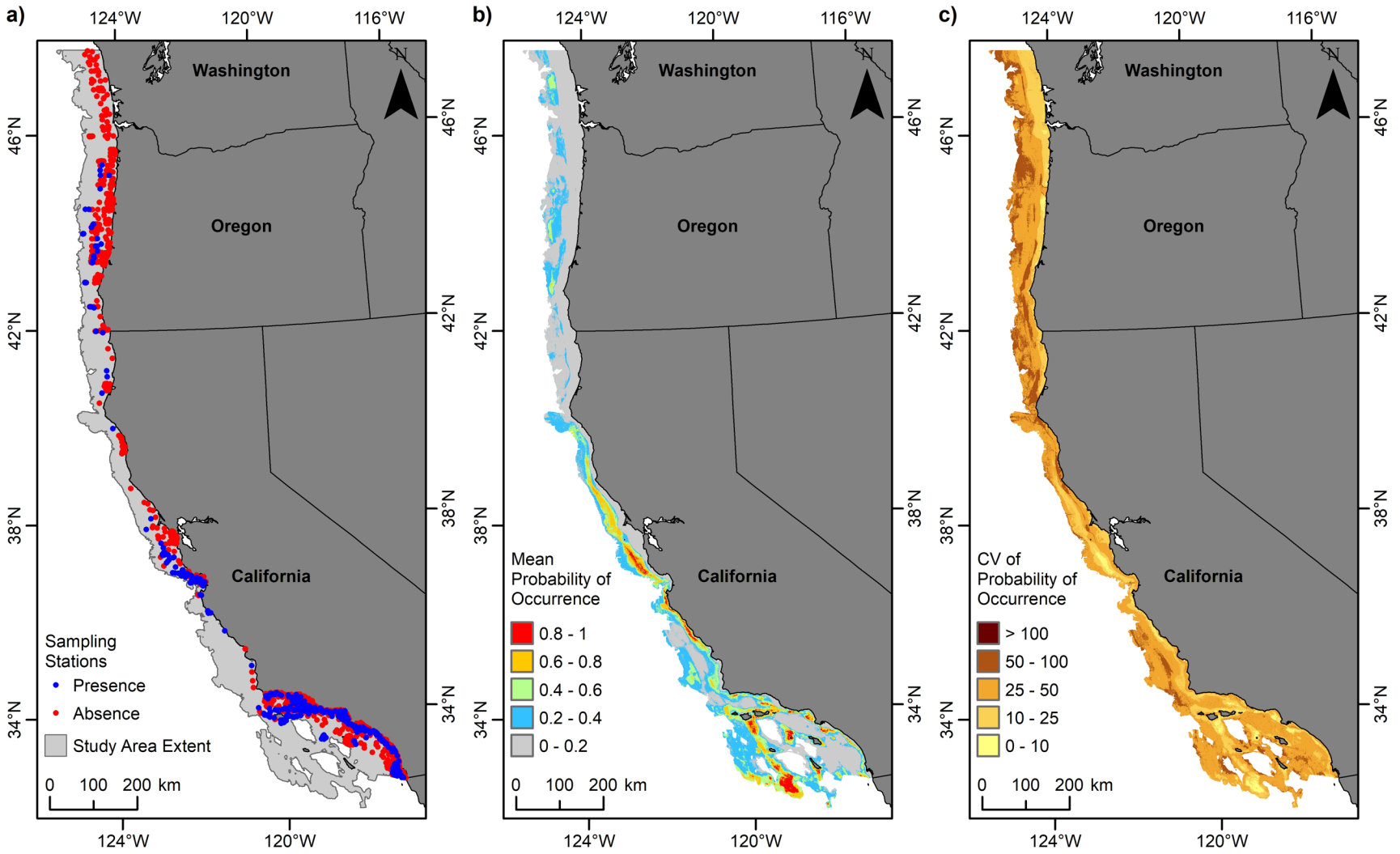

Figure 4.25. Predicted distribution of the polychaete *Chloeia pinnata* (Polychaeta, Amphinomida, Amphinomidae).
(a) Presence or absence of *C. pinnata* from grab samples at 2905 sampling stations within the study area offshore to 1,200 m depth; (b) mean predicted probability of *C. pinnata* occurrence; and (c) coefficient of variation of the predicted probability of *C. pinnata* occurrence.

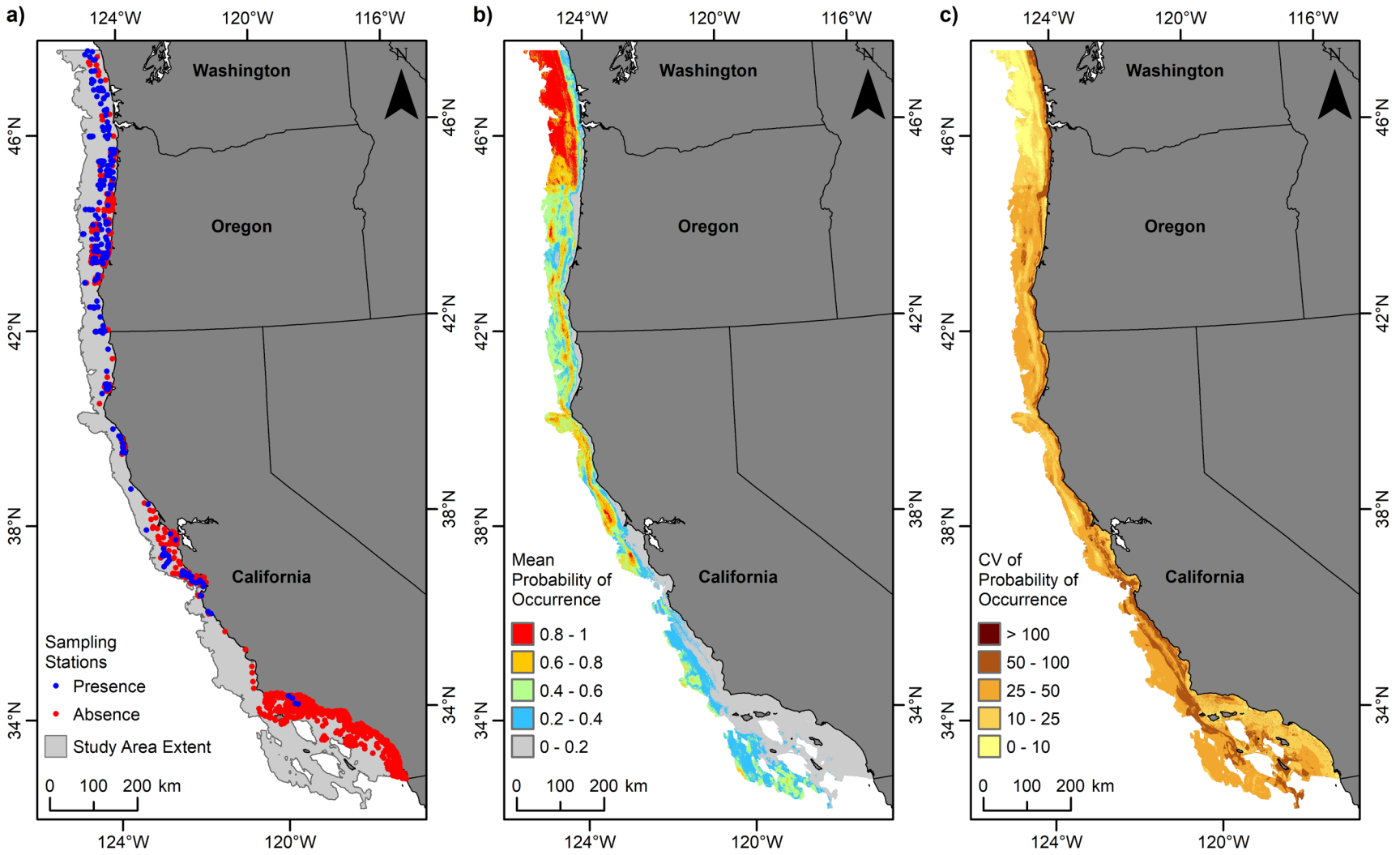

Figure 4.26. Predicted distribution of the polychaete *Galathowenia oculata* (Polychaeta, Sabellida, Oweniidae).
(a) Presence or absence of *G. oculata* from grab samples at 2905 sampling stations within the study area offshore to 1,200 m depth; (b) mean predicted probability of *G. oculata* occurrence; and (c) coefficient of variation of the predicted probability of *G. oculata* occurrence.

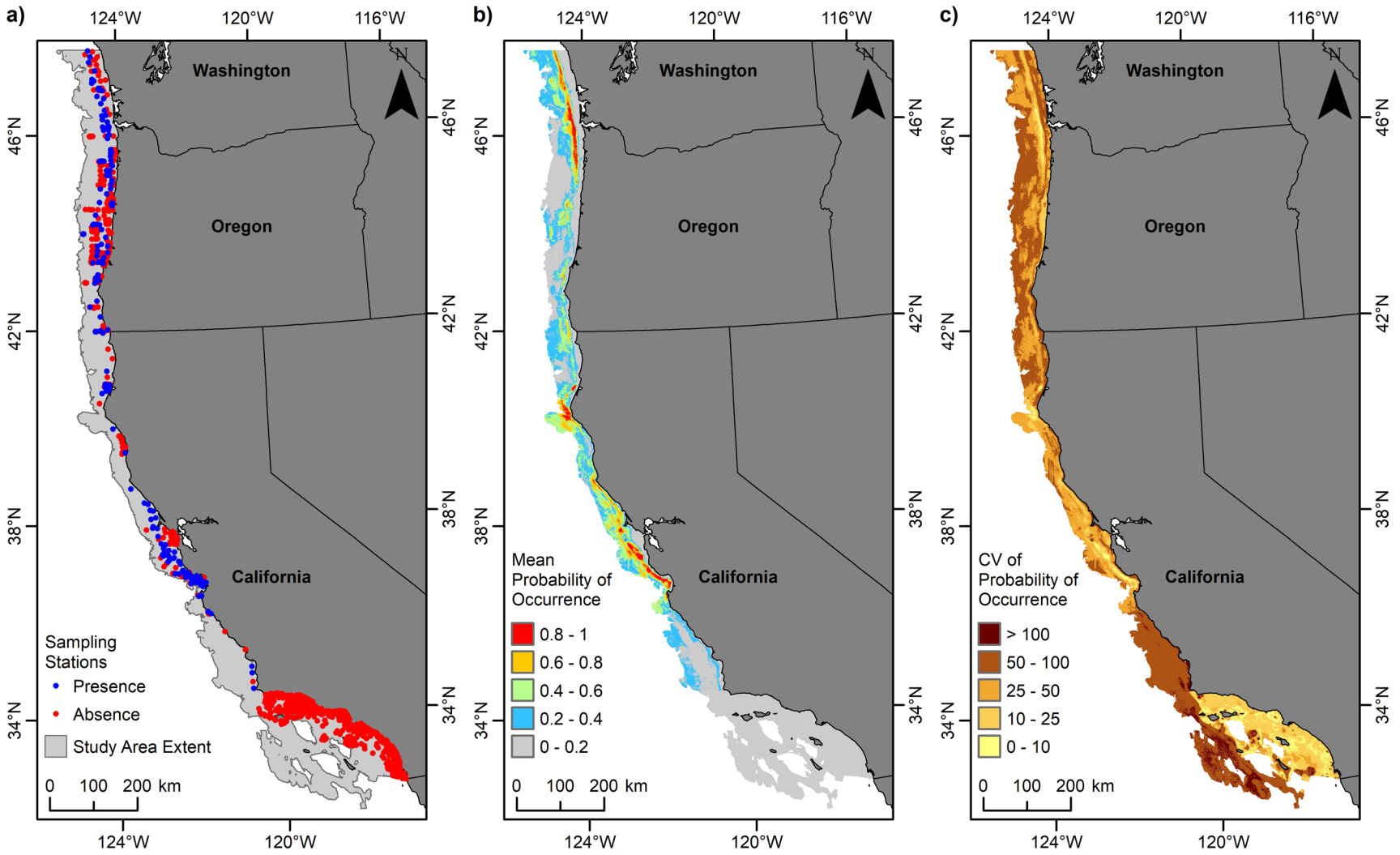

Figure 4.27. Predicted distribution of the polychaete *Glycera nana* (Polychaeta, Phyllodocida, Glyceridae).
(a) Presence or absence of *G. nana* from grab samples at 2905 sampling stations within the study area offshore to 1,200 m depth; (b) mean predicted probability of *G. nana* occurrence; and (c) coefficient of variation of the predicted probability of *G. nana* occurrence.

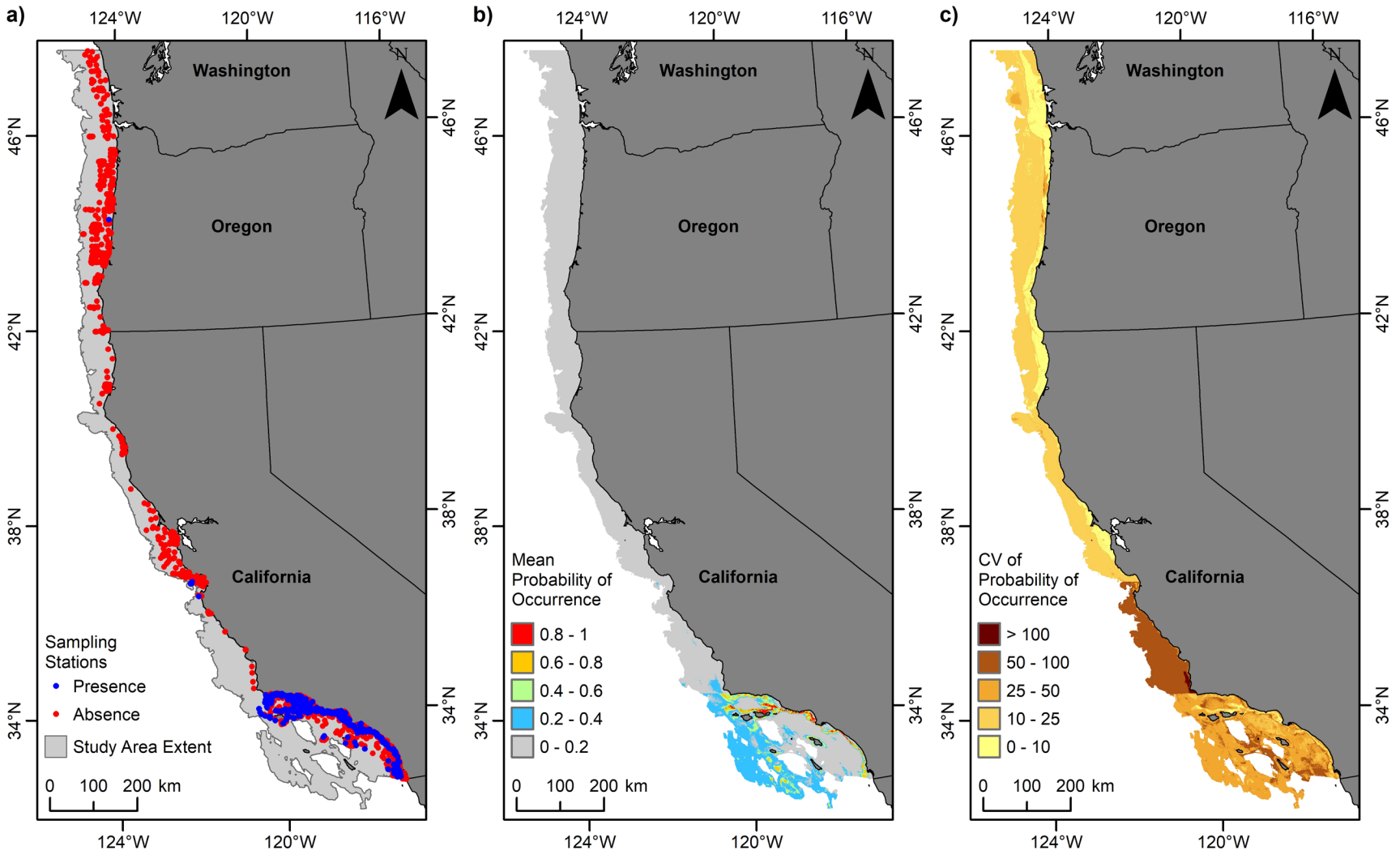

Figure 4.28. Predicted distribution of the polychaete *Glycera tesselata* (Polychaeta, Phyllodocida, Glyceridae).
(a) Presence or absence of *G. tesselata* from grab samples at 2905 sampling stations within the study area offshore to 1,200 m depth; (b) mean predicted probability of *G. tesselata* occurrence; and (c) coefficient of variation of the predicted probability of *G. tesselata* occurrence.

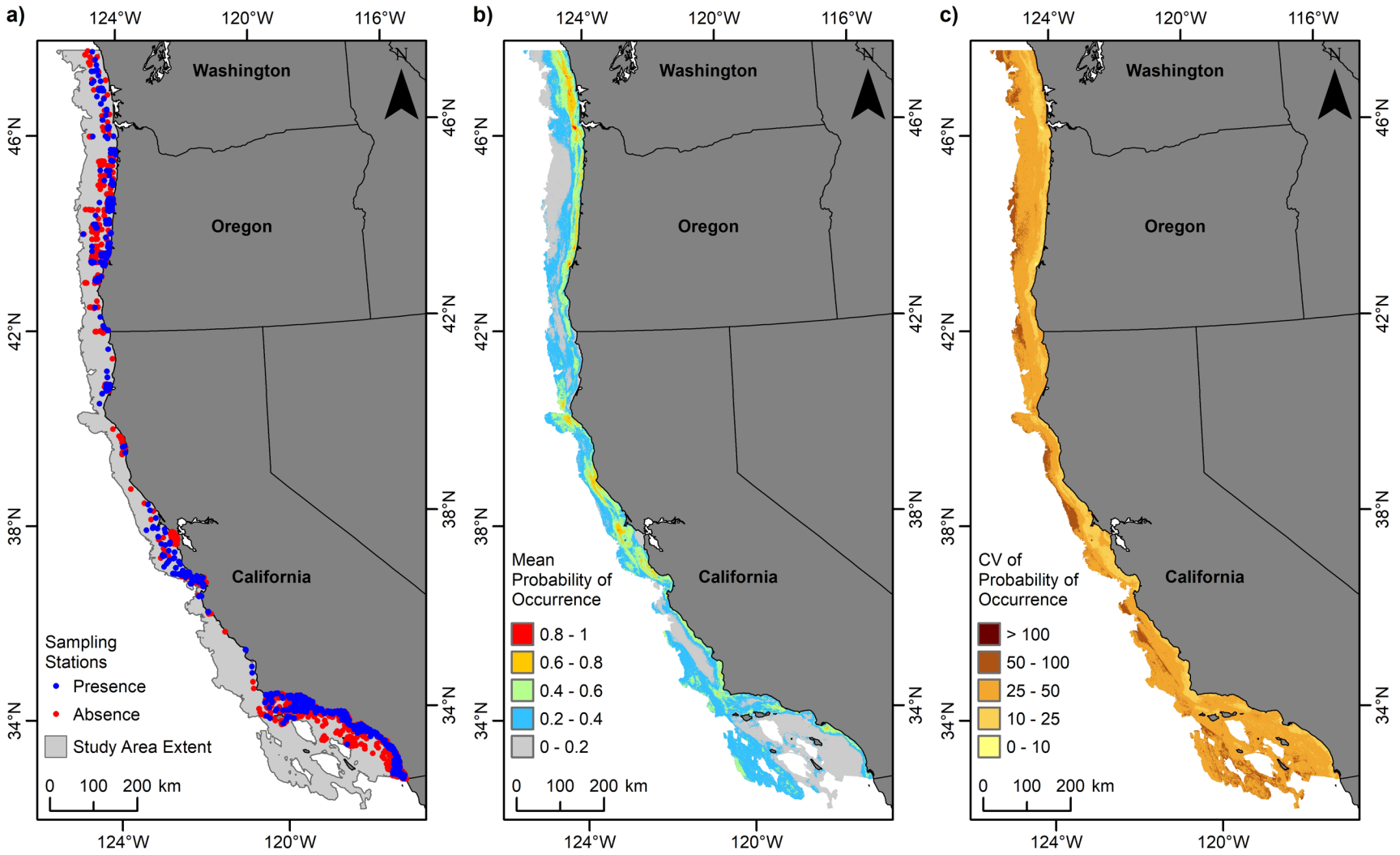

Figure 4.29. Predicted distribution of the polychaete *Glycinde armigera* (Polychaeta, Phyllodocida, Goniadidae).
(a) Presence or absence of *G. armigera* from grab samples at 2905 sampling stations within the study area offshore to 1,200 m depth; (b) mean predicted probability of *G. armigera* occurrence; and (c) coefficient of variation of the predicted probability of *G. armigera* occurrence.

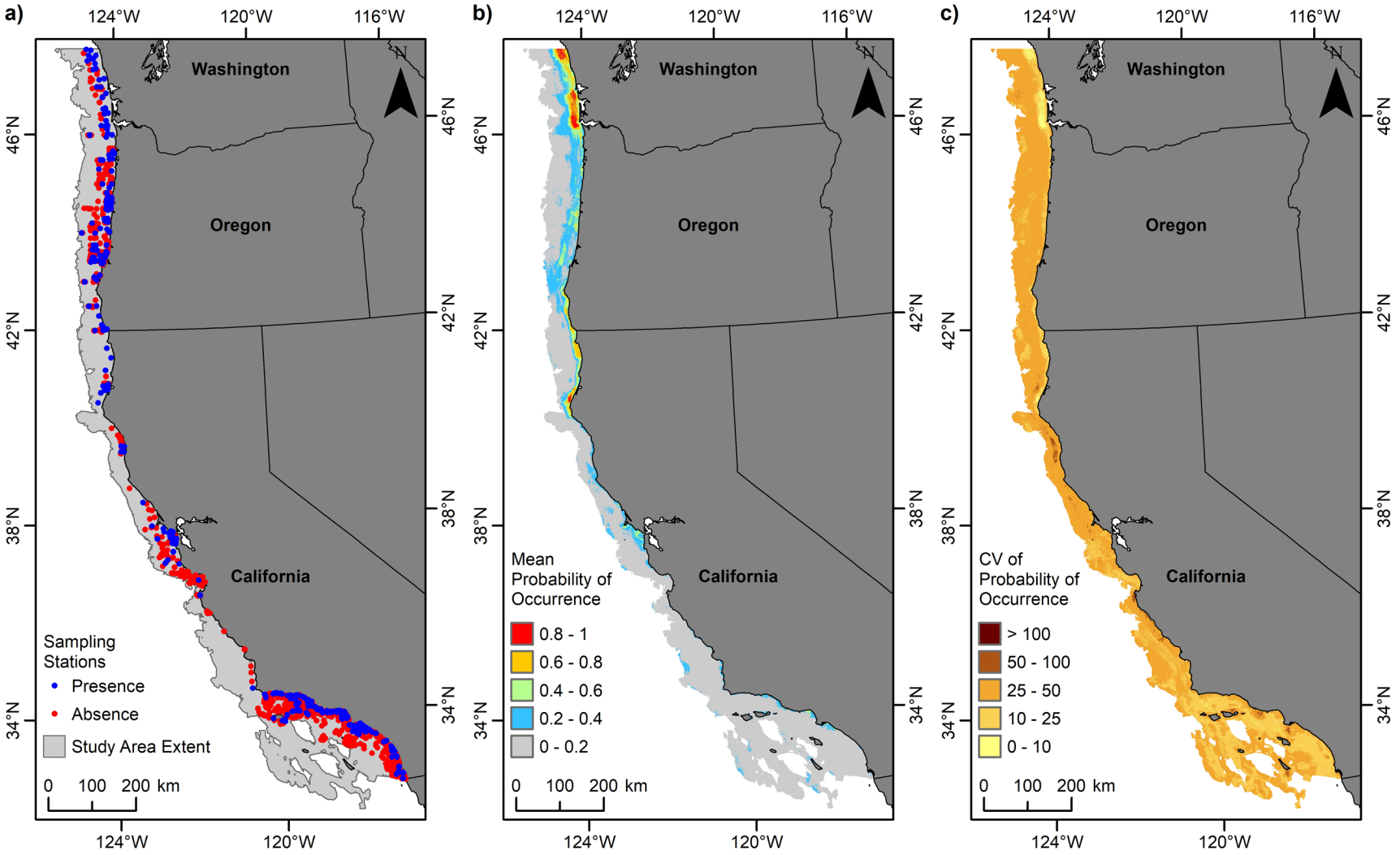

Figure 4.30. Predicted distribution of the polychaete *Leitoscoloplos pugettensis* (Polychaeta, Sedentaria, Orbiniidae).
(a) Presence or absence of *L. pugettensis* from grab samples at 2905 sampling stations within the study area offshore to 1,200 m depth; (b) mean predicted probability of *L. pugettensis* occurrence; and (c) coefficient of variation of the predicted probability of *L. pugettensis* occurrence.

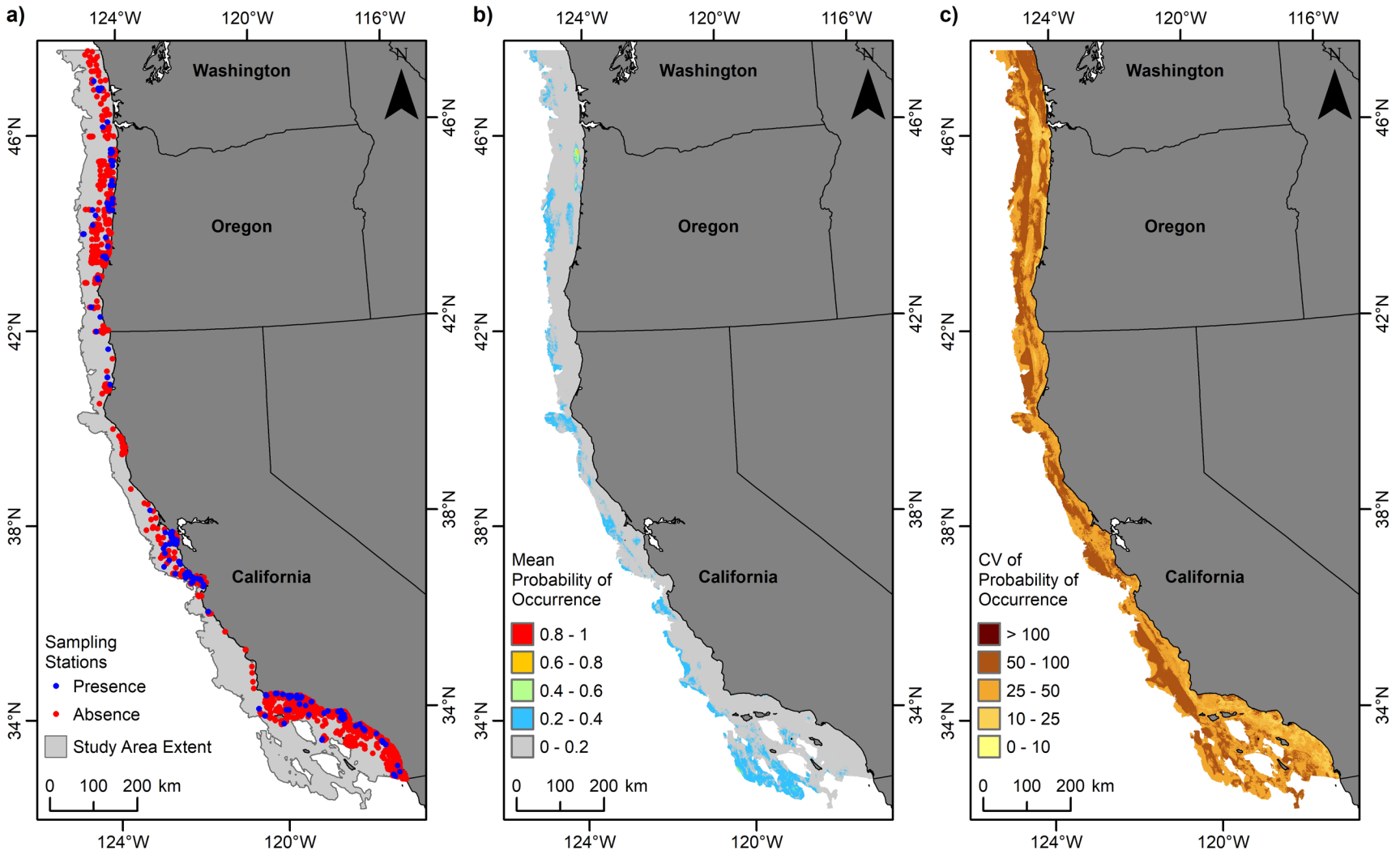

Figure 4.31. Predicted distribution of the polychaete *Magelona berkeleyi* (Polychaeta, Spionida, Magelonidae).
(a) Presence or absence of *M. berkeleyi* from grab samples at 2905 sampling stations within the study area offshore to 1,200 m depth; (b) mean predicted probability of *M. berkeleyi* occurrence; and (c) coefficient of variation of the predicted probability of *M. berkeleyi* occurrence.

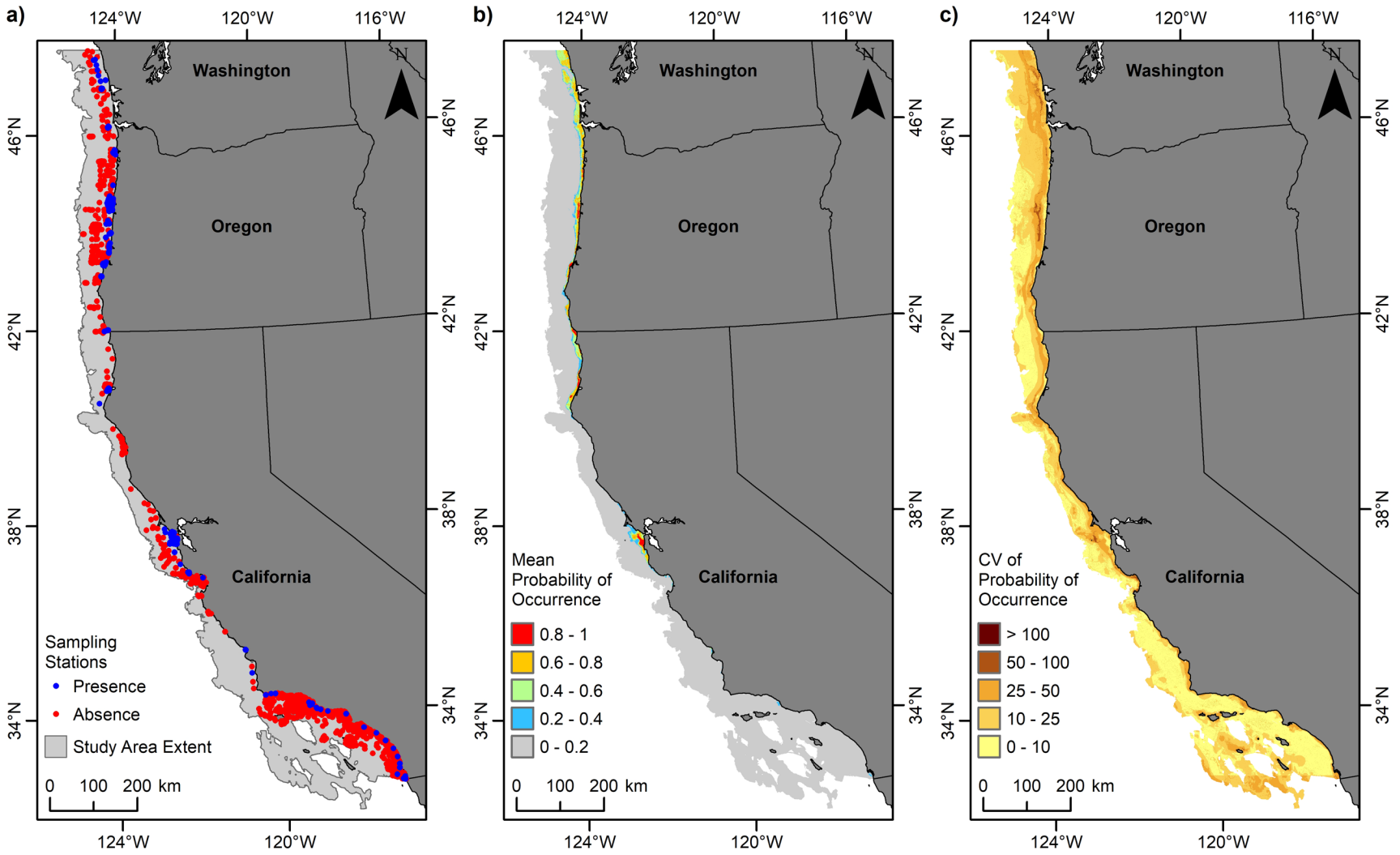

Figure 4.32. Predicted distribution of the polychaete *Magelona sacculata* (Polychaeta, Spionida, Magelonidae).
(a) Presence or absence of *M. sacculata* from grab samples at 2905 sampling stations within the study area offshore to 1,200 m depth; (b) mean predicted probability of *M. sacculata* occurrence; and (c) coefficient of variation of the predicted probability of *M. sacculata* occurrence.

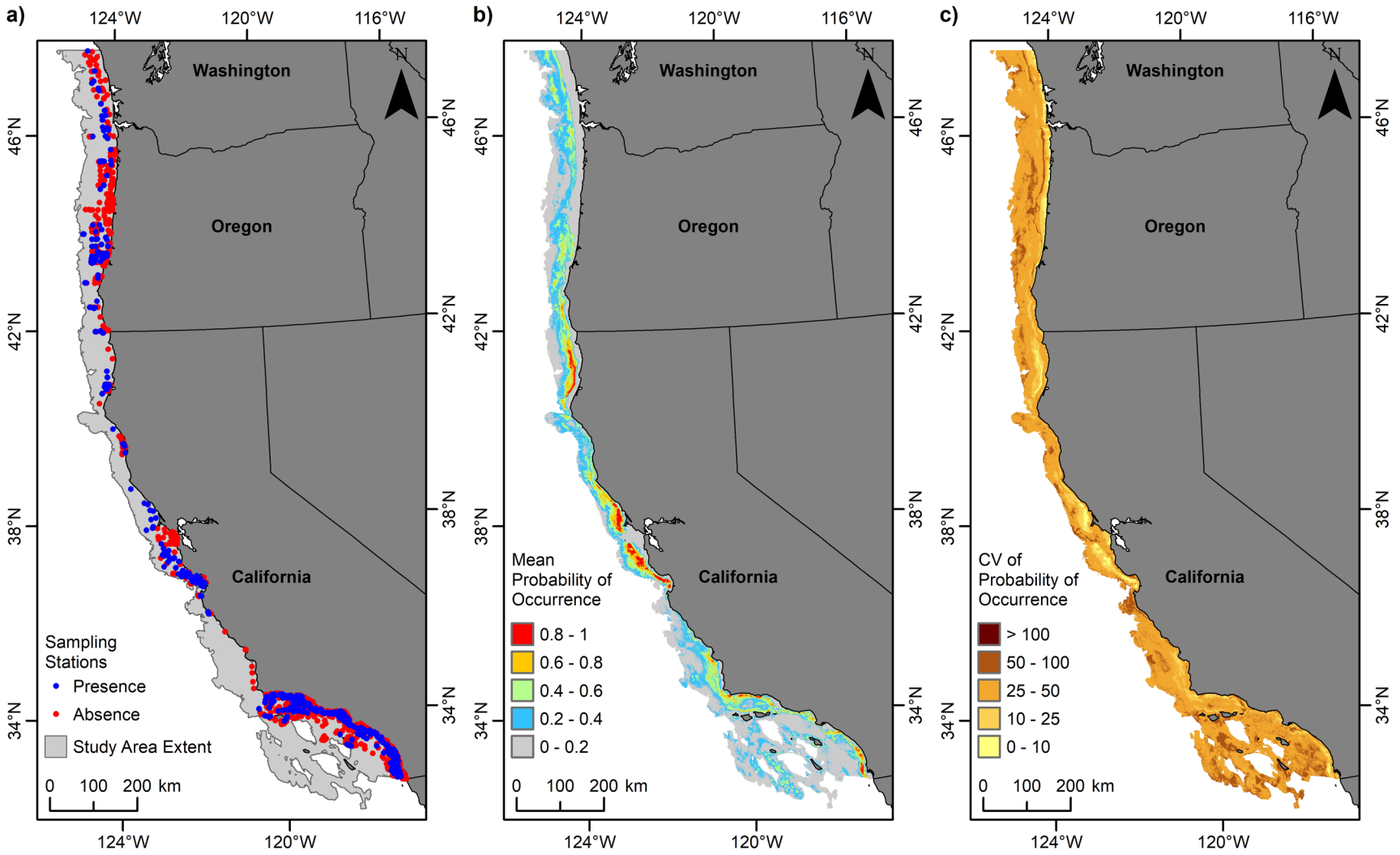

Figure 4.33. Predicted distribution of the polychaete *Maldane sarsi* (Polychaeta, Sedentaria, Maldanidae).
(a) Presence or absence of *M. sarsi* from grab samples at 2905 sampling stations within the study area offshore to 1,200 m depth; (b) mean predicted probability of *M. sarsi* occurrence; and (c) coefficient of variation of the predicted probability of *M. sarsi* occurrence.

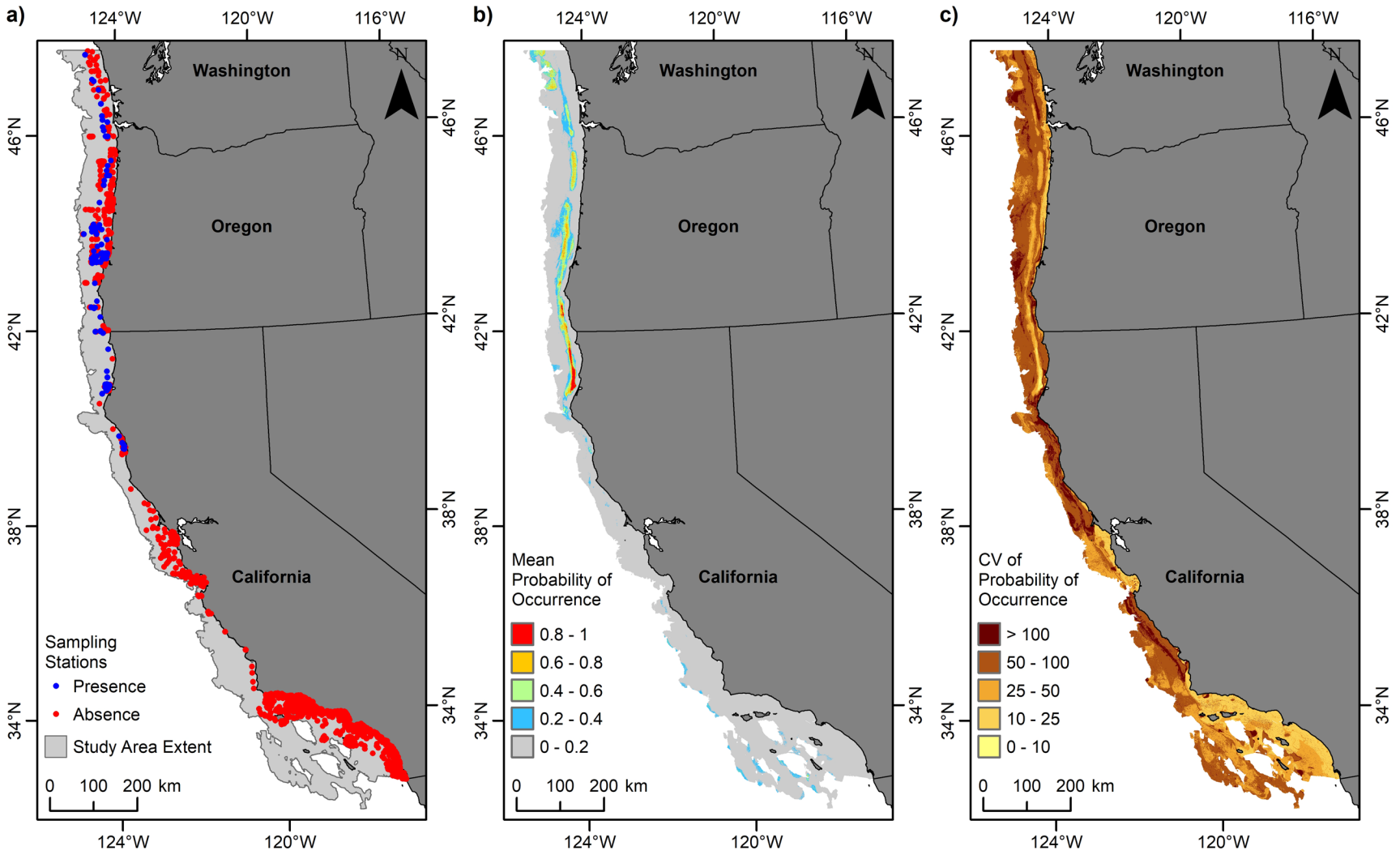

Figure 4.34. Predicted distribution of the polychaete *Ninoe gemmea* (Polychaeta, Eunicida, Lumbrineridae).
(a) Presence or absence of *N. gemmea* from grab samples at 2905 sampling stations within the study area offshore to 1,200 m depth; (b) mean predicted probability of *N. gemmea* occurrence; and (c) coefficient of variation of the predicted probability of *N. gemmea* occurrence.

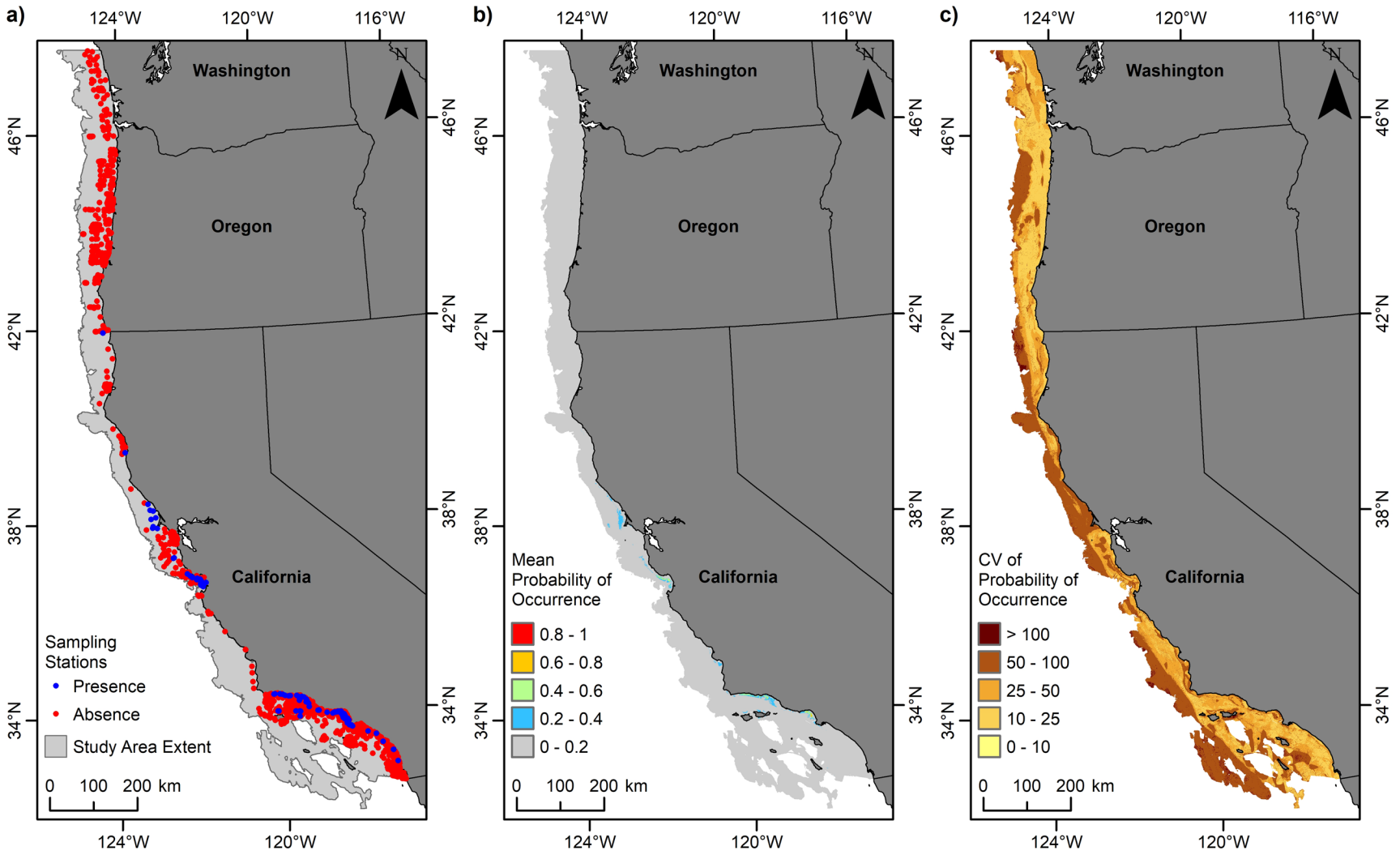

Figure 4.35. Predicted distribution of the polychaete *Ninoe tridentata* (Polychaeta, Eunicida, Lumbrineridae).
(a) Presence or absence of *N. tridentata* from grab samples at 2905 sampling stations within the study area offshore to 1,200 m depth; (b) mean predicted probability of *N. tridentata* occurrence; and (c) coefficient of variation of the predicted probability of *N. tridentata* occurrence.

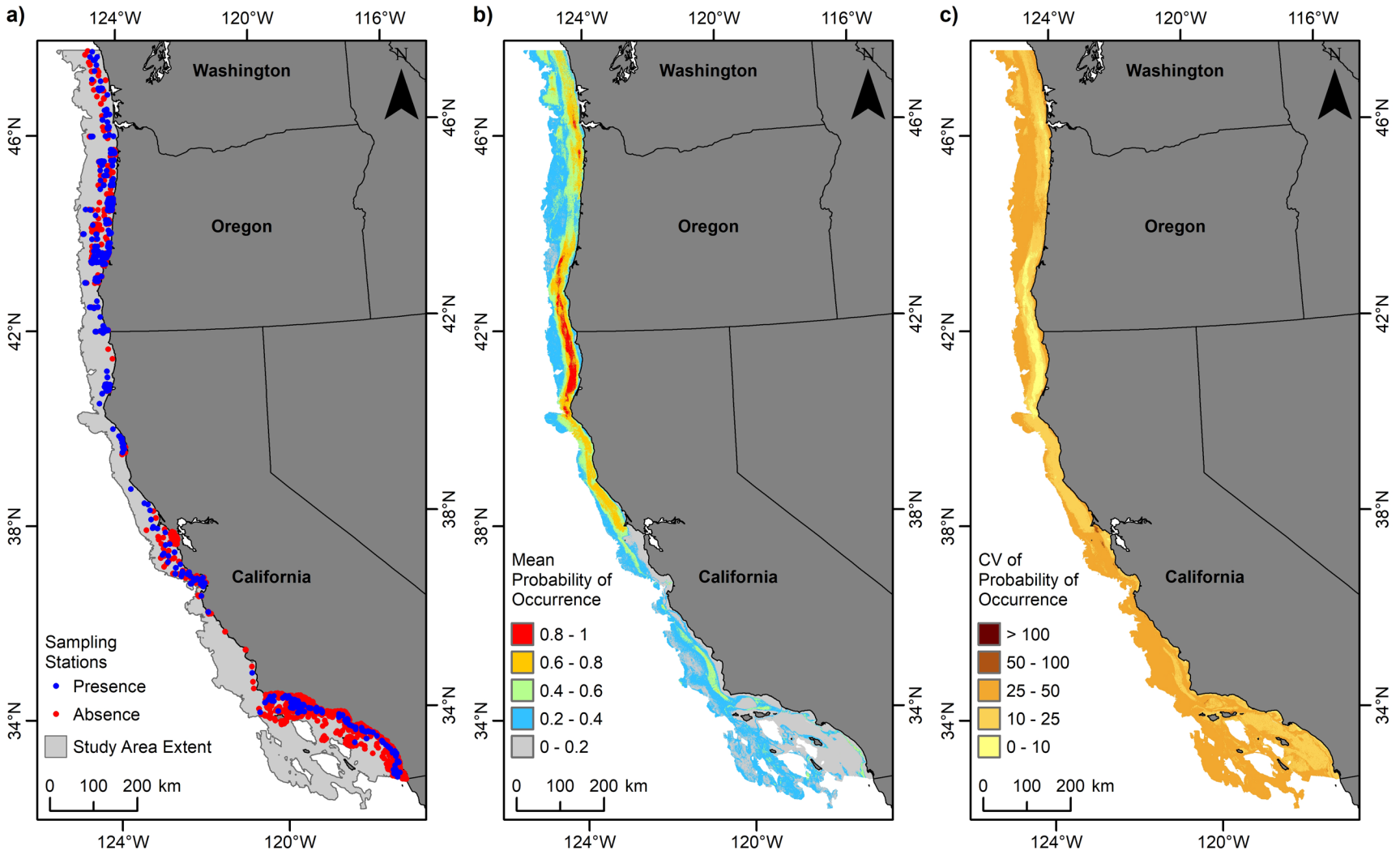

Figure 4.36. Predicted distribution of the polychaete *Onuphis iridescens* (Polychaeta, Eunicida, Onuphidae).
(a) Presence or absence of *O. iridescens* from grab samples at 2905 sampling stations within the study area offshore to 1,200 m depth; (b) mean predicted probability of *O. iridescens* occurrence; and (c) coefficient of variation of the predicted probability of *O. iridescens* occurrence.

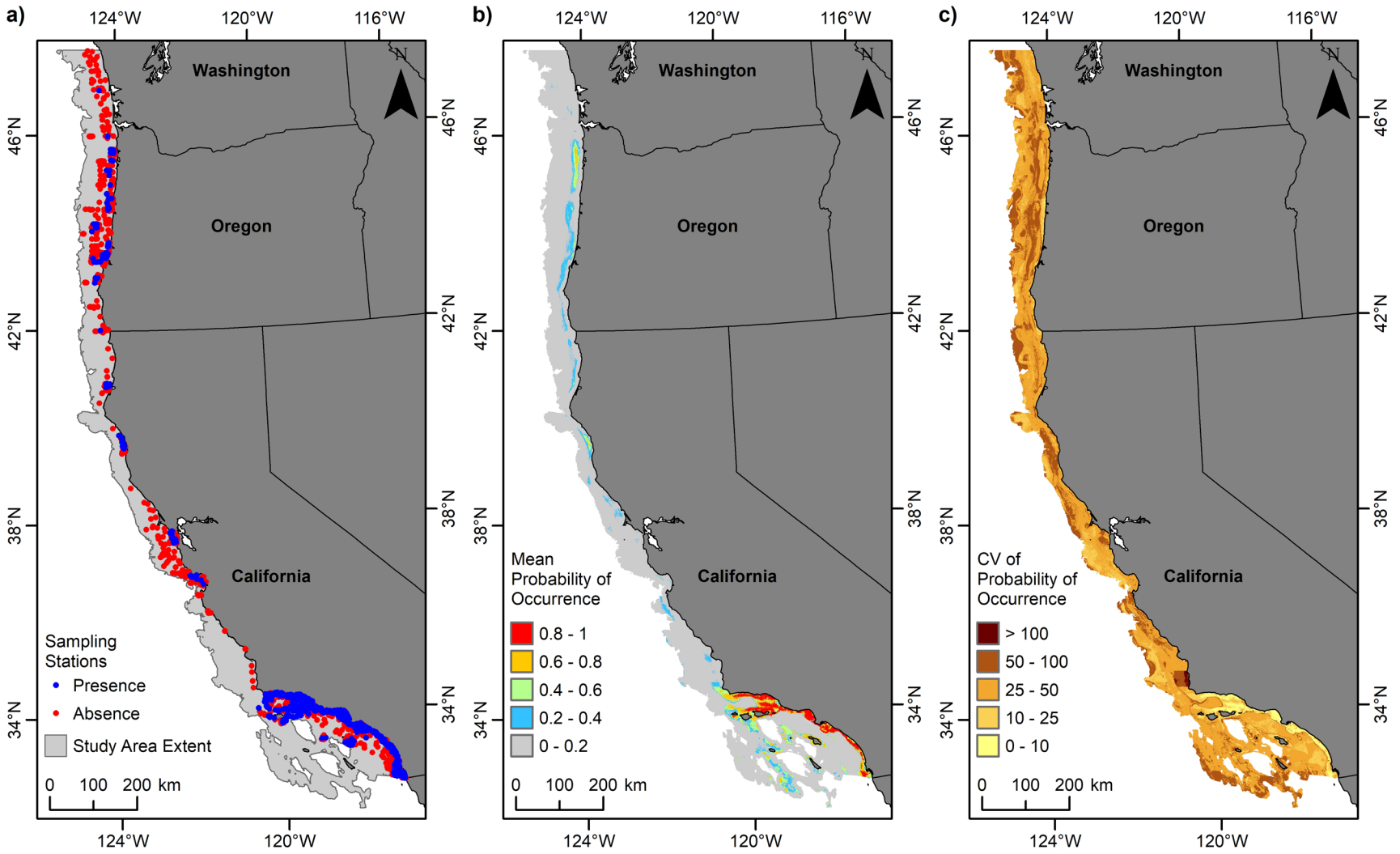

Figure 4.37. Predicted distribution of the polychaete *Paraprionospio alata* (Polychaeta, Spionida, Spionidae).
(a) Presence or absence of *P. alata* from grab samples at 2905 sampling stations within the study area offshore to 1,200 m depth; (b) mean predicted probability of *P. alata* occurrence; and (c) coefficient of variation of the predicted probability of *P. alata* occurrence.

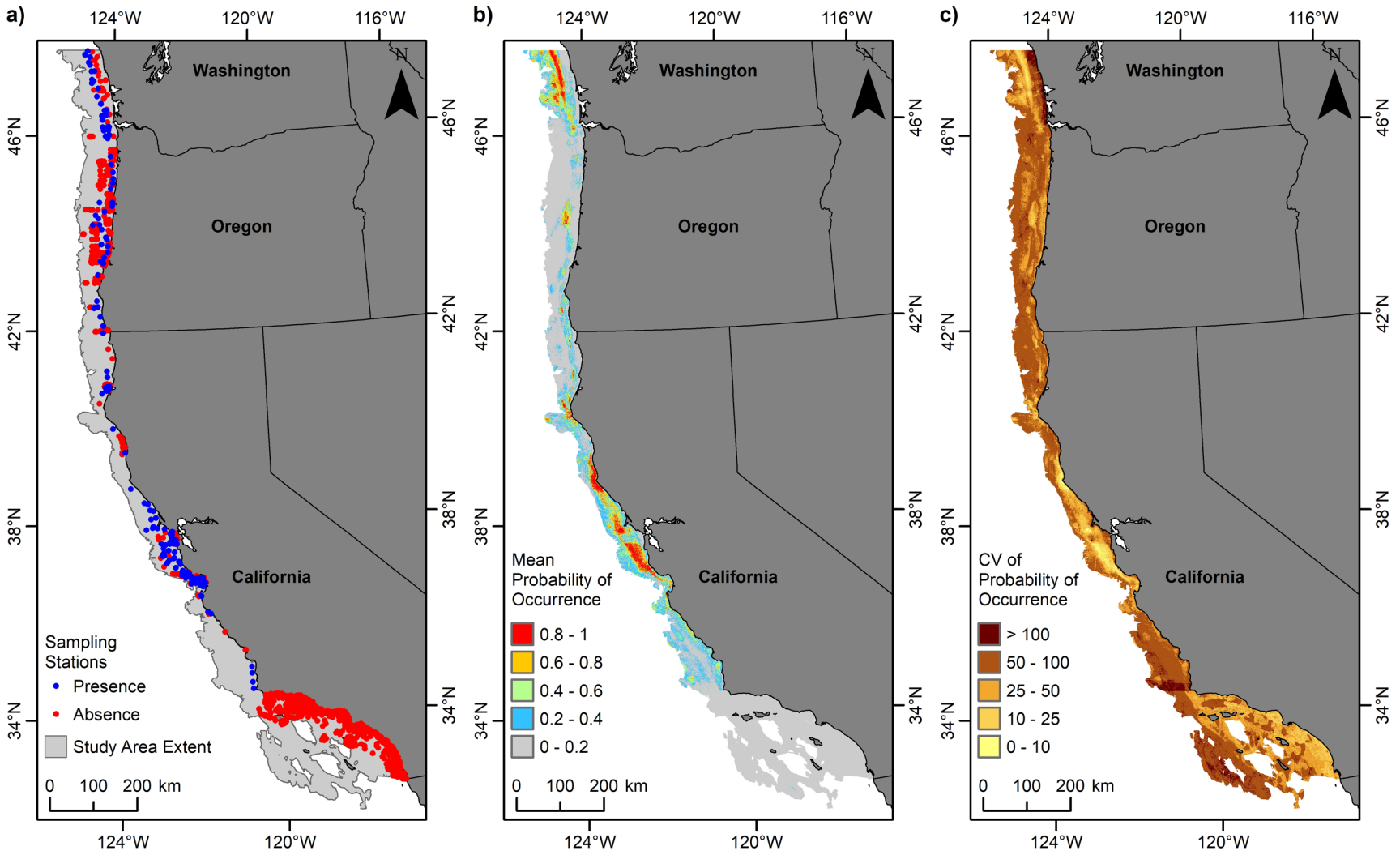

Figure 4.38. Predicted distribution of the polychaete *Paraprionospio pinnata* (Polychaeta, Spionida, Spionidae).
(a) Presence or absence of *P. pinnata* from grab samples at 2905 sampling stations within the study area offshore to 1,200 m depth; (b) mean predicted probability of *P. pinnata* occurrence; and (c) coefficient of variation of the predicted probability of *P. pinnata* occurrence.

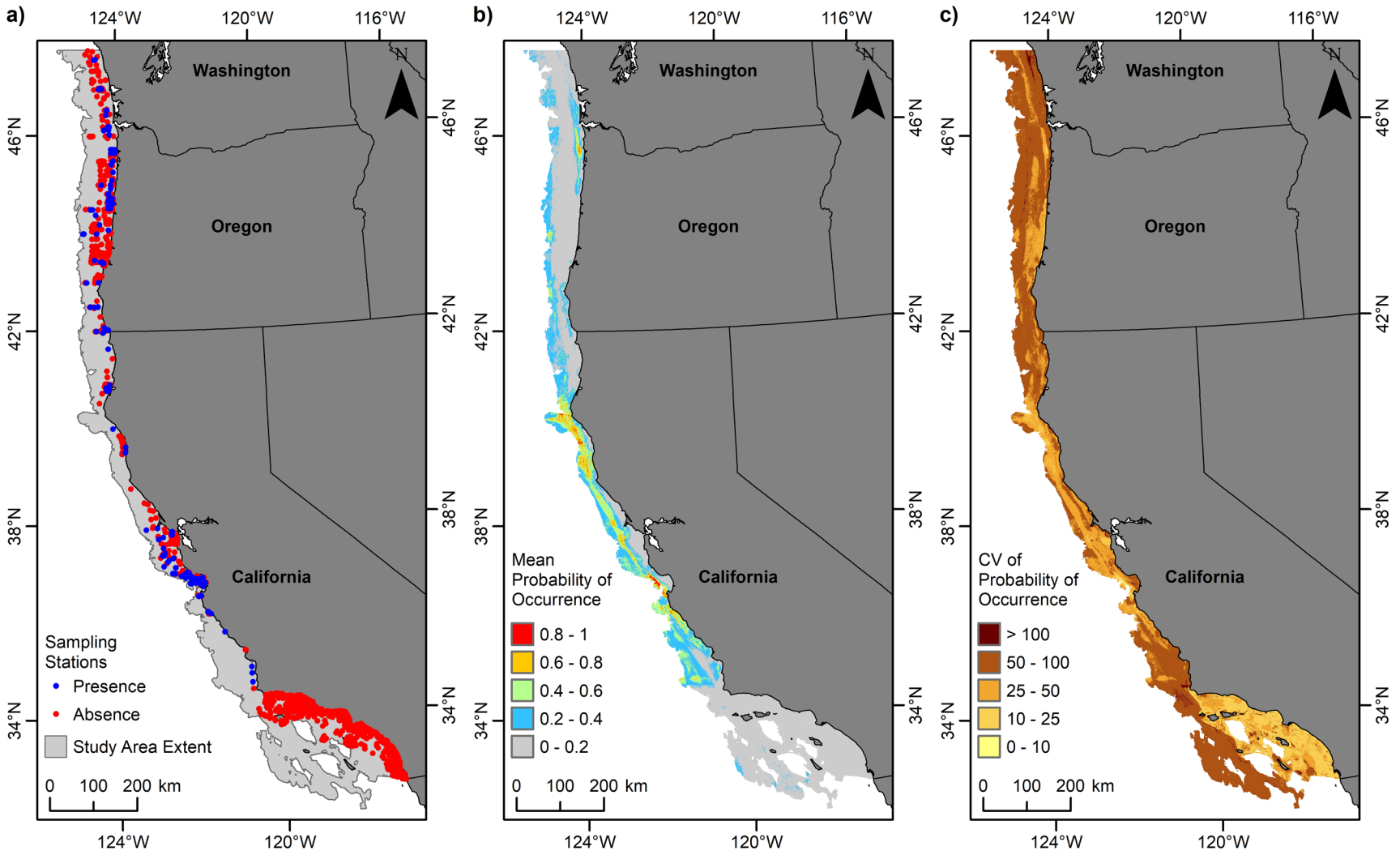

Figure 4.39. Predicted distribution of the polychaete *Polycirrus* (Polychaeta, Terebellida, Terebellidae).
(a) Presence or absence of *Polycirrus* from grab samples at 2905 sampling stations within the study area offshore to 1,200 m depth; (b) mean predicted probability of *Polycirrus* occurrence; and (c) coefficient of variation of the predicted probability of *Polycirrus* occurrence.

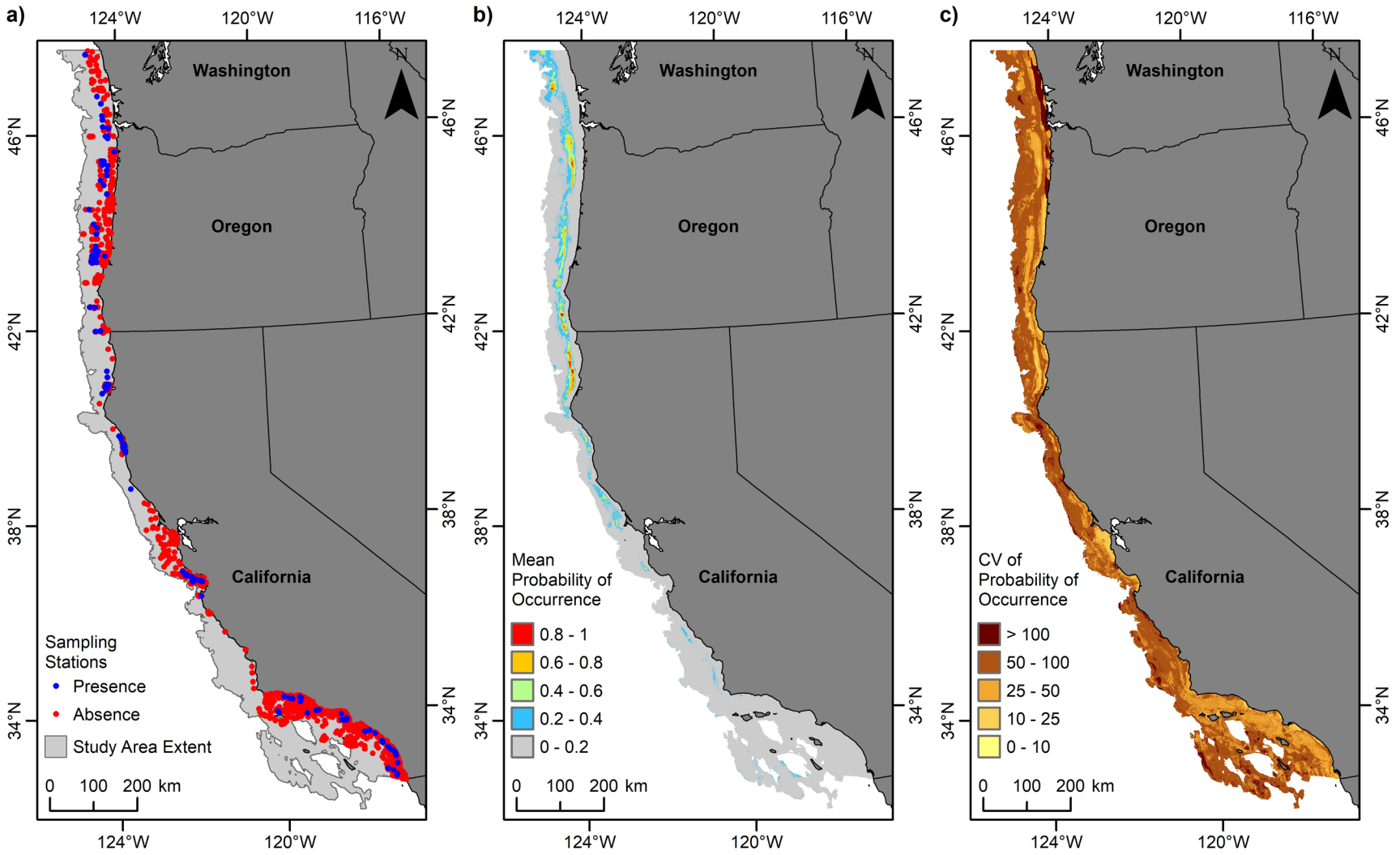

Figure 4.40. Predicted distribution of the polychaete *Praxillella gracilis* (Polychaeta, Sedentaria, Maldanidae).
(a) Presence or absence of *P. gracilis* from grab samples at 2905 sampling stations within the study area offshore to 1,200 m depth; (b) mean predicted probability of *P. gracilis* occurrence; and (c) coefficient of variation of the predicted probability of *P. gracilis* occurrence.

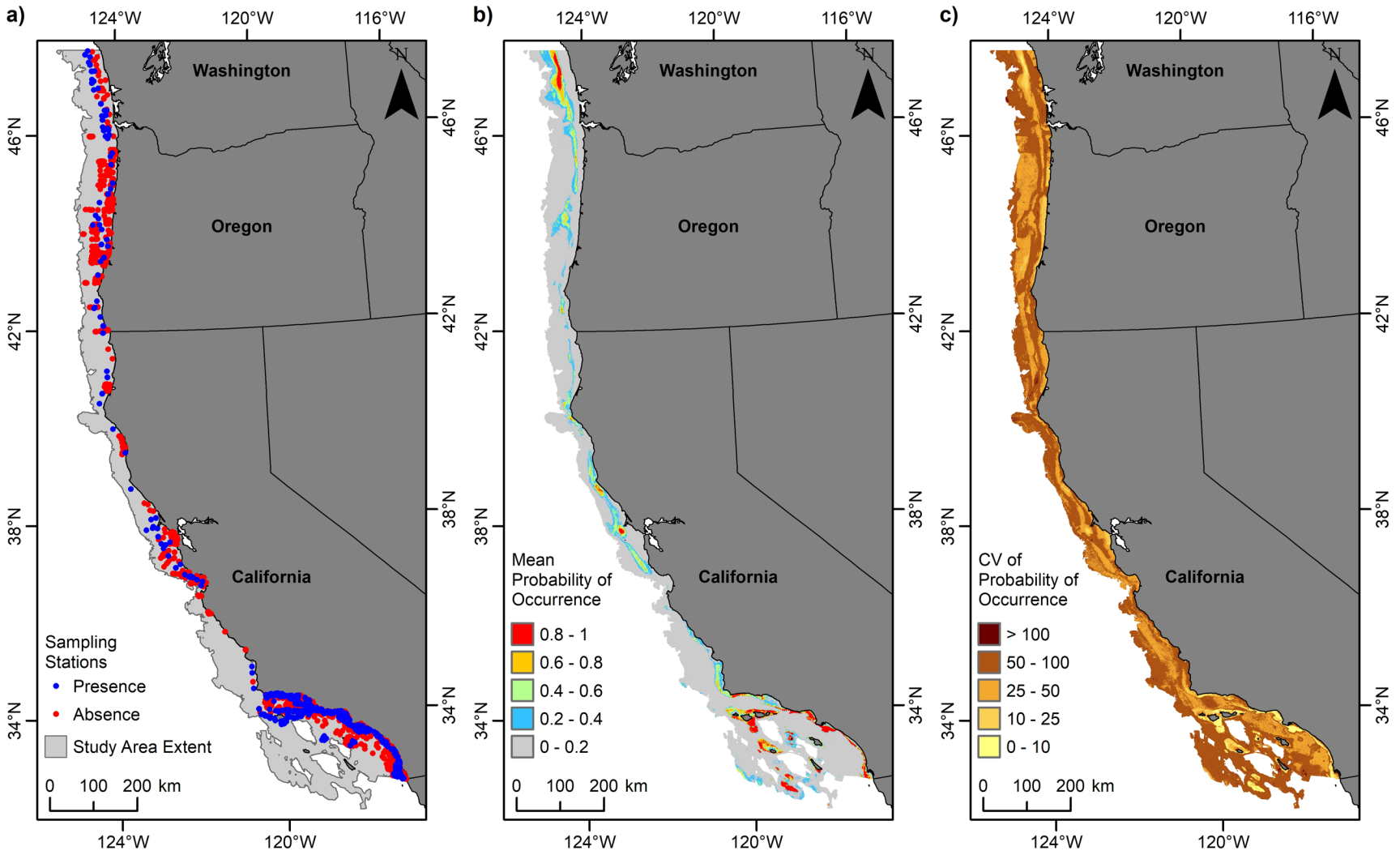

Figure 4.41. Predicted distribution of the polychaete *Prionospio jubata* (Polychaeta, Spionida, Spionidae).
(a) Presence or absence of *P. jubata* from grab samples at 2905 sampling stations within the study area offshore to 1,200 m depth; (b) mean predicted probability of *P. jubata* occurrence; and (c) coefficient of variation of the predicted probability of *P. jubata* occurrence.

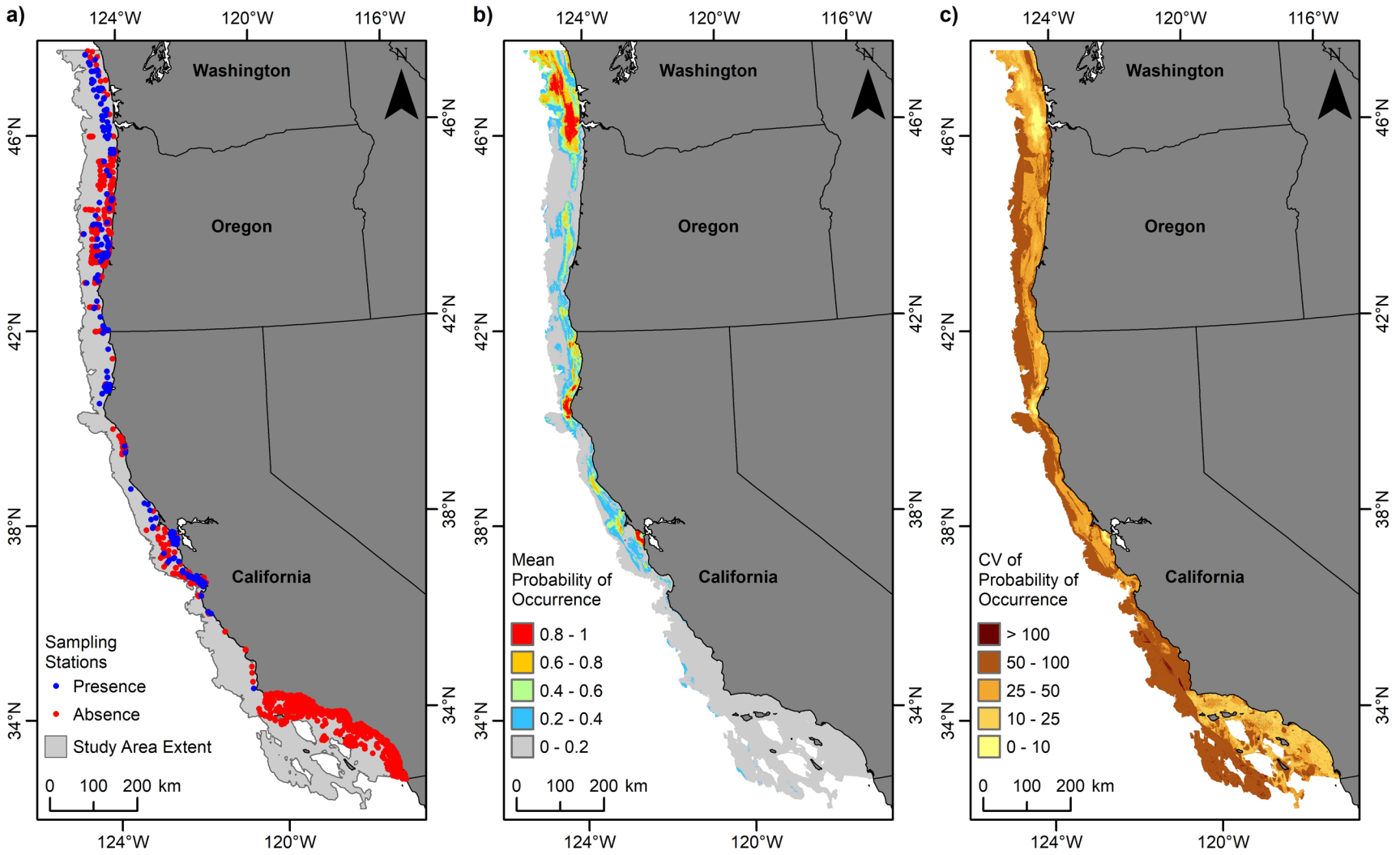

Figure 4.42. Predicted distribution of the polychaete *Scoletoma luti* (Polychaeta, Eunicida, Lumbrineridae).
(a) Presence or absence of *S. luti* from grab samples at 2905 sampling stations within the study area offshore to 1,200 m depth; (b) mean predicted probability of *S. luti* occurrence; and (c) coefficient of variation of the predicted probability of *S. luti* occurrence.

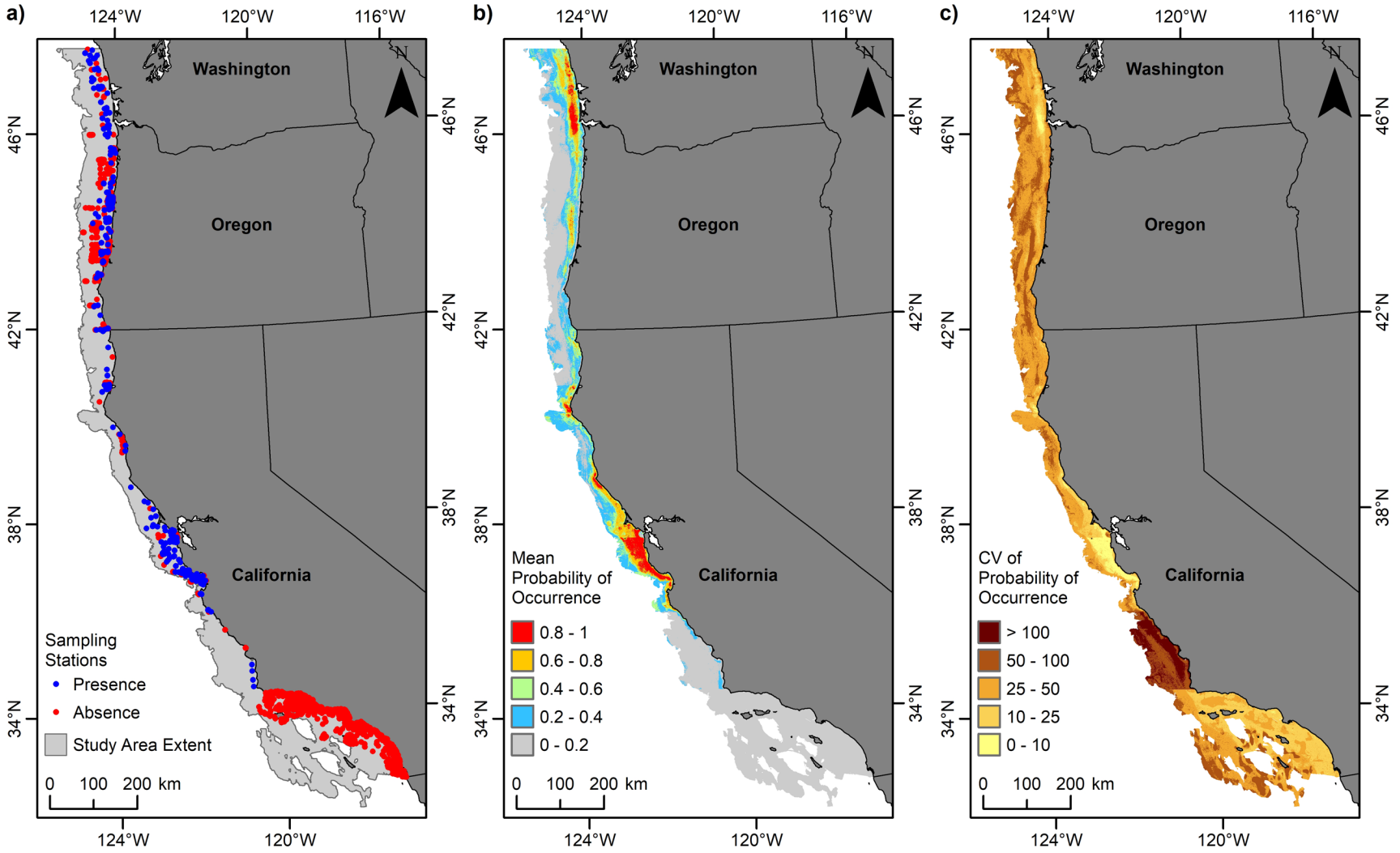

Figure 4.43. Predicted distribution of the polychaete *Spiophanes berkeleyorum* (Polychaeta, Spionida, Spionidae).
(a) Presence or absence of *S. berkeleyorum* from grab samples at 2905 sampling stations within the study area offshore to 1,200 m depth; (b) mean predicted probability of *S. berkeleyorum* occurrence; and (c) coefficient of variation of the predicted probability of *S. berkeleyorum* occurrence.

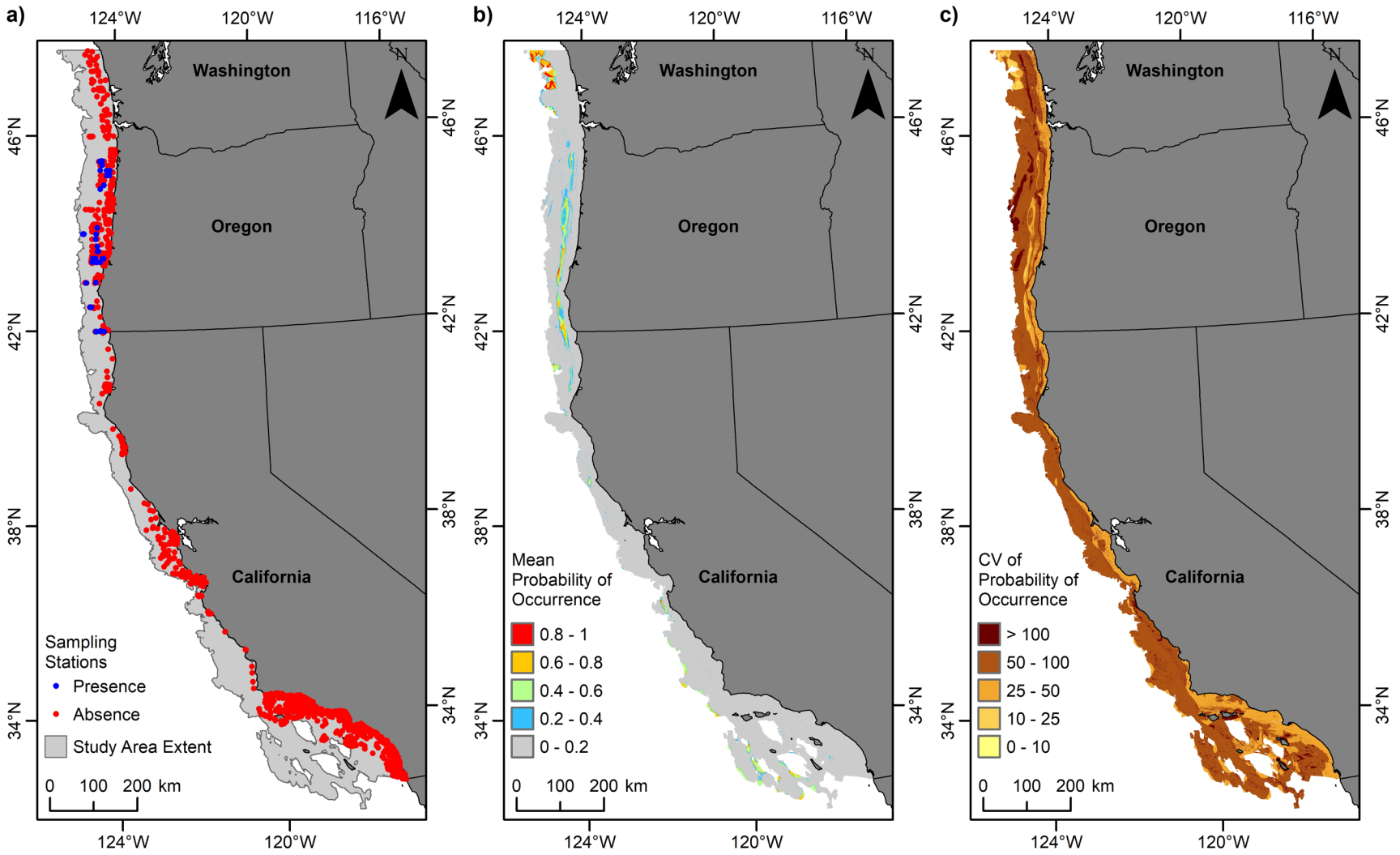

Figure 4.44. Predicted distribution of the polychaete *Sternaspis assimilis* (Polychaeta, Terebellida, Sternaspidae).
(a) Presence or absence of *S. assimilis* from grab samples at 2905 sampling stations within the study area offshore to 1,200 m depth; (b) mean predicted probability of *S. assimilis* occurrence; and (c) coefficient of variation of the predicted probability of *S. assimilis* occurrence.

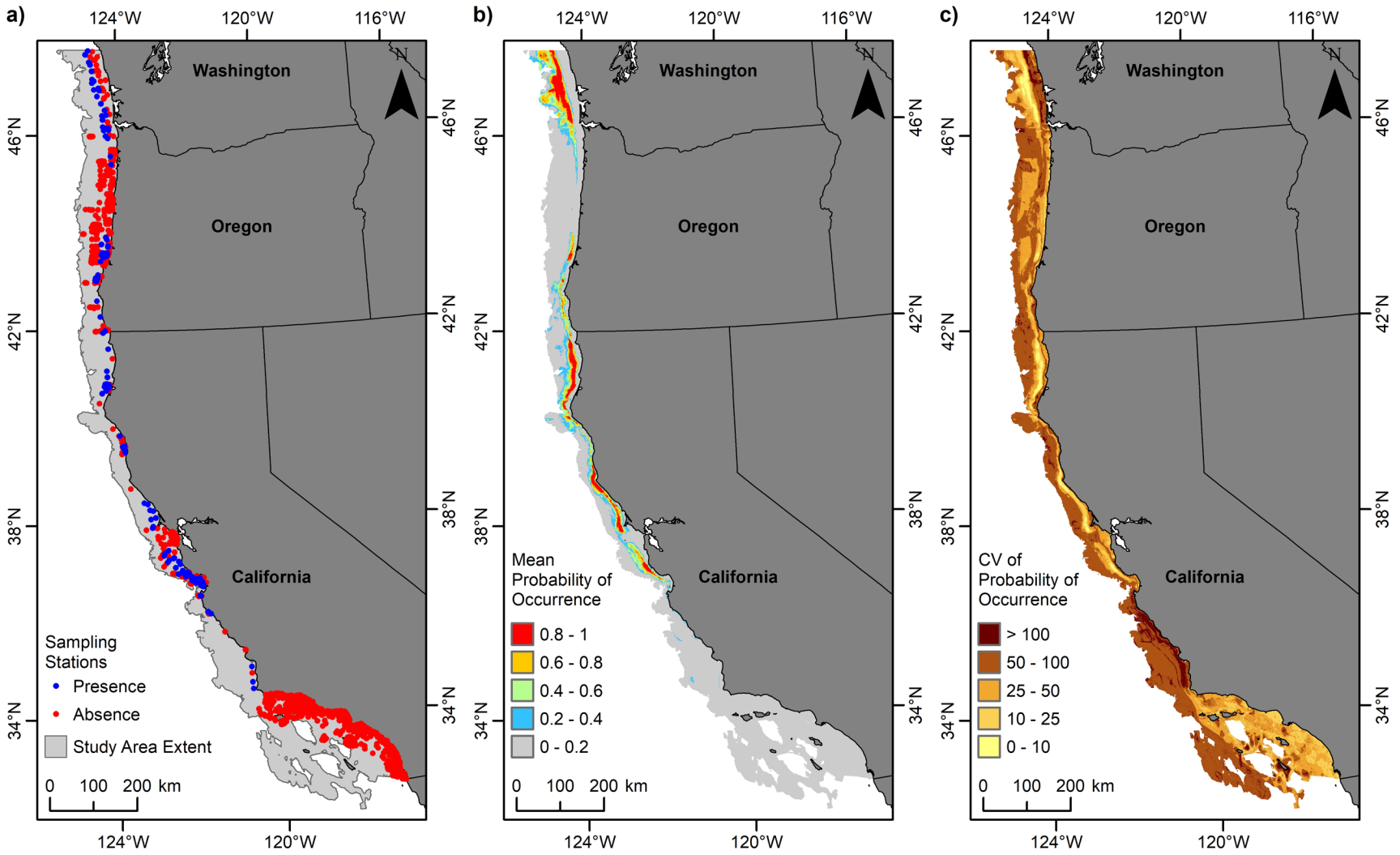

Figure 4.45. Predicted distribution of the polychaete *Sternaspis fossor* (Polychaeta, Terebellida, Sternaspidae).
(a) Presence or absence of *S. fossor* from grab samples at 2905 sampling stations within the study area offshore to 1,200 m depth; (b) mean predicted probability of *S. fossor* occurrence; and (c) coefficient of variation of the predicted probability of *S. fossor* occurrence.

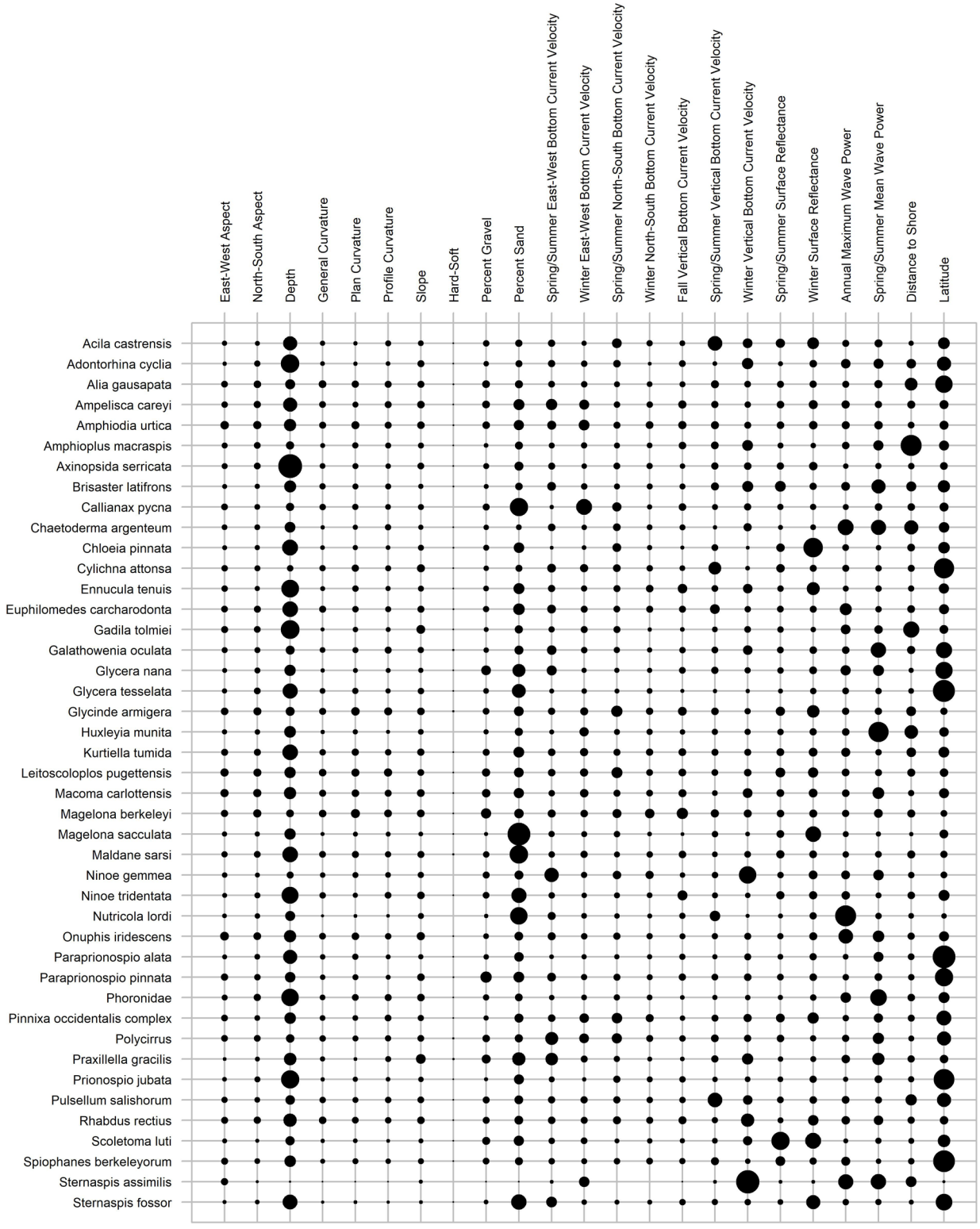

Figure 4.46. Relative importance of environmental predictor variables for each macrofauna taxon. The area of each circle is proportional to the mean relative contribution of the environmental predictor to model fitting.

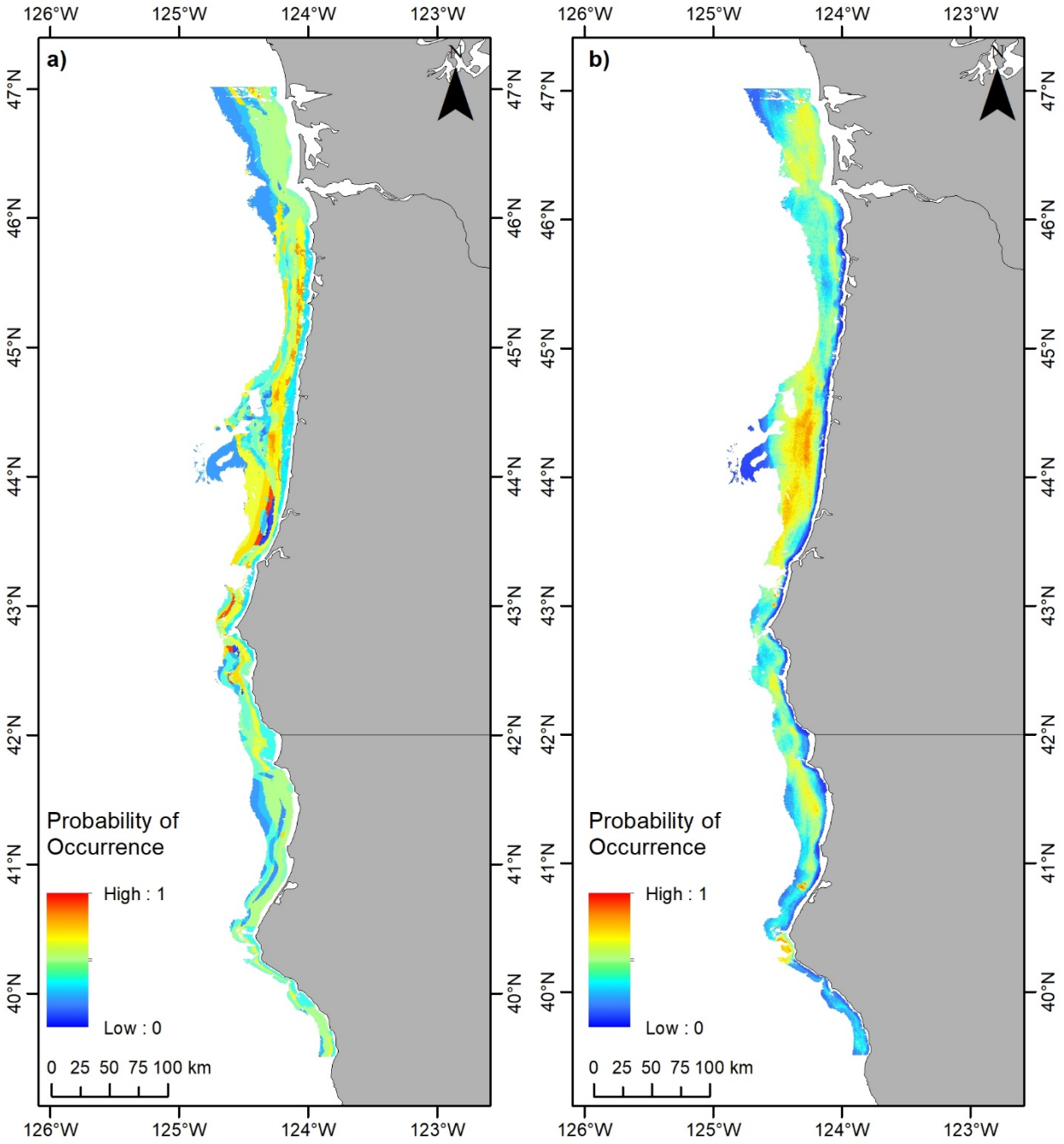

Figure 4.47. Comparison of model predictions for *Alia gausapata*.
Predicted probability of occurrence a) from Havron et al. (2017) and b) from this study, derived by unprojecting, resampling, and clipping the mean predicted probability of occurrence to match the grid from Havron et al. (2017).

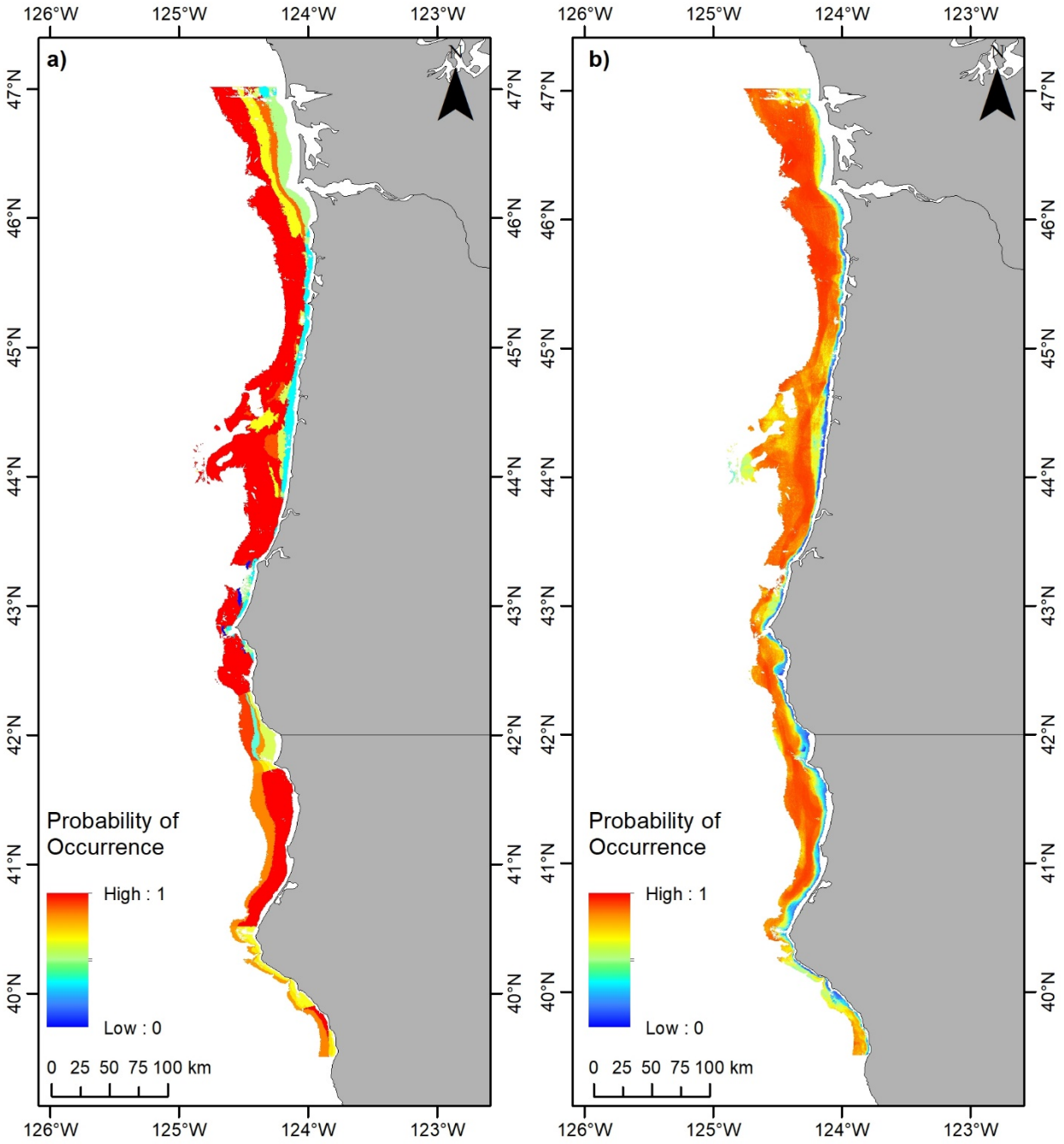

Figure 4.48. Comparison of model predictions for *Axinopsida serricata*.
Predicted probability of occurrence a) from Havron et al. (2017) and b) from this study, derived by unprojecting, resampling, and clipping the mean predicted probability of occurrence to match the grid from Havron et al. (2017).

5 References

ABA Consultants. 2000. MCI/WorldCom Southern Cross Monterey Bay Cable Landing, Technical Memorandum 5. Offshore Studies: Physical Oceanography and Marine Biology. Prepared for Natural Resources Consultants, CA. 207 pp.

Aiello-Lammens, M.E., R.A. Boria, A. Radosavljevic, B. Vilela, and R.P. Anderson. 2015. spThin: an R package for spatial thinning of species occurrence records for use in ecological niche models. Ecography 38(5): 541–545. doi:10.1111/ecog.01132

Akaike, H. 1974. A new look at the statistical model identification. IEEE Transactions on Automatic Control 19(6): 716–723. doi:10.1109/TAC.1974.1100705

Anderson, O.F., J.M. Guinotte, A.A. Rowden, D.M. Tracey, K.A. Mackay, and M.R. Clark. 2016. Habitat suitability models for predicting the occurrence of vulnerable marine ecosystems in the seas around New Zealand. Deep-Sea Research Part I: Oceanographic Research Papers 115: 265–292. doi:10.1016/j.dsr.2016.07.006

Baillon, S., J.-F. Hamel, V.E. Wareham, and A. Mercier. 2012. Deep cold-water corals as nurseries for fish larvae. Frontiers in Ecology and the Environment 10(7): 351–356. doi:10.1890/120022

Baillon, S., J.-F. Hamel, and A. Mercier. 2014. Diversity, distribution and nature of faunal associations with deep-sea pennatulacean corals in the Northwest Atlantic. PLoS One 9: e111519. doi:10.1371/journal.pone.0111519

Bergen, M., S.B. Weisberg, R.W. Smith, D.B. Cadien, A. Dalkey, D.E. Montagne, J.K. Stull, R.G. Velarde, and J.A. Ranasinghe. 2001. Relationship between depth, sediment, latitude, and the structure of benthic infaunal assemblages on the mainland shelf of southern California. Marine Biology 138: 637–647. doi:10.1007/s002270000469

Boria, R.A., L.E. Olson, S.M. Goodman, and R.P. Anderson. 2014. Spatial filtering to reduce sampling bias can improve the performance of ecological niche models. Ecological Modelling 275: 73–77. doi:10.1016/j.ecolmodel.2013.12.012

Breiman, L., J.H. Friedman, R.A. Olshen, and C.I. Stone. 1984. Classification and regression trees. Taylor & Francis, Belmont, CA. 368 pp.

Brodeur, R.D. 2001. Habitat-specific distribution of Pacific ocean perch (*Sebastes alutus*) in Pribilof Canyon, Bering Sea. Continental Shelf Research 21(3): 207–224. doi:10.1016/S0278-4343(00)00083-2

Bryan, T.L., and A. Metaxas. 2006. Distribution of deep-water corals along the North American continental margins: relationships with environmental factors. Deep-Sea Research Part I: Oceanographic Research Papers 53(12): 1865–1879. doi:10.1016/j.dsr.2006.09.006

Bryan, T.L., and A. Metaxas. 2007. Predicting suitable habitat for deep-water gorgonian corals on the Atlantic and Pacific Continental Margins of North America. Marine Ecology Progress Series 330: 113–126. doi:10.3354/meps330113

Buhl-Mortensen, L., A. Vanreusel, A.J. Gooday, L.A. Levin, I.G. Priede, P. Buhl-Mortensen, H. Gheerardyn, N.J. King, and M. Raes. 2010. Biological structures as a source of habitat heterogeneity

and biodiversity on the deep ocean margins. Marine Ecology 31(1): 21–50. doi:10.1111/j.1439-0485.2010.00359.x

Burnham, K.P., and D.R. Anderson. 2002. Model selection and multimodel inference: a practical information-theoretic approach. Springer-Verlag, New York. 488 pp.

Clarke, K.R., and R.N. Gorley. 2006. PRIMER v6: User Manual/Tutorial. PRIMER-E, Plymouth.

Clarke, K.R., P.J. Somerfield, and R.N. Gorley. 2008. Testing of null hypotheses in exploratory community analyses: similarity profiles and biota-environment linkage. Journal of Experimental Marine Biology and Ecology 366(1–2): 56–69. doi:10.1016/j.jembe.2008.07.009

Clarke, M.E., C.E. Whitmire, and M.M. Yoklavich. 2017. State of deep-sea coral and sponge ecosystems of the U.S. West Coast. pp. 112–155. In: T.F. Hourigan, P.J. Etnoyer, and S.D. Cairns. (eds.), The State of Deep-Sea Coral and Sponge Ecosystems of the United States. National Oceanic and Atmospheric Administration, NOAA Technical Memorandum NMFS-OHC-4. 467 pp. Available from: https://deepseacoraldata.noaa.gov/library/2017-state-of-deep-sea-corals-report (Accessed 8 June 2020)

Convention on Biological Diversity. 2009. Report of the expert workshop on scientific and technical guidance on the use of biogeographic classification systems and identification of marine areas beyond national jurisdiction in need of protection. Fourteenth meeting of the Subsidiary Body on Scientific, Technical and Technological Advice. Available from: http://aires-marines.uqar.ca/id/eprint/31/1/Rwebsa-wcar-01-ewbcsima-01-02%20CDB.pdf (Accessed 8 June 2020)

Cordes, E.E., S. Arnaud-Haond, O.-A. Bergstad, A.P. da Costa Falcão, A. Freiwald, J.M. Roberts, and P. Bernal. 2016. Chapter 42–Cold-Water Corals. pp. 803–816. In: United Nations (Ed.), The First Global Integrated Marine Assessment: World Ocean Assessment I. Cambridge University Press, Cambridge. 973 pp. doi:10.1017/9781108186148

Cressie, N.A.C. 1993. Statistics for spatial data (revised ed.). John Wiley & Sons. Inc., New York. 900 pp. doi:10.1002/9781119115151

Davies, A.J., and J.M. Guinotte. 2011. Global habitat suitability for framework-forming cold-water corals. PLoS One 6(4): e18483. doi:10.1371/journal.pone.0018483

De'ath, G. 2007. Boosted tress for ecological modeling and prediction. Ecology 88(1): 243–251. doi:10.1890/0012-9658(2007)88[243:BTFEMA]2.0.CO;2

De'ath, G., and K.E. Fabricius. 2000. Classification and regression trees: a powerful yet simple technique for ecological data analysis. Ecology 81(11): 3178–3192. doi:10.1890/0012-9658(2000)081[3178:CARTAP]2.0.CO;2

De Clippele, L.H., P. Buhl-Mortensen, and L. Buhl-Mortensen. 2015. Fauna associated with cold water gorgonians and sea pens. Continental Shelf Research 105: 67–78. doi:10.1016/j.csr.2015.06.007

Dong, C., L. Renault, Y. Zhang, J. Ma, and Y. Cao. 2017. Expansion of West Coast Oceanographic Modeling Capability. US Department of the Interior, Bureau of Ocean Energy Management, Pacific OCS Region. OCS Study BOEM 2017-055. 83 pp.

Du Preez, C. 2015. A new arc–chord ratio (ACR) rugosity index for quantifying three-dimensional landscape structural complexity. Landscape Ecology 30:181–192. doi:10.1007/s10980-014-0118-8

Du Preez, C., and V. Tunnicliffe. 2011. Shortspine thornyhead and rockfish (Scorpaenidae) distribution in response to substratum, biogenic structure and trawling. Marine Ecology Progress Series 425: 217–231. doi:10.3354/meps09005

Elith, J., J.R. Leathwick, and T. Hastie. 2008. A working guide to boosted regression trees. Journal of Animal Ecology 77(4): 802–813. doi:10.1111/j.1365-2656.2008.01390.x

Elith, J., S.J. Phillips, T. Hastie, M. Dudik, Y.E. Chee, and C.J. Yates. 2011. A statistical explanation of MaxEnt for ecologists. Diversity and Distributions 17(1): 43–57. doi:10.1111/j.1472-4642.2010.00725.x

EPA NCA. 2016. Coastal Data Search Engine. Website. US Environmental Protection Agency, National Coastal Assessment. Available from: https://oaspub.epa.gov/coastal/coast.search (Accessed 8 June 2020)

Etherington, L., P. van der Leeden, K. Graiff, D. Roberts, and B. Nickel. 2011. Summary of deep sea coral patterns and habitat modeling results from Cordell Bank, CA. Report to NOAA Deep-Sea Coral Research and Technology Program. NOAA Office of Marine Sanctuaries, Cordell Bank National Marine Sanctuary. 24 pp.

Etnoyer, P. NOAA National Centers for Coastal Ocean Science, Deep Coral Ecology Lab. Charleston, SC. Personal communication.

Etnoyer, P., and L.E. Morgan. 2003. Occurrences of habitat forming deep-sea corals in the Northeast Pacific Ocean. A Report to NOAA's Office of Habitat Conservation. Marine Conservation Biology Institute, Redmond, WA. 33 pp.

Etnoyer, P., and L. Morgan. 2005. Habitat-forming deep-sea corals in the Northeast Pacific Ocean. pp. 331-343. In: A. Freiwald, and J.M. Roberts (eds.), Cold-Water Corals and Ecosystems. Erlangen Earth Conference Series. Springer, Berlin, Heidelberg. 1243 pp. doi:10.1007/3-540-27673-4

Federal Register. 2018. Commercial leasing for wind power development on the Outer Continental Shelf (OCS) offshore California – call for information and nominations. Federal Register 83(203): 53096–53104.

Fielding, A.H., and J.F. Bell. 1997. A review of methods for the assessment of prediction errors in conservation presence/absence models. Environmental Conservation 24(1): 38–49. doi:10.1017/S0376892997000088

Fithian, W., and T. Hastie. 2013. Finite-sample equivalence in statistical models for presence-only data. Annals of Applied Statistics 7(4): 1917–1939. doi:10.1214/13-AOAS667

FAO. 2009. International Guidelines for the Management of Deep-Sea Fisheries in the High Seas. Food and Agriculture Organization. Rome. 73 pp. Available from: http://www.fao.org/3/i0816t/i0816t00.htm. (Accessed 4 June 2020).

Friedman, J.H. 2002. Stochastic gradient boosting. Computational Statistics and Data Analysis 38(4): 367–378. doi:10.1016/S0167-9473(01)00065-2

Friedman, J., T. Hastie, and R. Tibshirani. 2010. Regularization paths for generalized linear models via coordinate descent. Journal of Statistical Software 33(1): 1–22. doi:10.18637/jss/v033.io1

Gillett, D.J., L.L. Lovell, and K.C. Schiff. 2017. Southern California Bight 2013 Regional Monitoring Program: Volume VI. Benthic Infauna. Technical Report 971. Southern California Coastal Water Research Project. Costa Mesa, CA. 300 pp.

Goldfinger, C., S.K. Henkel, C. Romsos, A. Havron, and B. Black. 2014. Benthic habitat characterization offshore the Pacific Northwest, volume 1: evaluation of continental shelf geology. U.S. Department of the Interior, Bureau of Ocean Energy Management, Pacific OCS Region. OCS Study BOEM 2014-662.161 pp.

Greene, H.G., M. Yoklavich, R. Starr, V. O'Connell, W. Wakefield, D. Sullivan, J. McRea, and G. Cailliet. 1999. A classification scheme for deep seafloor habitats. Oceanologica Acta 22(6): 663–678. doi:10.1016/S0399-1784(00)88957-4

Guinotte, J.M., and A.J. Davies. 2014. Predicted deep-sea coral habitat suitability for the U.S. West Coast. PLoS One 9(4): e93918. doi:10.1371/journal.pone.0093918

Guinotte, J.M., S. Georgian, B.P. Kinlan, M. Poti, and A.J. Davies. 2017. Predictive Habitat Modeling for Deep-Sea Corals in U.S. Waters. pp. 211–235. In: T.F. Hourigan, P.J. Etnoyer, and S.D. Cairns (eds.), The State of Deep-Sea Coral and Sponge Ecosystems of the United States. NOAA Technical Memorandum NMFS-OHC-4. Silver Spring, MD. 467 pp.

Gullage, L., R. Devillers, and E. Edinger. 2017. Predictive distribution modelling of cold-water corals in the Newfoundland and Labrador region. Marine Ecology Progress Series 582: 57–77. doi:10.3354/meps12307

Halvorsen, R., S. Mazzoni, A. Bryn, and V. Bakkestuen. 2015. Opportunities for improved distribution modelling practice via a strict maximum likelihood interpretation of MaxEnt. Ecography 38(2): 172–183. doi:10.1111/ecog.00565

Havron, A.C., C. Goldfinger, S. Henkel, B.G. Marcot, C. Romsos, and L. Gilbane 2017. Mapping marine habitat suitability and uncertainty of Bayesian networks: a case study using Pacific benthic macrofauna. Ecosphere 8(7): e01859. doi:10.1002/ecs2.1859

Hawkes, N., M. Korabik, L. Beazley, H.T. Rapp, J.R. Xavier, and E. Kenchington. 2019. Glass sponge grounds on the Scotian Shelf and their associated biodiversity. Marine Ecology Progress Series 614: 91–109. doi:10.3354/meps12903

Henderson, M.J., D.D. Huff, and M.M. Yoklavich. In revision. Some demersal fish are more likely to co-occur with deep-sea corals and sponges even after accounting for depth and substratum. Marine Ecology Progress Series.

Henkel, S.K., C. Goldfinger, C. Romsos, L.G. Hemery, A. Havron, and K. Politano. 2014. Benthic Habitat Characterization Offshore the Pacific Northwest Volume 2: Evaluation of Continental Shelf Benthic Communities. US Department of the Interior, Bureau of Ocean Energy Management, Pacific OCS Region. OCS Study BOEM 2014-662. 218 pp.

Henkel, S.K., and W.G. Nelson. 2018. Assessment of spatial patterns in benthic macrofauna of the U.S. west coast continental shelf. Journal of Biogeography 45(12): 2701-2717. doi:10.1111/jbi.13451

Henkel, S.K., L. Gilbane, A.J. Phillips, and D.J. Gillett. 2020. Cross-shelf habitat suitability modeling for benthic macrofauna. US Department of the Interior, Bureau of Ocean Energy Management. OCS Study BOEM 2020-008. 71 pp.

Hernandez, P.A., C.H. Graham, L.L. Master, and D.L. Albert. 2006. The effect of sample size and species characteristics on performance of different species distribution modeling methods. Ecography 29(5): 773–785. doi:10.1111/j.0906-7590.2006.04700.x

Hijmans, R.J., and van Etten, J. 2018. raster: Geographic analysis and modeling with raster data. R package version 2.8-4. Website [Data downloaded 1 December 2018]. Available from: https://cran.r-project.org/web/packages/raster/index.html (Accessed 8 June 2020)

Hijmans, R.J., Phillips, S., Leathwick, J., and Elith, J. 2017. dismo: Species Distribution Modeling. R package version 1.1-4. Website [Data downloaded 1 December 2018]. Available from: https://cran.r-project.org/package=dismo (Accessed 5 June 2020)

Hogg, M.M., O.S. Tendal, K.W. Conway, S.A. Pomponi, R.W.M. van Soest, J. Gutt, M. Krautter, and J.M. Roberts. 2010. Deep-sea Sponge Grounds: Reservoirs of Biodiversity. UNEP-WCMC Biodiversity Series No. 32. UNEP-WCMC, Cambridge, UK. 88 pp.

Hosmer, D.W., and S. Lemeshow. 2000. Applied logistic regression, 2nd edition. John Wiley & Sons, Inc., New York. 383 pp. doi:10.1002/0471722146

Hourigan, T.F., P.J. Etnoyer, R.P. McGuinn, C. Whitmire, D.S. Dorfman, M. Dornback, S. Cross, and D. Sallis. 2015. An Introduction to NOAA's National Database for Deep-Sea Corals and Sponges. NOAA Technical Memorandum NOS NCCOS 191. Silver Spring, MD. 27 pp.

Hourigan, T.F., P.J. Etnoyer, and S.D. Cairns. 2017. The State of Deep-Sea Coral and Sponge Ecosystems of the United States. NOAA Technical Memorandum NMFS-OHC-4. Silver Spring, MD. 467 pp.

Howell, K.-L., N. Piechaud, A.-L. Downie, and A. Kenny. 2016. The distribution of deep-sea sponge aggregations in the North Atlantic and implications for their effective spatial management. Deep-Sea Research Part I: Oceanographic Research Papers 115: 309–320. doi:10.1016/j.dsr.2016.07.005

Huff, D.D., M.M. Yoklavich, M.S. Love, D.L. Watters, F. Chai, and S.T. Lindley. 2013. Environmental factors that influence the distribution, size, and biotic relationships of the Christmas tree coral *Antipathes dendrochristos* in the Southern California Bight. Marine Ecology Progress Series 494: 159–177. doi:10.3354/meps10591

HYCOM Consortium. 2018. HYCOM + NCODA Global 1/12° Reanalysis. Website [Data downloaded November 2017]. Available from: https://hycom.org/dataserver/gofs-3pt0/reanalysis (Accessed 8 June 2020)

Hyland, J., E. Baptiste, J. Campbell, J. Kennedy, R. Kropp, and S. Williams. 1991. Macroinfaunal communities of the Santa Maria Basin on the California outer continental shelf and slope. Marine Ecology Progress Series 78: 147–161. doi:10.3354/meps078147

Jenness, J. 2013. DEM Surface Tools. Jenness Enterprises. Website. Available from: http://www.jennessent.com/arcgis/surface_area.htm (Accessed 8 June 2020)

Jiménez-Valverde, A. 2012. Insights into the area under the receiver operating characteristic curve (AUC) as a discrimination measure in species distribution modeling. Global Ecology and Biogeography 21(4): 498-507. doi:10.1111/j.1466-8238.2011.00683.x

Kinlan, B.P., M. Poti, A.F. Drohan, D.B. Packer, D.S. Dorfman, and M.S. Nizinski. 2020. Predictive modeling of suitable habitat for deep-sea corals offshore the Northeast United States. Deep-Sea Research Part I: Oceanographic Research Papers 158: 103229. doi:10.1016/j.dsr.2020.103229

Krivoruchko, K. 2012. Empirical Bayesian Kriging. Website. Fall 2012 Edition. Esri. Redlands, CA, USA. Available from: https://www.esri.com/news/arcuser/1012/empirical-byesian-kriging.html (Accessed 8 June 2020)

Kutti, T., R.J. Bannister, and J.H. Fossa. 2013. Community structure and ecological function of deep-water sponge grounds in the Traenadypet MPA – Northern Norwegian continental shelf. Continental Shelf Research 69: 21–30. doi:10.1016/j.csr.2013.09.011

Laidig, T. NOAA National Marine Fisheries Service, Southwest Fisheries Science Center. Santa Cruz, CA. Personal communication.

Leal, M.C., J. Puga, J. Serodio, N.C.M. Gomes, and R. Calado. 2012. Trends in the discovery of new marine natural products from invertebrates over the last two decades – where and what are we bioprospecting? PLoS One 7(1): e30580. doi:10.1371/journal.pone.0030580

Li, J., and A.D. Heap. 2014. Spatial interpolation methods applied in the environmental sciences: a review. Environmental Modelling & Software 53: 173–189. doi:10.1016/j.envsoft.2013.12.008

Li, Y. CSS, Inc. and NOAA National Ocean Service, National Centers for Coastal Ocean Science. Silver Spring, MD. Personal communication.

Lobo, J.M., A. Jiménez-Valverde, and R. Real. 2008. AUC: a misleading measure of the performance of predictive distribution models. Global Ecology and Biogeography 17(2): 145–151. doi:10.1111/j.1466-8238.2007.00348.x

Maldonado, M., R. Aguilar, R.J. Bannister, J.J. Bell, K.W. Conway, P.K. Dayton, C. Díaz, J. Gutt, M. Kelly, E.L.R. Kenchington, S.P. Leys, S.A. Pomponi, H.T. Rapp, K. Rützler, O.S. Tendal, J. Vacelet, and C.M. Young. 2016. Sponge Grounds as Key Marine Habitats: A Synthetic Review of Types, Structure, Functional Roles, and Conservation Concerns. pp. 145–183. In: S. Rossi, L. Bramanti, A. Gori, and C. Orejas. (eds.), Marine animal forests: the ecology of benthic biodiversity hotspots. Springer International Publishing, Switzerland. 1366 pp. doi:10.1007/978-3-319-21012-4

Marine Research Specialists. 2016. Offshore Monitoring and Reporting Program: 2015 Annual Report. Report to the City of Morro Bay and Cayucos Sanitary District. 366 pp. Available from: http://www.morro-bay.ca.us/ArchiveCenter/ViewFile/Item/2757 (Accessed 2 May 2020)

Merow, C., M.J. Smith, and J.A. Silander, Jr. 2013. A practical guide to MaxEnt for modeling species' distributions: what it does, and why inputs and settings matter. Ecography 36(10): 1058–1069. Doi:10.1111/j.1600-0587.2013.07872.x

Nelson, W.G., J.L. Hyland, H. Lee II, C.L. Cooksey, J.O. Lamberson, F.A. Cole, and P.J. Clinton. 2008. Ecological Condition of Coastal Ocean Waters along the U.S. Western Continental Shelf: 2003. NOAA Technical Memorandum NOS NCCOS 79 and EPA 620/R-08/001. Charleston, SC. 137 pp.

NASA. 2018. OceanColor Web. Website. National Aeronautics and Space Administration, Goddard Space Flight Center, Ocean Biology Processing Group. Available from: https://oceancolor.gsfc.nasa.gov. (Accessed 8 June 2020)

NOAA NCEI. 2020. Bathymetric Data Viewer. Website [Data download 27 October 2017]. NOAA National Centers for Environmental Information. Available from: https://maps.ngdc.noaa.gov/viewers/bathymetry/ (Accessed 8 June 2020)

NOAA NGDC. 2003a. U.S. Coastal Relief Model Vol. 6 – Southern California. Website [Data downloaded 27 October 2017]. NOAA National Centers for Environmental Information, previously National Geophysical Data Center. doi:10.7289/V500001J. Available from: https://data.nodc.noaa.gov/cgi-bin/iso?id=gov.noaa.ngdc.mgg.dem:709 (Accessed 8 June 2020) …

NOAA NGDC. 2003b. U.S Coastal Relief Model Vol. 7 – Central Pacific. Website [Data downloaded 27 October 2017]. NOAA National Centers for Environmental Information, previously National Geophysical Data Center. doi:10.7289/V50Z7152. Available from: https://data.nodc.noaa.gov/cgi-bin/iso?id=gov.noaa.ngdc.mgg.dem:348 (Accessed 8 June 2020)

NOAA NGDC. 2003c. U.S. Coastal Relief Model Vol. 8 – Northwest Pacific. Website [Data downloaded 27 October 2017]. NOAA National Centers for Environmental Information, previously National Geophysical Data Center. doi:10.7289/V5H12ZXJ. Available from: https://data.nodc.noaa.gov/cgi-bin/iso?id=gov.noaa.ngdc.mgg.dem:288 (Accessed 8 June 2020)

NOAA NMFS. 2005. Pacific Coast Groundfish Fishery Management Plan, Essential Fish Habitat Designation and Minimization of Adverse Impacts, Final Environmental Impact Statement. NOAA National Marine Fisheries Service, Northwest Region, Seattle, WA.

NOAA NMFS. 2013. Groundfish Essential Fish Habitat Synthesis: A Report to the Pacific Fishery Management Council. NOAA National Marine Fisheries Service, Northwest Fisheries Science Center, Seattle, WA, April 2013. 107 pp. Available from: https://swfsc.noaa.gov/publications/CR/2013/2013NMFS.pdf (Accessed 8 June 2020)

NOAA CRCP. 2010. NOAA Strategic Plan for Deep-Sea Coral and Sponge Ecosystems: Research, Management, and International Cooperation. NOAA Coral Reef Conservation Program. NOAA Technical Memorandum CRCP 11. Silver Spring, MD. 67 pp. Available from: https://www.coris.noaa.gov/activities/deepsea_coral/ (Accessed 8 June 2020)

NOAA DSCRTP. 2019. NOAA National Database of Deep-Sea Corals and Sponges. Website [Data downloaded 20 March 2018]. NOAA National Marine Fisheries Service, Deep-Sea Coral Research and Technology Program. Available from: https://deepseacoraldata.noaa.gov/ (Accessed 8 June 2020)

NOAA NWS. 2018. WAVEWATCH III 30-Year Hindcast Phase 2. Website [Data downloaded 20 March 2018]. NOAA National Weather Service, National Centers for Environmental Prediction. Available from: https://polar.ncep.noaa.gov/waves/hindcasts/nopp-phase2.php (Accessed 8 June 2020)

NOAA NWFSC. 2016. Consolidated GIS Data Catalog and Online Registry for the 5-Year Review of Pacific Coast Groundfish EFH. NOAA National Marine Fisheries Service, Northwest Fisheries Science Center. Available from: https://www.nwfsc.noaa.gov/data/efh-catalog/ (Accessed 8 June 2020)

ODOE. 2018. 2018 Biennial Energy Report. Oregon Department of Energy. Salem, OR. 340 pp. Available from: https://energyinfo.oregon.gov/ber (Accessed 8 June 2020)

Pearson, R.G., C.J. Raxworthy, M. Nakamura, and A. Townsend Peterson. 2007. Predicting species distributions from small numbers of occurrence records: a test case using cryptic geckos in Madagascar. Journal of Biogeography 34(1): 102–117. doi:10.1111/j.1365-2699.2006.01594.x

PFMC. 2012. Pacific coast groundfish 5-year review of essential fish habitat. Report to Pacific Fishery Management Council. Phase 1: New information. September 2012. Portland, OR.

Phillips, S.J. 2017. A Brief Tutorial on Maxent. Website. Available from: https://biodiversityinformatics.amnh.org/open_source/maxent/ (Accessed 8 June 2020)

Phillips, S.J., M. Dudik, and R.E. Schapire. 2004. A maximum entropy approach to species distribution modeling. Proceedings of the 21st International Conference on Machine Learning, Banff, Canada. doi:10.1145/1015330.1015412

Phillips, S.J., R.P. Anderson, and R.E. Schapire. 2006. Maximum entropy modeling of species geographic distributions. Ecological Modelling 190(3–4): 231–259. doi:10.1016/j.ecolmodel.2005.03.026

Phillips, S.J., M. Dudik, J. Elith, C.H. Graham, A. Lehmann, J. Leathwick, and S. Ferrier. 2009. Sample selection bias and presence-only distribution models: implications for background and pseudo-absence data. Ecological Applications 19(1): 181–197. doi:10.1890/07-2153.1

Phillips, S.J., R.P. Anderson, M. Dudik, R.E. Schapire, and M.E. Blair. 2017. Opening the black box: an open-source release of Maxent. Ecography 40(7): 887–893. doi:10.1111/ecog.03049

Porter, A., and S. Phillips. 2016. Determining the Infrastructure Needs to Support Offshore Floating Wind and Marine Hydrokinetic Facilities on the Pacific West Coast and Hawaii. US Department of the Interior, Bureau of Ocean Energy Management, Pacific OCS Region, Camarillo, CA. OCS Study BOEM 2016-011. 238 pp.

Powell, A.N., M.E. Clarke, E. Fruh, J. Chaytor, H.M. Reiswig, and C.E. Whitmire. 2018. Characterizing the sponge grounds of Grays Canyon, Washington, USA. Deep-Sea Research Part II: Topical Studies in Oceanography 150: 146–155. doi:10.1016/j.dsr2.2018.01.004

Reid, J.A., J.M. Reid, C.J. Jenkins, M. Zimmerman, S.J. Williams, and M.E. Field. 2006. usSEABED: Pacific Coast (California, Oregon, Washington) offshore surficial-sediment data release: Website [Data downloaded 7 August 2017]. US Geological Survey Data Series 182, version 1.0. Available from: https://pubs.usgs.gov/ds/2006/182 (Accessed 8 June 2020)

Renner, I.W., and D.I. Warton. 2013. Equivalence of MAXENT and Poisson point process models for species distribution modeling in ecology. Biometrics 69(1): 274–281. doi:10.1111/j.1541-0420.2012.01824.x

Roberts, J.M., A.J. Wheeler, A. Freiwald, and S. Cairns. 2009. Cold-water corals: the biology and geology of deep-sea coral habitats. Cambridge University Press, New York. 351 pp. doi:10.1017/CBO9780511581588

Rooper, C.N., R. Wilborn, P. Goddard, K. Williams, R. Towler, and G.R. Hoff. 2018. Validation of deep-sea coral and sponge distribution models in the Aleutian Islands, Alaska. ICES Journal of Marine Science 75(1): 199–209. doi:10.1093/icesjms/fsx087

Rossi, S., L. Bramanti, A. Gori, and C. Orejas. 2017. An overview of the animal forests of the world. pp. 1–26. In: S. Rossi, L. Bramanti, A. Gori, and C. Orejas. (eds.), Marine animal forests: the ecology of benthic biodiversity hotspots. Springer International Publishing, Switzerland. 1366 pp. doi:10.1007/978-3-319-21012-4

Salgado, E.J., S.E. Nehasil, and P.J. Etnoyer. 2018. Distribution of deep-water corals, sponges, and demersal fisheries landings in Southern California, USA: implications for conservation priorities. PeerJ 6: e5697. doi:10.7717/peerj.5697

Salmi, M.S., H.P. Johnson, I. Leifer, and J.E. Keister. 2011. Behavior of methane seep bubbles over a pockmark on the Cascadia continental margin. Geosphere 7(6): 1273–1283. doi:10.1130/GES00648.1

Schiff, K., D. Greenstein, N. Dodder, and D.J. Gillett. 2016. Southern California Bight regional monitoring. Regional Studies in Marine Science 4: 34–46. doi:10.1016/j.rsma.2015.09.003

Sheng, W., and H. Li. 2017. A method for energy and resource assessment of waves in finite water depths. Energies 10(4): 460. doi:10.3390/en10040460

Sing, T., O. Sander, N. Beerenwinkel, and T. Lengauer. 2005. ROCR: visualizing classifier performance in R. Bioinformatics 21(20): 3940–3941. doi:10.1093/bioinformatics/bti623

Smith, R.W., M. Bergen, S.B. Weisberg, D. Cadien, A. Dalkey, D. Montagne, J.K. Stull, and R.G. Velarde. 2001. Benthic response index for assessing infaunal communities on the southern California mainland shelf. Ecological Applications 11(4): 1073–1087. doi:10.1890/1051-0761(2001)011[1073:BRIFAI]2.0.CO;2

Stone, R.P. 2014. The ecology of deep-sea coral and sponge habitats of the central Aleutian Islands of Alaska. NOAA National Marine Fisheries Service, Pacific Islands Fisheries Science Center. NOAA Professional Paper NMFS 16. Seattle, WA. 52 pp. doi:10.7755/PP.16

Stone, R.P., M.M. Masuda, and J.F. Karinen. 2014. Assessing the ecological importance of red tree coral thickets in the eastern Gulf of Alaska. ICES Journal of Marine Science 72(3): 900–915. doi:10.1093/icesjms/fsu190

Tittensor, D.P., A.R. Baco, P.E. Brewin, M.R Clark, M. Consalvey, J. Hall-Spencer, A.A. Rowden, T. Schlacher, K.I. Stocks, and A.D. Rogers. 2009. Predicting global habitat suitability for stony corals on seamounts. Journal of Biogeography 36(6): 1111–1128. doi:10.1111/j.1365-2699.2008.02062.x

Tobler, W. 1970. A computer movie simulating urban growth in the Detroit region. Economic Geography 46: 234–240. doi:10.2307/143141

UCSC. 2018. California Current System 31-Year Historical Reanalysis. UC Santa Cruz Ocean Modeling and Data Assimilation. Website. University of California, Santa Cruz. [Data received 13 September 2018]. Available from: https://oceanmodeling.ucsc.edu/reanalccs31/ (Accessed 8 June 2020)

US DOE. 2020. PacWave. Website. US Department of Energy, Water Power Technologies Office. Washington, D.C. Available from: https://www.energy.gov/eere/water/pacwave (Accessed 8 June 2020)

Valavi, R., J. Elith, J.J. Lahoz-Monfort, and G.-A. Gurutzeta. 2018. blockCV: an R package for generating spatially or environmentally separated folds for k-folds cross-validation of species distribution models. Methods in Ecology and Evolution 10(2): 225–232. doi:10.1111/2041-210X.13107

van Proosdij, A.S.J., M.S.M. Sosef, J.J. Wieringa, and N. Raes. 2016. Minimum required number of specimen records to develop accurate species distribution models. Ecography 39(6): 542–552. doi:10.1111/ecog.01509

Varela, S., R.P. Anderson, R. García-Valdés, and F. Fernández-González. 2014. Environmental filters reduce the effects of sampling bias and improve predictions of ecological niche models. Ecography 37(11): 1084–1091. doi:10.1111/j.1600-0587.2013.00441.x

Vierod, A.D.T., J.M. Guinotte, and A.J. Davies. 2014. Predicting the distribution of vulnerable marine ecosystems in the deep sea using presence-background models. Deep Sea Research Part II: Topical Studies in Oceanography 99: 6–18. doi:10.1016/j.dsr2.2013.06.010

Warren, D.L., and S.N. Seifort. 2011. Ecological niche modeling in Maxent: the importance of model complexity and the performance of model selection criteria. Ecological Applications 21(2): 335–342. doi:10.1890/10-1171.1

Weatherall, P., K.M. Marks, M. Jakobsson, T. Schmitt, S. Tani, J.E. Arndt, M. Rovere, D. Chayes, V. Ferrini, and R. Wigley. 2015. A new digital bathymetric model of the world's oceans. Earth and Space Science 2(8): 331–345. doi:10.1002/2015EA000107

Whitmire, C.E., and Clarke, M.E. 2007. State of deep coral ecosystems of the U.S. Pacific Coast: California to Washington. pp. 109–154. In: S.E. Lumsden, T.F. Hourigan, A.W. Bruckner, and G. Dorr. (eds.), The State of Deep Coral Ecosystems of the United States. NOAA Technical Memorandum CRCP-3. Silver Spring, MD. 365 pp. Available from: https://deepseacoraldata.noaa.gov/library/2007-dsc-status-report (Accessed 8 June 2020)

Whitmire, C.E., M.E. Clarke, M.M. Yoklavich, M.V. Everett, T.F. Hourigan, and S.D. Cairns. 2017. Deep-sea coral taxa in the U.S. West Coast region: depth and geographic distribution. Annex report. NOAA National Marine Fisheries Service. Available from: https://deepseacoraldata.noaa.gov/library/2017-state-of-deep-sea-corals-report (Accessed 8 June 2020)

Wiltshire, K.H., J.E. Tanner, F. Althaus, S.J. Sorokin, and A. Williams. 2018. Predicting environmental suitability for key benthic species in an ecologically and economically important deep-sea environment. Deep-Sea Research Part II: Topical Studies in Oceanography 157–158: 121–133. doi:10.1016/j.dsr2.2018.06.011

Winship, A.J., J.T. Thorson, M.E. Clarke, H.M. Coleman, B. Costa, S.E. Georgian, D. Gillett, A. Grüss, M.J. Henderson, T.F. Hourigan, D.D. Huff, N. Kreidler, J.L. Pirtle, J.V. Olson, M. Poti, C.N. Rooper, M.F. Sigler, S. Viehman, and C.E. Whitmire. 2020. Good practices for species distribution modeling of deep-sea corals and sponges: data collection, analysis, validation, and communication. Frontiers in Marine Science 7:303. doi:10.3389/fmars.2020.00303

WoRMS Editorial Board. 2019. World Register of Marine Species. Website. Flanders Marine Institute (VLIZ), Belgium. Available from: http://www.marinespecies.org (Accessed 8 June 2020) doi:10.14284/170

Yackulic, C.B., R. Chandler, E.F. Zipkin, J.A. Royle, J.D. Nichols, E.H.C. Grant, and S. Veran. 2013. Presence-only modelling using MAXENT: when can we trust the inferences? Methods in Ecology and Evolution 4(3): 236–243. doi:10.1111/2041-210x.12004

Yesson, C., M.L. Taylor, D.P. Tittensor, A.J. Davies, J. Guinotte, A. Baco, J. Black, J.M. Hall-Spencer, and A.D. Rogers. 2012. Global habitat suitability of cold-water octocorals. Journal of Biogeography 39(7): 1278–1292. doi:10.1111/j.1365-2699.2011.02681.x

Appendix A: Maps of the Environmental Predictor Variables

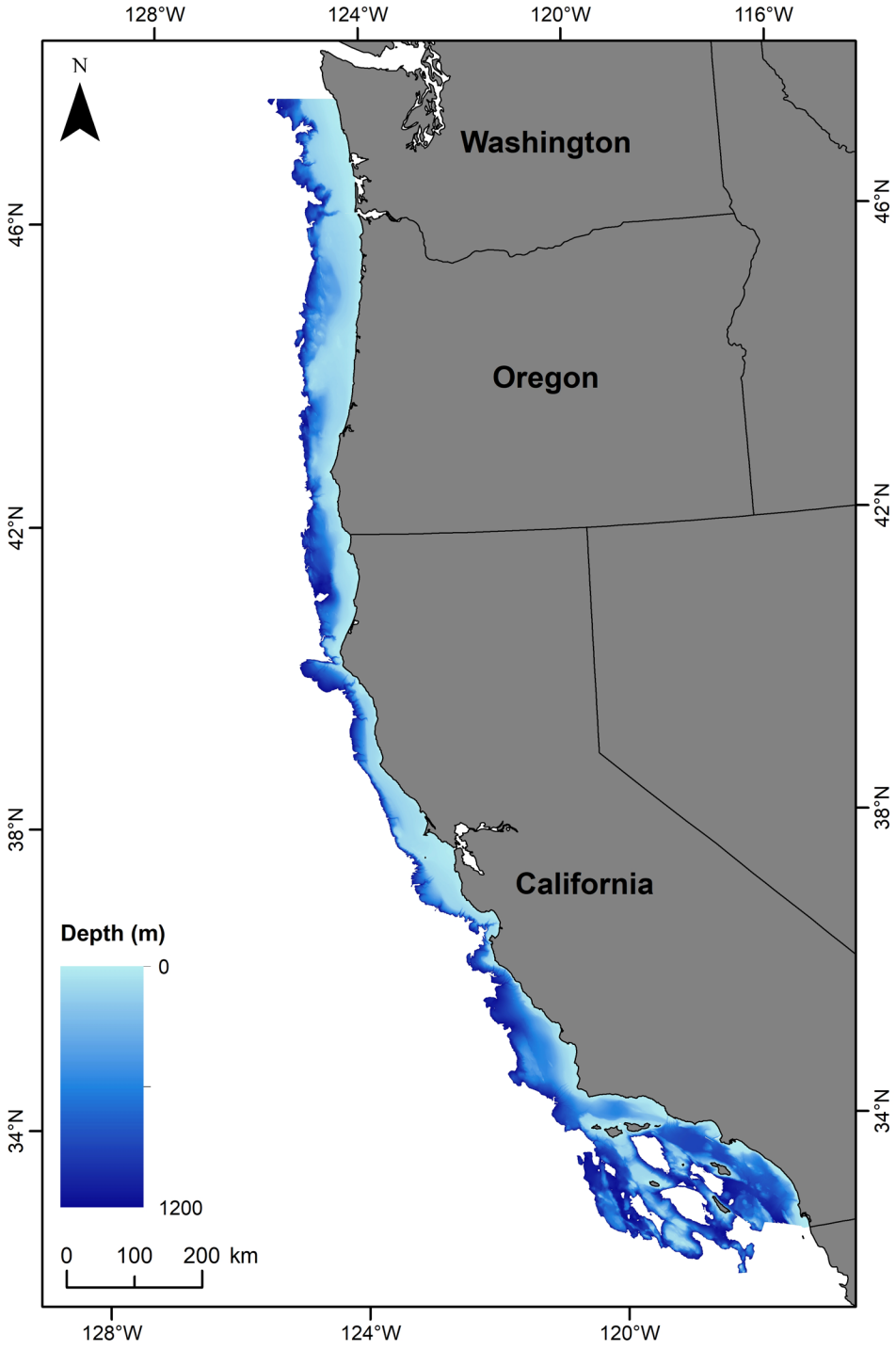

Figure A-1. Depth of the seafloor, 25 x 25 m resolution.

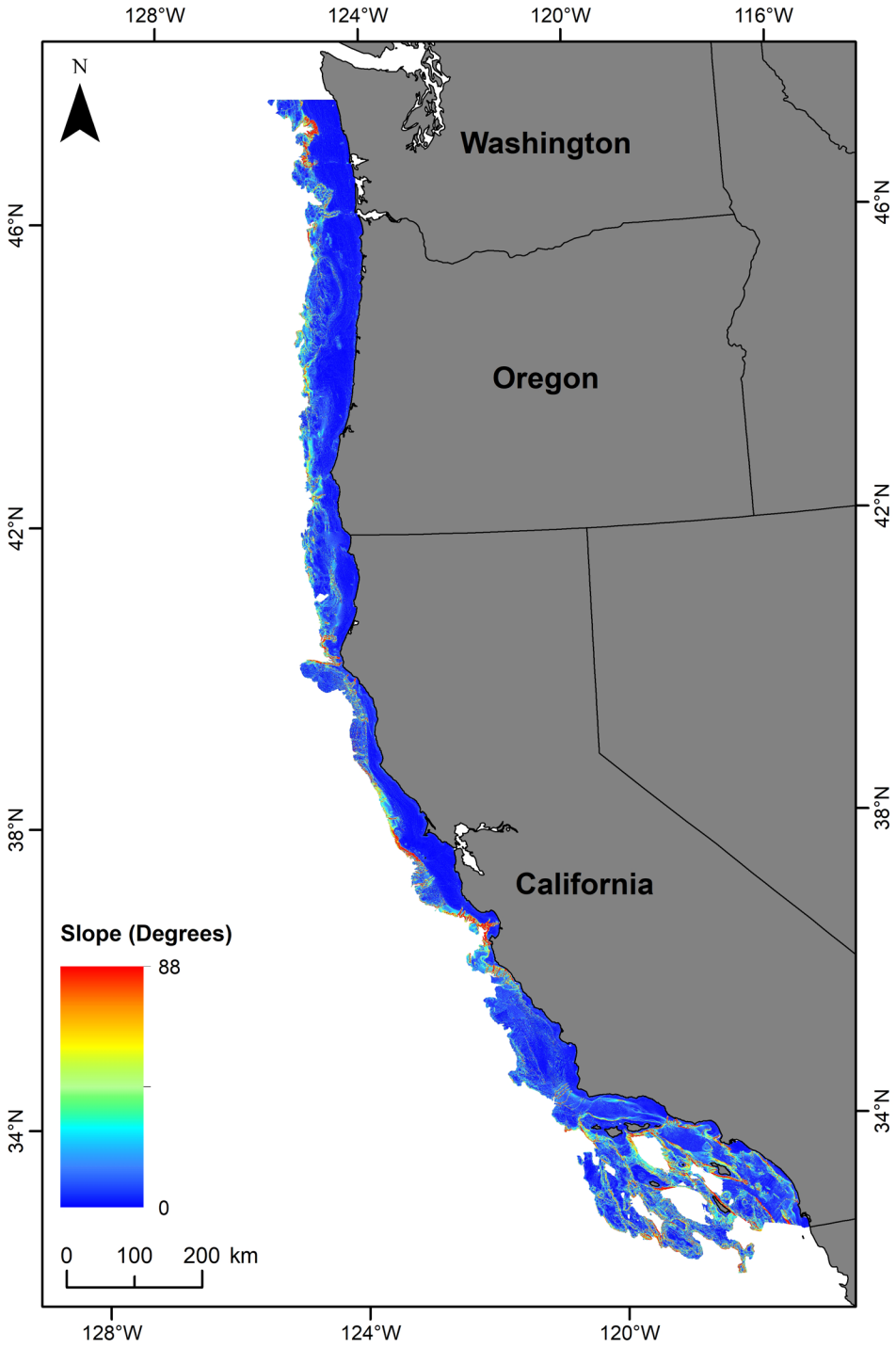

Figure A-2. Slope of the seafloor, 25 x 25 m resolution.

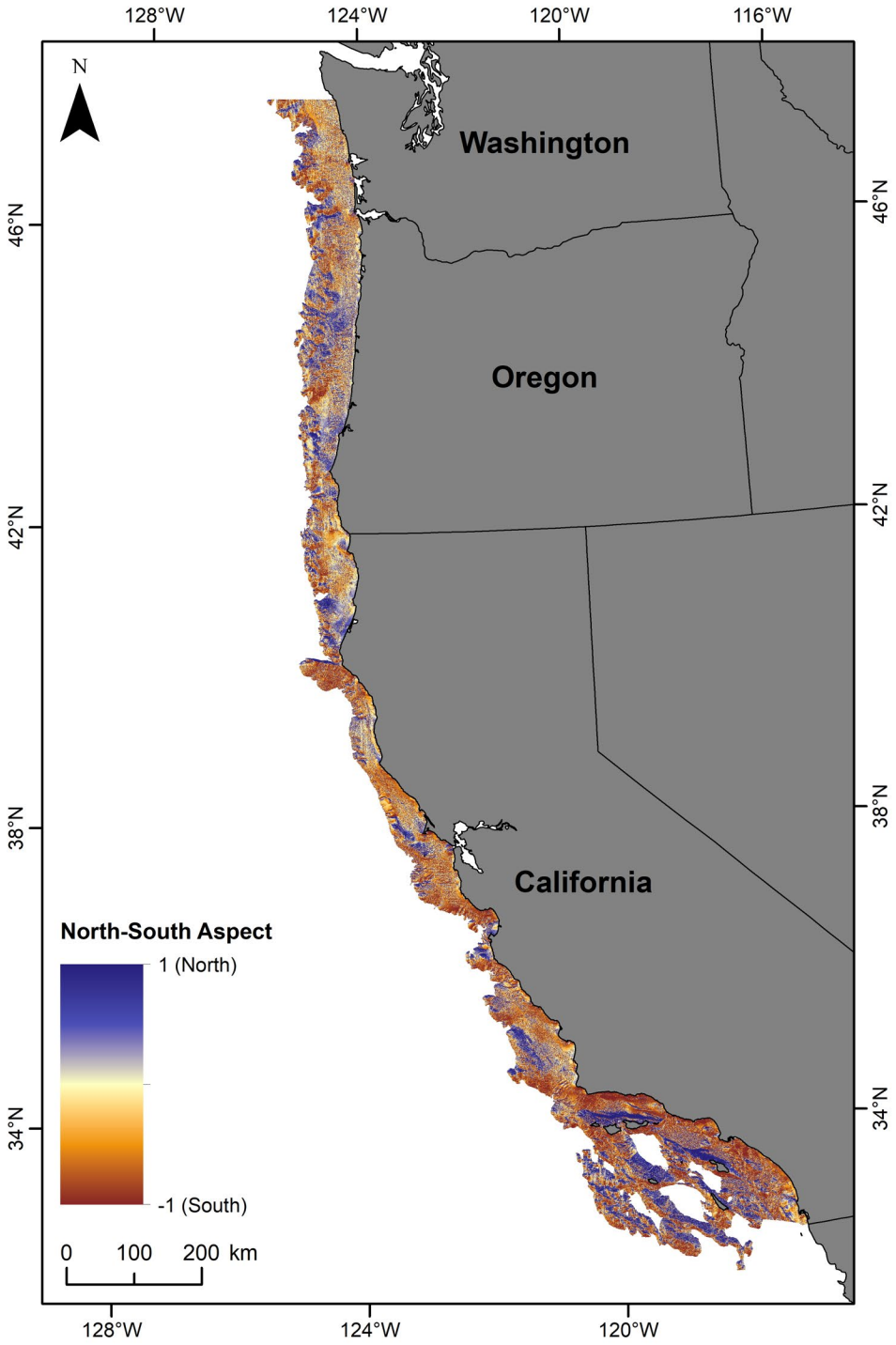

Figure A-3. North-south aspect (cosine of seafloor slope direction), 25 x 25 m resolution.

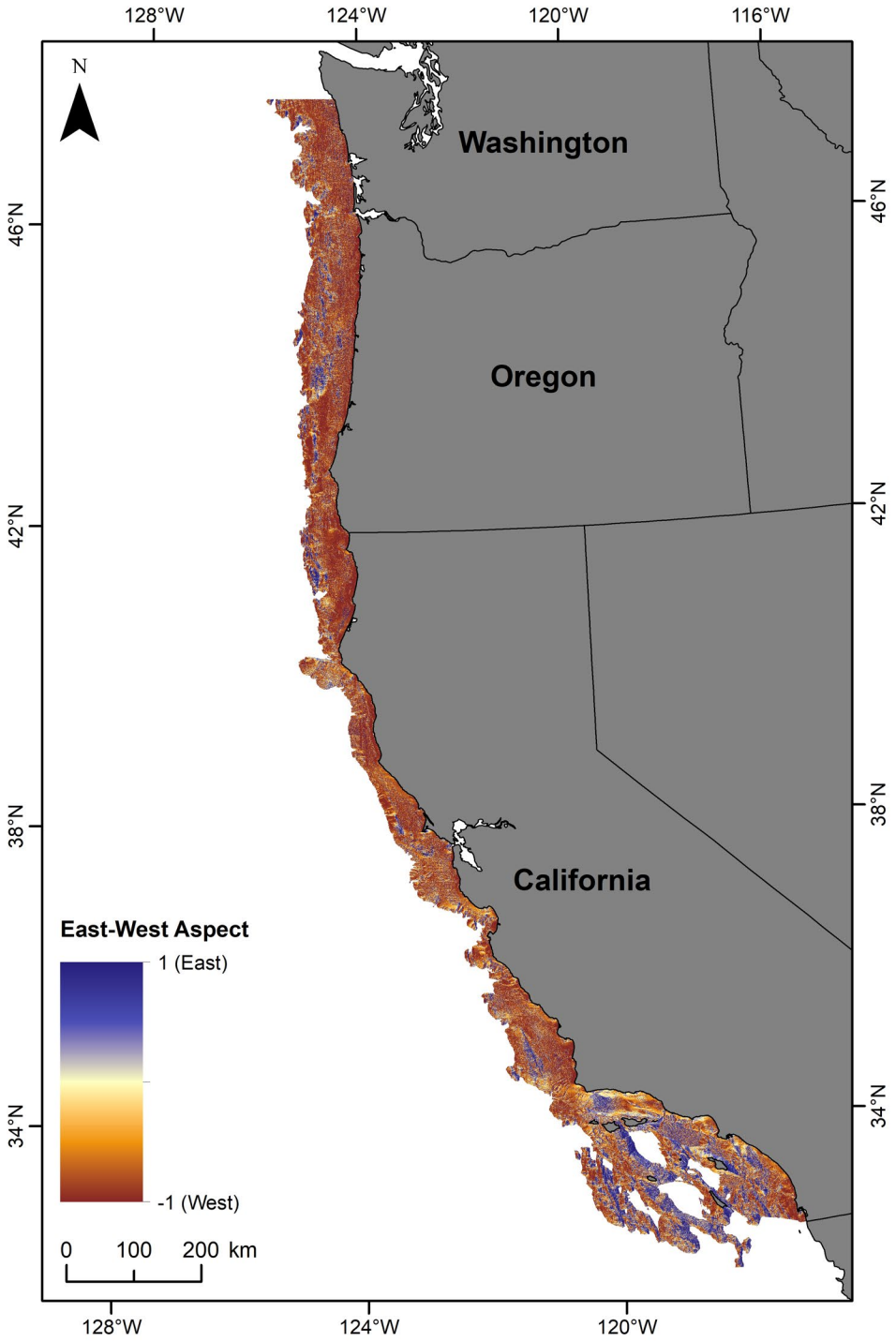

Figure A-4. East-west aspect (sine of seafloor slope direction), 25 x 25 m resolution.

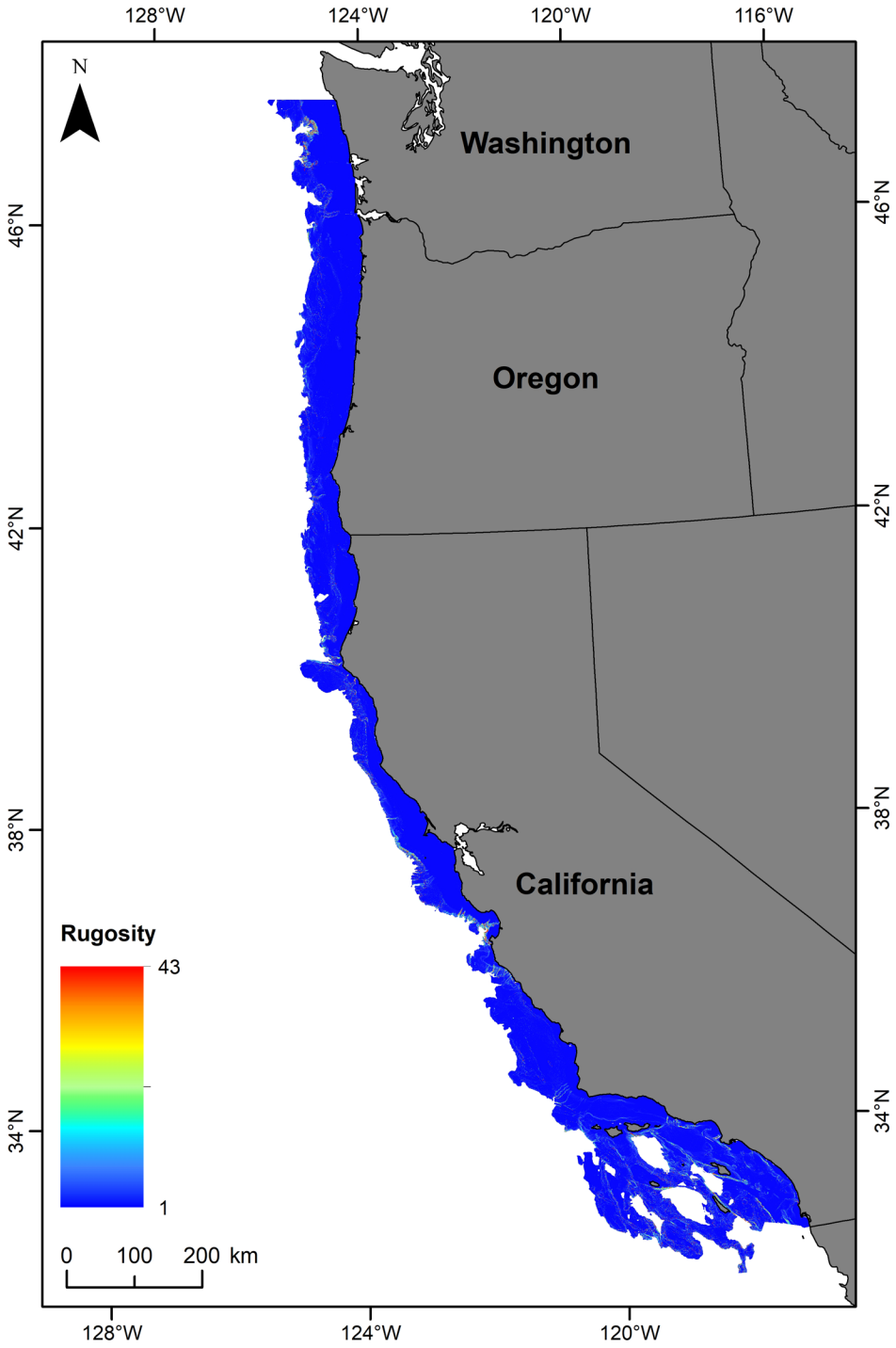

Figure A-5. Rugosity of the seafloor (surface ratio method), 25 x 25 m resolution.

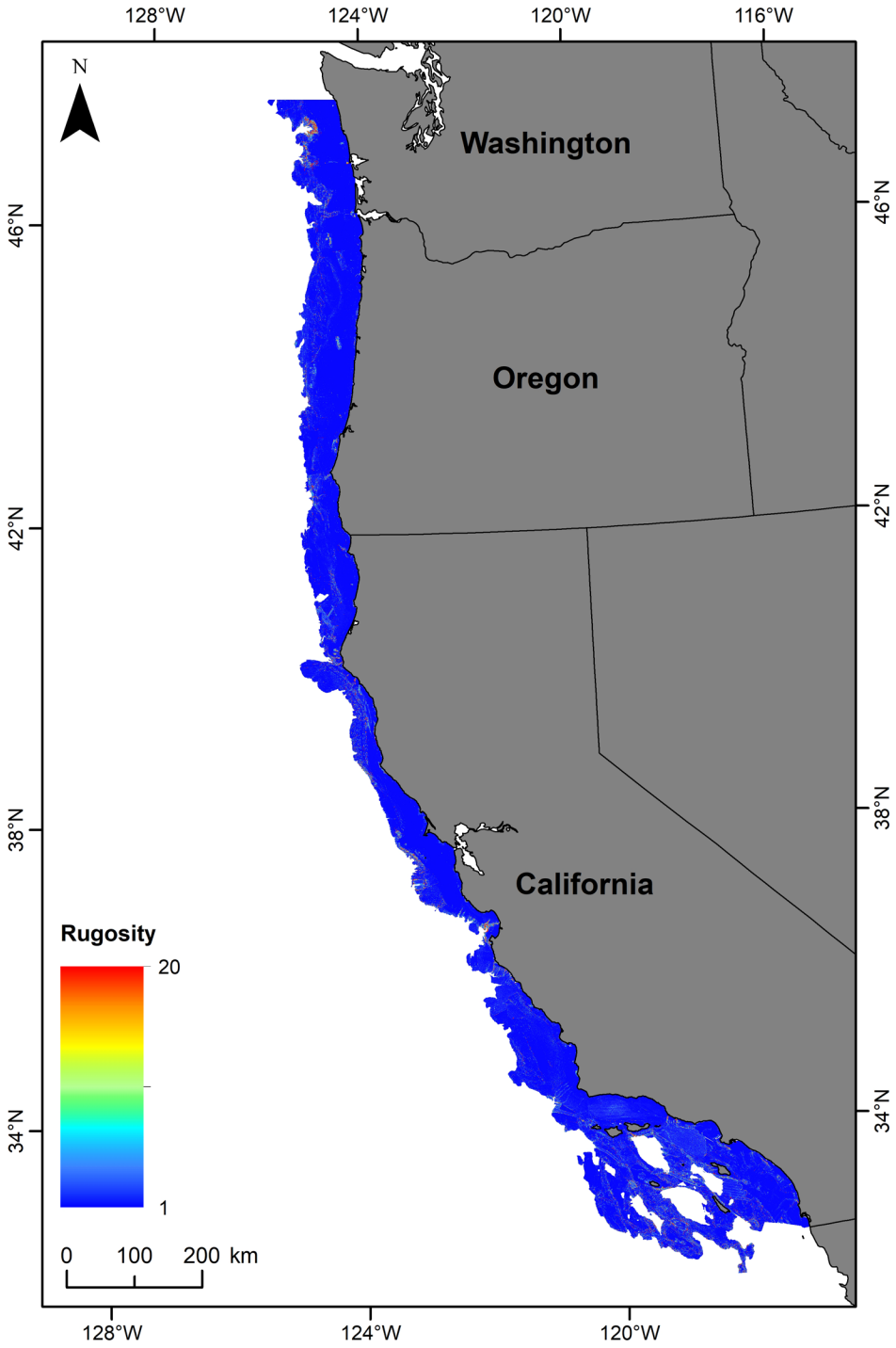

Figure A-6. Rugosity of the seafloor (arc-chord ratio method), 25 x 25 m resolution.

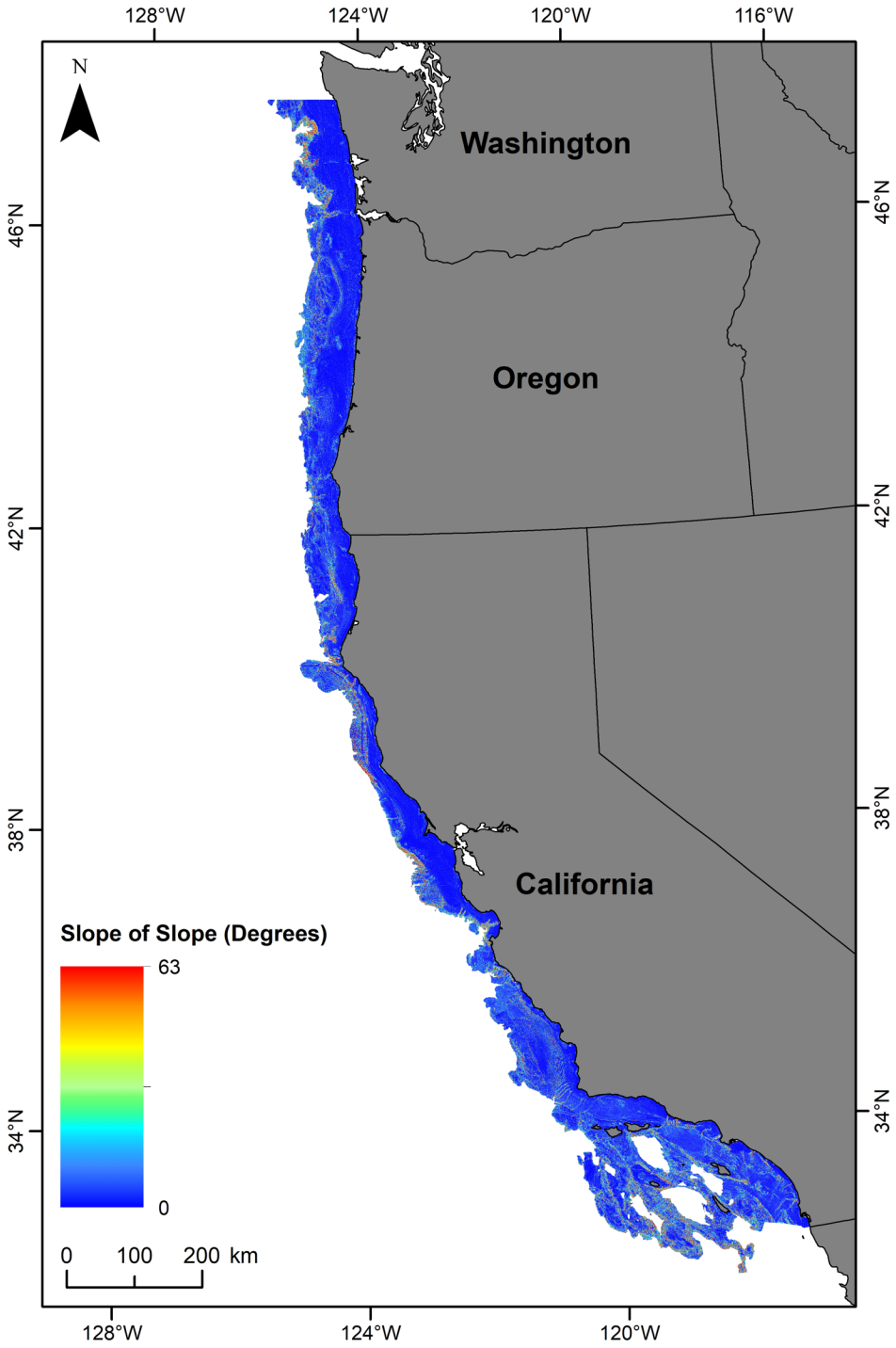

Figure A-7. Slope of slope of the seafloor, 25 x 25 m resolution.

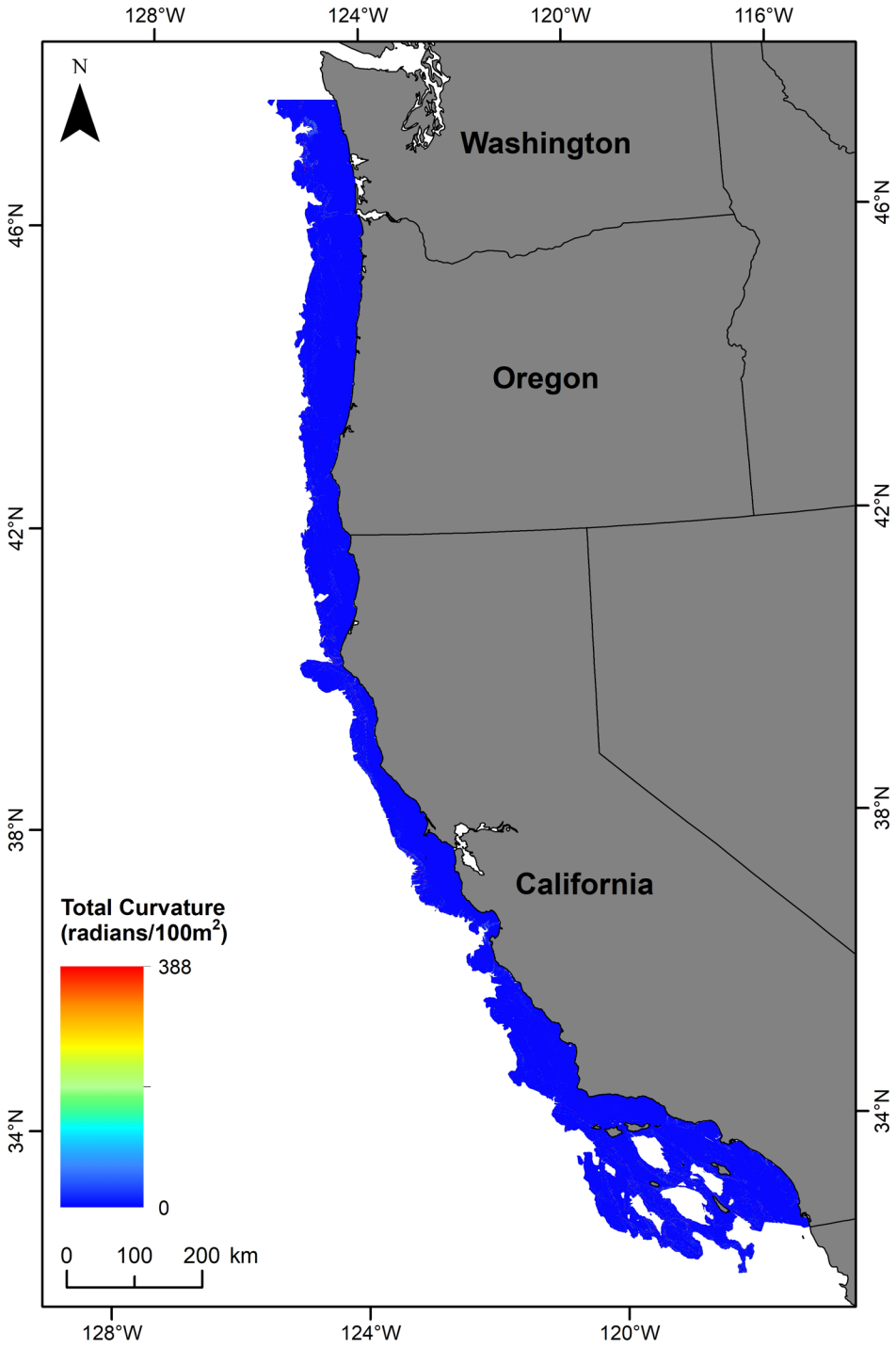

Figure A-8. Total curvature of the seafloor, 25 x 25 m resolution.

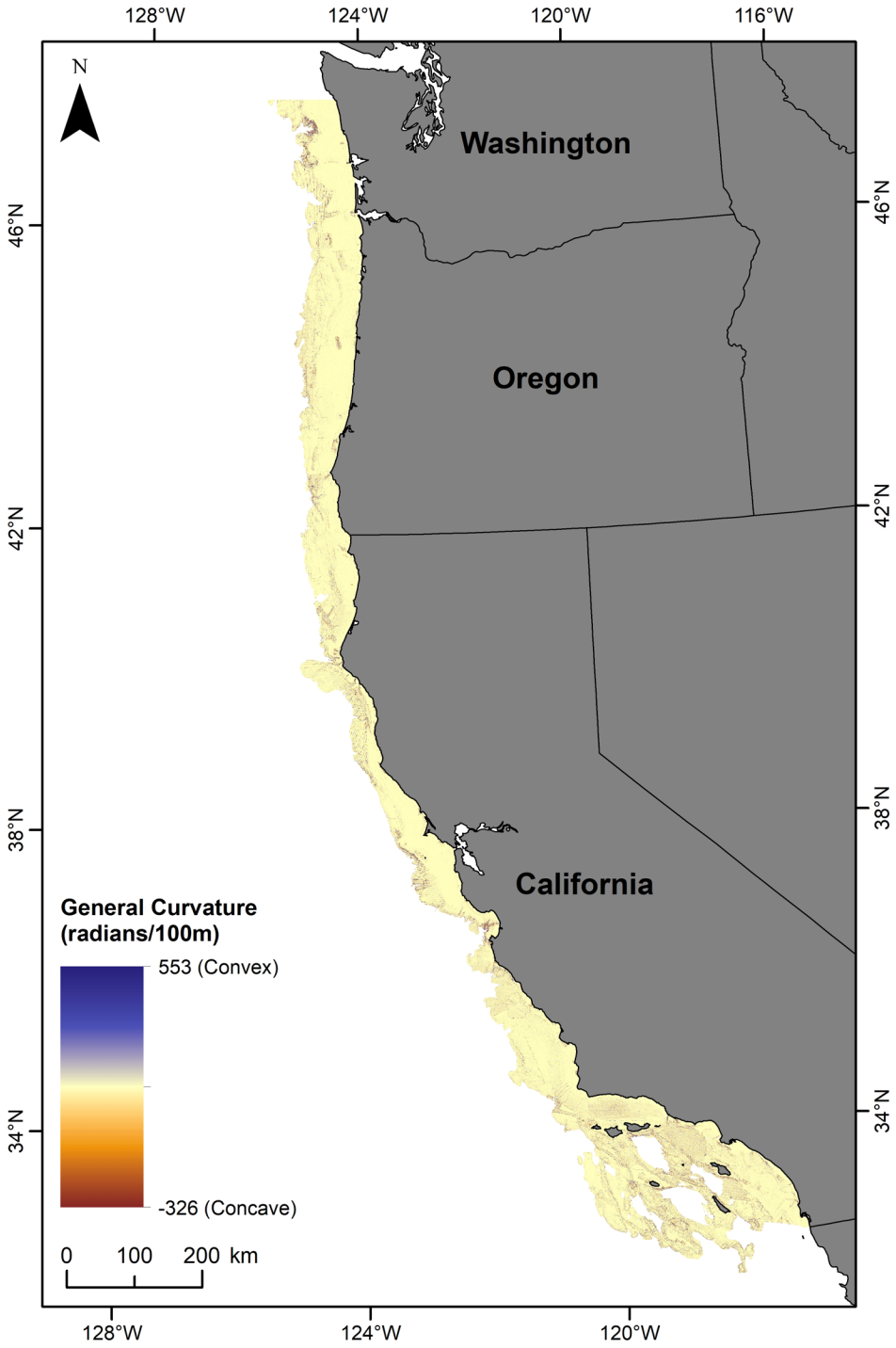

Figure A-9. General curvature of the seafloor, 25 x 25 m resolution.

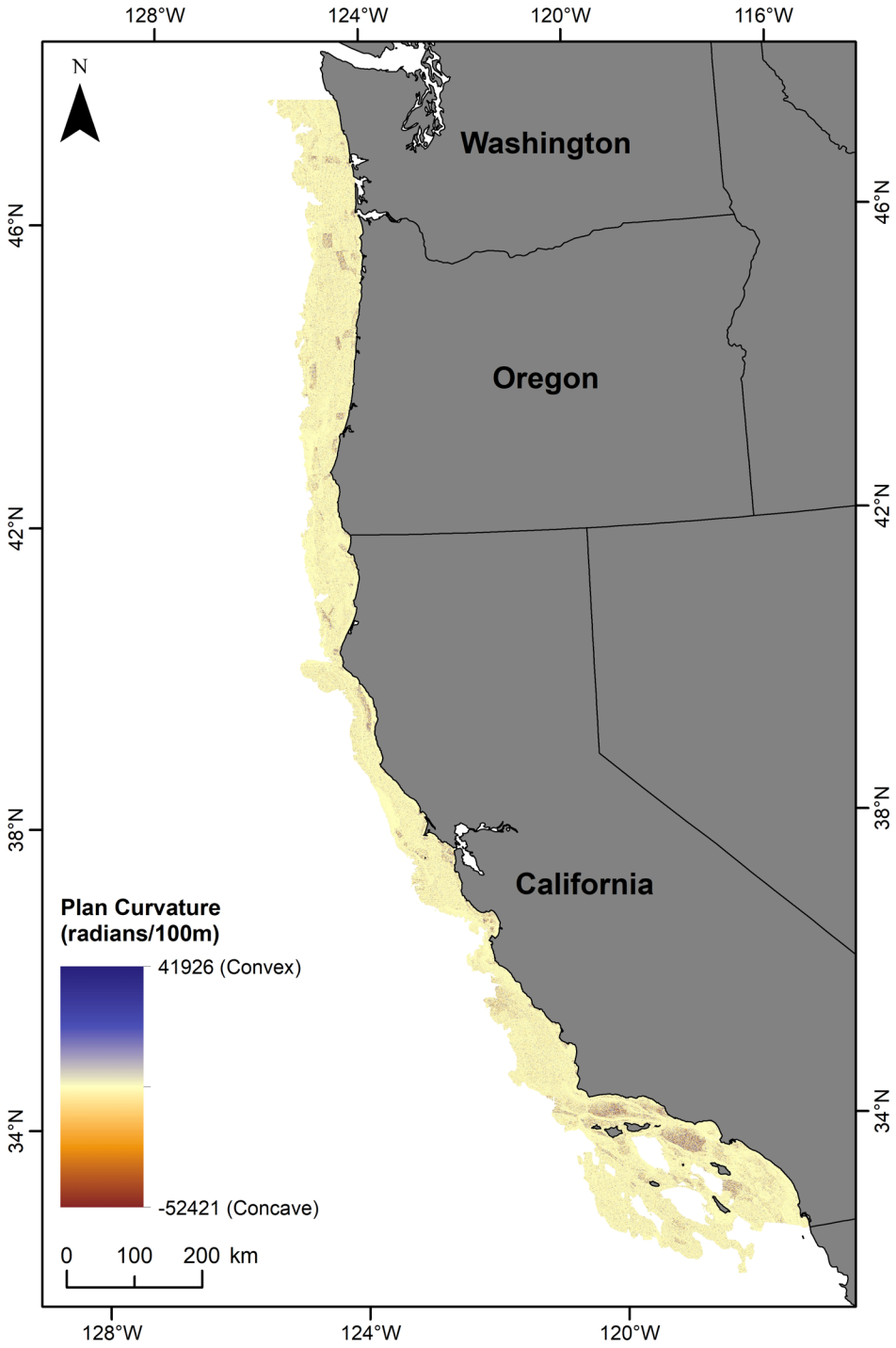

Figure A-10. Plan curvature of the seafloor, 25 x 25 m resolution.

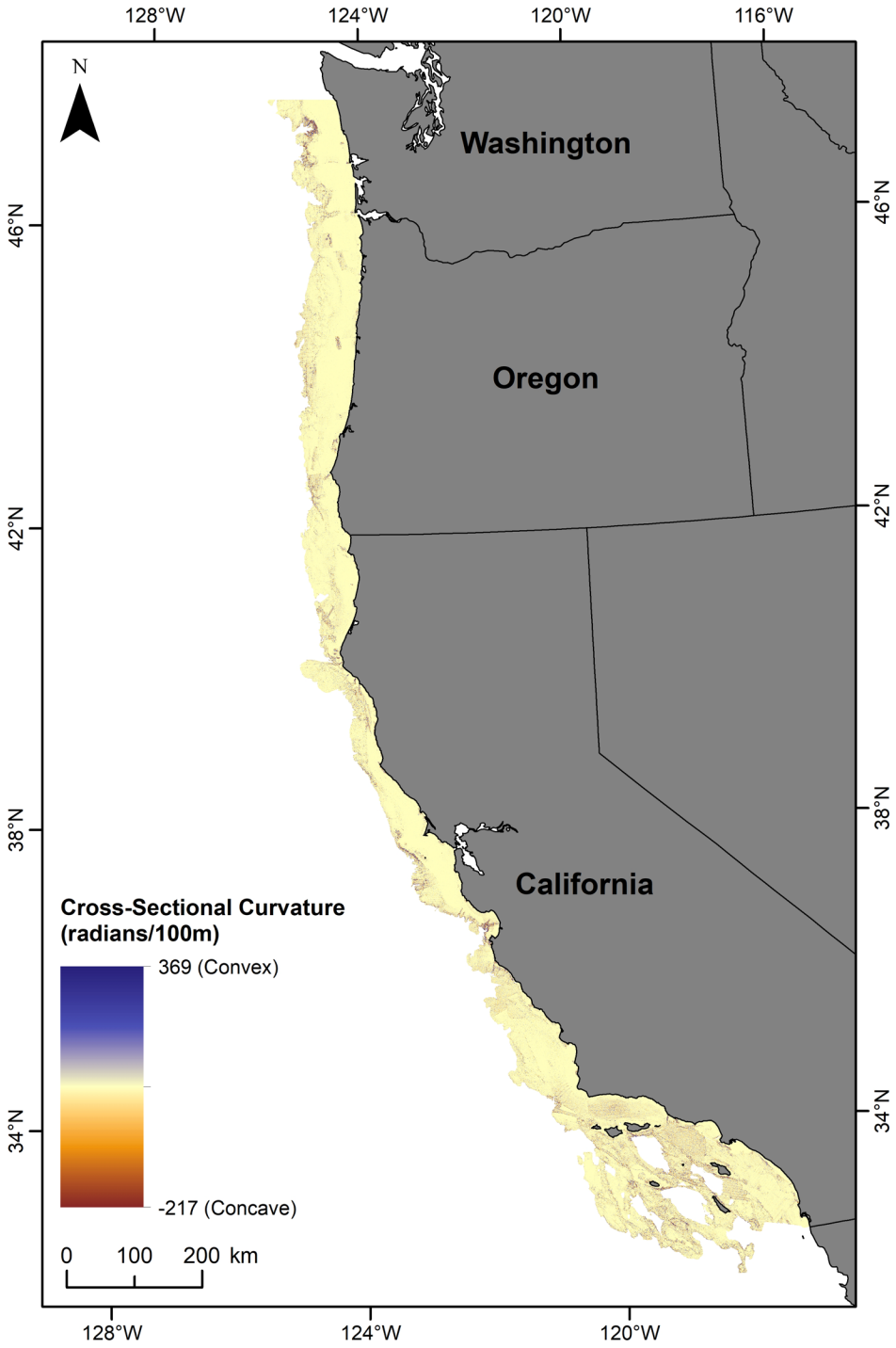

Figure A-11. Cross-sectional curvature of the seafloor, 25 x 25 m resolution.

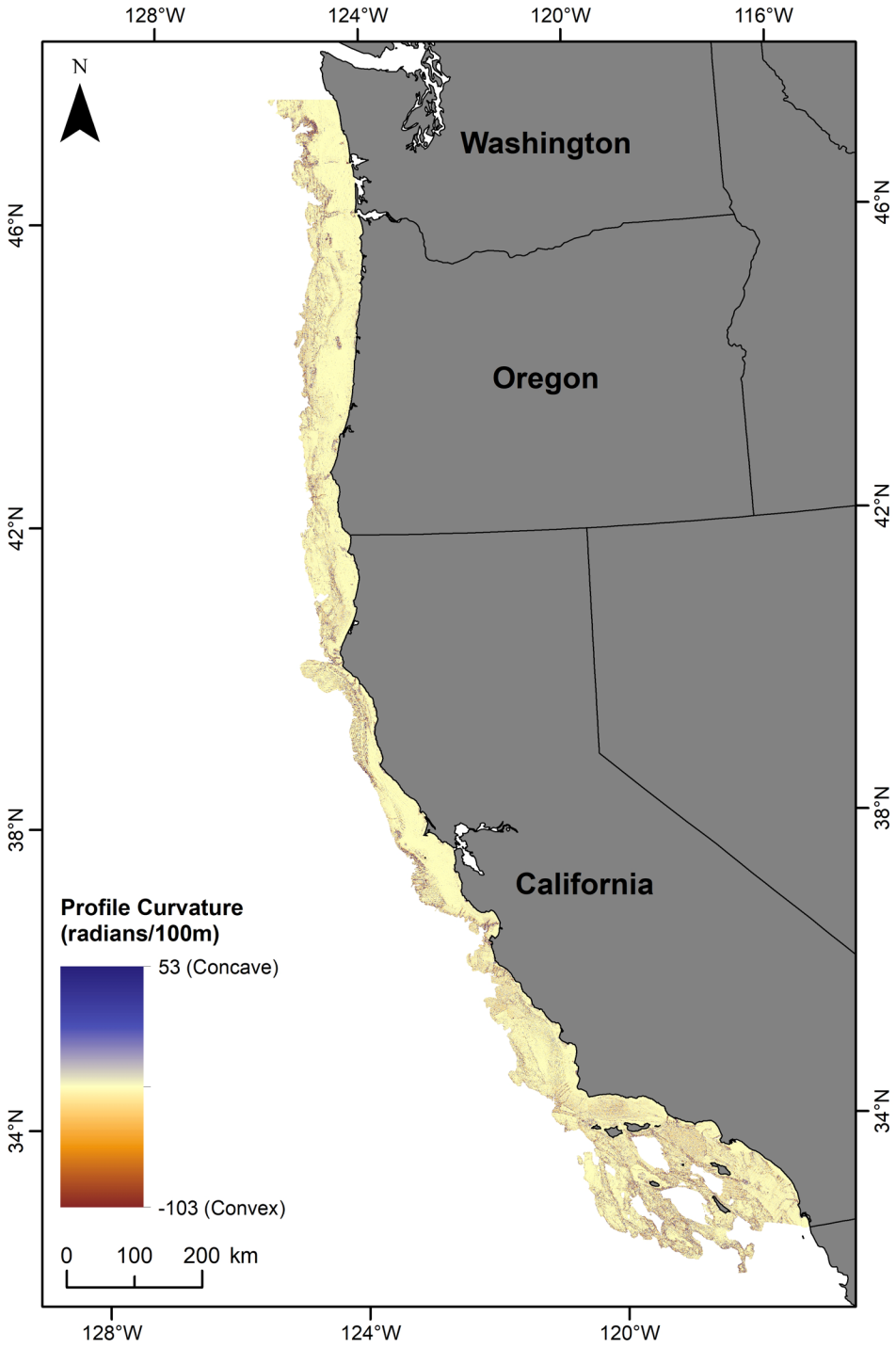

Figure A-12. Profile curvature of the seafloor, 25 x 25 m resolution.

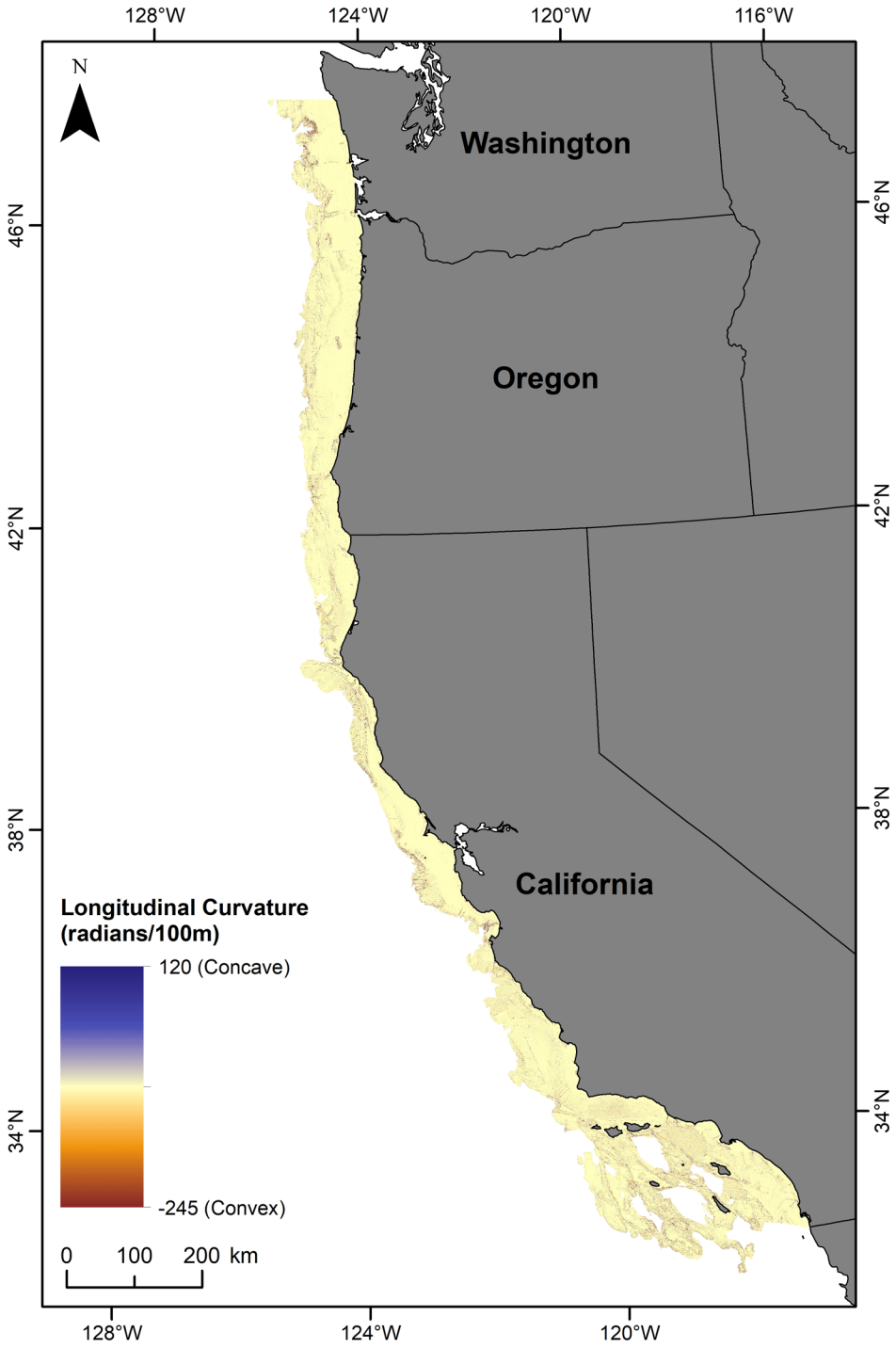

Figure A-13. Longitudinal curvature of the seafloor, 25 x 25 m resolution.

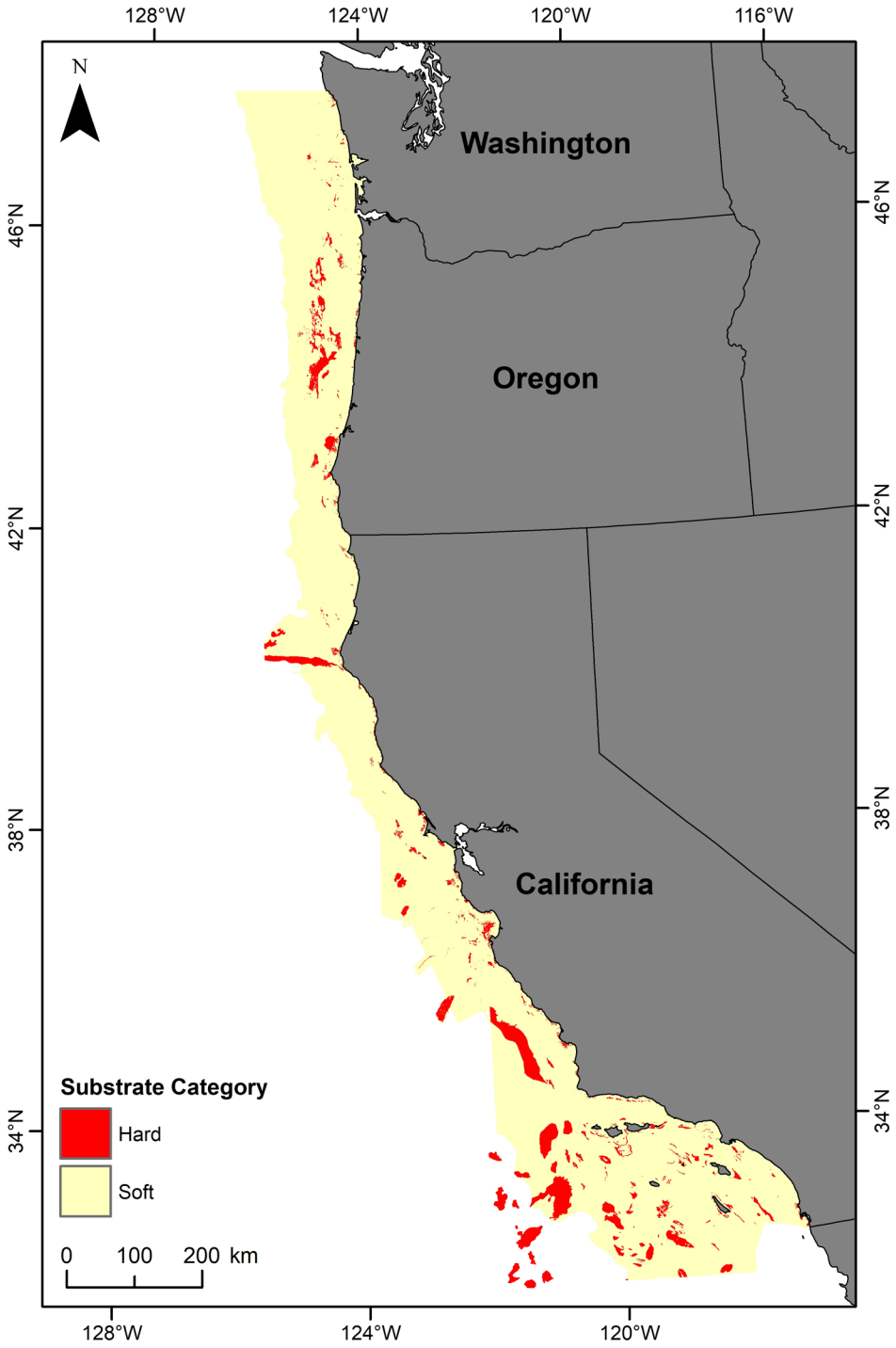

Figure A-14. Seafloor substrate (hard-soft), 25 x 25 m resolution.

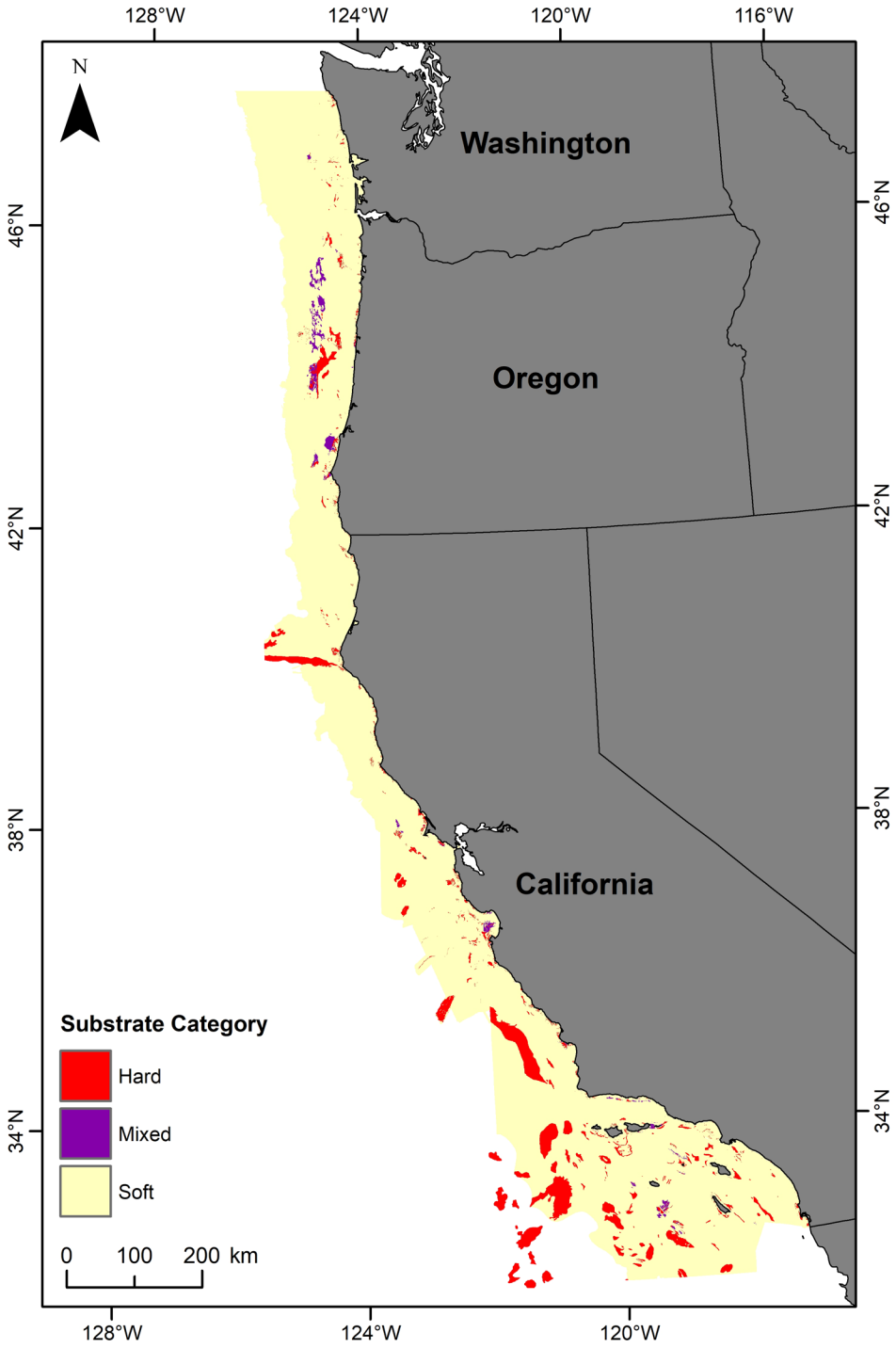

Figure A-15. Seafloor substrate (hard-mixed-soft), 25 x 25 m resolution.

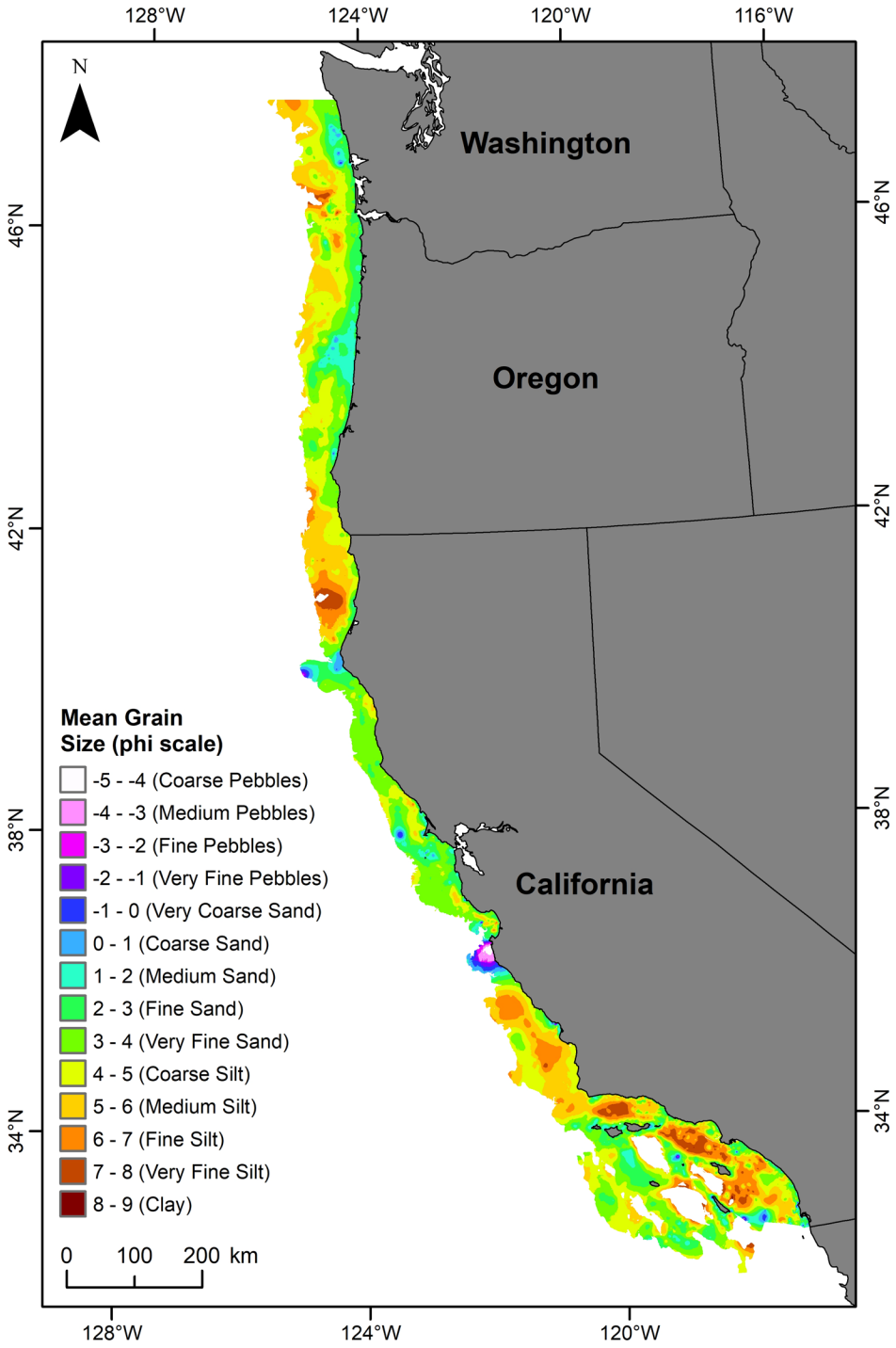

Figure A-16. Surficial sediment mean grain size, 25 x 25 m resolution.

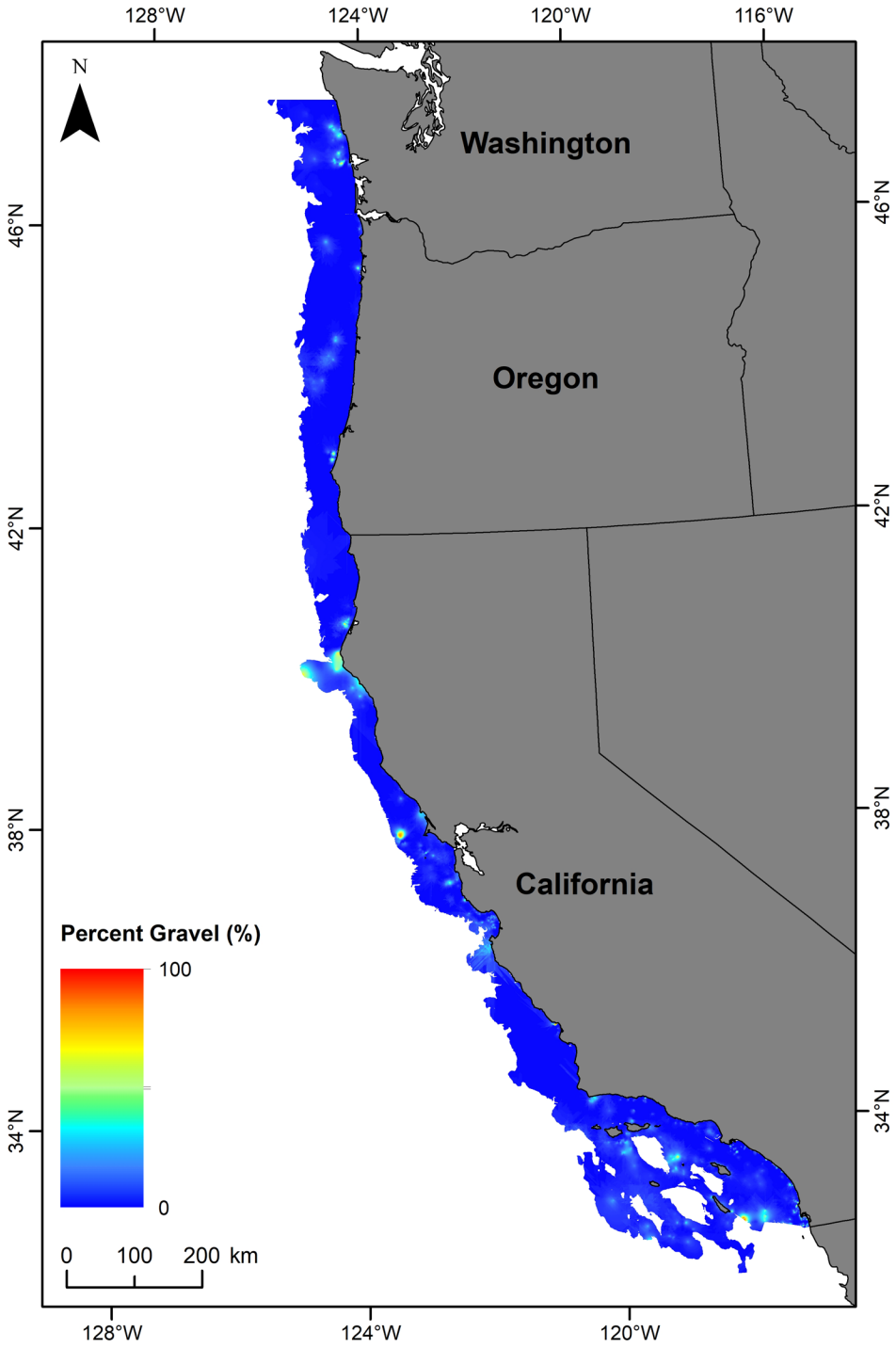

Figure A-17. Surficial sediment percent gravel, 25 x 25 m resolution.

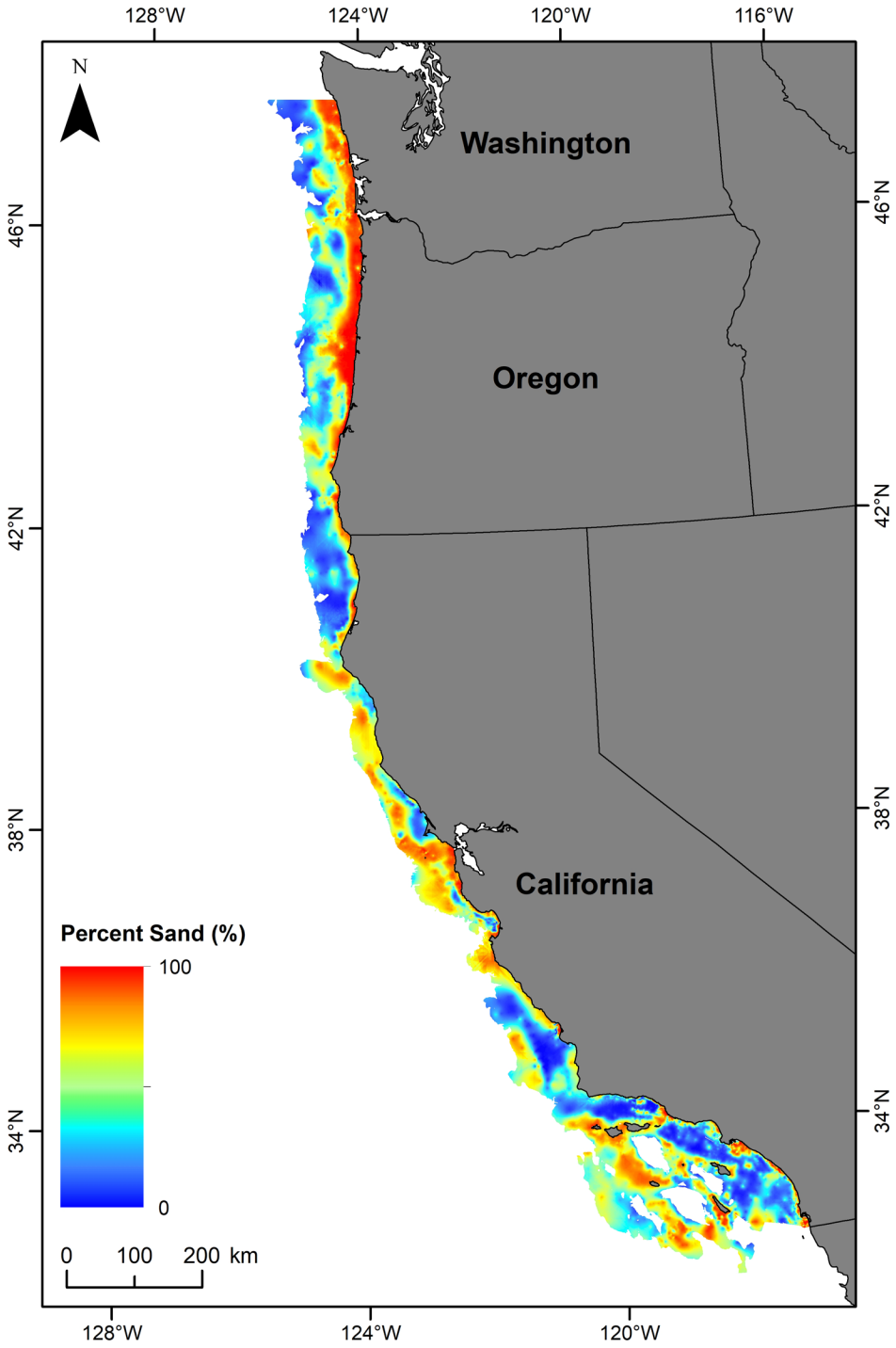

Figure A-18. Surficial sediment percent sand, 25 x 25 m resolution.

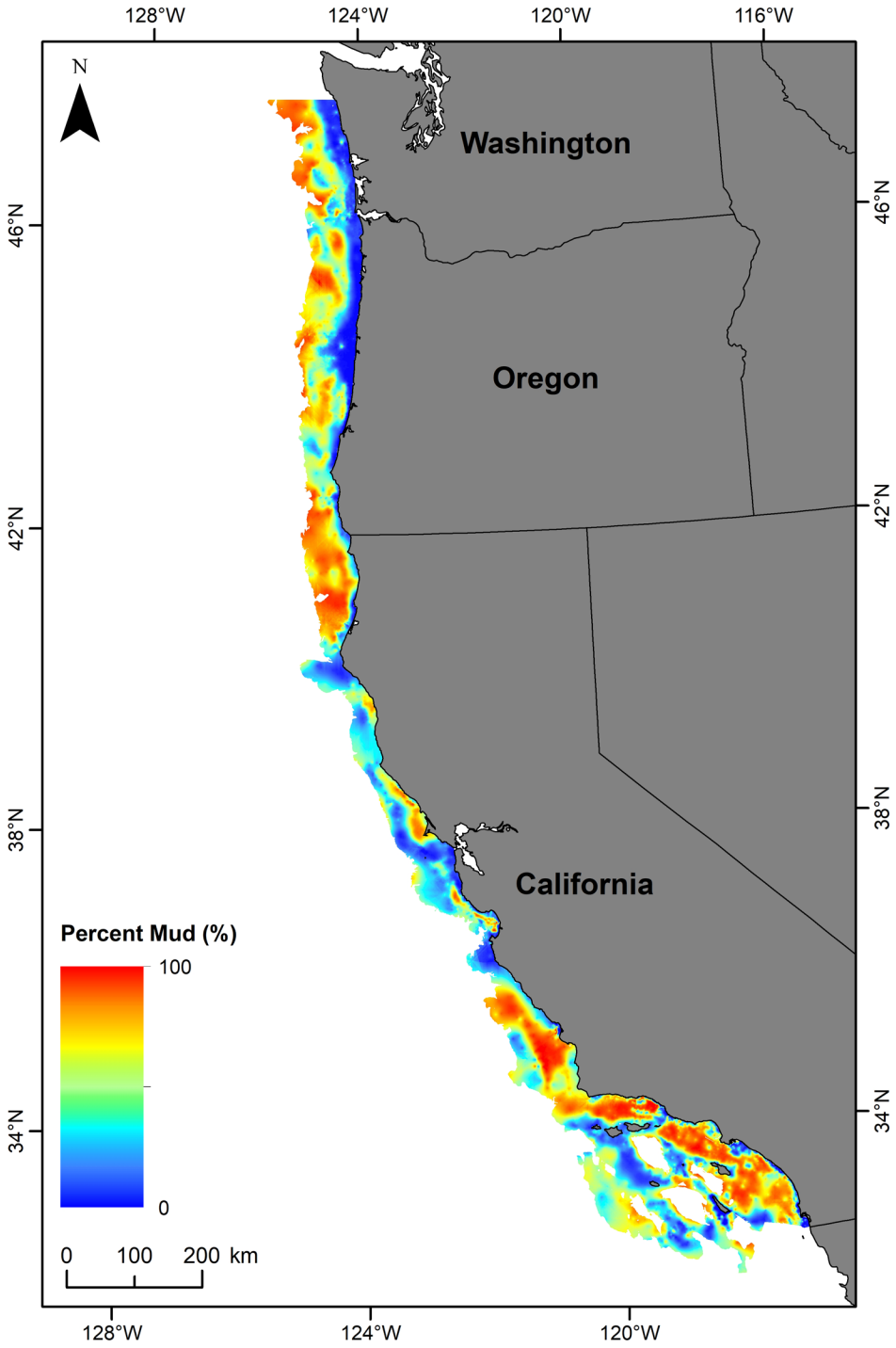

Figure A-19. Surficial sediment percent mud, 25 x 25 m resolution.

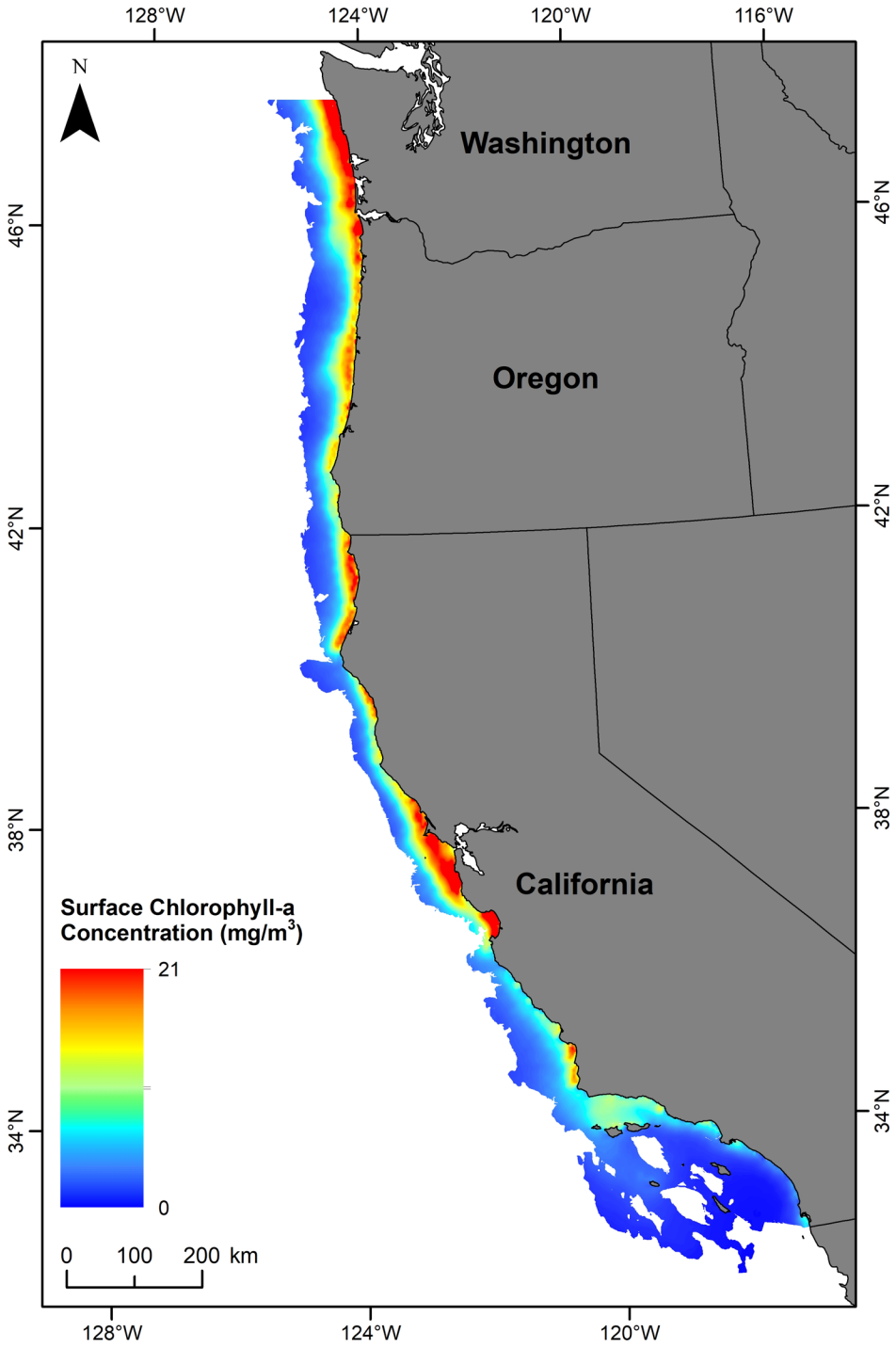

Figure A-20. Annual mean sea surface chlorophyll-a concentration, 200 x 200 m resolution.

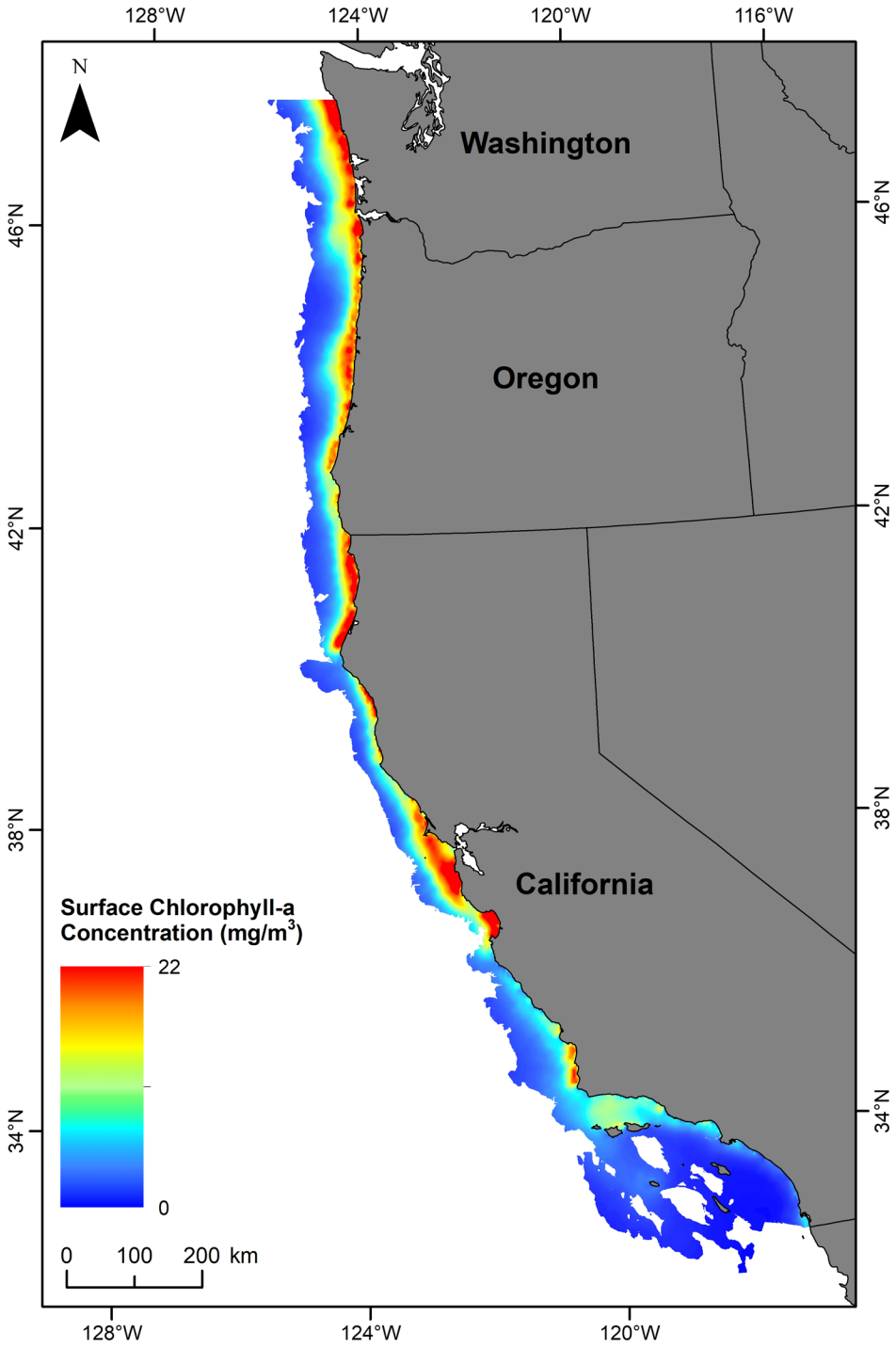

Figure A-21. Spring/summer mean sea surface chlorophyll-a concentration, 200 x 200 m resolution.

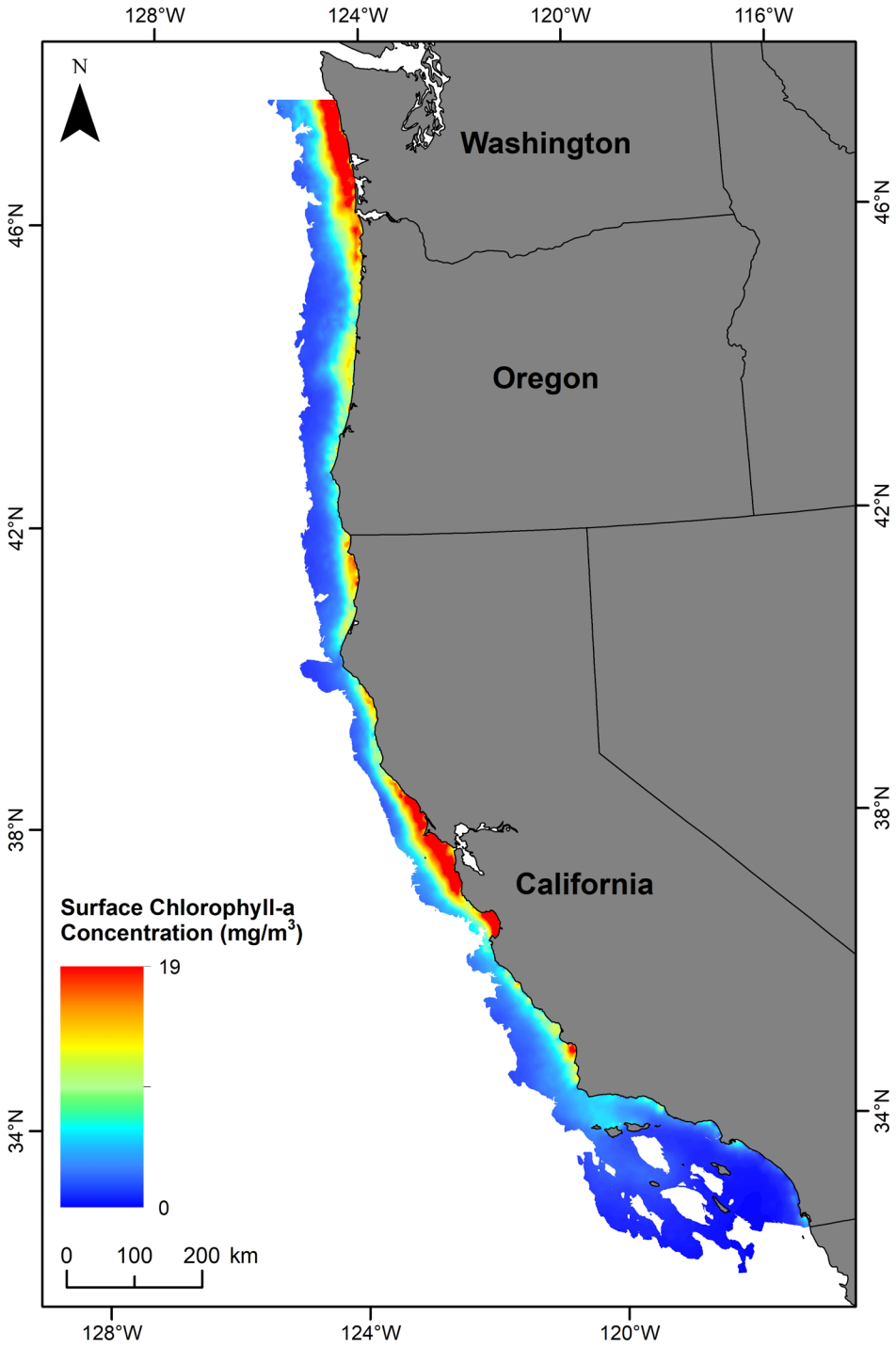

Figure A-22. Fall mean sea surface chlorophyll-a concentration, 200 x 200 m resolution.

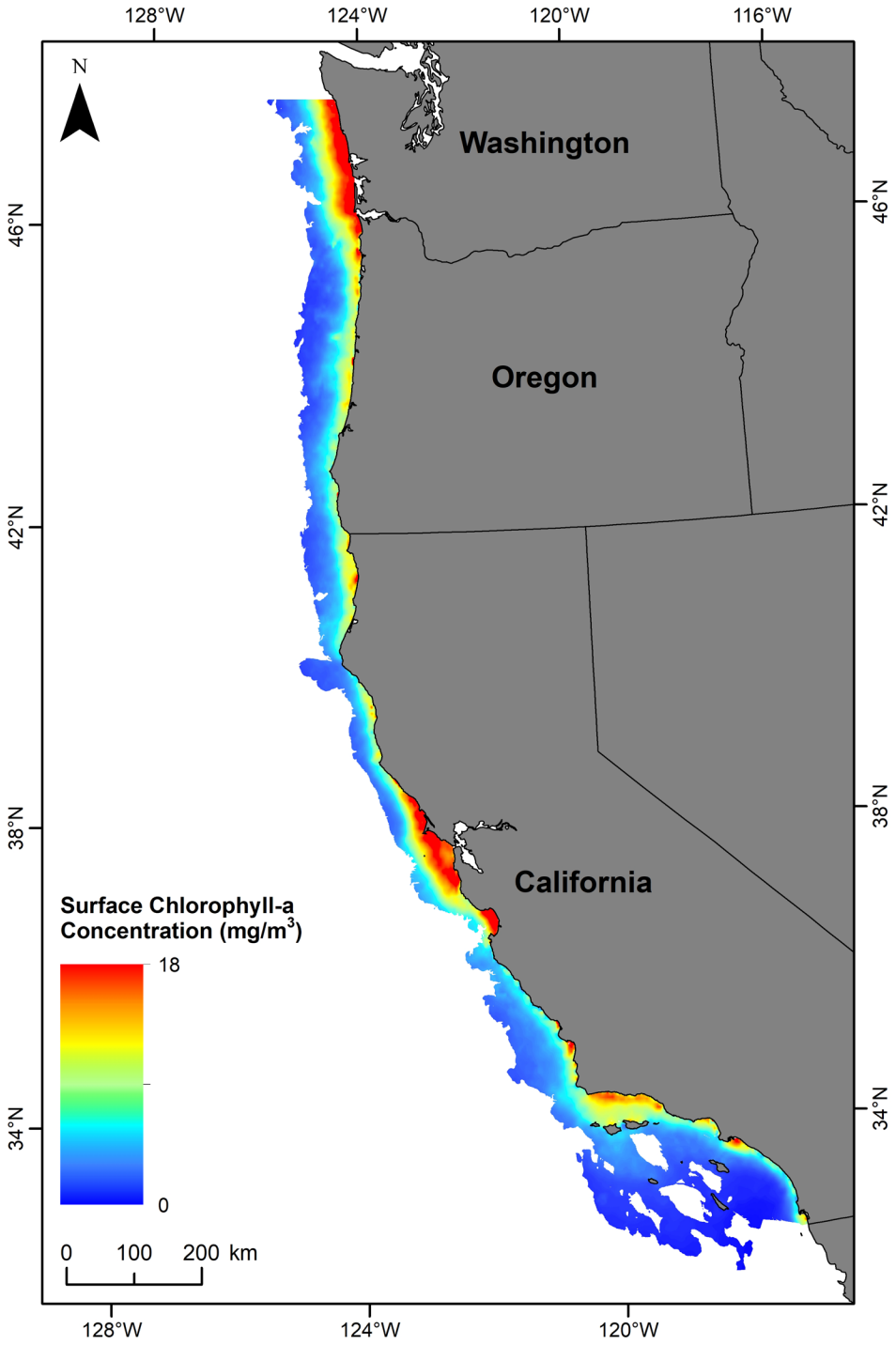

Figure A-23. Winter mean sea surface chlorophyll-a concentration, 200 x 200 m resolution.

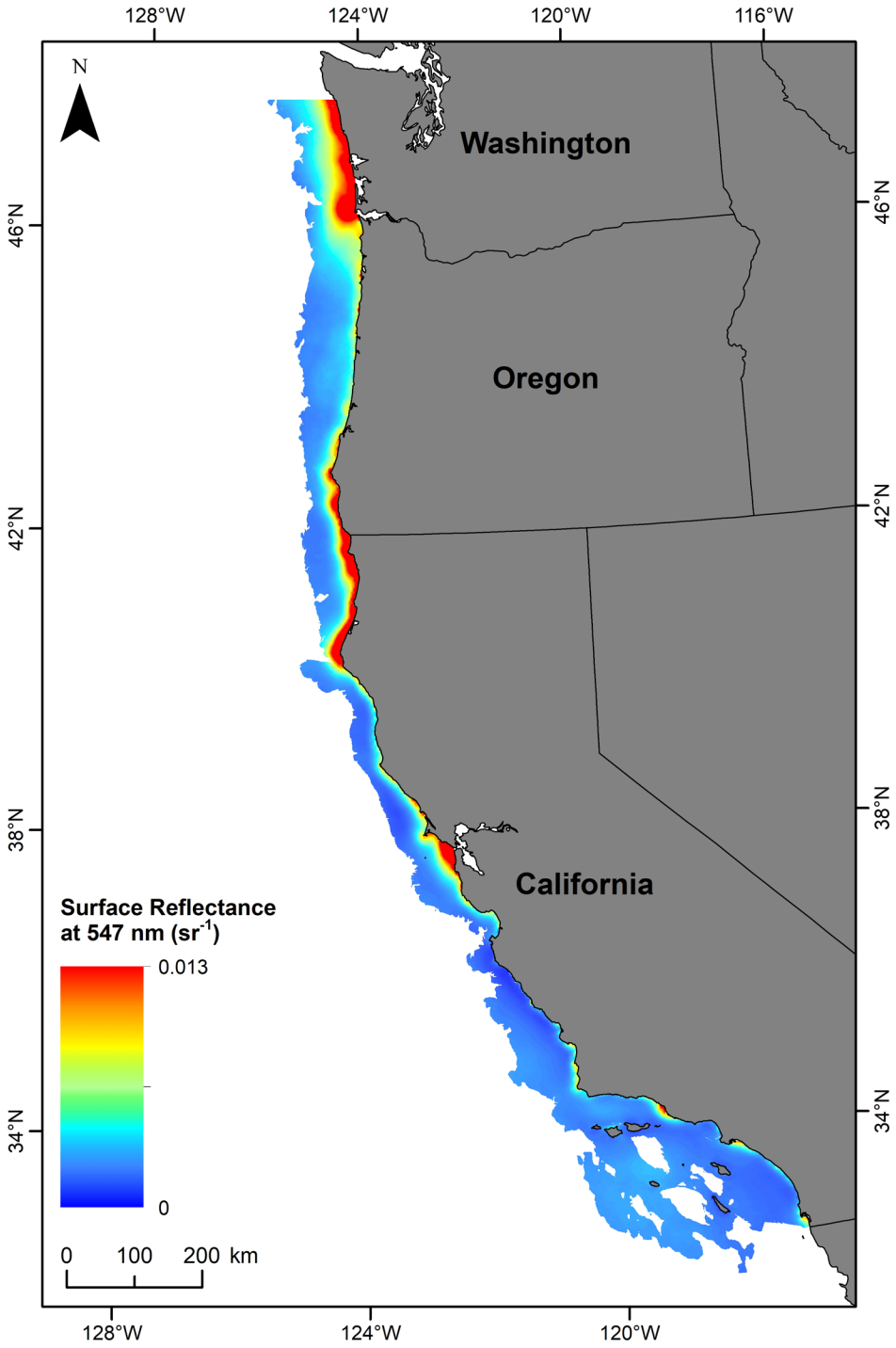

Figure A-24. Annual mean sea surface reflectance (547 nm), 200 x 200 m resolution.

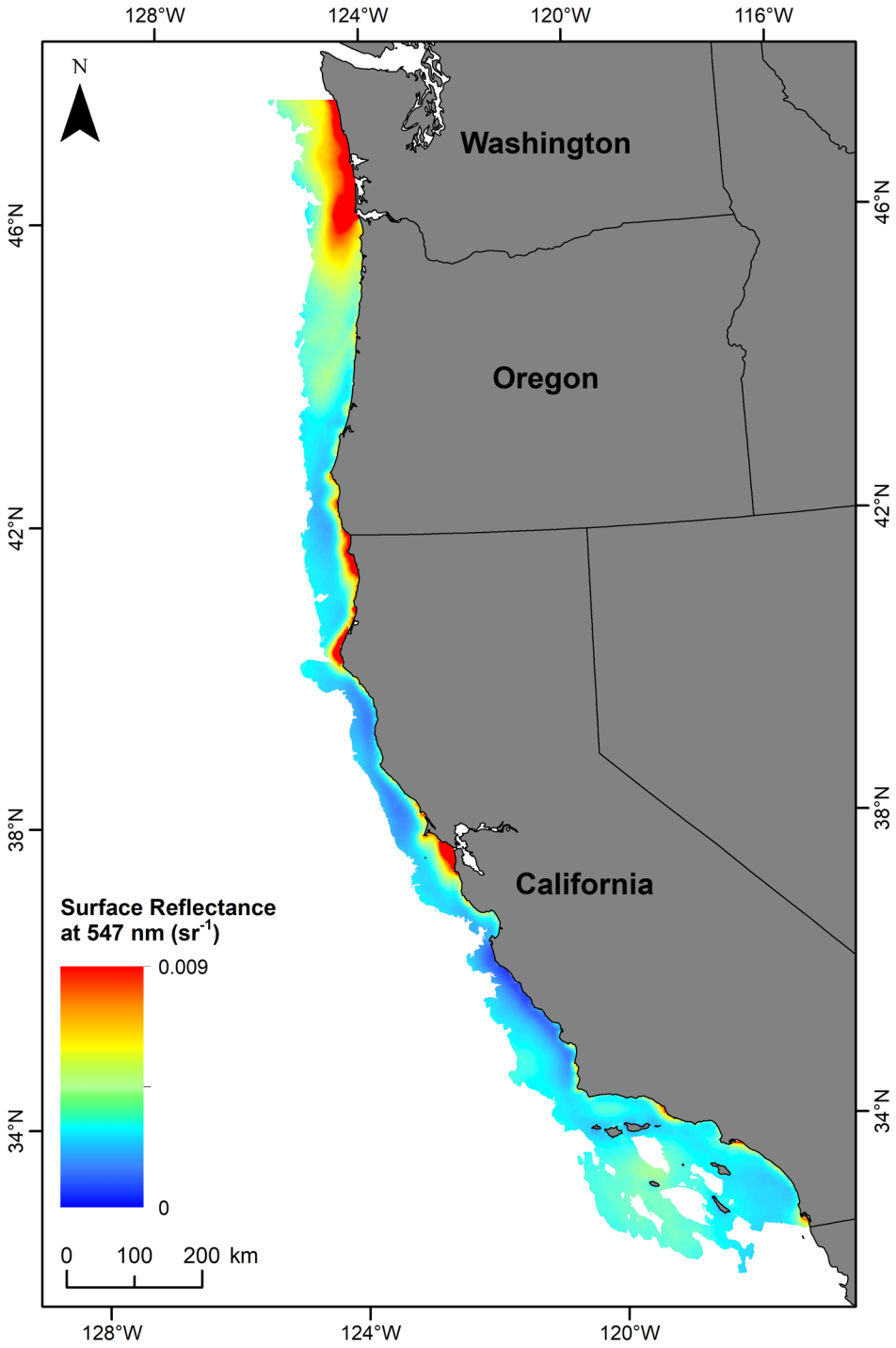

Figure A-25. Spring/summer mean sea surface reflectance (547 nm), 200 x 200 m resolution.

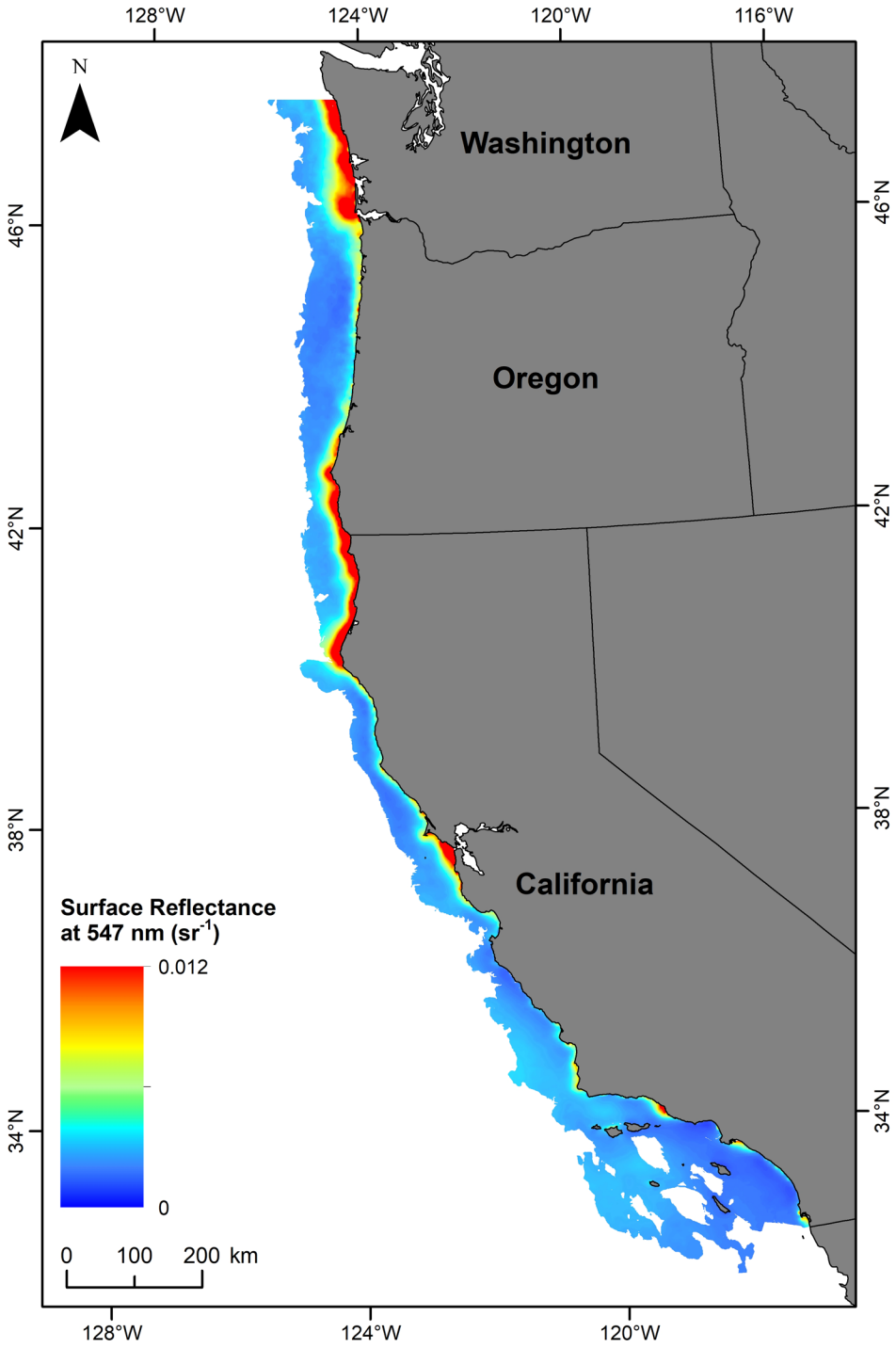

Figure A-26. Fall mean sea surface reflectance (547 nm), 200 x 200 m resolution.

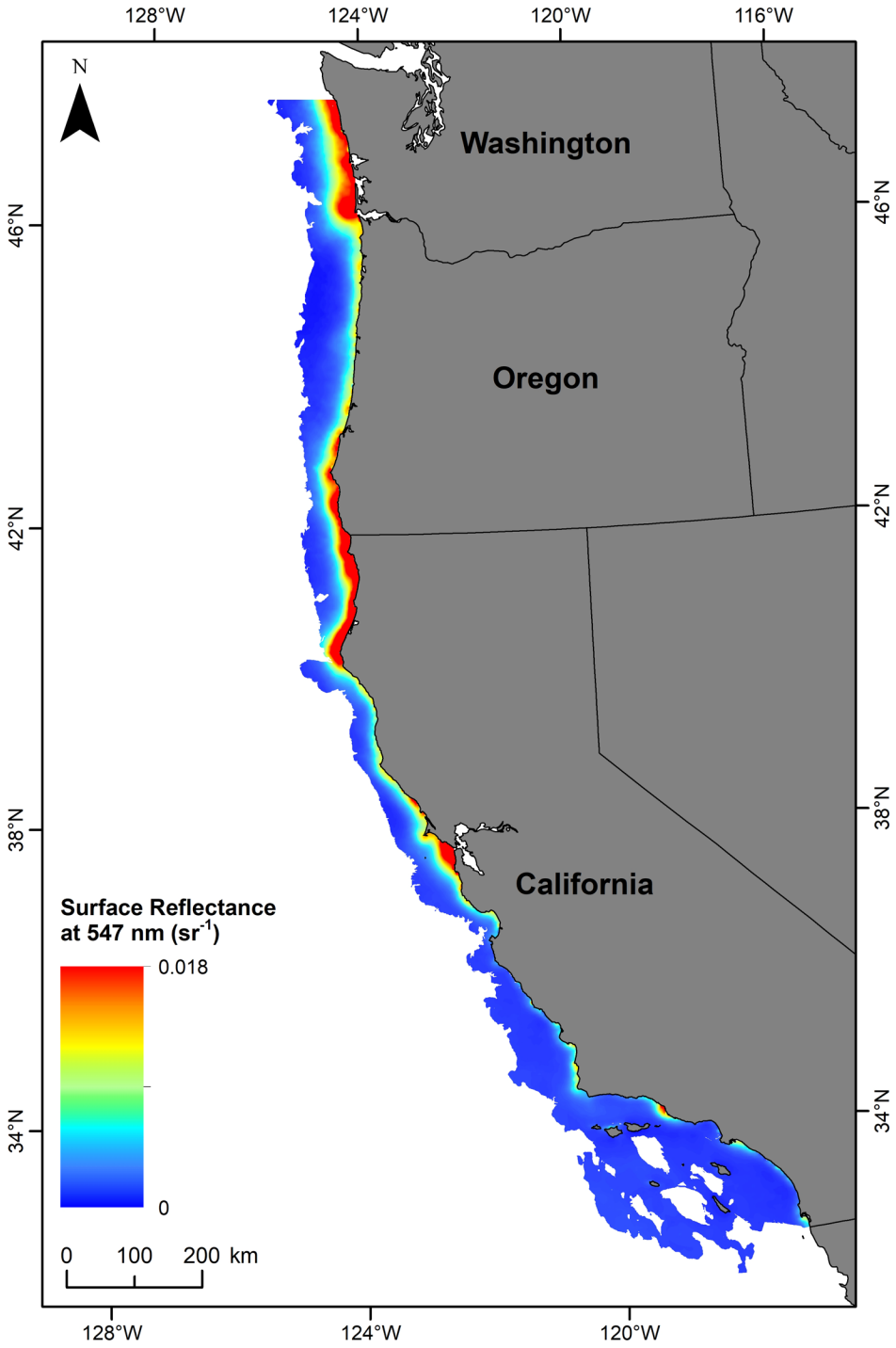

Figure A-27. Winter mean sea surface reflectance (547 nm), 200 x 200 m resolution.

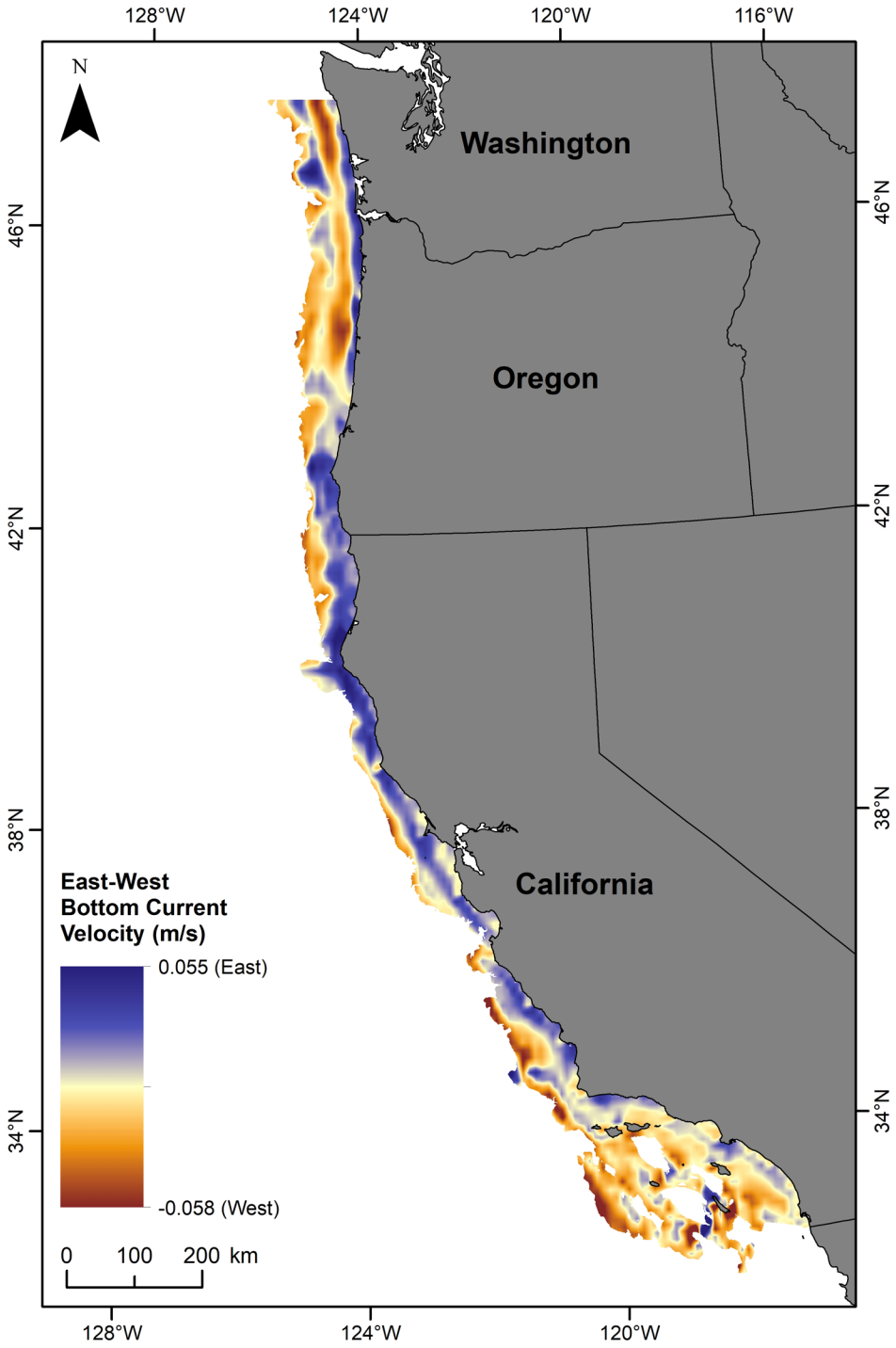

Figure A-28. Annual mean east-west bottom current velocity, 200 x 200 m resolution.

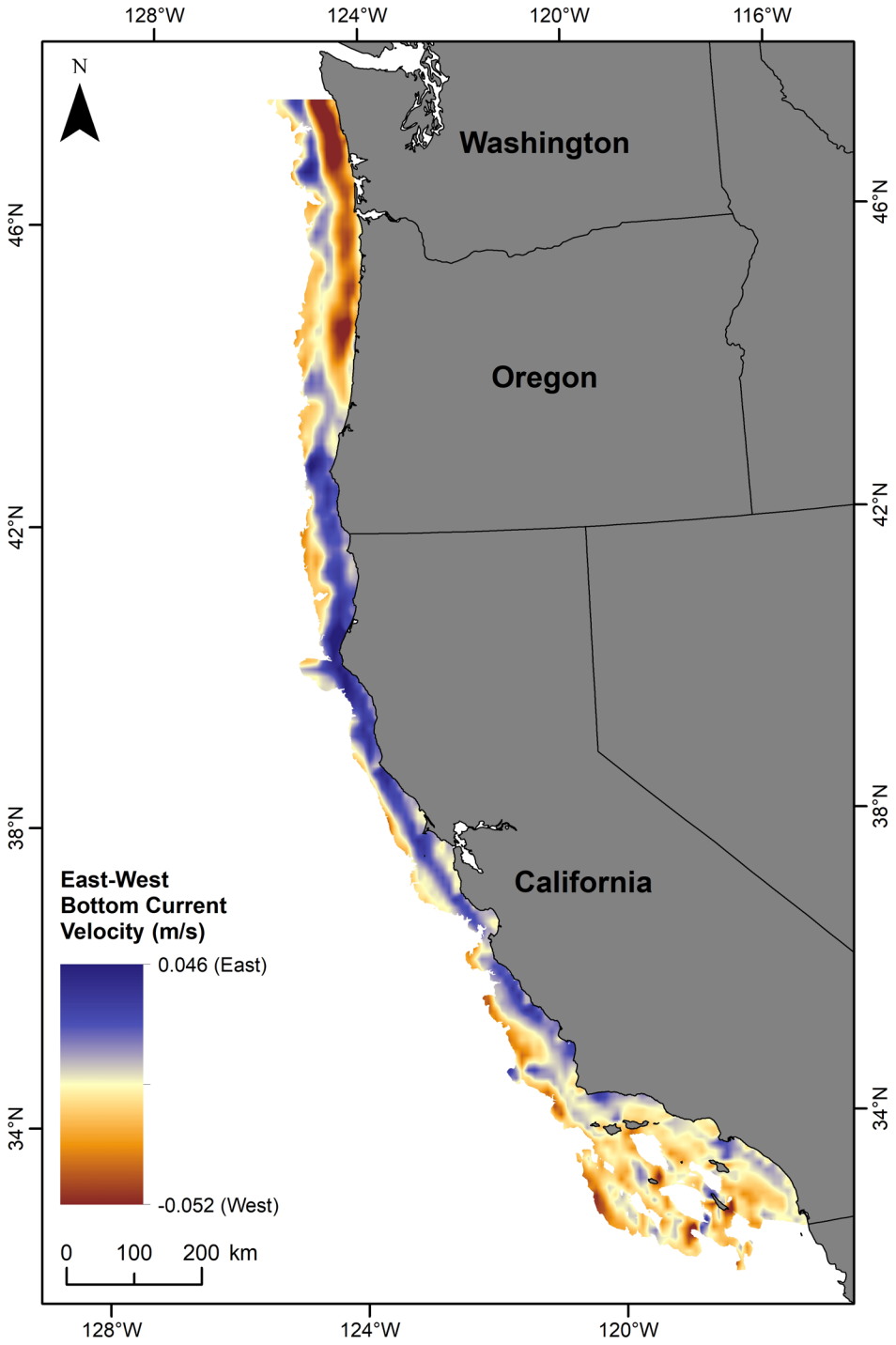

Figure A-29. Spring/summer mean east-west bottom current velocity, 200 x 200 m resolution.

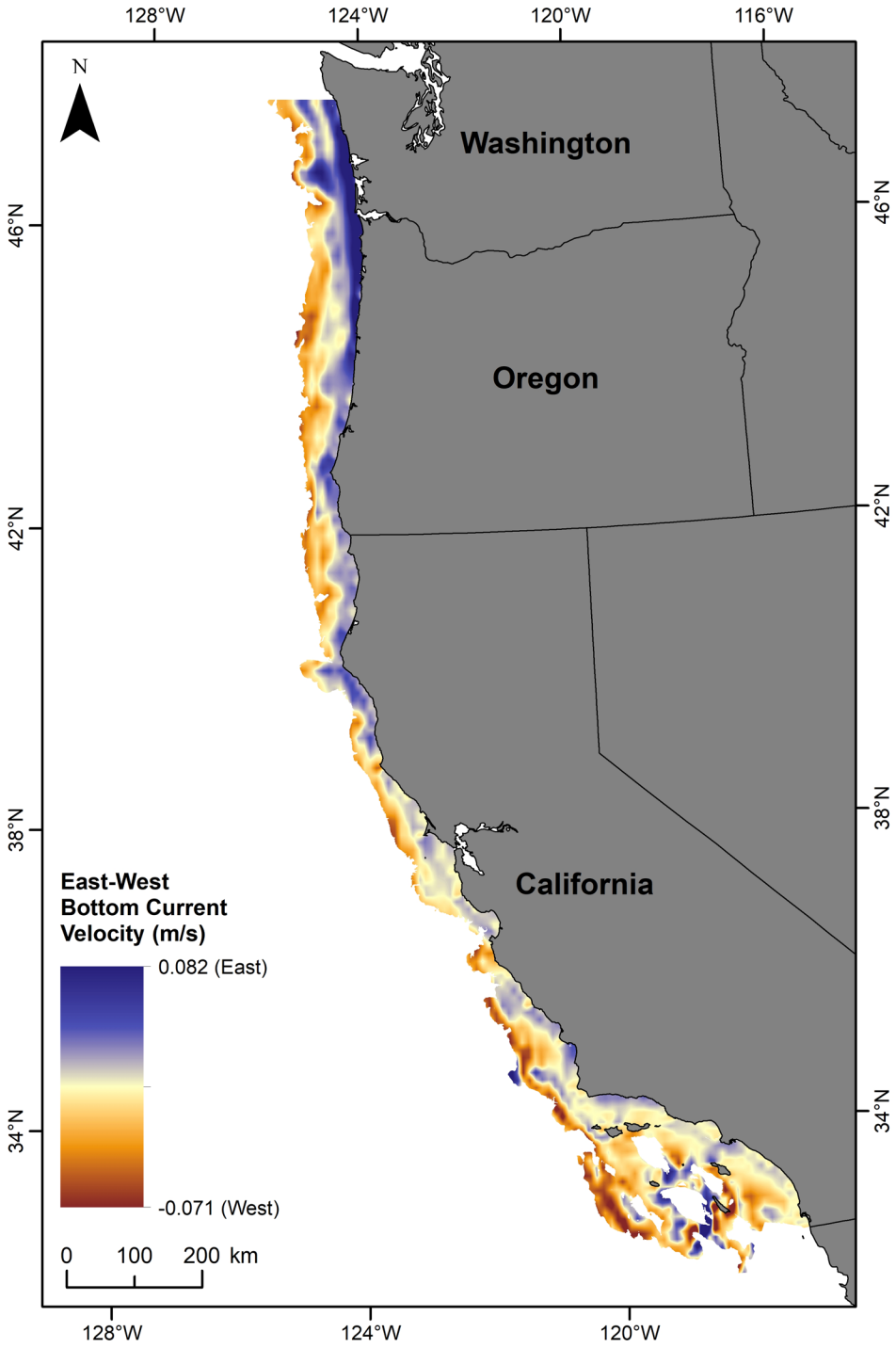

Figure A-30. Fall mean east-west bottom current velocity, 200 x 200 m resolution.

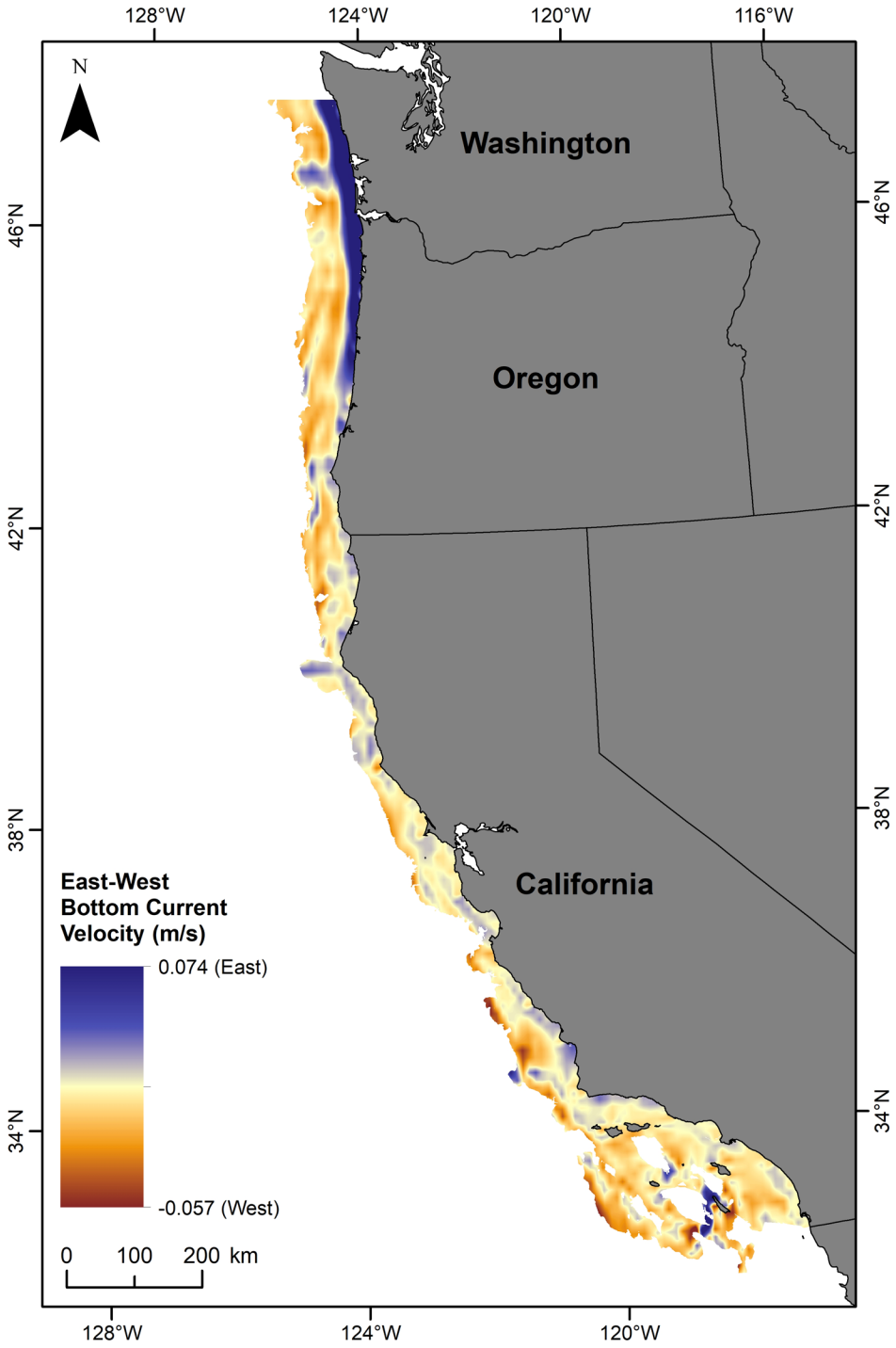

Figure A-31. Winter mean east-west bottom current velocity, 200 x 200 m resolution.

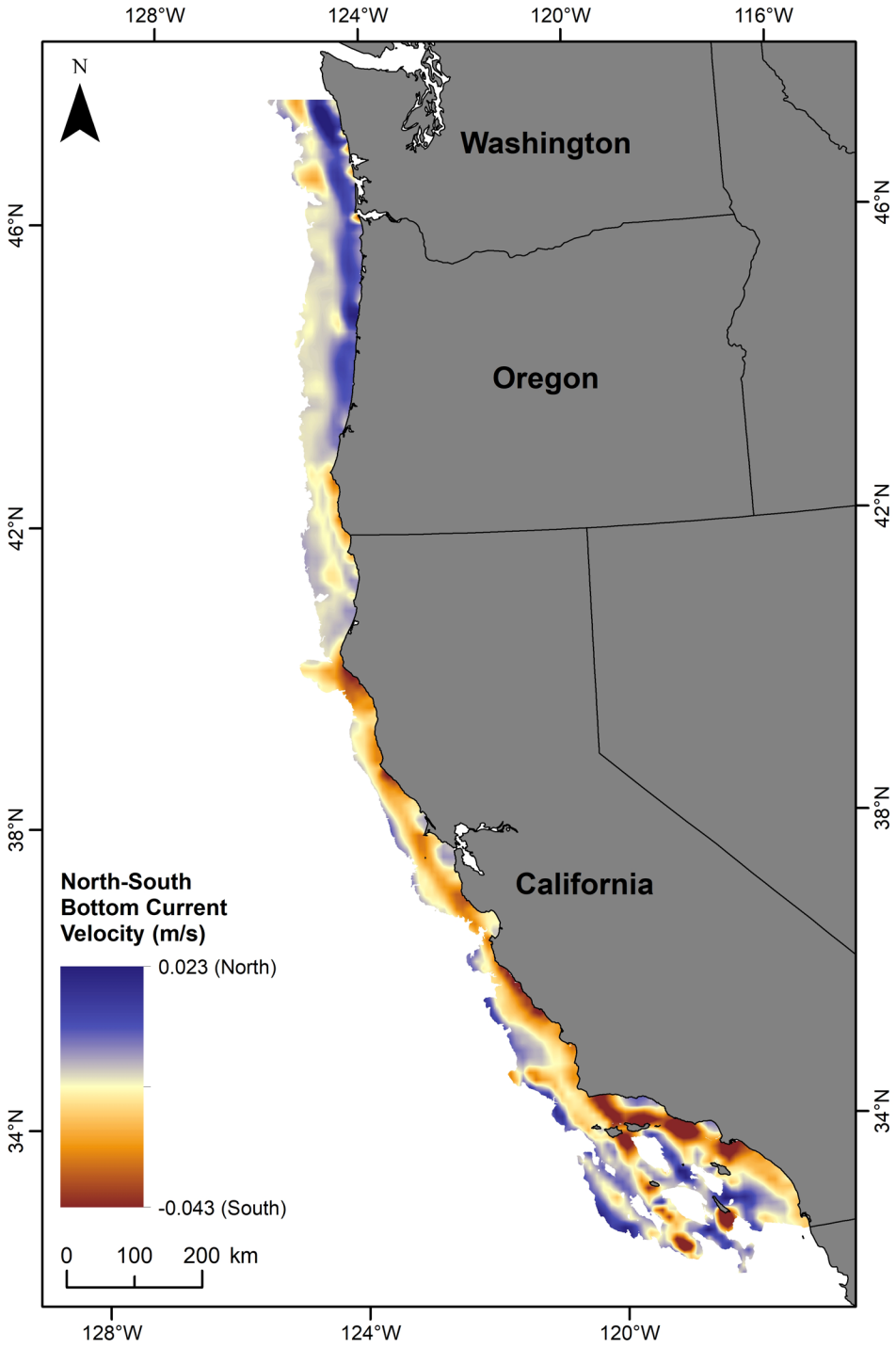

Figure A-32. Annual mean north-south bottom current velocity, 200 x 200 m resolution.

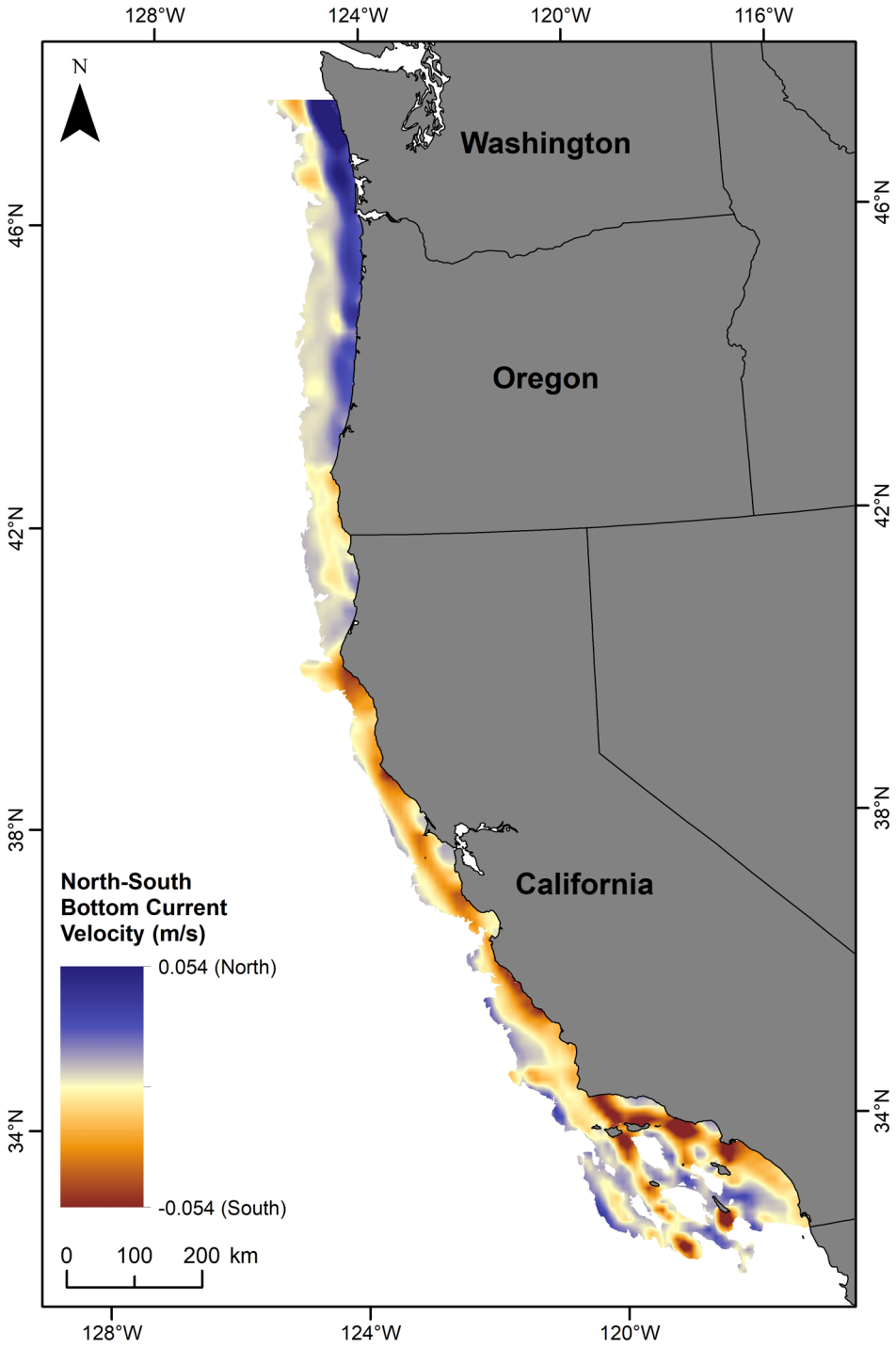

Figure A-33. Spring/summer mean north-south bottom current velocity, 200 x 200 m resolution.

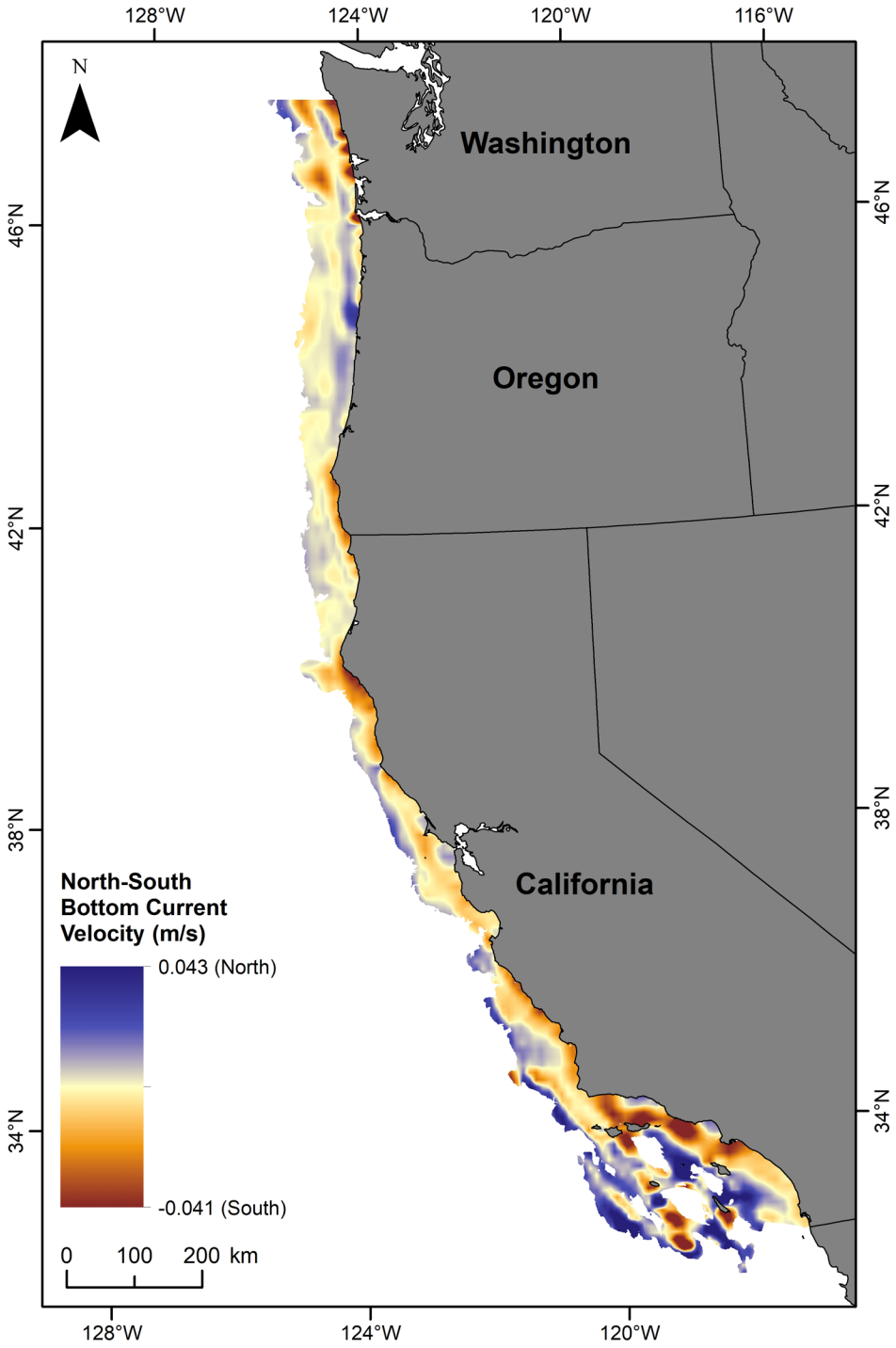

Figure A-34. Fall mean north-south bottom current velocity, 200 x 200 m resolution.

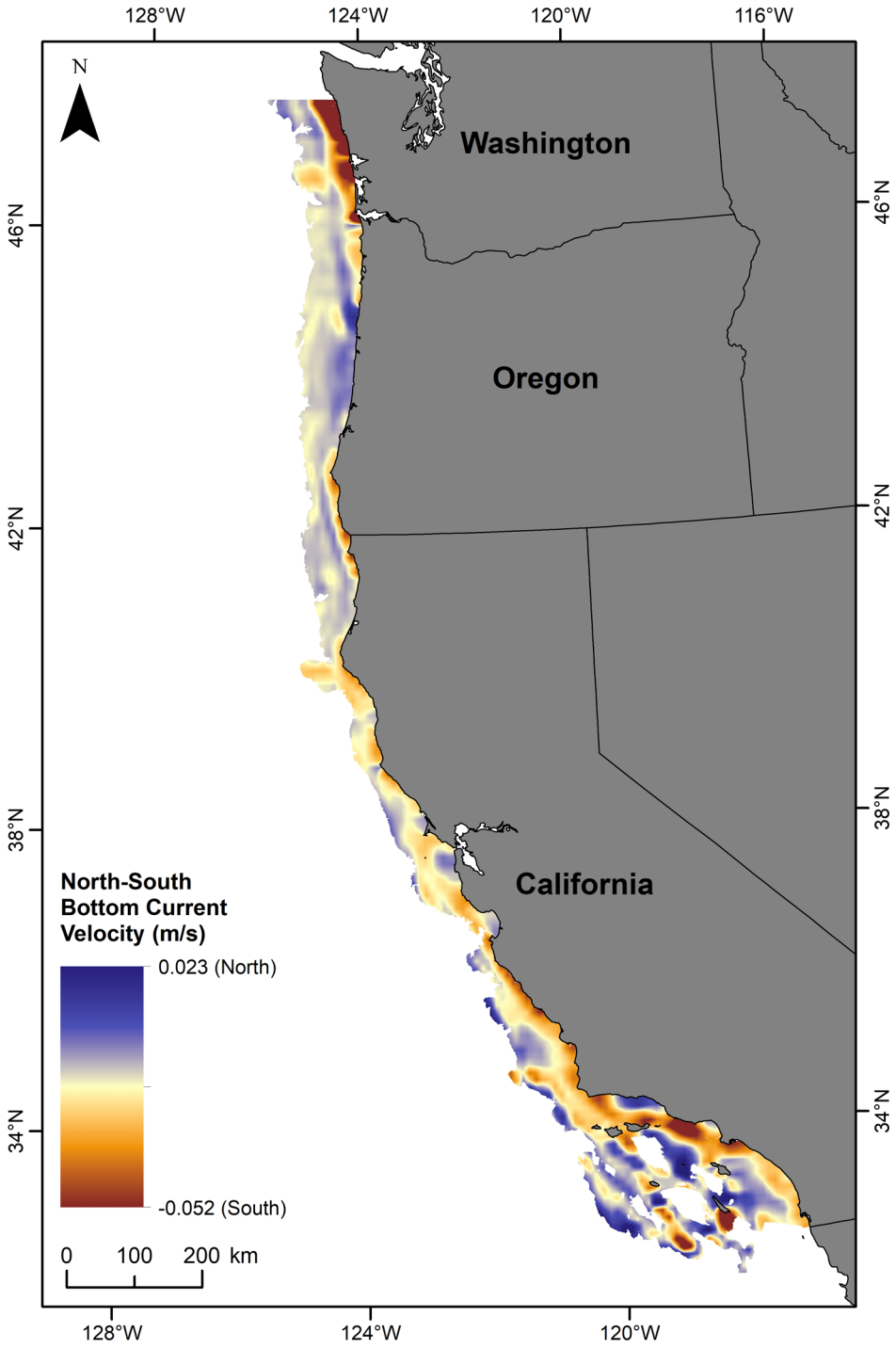

Figure A-35. Winter mean north-south bottom current velocity, 200 x 200 m resolution.

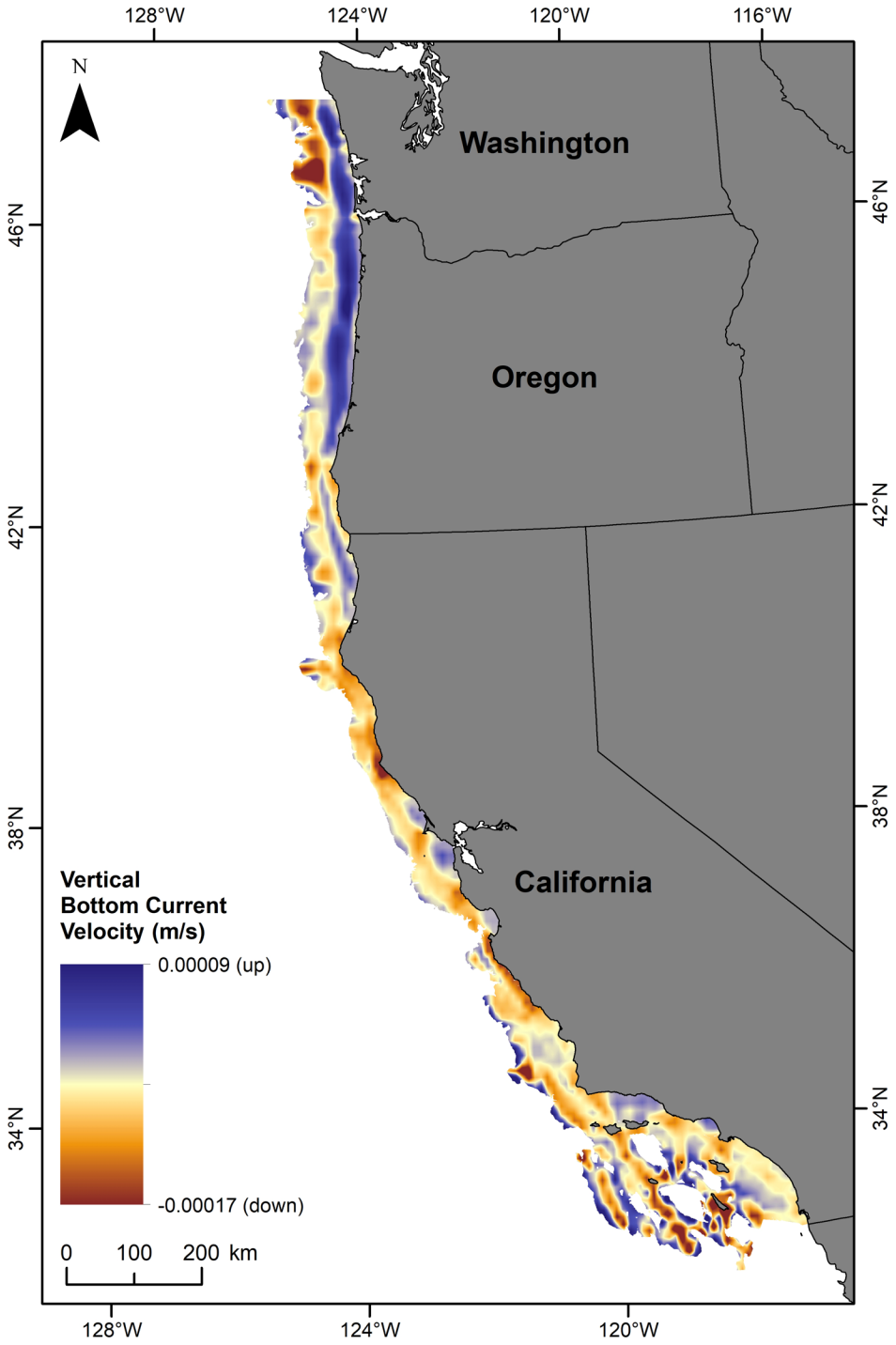

Figure A-36. Annual mean vertical bottom current velocity, 200 x 200 m resolution.

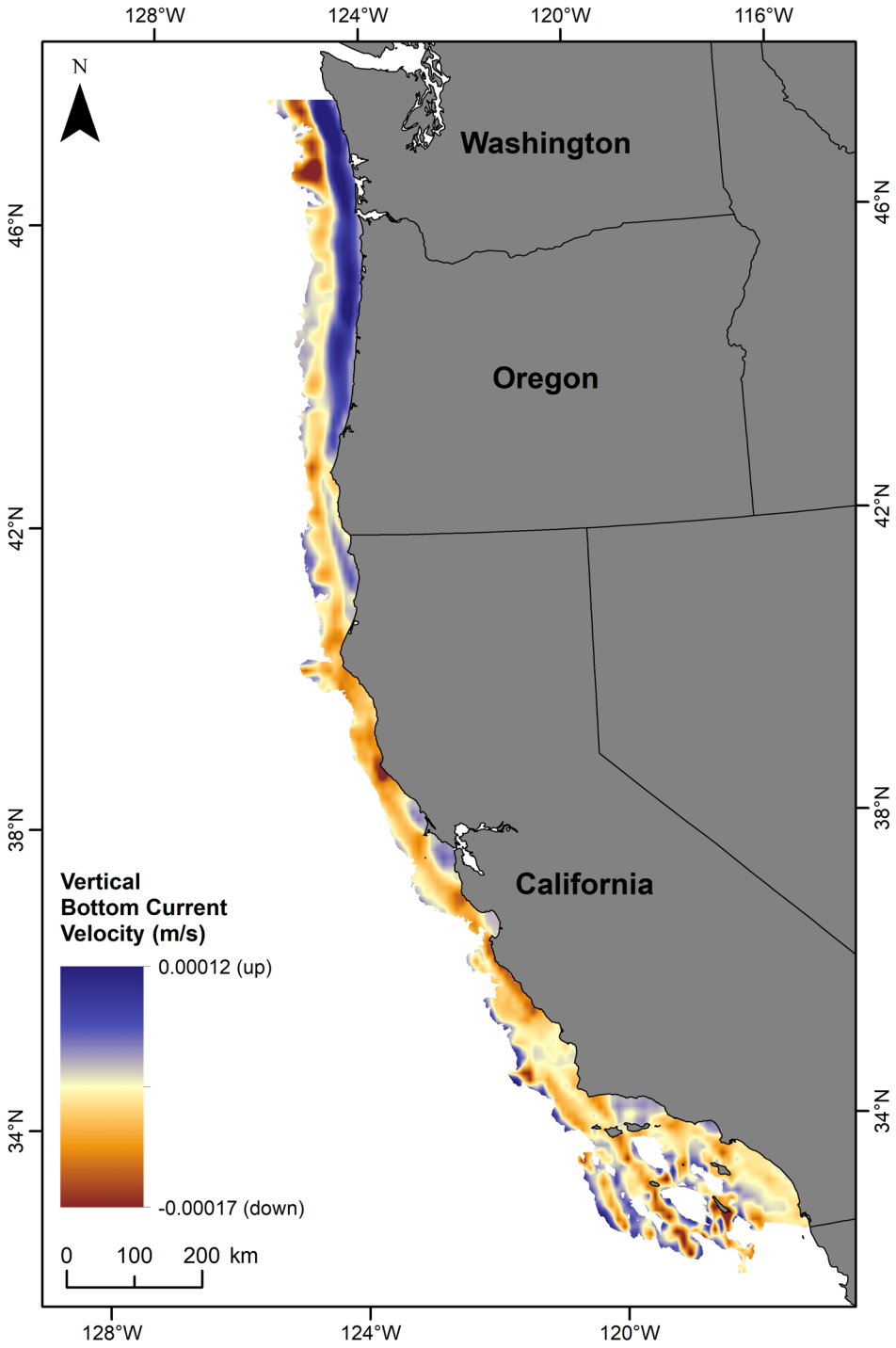

Figure A-37. Spring/summer mean vertical bottom current velocity, 200 x 200 m resolution.

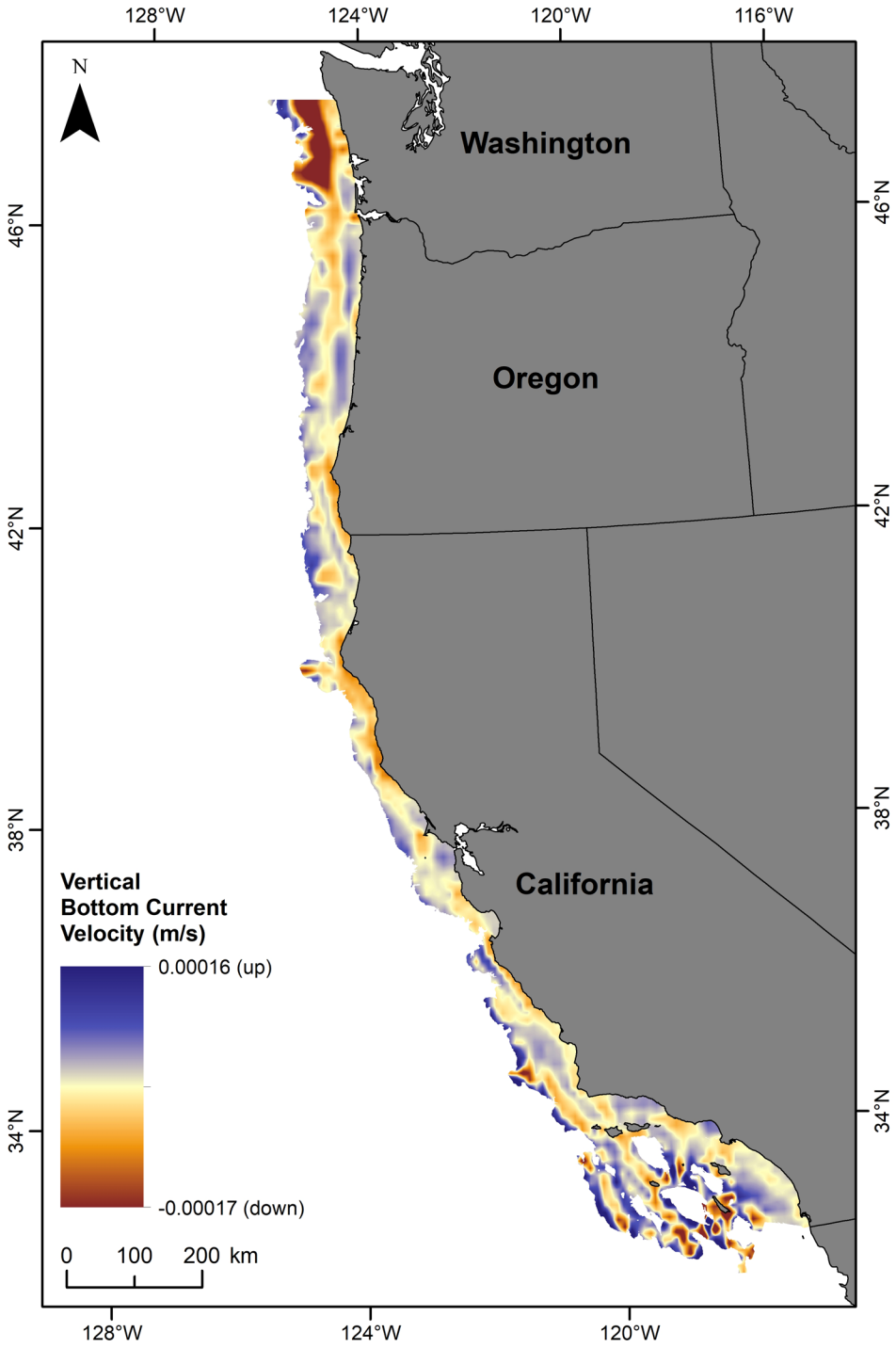

Figure A-38. Fall mean vertical bottom current velocity, 200 x 200 m resolution.

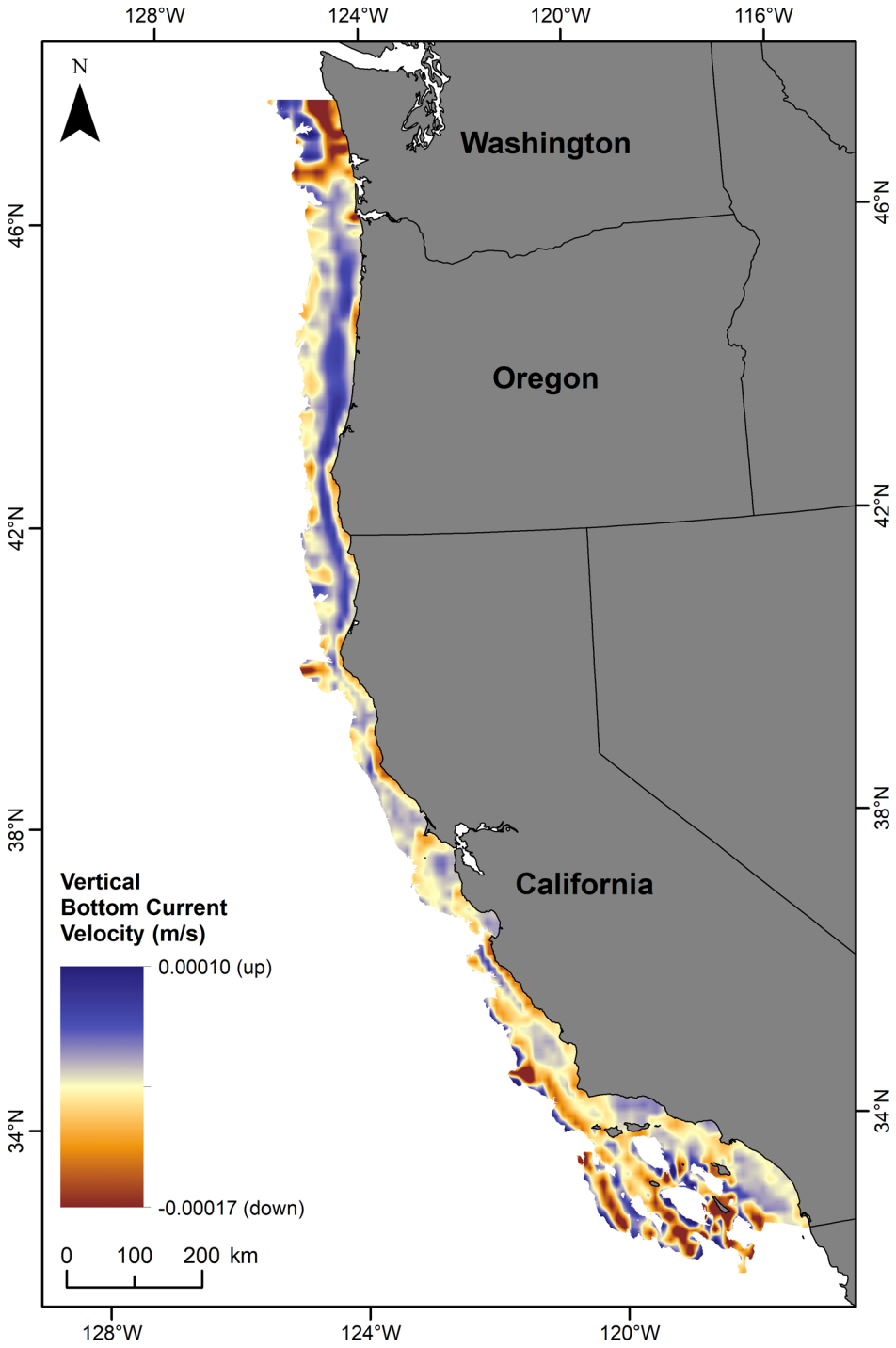

Figure A-39. Winter mean vertical bottom current velocity, 200 x 200 m resolution.

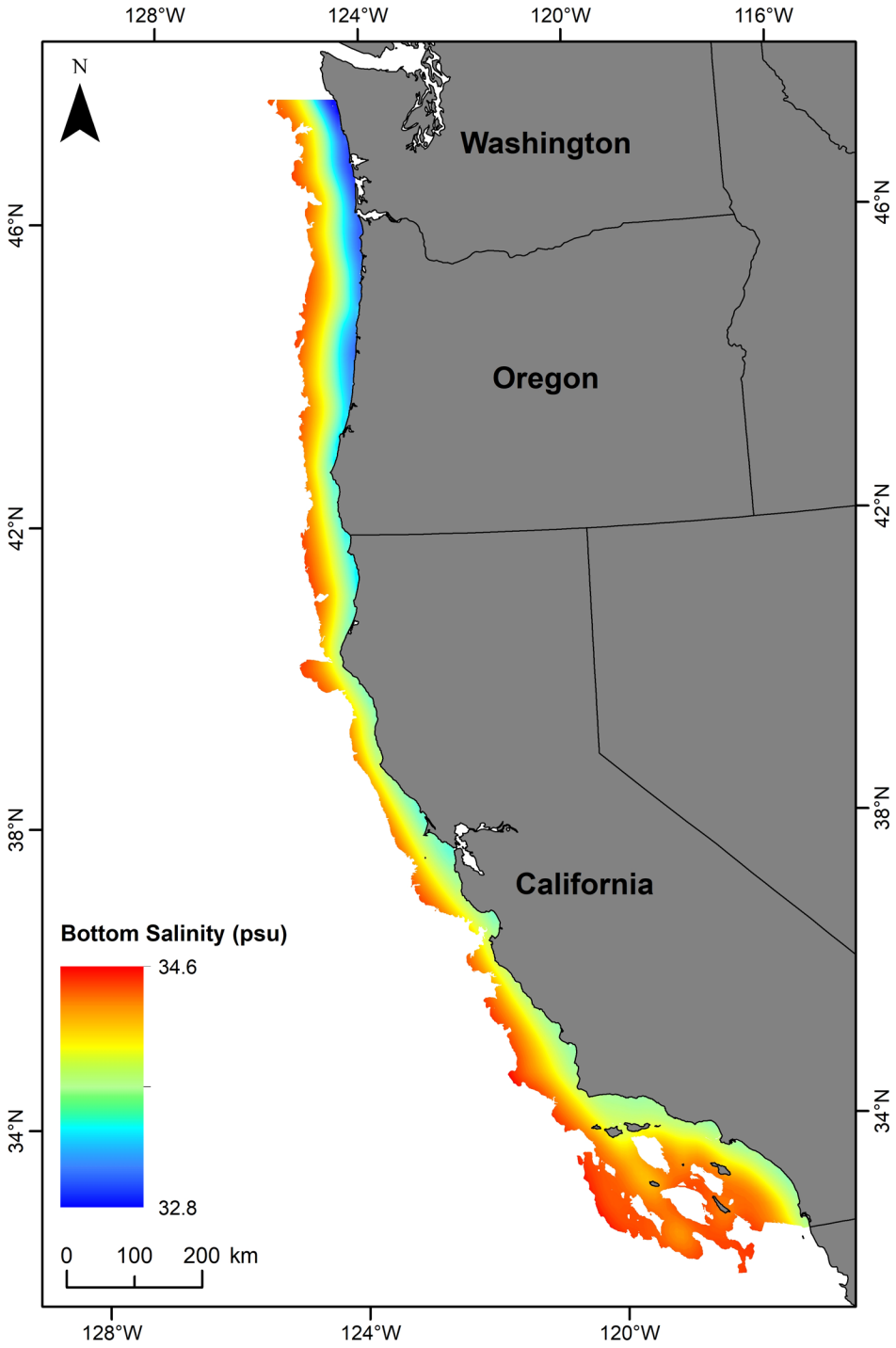

Figure A-40. Annual mean bottom salinity, 200 x 200 m resolution.

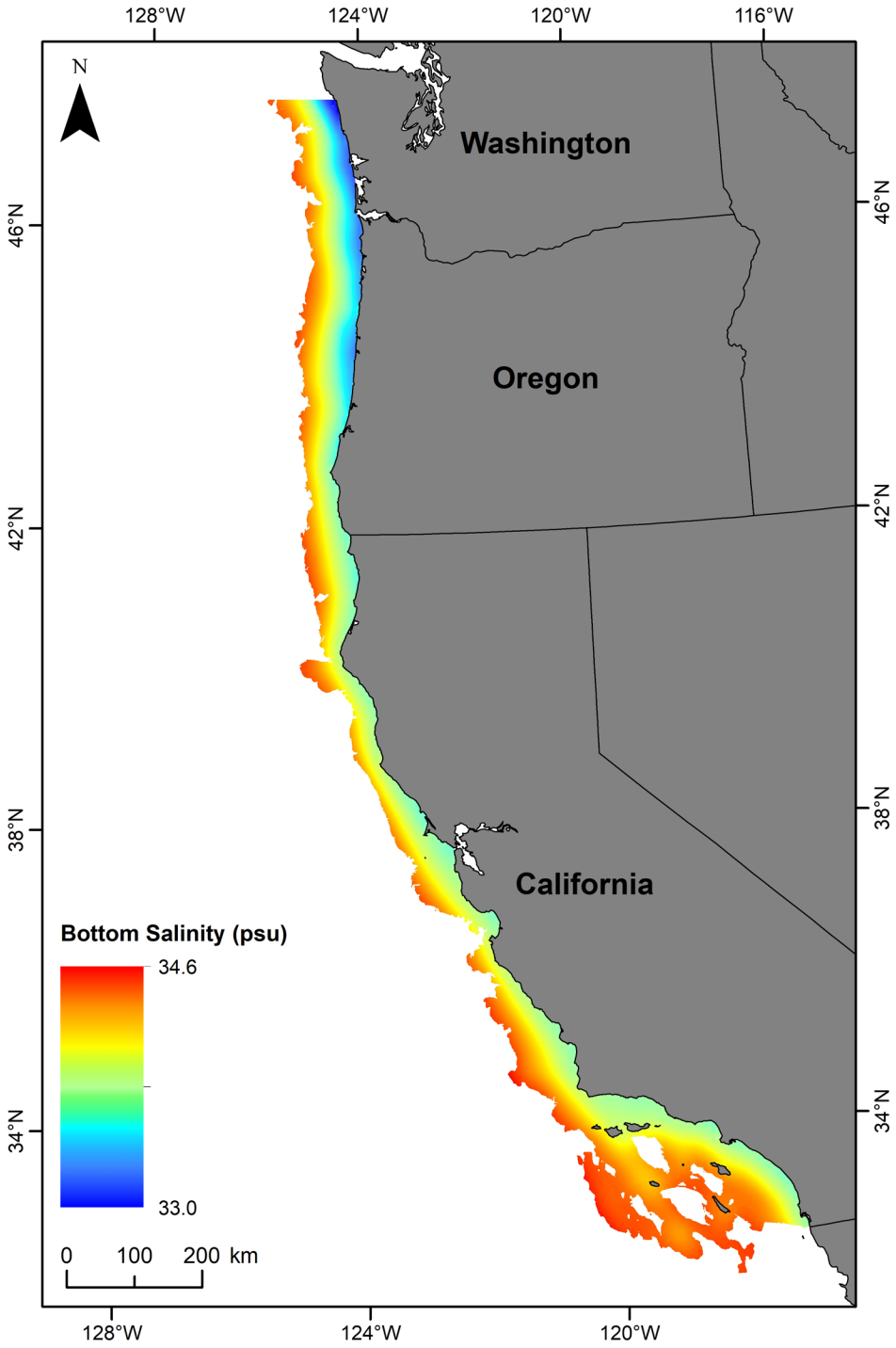

Figure A-41. Spring/summer mean bottom salinity, 200 x 200 m resolution.

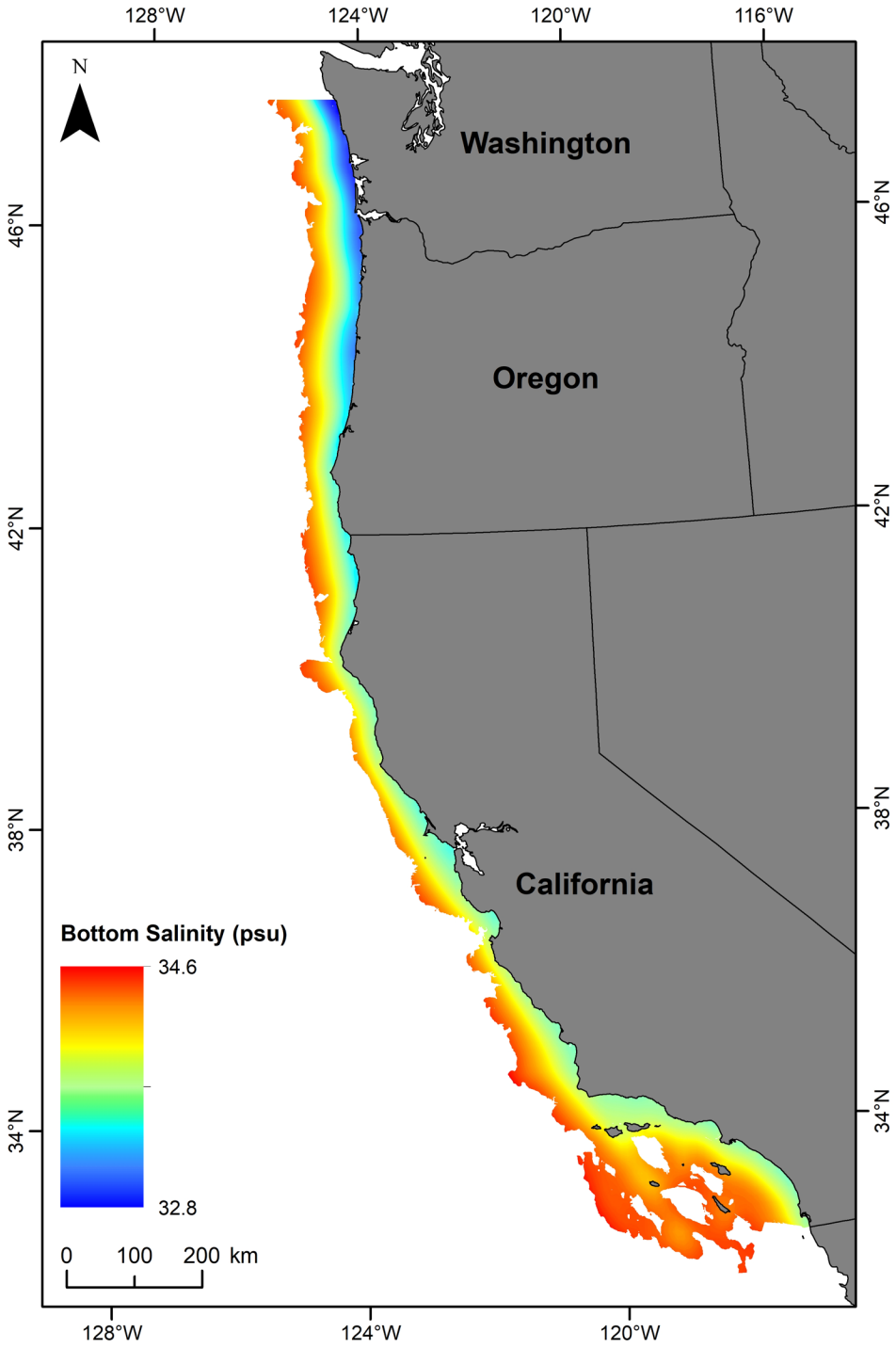

Figure A-42. Fall mean bottom salinity, 200 x 200 m resolution.

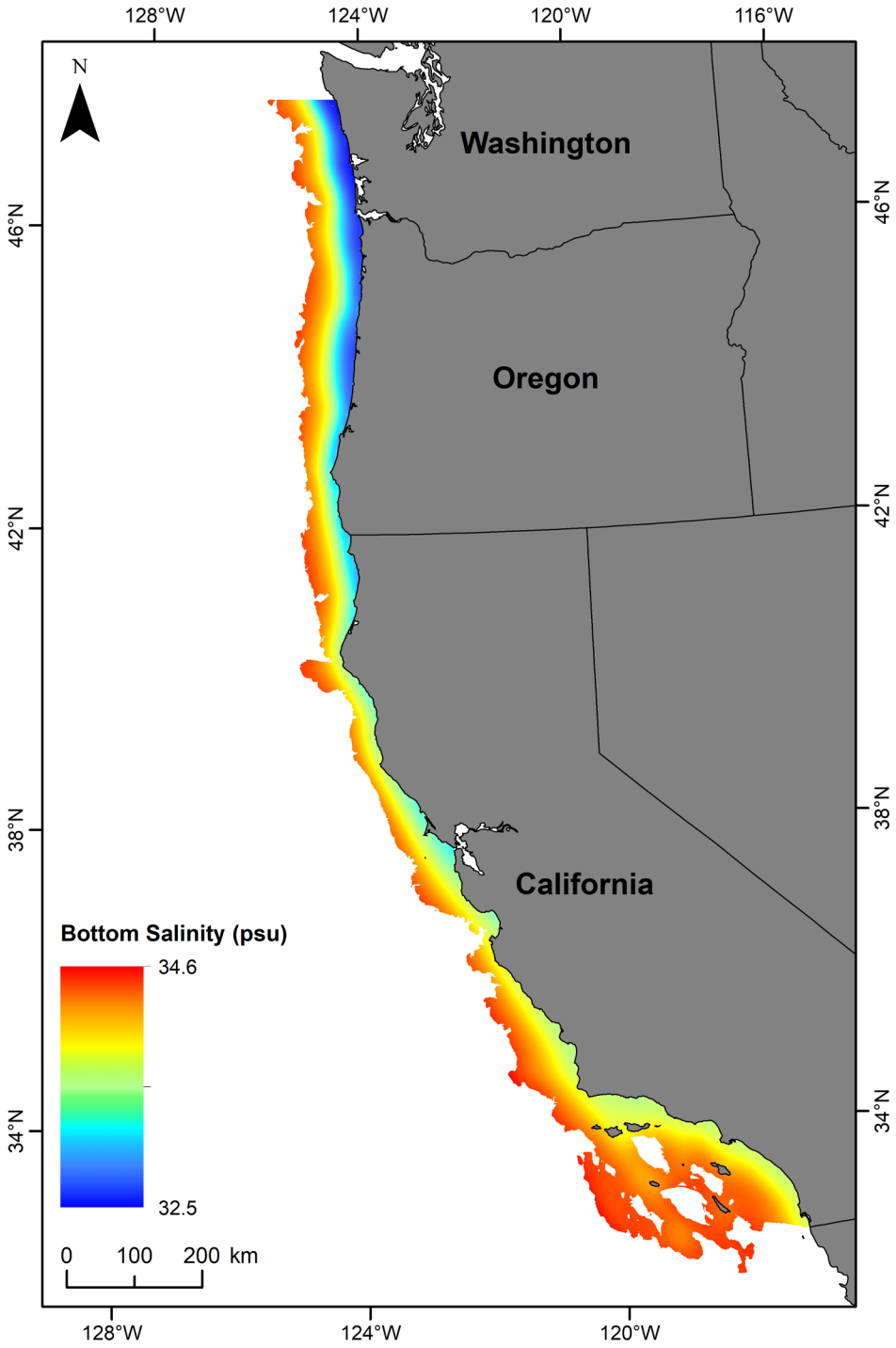

Figure A-43. Winter mean bottom salinity, 200 x 200 m resolution.

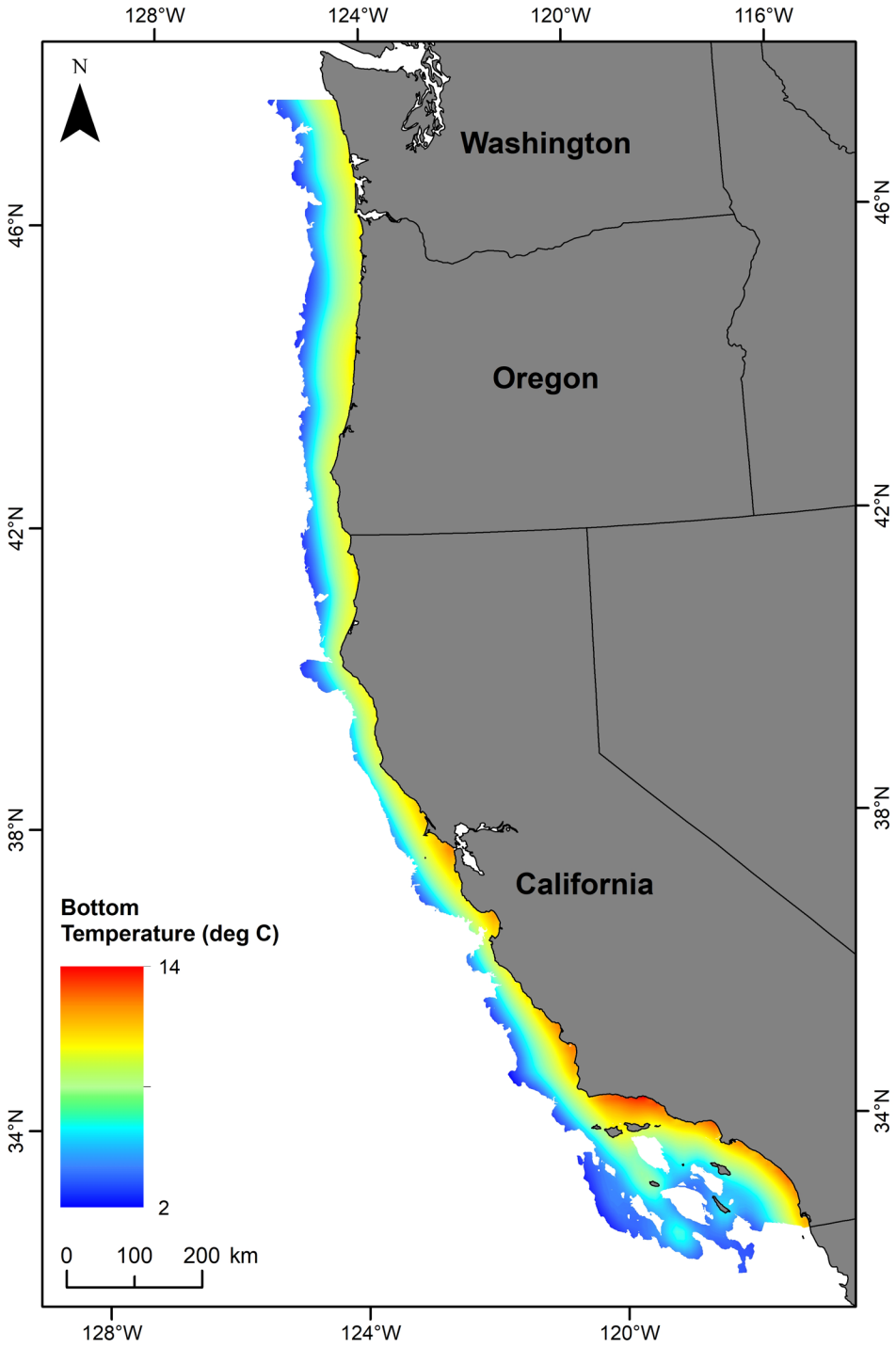

Figure A-44. Annual mean bottom temperature, 200 x 200 m resolution.

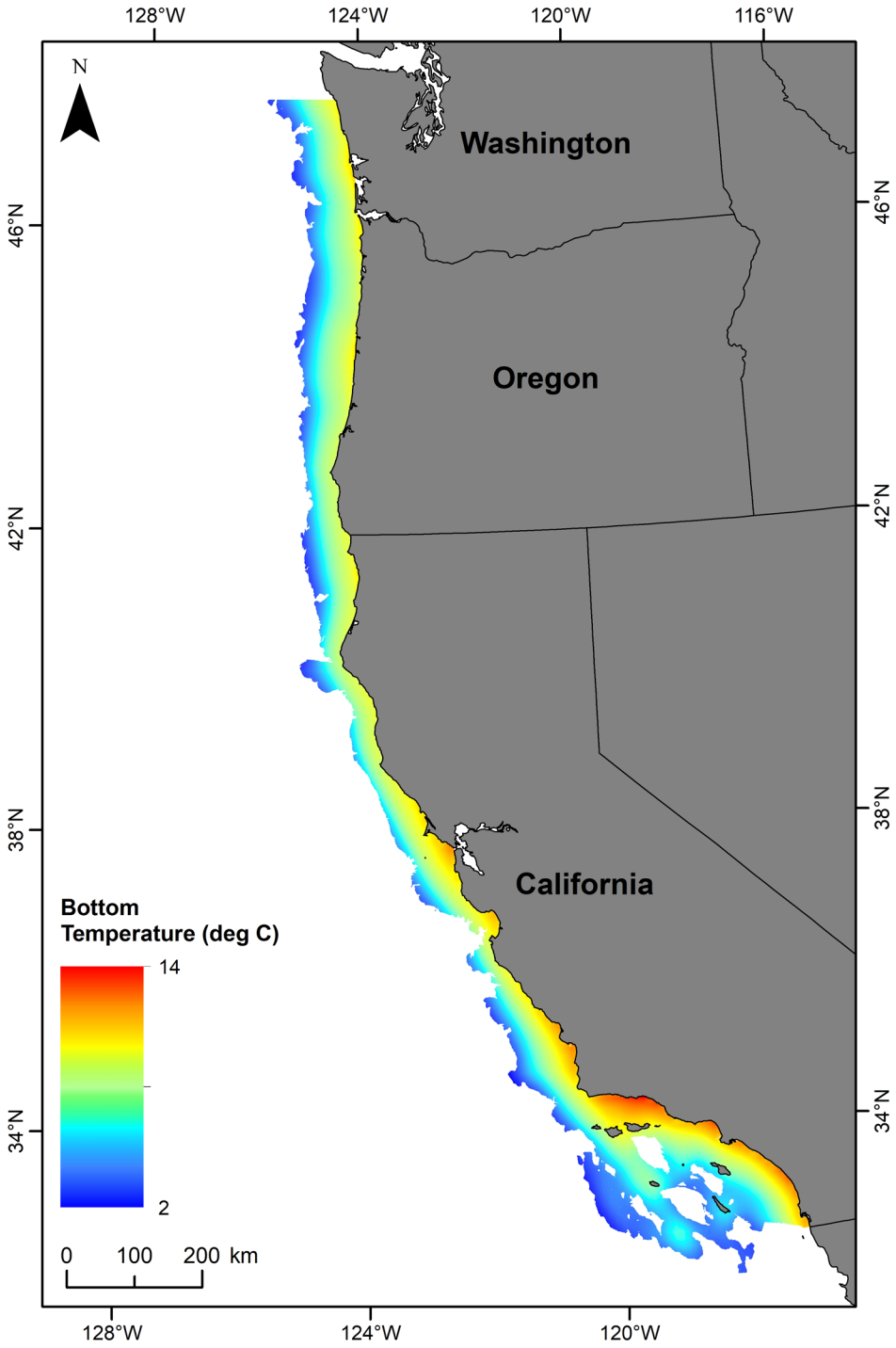

Figure A-45. Spring/summer mean bottom temperature, 200 x 200 m resolution.

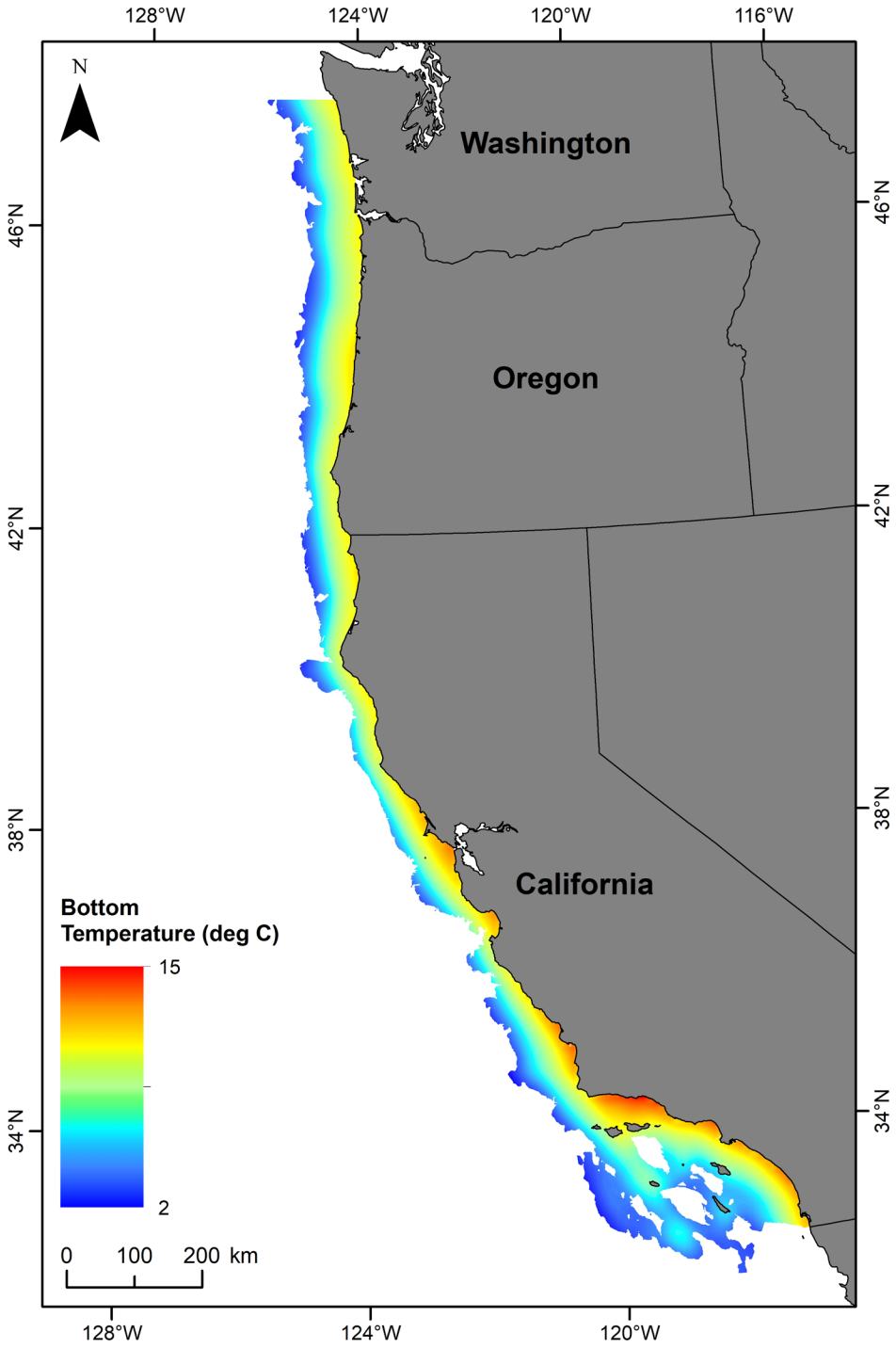

Figure A-46. Fall mean bottom temperature, 200 x 200 m resolution.

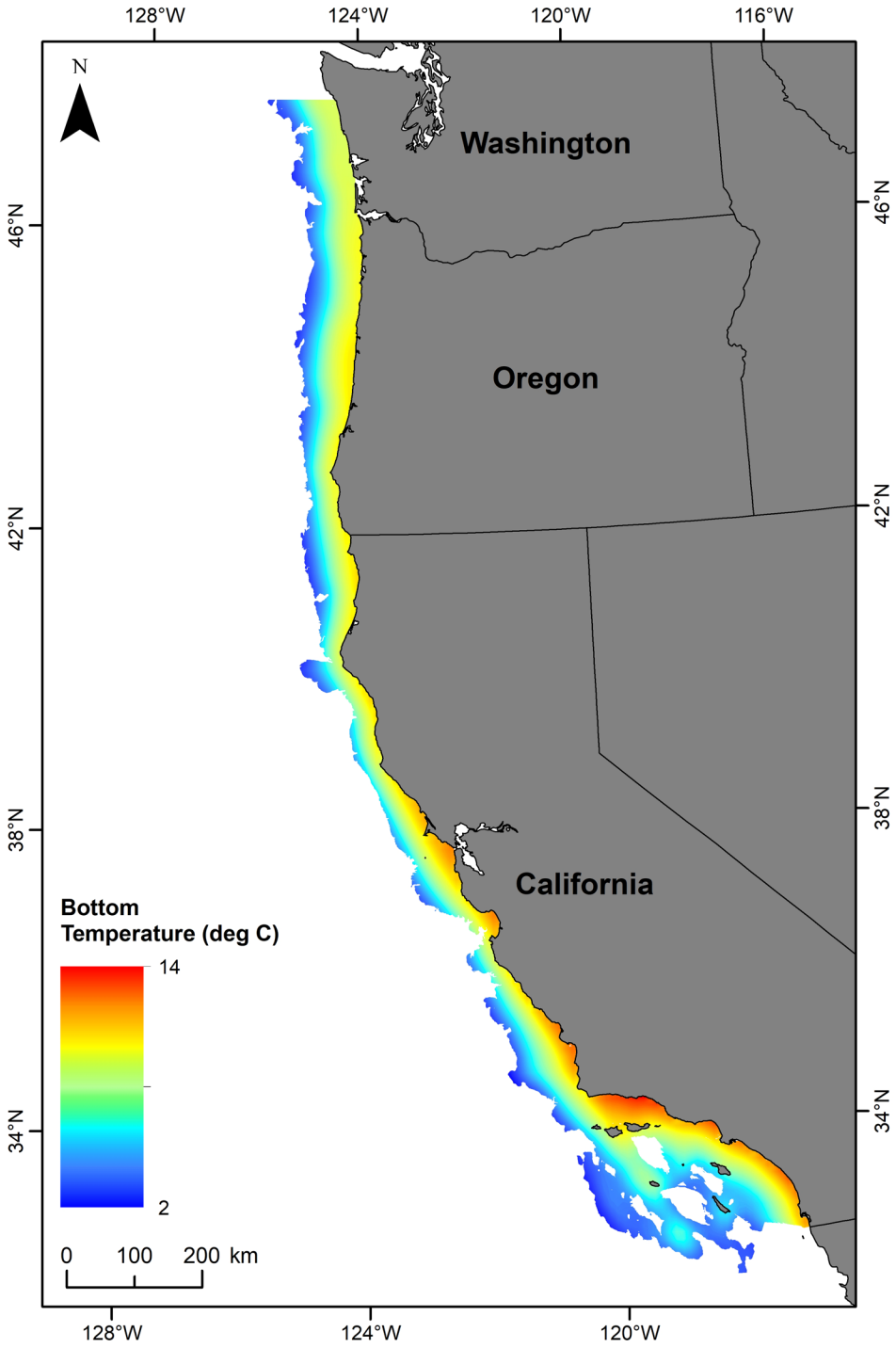

Figure A-47. Winter mean bottom temperature, 200 x 200 m resolution.

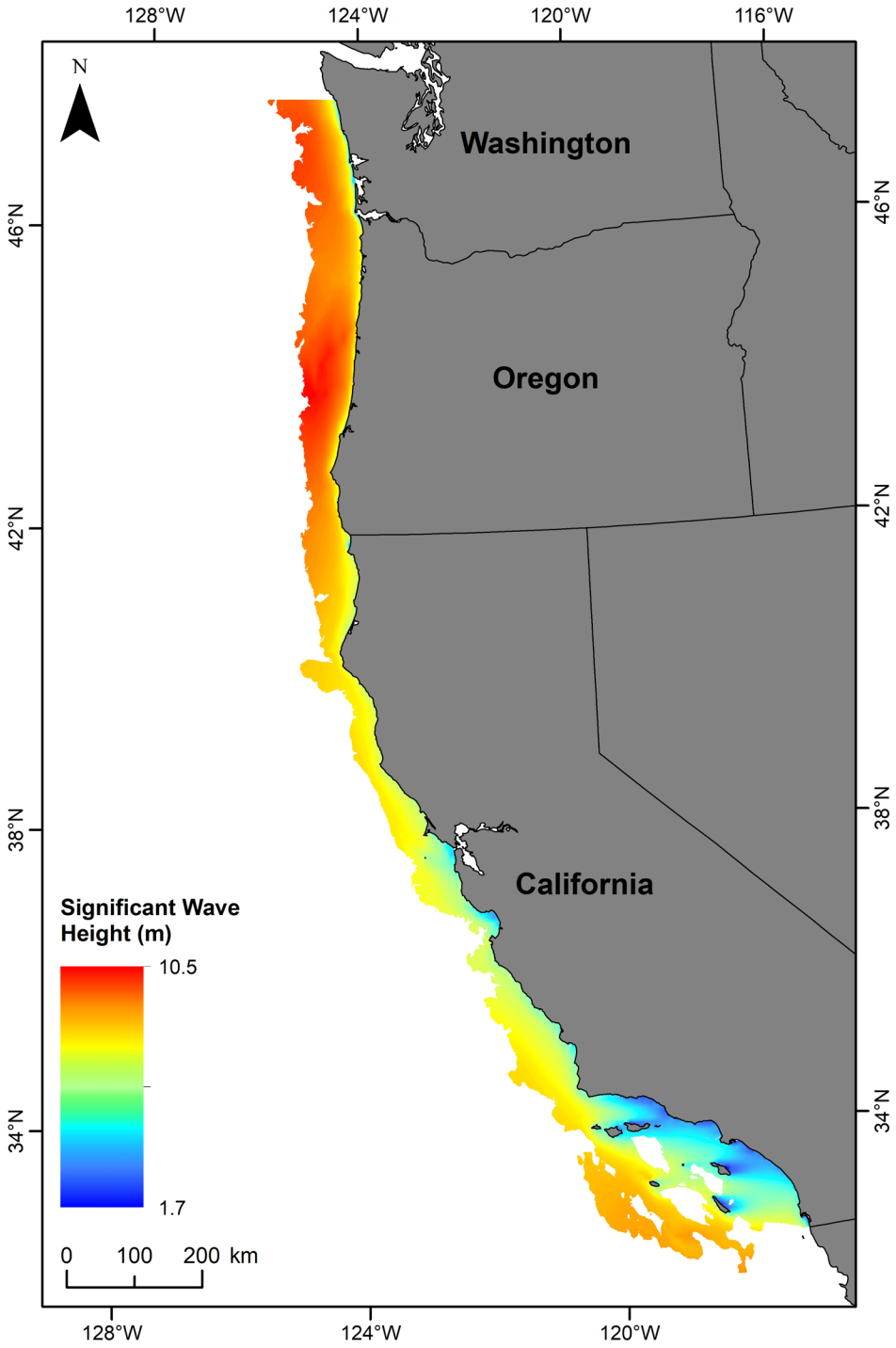

Figure A-48. Annual maximum significant wave height, 200 x 200 m resolution.

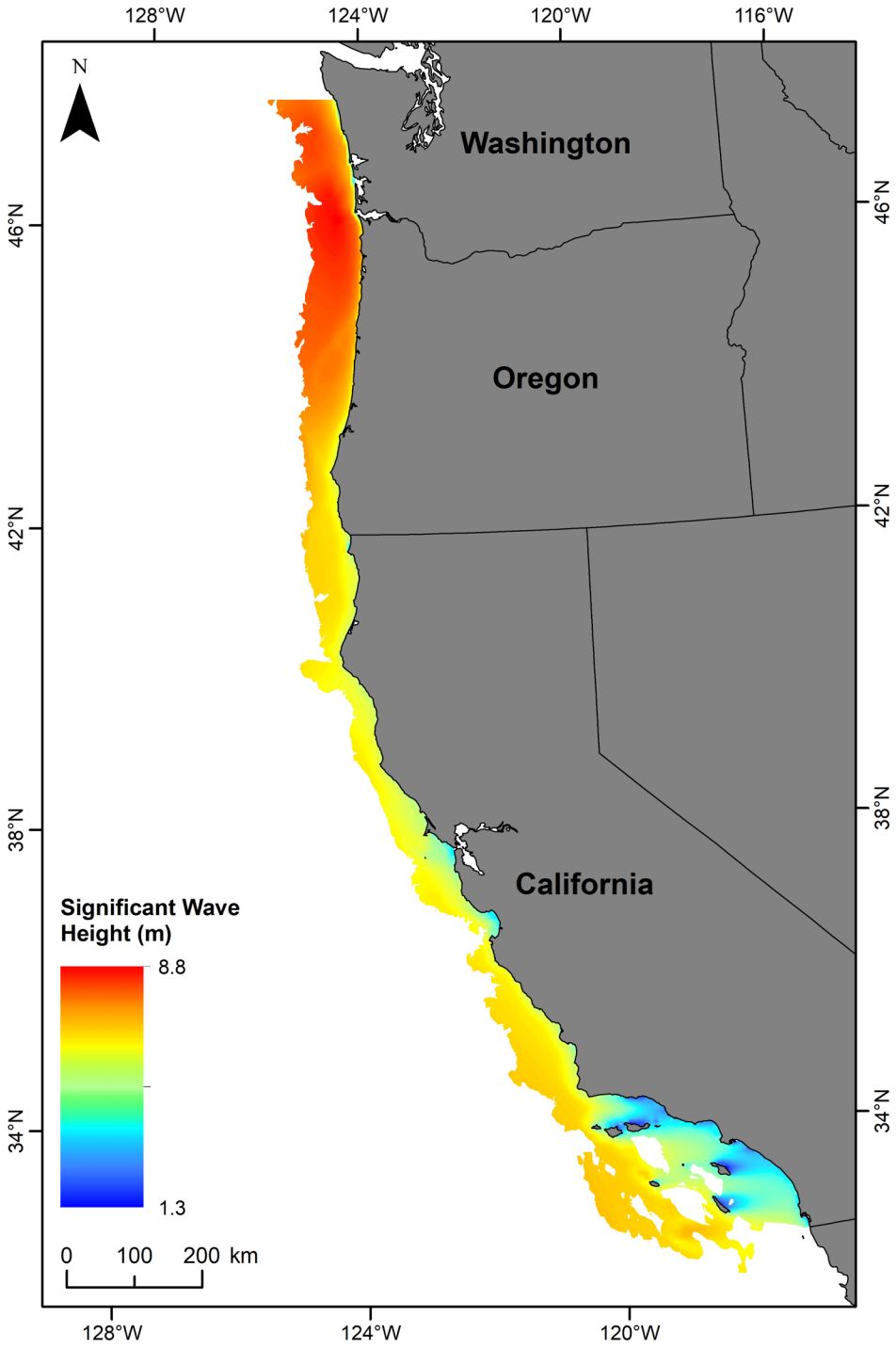

Figure A-49. Spring/summer maximum significant wave height, 200 x 200 m resolution.

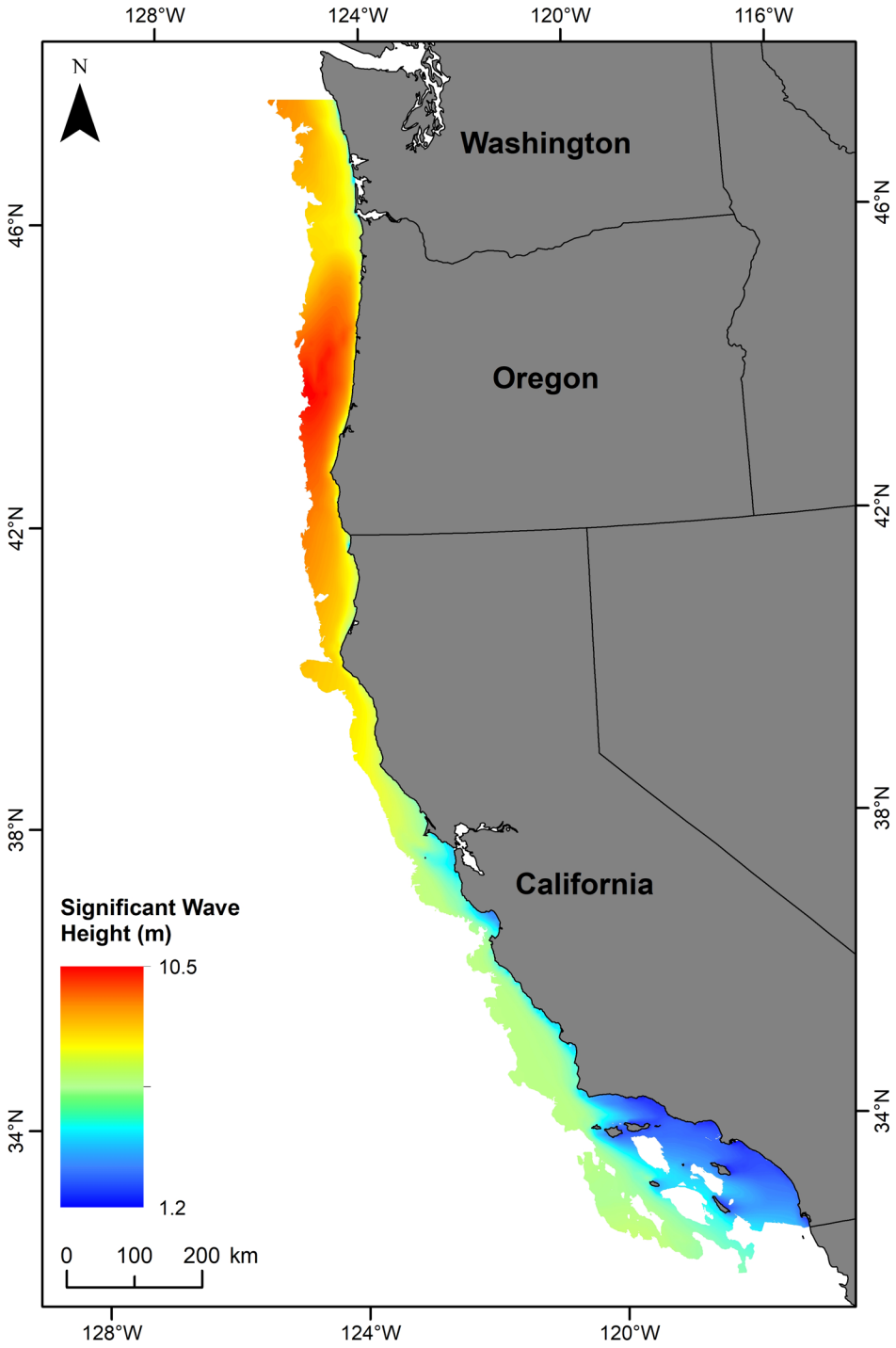

Figure A-50. Fall maximum significant wave height, 200 x 200 m resolution.

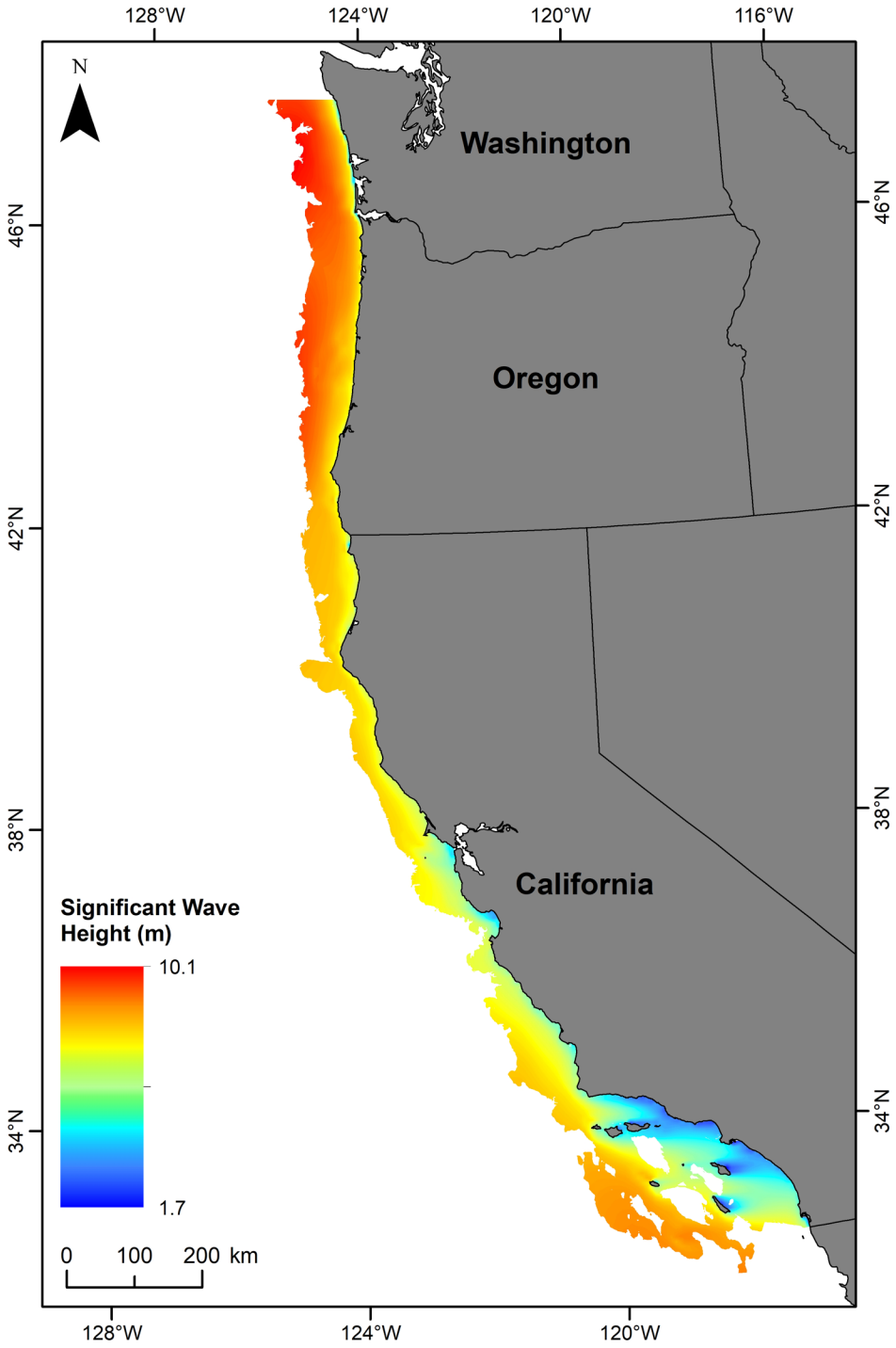

Figure A-51. Winter maximum significant wave height, 200 x 200 m resolution.

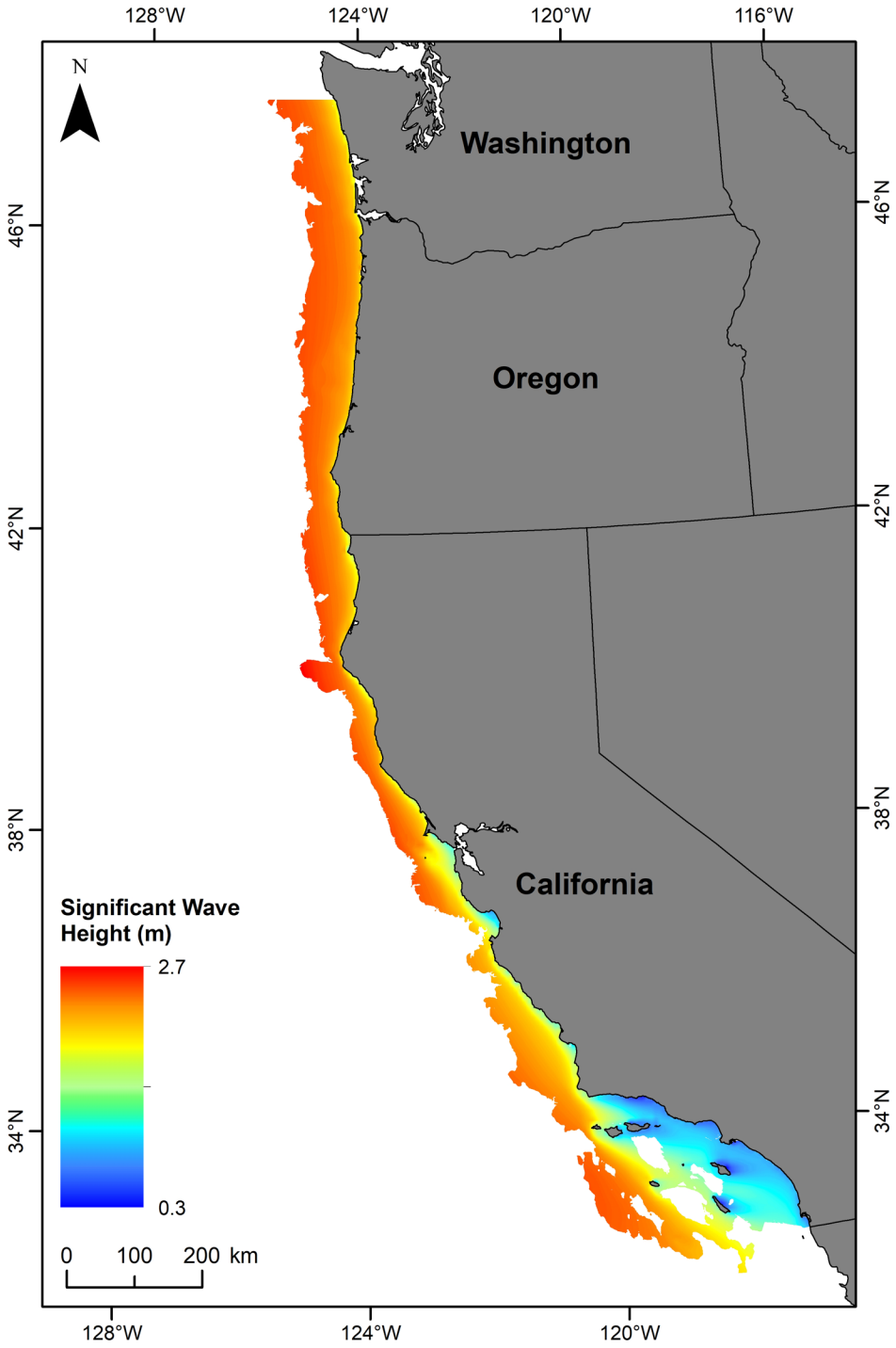

Figure A-52. Annual mean significant wave height, 200 x 200 m resolution.

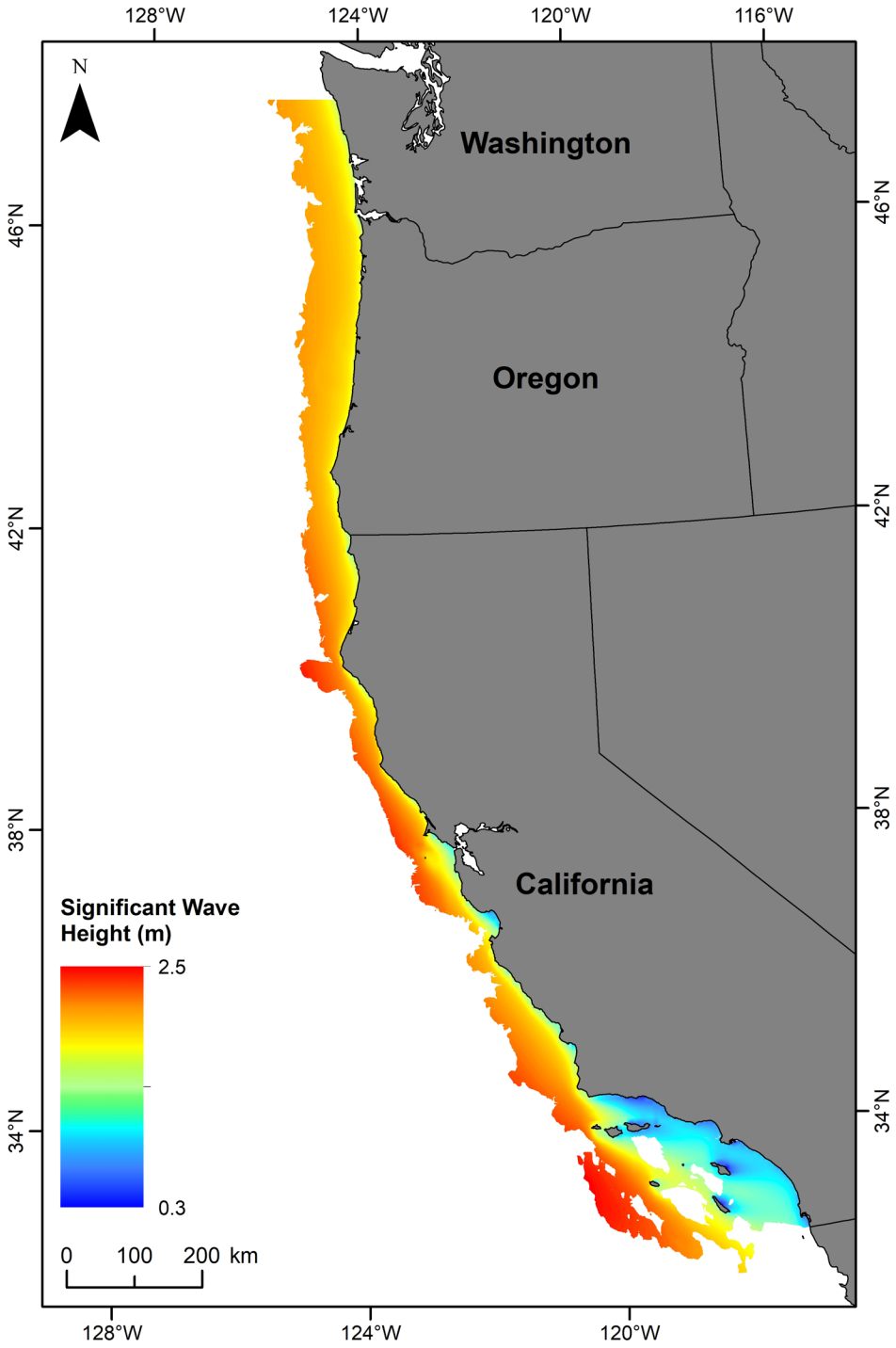

Figure A-53. Spring/summer mean significant wave height, 200 x 200 m resolution.

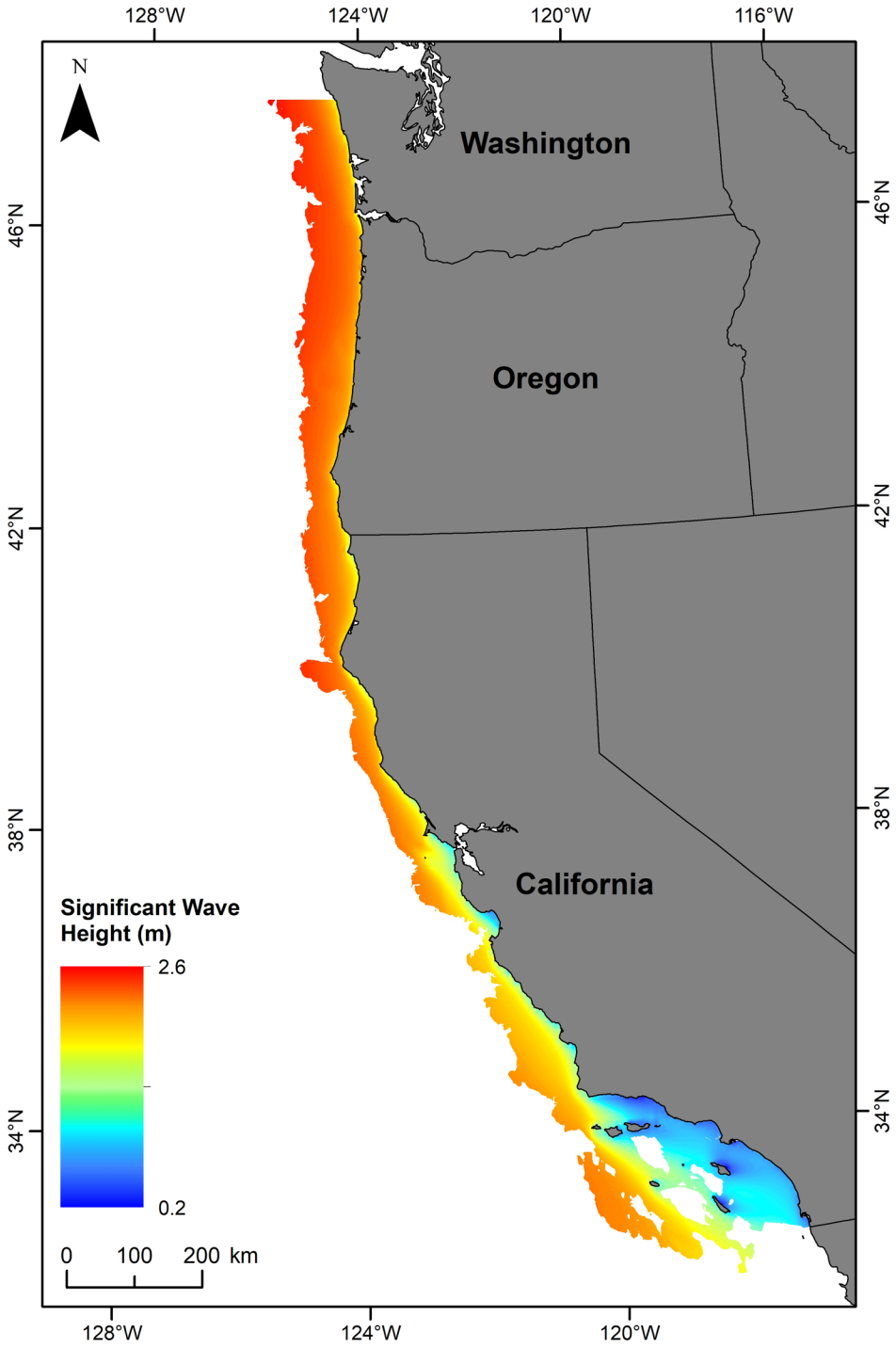

Figure A-54. Fall mean significant wave height, 200 x 200 m resolution.

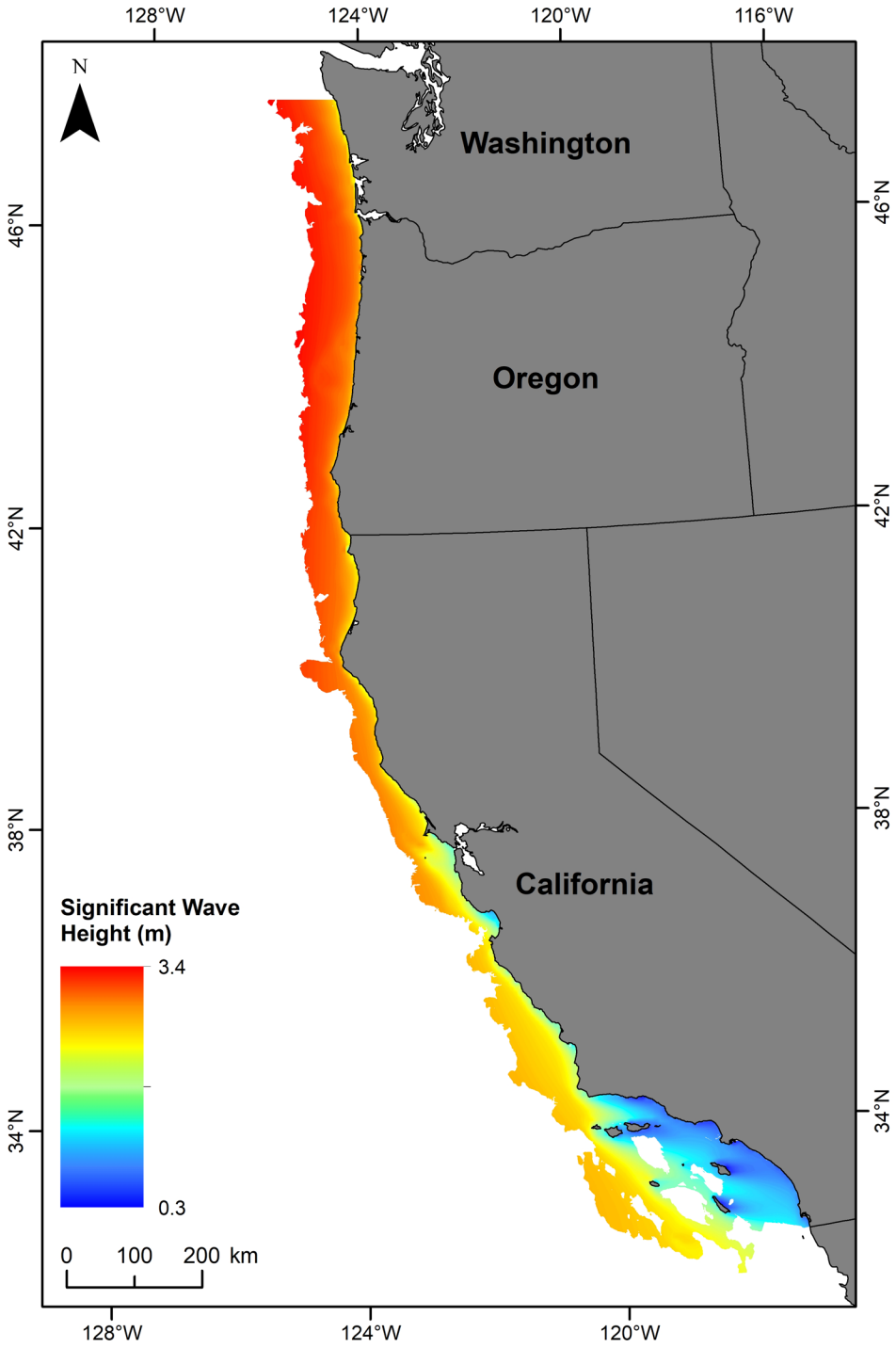

Figure A-55. Winter mean significant wave height, 200 x 200 m resolution.

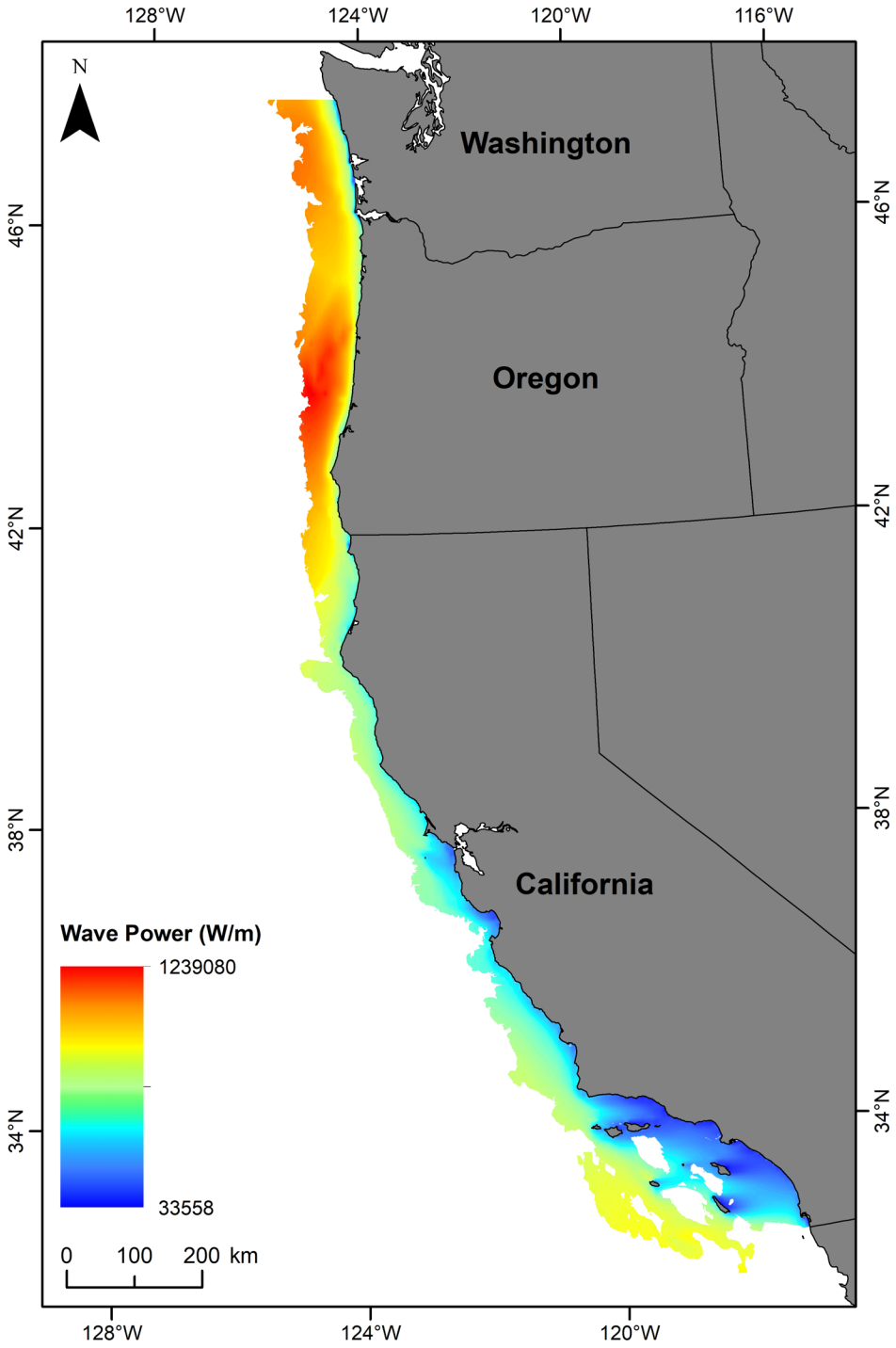

Figure A-56. Annual maximum wave power, 200 x 200 m resolution.

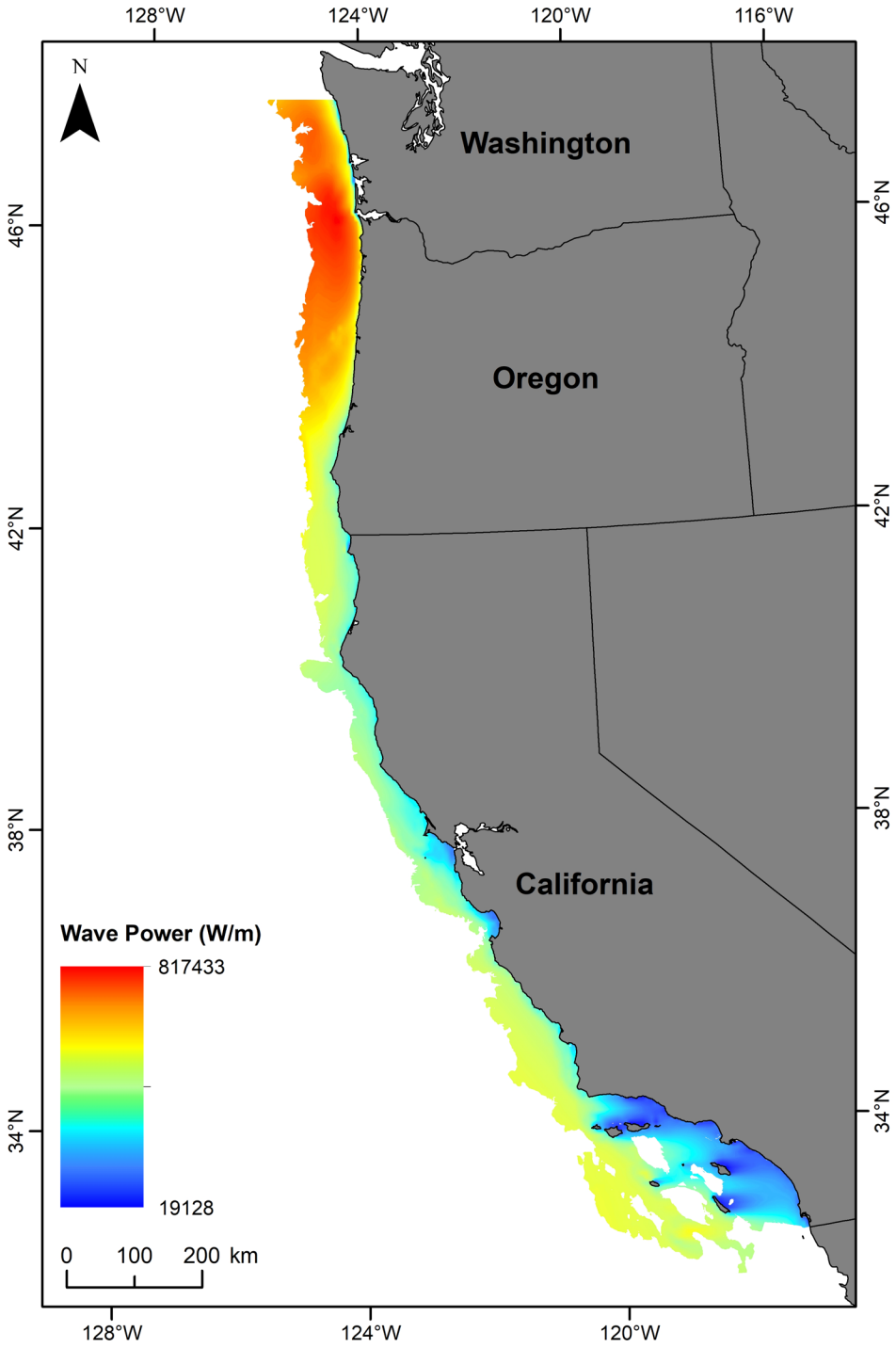

Figure A-57. Spring/summer maximum wave power, 200 x 200 m resolution.

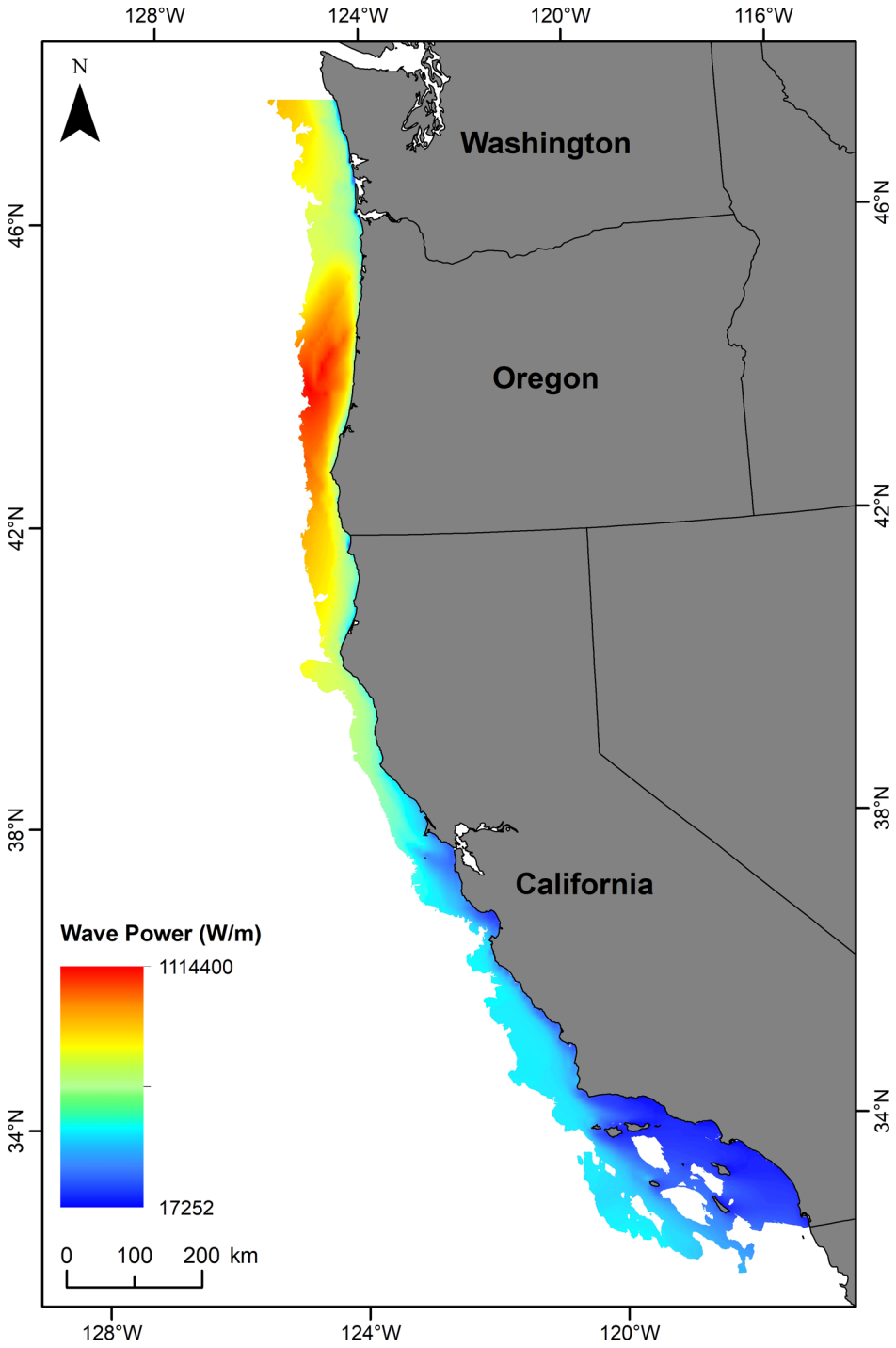

Figure A-58. Fall maximum wave power, 200 x 200 m resolution.

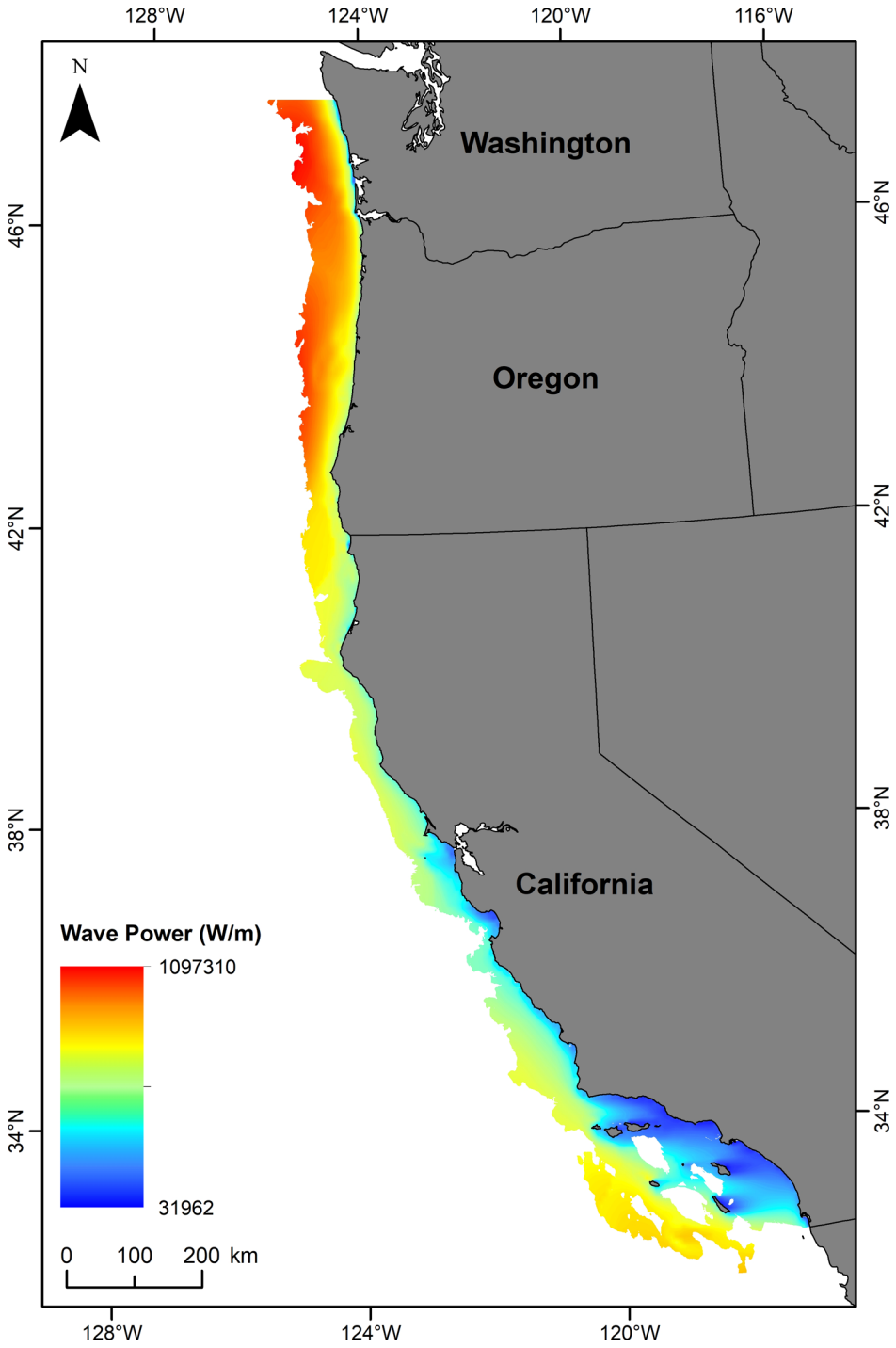

Figure A-59. Winter maximum wave power, 200 x 200 m resolution.

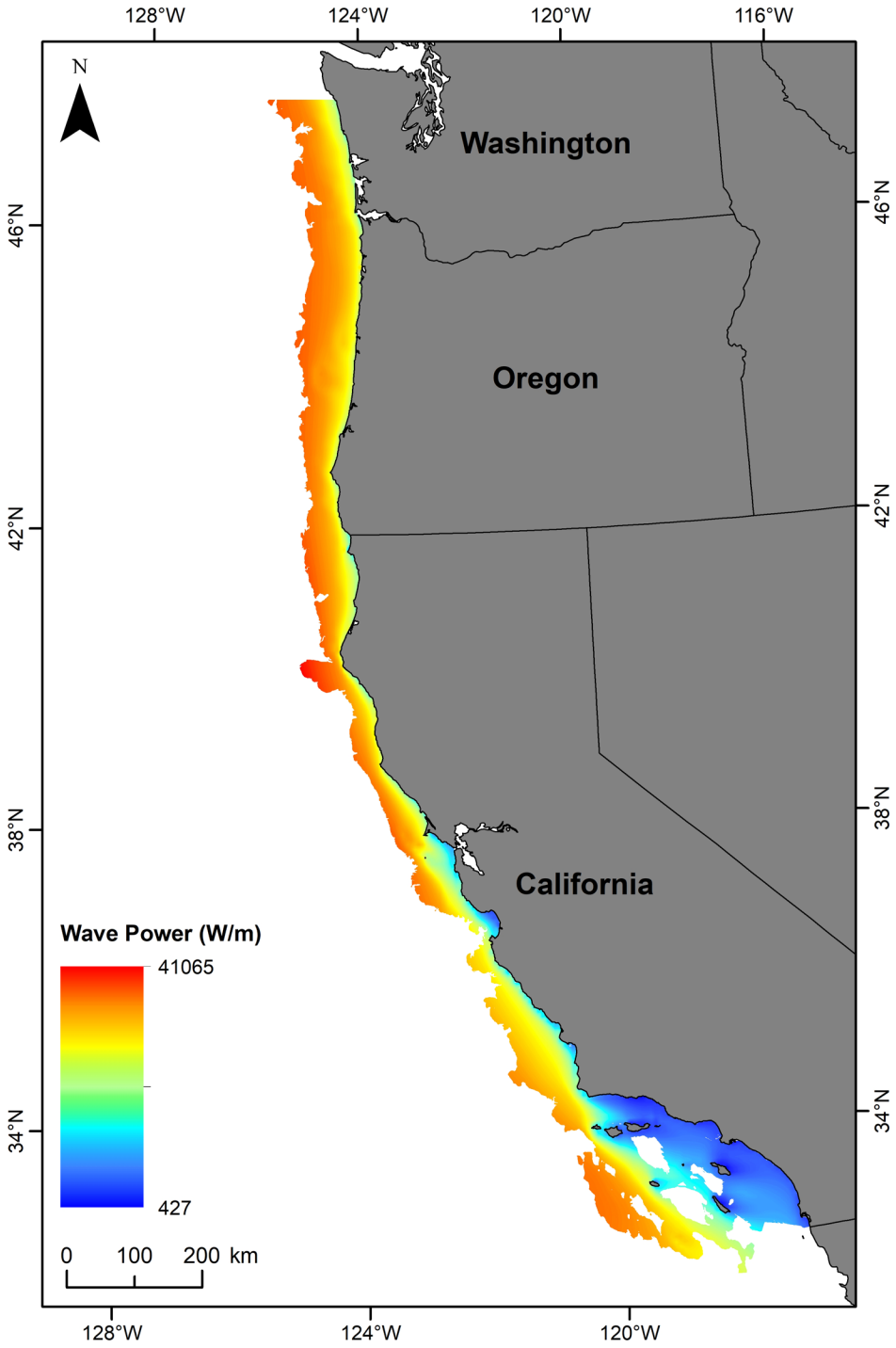

Figure A-60. Annual mean wave power, 200 x 200 m resolution.

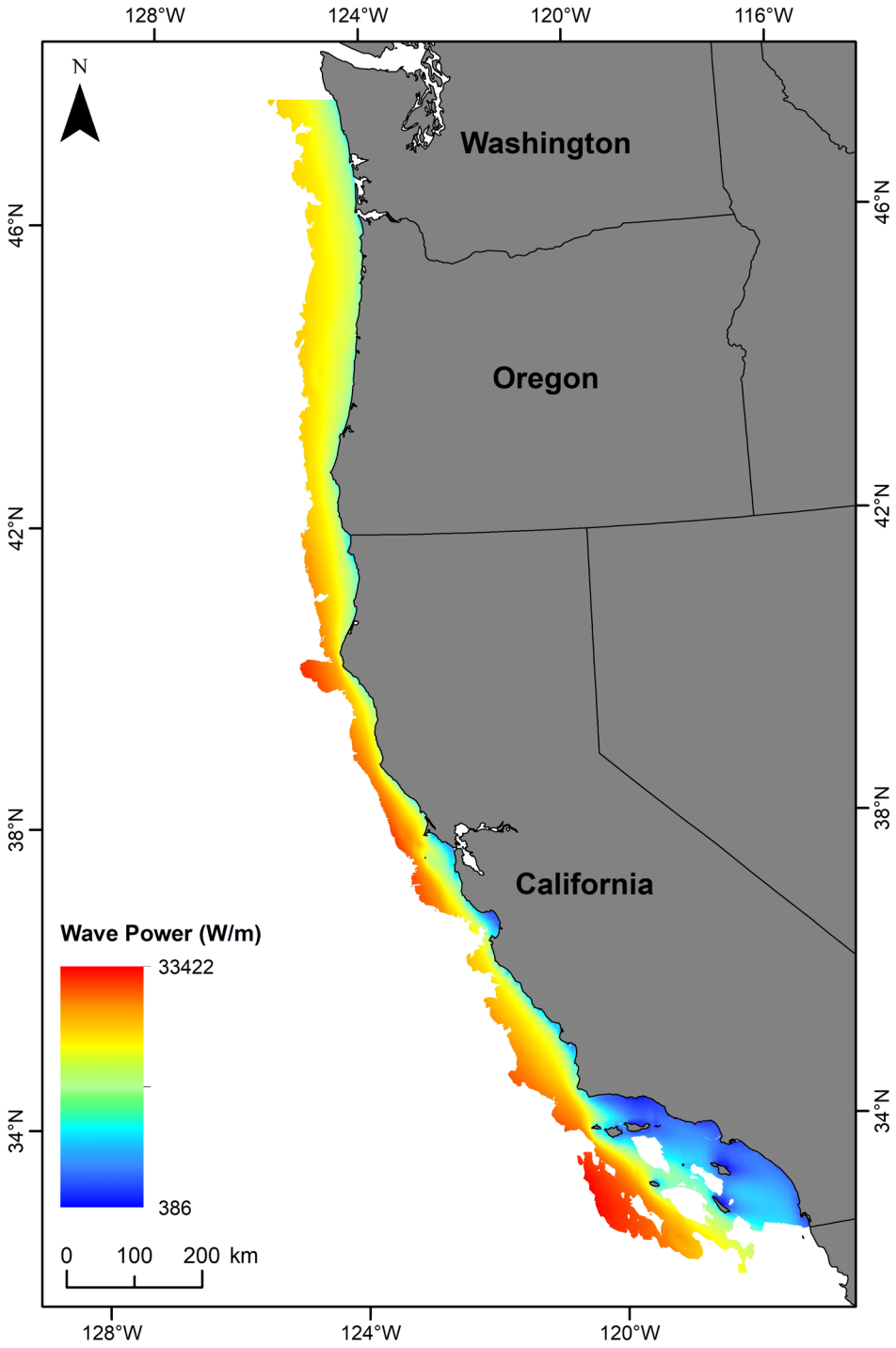

Figure A-61. Spring/summer mean wave power, 200 x 200 m resolution.

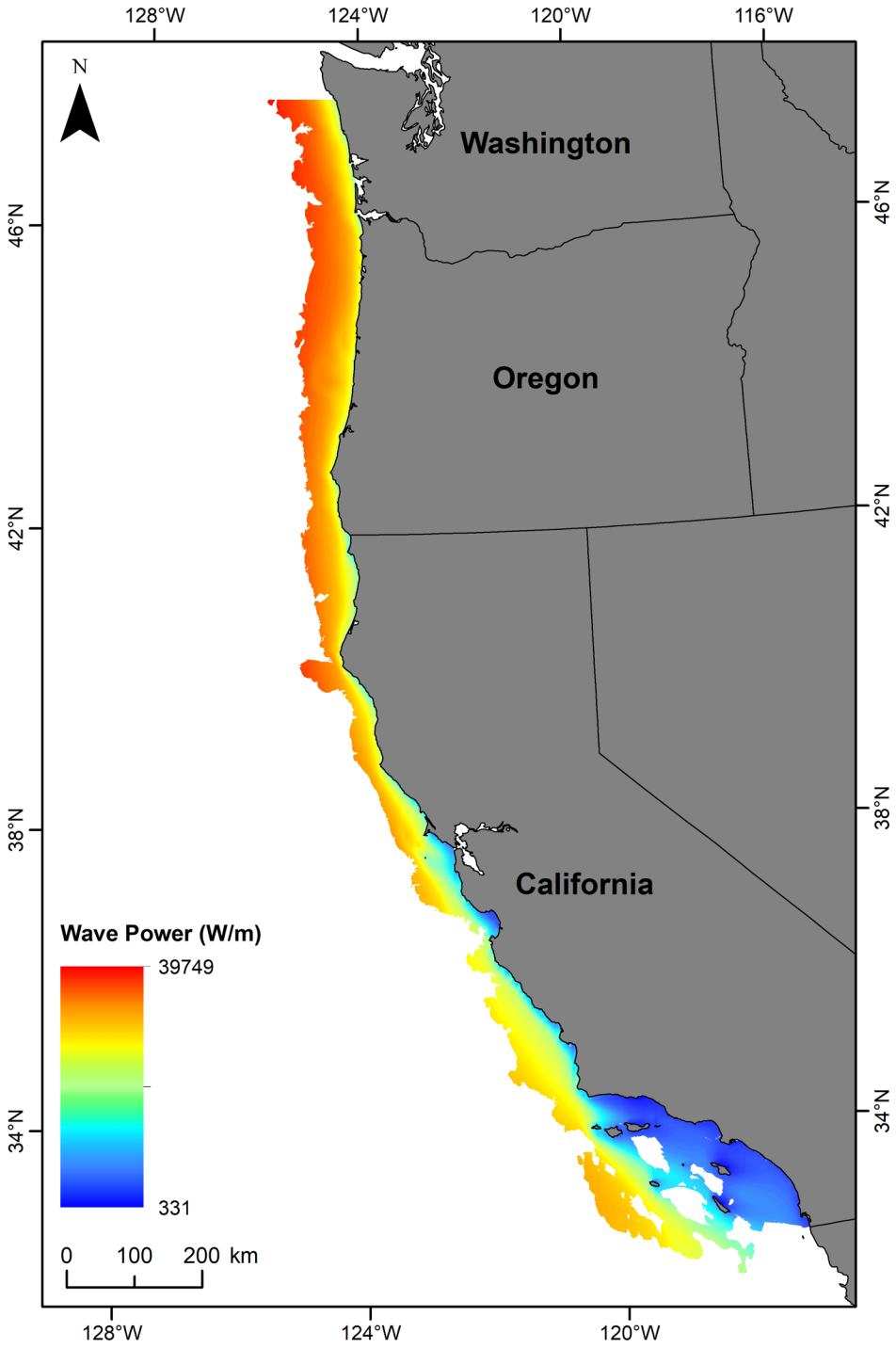

Figure A-62. Fall mean wave power, 200 x 200 m resolution.

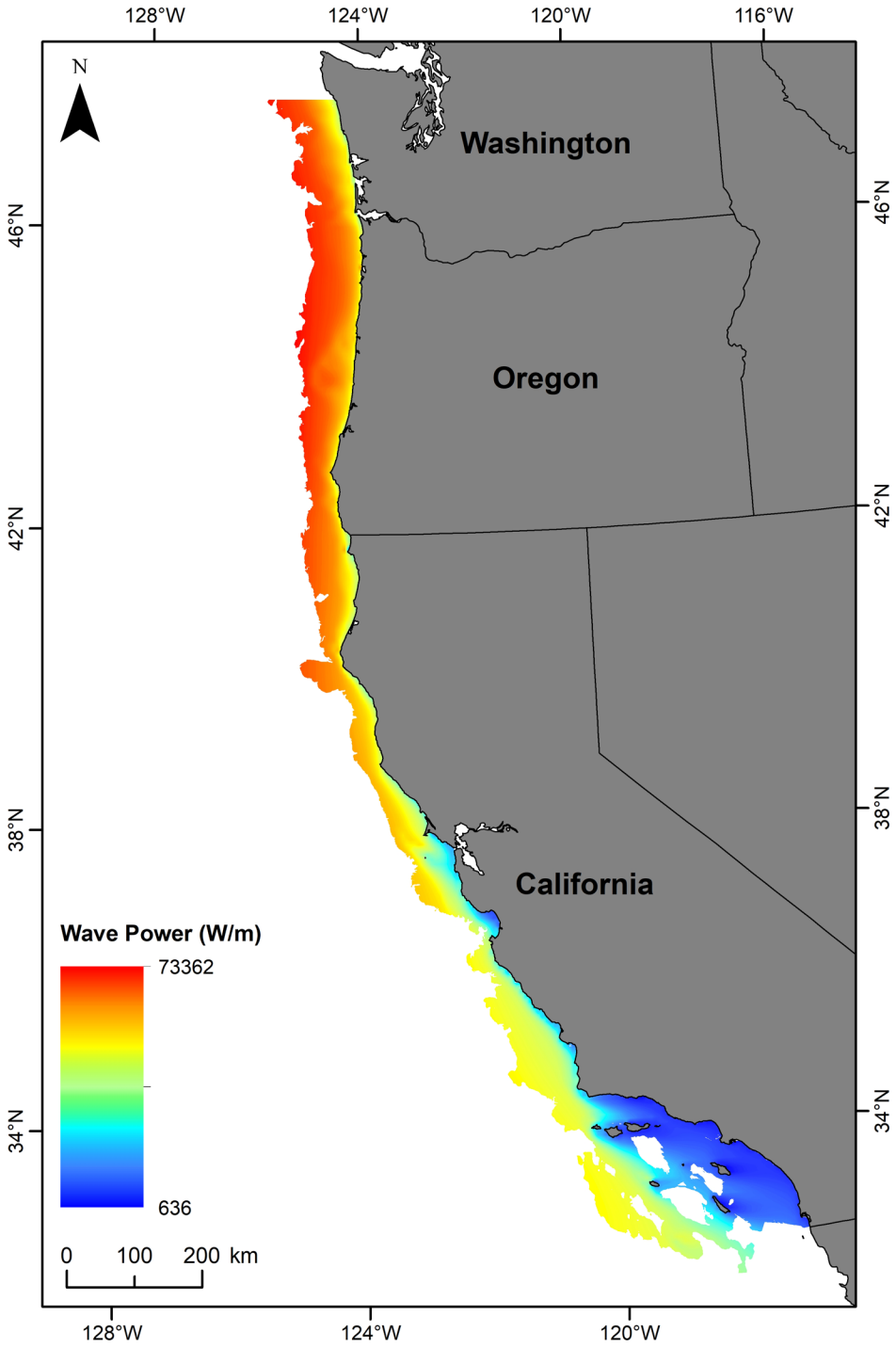

Figure A-63. Winter mean wave power, 200 x 200 m resolution.

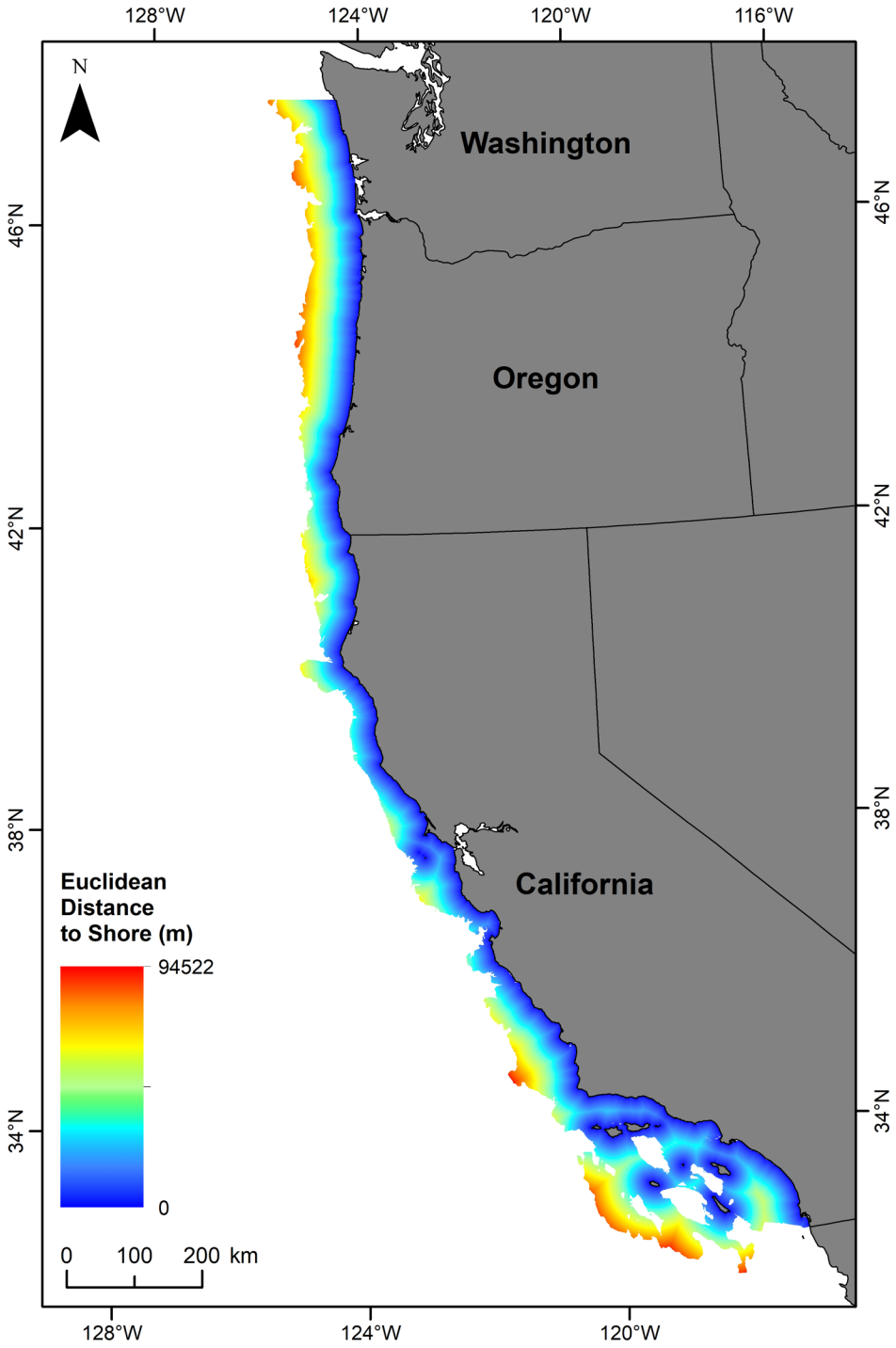

Figure A-64. Euclidean distance to shoreline, 200 x 200 m resolution.

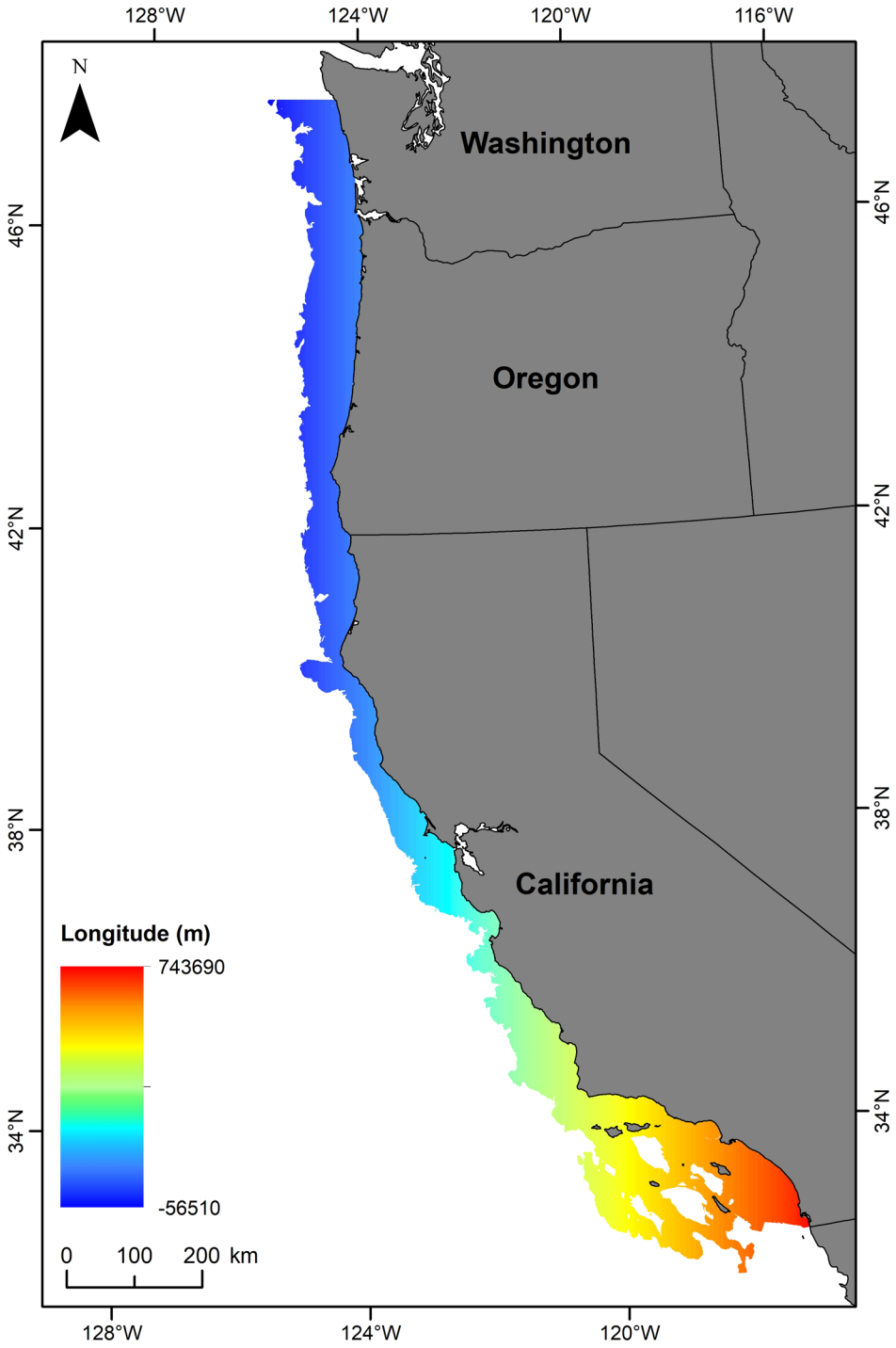

Figure A-65. Longitude (projected), 200 x 200 m resolution.

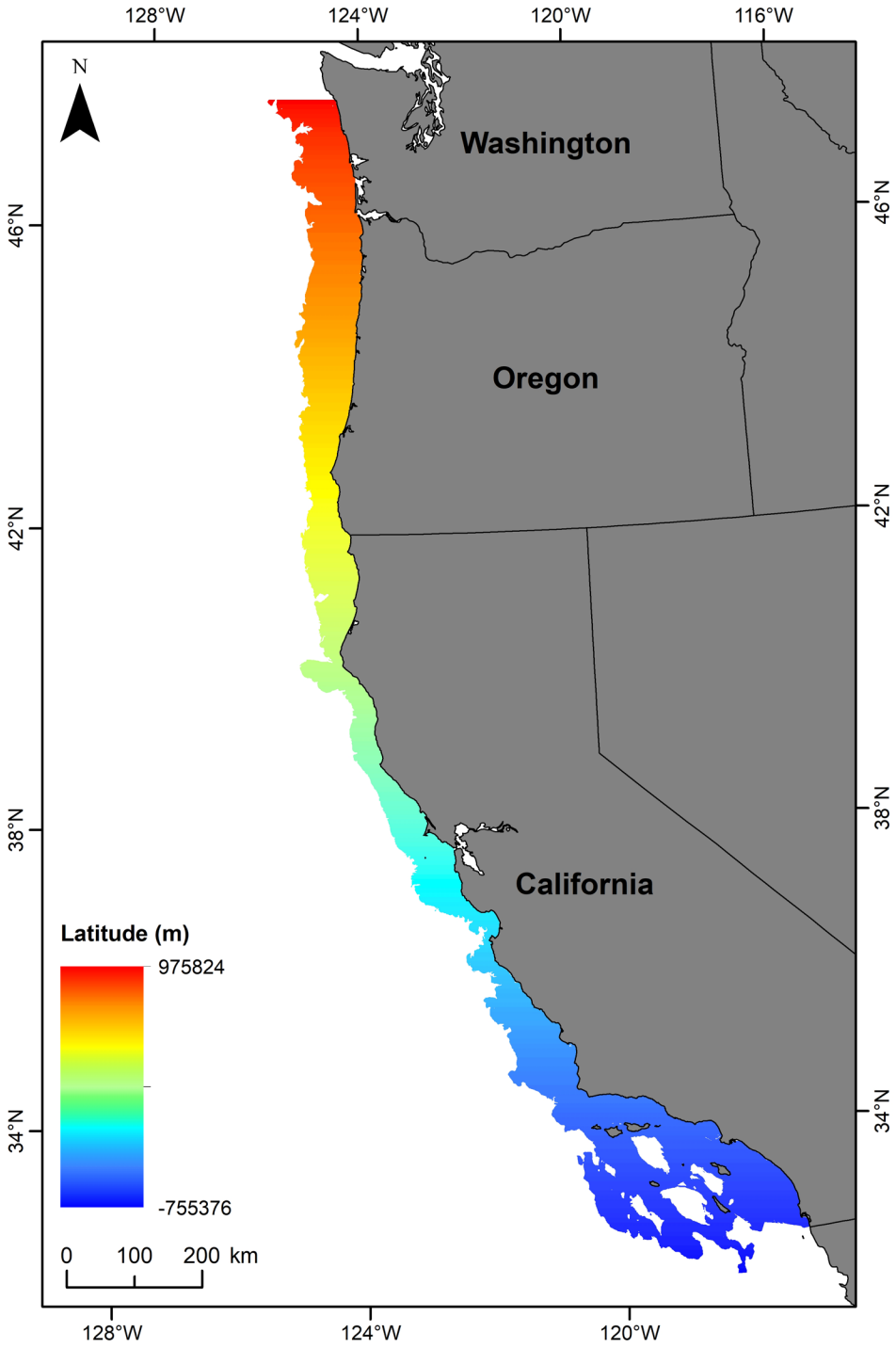

Figure A-66. Latitude (projected), 200 x 200 m resolution.

Appendix B: Table of Multibeam Bathymetry Datasets

Table B-1. Compilation of multibeam bathymetry datasets included in bathymetry synthesis.

Dataset	Data Source	Grid Resolution	Coordinate System
a_2mbathy	CSUMB	2 x 2 m	NAD83, UTM Zone 10N
a02_2mbath07	CSUMB	2 x 2 m	NAD83, UTM Zone 10N
a02_2mbath10	CSUMB	2 x 2 m	NAD83, UTM Zone 10N
bcn_5mallbath	CSUMB	5 x 5 m	NAD83, UTM Zone 10N
bcs_5mallbath	CSUMB	5 x 5 m	NAD83, UTM Zone 10N
br_5mallbty	CSUMB	5 x 5 m	NAD83 (CORS96), UTM Zone 11N
bss01_2mbathy	CSUMB	2 x 2 m	NAD83, UTM Zone 10N
bss02_2mbathy	CSUMB	2 x 2 m	NAD83, UTM Zone 10N
bss03_5mallbt	CSUMB	5 x 5 m	NAD83, UTM Zone 10N
bss04_5mallbt	CSUMB	5 x 5 m	NAD83, UTM Zone 10N
bss05_5mallbt	CSUMB	5 x 5 m	NAD83, UTM Zone 10N
bss06_5mallbt	CSUMB	5 x 5 m	NAD83, UTM Zone 10N
bss07_5mallbt	CSUMB	5 x 5 m	NAD83, UTM Zone 10N
bss08_5mallbt	CSUMB	5 x 5 m	NAD83, UTM Zone 10N
bss09_5mallbt	CSUMB	5 x 5 m	NAD83, UTM Zone 10N
bss10_5mallbt	CSUMB	5 x 5 m	NAD83, UTM Zone 10N
bss11_5mallbt	CSUMB	5 x 5 m	NAD83, UTM Zone 10N
bss12_5mallbt	CSUMB	5 x 5 m	NAD83, UTM Zone 10N
bss13_5mallbt	CSUMB	5 x 5 m	NAD83, UTM Zone 10N
c_p25mbathy	CSUMB	25 x 25 m	WGS84, UTM Zone 10N
cat_1mbathy	CSUMB	1 x 1 m	WGS84, UTM Zone 11N
cb2_3mbathy	CSUMB	3 x 3 m	WGS84, UTM Zone 10N
cbank_3mbathy	CSUMB	3 x 3 m	WGS84, UTM Zone 11N
cc_00_25mbath	CSUMB	25 x 25 m	WGS84, UTM Zone 10N

Dataset	Data Source	Grid Resolution	Coordinate System
cc_01_25mbath	CSUMB	25 x 25 m	WGS84, UTM Zone 10N
cc_02_25mbath	CSUMB	25 x 25 m	WGS84, UTM Zone 10N
cc_03_25mbath	CSUMB	25 x 25 m	WGS84, UTM Zone 10N
cc_05_25mbath	CSUMB	25 x 25 m	WGS84, UTM Zone 10N
cc_06_25mbath	CSUMB	25 x 25 m	WGS84, UTM Zone 10N
cc_07_25mbath	CSUMB	25 x 25 m	WGS84, UTM Zone 10N
cc_08_25mbath	CSUMB	25 x 25 m	WGS84, UTM Zone 10N
cc_09_25mbath	CSUMB	25 x 25 m	WGS84, UTM Zone 10N
cc_10_25mbath	CSUMB	25 x 25 m	WGS84, UTM Zone 10N
cc_11_25mbath	CSUMB	25 x 25 m	WGS84, UTM Zone 10N
cc_ba1_5mallb	CSUMB	5 x 5 m	NAD83, UTM Zone 10N
cc_ba2_5mallb	CSUMB	5 x 5 m	NAD83, UTM Zone 10N
cc_ba3_25mbth	CSUMB	25 x 25 m	NAD83, UTM Zone 10N
cc_bb_5mallbt	CSUMB	5 x 5 m	NAD83, UTM Zone 10N
cc_bc_5mallbt	CSUMB	5 x 5 m	NAD83, UTM Zone 10N
cc_bd_2mbthy	CSUMB	2 x 2 m	NAD83, UTM Zone 10N
cc_be_25mbthy	CSUMB	25 x 25 m	NAD83, UTM Zone 10N
cc_bf_25mbthy	CSUMB	25 x 25 m	NAD83, UTM Zone 10N
cc_bg_25mbthy	CSUMB	25 x 25 m	NAD83, UTM Zone 10N
cc_bh_25mbthy	CSUMB	25 x 25 m	NAD83, UTM Zone 10N
cc_bi_25mbath	CSUMB	25 x 25 m	NAD83, UTM Zone 10N
cc_bj_25mbth	CSUMB	25 x 25 m	NAD83, UTM Zone 10N
cc2a01_2mbath	CSUMB	2 x 2 m	NAD83, UTM Zone 10N
cc2a03_2mbath	CSUMB	2 x 2 m	NAD83, UTM Zone 10N
cc2a04_2mbath	CSUMB	2 x 2 m	NAD83, UTM Zone 10N
cc2a05_2mbath	CSUMB	2 x 2 m	NAD83, UTM Zone 10N
cc2a06_2mbath	CSUMB	2 x 2 m	NAD83, UTM Zone 10N
cc2a07_2mbath	CSUMB	2 x 2 m	NAD83, UTM Zone 10N

Dataset	Data Source	Grid Resolution	Coordinate System
cc2a08_2mbath	CSUMB	2 x 2 m	NAD83, UTM Zone 10N
cc2a09_2mbath	CSUMB	2 x 2 m	NAD83, UTM Zone 10N
cc2a10_2mbath	CSUMB	2 x 2 m	NAD83, UTM Zone 10N
cc2a11_2mbath	CSUMB	2 x 2 m	NAD83, UTM Zone 10N
cc2b01_2mbath	CSUMB	2 x 2 m	NAD83, UTM Zone 10N
cc2b02_2mbath	CSUMB	2 x 2 m	NAD83, UTM Zone 10N
cc2b03_2mbath	CSUMB	2 x 2 m	NAD83, UTM Zone 10N
cc2b04_2mbath	CSUMB	2 x 2 m	NAD83, UTM Zone 10N
cc2b05_2mbath	CSUMB	2 x 2 m	NAD83, UTM Zone 10N
cc2b06_2mbath	CSUMB	2 x 2 m	NAD83, UTM Zone 10N
cc2b07_2mbath	CSUMB	2 x 2 m	NAD83, UTM Zone 10N
cc2b08_2mbath	CSUMB	2 x 2 m	NAD83, UTM Zone 10N
cc2b09_2mbath	CSUMB	2 x 2 m	NAD83, UTM Zone 10N
cc2b10_2mbath	CSUMB	2 x 2 m	NAD83, UTM Zone 10N
cc2b11_2mbath	CSUMB	2 x 2 m	NAD83, UTM Zone 10N
cc2b12_2mbath	CSUMB	2 x 2 m	NAD83, UTM Zone 10N
cc2b13_2mbath	CSUMB	2 x 2 m	NAD83, UTM Zone 10N
ci01all_5mbty	CSUMB	5 x 5 m	NAD83, UTM Zone 11N
ci02all_5mbty	CSUMB	5 x 5 m	NAD83, UTM Zone 11N
ci03all_5mbty	CSUMB	5 x 5 m	NAD83, UTM Zone 11N
ci04all_5mbty	CSUMB	5 x 5 m	NAD83, UTM Zone 11N
ci05all_5mbty	CSUMB	5 x 5 m	NAD83, UTM Zone 11N
ci06all_5mbty	CSUMB	5 x 5 m	NAD83, UTM Zone 11N
ci07all_5mbty	CSUMB	5 x 5 m	NAD83, UTM Zone 11N
ci08all_5mbty	CSUMB	5 x 5 m	NAD83, UTM Zone 11N
ci09all_5mbty	CSUMB	5 x 5 m	NAD83, UTM Zone 11N
ci10all_5mbty	CSUMB	5 x 5 m	NAD83, UTM Zone 11N
ci11all_5mbty	CSUMB	5 x 5 m	NAD83, UTM Zone 11N

Dataset	Data Source	Grid Resolution	Coordinate System
ci12all_5mbty	CSUMB	5 x 5 m	NAD83, UTM Zone 11N
cmb_n_2mbathy	CSUMB	2 x 2 m	NAD83, UTM Zone 10N
cmb_s_2mbathy	CSUMB	2 x 2 m	NAD83, UTM Zone 10N
cp_3mbathy	CSUMB	3 x 3 m	WGS84, UTM Zone 10N
dp_10mbathy	CSUMB	10 x 10 m	NAD83 (CORS96), UTM Zone 11N
ec_ob_2mbathy	CSUMB	2 x 2 m	WGS84, UTM Zone 10N
fi_5mallbathy	CSUMB	5 x 5 m	NAD83 (CORS96), UTM Zone 10N
gi_3mbathy	CSUMB	3 x 3 m	WGS84, UTM Zone 11N
gp_2mbathy	CSUMB	2 x 2 m	WGS84, UTM Zone 10N
h11875all5mbt	CSUMB	5 x 5 m	NAD83, UTM Zone 11N
h11876all5mbt	CSUMB	5 x 5 m	NAD83, UTM Zone 11N
h11877all5mbt	CSUMB	5 x 5 m	NAD83, UTM Zone 11N
h11878all5mbt	CSUMB	5 x 5 m	NAD83, UTM Zone 11N
h11879all5mbt	CSUMB	5 x 5 m	NAD83, UTM Zone 11N
h11880all5mbt	CSUMB	5 x 5 m	NAD83, UTM Zone 11N
h11881all5mbt	CSUMB	5 x 5 m	NAD83, UTM Zone 11N
h11882all5mbt	CSUMB	5 x 5 m	NAD83, UTM Zone 11N
h11883all5mbt	CSUMB	5 x 5 m	NAD83, UTM Zone 11N
h11891all5mbt	CSUMB	5 x 5 m	NAD83, UTM Zone 11N
h11950all5mbt	CSUMB	5 x 5 m	NAD83, UTM Zone 11N
h11951all5mbt	CSUMB	5 x 5 m	NAD83, UTM Zone 10N
h11952all5mbt	CSUMB	5 x 5 m	NAD83, UTM Zone 10N
h11953all5mbt	CSUMB	5 x 5 m	NAD83, UTM Zone 10N
h966_5mallbty	CSUMB	5 x 5 m	NAD83, UTM Zone 10N
h967_5mallbty	CSUMB	5 x 5 m	NAD83, UTM Zone 10N
h968_5mallbty	CSUMB	5 x 5 m	NAD83, UTM Zone 10N
h969_5mallbty	CSUMB	5 x 5 m	NAD83, UTM Zone 10N
h970_5mallbty	CSUMB	5 x 5 m	NAD83, UTM Zone 10N

Dataset	Data Source	Grid Resolution	Coordinate System
h971_5mallbty	CSUMB	5 x 5 m	NAD83, UTM Zone 10N
h972_5mallbty	CSUMB	5 x 5 m	NAD83, UTM Zone 10N
h973_5mallbty	CSUMB	5 x 5 m	NAD83, UTM Zone 10N
h974_5mallbty	CSUMB	5 x 5 m	NAD83, UTM Zone 10N
h975_5mallbty	CSUMB	5 x 5 m	NAD83, UTM Zone 10N
h976_5mallbty	CSUMB	5 x 5 m	NAD83, UTM Zone 10N
h977_5mallbty	CSUMB	5 x 5 m	NAD83, UTM Zone 10N
h978_1_2mbthy	CSUMB	2 x 2 m	NAD83, UTM Zone 10N
h978_2_2mbthy	CSUMB	2 x 2 m	NAD83, UTM Zone 10N
h979_2mbthy	CSUMB	2 x 2 m	NAD83, UTM Zone 10N
h980_2mbthy	CSUMB	2 x 2 m	NAD83, UTM Zone 10N
h981_2mbthy	CSUMB	2 x 2 m	NAD83, UTM Zone 10N
h982_2mbthy	CSUMB	2 x 2 m	NAD83, UTM Zone 10N
h983_2mbthy	CSUMB	2 x 2 m	NAD83, UTM Zone 10N
h984_1_2mbthy	CSUMB	2 x 2 m	NAD83, UTM Zone 10N
h984_2_2mbthy	CSUMB	2 x 2 m	NAD83, UTM Zone 10N
h984_5mbthy	CSUMB	5 x 5 m	NAD83, UTM Zone 10N
h985_2mbthy	CSUMB	2 x 2 m	NAD83, UTM Zone 10N
hp_2mbathy	CSUMB	2 x 2 m	WGS84, UTM Zone 10N
ib_2mbathy	CSUMB	2 x 2 m	NAD83 (CORS96), UTM Zone 11N
kp_25mbathy	CSUMB	25 x 25 m	WGS84, UTM Zone 10N
lj_2mbathy	CSUMB	2 x 2 m	NAD83 (CORS96), UTM Zone 11N
ljn_2mbathy	CSUMB	2 x 2 m	WGS84, UTM Zone 11N
lp_5mallbathy	CSUMB	5 x 5 m	NAD83, UTM Zone 10N
m_c25mbathy	CSUMB	25 x 25 m	WGS84, UTM Zone 10N
mac02_2mbathy	CSUMB	2 x 2 m	WGS84, UTM Zone 10N
mb_2mbathy	CSUMB	2 x 2 m	NAD83 (CORS96), UTM Zone 11N
mc_3mbathy	CSUMB	3 x 3 m	WGS84, UTM Zone 10N

Dataset	Data Source	Grid Resolution	Coordinate System
mp_10mbathy	CSUMB	10 x 10 m	NAD83, UTM Zone 10N
nmb1_2mbathy	CSUMB	2 x 2 m	NAD83, UTM Zone 10N
nmb2_2mbathy	CSUMB	2 x 2 m	NAD83, UTM Zone 10N
p_s25mbathy	CSUMB	25 x 25 m	WGS84, UTM Zone 10N
pc05_2mbathy	CSUMB	2 x 2 m	WGS84, UTM Zone 10N
pl_25mbathy	CSUMB	25 x 25 m	WGS84, UTM Zone 10N
pl_5mbathy	CSUMB	5 x 5 m	NAD83, UTM Zone 10N
pln_2mbathy	CSUMB	2 x 2 m	NAD83 (CORS96), UTM Zone 11N
pls_2mbathy	CSUMB	2 x 2 m	NAD83 (CORS96), UTM Zone 11N
ps_1mbathy	CSUMB	1 x 1 m	WGS84, UTM Zone 10N
PS_2mbathy	CSUMB	2 x 2 m	WGS84, UTM Zone 10N
ptcab_1mbathy	CSUMB	1 x 1 m	WGS84, UTM Zone 10N
s_5mbathy	CSUMB	5 x 5 m	NAD83, UTM Zone 10N
sb_2mbathy	CSUMB	2 x 2 m	NAD83 (CORS96), UTM Zone 10N
sbc_a_2mbathy	CSUMB	2 x 2 m	WGS84, UTM Zone 11N
sbc_b_2mbathy	CSUMB	2 x 2 m	WGS84, UTM Zone 11N
sbc_c_2mbathy	CSUMB	2 x 2 m	WGS84, UTM Zone 11N
sbc_d_2mbathy	CSUMB	2 x 2 m	WGS84, UTM Zone 11N
sbc_e_2mbathy	CSUMB	2 x 2 m	WGS84, UTM Zone 11N
sbc_f_2mbathy	CSUMB	2 x 2 m	WGS84, UTM Zone 11N
sbc_g_2mbathy	CSUMB	2 x 2 m	WGS84, UTM Zone 11N
sbc_h_2mbathy	CSUMB	2 x 2 m	WGS84, UTM Zone 11N
sbi_3mbathy	CSUMB	3 x 3 m	WGS84, UTM Zone 11N
scc01_2mbathy	CSUMB	2 x 2 m	NAD83, UTM Zone 10N
scc02_2mbathy	CSUMB	2 x 2 m	NAD83, UTM Zone 10N
scc03_5mallbt	CSUMB	5 x 5 m	NAD83, UTM Zone 10N
scc04_5mallbt	CSUMB	5 x 5 m	NAD83, UTM Zone 10N
scc05_5mallbt	CSUMB	5 x 5 m	NAD83, UTM Zone 10N

Dataset	Data Source	Grid Resolution	Coordinate System
scc07_5mallbt	CSUMB	5 x 5 m	NAD83, UTM Zone 10N
scc08_5mallbt	CSUMB	5 x 5 m	NAD83, UTM Zone 10N
scc09_5mallbt	CSUMB	5 x 5 m	NAD83, UTM Zone 10N
scc10_5mallbt	CSUMB	5 x 5 m	NAD83, UTM Zone 10N
scc11_5mallbt	CSUMB	5 x 5 m	NAD83, UTM Zone 10N
scc12_2mbathy	CSUMB	2 x 2 m	NAD83, UTM Zone 10N
scc13_2mbathy	CSUMB	2 x 2 m	NAD83, UTM Zone 10N
scc14_2mbathy	CSUMB	2 x 2 m	NAD83, UTM Zone 10N
scc15_2mbathy	CSUMB	2 x 2 m	NAD83, UTM Zone 10N
scc16_2mbathy	CSUMB	2 x 2 m	NAD83, UTM Zone 10N
scc17_2mbathy	CSUMB	2 x 2 m	NAD83, UTM Zone 10N
scc18_2mbathy	CSUMB	2 x 2 m	NAD83, UTM Zone 10N
scc19_2mbathy	CSUMB	2 x 2 m	NAD83, UTM Zone 10N
scc20_2mbathy	CSUMB	2 x 2 m	NAD83, UTM Zone 10N
scc21_2mbathy	CSUMB	2 x 2 m	NAD83, UTM Zone 10N
scc22_2mbathy	CSUMB	2 x 2 m	NAD83, UTM Zone 10N
scc23_2mbathy	CSUMB	2 x 2 m	NAD83, UTM Zone 10N
scc24_2mbathy	CSUMB	2 x 2 m	NAD83, UTM Zone 10N
scc25_2mbathy	CSUMB	2 x 2 m	NAD83, UTM Zone 10N
scc26_2mbathy	CSUMB	2 x 2 m	NAD83, UTM Zone 10N
scc27_2mbathy	CSUMB	2 x 2 m	NAD83, UTM Zone 10N
scc28_2mbathy	CSUMB	2 x 2 m	NAD83, UTM Zone 10N
scia_5mallbty	CSUMB	5 x 5 m	NAD83 (CORS96), UTM Zone 11N
scib_5mallbty	CSUMB	5 x 5 m	NAD83 (CORS96), UTM Zone 11N
scicp_2mbathy	CSUMB	2 x 2 m	NAD83 (CORS96), UTM Zone 11N
scid_5mallbty	CSUMB	5 x 5 m	NAD83 (CORS96), UTM Zone 11N
scidcp_2mbath	CSUMB	2 x 2 m	NAD83 (CORS96), UTM Zone 11N
sciep_2mbathy	CSUMB	2 x 2 m	NAD83 (CORS96), UTM Zone 11N

Dataset	Data Source	Grid Resolution	Coordinate System
scifn_5mallbt	CSUMB	5 x 5 m	NAD83 (CORS96), UTM Zone 11N
scifs_5mallbt	CSUMB	5 x 5 m	NAD83 (CORS96), UTM Zone 11N
scig_5mallbty	CSUMB	5 x 5 m	NAD83 (CORS96), UTM Zone 11N
scignr_2mbath	CSUMB	2 x 2 m	NAD83 (CORS96), UTM Zone 11N
scilp_2mbathy	CSUMB	2 x 2 m	NAD83 (CORS96), UTM Zone 11N
scimp_2mbathy	CSUMB	2 x 2 m	NAD83 (CORS96), UTM Zone 11N
scinr_2mbathy	CSUMB	2 x 2 m	NAD83 (CORS96), UTM Zone 11N
scisr_2mbathy	CSUMB	2 x 2 m	NAD83 (CORS96), UTM Zone 11N
sciwc_5mallbt	CSUMB	5 x 5 m	NAD83 (CORS96), UTM Zone 11N
scpt_2mbathy	CSUMB	2 x 2 m	WGS84, UTM Zone 11N
sf_1mbathy	CSUMB	1 x 1 m	WGS84, UTM Zone 10N
sf_2mbathy	CSUMB	2 x 2 m	WGS84, UTM Zone 10N
sfn_2mbathy	CSUMB	2 x 2 m	WGS84, UTM Zone 10N
sfne_1mbathy	CSUMB	1 x 1 m	WGS84, UTM Zone 10N
sfnw_1mbathy	CSUMB	1 x 1 m	WGS84, UTM Zone 10N
sfse_1mbathy	CSUMB	1 x 1 m	WGS84, UTM Zone 10N
sfse_2mbathy	CSUMB	2 x 2 m	WGS84, UTM Zone 10N
sfsw_1mbathy	CSUMB	1 x 1 m	WGS84, UTM Zone 10N
sfsw_2mbathy	CSUMB	2 x 2 m	WGS84, UTM Zone 10N
shb_1mbathy	CSUMB	1 x 1 m	WGS84, UTM Zone 10N
smb13_2mbathy	CSUMB	2 x 2 m	WGS84, UTM Zone 11N
smb14_2mbathy	CSUMB	2 x 2 m	WGS84, UTM Zone 11N
smb15_2mbathy	CSUMB	2 x 2 m	WGS84, UTM Zone 11N
smb16_2mbathy	CSUMB	2 x 2 m	WGS84, UTM Zone 11N
sni01_5mallbt	CSUMB	5 x 5 m	NAD83 (CORS96), UTM Zone 11N
sni02_5mallbt	CSUMB	5 x 5 m	NAD83 (CORS96), UTM Zone 11N
sni03_2mbathy	CSUMB	2 x 2 m	NAD83 (CORS96), UTM Zone 11N
sni04_2mbathy	CSUMB	2 x 2 m	NAD83 (CORS96), UTM Zone 11N

Dataset	Data Source	Grid Resolution	Coordinate System
sni05_2mbathy	CSUMB	2 x 2 m	NAD83 (CORS96), UTM Zone 11N
sni06_5mallbt	CSUMB	5 x 5 m	NAD83 (CORS96), UTM Zone 11N
sni07_5mallbt	CSUMB	5 x 5 m	NAD83 (CORS96), UTM Zone 11N
sni08_5mallbt	CSUMB	5 x 5 m	NAD83 (CORS96), UTM Zone 11N
sni09_5mallbt	CSUMB	5 x 5 m	NAD83 (CORS96), UTM Zone 11N
sni10_5mallbt	CSUMB	5 x 5 m	NAD83 (CORS96), UTM Zone 11N
sni11_5mallbt	CSUMB	5 x 5 m	NAD83 (CORS96), UTM Zone 11N
sni12_2mbathy	CSUMB	2 x 2 m	NAD83 (CORS96), UTM Zone 11N
sob01_2mbathy	CSUMB	2 x 2 m	NAD83 (CORS96), UTM Zone 11N
sob02_2mbathy	CSUMB	2 x 2 m	NAD83 (CORS96), UTM Zone 11N
sob03_2mbathy	CSUMB	2 x 2 m	NAD83 (CORS96), UTM Zone 11N
socy_3mbathy	CSUMB	3 x 3 m	WGS84, UTM Zone 10N
sp_25mbathy	CSUMB	25 x 25 m	WGS84, UTM Zone 10N
sp_3mbathy	CSUMB	3 x 3 m	WGS84, UTM Zone 10N
sr_25mbathy	CSUMB	25 x 25 m	WGS84, UTM Zone 10N
tb3mbathy_dp	CSUMB	3 x 3 m	WGS84, UTM Zone 11N
yp_25mbathy	CSUMB	25 x 25 m	WGS84, UTM Zone 10N
H11965_MB_5m_MLLW_combined	Fugro Pelagos	5 x 5 m	WGS84, UTM Zone 10N
H12109_MB_2m_MLLW_Combined	Fugro Pelagos	2 x 2 m	NAD83, UTM Zone 10N
H12110_MB_2m_MLLW_combined	Fugro Pelagos	2 x 2 m	NAD83, UTM Zone 10N
H12111_MB_2m_MLLW_Combined	Fugro Pelagos	2 x 2 m	WGS84, UTM Zone 10N
H12113_MB_2m_MLLW_combined	Fugro Pelagos	2 x 2 m	NAD83, UTM Zone 10N
MBARI_Axial_Volcano_20m	MBARI	20 x 20 m	WGS84
MBARI_Axial_Volcano_40m	MBARI	40 x 40 m	WGS84
MBARI_Central_Gorda_Ridge_40m	MBARI	40 x 40 m	WGS84
MBARI_Cleft_Segment_A_30m	MBARI	30 x 30 m	WGS84
MBARI_Cleft_Segment_B_20m	MBARI	20 x 20 m	WGS84
MBARI_Cleft_Segment_C_5m	MBARI	5 x 5 m	WGS84

Dataset	Data Source	Grid Resolution	Coordinate System
MBARI_Cleft_Segment_D_5m	MBARI	5 x 5 m	WGS84
MBARI_Davidson_Seamount_30m	MBARI	30 x 30 m	WGS84
MBARI_Davidson_Summit_20m	MBARI	20 x 20 m	WGS84
MBARI_Eel_River_Basin_10m	MBARI	10 x 10 m	WGS84
MBARI_Escanaba_Trough_40m	MBARI	40 x 40 m	WGS84
MBARI_Guide_Seamount_20m	MBARI	20 x 20 m	WGS84
MBARI_Guide_to_Gumdrop_Seamounts_30m	MBARI	30 x 30 m	WGS84
MBARI_Mendocino_Fracture_Zone_20m	MBARI	20 x 20 m	WGS84
MBARI_Monterey_Bay_40m	MBARI	40 x 40 m	WGS84
MBARI_Monterey_Bay_Ascension_Slope_25m	MBARI	25 x 25 m	WGS84
MBARI_Monterey_Bay_Lower_Lucia_Canyon_25m	MBARI	25 x 25 m	WGS84
MBARI_Monterey_Bay_Monterey_Canyon_25m	MBARI	25 x 25 m	WGS84
MBARI_Monterey_Bay_Sur_Ridge_Sur_Canyon_25m	MBARI	25 x 25 m	WGS84
MBARI_Monterey_Bay_Upper_Lucia_Canyon_25m	MBARI	25 x 25 m	WGS84
MBARI_North_Gorda_Ridge_40m	MBARI	40 x 40 m	WGS84
MBARI_Oregon_Margin_40m	MBARI	40 x 40 m	WGS84
MBARI_Oregon_Margin_B_10m	MBARI	10 x 10 m	WGS84
MBARI_Oregon_Margin_C_10m	MBARI	10 x 10 m	WGS84
MBARI_Oregon_Margin_D_10m	MBARI	10 x 10 m	WGS84
MBARI_Oregon_Margin_E_10m	MBARI	10 x 10 m	WGS84
MBARI_Oregon_Margin_F_10m	MBARI	10 x 10 m	WGS84
MBARI_Oregon_Margin_G_10m	MBARI	10 x 10 m	WGS84
MBARI_Oregon_Margin_H_10m	MBARI	10 x 10 m	WGS84
MBARI_Oregon_Margin_I_10m	MBARI	10 x 10 m	WGS84
MBARI_Pioneer_Seamount_20m	MBARI	20 x 20 m	WGS84
MBARI_President_Jackson_Seamounts_30m	MBARI	30 x 30 m	WGS84
MBARI_Santa_Barbara_Basin_20m	MBARI	20 x 20 m	WGS84
MBARI_Santa_Barbara_Basin_40m	MBARI	40 x 40 m	WGS84

Dataset	Data Source	Grid Resolution	Coordinate System
MBARI_Santa_Barbara_Basin_Arguello_and_Concepcion_Canyon_Systems_20m	MBARI	20 x 20 m	WGS84
MBARI_Santa_Barbara_Basin_Canyons_Offshore_of_Point_Arguello_10m	MBARI	10 x 10 m	WGS84
MBARI_Santa_Barbara_Basin_Canyons_Offshore_of_Point_Concepcion_10m	MBARI	10 x 10 m	WGS84
MBARI_Santa_Barbara_Basin_Channel_Islands_Slope_East_10m	MBARI	10 x 10 m	WGS84
MBARI_Santa_Barbara_Basin_Channel_Islands_Slope_West_10m	MBARI	10 x 10 m	WGS84
MBARI_Santa_Barbara_Basin_Offshore_of_Goleta_10m	MBARI	10 x 10 m	WGS84
MBARI_Santa_Barbara_Basin_Rodriguez_Seamount_40m	MBARI	40 x 40 m	WGS84
MBARI_Santa_Barbara_Basin_Rodriguez_Summit_15m	MBARI	15 x 15 m	WGS84
MBARI_Santa_Barbara_Basin_Santa_Barbara_Anticline_10m	MBARI	10 x 10 m	WGS84
MBARI_Taney_Seamounts_40m	MBARI	40 x 40 m	WGS84
MBARI_Vance_Seamounts_40m	MBARI	40 x 40 m	WGS84
H11723_5m_Combined_MLLW_4of4	NOAA NOS	5 x 5 m	NAD83, UTM Zone 10N
H11744_50cm_MLLW_1of11	NOAA NOS	50 x 50 cm	NAD83, UTM Zone 10N
H11744_50cm_MLLW_2of11	NOAA NOS	50 x 50 cm	NAD83, UTM Zone 10N
H11744_50cm_MLLW_3of11	NOAA NOS	50 x 50 cm	NAD83, UTM Zone 10N
H11744_1m_MLLW_9of11	NOAA NOS	1 x 1 m	NAD83, UTM Zone 10N
H11744_1m_MLLW_10of11	NOAA NOS	1 x 1 m	NAD83, UTM Zone 10N
H11744_1m_MLLW_11of11	NOAA NOS	1 x 1 m	NAD83, UTM Zone 10N
H11939_MBVB_2m_MLLW_Combined	NOAA NOS	2 x 2 m	NAD83, UTM Zone 10N
H11989_MB_2m_MLLW_combined	NOAA NOS	2 x 2 m	WGS84, UTM Zone 10N
SH15_SH16a_RL16_SH17_8m_MLLW_FINAL	NOAA NOS	8 x 8 m	WGS84, UTM Zone 10N
W00306_MB_32m_MLLW_Combined	NOAA NOS	32 x 32 m	WGS84, UTM Zone 10N
W00311_MB_32m_MLLW_Combined	NOAA NOS	32 x 32 m	NAD83, UTM Zone 10N
H13082_2m_DN280	NOAA NOS	2 x 2 m	NAD83, UTM Zone 10N
H13083_2m_DN280	NOAA NOS	2 x 2 m	NAD83, UTM Zone 10N
EX0801_MB_10m_UTM_Zone10N	NOAA OER	10 x 10 m	WGS84, UTM Zone 10N
EX0903_Mendocino_Central_bathy	NOAA OER	50 x 50 m	WGS84
EX0903_Mendocino_East_bathy	NOAA OER	50 x 50 m	WGS84

Dataset	Data Source	Grid Resolution	Coordinate System
EX0903_Mendocino_West_bathy	NOAA OER	50 x 50 m	WGS84
EX0904_Geog_LatLong_50m_All	NOAA OER	50 x 50 m	WGS84
EX0905_Geog_LatLong_100m_All	NOAA OER	100 x 100 m	WGS84
EX0907_Geog_LatLong_50m_Sanctuary	NOAA OER	50 x 50 m	WGS84
EX1101_MB_FNL_CINMS_30m_WGS84	NOAA OER	30 x 30 m	WGS84
EX1101_MB_FNL_Hancock_109_Seamnts_25m_WGS84	NOAA OER	25 x 25 m	WGS84
EX1101_MB_FNL_PatchTest_50m_WGS84	NOAA OER	50 x 50 m	WGS84
EX1101_MB_FNL_SanJuanSeamnt_75m_WGS84	NOAA OER	75 x 75 m	WGS84
EX1101_MB_FNL_SouthMBNMS_25m_WGS84	NOAA OER	25 x 25 m	WGS84
EX1101_MB_FNL_SurRidge_30m_WGS84	NOAA OER	30 x 30 m	WGS84
EX1102_MB_FNL_50m_WGS84	NOAA OER	50 x 50 m	WGS84
heceta_10m	NOAA PMEL	10 x 10 m	WGS84, UTM Zone 10N
tn173_30m	NOAA PMEL	30 x 30 m	WGS84, UTM Zone 10N
ocnms_multibeam_2011	NOAA OCNMS	8 x 8 m	NAD83, UTM Zone 10N
W00262_MB_2m_MLLW_Combined	NOAA OCNMS	2 x 2 m	NAD83, UTM Zone 10N
odfw_sl_n	ODFW	2.4 x 2.4 m	WGS84, UTM Zone 10N
odfw_sl_s	ODFW	2.4 x 2.4 m	WGS84, UTM Zone 10N
W00341_MB_MLLW_16m_east	OET	16 x 16 m	NAD83, UTM Zone 10N
W00341_MB_MLLW_16m_west	OET	16 x 16 m	NAD83, UTM Zone 11N
NA078_20160831_40m_UTM10N	OET	40 x 40 m	WGS84, UTM Zone 10N
NA078_20160901_50m_UTM10N	OET	50 x 50 m	WGS84, UTM Zone 10N
NA078_20160904_30m_UTM10N	OET	30 x 30 m	WGS84, UTM Zone 10N
NA078_20160904_deadseep_15m_UTM10N	OET	15 x 15 m	WGS84, UTM Zone 10N
NA078_20160906_mound_15m_UTM11N	OET	15 x 15 m	WGS84, UTM Zone 11N
NA078_20160906_WSanPedroChannel_20m_UTM11N	OET	20 x 20 m	WGS84, UTM Zone 11N
W00418_MB_MLLW_16m_cube	OET	16 x 16 m	NAD83, UTM Zone 10N
NA079_20170505_SantaCruzBasin_25m_UTM11N	OET	25 x 25 m	WGS84, UTM Zone 11N
NA080_20170509_SantaCruzBasin_25m_srf	OET	25 x 25 m	WGS84, UTM Zone 11N

Dataset	Data Source	Grid Resolution	Coordinate System
NA080_20170511_SanMiguelSouth_20m_srf	OET	20 x 20 m	WGS84, UTM Zone 10N
NA080_20170511_SouthSantaRosa_25m_srf	OET	25 x 25 m	WGS84, UTM Zone 10N
NA080_20170511_Transit2SantaRosa_25m_srf	OET	25 x 25 m	WGS84, UTM Zone 11N
NA080_20170513_PilgrimBank_15m_srf	OET	15 x 15 m	WGS84, UTM Zone 11N
NA080_20170516_DavidsonSeamount_50m_srf	OET	50 x 50 m	WGS84, UTM Zone 10N
NA080_20170518_PioneerCanyon_10m_srf	OET	10 x 10 m	WGS84, UTM Zone 10N
NA080_20170520_FarallonEscarpment_10m_srf	OET	10 x 10 m	WGS84, UTM Zone 10N
NA080_20170523_BodegaCanyon_20m_srf	OET	20 x 20 m	WGS84, UTM Zone 10N
NA080_20170523_SWCordellBank_20m_srf	OET	20 x 20 m	WGS84, UTM Zone 10N
NA080_20170523_Transit2CordellBank_10m_srf	OET	10 x 10 m	WGS84, UTM Zone 10N
NA080_20170524_BoxCanyon_40m_srf	OET	40 x 40 m	WGS84, UTM Zone 10N
NA080_20170524_NorthBodegaCanyon_30m_srf	OET	30 x 30 m	WGS84, UTM Zone 10N
NA080_20170524_PMEL_CanyonSouth_10m_srf	OET	10 x 10 m	WGS84, UTM Zone 10N
NA080_20170526_SouthOregon2_10m_srf	OET	10 x 10 m	WGS84, UTM Zone 10N
NA080_20170529_PMEL_SouthOregon1_30m_srf	OET	30 x 30 m	WGS84, UTM Zone 10N
NA082_20170629_OCNMS_15m_srf	OET	15 x 15 m	WGS84, UTM Zone 10N
NA086_20170827_JDF_5m_srf	OET	5 x 5 m	WGS84, UTM Zone 10N
NA086_20170830_JDF_South_10m_srf	OET	10 x 10 m	WGS84, UTM Zone 10N
NA086_20170904_QuinaultCanyon_10m_srf	OET	10 x 10 m	WGS84, UTM Zone 10N
NA088_20170913_Astoria_Canyon_30m_srf	OET	30 x 30 m	WGS84, UTM Zone 10N
NA088_20170920_Santa_Rosa_10m_srf	OET	10 x 10 m	WGS84, UTM Zone 10N
NA088_20170921_SantaCruzNorth_5m_srf	OET	5 x 5 m	WGS84, UTM Zone 11N
NA088_20170922_USGS_Catalina_25m_srf	OET	25 x 25 m	WGS84, UTM Zone 11N
NA088_20170923_Potato_Bank_5m_srf	OET	5 x 5 m	WGS84, UTM Zone 11N
NA088_20170927_TannerBank_7m_srf	OET	7 x 7 m	WGS84, UTM Zone 11N
NA088_20170929_USGS_40MileBank_15m_srf	OET	15 x 15 m	WGS84, UTM Zone 11N
Fortythree_fathom_bank_10m	OSU ATSML	10 x 10 m	WGS84, UTM Zone 11N
BandonArago_Combined_4m	OSU ATSML	4 x 4 m	WGS84, UTM Zone 10N

Dataset	Data Source	Grid Resolution	Coordinate System
blanco_4m	OSU ATSML	4 x 4 m	WGS84, UTM Zone 10N
BlancoBlacklock_Combined_4m	OSU ATSML	4 x 4 m	WGS84, UTM Zone 10N
BOEM_Nehalem_8m	OSU ATSML	8 x 8 m	WGS84, UTM Zone 10N
BOEM_Newport_in_shlf_8m	OSU ATSML	8 x 8 m	WGS84, UTM Zone 10N
Cape_Arago_4m	OSU ATSML	4 x 4 m	WGS84, UTM Zone 10N
capefalcon_4m	OSU ATSML	4 x 4 m	WGS84, UTM Zone 10N
Cherry_Bank_10m	OSU ATSML	10 x 10 m	WGS84, UTM Zone 11N
coquille_15m	OSU ATSML	15 x 15 m	WGS84, UTM Zone 10N
Depoe_Bay_extension_usgs_ex_4m	OSU ATSML	4 x 4 m	WGS84, UTM Zone 10N
eureka_18m_bt	OSU ATSML	18 x 18 m	WGS84, UTM Zone 10N
Florence_Combined_4m	OSU ATSML	4 x 4 m	WGS84, UTM Zone 10N
graysbank_8m	OSU ATSML	8 x 8 m	WGS84, UTM Zone 10N
H12122_Combined_4m	OSU ATSML	4 x 4 m	WGS84, UTM Zone 10N
H12122Plus_Combined_4m	OSU ATSML	4 x 4 m	WGS84, UTM Zone 10N
H12123_Combined_4m	OSU ATSML	4 x 4 m	WGS84, UTM Zone 10N
H12124_Combined_8m	OSU ATSML	8 x 8 m	WGS84, UTM Zone 10N
H12125_Combined_4m	OSU ATSML	4 x 4 m	WGS84, UTM Zone 10N
H12126_Combined_8m	OSU ATSML	8 x 8 m	WGS84, UTM Zone 10N
H12127_Combined_8m	OSU ATSML	8 x 8 m	WGS84, UTM Zone 10N
H12128_Combined_8m	OSU ATSML	8 x 8 m	WGS84, UTM Zone 10N
H12129_Combined_4m	OSU ATSML	4 x 4 m	WGS84, UTM Zone 10N
h12130_4m_bth	OSU ATSML	4 x 4 m	WGS84, UTM Zone 10N
h12131_4m_bth	OSU ATSML	4 x 4 m	WGS84, UTM Zone 10N
humbug_bathy	OSU ATSML	4 x 4 m	WGS84, UTM Zone 10N
Lakeside_Combined_4m	OSU ATSML	4 x 4 m	WGS84, UTM Zone 10N
Netarts_Combined_4m	OSU ATSML	4 x 4 m	WGS84, UTM Zone 10N
Newport_sitz_4m	OSU ATSML	4 x 4 m	WGS84, UTM Zone 10N
NewportDepoe_Combined_4m	OSU ATSML	4 x 4 m	WGS84, UTM Zone 10N

Dataset	Data Source	Grid Resolution	Coordinate System
nsaf_8m_bthy	OSU ATSML	8 x 8 m	WGS84, UTM Zone 10N
Osborn_Bank_10m	OSU ATSML	10 x 10 m	WGS84, UTM Zone 11N
Pilgrim_Kidney_Banks_10m	OSU ATSML	10 x 10 m	WGS84, UTM Zone 11N
Potato_Bank_10m	OSU ATSML	10 x 10 m	WGS84, UTM Zone 11N
Seal_Rock_southbeach_4m	OSU ATSML	4 x 4 m	NAD83, UTM Zone 10N
seaside_4m	OSU ATSML	4 x 4 m	WGS84, UTM Zone 10N
Seaside_Combined_8m	OSU ATSML	8 x 8 m	WGS84, UTM Zone 10N
SiletzFill_Combined_4m	OSU ATSML	4 x 4 m	WGS84, UTM Zone 10N
siltcoos_4m_b	OSU ATSML	4 x 4 m	WGS84, UTM Zone 10N
stonewall_2m	OSU ATSML	2 x 2 m	WGS84, UTM Zone 10N
Tanner_Bank_20m	OSU ATSML	20 x 20 m	WGS84, UTM Zone 11N
TN149_Nehalem_Bank_n_5m	OSU ATSML	5 x 5 m	WGS84, UTM Zone 10N
TN149_Nehalem_Bank_s_5m	OSU ATSML	5 x 5 m	WGS84, UTM Zone 10N
wa_inshore_2m	OSU ATSML	2 x 2 m	WGS84, UTM Zone 10N
wa_offshr_25m	OSU ATSML	25 x 25 m	WGS84, UTM Zone 10N
wa_shelf_8m	OSU ATSML	8 x 8 m	WGS84, UTM Zone 10N
wa_sponge_8m	OSU ATSML	8 x 8 m	WGS84, UTM Zone 10N
rf_island_2m	POORT	2 x 2 m	WGS84, UTM Zone 10N
merged_bathymetry_north_borderland_25m	USGS	25 x 25 m	GRS80, UTM Zone 11N
Columbia_River_mouth_1m	USGS	1 x 1 m	NAD83, UTM Zone 10N
DrakesBay_2m	USGS	2 x 2 m	NAD83, UTM Zone 10N
East_SB_channel_block_a_2m	USGS	2 x 2 m	NAD83, UTM Zone 11N
East_SB_channel_block_b_2m	USGS	2 x 2 m	NAD83, UTM Zone 11N
East_SB_channel_block_c_2m	USGS	2 x 2 m	NAD83, UTM Zone 11N
East_SB_channel_block_d_2m	USGS	2 x 2 m	NAD83, UTM Zone 11N
East_SB_channel_block_e_2m	USGS	2 x 2 m	NAD83, UTM Zone 11N
East_SB_channel_block_f_2m	USGS	2 x 2 m	NAD83, UTM Zone 11N
East_SB_channel_block_g_2m	USGS	2 x 2 m	NAD83, UTM Zone 11N

Dataset	Data Source	Grid Resolution	Coordinate System
Elwah_River_Delta_East_1m	USGS	1 x 1 m	WGS84, UTM Zone 10N
Elwah_River_Delta_Mid_1m	USGS	1 x 1 m	WGS84, UTM Zone 10N
Elwah_River_Delta_West_1m	USGS	1 x 1 m	WGS84, UTM Zone 10N
Farallon_Escarpment_10m	USGS	10 x 10 m	NAD83, UTM Zone 10N
Gulf_of_Santa_Catalina_20m	USGS	20 x 20 m	NAD83, UTM Zone 11N
HuenemeCanyon_2m	USGS	2 x 2 m	WGS84, UTM Zone 11N
Los_Angeles_Margin_16m	USGS	16 x 16 m	NAD83, UTM Zone 11N
MontereyCanyon_2m	USGS	2 x 2 m	NAD83(2011), UTM Zone 10N
N_Santa_Barbara_Channe_2m	USGS	2 x 2 m	NAD83, UTM Zone 10N
NChannelIslands_NorthArea_Bathy_5m	USGS	5 x 5 m	WGS84, UTM Zone 11N
North_Monterey_Bay_Block1_2m	USGS	1 x 1 m	NAD83, UTM Zone 10N
North_Monterey_Bay_Block2_2m	USGS	2 x 2 m	NAD83, UTM Zone 10N
Offshore_Aptos_2m	USGS	2 x 2 m	NAD83, UTM Zone 10N
Offshore_Aptos_5m	USGS	5 x 5 m	NAD83, UTM Zone 10N
Offshore_Aptos_CSUMB_3m	USGS	3 x 3 m	NAD83, UTM Zone 10N
Offshore_BodegaHead_2m	USGS	2 x 2 m	NAD83, UTM Zone 10N
Offshore_Bolinas_2m	USGS	2 x 2 m	NAD83, UTM Zone 10N
Offshore_Fort_Ross_2m	USGS	2 x 2 m	NAD83, UTM Zone 10N
Offshore_Pacifica_2m	USGS	2 x 2 m	NAD83, UTM Zone 10N
Offshore_PigeonPoint_2m	USGS	2 x 2 m	NAD83, UTM Zone 10N
Offshore_Salt_Point_2m	USGS	2 x 2 m	NAD83, UTM Zone 10N
Offshore_San_Francisco_2m	USGS	2 x 2 m	NAD83, UTM Zone 10N
Offshore_SanGregorio_2m	USGS	2 x 2 m	WGS84, UTM Zone 10N
Offshore_SantaCruz_2m	USGS	2 x 2 m	NAD83, UTM Zone 10N
Offshore_Tomales_Point_2m	USGS	2 x 2 m	NAD83, UTM Zone 10N
Offshore_Ventura_2m	USGS	2 x 2 m	WGS84, UTM Zone 11N
Oregon_OCS_Coos_Bay_12m	USGS	12 x 12 m	WGS84, UTM Zone 10N
Rittenburg_Bank_2m	USGS	2 x 2 m	NAD83, UTM Zone 10N

Dataset	Data Source	Grid Resolution	Coordinate System
s_ca_merged_intercontinental_25mbathy	USGS	25 x 25 m	NAD83, UTM Zone 11N
San_Diego_Margin_8m	USGS	8 x 8 m	WGS84, UTM Zone 11N
SB_chanwest_1m	USGS	1 x 1 m	WGS84, UTM Zone 11N
SB_chaneast_1m	USGS	1 x 1 m	WGS84, UTM Zone 11N
SB_chancen_1m	USGS	1 x 1 m	WGS84, UTM Zone 11N
sbchannel_10mbathy	USGS	10 x 10 m	NAD83, UTM Zone 11N
SD_OC_Offshore_25m_bathy	USGS	25 x 25 m	WGS84, UTM Zone 11N
Tomales_Bay_4m	USGS	4 x 4 m	WGS84, UTM Zone 10N
tn177_35m	UW	35 x 35 m	WGS84, UTM Zone 10N
tn207_35m	UW	35 x 35 m	WGS84, UTM Zone 10N
tn252_n_50m	UW	50 x 50 m	WGS84, UTM Zone 10N

CSUMB – California State University, Monterey Bay
MBARI – Monterey Bay Aquarium Research Institute
NOAA NOS – National Oceanic and Atmospheric Administration, National Ocean Service
NOAA OER – NOAA Office of Exploration and Research
NOAA OCNMS – NOAA Olympic Coast National Marine Sanctuary
NOAA PMEL – Pacific Marine Environmental Laboratory
ODFW – Oregon Department of Fish and Wildlife
OET – Ocean Exploration Trust
OSU ATSML – Oregon State University Active Tectonics and Seafloor Mapping Lab
POORT – Port Orford Ocean Research Team
USGS – US Geological Survey
UW – University of Washington

Department of the Interior (DOI)

The Department of the Interior protects and manages the Nation's natural resources and cultural heritage; provides scientific and other information about those resources; and honors the Nation’s trust responsibilities or special commitments to American Indians, Alaska Natives, and affiliated island communities.

Bureau of Ocean Energy Management (BOEM)

The mission of the Bureau of Ocean Energy Management is to manage development of U.S. Outer Continental Shelf energy and mineral resources in an environmentally and economically responsible way.

BOEM Environmental Studies Program

The mission of the Environmental Studies Program is to provide the information needed to predict, assess, and manage impacts from offshore energy and marine mineral exploration, development, and production activities on human, marine, and coastal environments. The proposal, selection, research, review, collaboration, production, and dissemination of each of BOEM’s Environmental Studies follows the DOI Code of Scientific and Scholarly Conduct, in support of a culture of scientific and professional integrity, as set out in the DOI Departmental Manual (305 DM 3).